NOAA Technical Report NESDIS 57

WATER VAPOR IMAGERY

INTERPRETATION AND APPLICATIONS TO WEATHER ANALYSIS AND FORECASTING

Roger B. Weldon
and
Susan J. Holmes
Office of Research and Applications
Physical Science Branch

Washington, D.C.
April 1991

U. S. DEPARTMENT OF COMMERCE
Robert A. Mosbacher, Secretary

National Oceanic and Atmospheric Administration
John A. Knauss, Under Secretary

National Environmental Satellite, Data, and Information Service
Thomas N. Pyke, Jr., Assistant Administrator

ABSTRACT

In Part One, satellite radiation measurements in the 6.7μm and 7.3μm bands are compared to atmospheric moisture and temperature soundings. Concepts developed from a computer model of radiation transfer are related to satellite observations and radiosonde data. In Part Two, patterns and features observed on 6.7μm satellite imagery are related to atmospheric wind and temperature fields. Applications of water vapor imagery to weather analysis and forecasting are suggested.

Overview

Satellite measurements of radiation in the 6.7μm and 7.3μm infrared bands are significantly affected by water vapor suspended in the atmosphere. The individual measurements by the satellite instruments may be assigned gray shades or colors and displayed in arrays as images. Since these images are well correlated to the temperature of the atmospheric moisture, they are referred to as "water vapor imagery." The purpose of our studies and this presentation is to enable more accurate interpretation of water vapor imagery.

The interpretation problem may be divided into two fundamental questions in regard to the imagery. Each individual pixel on an image represents a single scalar value measured by the satellite, and displayed as some specific gray shade or color. The first question is: what information does this gray shade or color provide in regard to the vertical distributions of moisture and temperature in the path of the radiation? Many pixels in an array produce patterns and features of gray shades or colors. The second question is: how do these patterns and their changes with time relate to atmospheric circulation systems and processes? This presentation is divided into two parts, based upon the two fundamental questions. Part One, approximately 25% of the total number of pages, addresses the first question on image gray shades. The second question, on image patterns and their changes, is addressed by Part Two, which accounts for the remaining 75% of the pages.

Reading Sequence

Either Part One or Part Two may be read independently of the other. Within each part, successful interpretation of the imagery may require knowledge of concepts presented in the other part; however, this information is generally provided when required. For those readers of Part Two only, a special discussion of image grade shade interpretation is provided at the end of Part One. The discussion, "IMAGE GRAY SHADES - A GUIDE TO INTERPRETATION" is not a direct summary of Part One. Although the same problem of image gray shade interpretation is addressed, the section is written from a perspective independent of Part One.

PART ONE

Radiation Effects From Varied Moisture and Temperature Soundings

A computer model of radiation transfer is applied to examine the various factors affecting radiation measurements. Controlled sets of simulated moisture and temperature profiles are examined, using the model to predict the satellite measured "brightness temperatures" and to compare the different origins of radiation contributing to the measurements. Although the use of the model provided detailed analysis of the radiation origins, it did not provide actual measurements. Therefore, qualitative concepts derived by studies of simulated soundings were evaluated using satellite imagery and corresponding radiosonde data. Case studies are examined, comparing satellite imagery, radiosonde data, and radiation model computations from the radiosonde measurements.

Although the information presented in Part One is quantitative, the primary objective is to provide qualitative relationships and concepts that may be applied to estimating vertical moisture and temperature distributions from image gray shades.

PART TWO

Patterns and Features on 6.7μm Water Vapor Imagery

Individual images and sequences of imagery from geostationary satellites are shown to illustrate and compare common patterns and their changes with time. Selected analyses of wind, temperature, and pressure fields are overlain on images to illustrate empirical relationships between image patterns and atmospheric circulation systems. In Section A, basic types of boundaries commonly observed on water vapor imagery are described and compared. In Section B, commonly observed changes with time of boundaries and other image features are illustrated and related to their associated atmospheric processes. In Section C, water vapor imagery associated with cyclogenesis are examined; and, in Section D, the image features related to upper air troughs, ridges, and jet streams are illustrated and compared. Finally, in Section E, some tropical applications of water vapor imagery are suggested.

The basic method of presentation of Part Two is to show and describe, and to identify empirical relationships between imagery and circulation systems. However, considerable effort has been made to provide perspective derived from observing many times the number of cases as those shown. We have attempted to emphasize the most common features and changes, but have discussed exceptions and variations. We have also attempted to provide the degree of reliability of the empirical relationships illustrated and described.

General Outline

PART ONE
RADIATION EFFECTS FROM VARIED MOISTURE AND TEMPERATURE SOUNDINGS

SECTION A FACTORS THAT AFFECT THE SATELLITE MEASURED RADIATION

SECTION B MOIST LAYERS - THEIR EFFECTS ON RADIATION MEASUREMENTS

SECTION C CASE STUDIES - WATER VAPOR IMAGES AND RADIOSONDE DATA

IMAGE GRAY SHADES - A GUIDE TO INTERPRETATION

PART TWO
PATTERNS AND FEATURES ON 6.7μm WATER VAPOR IMAGERY

SECTION A BASIC TYPES OF BOUNDARIES

SECTION B EVOLUTION OF FEATURES

SECTION C CYCLOGENESIS AND STORM EVOLUTION

SECTION D MOISTURE PATTERNS OF SPECIFIC CIRCULATION SYSTEMS AND FEATURES

SECTION E TROPICAL APPLICATIONS

Table Of Contents

PART ONE
RADIATION EFFECTS FROM VARIED MOISTURE AND TEMPERATURE SOUNDINGS

SECTION A FACTORS THAT AFFECT THE SATELLITE MEASURED RADIATION 2

1. INTRODUCTION - RADIATION MEASUREMENTS IN IMAGE FORMAT 2
2. ANALYSIS OF A SINGLE RADIATION MEASUREMENT 5
3. BASIC FACTORS THAT INFLUENCE THE RADIATION MEASUREMENTS. 7
   - a. The Wavelength of the Radiation 7
   - b. The Amount of Water Vapor Within the Path of the Radiation 7
   - c. The Vertical Location of the Moisture 9
   - d. The Temperature of the Air Column 11
4. SUMMARY - SECTION A 13

SECTION B MOIST LAYERS - THEIR EFFECTS ON RADIATION MEASUREMENTS 14

1. BRIGHTNESS TEMPERATURES FROM VARIED MOISTURE DISTRIBUTIONS 14
   - Background Moisture
   - "Deep" Moist Layers
   - "High" Moist Layers
   - Four Single Moist Layers Compared
2. RADIATION FROM SHALLOW MOIST LAYERS AT VARIED HEIGHTS 18
   - a. Radiation From Fourteen Moist Layers 18
   - b. The "Crossover" Effect 19
   - c. Variations of Humidity Within The Moist Layers 21
   - d. 7.3μm Radiation Characteristics From The 14 Moist Layers 21
3. A COMPARISON OF SINGLE LAYER RADIATION RESULTS 23
4. COMBINATIONS OF 100mb THICK MOIST LAYERS 23
5. SUMMARY - SECTION B 25

SECTION C CASE STUDIES - WATER VAPOR IMAGES AND RADIOSONDE DATA 26

1. TWO SIGNIFICANT LIMITATIONS OF THE TRANSMITTED RADIOSONDE DATA 26
2. GENERAL COMPARISON - 6.7μm GOES IMAGERY AND RADIOSONDE DATA. 28
   - a. Case Discussion - 19 May 1983 30
   - b. Case Study - 03 May 1983 32
3. COMPARISON - RADCOM RESULTS, IMAGE BRIGHTNESS, AND RADIOSONDE MOISTURE 37
   - a. Case Study - 26 May 1982 37
     - General Description
     - Cloud Conditions Along The Cross Section
     - General Comparison - Cross Section Soundings And Imagery
     - The Origin Of Radiation Reaching The Satellite - Moist Layers
4. VARIED CHANNEL COMPARISON - POLAR ORBITING AND GOES SATELLITE IMAGERY 42
   - a. Case Study - 20 December 1983 42
     - "Brightness Index" - Explanation and Comparison to "Image Brightness"
     - General Description - The 20 December 1983 Circulation Systems
     - Cloud Conditions
     - The Water Vapor Imagery
     - Radiosonde Data Compared to Imagery
     - The Effects Of Very Cold Air
     - The Effects Of Large Temperature Inversions
   - b. Case Study - 19 October 1982. 51
     - General Description
     - The Water Vapor Imagery And Radiosonde Moisture Distributions
     - A Mountain Effect On Water Vapor Imagery

IMAGE GRAY SHADES - A GUIDE TO INTERPRETATION 53

- a. Radiation Concepts 53
- b. 6.7μm Imagery 53
- c. Image Gray Shades And The "Topographic" Concept 53
- d. Primary Exceptions To The Topographic Concept. 55
- e. Clouds 56
- f. Gray Shade Interpretation - A Practical Guide 57

PART TWO
PATTERNS AND FEATURES ON 6.7μm WATER VAPOR IMAGERY

SECTION A BASIC TYPES OF BOUNDARIES 61

1. HEAD BOUNDARIES 63
   - a. "Head Blocking" - A General Concept 63
   - b. "Head Boundaries" of Synoptic Scale Systems 64
     - Image Characteristics of Head Boundaries
     - Upper Air Analysis Features Related to Head Boundaries
2. BOUNDARIES ON THE FORWARD SIDES OF UPPER AIR TROUGHS 66
   - a. Parallel Jet Stream Boundaries 67
   - b. Dry Surge Boundaries 69
     - Image Features
     - Relationships to the Wind Field
   - c. "Baroclinic Leaf" Boundaries 71
3. BASE SURGE BOUNDARIES 72
4. INSIDE BLOCKING -"INSIDE" BOUNDARIES 75
5. RETURN MOISTURE AND RESIDUAL EFFECTS 77
   - a. Introduction 77
   - b. A "Return Moisture" Boundary 77
   - c. Boundary Changes and Residual Effects 79
6. SUMMARY - BOUNDARIES 80

SECTION B EVOLUTION OF FEATURES 85

1. "DARK" REGIONS AND "DARKENING" WITH TIME 85
   - a. Darkening With Time in Westerly Wind Regimes 86
     - Dry Surge Darkening
     - Head Darkening
   - b. Base Darkening 90
2. ANTICYCLOGENESIS - INSIDE BOUNDARY EVOLUTION 95
   - a. Blocking System - Spring Season 95
     - Inside Boundary Formation and Characteristics
     - Vertical Variations and Vertical Phase Differences
   - b. Moving System - Winter Season 100
   - c. Inside Perturbations - Reverse Image Patterns 103
3. A "CUT-OFF" CYCLONE WITH A "ROLL-OVER" SYSTEM EVOLUTION 104
   - a. Overview - "Blocking Regimes" and System Evolutions 104
     - Two Basic Types of Blocking Regime Formations
     - Two Common Types of Evolution of Large Blocking Regimes
   - b. Introduction to the Case Study 106
     - Imagery and Analyses
     - Image Patterns Near the Mature Phase of the "Roll-Over" Cycle
   - c. System Evolution - "Roll-Over" Cycle 109
   - d. Moisture Pattern Changes Related to the Opening of the Cut-Off Low 121
   - e. Summary and Perspective 121
4. A COMBINATION BLOCKING REGIME WITH A "BUILD-BACK" EVOLUTION 123

SECTION C CYCLOGENESIS AND STORM EVOLUTION 125

1. A BASIC STORM SYSTEM DEVELOPMENT AND EVOLUTION 125
   - a. The Formation of a "Baroclinic Leaf" Cloud System 127
   - b. The "Baroclinic Leaf" System and Related Analyses 129
     - Low Level Conditions
     - "Leaf" Characteristics - Water Vapor Imagery
     - The Convex Boundary of the "Leaf"
     - The Concave Boundary of the "Leaf"
     - General Analyses and Image Features
   - c. The Cyclogenesis Phase of the Storm Evolution 131
     - "Leaf" to "Comma" Evolution with "Cusp" Formation
     - Related Surface and Upper Air Analyses
     - Boundary Evolutions - Water Vapor Imagery
   - d. The Mature Storm Phase 141
2. A "CUT-OFF LOW" DEVELOPMENT WITH A DARK CORE REGION 142
3. A DEVELOPMENT WITH VERY RAPID DEEPENING SURFACE CYCLOGENESIS 144
   - a. A "Very Rapidly Deepening" Storm - The Surface Low Center Track 144
   - b. The "Leaf" Phase of Development 144
   - c. The "Leaf" to "Open Comma" Transition 147
   - d. The "Slotted Storm" Phase 148

SECTION D MOISTURE PATTERNS OF SPECIFIC CIRCULATION SYSTEMS AND FEATURES 150

1. CYCLONES - THEIR PATTERNS ON WATER VAPOR IMAGERY . . . 150
   a. Combination Moist-Dry Core Systems - the Most Common Condition . . . 150
   b. Spiral Moisture Patterns with Cyclones . . . 151
   c. Dark or Dry Core Cyclones . . . 152
   d. Light or Moist Core Cyclones . . . 153
   e. "Vorticity Eye Features" . . . 154
2. ANTICYCLONES AND RIDGES . . . 155
   a. Closed Anticyclones . . . 155
   b. Open Ridges . . . 156
      Basic Convex Poleward Boundary
      Split Ridges - Apex on Poleward Boundary
      Head Ridges to Left of Primary Jet Axis
3. JET STREAMS - RELATED PATTERNS ON WATER VAPOR IMAGERY . . . 160
   a. Introduction . . . 160
      Three Types of Jet Stream Structure . . . 160
         Channeled Jet Structure
         NVA Type Advection Jet Structure
         PVA Type Advection Jet Structure
      Some General Observations on Relating Water Vapor Imagery And Jet Streams . . . 161
         Parcel Motion Vectors
         Three Methods of Locating Jet Core Regions on Satellite Imagery
   b. Jet Stream Conditions Related to Common Image Patterns . . . 162
      Boundaries On The Forward Sides Of Upper Air Troughs . . . 162
         Straight Boundaries
         "Cyclonically" Curved Or "Concave" Boundaries
         "Convex" And "S" Shaped Boundaries
      Boundaries Associated With Blocking Circulation Regimes . . . 169
         Inside Boundaries - "Roll-Over" Ridge With Anticyclogenesis
         "Head" Boundaries - "Build-Back" Ridge With Cyclogenesis
         Boundary Combinations - "Head" And "Inside" - The "Omega Block"
      Boundaries And Slots On The West Side Of Closed Lows . . . 171
      Boundaries Oriented Generally West To East . . . 174
         Boundaries At The Base Of Troughs
         Boundaries Over The Poleward Sides Of Ridges
         Straight Or Zonal Boundaries
   c. Change With Time and System Interactions . . . 176
      Changes Associated With Thermal Ridge Developments . . . 176
      Thermal Trough Intensification . . . 178
      Interactions - Thermal Ridge And Thermal Trough . . . 178
      Interactions - Thermal Ridge To Thermal Ridge . . . 179
      Interactions - Thermal Trough To Thermal Trough . . . 179
      A Summary Of Jet Stream Changes And Interactions . . . 181

SECTION E TROPICAL APPLICATIONS . . . 183

1. LARGE SCALE FEATURES . . . 184
   a. Large Tropical Dark Regions . . . 184
   b. Dark Regions Over Land . . . 187
2. SOME SYNOPTIC SCALE FEATURES AT TROPICAL LOCATIONS . . . 188
   a. An Upper Air Cyclone with Core Convection . . . 188
   b. Inside Blocking Regimes at Low Latitudes . . . 190
3. SYNOPTIC SCALE FEATURES UNIQUE TO TROPICAL LATITUDES . . . 192
   a. A Base Surge Boundary and Weather Regime Change . . . 192
   b. Base Surge Across the Equator . . . 195
   c. Cloud Conditions Affected by System of Opposite Hemisphere . . . 195
   d. Dry Blocking Regimes Across the Equator . . . 195
   e. Perturbations on the ITCZ Moisture Boundaries . . . 195
4. WATER VAPOR IMAGE PATTERNS RELATED TO TROPICAL CYCLOGENESIS . . . 199
   a. Model Patterns of Favorable Image Conditions . . . 200
   b. A Tropical Cyclone Formation in the "Base Ridge" Location . . . 203
   c. An "RE1" Formation and Westerly Jet Stream Break-Through . . . 207
   d. A Base Surge Effect on an Existing Organized Convective System . . . 209
   e. A Category I "Hybrid" Type of Tropical Cyclone Development . . . 210

This page intentionally left blank

PART ONE

RADIATION EFFECTS FROM VARIED MOISTURE AND TEMPERATURE SOUNDINGS

SECTION A

FACTORS THAT AFFECT THE SATELLITE MEASURED RADIATION

Instruments on the NOAA satellites measure radiation in several different wavelengths within the infrared range of the spectrum. In some of these wavelength ranges, or "bands", the radiation reaching the satellite is significantly absorbed and reradiated by water in its gaseous state. Therefore, water suspended in the atmosphere needn't be in droplet or ice crystal form to be detected by the satellite.

Within the infrared bands, including the "water vapor" channels, radiation will be emitted by solid objects such as cloud elements, precipitation, and the surface of the earth. The intensity of the radiation is closely correlated to the temperature of the objects or substance from which the radiation is emitted. Thus, by measuring the intensity of the radiation arriving from below, the satellite instrument can detect the temperatures of such things as cloud tops, land, and sea surfaces. However, if water vapor exists between the object and the satellite, it will absorb a portion of the upcoming radiation and reradiate. Since temperature usually varies considerably along the "vertical" path to the satellite, this reradiation by the water vapor will occur at a different energy level.

The water vapor will usually radiate at a lesser energy level, since it is commonly cooler than the earth's surface or cloud tops radiating from below. Generally, the effect of the water vapor existing in the path to the satellite is to reduce the net intensity of the radiation reaching the satellite. The satellite will detect a colder temperature because of the water vapor's presence. It is be this method, that the satellite detects the moisture suspended in the atmosphere.

Note, however, that the effect could be the opposite, if - for example - abundant moisture were present within a strong temperature inversion. Although such net warming by the moisture occurs, it is not prevalent. Generally, with strong temperature inversions, the top of the moisture coincides with the base of the inversion; or, the moisture extends through the inversion into the cooler air above. The "warming" effect occurs most frequently over continents during winter with intense radiational cooling or strong poleward advection of air above the boundary layer.

1. INTRODUCTION - RADIATION MEASUREMENTS IN IMAGE FORMAT

Each measurement of the intensity of the upcoming radiation may be converted to a temperature value. A temperature measured by this process shall be referred to as "brightness temperature". The radiation measurement may also be assigned a gray shade and displayed as a single "pixel", as part of a large array of pixels in mapped format to produce imagery. On common water vapor imagery, white indicates very low energy radiation, or very cold brightness temperature; and, black indicates high energy warm brightness temperature.

Of the "water vapor" infrared channels available on current NOAA satellites, bands in the 6.7 and 7.3 micrometer wavelengths are most commonly displayed and used in image format. Of these two bands, the 6.7μm radiation is more highly absorbed by water vapor, and is more sensitive to differences in the amount of water vapor in the path.

Shown on **Figure 1** are images for the same time and area. The image in **Figure 1a** is of 6.7μm radiation, which may be compared to an image of "standard" or "window" infrared radiation in **Figure 1b**. High cold clouds appear very similar on "water vapor" imagery as on the "standard IR" imagery, except that the borders are generally not as well defined. On 6.7μm imagery, middle and low cloud patterns are generally modified or totally obscured by reradiation from the water vapor above them.

Considering the portion of **Figure 1a** where high clouds are not a significant factor; what do the various gray shades and their patterns represent in regard to atmospheric constituents and conditions? Some common generalizations are the following. The gray shades represent:

- The humidity at some specific level or surface in the atmosphere, such as 400mb.
- The amount of moisture through a vertical column of the atmosphere, such as total water or precipitable water
- A topography of the height of the significant moisture in the atmosphere.
- The relative humidity.

Although some of the simplifications have merit, none of them are correct. The topography representation is perhaps the best of the list as a generalization. In a simple sentence, the satellite instrument indicates the temperature of the moisture that it "sees".

The complicating factor is: what does the satellite "see"?

The water vapor is not opaque to the radiation. The degree of penetration by the radiation through the water vapor varies considerably, depending upon the relative concentration or density of the water vapor. For most practical purposes, water vapor is nearly opaque to 6.7μm radiation, only when it is highly concentrated in nearly saturated warm air, such as a tropical marine layer. But, in nearly saturated cold upper tropospheric air, water vapor is nearly transparent to the same radiation.

In general, radiation reaching the satellite from water vapor, does not arrive from a single surface or level, but from some layer of finite depth. Water vapor - in its most common concentrations - is semitransparent to the radiation. Therefore, the brightness temperature measured by the satellite is a "net" temperature of some layer of moisture, not the temperature of any single surface or level.

The more densely concentrated is the water vapor, the more shallow is the layer from which radiation arrives at the satellite. The concept is similar to a person looking into fog. The depth of visibility decreases as the density of the fog increases. We can think of the satellite "seeing" down into the water vapor in a similar manner; but, it senses or "sees" temperature instead of visible light.

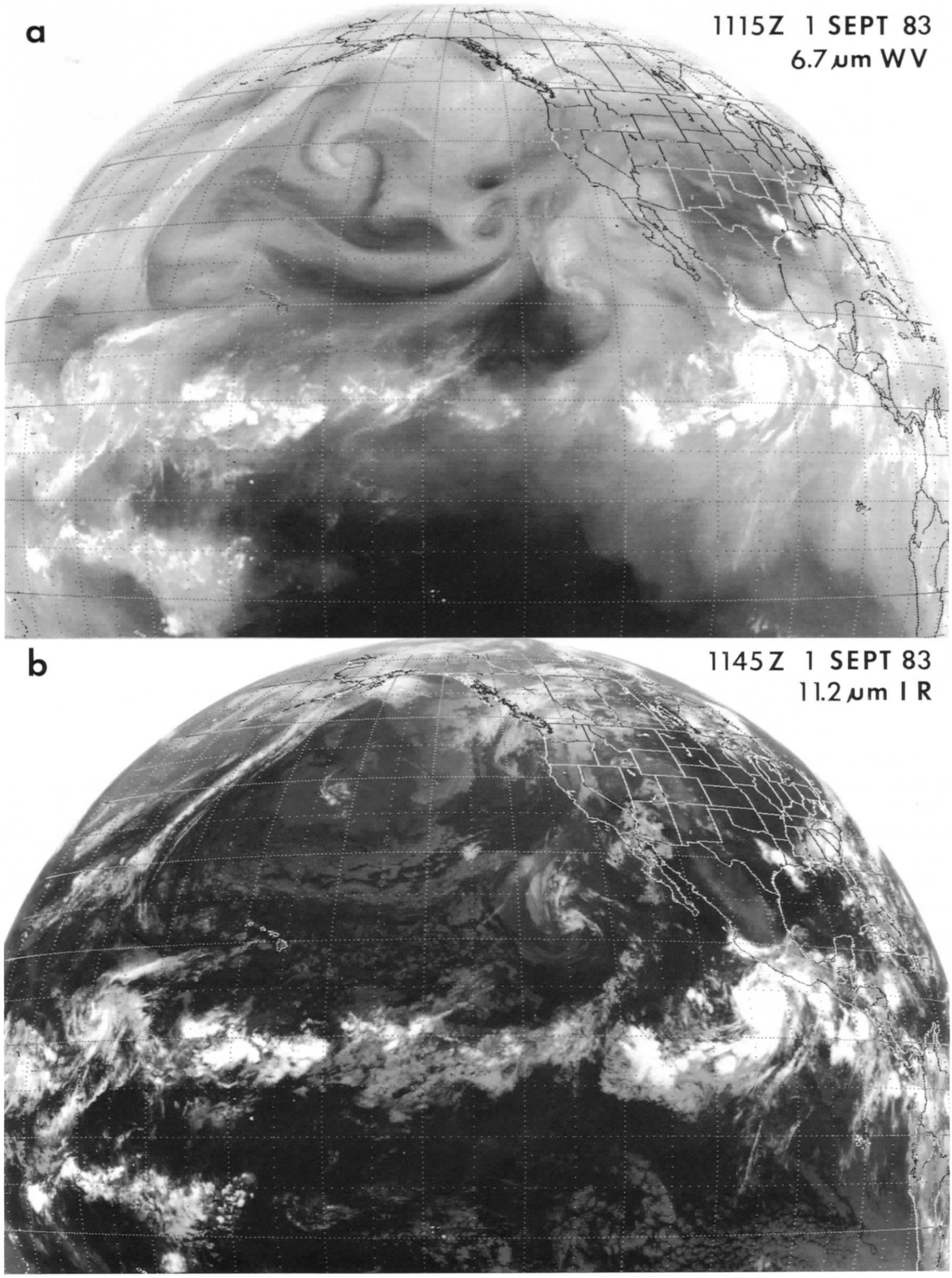

Figure 1

IMAGE COMPARISON

Fig. 1a. 6.7μm Water Vapor Image, 1115Z 01 September 1983, GOES West,

Fig. 1b. "Window" Infrared, 11.2μm Image, 1145Z 01 September 1983, GOES West.

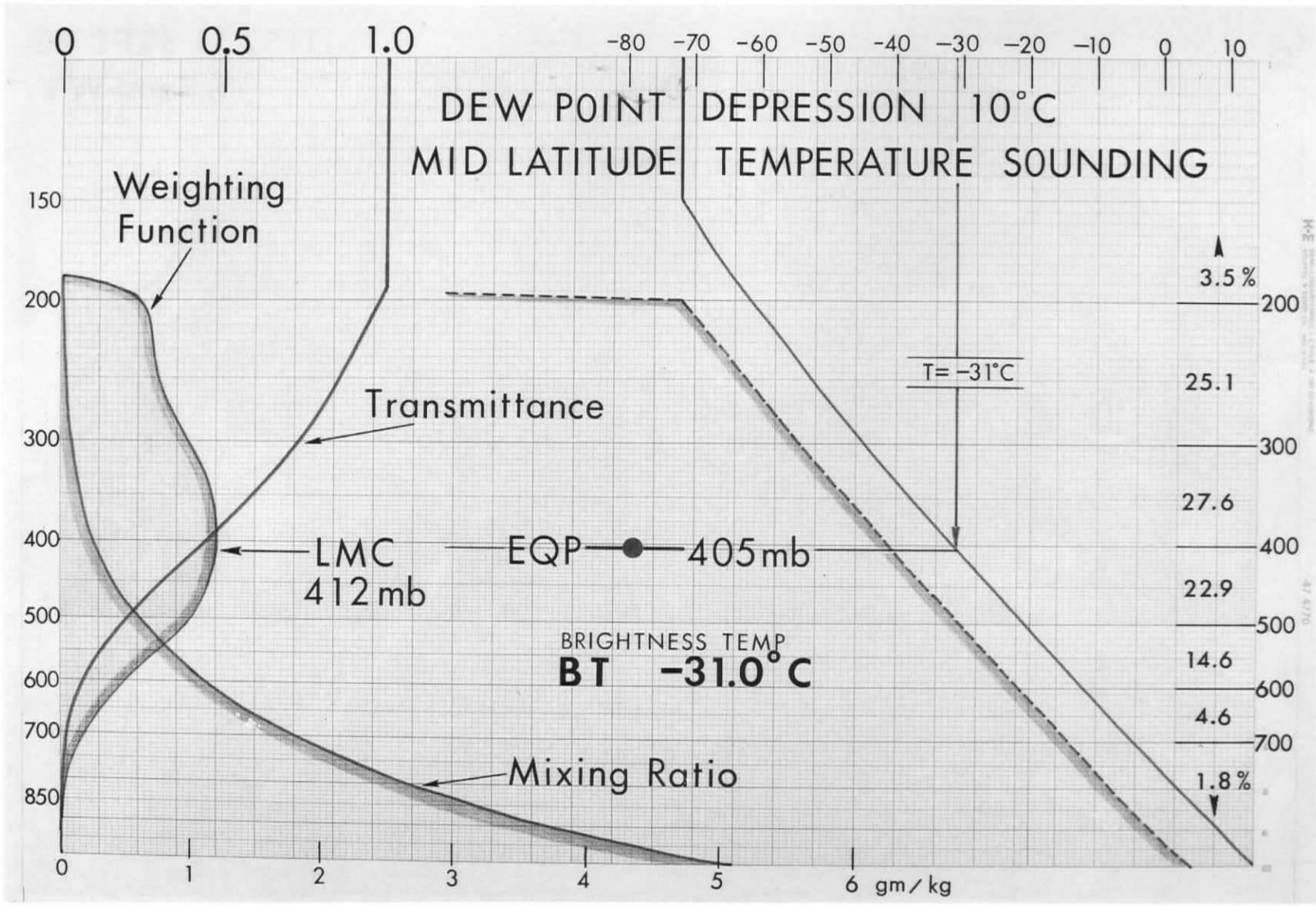

Figure 2 **MID-LATITUDE TEMPERATURE SOUNDING - RADIATION ANALYSIS**
Plotted on the right side of the graph are curves of Air Temperature (solid line) and Dewpoint Temperature (dashed line). The vertical scale of this graph and others of Part One is logarithmic pressure in millibars. The scale for Weighting Function is shown on **Figure 9**.

BT - Brightness Temperature

The brightness temperature computed by the RADCOM model - degrees Celsius (°C).

Mixing Ratio

A measurement of moisture by mass - the ratio of gaseous water in grams to the mass of dry air in kilograms

Transmittance

A ratio from zero to one which describes the rate of absorption of radiation as it passes upward through the atmosphere. Transmittance, at a given level, is the ratio of all the radiation arriving from below that level which penetrates to the satellite. Or, transmittance describes how much absorption will be accomplished on the radiation reaching that level, by all of the water vapor above that level. [For example: At 150mb the transmittance is 1.0. All of the radiation arriving from below 150mb will reach the satellite. At 500mb only 21% of the radiation arriving from below will pass through the moisture above and reach the satellite].

Weighting Function

The percentage of total radiation reaching the satellite which is contributed by each 300 meter layer of the atmosphere. It illustrates the relative vertical contribution of radiation by moisture suspended in the atmosphere. It does not reveal the percentage of radiation contributed by the earth's surface. That is stated separately when applicable. From the model, weighting function is derived from the vertical change of transmittance. The weighting function curves are smoothed from 300m layer values plotted at layer midpoints.

LMC - Level of Maximum Contribution

The altitude of the maximum weighting function value, expressed as the pressure surface at the center of the particular 300m layer having the maximum contribution. (Excluding any contribution by the earth's surface).

EQP - Equivalent Pressure

The pressure surface at which the air temperature equals the brightness temperature.

2. ANALYSIS OF A SINGLE RADIATION MEASUREMENT

In Sections A and B of Part One, radiation characteristics are examined using the "RADCOM" computer model (See References 1 and 2). This computer model simulates the transmittance of radiation by water vapor in the atmosphere, and provides an estimation of the "brightness temperature" that would be measured by the satellite for any given vertical distribution of moisture, temperature, and pressure. The model also provides detailed information on the origin of radiation reaching the satellite.

A water vapor image consists of a large array of individual pixels. The gray shade or color assigned to each pixel is determined by a single measurement of the radiation arriving from a relatively small area in the view of the satellite. For a given wavelength, such as 6.7μm, each measurement provides a single scalar value of radiation intensity. The basic question to be addressed here is: what distribution of moisture and temperature in the atmosphere contributed to that radiation measurement? We shall reverse this procedure, temporarily. The "RADCOM" model will be used to compute the radiation measurements for controlled sets of moisture and temperature soundings.

Consider a single distribution of moisture and temperature, and its contribution to the net radiation reaching the satellite, as estimated by the computer model. On the right side of **Figure 2**, an atmospheric sounding is shown by plotted curves of air temperature and dewpoint temperature. Moisture is present between 1000mb and 200mb, with a constant 10°C dewpoint depression. The air temperature is nearly identical to the U.S. Standard Atmosphere, but with a higher colder tropopause. Computed data shown on the figure are for 6.7μm radiation. The computed brightness temperature for 6.7μm radiation transmitted through this moisture is -31.0°C. The computer model estimated that this value is equivalent to the radiation measurement that would be made by the satellite for an area of such atmospheric conditions. On a typical image display, as those shown here, the -31.0°C brightness temperature would be assigned a very light gray shade.

In addition to the temperature and dewpoint temperature curves shown on **Figure 2**, there are several other curves and plotted data that will be used on subsequent illustrations. Explanations of those curves and data are provided in the expanded caption with **Figure 2**. We direct your attention to that information for reference to subsequent figures and discussion.

It is useful to examine some of the details that contributed to the -31.0°C brightness temperature. In addition to the dewpoint temperature plot on the figure, the moisture distribution is illustrated by mixing ratio. The water content - by mass - decreases rapidly with increasing altitude. Note that 48.7% of the total water content is below 850mb; 77.5% is below 700mb, and 92.5% is below 550mb.

At 550mb, the transmittance is 0.13. Only 13% of the radiation from the 92.5% of the water vapor penetrates to the satellite. This illustrates why the gray shade differences on imagery are not well correlated with total precipitable water. In this specific sounding, the transmittance is nearly zero at 850mb. The moisture below 850mb - almost half of the total water - could be removed from the column, and the brightness temperature would not vary significantly from the -31°C value. If low clouds were present, even with tops as high as 700mb where the transmittance is 0.02; their presence would not be detectable on standard 6.7μm imagery. Note that this is true with the mid and high level moisture present as shown in this particular sounding - not under other atmospheric conditions.

The weighting function curve of **Figure 2** indicates the relative contribution by moisture at various levels to the total radiation reaching the satellite. The weighting function - or relative contribution - increases downward as the amount of moisture increases. However, continuing downward, the accumulative effect of the moisture above absorbing more and more radiation, also increases. At some point, the absorption effect overpowers the increased moisture effect; and the contribution reaches a peak value. This level of maximum weighting function - the "LMC" - occurs at 412mb for the sounding in **Figure 2**.

The "equivalent pressure", where the air temperature is equal to -31°C, occurs at 405mb. That is the level where the water vapor radiates at the same intensity indicated by the brightness temperature. Note however, by the weighting function curve, that large amounts of the radiation are contributed by the moisture through a very deep layer of the atmosphere. The percentages of total radiation contributed by 100mb thick layers are shown at the right side of the figure.

When moisture is present through a relatively deep layer of the middle and upper troposphere, as in this sounding, radiation reaching the satellite is contributed from a relatively deep layer; and, the existence of moisture above prevents the detection of low level moisture and clouds. Soundings similar to that on **Figure 2** do sometimes occur in the real atmosphere. Commonly, however, moisture in the atmosphere is distributed in one or more layers, with more complex vertical variations. Layered distributions will be considered in Section B, and illustrated in case studies in Section C. The more complex moisture distributions and radiosonde observations are easier to understand if the factors that influence radiation measurements are considered first individually.

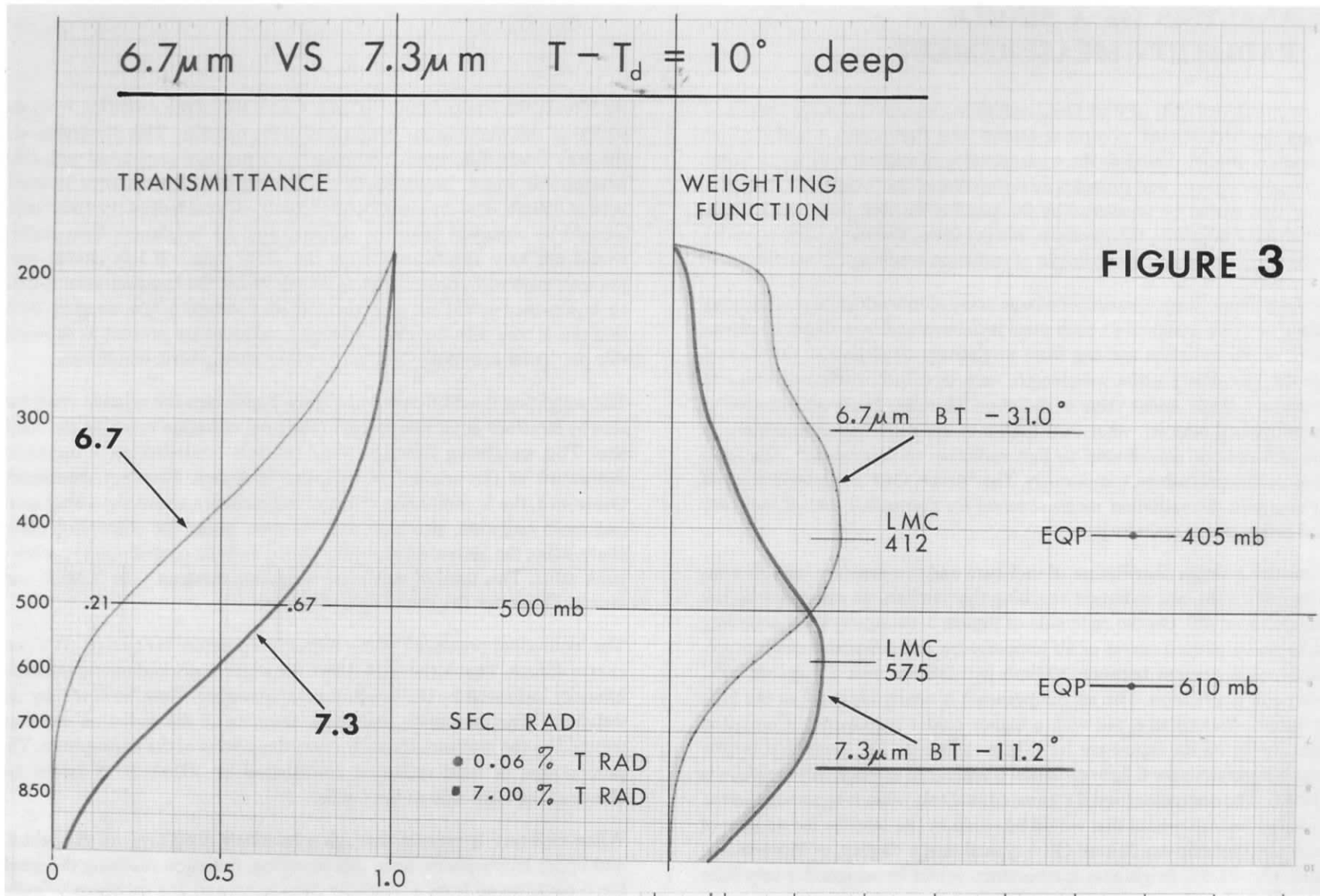
6.7μm VS 7.3μm T − Td = 10° deep
TRANSMITTANCE
WEIGHTING FUNCTION
FIGURE 3
200
300
400
500
600
700
850
6.7
7.3
.21
.67
500 mb
SFC RAD
0.06 % T RAD
7.00 % T RAD
6.7μm BT −31.0°
LMC 412
EQP 405 mb
LMC 575
EQP 610 mb
7.3μm BT −11.2°
0
0.5
1.0

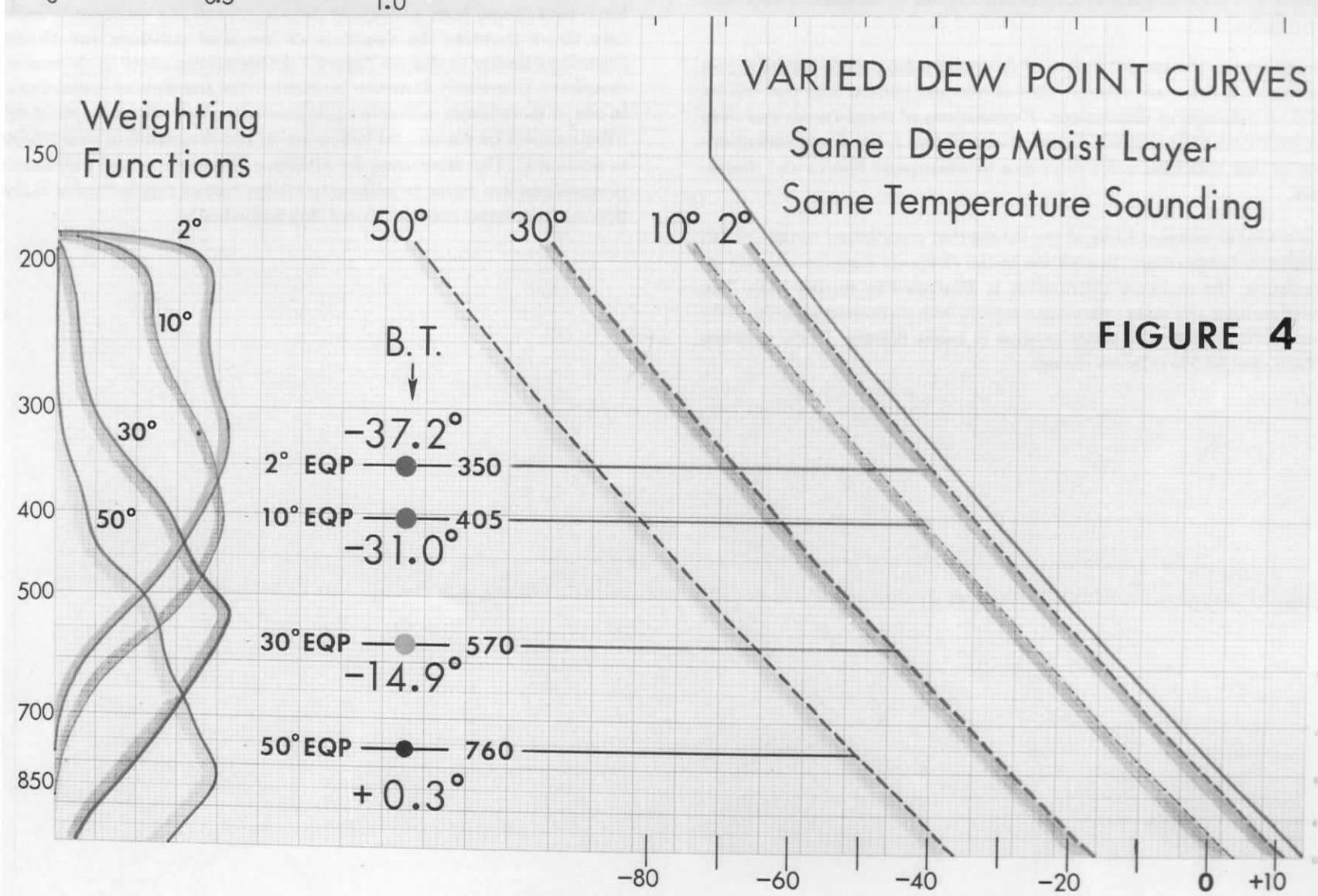
VARIED DEW POINT CURVES
Same Deep Moist Layer
Same Temperature Sounding
Weighting Functions
FIGURE 4
150
200
300
400
500
700
850
2°
10°
30°
50°
B.T.
−37.2°
2° EQP 350
10° EQP 405
−31.0°
30° EQP 570
−14.9°
50° EQP 760
+0.3°
−80
−60
−40
−20
0
+10

3. BASIC FACTORS THAT INFLUENCE THE RADIATION MEASUREMENTS

Radiation reaching the satellite is affected by a complex set of variables. From those, we have defined four basic factors: the radiation wavelength, the amount of water vapor in the radiation path, the vertical location of the water vapor, and the temperature of the water vapor. It is useful to consider the effect of each factor individually on the radiation measurements.

a. The Wavelength of the Radiation

On **Figure 3**, characteristics of 6.7μm and 7.3μm radiation are compared for the same distribution of moisture and temperature. The sounding used is the same as that of **Figure 2**, a constant 10° dewpoint depression through a deep vertical layer.

Plots of transmittance and weighting function for 7.3μm radiation are superimposed with those already shown for 6.7μm radiation. The computed intensity of 7.3μm radiation from the same sounding is equivalent to a brightness temperature of -11.2°C compared to -31.0°C for 6.7μm radiation.

Observing 7.3μm radiation, the satellite "sees" lower into the moisture. A larger amount of the higher energy radiation from the lower warmer moisture penetrates upward to the satellite at the 7.3μm wavelength.

The 7.3μm radiation is absorbed less by the water vapor than the 6.7μm radiation. Note that the earth's surface contributed 7% of the total 7.3μm radiation; whereas, the surface contribution to the total 6.7μm radiation was insignificant.

Comparing the weighting function curves, recall that only 1.8% of the total 6.7μm radiation reached the satellite from below 700mb. A relatively large portion of the 7.3μm radiation is contributed by the moisture below 700mb. Differences in low level moisture and cloudiness, which are undetectable on 6.7μm imagery, will be detected by 7.3μm measurements.

In this case, the exact same distribution of moisture and temperature was used. Only the wavelength of the radiation was varied; the other factors were held constant. Although a very significant factor to the radiation intensity, the wavelength of the radiation is a factor which we control.

b. The Amount of Water Vapor Within the Path of the Radiation

The amount or quantity of moisture in the radiation's path, or the water content in the vertical column, directly affects how much of the radiation is absorbed, and where in the vertical the absorption occurs. Thus, the amount and vertical distribution of the reradiation by the water vapor is affected. There are two basic ways to vary the amount of moisture present. The humidity within a given layer may be varied; or, the thickness of the layer may be changed. However, if the thickness is changes, so also is the vertical location or distribution of the moisture.

Variation of the humidity is illustrated on **Figure 4**. The same temperature sounding and the same vertical thickness of the moist layer as in previous examples are used. In this case the dewpoint temperature curve is varied by using constant dewpoint depressions of 2°, 10°, 30°, and 50°. Although dewpoint depressions are used to establish the vertical distribution of moisture, it is the absolute humidity which is of concern here. The relative humidity is significant only from the standpoint of limiting the availability of moisture for a given temperature curve.

Brightness temperatures, equivalent pressures, and weighting function curves are shown for 6.7μm radiation. Note by the weighting function curves, that, as the humidity of the layer is decreased, the level of maximum contribution is lowered. With very dry air, a large portion of the radiation reaching the satellite is from low levels. Since the air temperature decreases significantly with increasing altitude, the radiation from low levels is of higher intensity. The brightness temperature for the 50° dewpoint depression case is +0.3°C, and a large portion of the surface radiation penetrated to the satellite. For the most moist case - with the 2° dewpoint depression - virtually no radiation from below 700mb penetrated to the satellite, and the brightness temperature is -37.2°. On standard enhanced water vapor imagery, the gray shades would range from nearly white, to very dark gray, for these cases.

Consider also the water vapor's effect of limiting the amount of radiation reaching the satellite form the earth's surface. This is indicated by the difference between surface temperature (+14.0°C) and the brightness temperature. In the driest case, the absorption and reradiation by the moisture, reduced the temperature by almost 14°. For the most humid case, the reduction was 51°.

Figure 3

6.7μm AND 7.3μm RADIATION DATA FROM THE SAME SOUNDING
Plotted curves are Transmittances and Weighting Functions. Percentage contributions of radiation from the earth's surface are shown under "SFC RAD".

Figure 4

VARIED DEWPOINT DEPRESSIONS WITH FIXED TEMPERATURE SOUNDING
The same air temperature sounding as that of **Figure 2** is evaluated with 4 different dewpoint depressions constant between 1000mb and 200mb. Results are for 6.7μm radiation.

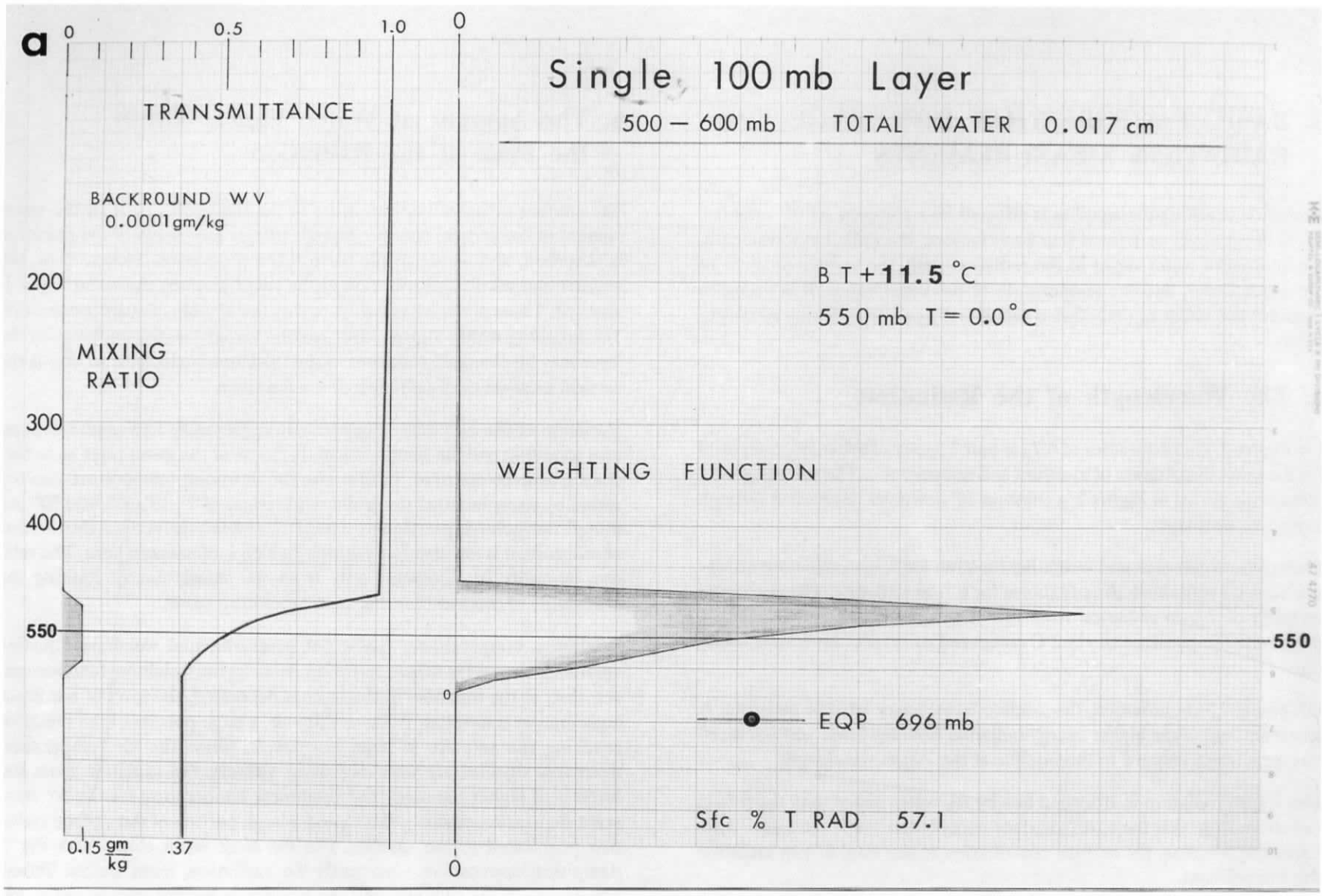
a
0
0.5
1.0
0
Single 100 mb Layer
500 — 600 mb TOTAL WATER 0.017 cm
TRANSMITTANCE
BACKROUND WV
0.0001gm/kg
200
300
400
550
MIXING
RATIO
B T + 11.5 °C
550 mb T = 0.0 °C
WEIGHTING FUNCTION
550
0
EQP 696 mb
Sfc % T RAD 57.1
0.15 gm/kg
.37
0

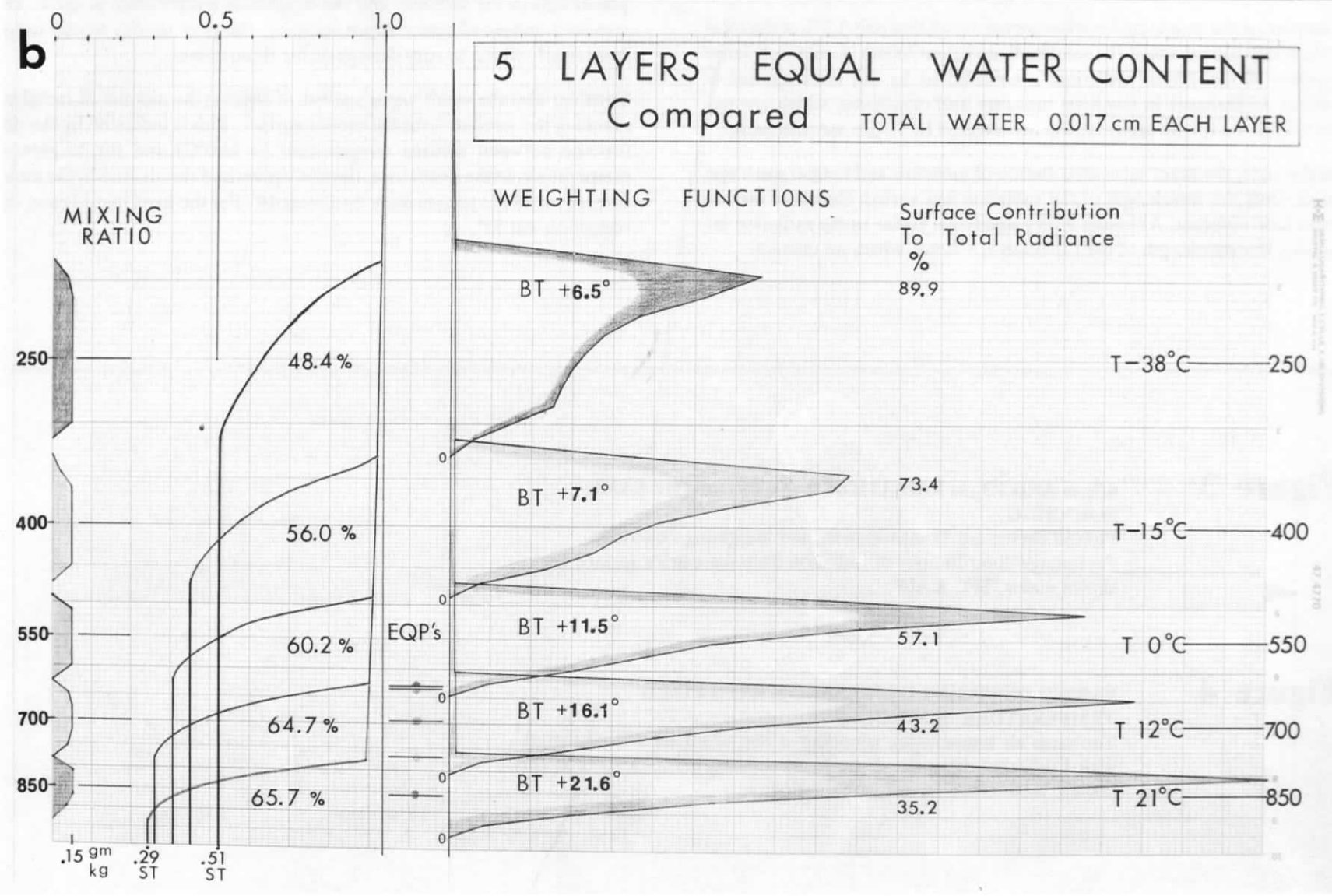
b
0
0.5
1.0
5 LAYERS EQUAL WATER CONTENT
Compared TOTAL WATER 0.017 cm EACH LAYER
MIXING
RATIO
WEIGHTING FUNCTIONS
Surface Contribution
To Total Radiance
%
BT +6.5°
89.9
250
48.4 %
T −38°C
250
BT +7.1°
73.4
400
56.0 %
T −15°C
400
550
60.2 %
EQP's
BT +11.5°
57.1
T 0°C
550
700
64.7 %
BT +16.1°
43.2
T 12°C
700
850
65.7 %
BT +21.6°
35.2
T 21°C
850
.15 gm/kg
.29 ST
.51 ST

c. The Vertical Location of the Moisture

On **Figure 5a**, computed 6.7μm radiation data are displayed for a single layer of moisture, approximately 100mb thick, centered at 550mb. The moisture within the layer is of constant mixing ratio at 0.15 grams per kilogram. The air above and below the layer contains a "background" moisture of 0.0001 grams per kilogram. The mixing ratio is plotted on the left side of **Figure 5a**.

The temperature sounding, not shown on the figure, is a low latitude or summer season sounding with a surface temperature of +29°C. This was used to prevent saturation at high levels when the moist layer is moved to different vertical locations.

The total water content of the single layer sounding is only 0.017 cm. Note by the transmittance curve that 37% of the surface radiation penetrates to the satellite. The large change in transmittance is through the depth of the moist layer. Note by the weighting function that, although there is a slight contribution of radiation by the background moisture above the moist layer; the primary sources of radiation reaching the satellite are the moist layer and the earth's surface. The resulting measured radiation intensity, indicated by the brightness temperature, is derived partly by the reradiation from the relatively cool moist layer, and partly from the very warm earth's surface.

Data on **Figure 5b** illustrate the same moist layer at five different vertical locations, with the same temperature sounding. Note that **Figure 5b** does not illustrate one sounding with five moist layers; it shows results from five soundings, each with one moist layer in a different location. Five cases are compared on one figure.

On the figure, mixing ratio, transmittance, and weighting function are shown. The case with the moist layer in the middle location, centered on 550mb, has been discussed and illustrated. Data from two higher and two lower locations are shown.

As the moist layer is raised to higher locations, brightness temperature decreases. Since the air temperature decreases with height, the higher water vapor radiates with lower intensity. However, compare the difference in brightness temperature between the highest and lowest locations with the differences in air temperatures at layer midpoints. From the lowest to the highest position, air temperature decreases by 59°C, and the brightness temperature decreases by only 15.1°C. For the lowest layer, the brightness temperature and the midpoint air temperature are nearly identical. But, for the highest layer, the brightness temperature is 44° warmer than the 250mb air temperature.

The brightness temperature decreases when the layer is moved to higher altitudes, but not nearly as much as the air temperature. There are two reasons for this difference: (1) The same moist layer, when located at lower altitudes at greater density, absorbs and reradiates significantly more of the radiation arriving from below. Note the amount of reduction of transmittance by each of the moist layers. Moisture in the highest position reduces the transmittance by 48.4%. Reduction by the moist layer in the lowest position is 65.7%. This difference in absorption results in a contribution to the total radiation by the surface of 29% for the lowest layer and 51% for the highest layer. (2) The intensity of the radiation is related to the temperature of the emitting substance through the Planck Function. This provides greater weight to the surface contribution of radiation, since it is emitted at the warmest temperature. Surface contribution to total "radiance" is listed on the figure. The term "radiance" is the intensity of the radiation, after the temperature or Planck Function of the emitting substance has been taken into account. Whereas the earth's surface contributed 51% of the total radiation for the highest layer; it contributed 89.9% of the total radiance.

In summary, the same mass of water vapor will absorb and reradiate more of the upcoming radiation when it is located lower in the atmosphere at greater pressure and density.

The most significant effect of this fact is that higher level moist layers do not yield brightness temperatures representative of their air temperature. This concept is even more amplified in the atmosphere for an additional reason. Generally, moist air at high levels has significantly less water content than lower altitude moist air. Change of moisture with height is more likely of constant dewpoint depression, than of constant, mixing ratio. This additional effect will be illustrated in Section B.

Figure 5

MOIST LAYERS OF EQUAL WATER CONTENT AND VERTICAL THICKNESS

Radiation data for five moist layers are shown. Each layer has 0.17cm of water content and is 100mb in vertical depth. The vertical locations vary. Plotted curves of Mixing Ratio, Transmittance, and Weighting Function are shown for the layers at each vertical location, individually, with a fixed temperature sounding.

Fig. 5a. Data for layer centered at 550mb.

Fig. 5b. Data shown for layers at all 5 locations compared. Numbers plotted under transmittance curves are the percentage reduction of transmittance caused by the atmospheric moisture.

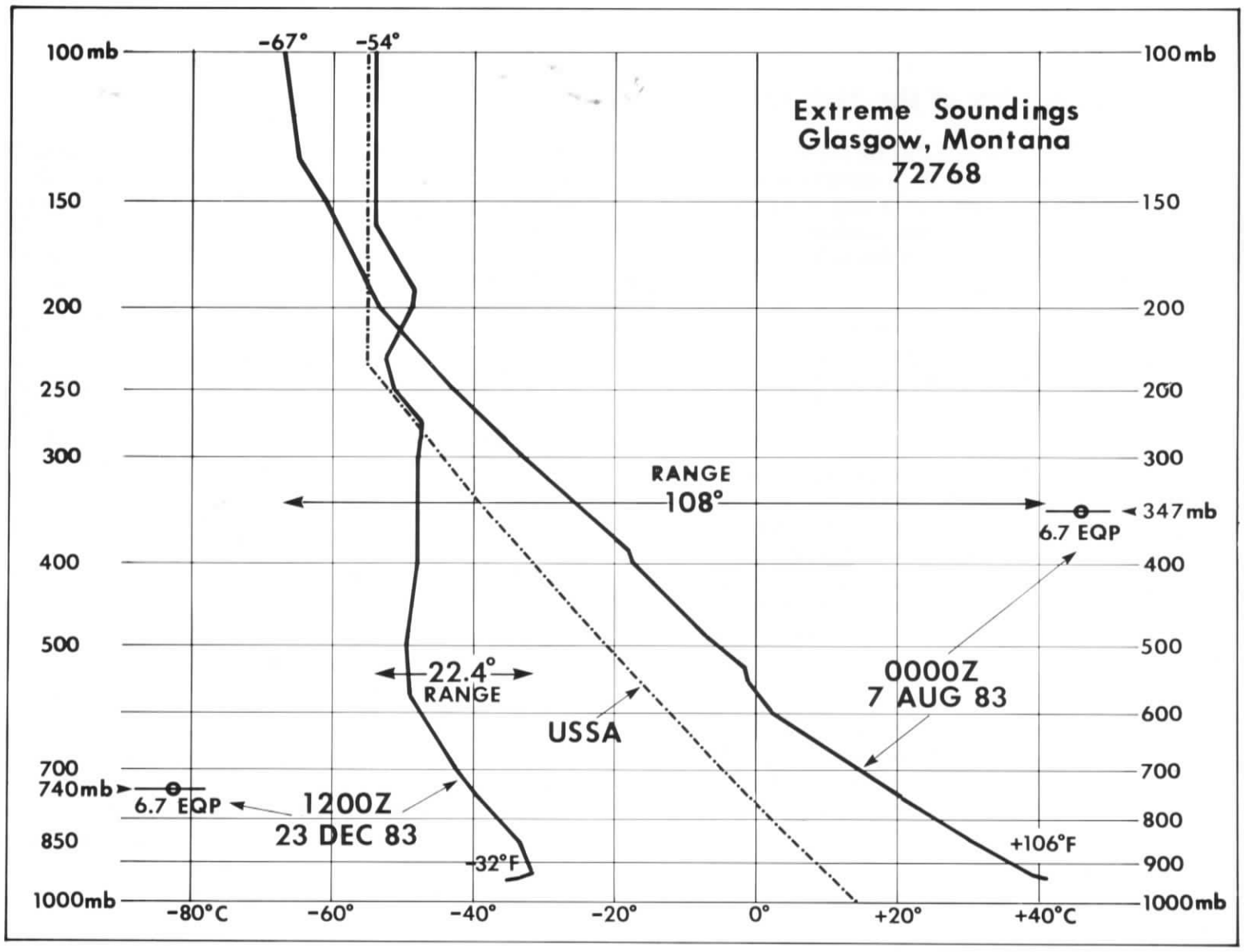

	GLASGOW, MONTANA SOUNDINGS	1200Z 23 DECEMBER 83	0000Z 07 AUGUST 83
MOISTURE DATA	Average Dewpoint Depression	3°C	15°C
	Minimum Dewpoint Depression	1° (850 mb)	6° (594 mb)
	Total Water Content	0.055 cm	2.019 cm
COMPUTED RADIATION DATA	6.7μm Brightness Temperature	-39.9°C	-24.5°C
	Equivalent Pressure	740 mb	347 mb
	Surface Radiation Contribution	14.0 %	0.0 %

Figure 6

EXTREME TEMPERATURE SOUNDINGS

Graph Two air temperature soundings from Glasgow, Montana are plotted with the U.S. Standard Atmosphere sounding, labeled "USSA". Air temperature ranges within each Glasgow sounding are indicated by horizontal arrows.
Equivalent Pressures (EQP) were derived from 6.7μm brightness temperatures.

Table All data were computed from the radiosonde soundings. Surface radiation contributions are percent of the total radiation reaching the satellite.

d. The Temperature of the Air Column

In the previous examples, variations of wavelength, amount of moisture, and vertical location of the moisture resulted in different radiation intensities or brightness temperatures. Variation of those factors changed the absorption characteristics of the radiation, and caused the radiation to reach the satellite from different origins. This alone does not change the net radiation intensity or the brightness temperature. Those changes occur only if radiation emitting substances at the different origins are at different temperatures. Had the temperature soundings used in the previous examples been isothermal, and equal to the surface temperature, no brightness temperature differences would have occurred.

The temperature soundings used were held constant; but, they were not isothermal. Temperature changed in the vertical. It was this change in temperature, in combination with the variation of absorption characteristics, that resulted in the different brightness temperatures.

If the radiation wavelength and the distribution of moisture in the air column are held constant; but, the air temperature is varied, the net radiation intensity and brightness temperature will vary accordingly. Warming the entire sounding, and the earth's surface temperature, by the same amount will result in a nearly identical increase of brightness temperature. It should be noted that the temperature changes to the sounding and the brightness temperature are not exactly identical. A slight change in absorption characteristics occurs because of the density change of the air column.

In the atmosphere, changes in the temperature of the air column occur with changes in season of the year, differences of latitude, and with varied circulation systems.

Three temperature soundings are shown on **Figure 6**. One is that of the U.S. Standard Atmosphere. The other two, although from the same observation site and the same year, represent extremely cold and warm samples of atmospheric soundings. Based upon thousands of soundings observed, these represent a practical range between the warmest and coldest conditions likely to be encountered in the process of image interpretation. The soundings have not been extended above 100mb, since water vapor at higher altitudes is generally not significant to 6.7 or 7.3μm radiation measurements. Note that there are some exceptions to that at tropical latitudes in the vicinity of deep convective weather complexes.

The computed 6.7μm brightness temperature for the summer sounding is -24.5°C. Since the air temperature range in the sounding is 108°C, there is a potentially large range in brightness temperatures, depending upon the amount and vertical location of moisture. If the sounding were extremely dry, brightness temperatures near +20°C might be observed. With nearly saturated, but cloud-free conditions, brightness temperatures near -35°C might occur. On imagery, gray shades can vary from nearly black to very light gray with such temperature soundings.

On the winter sounding on **Figure 6**, the range between maximum and minimum temperatures is only 22.4°C. This alone extremely limits the possible range of brightness temperatures. Since the maximum temperature in the sounding is only -31.5°C, brightness temperatures are limited to the very cold ranges. The computed 6.7μm brightness temperature is near -40°C, one of the coldest encountered in our studies. Although relatively moist with respect to the air temperature, the sounding had the smallest water content of all atmospheric soundings observed in our project. With such air temperatures, regardless of the humidity, the range of brightness temperatures and image gray shades is very small.

In the soundings shown on **Figure 6**, both the season and the circulation system environment varied to extremes. The summer sounding was within an upper air ridge, and the winter sounding was in a deep cold low. The 500mb heights were 5990m and 4990m respectively.

Although seasonal differences in temperature soundings are important to radiation measurements, they are not greatly significant to the problems of image interpretation. The season is known.

	Seven Islands	Key West
TOTAL WATER	0.11cm	4.61cm
6.7 µm		
Brightness Index	68	65
Brightness Temperature	-36.2°	-30.7°
Surface Radiation	7%	0%
7.3 µm		
Brightness Index	63	45
Brightness Temperature	-30.0°	-12.3°
Surface Radiation	50%	0.1%
11.1 µm		
Brightness Index (I.R. by Surface)	58	15

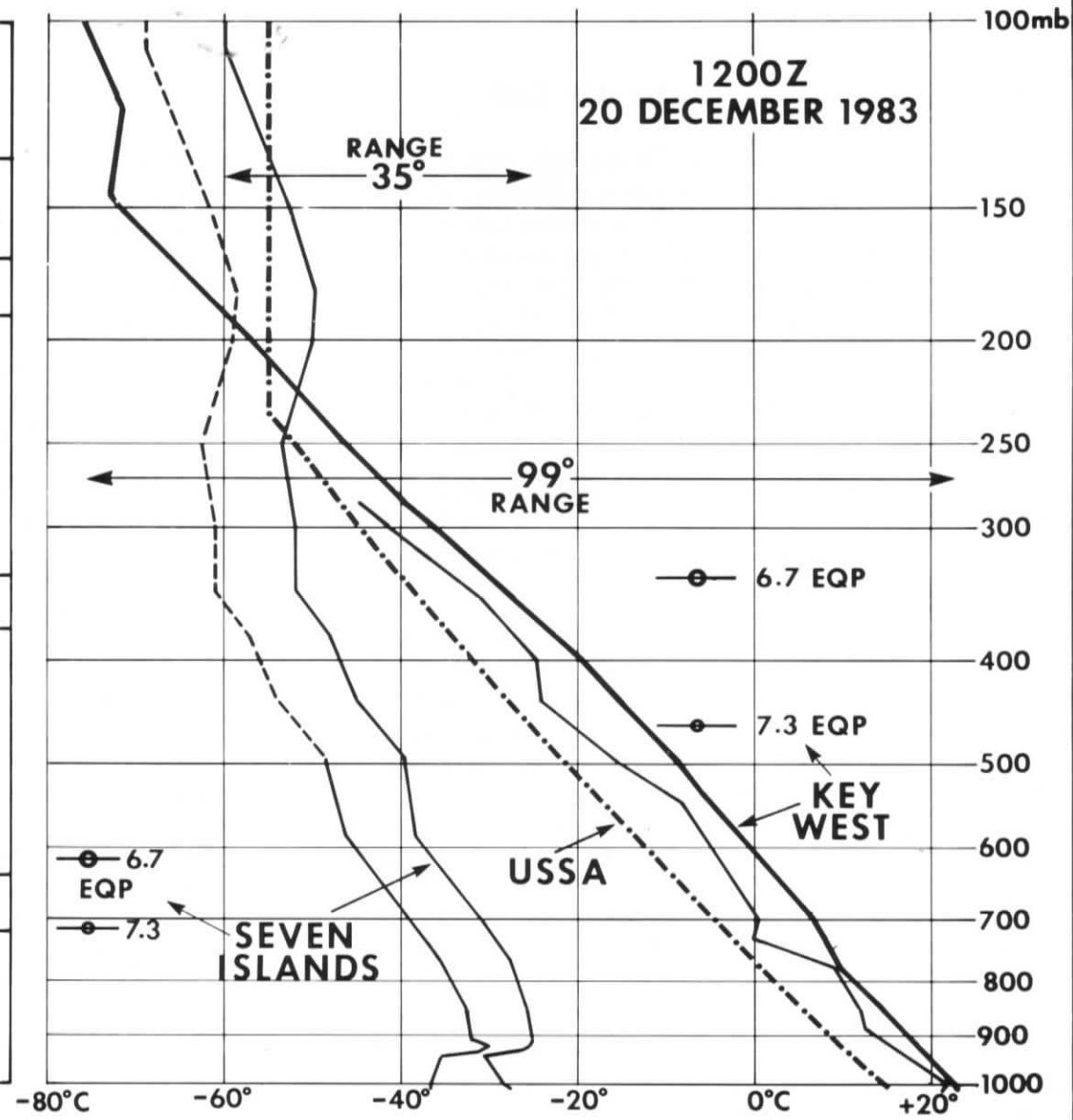

Figure 7

COMPARISON OF COLD AND WARM SOUNDINGS - SAME TIME AND DATE

Graph Air temperature and dewpoint temperature soundings from 1200Z 20 December 1983 are shown for Seven Islands, Quebec, and Key West, Florida. The U.S. Standard Atmosphere air temperature sounding is included - labeled "USSA". Equivalent Pressures (EQP) are plotted for both sites from 6.7µm and 7.3µm brightness temperatures computed from the radiosonde data. Air temperature ranges within each radiosonde sounding are shown by horizontal arrows.

Table "Brightness Indices" were measured from NOAA-7 satellite data. Larger numbers indicate lighter gray shades (see text). Values of "total water" content, "brightness temperatures", and "surface radiation" contribution were computed from radiosonde data. "Surface radiation" is the percentage of the total radiation reaching the satellite that was contributed by the surface (RADCOM Model derivation).

Shown on **Figure 7**, are two soundings from the same time and date. The U.S. Standard Atmosphere temperature sounding is included for comparison. The sounding from Seven Islands, Quebec is compared with that from Key West, Florida. Although the relative humidities of the soundings are similar, the Canadian sounding contains only 0.11 cm of total water compared to 4.61 cm at Key West. Data for both 6.7µm and 7.3µm radiation are shown on the figure, including computed brightness temperatures from the RADCOM model, and "Brightness Index" derived from radiation measurements from the NOAA-7 polar orbiting satellite. "Brightness Index" is a normalized index of 100 points based upon the "count" values transmitted by the satellite. Zero is equivalent to the warmest value, and 100 is equivalent to the coldest value. The data were not converted to brightness temperatures.

Consider the 6.7µm radiation data. Although the Seven Islands sounding is very dry, compared to the very moist Key West sounding; it had the lighter gray shade and the colder computed brightness temperature. Both soundings produced relatively cold brightness temperatures. Most of the radiation arriving at the satellite from the Key West sounding was from moisture above 400mb where the air is cold. From the Seven Islands site, most of the radiation arrived from below 500mb, and 7% of the surface radiation penetrated to the satellite. However, both the air and the surface temperature are very cold at the Canadian site. Brightness temperatures are cold at Key West because of the absorption and reradiation by moisture in the cold air aloft, and at Seven Islands because of the cold sounding and surface.

Radiation in the 7.3μm band is able to penetrate the water vapor to a greater extent than the 6.7μm radiation. At Seven Islands, this causes little difference in the brightness temperature, because the lower level air is also cold, and the ground is cold. But, from Key West, the 7.3μm radiation arrives to the satellite from warmer air, producing a much warmer brightness temperature than by 6.7μm radiation. The brightness indices, from NOAA-7 measurements, indicate similar results.

Differences in sounding temperatures because of latitude are significant; but, the changes occur over large distances. The temperature differences most important to image interpretation are those related to the mid and upper tropospheric circulation systems. These are of such magnitude to greatly enhance, or - quite commonly - reverse the mean latitudinal gradients. The sounding temperature differences related to circulation systems will be thoroughly illustrated and discussed in Section C using imagery with atmospheric soundings and analyses.

4. SUMMARY - SECTION A

Radiation intensity measured at the satellite, also referred to as "radiance", may be converted to brightness temperature or to image gray shade. Radiation arriving at the satellite in the infrared bands may be from the surface of the earth, from cloud tops, from water vapor, or some combination of the three. If little or no water vapor exists above, the brightness temperature will be representative of the cloud top or surface temperature.

If water vapor is present above the clouds, or if no clouds are present, energy will be reradiated by the water vapor which is usually at colder temperatures.

Radiation to the satellite from water vapor is emitted from some layer of finite vertical extent. The depth of the moist layer contributing radiation to the satellite is dependent upon the amount and density of the moisture existing in the radiation's path.

Several basic factors affecting the behavior of radiation may be considered. Although several of the factors usually vary in combination in the atmosphere, knowledge of their individual effects is useful to the understanding of water vapor imagery.

WAVELENGTH OF THE RADIATION

Of the operational "water vapor" channels on current weather satellites, the 6.7μm and 7.3μm bands are most commonly used in image format. Of these, 6.7μm radiation is more highly absorbed by moisture. Therefore, smaller amounts of moisture, commonly at higher altitudes, are detected by 6.7μm radiation than by 7.3μm radiation. However, because of this, low level features are usually obscured on 6.7μm imagery.

THE AMOUNT OF WATER VAPOR IN THE PATH OF THE RADIATION

Increased amounts of moisture or water content in the radiation's path accomplish more absorption of the radiation arriving from lower levels. Therefore, if the air temperature decreases with height, larger amounts of moisture result in colder brightness temperatures.

THE VERTICAL LOCATION OF THE MOISTURE

Since the vertical change of air temperature is commonly very large, moisture at high altitudes reradiates at low intensity contributing to colder brightness temperatures than at low altitudes. But, moisture in higher less dense air absorbs less radiation than the same amount at lower altitudes. Therefore, the brightness temperatures from moist layers at high altitudes are significantly warmer than the air temperatures at those altitudes.

THE TEMPERATURE OF THE AIR COLUMN

The vertical change of air temperature, which is generally large, is necessary for the production of different brightness temperatures by varied moisture distributions. For the same atmospheric moisture conditions, warming or cooling of the temperature sounding will produce corresponding changes in the brightness temperature. Very cold air temperature soundings, such as those at high latitudes during winter on the cyclonic side of the jet stream, also have very small vertical changes of temperature. Therefore, changes of moisture cannot produce large changes in brightness temperature, or large variations of gray shade on images. Low latitude soundings, or summer season soundings in upper air anticyclones, have very large vertical temperature ranges. Very large gray shade variations can be produced by different moisture distributions.

No valid simplified explanation exists for the relationship between atmospheric conditions and variations of brightness temperatures, such as those displayed as gray shade patterns on water vapor imagery. The net intensity of the radiation arriving at the satellite is dependent upon the amount and vertical location of the moisture in combination with the air and surface temperatures.

In the next section, moisture in varied layers shall be examined. The temperature sounding and wavelength will be held constant; but, the amount and vertical location of the moisture will vary in combinations.

SECTION B

MOIST LAYERS - THEIR EFFECTS ON RADIATION MEASUREMENTS

In Section A, factors affecting the radiation reaching the satellite were varied individually. In this section, radiation characteristics will be examined from varied layers of moisture. Both the vertical location and the amount of the moisture will be varied in combinations.

1. BRIGHTNESS TEMPERATURES FROM VARIED MOISTURE DISTRIBUTIONS

On **Figure 8**, brightness temperatures and equivalent pressures computed by the RADCOM radiation model are compared from 29 moisture distributions. Each bar on the figure indicates a layer of moisture with a constant dewpoint depression. The vertical extent of the moist layer is indicated by the length of the bar. Pressure is shown at the left side of the graph. The relative humidity of the moist layer is implied by the width of the bar, and the dewpoint depression is labeled just above or below each bar.

The same air temperature sounding was used for all 29 moisture distributions. It is nearly identical to that of the U.S. Standard Atmosphere, but with a higher colder tropopause. Air temperatures for all layer boundaries are shown on the right side of the graph.

Computed brightness temperatures for 6.7μm radiation are listed across the top of the figure, and those for 7.3μm radiation are along the bottom. Equivalent pressures - where the air temperature equals the brightness temperature - are indicated by horizontal lines and dots for each column. Since no temperature inversion was present in the sounding, vertically higher equivalent pressures indicate colder brightness temperatures; and, the 6.7μm equivalent pressures are in all cases at higher altitude than those of 7.3μm radiation for each sounding.

BACKGROUND MOISTURE

For each of the 29 moisture distributions, the air is not totally dry above or below the indicated moist layer. A "background" moisture is present. The background moisture alone is included as one of the "deep" layer cases, labeled "BR". It was chosen as a result of experiments comparing real radiosonde soundings and satellite radiation data. Although the dewpoint depression is not constant, the moisture is equivalent to a 50° constant depression between 100 & 1000mb. As will be shown, this is sufficient moisture - especially at lower altitudes - to affect the net radiation of the moist layer cases.

"DEEP" MOIST LAYERS

Counting from left on **Figure 8**, the first five cases compare moisture at different humidities through a deep vertical layer of the atmosphere. Three of the "deep" layer cases were discussed in Section A. They are included in **Figure 8** for comparison to the single and multiple layer cases. The "deep" layer cases also provide an indication of the extreme cases for the particular temperature sounding.

Note that, if the atmosphere contained absolutely no moisture, the brightness temperature would be equal to the surface black body temperature which is +14.0°C for this set of cases. The driest sounding of the set is the "background" case labeled "BR". The brightness temperature for 6.7μm radiation for this case is 0.0°C. Although the sounding contained only 0.032 cm of total water, the absorption and reradiation by the water vapor reduced the brightness temperature to a value 14°C colder than the surface temperature.

The brightness temperature for the less highly absorbed 7.3μm radiation was +9.8°C - a reduction of only 4.2° from the surface temperature.

Of the 29 cases, the sounding with the greatest water content is the "deep" 2° dewpoint depression case, which produced a brightness temperature of -37.2°C. Thus, the range between the warmest and coldest of the 6.7μm brightness temperatures is 37.2°.

The 30° dewpoint depression case shown of the far left represents another form of extreme. That is the largest value of dewpoint depression routinely reported by radiosonde stations. Note that the 6.7μm brightness temperature for that sounding is -14.9°C which is 40% along the range from the warmest to the coldest cases. This is a significant problem in comparing water vapor imagery to radiosonde data; and will be discussed in Section C.

"HIGH" MOIST LAYERS

In this set, the moisture extends from 200 through 300mb. Four cases of varied humidity are shown; dewpoint depressions are 15, 10, 5 and 2°. All four cases have the identical background moisture below 300mb.

Note that the brightness temperatures are all considerably warmer than the air temperatures within the layer. The equivalent pressures are well below the altitude of the moist layer.

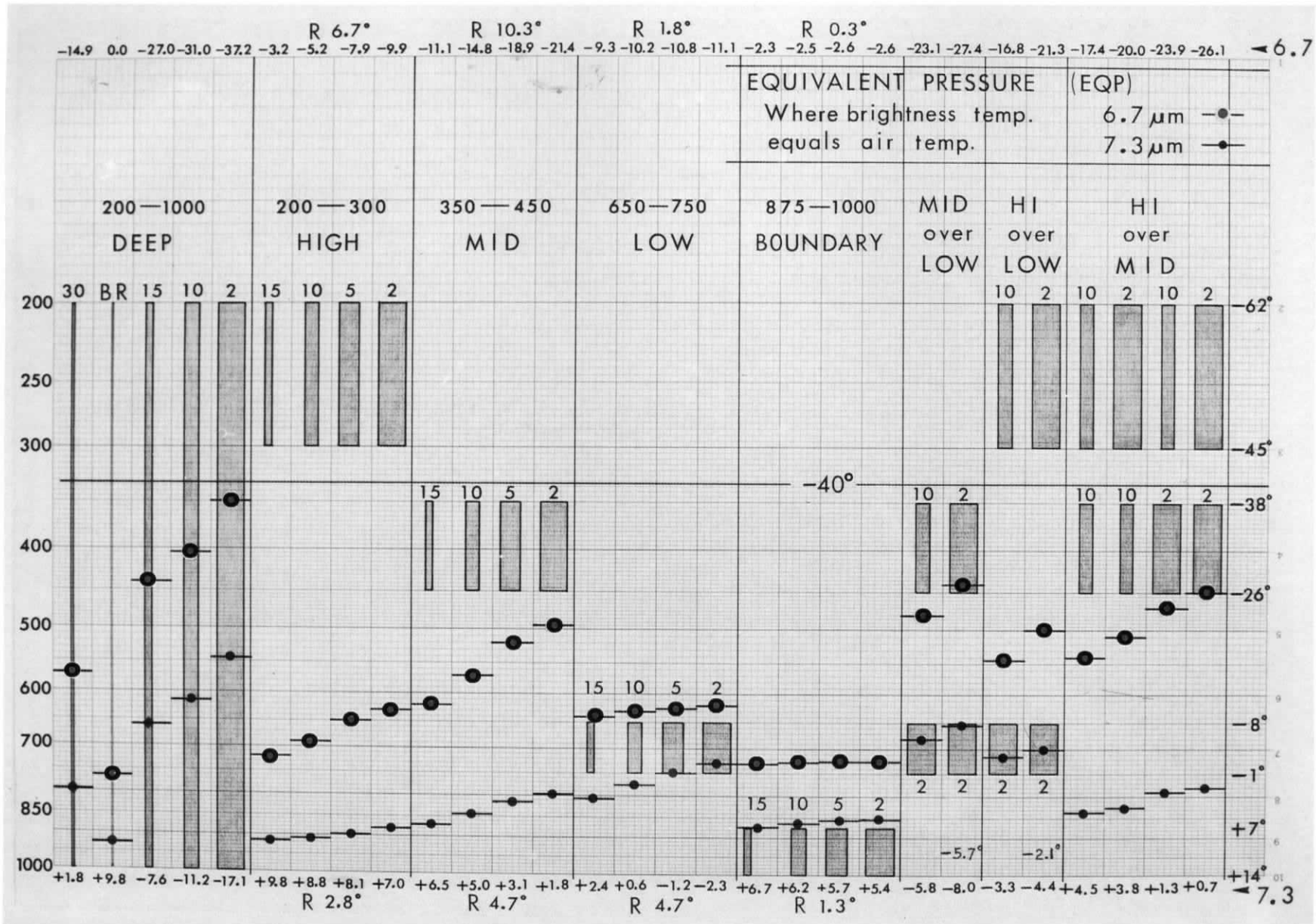

Figure 8 **VARIED MOIST LAYERS**

29 moisture distributions arranged in 8 sets are indicated by shaded bars on a vertical scale of logarithmic pressure. A single fixed air temperature sounding was used for all cases.

Vertical Scale	Left side = pressure in millibars Right side = air temperature (fixed with respect to pressure for this case)
Shaded Bars	Length = vertical depth of moist layer at constant dewpoint depression Width = implies the relative humidity - constant dewpoint depression indicated by numbers immediately above or below bars, (except second case, labeled "BR" - see text).
Computed Brightness Temperatures	6.7μm along the top of the graph 7.3μm along the bottom of the graph
Equivalent Pressures	6.7μm indicated by horizontal line with large dot 7.3μm indicated by horizontal line with small dot (all 6.7μm EQP's at higher altitudes than 7.3μm EQP's of same case)
Moist Layers in Sets	The moisture distributions are arranged in 8 "sets" divided by lines and labeled above the shaded bars. Brightness temperature "ranges" within some sets are indicated at the top and bottom of the graph by numbers prefixed by "R". Those sets are HIGH, MID, LOW, and BOUNDARY.

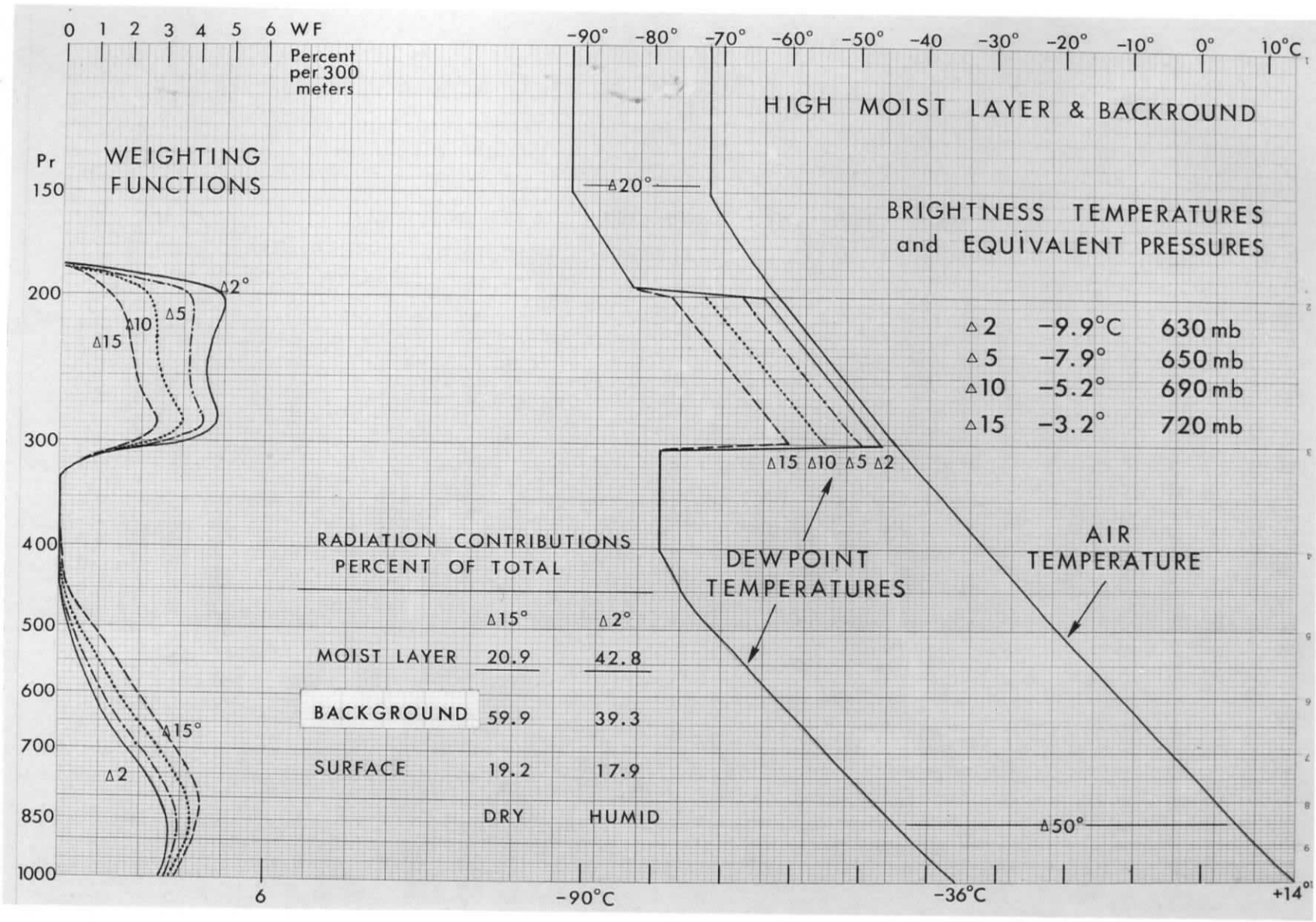

Figure 9

HIGH MOIST LAYERS
Computed data from the 4 cases of the "High" layer set of the **Figure 8** bar graph are shown. Moisture between 300mb and 200mb is varied by constant dewpoint depressions of 2°C, 5°C, 10°C, and 15°C. Weighting functions are plotted on the left. The scale above the graphs is percent of the total radiation arriving at the satellite from each 300m layer of the atmospheric moisture. Other plots are dewpoint temperature and air temperature. "Background" moisture, present above and below the moist layers is indicated by the dewpoint temperature curve. Percentages of the total radiation contributed by the 300-200mb moist layer, the "background" moisture, and the earth's surface are shown for the dry and moist cases (15° and 2°C dewpoint depressions).

Figure 9 shows the weighting functions and other information for the four "high" layer cases. The weighting functions indicate the relatively large contribution by the lower level background moisture. For the two drier cases of the set, the level of maximum contribution by the atmospheric radiation is below 800mb. The table included on the figure lists the percentages of total radiation contributed by the moist layer, the background moisture, and the earth's surface. Even for the most humid of the cases, nearly 18% of the total radiation arrives from the surface, and over 39% from the background moisture below the moist layer. The weighting function shows that most of the background contribution originated from the very warm lower portion of the atmosphere.

It is useful to compare the brightness temperatures of the "high" moist layer set with that produced by the background moisture alone. For the driest case, and for 6.7μm radiation, the presence of the "high" layer reduced the brightness temperature by only 3.2°C from that of the background alone. The nearly saturated "high" layer cooled the brightness temperature by nearly 10°C. Such differences are sufficient for the detection of the high moisture on imagery, especially if the high layer had well defined horizontal boundaries. However, with 7.3μm imagery, only the most humid of the "high" layer cases is likely to be detectable. In all cases, the gray shade produced by the "high" layer would be very unrepresentative of the air temperature between 200mb and 300mb. This is characteristic of radiation from high level moist layers, even if the humidity is extremely large with tropical air temperatures.

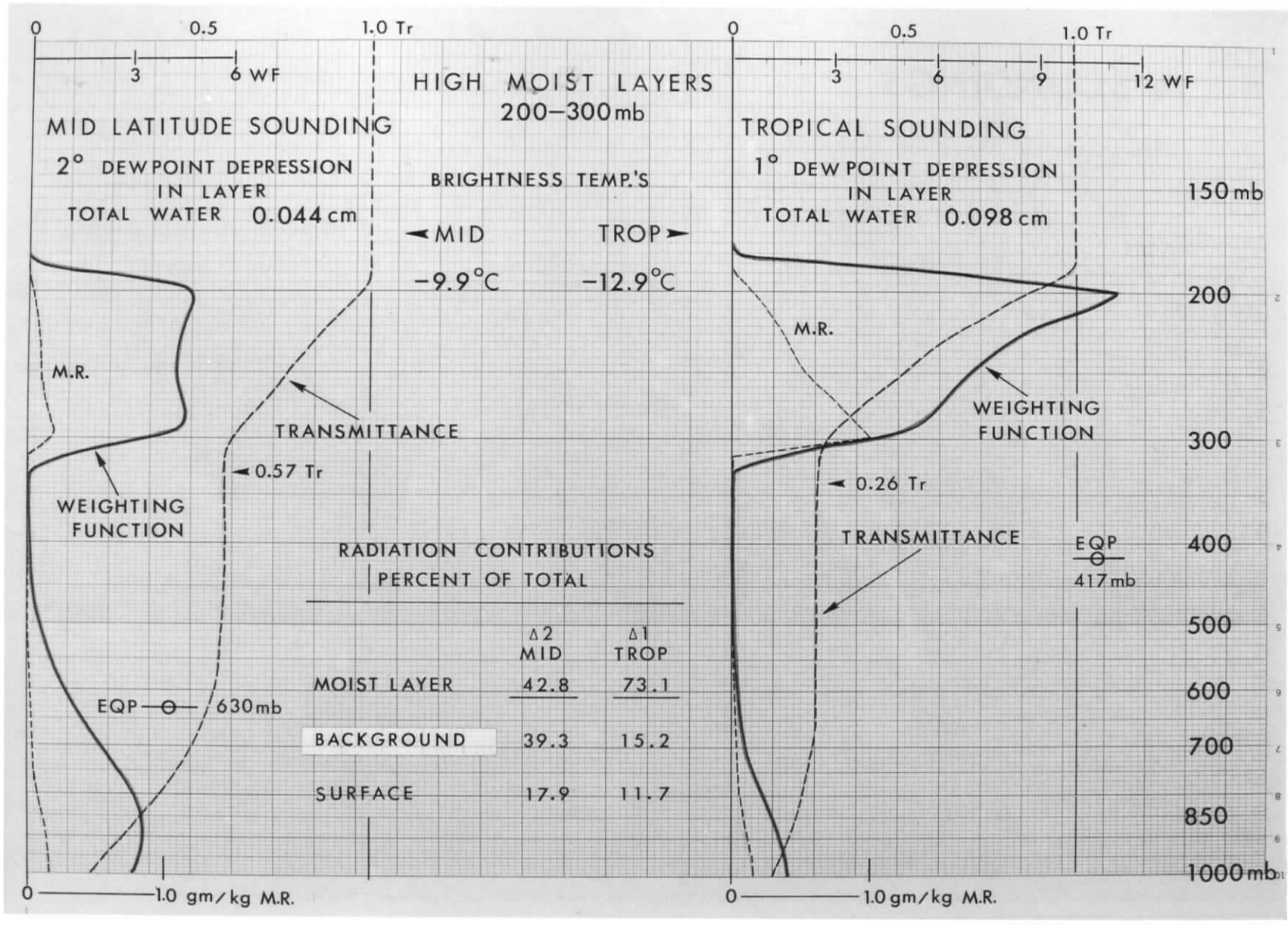

Figure 10 **HIGH MOIST LAYERS - MID-LATITUDE AND TROPICAL TEMPERATURE SOUNDINGS**
Plotted curves include Mixing Ratio (thin dashed lines - bottom scale), Weighting Function (solid lines) and Transmittance (thick dashed lines). Top scales are WF - Weighting Function, TR - Transmittance. Data on the left side of the graph, labeled "MID", are from the same 2°C dewpoint depression case on **Figure 9**. Right side data (TROP) are from a tropical air temperature sounding with a 1°C dewpoint depression between 300mb and 200mb.

On **Figure 10**, radiation data from the 2° dewpoint depression case of the bar graph are compared with those from a tropical temperature sounding with a 1° dewpoint depression. In both cases, the moist layer extends from 200mb to 300mb; but the water content of the tropical case is more than twice that of the mid-latitude bar graph case. As shown by the plots of transmittance, the increased moisture of the tropical case greatly increases the absorption accomplished by the high layer. This changes the equivalent pressure from 630mb to 417mb. However, since the air temperature of the tropical sounding averages 15°C warmer; the increased absorption decreases the brightness temperature by only 3° to -12.9°C.

If such a tropical moist layer were extended upward to the tropical tropopause, an additional three to six degrees reduction of brightness temperature could occur. That would yield 6.7μm brightness temperatures in the -18 to -20°C range for moisture entirely above 300mb; but, this is still much warmer than the air temperatures at those altitudes.

Because of their unrepresentative brightness temperatures, high moist layers provide a significant exception to the "topographic" concept listed in Section A as one of the "simplified" explanations of water vapor imagery. Evaluate the "topographic" concept by comparing the equivalent pressures of **Figure 8** to the vertical distributions of moisture.

FOUR SINGLE MOIST LAYERS COMPARED

On the bar graph of **Figure 8**, consider the brightness temperatures and equivalent pressures of the single moist layers labeled: "HIGH, MID, LOW and BOUNDARY". Each set contains the same variation of dewpoint depressions; but, as the layers are lowered in altitude, their water content and density increase.

Of the four sets, the brightness temperatures are most representative of the air temperature at the "low" layer centered on 700mb, when 6.7μm radiation is used. Unlike the "high" layers, the "low" moist layers absorb and reradiate a very large proportion of the radiation reaching ;the satellite. In all four cases of the "low" layer set, less than 5% of the radiation reaching the satellite penetrates from below the layer. Note that the 6.7μm brightness temperatures from the "low" layer set are similar in value to those from the "high" layer. The coldest 6.7μm brightness temperatures from the single moist layers are those from the "mid" layer set. The "low" layer produces the coldest 7.3μm brightness temperatures.

Note also, the range of brightness temperatures between the maximum and minimum dewpoint depressions within each of the four single layers; or, compare the differences in altitude of the corresponding equivalent pressures. The brightness temperature ranges are shown at the top and bottom of the figure, preceded by the letter "R". The ranges are an indication of the satellite's "ability" to distinguish the differences in humidity within each of the moist layers.

Of the four moist layers, the maximum range in 6.7μm brightness temperatures is 10.3°C from the "mid" layer. The range is also significant for the "high" layer. Differences in water content would be relatively easily detected by satellite measurements for the "high" and "mid" layers; but, the small ranges from the "low" and "boundary" layers indicate that different humidities there would be difficult to detect.

Examination of the four moist layers indicates that for 6.7μm radiation, a moist layer at some mid-tropospheric altitude would yield the coldest brightness temperatures, and the maximum range for different humidities. This concept may be better defined and understood by considering a greater number of layers under better controlled conditions.

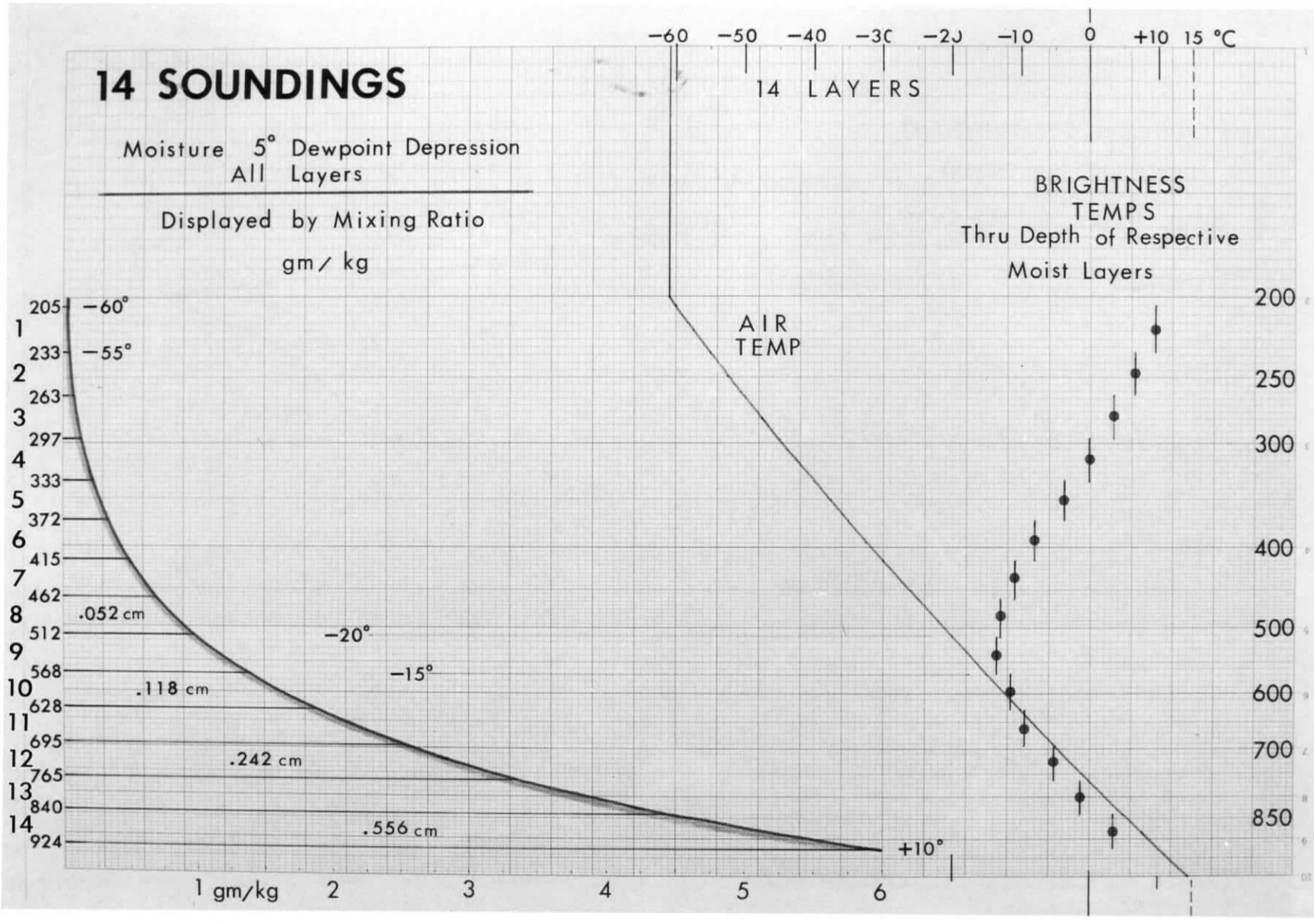

Figure 11 **14 SOUNDINGS**
The plotted air temperature sounding with a constant 5°C dewpoint depression was divided into 14 layers by 5°C air temperature intervals from +10°C to -60°C. Along the left side of the graph, layers are numbered with their pressure boundaries indicated. Moisture is shown by Mixing Ratio (left curve - bottom scale). Brightness temperatures for moisture present only in individual layers are shown by vertical bars with dots at respective layer mid-points (plotted on the same temperature scale as the air temperature).

2. RADIATION FROM SHALLOW MOIST LAYERS AT VARIED HEIGHTS

a. Radiation From Fourteen Moist Layers

The temperature sounding displayed on **Figure 11** is identical to the U.S. Standard Atmosphere between 233mb and 1000mb. The tropopause has been raised to 200mb and cooled to -61°C. Moisture in the sounding is equivalent to a constant five degree dewpoint depression, but is displayed by a plot of mixing ratio.

In this experiment, the sounding is not used intact. Instead, the moisture is divided into 14 individual layers which are defined by temperature at five degree increments between +10°C and -60°C. Temperature was chosen as the basic reference for layer boundaries instead of pressure, because of its greater importance to radiation measurements. However, since the temperature sounding is fixed for the experiment; pressure boundaries can also be assigned. They are shown on the left of the figure.

Radiation data were computed for each of the fourteen moist layers individually along with a fixed temperature sounding and a background moisture of 0.0001 gm/kg mixing ratio above and below the moist layer. Brightness temperatures for 6.7μm radiation from each of the 14 soundings are plotted on the same scale as the air temperature on **Figure 11**. Each brightness temperature is indicated by a line through the depth of the corresponding moist layer, and is highlighted by a dot at the center of the layer.

Consider sounding #1 in which the moist layer is located at the highest altitude where the air temperatures range from -55° to -60°C. The computed brightness temperature for this sounding is +9.5°C. The coldest brightness temperature, -13.5°C, was produced by sounding #9 with the moist layer centered on 540mb and the air temperature between -15° and -20°C. The moist layer at the lowest altitude in sounding #14 produced a brightness temperature of +3.5°C. As indicated on the graph, this is slightly cooler than the air temperature of the moist layer which ranged from +10° to +5°C.

From the lower layers, the net radiation reaching the satellite produces a brightness temperature that is slightly colder than the air temperatures at the top of the moist layer. Although the background moisture is very small, its accumulative effect above the lower moist layers contributes to slightly colder brightness temperatures than the air temperatures of the corresponding layers.

As was the case with the four single layers of the **Figure 8** bar graph, the high layers with the coldest air temperatures do not produce the coldest brightness temperatures. The moist layer in the highest coldest air yields the warmest brightness temperature. As the moist layer is lowered, the brightness temperatures decrease, reaching a minimum value in the middle troposphere; then increase for lower altitudes. In this case, with more layers in the sample, the altitude which produces the coldest brightness temperature is better defined. It shall be referred to as the "crossover altitude".

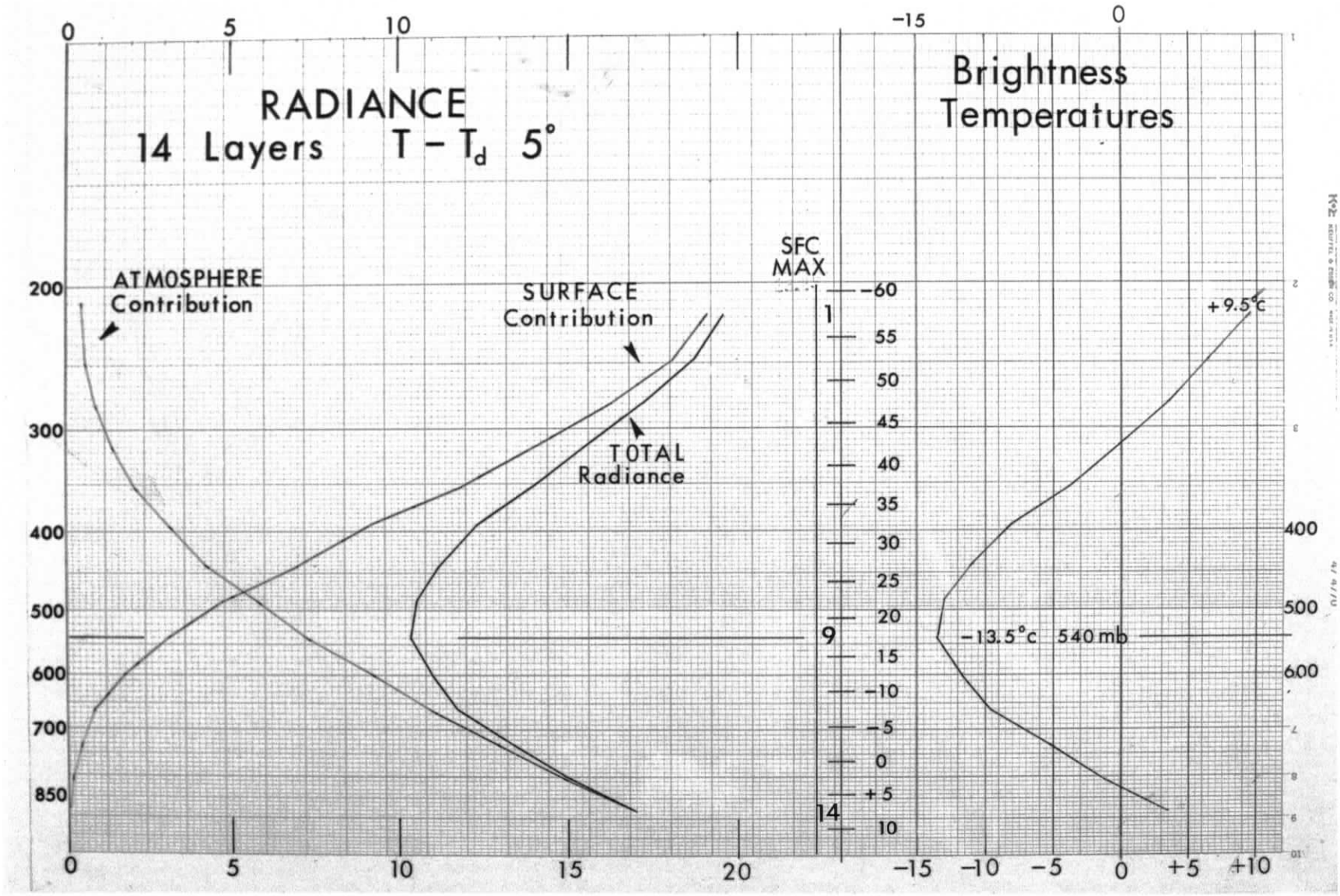

Figure 12 **CROSSOVER EFFECT FROM 14 MOIST LAYER SOUNDINGS**
Left side curves are Radiance (bottom scale, units of Planck Function). For each of the 14 layers, the atmospheric radiance plus the earth's surface radiance is equal to the total radiance. Brightness temperatures (directly proportional to total radiance) are plotted on the right (units degrees Celsius). Vertical scales of pressure (left) and air temperature (center). "SFC MAX" applies to the radiance and indicates the value produced by the earth's surface at 15°C (the maximum attainable value for the fixed temperature regime used).

b. The "Crossover" Effect

The term "crossover" refers to the reversal in roles between the radiation passing through the moist layer from below, and the radiation emitted by the moist layer itself.

The concept may be illustrated by **Figure 12** where results from the same 14 soundings of **Figure 11** are displayed. The same 6.7μm brightness temperatures are shown on an expanded scale at the right side of the figure. They are plotted at layer midpoints and connected by a line.

On the left side of the figure are plots of "radiance" - a term for the intensity of the radiation. The "radiance" value includes the temperature or Planck Function of the substance from which the radiation is emitted. Three values of RADIANCE are plotted for each of the 14 soundings:

- "**Total Radiance**" - the net radiation intensity from which the brightness temperature is derived.
- "**Surface Contribution**" - that portion of the total radiance contributed by the earth's surface.
- "**Atmospheric Contribution**" - that portion of the total radiance contributed by the atmosphere - both the moist layer and the background moisture.

For each sounding or each moist layer, the sum of the **Atmospheric Contribution** and the **Surface Contribution** is equal to the **Total Radiance**.

Consider the radiance values from sounding #1 with the moist layer at the highest altitude. The **Atmospheric Contribution** to the total radiance is very small for two reasons: (1) The amount of water vapor in the moist layer is small, and the amount of absorption and reradiation accomplished by the layer is small. (2) That small amount of radiation is emitted at very low energy levels because of the very cold air temperatures. Approximately 85% of the radiation reaching the satellite is from the earth's surface radiating at very warm temperature, which further increases the radiance. Therefore, the **Surface Contribution** dominates the **Atmospheric Contribution** for the highest moist layer.

As the moist layer is lowered, and the quantity and temperature of the water vapor increases, the atmospheric contribution increases. Also because of the increased absorption by the moist layers, the surface contribution decreases. As the layer is lowered to near 500mb, the atmospheric contribution begins to dominate; and, as the layer is lowered farther, the total radiance reaches a minimum value and increases downward with the increasing air temperature of the moist layer.

The "crossover effect" refers to the reversal of dominance between the atmospheric and surface contributions. It is this effect that causes the total radiance to yield a minimum value for sounding #9 with the moist layer centered at 540mb. Layer #9 may be referred to as the "crossover layer", or 540mb as the "crossover altitude". Note that the actual crossing of the atmospheric and surface contribution curves occurs above 540mb. This difference is primarily an effect of the background moisture which tends to slightly increase the atmospheric contribution and decrease the surface contribution; thus, raising the curve crossing. If the background moisture were decreased, and the number of moist layers in the sample increased; the crossing level of the contribution curves would approach the level of minimum total radiance.

For this particular set of 14 moist layers, the "crossover altitude" is 540mb for 6.7μm radiation. The moist layer centered at 540mb would produce the coldest brightness temperature and the lightest gray shade on satellite imagery. However, variation of the amount of moisture within the moist layers would change the amount of absorption and affect the "crossover altitude". Such variations were examined and are illustrated by samples on **Figure 13**.

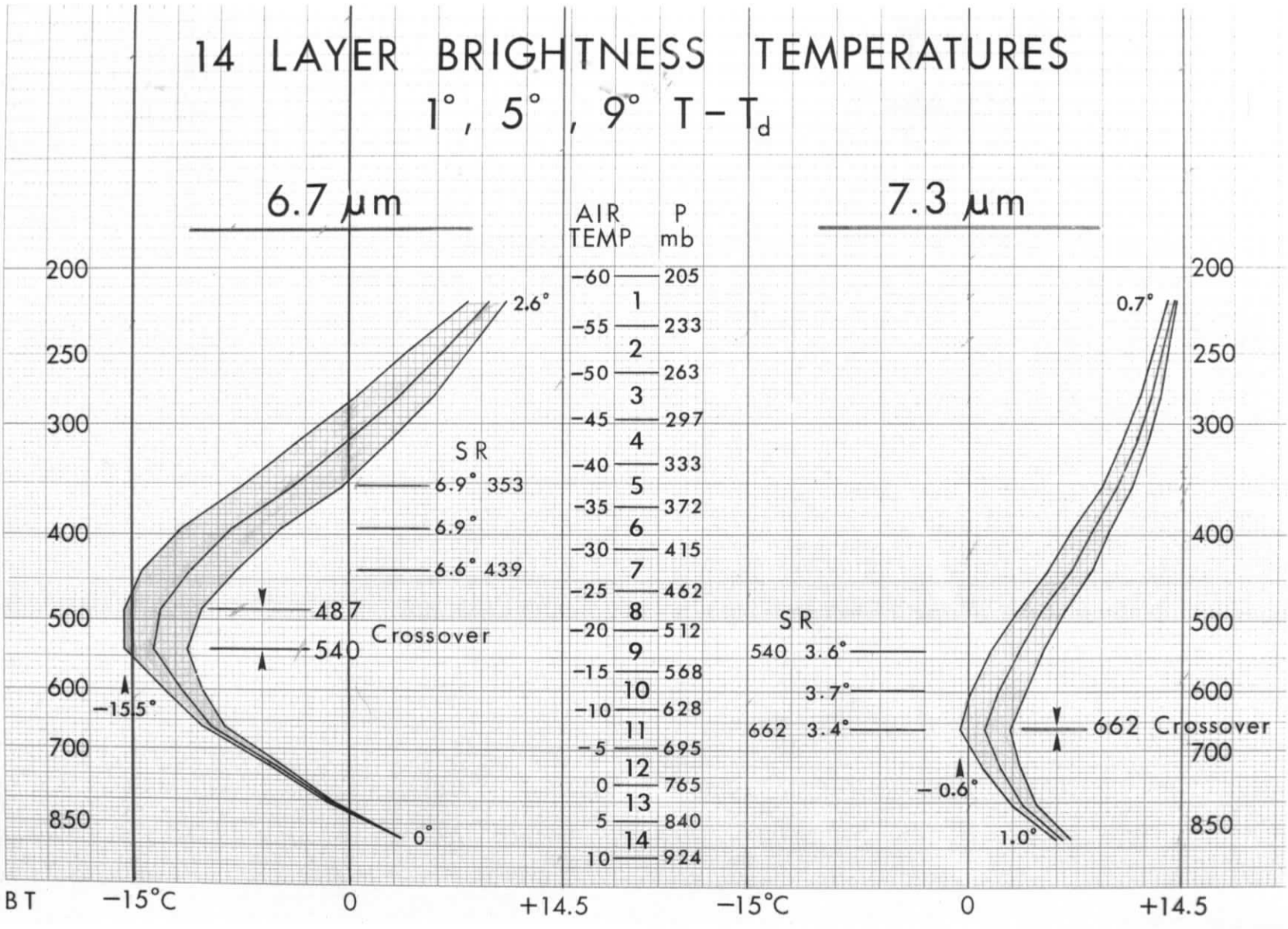

Figure 13 **BRIGHTNESS TEMPERATURE VARIATIONS FROM MOIST LAYERS**
The 6.7μm brightness temperatures from 14 moist layers are shown for dewpoint depressions of 1°C (left), 5°C (center - same as **Figures 11** and **12**), and 9°C (right). A corresponding set of 7.3μm brightness temperatures are shown for the same 42 soundings. Values labeled "S.R." are "sensitivity range" (the brightness temperature difference between the 9°C and 1°C dewpoint depression soundings for any given layer). The central vertical scale indicates layer numbers and layer boundary air temperatures and pressures.

CHANGES OF 6.7μm RADIATION ORIGIN BY REDUCING LAYER HUMIDITY

PERCENT CONTRIBUTIONS OF RADIATION FROM 3 SOURCES AND CHANGES WITH INCREASED DEWPOINT DEPRESSIONS

SELECTED LAYERS	MOIST LAYER			SURFACE			BACKGROUND			B.T. INCREASE
	1°	9°	LOSS	1°	9°	GAIN	1°	9°	GAIN	S.R.
LAYER #2	26.5	16.4	-10.1	72.3	81.9	+ 9.6	1.2	1.7	+0.5	4.0°C
LAYER #6	65.8	51.6	-14.2	32.4	46.5	+14.1	1.8	1.9	+0.1	6.9°C
LAYER #12	95.0	92.6	- 2.4	1.1	3.4	+ 2.3	3.9	4.0	+0.1	0.8°C

TABLE 1

c. Variations of Humidity Within The Moist Layers

On **Figure 13**, brightness temperatures from 42 soundings are plotted for both 6.7μm radiation and 7.3μm radiation. Consider first the results from 6.7μm radiation, which are displayed on the left. The brightness temperature curves represent the same 14 moist layers, but with three different dewpoint depressions for each layer. The central curve, from five degree dewpoint depressions, is the same as shown on **Figure 12**. The cooler brightness temperatures plotted to the left are from layers nearly saturated with a one degree depression; and those on the right are from layers with a nine degree depression.

The "crossover altitude" is not greatly changed by the variation of humidity within the layers. From the nearly saturated set, the minimum brightness temperature was -15.5°C produced by both layers #8 and #9. From the drier nine degree dewpoint depressions, the "crossover" occurred at layer #9 as was the case from the original five degree depression set. If the three curves were smoothed, they would imply a gradual rise in "crossover altitude" with increasing humidity in the layers.

"Sensitivity Range" - The Detection of Layer Humidity

As discussed with the "crossover effect", relatively large differences of brightness temperature are produced by the different moist layers at different vertical locations. Consider now the brightness temperature differences produced by changes of humidity within each layer.

Definition - "Sensitivity Range"

The difference between the brightness temperature produced by 9° dewpoint depression sounding and that produced by 1° dewpoint depression sounding in each moist layer is defined as the "sensitivity range", labeled "SR" on **Figure 13**. It provides a quantitative indication of the satellite's ability to detect differences of humidity or water content within the layers; but, it is not a measure of those differences.

Vertical Variation of "Sensitivity Range"

This is shown graphically on **Figure 13** by the distance between the brightness temperature curves from the one and nine degree dewpoint depression cases of each layer. With 6.7μm radiation, there is a large variation of "sensitivity range" with altitude, especially between the middle and low layers. The 6.7μm radiation is very "sensitive" to the differences of humidity in the layers near 400mb. But, at low levels, where the differences of water content in the layers is much larger; they are barely detectable by the 6.7μm radiation.

Reason For The Vertical Variation

With the air temperature sounding fixed, different brightness temperatures are dependent upon the radiation arriving at the satellite from different origins. On Table 1, 6.7μm radiation data are listed from sample moist layers near 250mb, 400mb and 700mb. Percentages of radiation reaching the satellite from the moist layer, the background moisture, and the earth's surface, are displayed for each sounding. As the humidity of the layer is reduced, the contribution from the layer decreases, and the contribution by the warmer earth's surface increases. This produces an increase in brightness temperature. At layer #6, a relatively large change in the radiation origin produces a 6.9°C increase in the brightness temperature. At low layers, where even the drier relative humidity absorbs a large percentage of the radiation, only a small change in origin occurs with the change of water content. At layer #12, the change of brightness temperature is less than one degree.

Importance And Usefulness Of "Sensitivity Range" And Its Variation

The "sensitivity range" provides another important characteristic of the radiation in both wavelengths. Consider the sensitivity of 6.7μm radiation to layer humidity differences. Observations of 6.7μm imagery have shown that a layer of moisture at high or middle levels is more likely to have a textured or uneven gray shade appearance than a layer at low altitudes. Small horizontal scale differences of humidity within a middle or high layer can be detected by the satellite, providing that the horizontal resolution capability of the instrument is sufficient. At low altitudes, where the "sensitivity range" is very small, similar localized differences are less likely to be detected; and, the layer tops have a regular appearance.

A common dilemma encountered in image interpretation is that of estimating the altitude of a moist layer. Note on **Figure 13**, that a 6.7μm brightness temperature of 0°C could be produced by a layer of moisture near 850mb where the air temperature is similar, or near 300mb where the air is much colder. Two such layers would have identical gray shades on imagery; however, the high layer is more likely to have an uneven appearance caused by localized differences of humidity within the layer.

The ability to detect humidity differences within a moist layer can be significant in other ways. Consider a situation where mountain waves are present without clouds. If the waves are confined to specific altitudes, or if moisture is present only in specific layers; the detection of the waves on water vapor imagery can depend upon the "sensitivity range" and its vertical variation for the particular wavelength being measured.

d. 7.3μm Radiation Characteristics From The 14 Moist Layers

On the right side of **Figure 13**, 7.3μm brightness temperatures from the same 42 soundings are displayed. Since 7.3μm radiation is less easily absorbed by water vapor than is 6.7μm radiation, the atmospheric contribution to the total radiance is less for each of the 14 layers. Therefore, the 7.3μm brightness temperatures are all less than those from 6.7μm radiation; and the dominance by the atmospheric contribution over the surface contribution occurs at a lower level. This results in lower crossover altitudes. For all three dewpoint depressions, the 7.3 crossover altitude occurs at layer #11 - centered on 662mb. At middle and high layers, the 7.3μm radiation is less sensitive to the differences in layer humidity than is 6.7μm radiation. But, at low altitudes, the sensitivity range of the 7.3μm radiation remains significantly large. Differences in low level humidity can be detected.

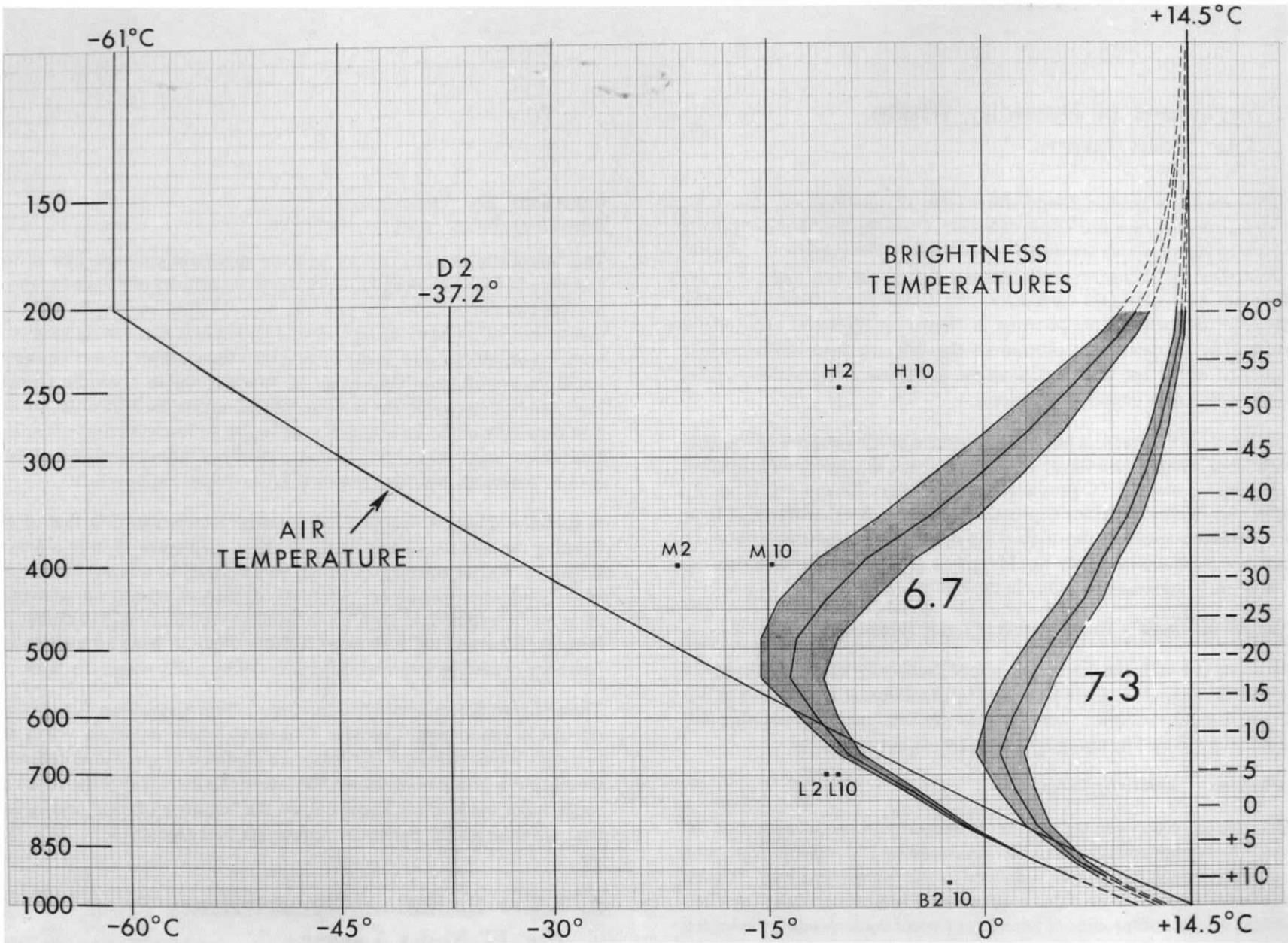

Figure 14 **LAYER BRIGHTNESS TEMPERATURES COMPARED TO AIR TEMPERATURES**
The same sets of brightness temperatures of **Figure 13** are plotted with the air temperature sounding. The standard air temperature scale is doubled.

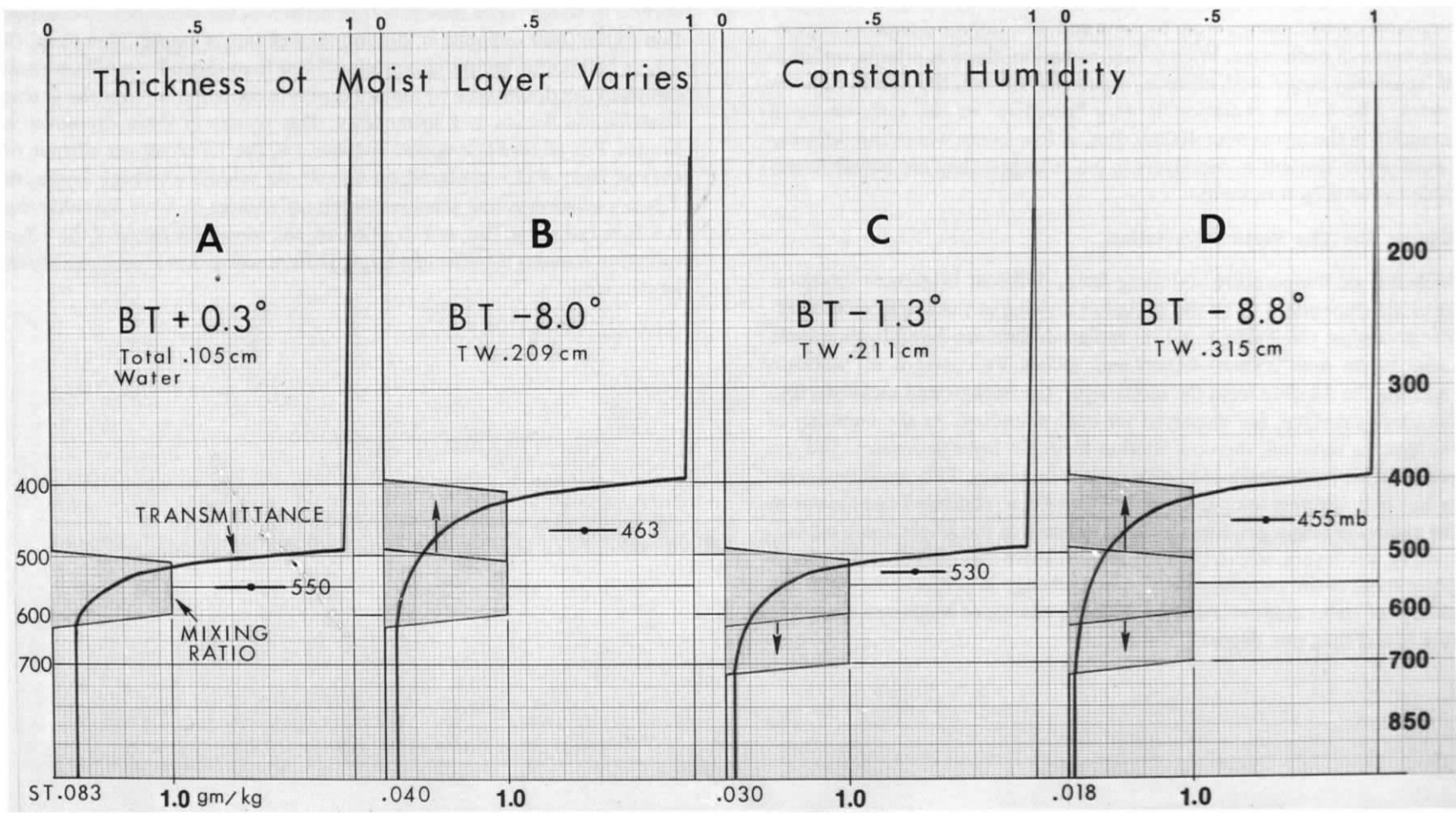

Figure 15 **COMBINED LAYERS OF CONSTANT WATER CONTENT**
Moist layers of 100mb depth and 1.0 gm/kg mixing ratio are displayed by plots of Mixing Ratio. Single layer centered at 550mb is shown on left. The layer is extended upward, downward, and in both vertical directions for cases B, C, and D.

3. A COMPARISON OF SINGLE LAYER RADIATION RESULTS

On **Figure 14**, the brightness temperature curves for both radiation bands are plotted on the same temperature scale along with the air temperature sounding used for all single layer cases. Also included on **Figure 14** are selected brightness temperatures from the bar graph shown on **Figure 8**. Of the soundings previously discussed, the coldest brightness temperature computed was -37.2°C. This was for 6.7μm radiation from the "deep" layer bar graph case with a 2° dewpoint depression. For comparison, this brightness temperature is shown on **Figure 14** by a line labeled "D2". It represents the coldest brightness temperature computed from the air temperature sounding shown.

Consider the curves on **Figure 14** representing 7.3μm radiation. As the altitude of the moist layers is decreased from the highest level, the absorption by the layers increases; and, the surface contribution to the total radiation decreases. Thus, the brightness temperatures approach the air temperature, which is colder than the surface temperature. However, as the altitude is lowered, the air temperature increases. Therefore, the brightness temperatures reach a minimum value at the "crossover altitude". Below there, the brightness temperatures increase along with increasing air temperature and the temperature of the moisture within that air. If the absorption of the moist layers is increased, colder brightness temperatures and a higher "crossover altitude" occur. This increased absorption can be attained by decreasing the dewpoint depressions within the moist layers, or by changing to 6.7μm radiation which is more easily absorbed by the same amount of water vapor. Thus, the set of curves for 6.7μm radiation have colder brightness temperatures and higher "crossover altitudes".

Increased absorption can also be attained by increasing the thickness of the individual layers. The layers of moisture illustrated on the bar graph of **Figure 8** were 100mb in thickness. Recall that the "high" moist layers from that set extended from 300mb to 200mb. On **Figure 14**, 6.7μm brightness temperatures from the high layers with dewpoint depression of 2°C and 10°C are plotted as "H2" and H10". Similarly, pairs of brightness temperatures from the 2° and 10° dewpoint depression cases are plotted for the "mid", "low" and "boundary" layers. Although there are only four layers, their crossover and sensitivity range effects are apparent. With the increased moisture of the thicker layers, the overall brightness temperatures are colder with a higher "crossover altitude" and increased "sensitivity range"

To examine layers of even greater thickness defeats the "layer" concept, and is of little practical value. As an extreme example, consider the thickness required of a "high" layer which absorbs all of the 6.7μm radiation arriving from below. With the top of the moisture at 200mb and a nearly saturated tropical temperature sounding, the layer would have to extend downward to 600mb.

Specific results of the 14 layer experiment are arbitrary, since they would vary with different conditions such as layer thickness, number of layers, and the temperature sounding. However, the basic concepts involved, such as the crossover effect and the sensitivity range, are fundamental to the process of radiation measurements from moist layers. The experiment also provides a quantitative comparison of the characteristics of 6.7 and 7.3μm radiation with different vertical distributions of water vapor.

4. COMBINATIONS OF 100mb THICK MOIST LAYERS

On the bar graph of **Figure 8** are eight combinations of "high", "mid" and "low" moist layers. Although there are numerous comparisons to consider, we shall limit our discussion to 6.7μm radiation results and to layers with two degree dewpoint depressions. We may compare the brightness temperatures of the three selected combinations with that of the "mid" layer only. These are listed below for convenience.

Soundings	6.7μm Brightness Temperatures
Mid only	-21.4°C
High over **Low**	-21.3°C
High over **Mid**	-26.1°C
Low under **Mid**	-27.4°C

The brightness temperature from the **Mid** layer alone is equal to the air temperature near 500mb. Note that the **High** over **Low** combination yields an almost identical brightness temperature and equivalent pressure. The net radiation from the two moist layers implies moisture at middle levels where only the relatively dry background humidity exists. This further illustrates a common problem for image interpretation. In addition to the use of image patterns and time-lapse motion, comparing measurements from more than one water vapor channel may resolve such problems.

Compare the brightness temperatures from the **Mid** layer alone to those from the **Mid** and one additional layer. In both cases shown, the increased absorption by the additional layer results in colder brightness temperatures. The additional layer prevents a portion of the high intensity radiation from the surface and very low levels from reaching the satellite. Note that - in these samples - the addition of the **Low** layer under the **Mid**, produced a cooler brightness temperature than the addition of the **High** layer over the **Mid**. The result may appear suspicious, since the moisture in the **High** layer is significantly colder than that in the **Low** layer. Several factors, acting in combination, contributed to the colder brightness temperature from the **Low** under **Mid** sounding. The absorption accomplished by the **Low** layer is much greater than that by the **High** layer because of the larger amount and density of moisture; and, the background moisture has a larger cooling effect on the **Low-Mid** results. A brief examination of layer combinations under controlled conditions is useful. Consider the layers shown in **Figure 15**.

In the soundings illustrated by **Figure 15**, the depth of the moist layer is increased upward, downward, and in both directions. The effect is identical to placing additional moist layers adjacent to the original. For these cases, conditions were established to eliminate some of the complications present with the bar graph layers. The mixing ration is held constant at 1.0 gm/kg through the depth of the moist layers, and the background moisture is reduced to a constant 0.0001 gm/kg, to minimize its effect. The temperature sounding is constant for all 4 cases, but is different from that used in the bar graph cases. It is a summer season - or low latitude - sounding which averages 15°C warmer than the temperatures of the U.S. Standard Atmosphere. The surface temperature is +29.0°C. This warmer sounding, which was chosen to allow more water content in the layers, affects the absolute value of the brightness temperatures, but does not alter the conclusions. Displayed on the figure, for each sounding, are mixing ratio, transmittance and equivalent pressure.

Sounding "A"

In sounding "A", a single moist layer extends from 500mb to 600mb. From a relative humidity aspect, the sounding represents a dewpoint depression of 4°C with respect to the U.S. Standard Atmosphere temperature at 500mb. The 6.7μm brightness temperature of 0.3°C is equal to the air temperature at 550mb - the layer midpoint. As shown by the transmittance plot, slightly more than 8% or the radiation from below the layer penetrates to the satellite.

Sounding "B"

The moist layer of sounding "B" is extended upward to 400mb. The total water content and pressure thickness of the resulting layer are double those of sounding "A". This is equivalent to placing a second nearly identical moist layer above the original, except that the volume occupied is greater and the density less. Since the additional layer is in colder air, and even less radiation from below 600mb penetrates to the satellite; the brightness temperature is colder by 8.3°C. Both the increased absorption and the colder temperature of the additional moisture act to reduce the brightness temperature.

Sounding "C"

In sounding "C" the water content is nearly identical to that of sounding "B"; but, the layer is extended downward to 700mb instead of upward. The brightness temperature is again cooler than that of case "A", but only by 1.6°C in this case. Although the increased absorption is greater than that of case "B", the additional moisture is in warmer air. Compared to case "A", both cases "B" and "C" reduce the percentage of high intensity surface radiation reaching the satellite; thus, both produce cooler brightness temperatures. Although the additional lower layer of case "C" was warmer than the layer in case "A", it is significantly colder than the surface.

Sounding "D"

In this case, the moisture is extended both upward and downward. This produces the coldest brightness temperature of the four cases. However, compare case "D" with "B". In sounding "B", moisture was present from 400 to 600mb. Extending the moisture on downward to 700mb reduces the brightness temperature by less than one degree from -8.0° to -8.8°C. Additional moisture below "B" has less effect than below "A".

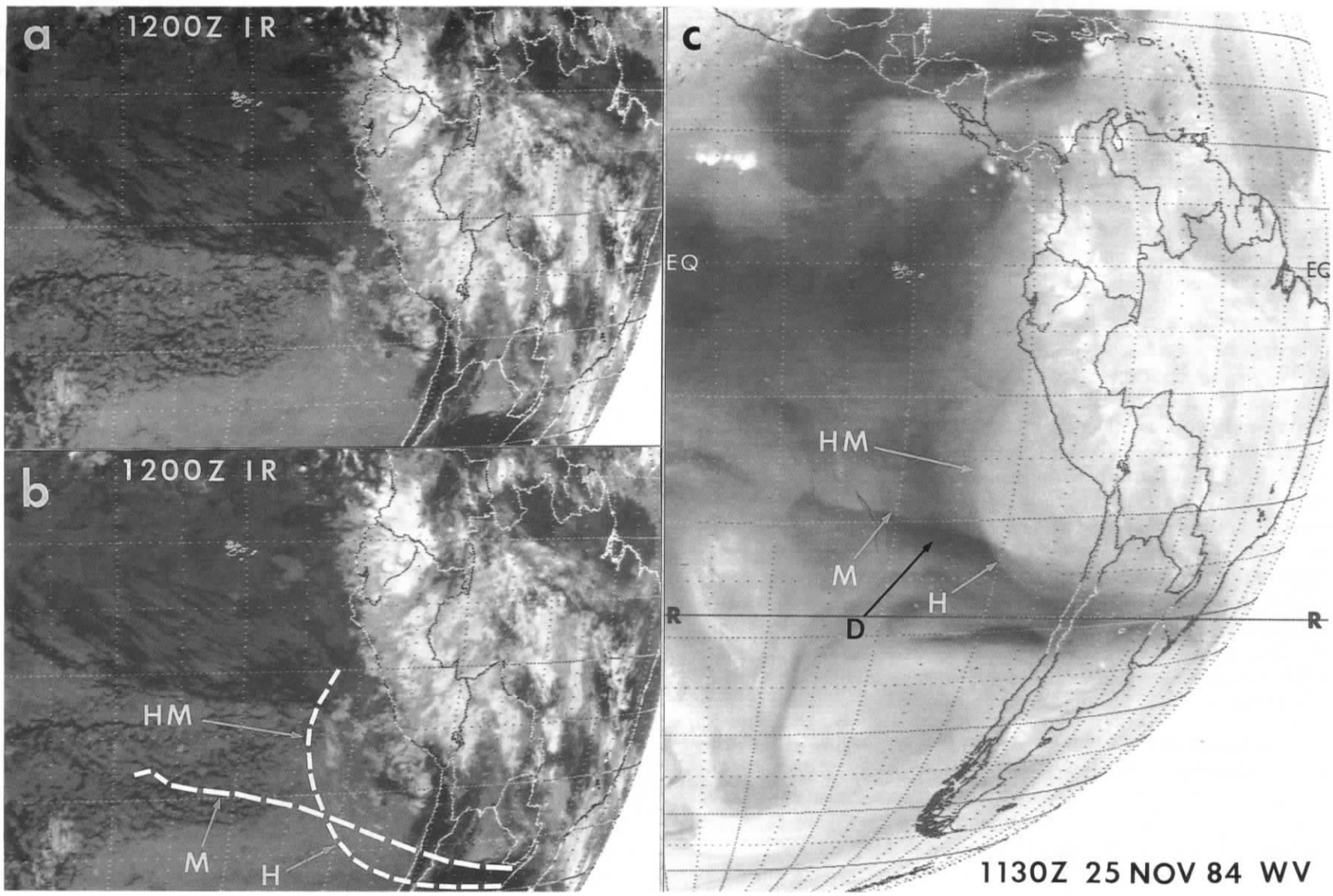

Figure 16 IMAGE EXAMPLE OF COMBINED MOIST LAYERS

Figs. 16a and 16b. Identical window infrared images (16b annotated) 1200Z 25 November 1984, GOES Central. Dashed lines correspond to moisture boundaries labeled on the water vapor image of **Fig. 16c.**

Fig. 16c. 6.7μm water vapor, 1130Z 25 November 1984, GOES Central. Line "R-R" indicates the southern boundary of the infrared images (data not received south of there).

On **Figure 16**, a 6.7μm water vapor image is shown on the right side. On the left, an infrared image is repeated, with and without notation. The line "R-R" on the water vapor image indicates the southern border of the infrared image which was not received south of there.

Over the Pacific Ocean west of South America, a large region of moisture in the upper middle troposphere is bounded on its southern side by boundary "M". Another boundary, "HM" is located over the upper middle level moisture. Very high level moisture from the convective cloudiness over South America has spread westward and poleward, and is bounded by "HM" on its west side. As that cold high level moist air spread poleward and turned into the westerlies, it passed over boundary "M". South of there, the high level boundary is present at "H". That portion of the high level moisture south of "M" displays significantly darker gray shades, compared to that north of "M".

This case is an example of radiation arriving at the satellite from different combinations of moist layers. East of "HM", part of the radiation arrives from the upper middle level moisture under the cold high moisture. The combination produces relatively cold brightness temperatures and a light gray shade. Where the high level moisture passes south of "M", it overlies a slot "D" in which the air is dry at middle levels. The radiation from there combines with that of the thin high level moisture to produce a medium gray shade. Note that the stratocumulus clouds within the marine layer, shown on the infrared image, are not apparent on the water vapor image, even where the middle and upper levels are relatively dry.

5. SUMMARY - SECTION B

The satellite measures only the intensity of radiation arriving from below. It does not detect the origin of the radiation. If the intensity is converted to brightness temperature, the relative vertical location of the emitting substance may be estimated. However, the same net radiation intensity at the satellite may be produced by various combinations of air temperature, humidity and vertical distributions of moisture. This is particularly significant when moisture is distributed in single or multiple layers.

RANGE OF BRIGHTNESS TEMPERATURES

The range of brightness temperature, computed or measured, is limited at the warm end by the skin temperature of the earth's surface; or, in some cases, by moisture or clouds at the top of a strong temperature inversion. With no middle or high clouds present, the coldest 6.7μm brightness temperatures computed or measured in our studies were near -45°C.

A practical range of 6.7μm brightness temperatures, from cloud-free conditions, is from - 45°C to +20°C. A similar practical range for 7.3μm radiation with mid or low latitude temperature soundings is smaller - from - 20°C to +25°C. However, with very dry cold temperature soundings, such as over continents in winter, 7.3μm brightness temperatures can be as cold as those of 6.7μm radiation.

THE "CROSSOVER" EFFECT

When moisture is arranged in layers, the brightness temperature measured by the net radiation reaching the satellite is often unrepresentative of the air temperature of the layers. Layers of moisture at high altitudes produce relatively warm brightness temperatures, since much of the high intensity radiation from lower warmer sources penetrates through the layer. Low level moist layers, which often absorb all or most of the upcoming radiation, produce warm brightness temperatures because the moist layer itself is warm. Because of the "crossover" effect between radiation penetrating from below, and radiation from the moist layer, the coldest brightness temperatures are produced by moist layers at middle altitudes. Since 6.7μm radiation is more easily absorbed by water vapor, its "crossover" altitude is higher than that of 7.3μm radiation. A 14 layer experiment was composed of moist layers with air temperatures and humidities commonly observed in the atmosphere. For such layers, the coldest 6.7μm brightness temperatures are most likely to be produced by moisture located near 500mb. Those for 7.3μm radiation are most likely from moisture just above 700mb.

THE "SENSITIVITY RANGE"

The net radiation intensity reaching the satellite in the 6.7μm band is very sensitive to differences in humidity within middle and high moist layers. The "sensitivity range" is a maximum near 400mb. However, differences of water content in low moist layers - typically those below 700mb - are not easily detected by 6.7μm radiation measurements. The "sensitivity range" of 7.3μm radiation is overall less than that of 6.7μm radiation; however, it remains sufficiently large at low levels to detect differences in humidity commonly found there.

MULTIPLE MOIST LAYERS

If no significant air temperature inversion is present, the addition of a moist layer either above - or below - an original moist layer will produce a colder brightness temperature. If a layer is added under an original moist layer with very large water content and density, such that all or most of the upcoming radiation is already absorbed; then, no appreciable reduction of brightness temperature will occur.

SECTION C

CASE STUDIES - WATER VAPOR IMAGES AND RADIOSONDE DATA

In this section, three basic categories of data will be compared.

- Water vapor imagery from NOAA-7 and GOES satellites
- Radiosonde soundings as transmitted operationally
- RADCOM model computations from radiosonde data

There are a number of complications involved in this comparison, many of which are of minor consequence, and some of significance.

In regard to the imagery, we really do not know exactly what the satellite is measuring. Even if the radiation theory, instrumentation, and data handling system were perfect, there are other problems such as horizontal resolution and the non vertical radiation path. The measured data used to produce imagery were not temperature calibrated. For quantitative comparisons, two types of brightness indices will be used. These will be explained as they are introduced into the discussion.

Although radiosonde soundings do not provide accurate vertical distributions of moisture, they are the basic data source commonly available to persons using satellite imagery; and, their use enabled us to examine a very large data sample. Two very significant limitations to the radiosonde moisture data will be discussed.

The RADCOM computed radiation data are dependent upon the accuracy of the model and the limitations of the radiosonde data.

Literally thousands of upper air soundings were compared with imagery from several satellites. In some cases, as will be shown, data from all three basic categories were compared, including imagery from two satellites. Apparent contradictions were observed among the different data sources. However, in general, results from the three basic categories of data were in agreement. The empirical comparisons confirmed the value of the RADCOM model, and enhanced the reliability of the conclusions in Sections A and B.

1. TWO SIGNIFICANT LIMITATIONS OF THE TRANSMITTED RADIOSONDE DATA

The upper air moisture data are limited to dewpoint depressions of less than 30°C. From most observing sites, moisture data were not available for air temperatures colder than - 40°C. We did examine moisture data for a one week period from western United States observing sites, which was extended to air temperatures of -60°C. Data were also available routinely from some upper air observing sites that transmit dewpoint depressions to 100mb.

Both limitations represent problems in relating radiosonde data to water vapor imagery.

The 30° Dewpoint Depression Limit

When a 30° dewpoint depression is transmitted, we can assume that the dewpoint depression is exactly 30°, or anything greater than 30°. We can assume that the air is relatively dry; but, we do not know the humidity. With a summer season or tropical temperature sounding, the total water content could be as much as 1 cm which is approximately 10 times as much as a typical mid winter continental sounding.

Consider the effect of a 30°C dewpoint depression moisture profile on 6.7μm radiation measurements. On **Table 2**, computed radiation data are listed for a mid-latitude temperature sounding with humidity ranging from nearly saturated to zero water content. The computed 6.7μm brightness temperature for a 30°C dewpoint depression sounding is near - 15°C, which is a relatively cool value compared to the range between the humid and dry cases. This can be related to the gray shade scale of 6.7μm water vapor imagery transmitted operationally from GOES satellites. Using a gray shade scale of 100 digits, such that black = 0 and white = 100; we estimate that a brightness temperature computed at -15°C would be equivalent to approximately 40 on the gray shade scale.

The computations indicate that a 30°C dewpoint depression sounding is not exceptionally dry with respect to 6.7μm radiation measurements. This is confirmed by comparing satellite imagery to radiosonde soundings. Significant gray shade differences are observed above radiosonde soundings reporting similar air temperatures and 30°C dewpoint depressions above the boundary layer. The problem is most common at low latitudes.

With the 30°C dewpoint depression limit to radiosonde moisture data, in relatively dry warm atmospheric conditions, the radiosonde data cannot reveal moisture differences detected by 6.7 μm satellite data.

The dew point depression limit is also significant when using RADCOM computations from radiosonde data. It was found through experimentation that substituting 50°C dewpoint depressions for those reported at 30°C in the sounding data, produced the best correlations between computed radiation intensities and satellite imagery. Therefore, this substitution was adopted as a standard procedure for RADCOM computations from radiosonde data.

The -40°C Air Temperature Limit to Reporting Moisture Data

With the very sensitive 6.7μm radiation, moisture in air cooler than -40°C is sufficient to produce significant differences in brightness temperature or image gray shades. This is important with nearly saturated moist layers in the upper troposphere, such as along the equatorward side of the jet stream over an upper air ridge.

Although such cold high altitude moist layers do not produce brightness temperatures representative of their air temperature, they can produce significant differences in image gray shade, especially when the air is relatively dry at middle levels. To provide a quantitative range of this effect, radiation data were computed for mid and low latitude soundings with moisture at 1°C dewpoint depression from the altitude of -40°C air temperature to the tropopause. For these computations, the same "background moisture" as used in the bar graph sounding of **Figure 10**, was present below the cold high moisture. The 6.7μm radiation data computed from these cases are shown in **Table 3**.

Brightness temperatures from soundings with nearly saturated air colder than -40°C can be compared to soundings with "background moisture" only. In the tropical case, the sounding with the high level moisture produces a brightness temperature which was 17.1°C colder than that produced by the background moisture alone. Although the reduction produced by the mid-latitude samples is slightly less, such differences would be significant to image interpretation.

As in the case of the 30°C dewpoint depression limitation, this second limitation presents a problem in comparing water vapor imagery with radiosonde data. It is more significant to 6.7μm imagery than to 7.3μm imagery.

Computed Radiation Data From Mid-Latitude Temperature Sounding

Moisture		6.7 μm		7.3 μm	
Dewpoint Depression 1000-200mb	Total Water Content	Brightness Temperature	Surface Radiation Contribution	Brightness Temperature	Surface Radiation Contribution
1°	2.577 cm	- 38.4°C	0.0%	- 18.0°C	0.6%
30°	0.245 cm	- 14.9°C	1.5%	+ 1.8°C	25.5%
50°	0.034 cm	+ 0.3°C	18.7%	+ 9.8°C	62.5%
Dry	0.0 cm	+ 14.0°C	100.0%	+ 14.0°C	100.0%

Tropopause -62°C 200 mb Surface Temperature + 14.0°C 1000 mb

TABLE 2

Maximum Effects by Moisture in Air Colder Than -40°C

	Soundings		Depth of Moist Layer	Surface Radiation Contribution	Total Water Content	6.7μm Brightness Temperatures
Mid-Latitude Temperature Soundings Surface: + 14°C at 1000 mb Tropopause: -62°C at 200 mb	Background Moisture Only No Moist Layer		0	19.5%	0.032 cm	0.0°C
	Cold Moist Layer 1°C Dewpoint Depression	200 mb -62°C 333 mb -40°C	133 mb	16.5%	0.054 cm	-14.3°C
	Cold Moist Layer 1°C Dewpoint Depression	100 mb -62°C 333 mb -40°C	233 mb	16.1%	0.059 cm	-15.8°C
Tropical Temperature Soundings Surface: + 29°C at 1000 mb Tropopause: -82°C at 100 mb	Background Moisture Only No Moist Layer		0	18.9%	0.032 cm	+ 15.2°C
	Cold Moist Layer 1°C Dewpoint Depression	100 mb -82°C 238 mb -40°C	138 mb	16.3%	0.056 cm	- 1.9°C

Soundings have same background moisture as bar graph soundings of **Figure 10**.

TABLE 3

2. GENERAL COMPARISON - 6.7μm GOES IMAGERY AND RADIOSONDE DATA

On **Figure 17**, a water vapor image valid at 1130Z 19 May 1983 is shown with a 1200Z infrared image. A close-up view of the same water vapor image is shown on **Figure 18a**, and with a 300mb analysis superimposed on **Figure 18b**.

In this section, an index called "image brightness" will be used in the discussion of GOES water vapor images.

IMAGE BRIGHTNESS

Image Brightness is a quantitative representation of image gray shades, consisting of whole numbers from 0-100, where the warmest or darkest gray shade attainable on the image is equal to zero, and the lightest or coldest shade attainable is equal to 100. The image brightnesses were measured from imagery, not obtained from digital data. Therefore, they were normalized to each individual image, on which they were measured. The image brightness was not intended for comparing gray shades among different images, but to provide a quantitative comparison of gray shades on a single image. The image brightnesses cannot be converted to brightness temperatures, and serve only as an indication of relative gray shade differences.

Some values of image brightness have been plotted on the images of **Figure 18**. They are plotted directly over the points where the measurements were made. Note on **Figure 18a** that the brightest, or coldest, value measured on the image was an image brightness of 100 over the thunderstorm tops south of Guatemala (See **Figure 19**). The warmest, or darkest, value on the image was an image brightness of 12 east of Florida. In these two extreme value locations, the measurements were made at the locations of the star symbols.

Although it is not necessarily a disadvantage, we tend to observe relative differences in gray shades, rather than absolute values, when we observe an image. This can be illustrated by comparing some of the image brightness values plotted on the image. Note the value of 71 plotted over the Atlantic Ocean east of Delaware. It is located in an area of relatively lighter gray shades with respect to the surrounding areas. Another value of 71 is located over Utah in an area of relatively darker gray shades. Without quantitative measurements, we might expect the area over Utah to be darker than that of the eastern location.

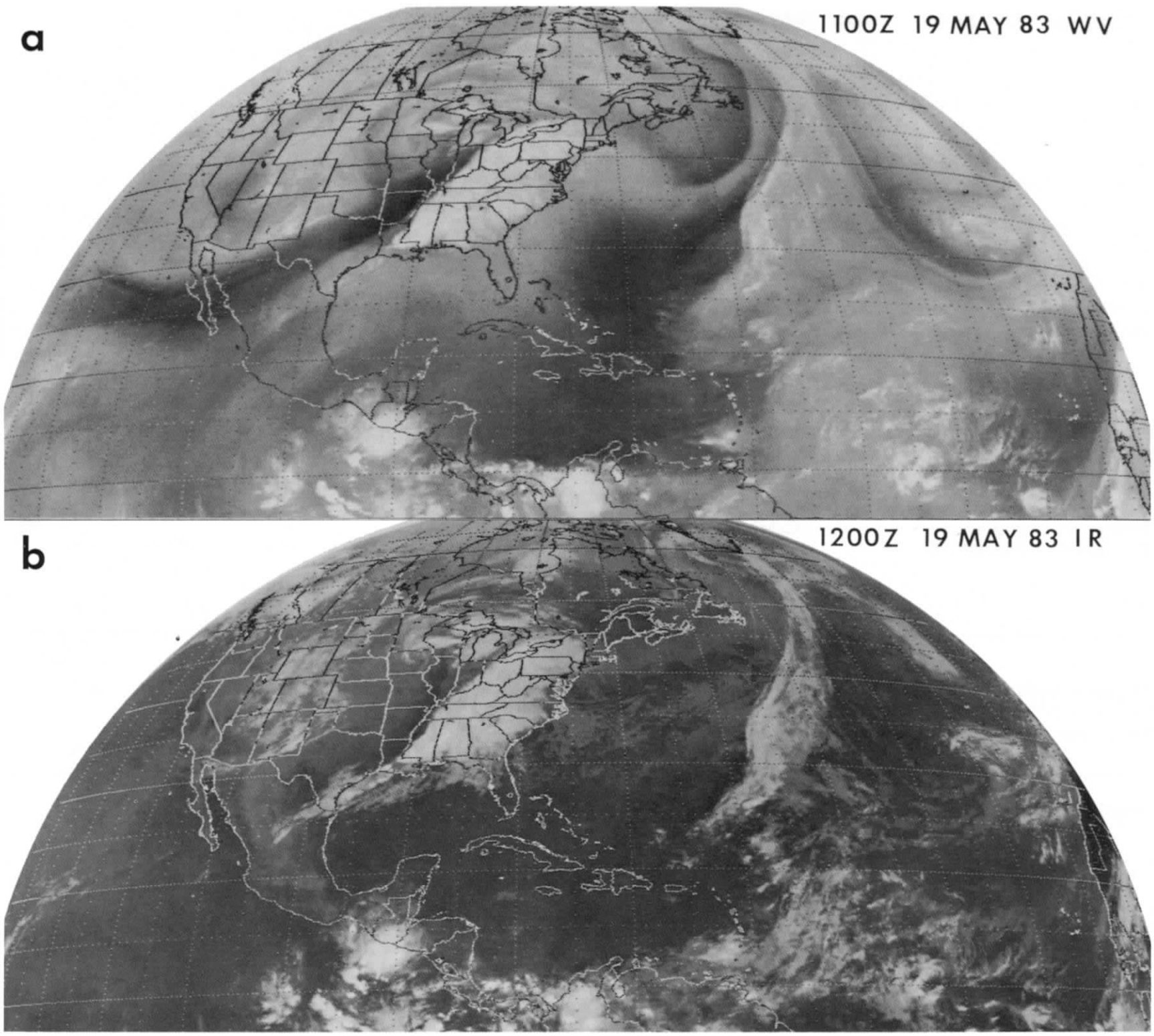

Figure 17 **WATER VAPOR INFRARED IMAGE COMPARISON - LARGE VIEW**
Fig. 17a. 6.7μm Water Vapor Image, 1100Z 19 May 1983, GOES East,
Fig. 17b. 11.2μm Infrared Image, 1200Z 19 May 1983, GOES East.

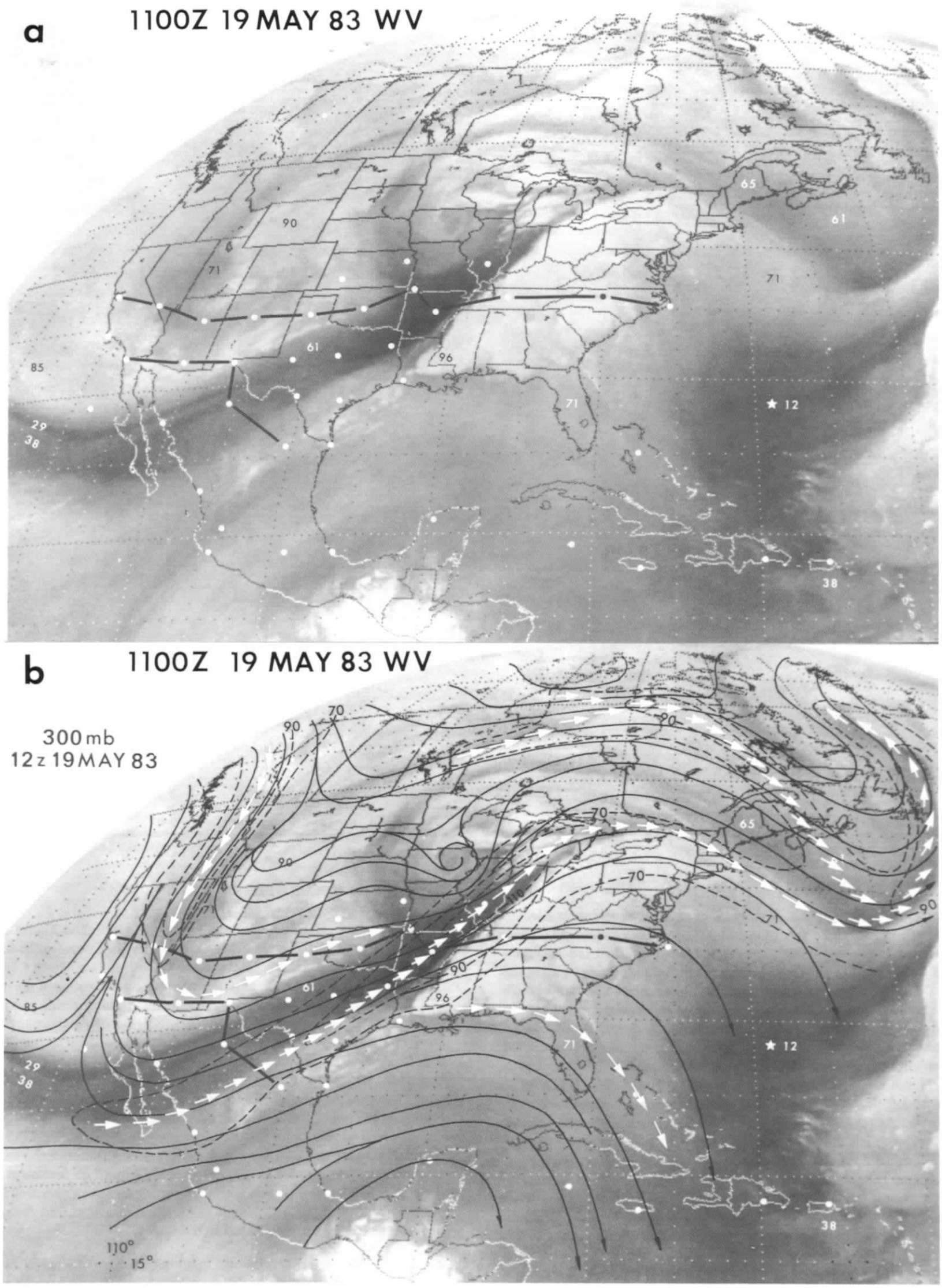

Figure 18 **WATER VAPOR IMAGES WITH CROSS SECTION LOCATIONS AND 300mb ANALYSIS**

Fig. 18a. Values of Image Brightness (digits), Radiosonde Sites (dots)
Connected sites indicate cross section locations.

Fig. 18b. 300mb Analysis: streamlines (solid black lines), Isotachs (dashed black lines labeled in knots), Axes of maximum 300mb wind speeds (white arrows).

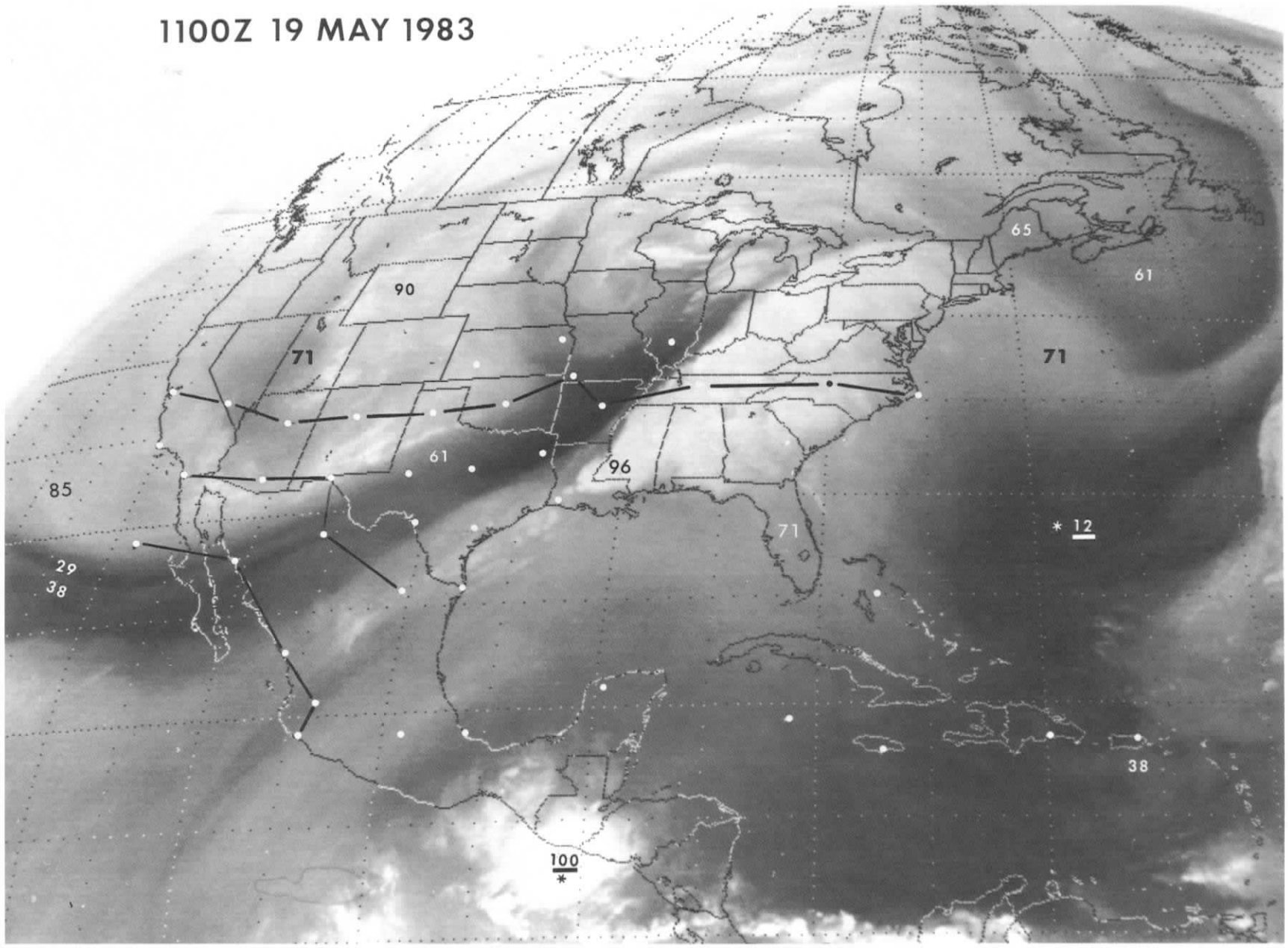

Figure 19 **WATER VAPOR IMAGE (REPEAT OF FIGURE 18a)**
6.7μm Water Vapor Image, 1100Z 19 May 1983, GOES East with Image Brightnesses, Radiosonde Sites, and Cross Section Locations.

DEWPOINT DEPRESSION VERTICAL CROSS SECTIONS

Also plotted on the images of **Figures 18 and 19**, are white dots at selected radiosonde sights. Three sets of radiosonde sites are connected by black lines. The northern two of these correspond to two moisture cross sections shown on **Figure 20**. We tried a number of techniques for comparing the vertical moisture profiles among a group of radiosonde sites. Although each display technique had advantages and disadvantages, we chose the type shown on **Figure 20**. The cross sections display dewpoint depressions plotted on a vertical pressure scale. Each radiosonde site is represented by a column with a horizontal temperature scale of 30°C width. Within each column, dewpoint depressions are plotted from right to left. A value on the far left side of the column indicates a dewpoint depression of 30°C, and one on the far right indicates a zero depression. Within each column, the area to the left of the depression plot is shaded. Where the shading approaches the right side of a column, the air is relatively moist. The top of each data column is at the -40°C air temperature. In some of the subsequent cases to be discussed, air temperature isotherms are added to the columns at 10°C intervals, and different shadings are used for different temperature ranges. The numbers above each column on **Figure 20** are image brightnesses measured as near to the radiosonde site as possible. Since many sites are located near grid borders or coastal map grids, it was not possible to measure the values directly over the site. Such measurements were made on the downwind side.

a. Case Discussion - 19 May 1983

The water vapor image of **Figure 18** has been repeated on **Figure 19** for easy comparison to the cross sections of **Figure 20**. Compare the longer cross section from Oakland, California to Cape Hatteras, North Carolina to the water vapor image. Generally, the simple consideration of the image as a "topographic" view of the moisture appears valid. Viewing from west to east along the cross section, the image shades become darker at Desert Rock (DRA) and Winslow (INW). The shades then lighten eastward until becoming even darker at Monett (UMN) and Little Rock (LIT). The brightest sites are east of there at Nashville (BNA) and Greensboro (GSO). Comparison of the IR and WV images indicates that these two sites were covered with cold high clouds. Generally, Image Brightness greater than 90 are observed with areas of thick cirrus clouds. Some exceptions occur at tropical latitudes and over very cold regions during winter. Values in the eighties are common with abundant upper level moisture and no clouds, such as over Oakland in this case. The only cloudiness reported from ground observations near Oakland were patches of stratus, and no middle high clouds can be seen on the infrared imagery.

Comparing the cross sections and the image in more detail illustrates some of the concepts discussed in Sections A and B, and introduces the complications of cloudiness. Notice that the Image Brightness was measured at 71 over both Cape Hatteras and Desert Rock. At Cape Hatteras, surface observations, IR and VIS imagery, and examination of the sounding indicate that stratocumulus clouds were present with the base near 850mb and the top near 821mb. No clouds were present above that,

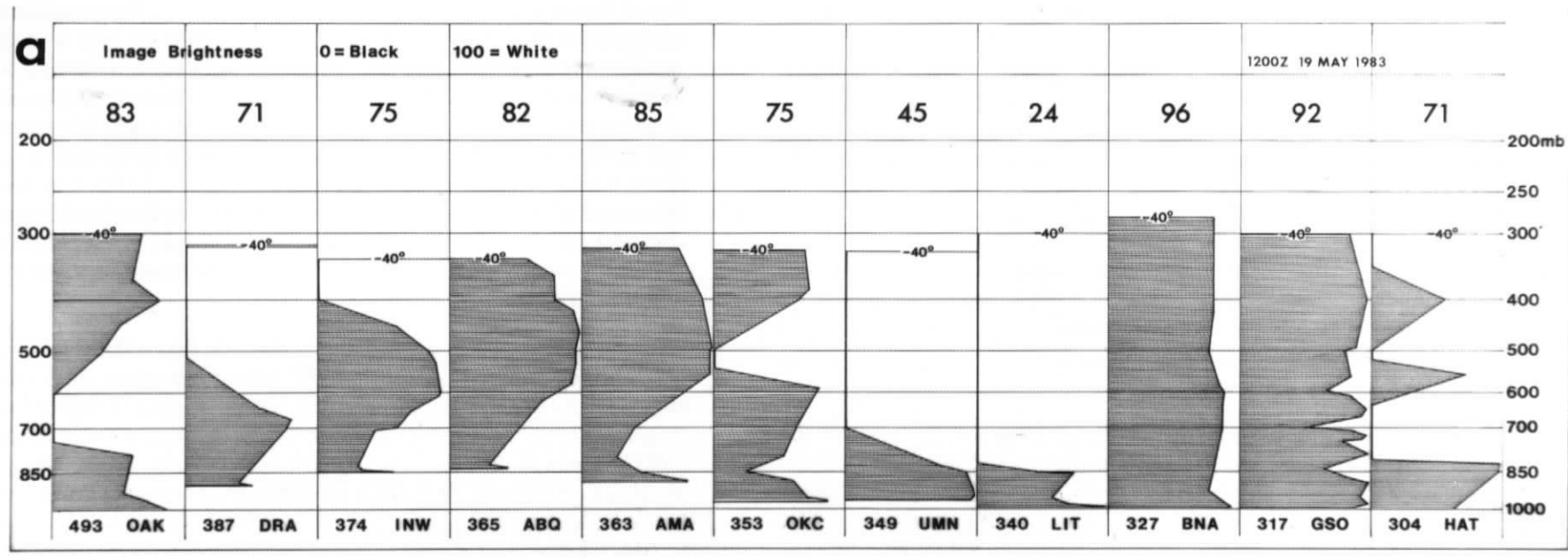

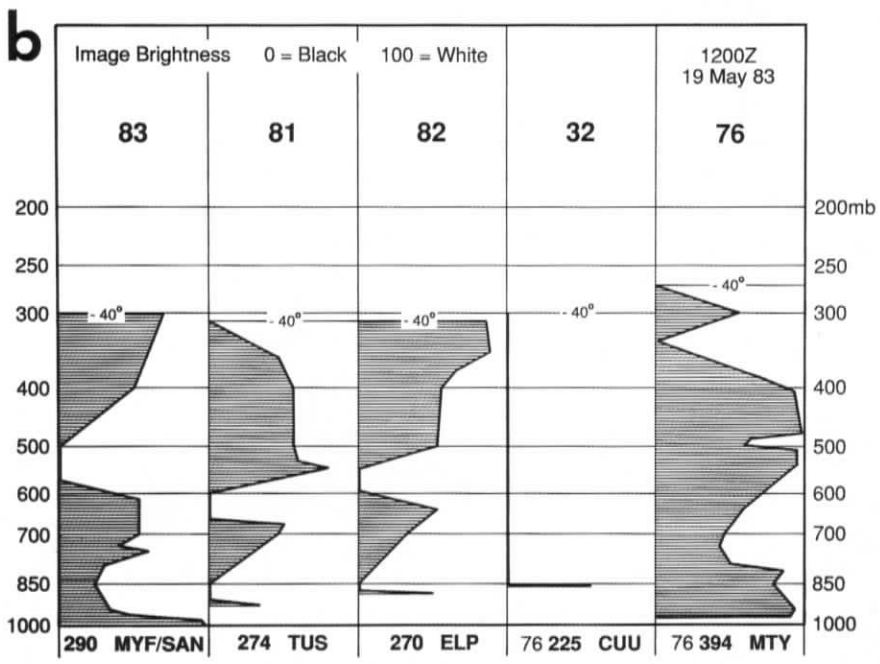

Figure 20

DEWPOINT DEPRESSION CROSS SECTIONS
Dewpoint depressions from radiosonde soundings plotted on 30°C wide columns with a logarithmic vertical pressure scale. See text for detailed explanation.

but at least two moist layers were present. The surface observation at Las Vegas and other imagery indicate that no clouds were present over Desert Rock. A single layer of moisture is present from just below 500mb to the surface with a minimum dewpoint depression of 6°C at 670mb. This case illustrates the concept shown in the bar graph of **Figure 8**, that the same brightness temperatures can be contributed by different moisture distributions. The topographic simplification would imply a lighter gray shade over Cape Hatteras; however, with moisture in layers above 600mb, the net contribution of the moist layers is warmer than their corresponding air temperatures. A reasonable questions is introduced. If the equal gray shades at the two sites were noted from imagery and no sounding data were available, would we have been able to guess that different vertical moisture distributions were present? Such a determination would have been made in general based upon the differences in the upper air circulation environments. Although this difference can be seen on the imagery alone, the 300mb analysis is shown on **Figure 18b** superimposed on the water vapor image. Cape Hatteras is located near the ridge axis well south of where the jet axis crosses the ridge. In that environment, multiple layers of moisture with very dry layers between them are likely through the troposphere. A location such as Desert Rock near the axis of a cyclonically curved northerly jet stream would likely have a single deep layer of moisture below 400mb with dry air above.

Another comparison of interest is that between Winslow (INW) and Oklahoma City (OKC). The Image Brightness over both of these sites was measured at 75. Although the same concept is involved as in the last comparison, the moisture cross section implies a lighter gray shade at Oklahoma City. In this case, cloud cover is an important factor. Skies were clear over Oklahoma City. Winslow reported nine tenths middle cloud cover. Cloud top temperature measure on infrared imagery over Winslow was -20°C, equal to the air temperature at 485mb. With this relatively high level radiation source at Winslow, the equal gray shades are reasonable.

Consider the relatively dark or warm zone which extends from west of the Baja Peninsula to northern Indiana. With such warm zones on 6.7μm imagery, mid-tropospheric moisture is generally absent. However, gray shade differences and patterns can be seen within the relatively dark region. In this case, Image Brightness within the zone range from 22 just south of Little Rock, Arkansas to 61 in west Texas. Such differences are generally related to low level moisture and surface differences, and to the presence of high level moist layers which are relatively thin or of relatively low humidities. In the two cross sections shown on **Figure 20**, three stations are located within the dark zone: Monet, Missouri (UMN), Little Rock, Arkansas (LIT), and Chihuahua, Mexico (CUU). Monett has the lightest gray shade of the three and the most low level moisture. Little Rock has the darkest gray shade - an Image Brightness of 24. Chihuahua reported the driest sounding with an Image Brightness of 32. In such a case, the 30°C dewpoint limitation for radiosonde moisture reports could be a factor. However, in this case, the difference is likely in the low level conditions. Little Rock reported a surface air temperature of +13.8°C and had a measured IR temperature of +12°C. Chihuahua, at 1429 feet elevation, reported a surface air temperature of +9.2°C and had a measured IR image temperature of +7°C.

At other locations within the dark zone, high level moisture was a factor. The thin gray band just north of Chihuahua, which passed over the radiosonde site at Guaymas, Mexico was caused by a high moist layer. Also, the slightly lighter gray shades over west Texas were caused by high level moisture extending over the dry mid-troposphere.

Comparison of the image gray shades to the dewpoint depressions of the San Diego (SAN) to Monterey (MTY) cross section raises a question between the conditions at Monterey and Tucson (TUS). Cloud cover is again the significant factor. There are overcast cloud conditions over Monterey. The infrared image cloud top temperature was -19°C which corresponds to an air temperature at 410mb. This indicates that the large amount of moisture below that level would be of no significance to the 6.7μm brightness temperature. On the IR imagery, cirrus clouds are present near Tucson. It is likely that significant moisture is present a high altitudes colder than -40°C.

b. Case Study - 03 May 1983

On **Figure 21**, a 6.7μm water vapor image valid at 2300Z 03 May 1983 is shown with radiosonde sites and cross section locations. A larger area view of the same image is shown on **Figure 23**, compared to an infrared image, and on **Figure 25** with a 300mb analysis valid at 0000Z 4 May 83. The three northern cross sections indicated on **Figure 21** are shown on **Figure 22**, and the southernmost one is shown on **Figure 24**.

On the water vapor image of **Figure 21**, images brightnesses were not plotted; however, the darkest value on the image was 31 located off the east coast of Nicaragua. The brightest value was 99 at the thunderstorm top over western Venezuela. Over the United States, the warmest value was 36 over central Louisiana.

Consider the longest cross section on **Figure 22**, which extends from San Diego (SAN) to Charleston (CHS). Generally, the "topographic" representation appears valid, with the four central sites reporting 30° dewpoint depressions above single moist layers. High clouds are present over the two easternmost sites, and at Tucson (TUS). There are cirrus clouds just west of San Diego and north of El Paso. The topographic concept is most valid for those sites with a single moist layer below 500mb, as suggested by the 14-layer RADCOM data of Section B. The image brightness values for those sites (plotted on **Figure 22**) range from 72 at Amarillo (AMA) where the air temperature at the top of the moist layer was -11°C at 601mb, to 39 at Lake Charles (LCH) with an air temperature of +8.6°C at 829mb.

A common exception to the topographic concept is illustrated on the cross section from Guadalupe (IGP) to Lake Charles (LCH). Guadalupe, which reported only standard levels, is located under relatively thick middle and high clouds. There were no clouds directly over any of the other sites of the cross section. The four middle sites of the series are under high moisture to the right of the jet stream axis passing over a shallow amplitude ridge (See **Figure 25**). The Image Brightnesses increase from 62 at Victoria (VCT) to 83 at Chihuahua (CUU). Although the tops of the moisture at the stations are not reported because of the -40°C air temperature limitation, the change in the image brightness is most likely a result of the thickness of the moist layer. Air temperatures of the four middle sites are nearly identical between 300 and 100mb, and the tropopauses are above 100mb. Even if there are differences in the tops of the moisture at the sites, it would not likely produce such a significant difference in the Image Brightnesses.

As in the last case, comparison of the radiosonde data with the imagery in detail presents some puzzles. Consider the northernmost cross section shown on **Figure 23**. Based upon the dewpoint data, a higher Image Brightness might be expected at Nashville (BNA) than at Oklahoma City (OKC). Nashville has overcast clouds with tops near 700mb. The same cloud deck was present at both 2300 and 0000Z. Oklahoma City was cloud free at both times. Nashville is located at the western side of the dark zone or "slot" observed on the water vapor image at 2300Z. The moist region west of Nashville ranges in depth from 600mb to 300mb with thickness increasing toward the northwest border. Careful analysis indicates that the eastern border of the moist region moved over Nashville at approximately 2320Z. The discrepancy was caused by movement of the systems during the one hour time difference between the water vapor image and the sounding data. Other factors involved were that the map grid was 12 nm too far south, the satellite angle of view causes something located at 400mb to appear too far northwest of its vertical position, the release time of the balloon, and the movement of the balloon before reaching 400mb. Such problems are common when comparing radiosonde data and imagery when the site is near a border in the gray shades.

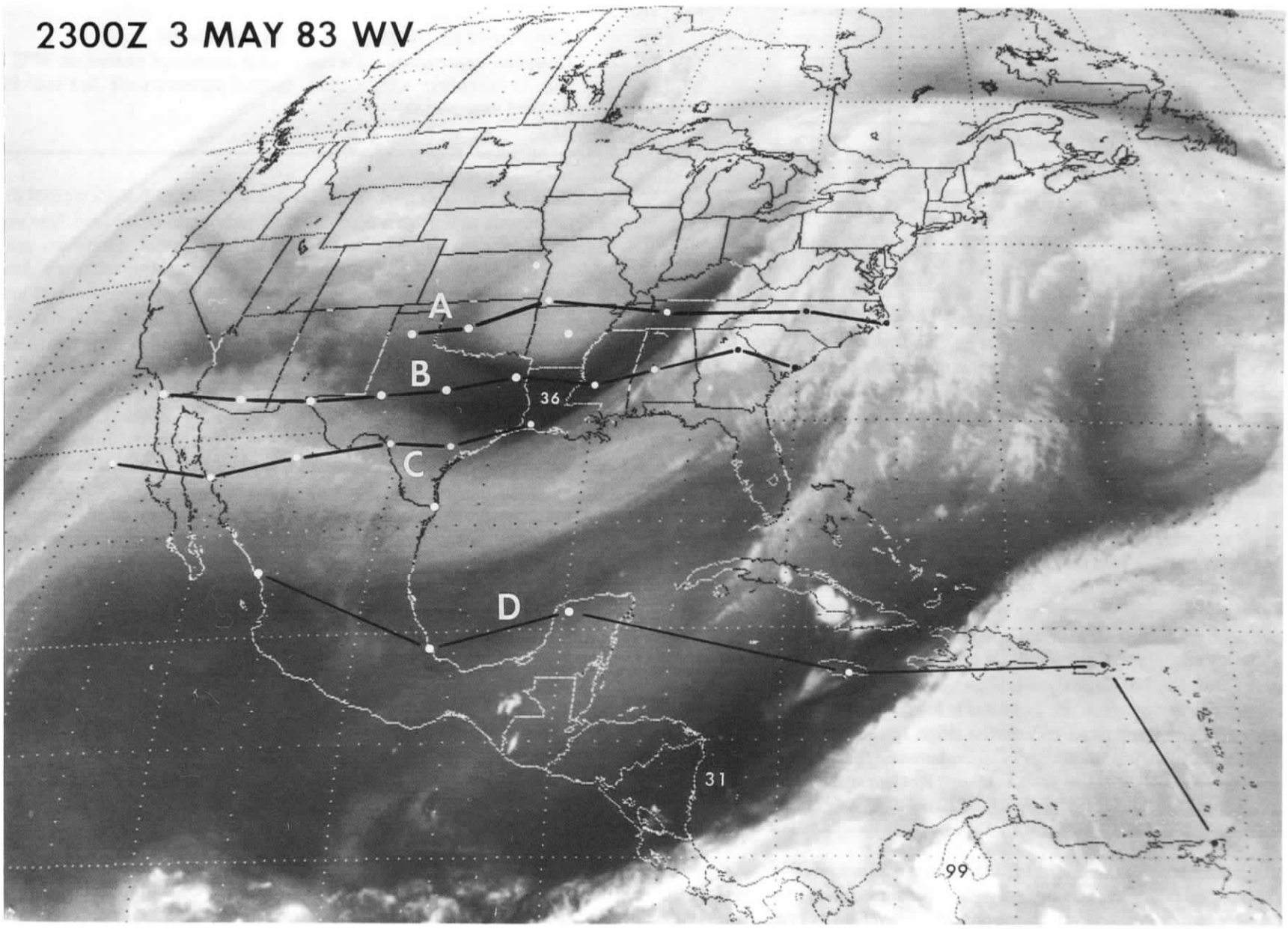

Figure 21 **WATER VAPOR IMAGE WITH CROSS SECTION LOCATIONS**
6.7μm Water Vapor Image, 2300Z 03 May 1983, GOES East, Dots - Radiosonde Sites. Connected sites are cross section locations. Digits - Image Brightness.

Vertical Scale: logarithmic pressure millibars
Horizontal Scale: 30°C per column
Dewpoint Depressions: Air temperature minus dewpoint temperature plotted from right to left in each column
Shaded portions: Relatively Moist Conditions (30°C minus the dewpoint depression)
Maximum altitude of data for each column is at the reported - 40°C air temperature.

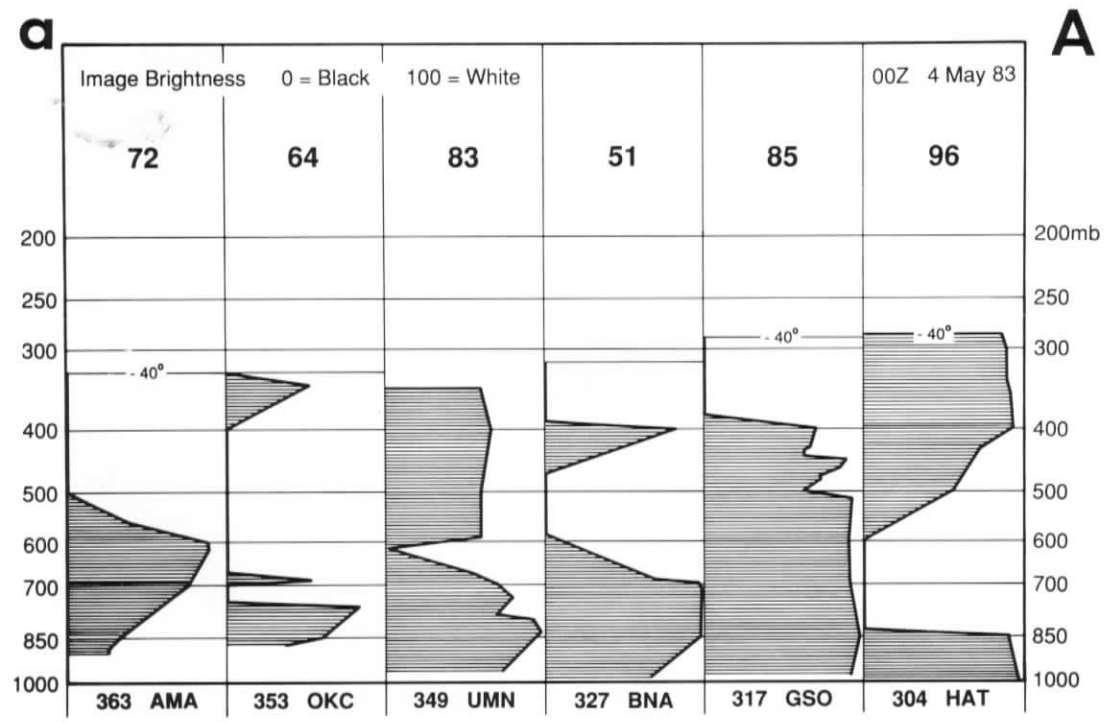

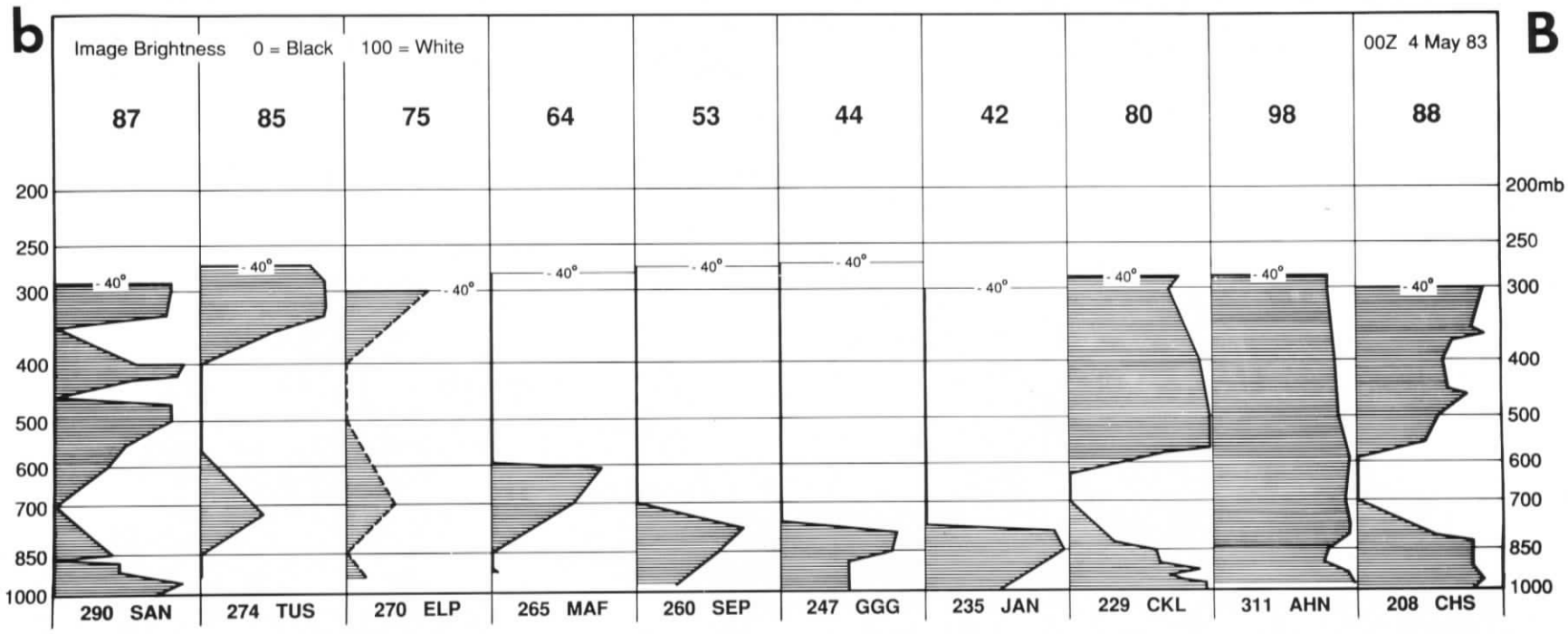

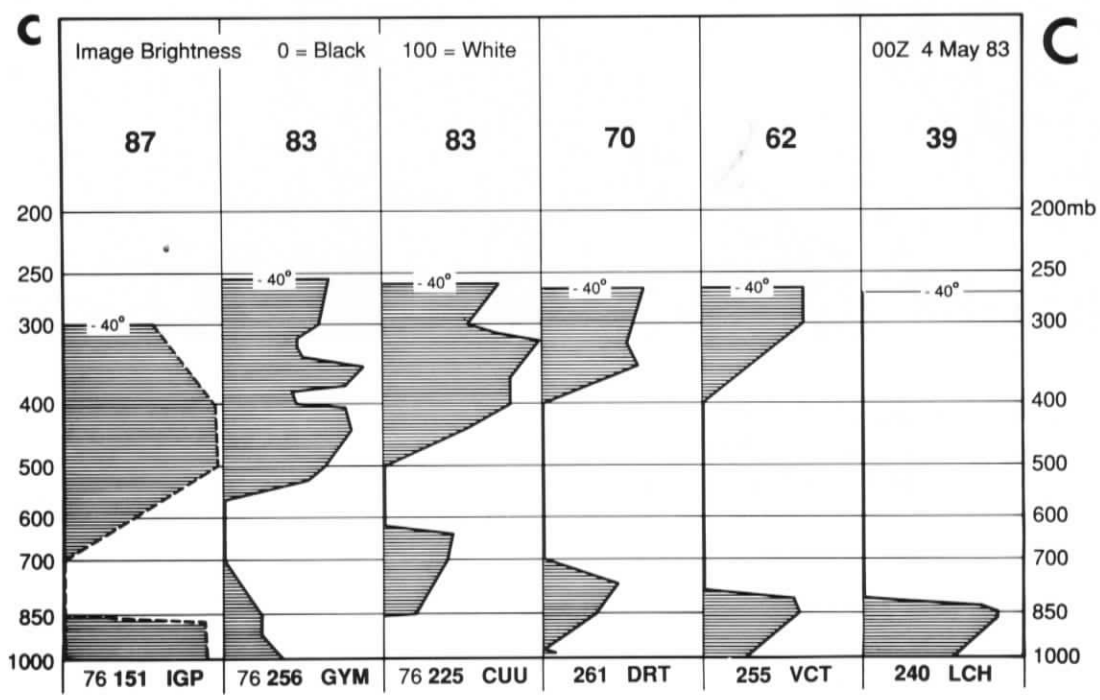

Figure 22

DEWPOINT DEPRESSION CROSS SECTIONS

A. Amarillo, Texas to Cape Hatteras, North Carolina
B. San Diego, California to Charleston, South Carolina
C. Guadalupe Island, Mexico to Lake Charles, Louisiana

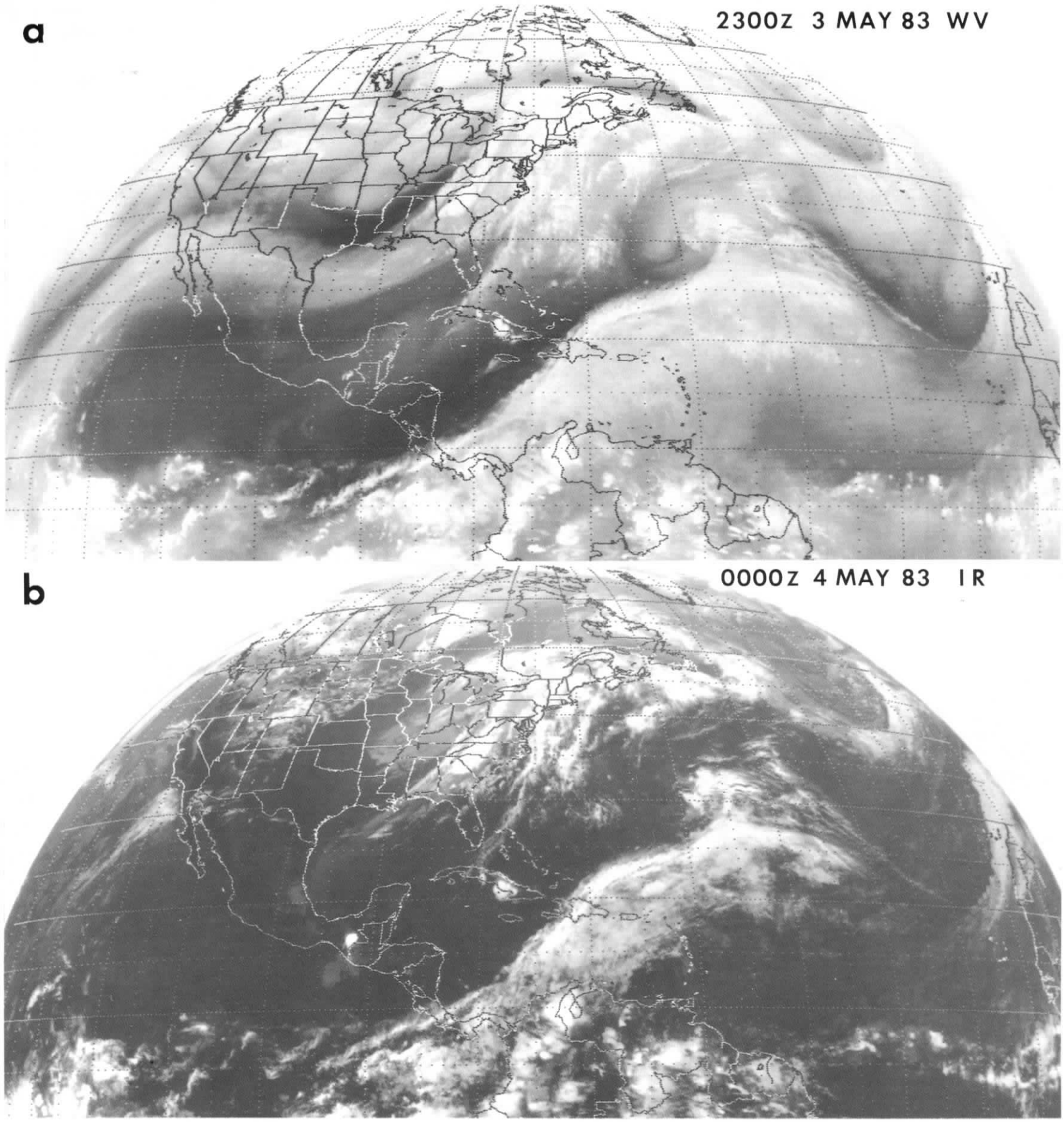

Figure 23 **WATER VAPOR - INFRARED IMAGE COMPARISON**
Fig. 23a. 6.7μm water vapor image, 2300Z 03 May 1983, GOES East,
Fig. 23b. 11.2μm infrared image, 0000Z 04 May 1983, GOES East.

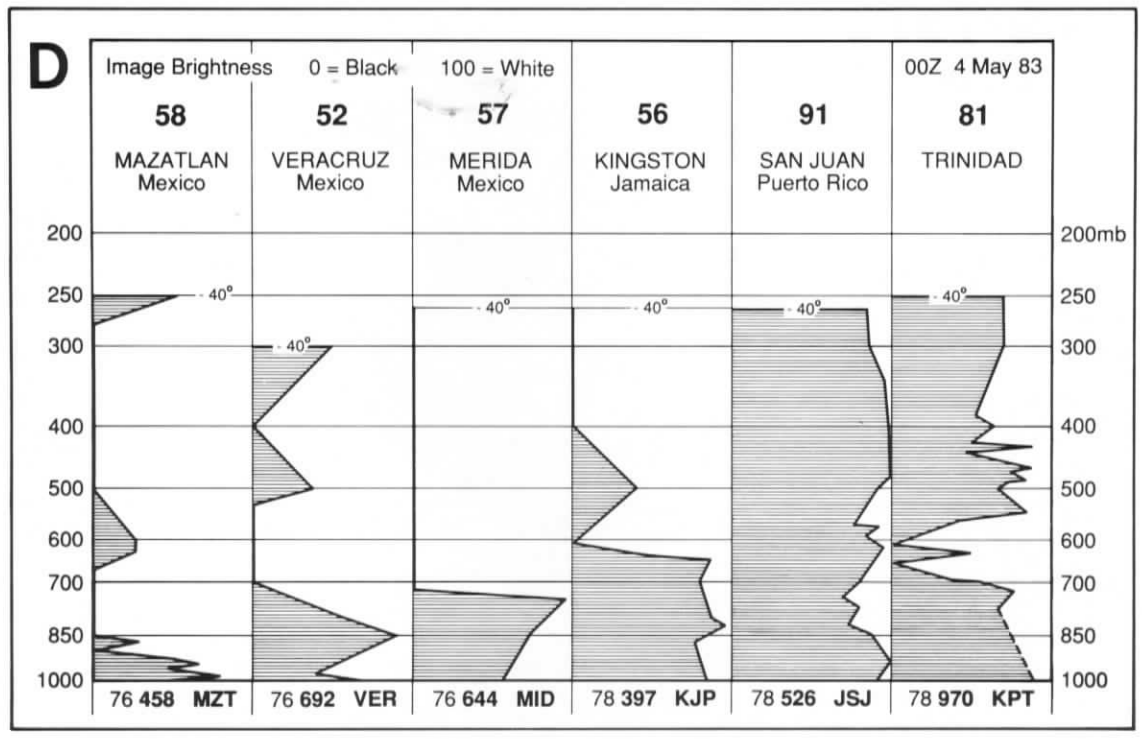

Figure 24 **DEWPOINT DEPRESSION CROSS SECTION - TROPICAL SITES**
Cross Section D - Mazatlan, Mexico to Trinidad.

The southernmost cross section shown on the water vapor image is displayed on **Figure 24**. In general the sounding data are in agreement with the imagery. The four westernmost sites have Image Brightnesses in the 50's. San Juan (JSJ) is under thick cirrus clouds with an Image Brightness of 91, and Trinidad (KPT) although free of middle and high clouds - has deep moisture and an Image Brightness of 81. The primary question regarding this group of sites is why the Image Brightness of Merida, Mexico (MID) is so large (cold)? The single moist layer reported is below the base of an inversion. The air temperature at the top of the moist layer is +12°C. In regions of warm air temperatures and relatively dry soundings, the 30°C dewpoint depression limitation is often a factor. This, however, is not logical in this case when Merida is compared to Veracruz and Kingston. In this case, the "cooling" at Merida is most likely caused by the presence of volcanic debris which can be seen on visible imagery over the site. Such areas of debris suspended in the air have been observed on both 6.7μm and 7.3μm water vapor imagery, while undetectable on window IR.

At Kingston, the air temperature at the top of the moist layer is +3.4°C at 647mb, but some moisture is also present at 500mb remaining from convective cells which were present earlier in the afternoon. This is in reasonable agreement with the 56 Image Brightness.

It is useful to summarize some of the findings from the 03 and 19 May 1983 cases. Considering the comparisons between imagery and radiosonde data where no middle or high clouds were present, dark gray shades (IB less than 45) imply moisture confined to the low layers - typically below 700mb depending upon the latitude. light gray shades (IB more than 75) imply that moisture is present in the upper middle troposphere, typically between 500 and 300mb. The medium gray shades (IB 45-75) present the greatest problem in interpretation. Generally in this middle range, moisture is not present in the upper middle troposphere, at least not in thick layers or at large relative humidities. However, the moisture may be high, low, or both. Compare on **Figure 22**, Amarillo (IB = 72) and Del Rio (IB = 70) or Midland (IB = 64) with Victoria (IB = 62). This difficulty in interpretation was indicated by the RADCOM computations discussed in Section B and illustrated by the bar graph (**Figure 8**).

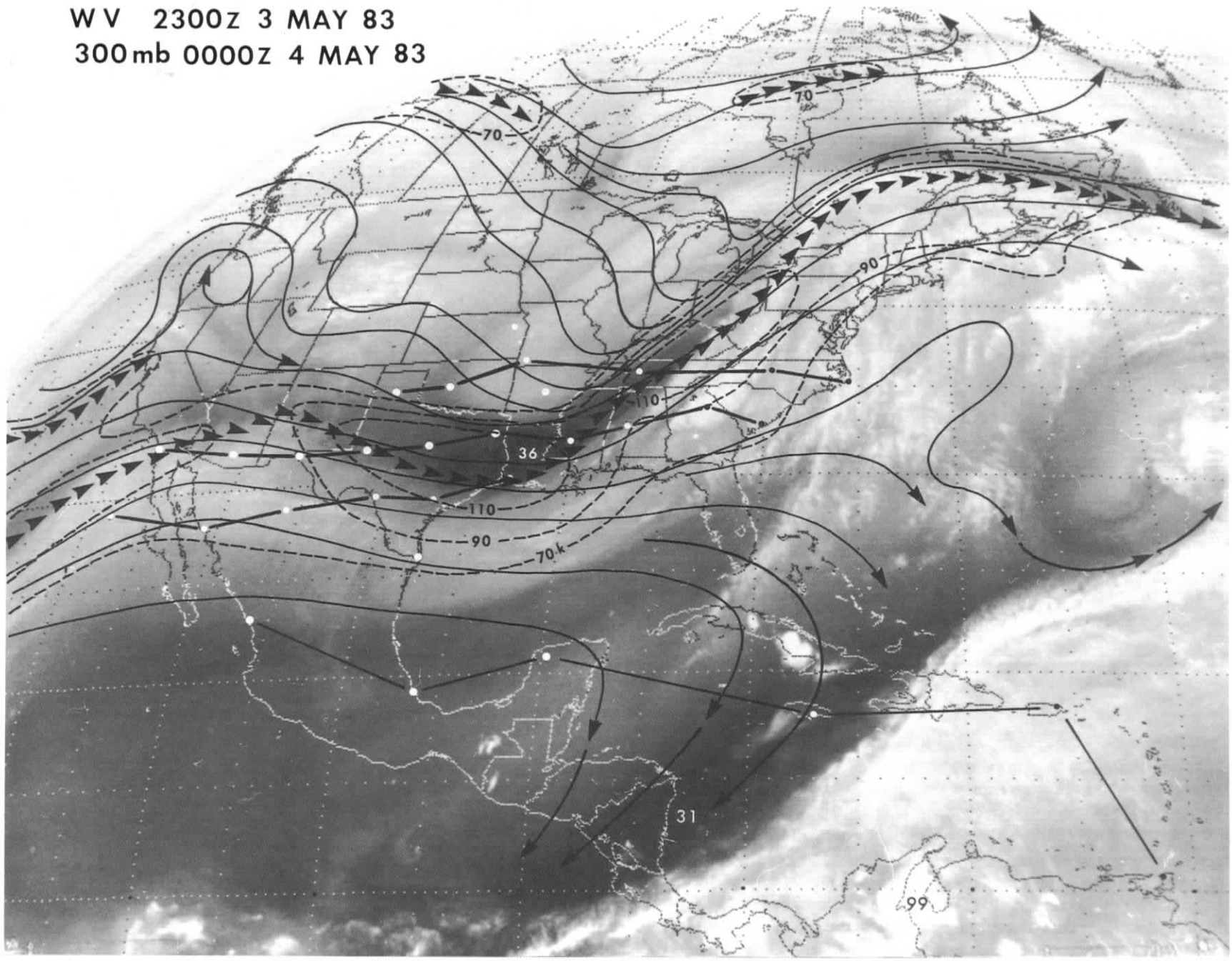

Figure 25

WATER VAPOR IMAGE WITH 300mb ANALYSIS
6.7μm water vapor image, 2300Z 03 May 1983, GOES East,
300mb Analysis: 0000Z 04 May 1983,
Solid black lines: streamlines,
Dashed black lines: isotachs, labeled in knots,
Black arrowheads: axes of 300mb maximum wind speeds.
Same cross section locations as indicated on **Figure 21**.

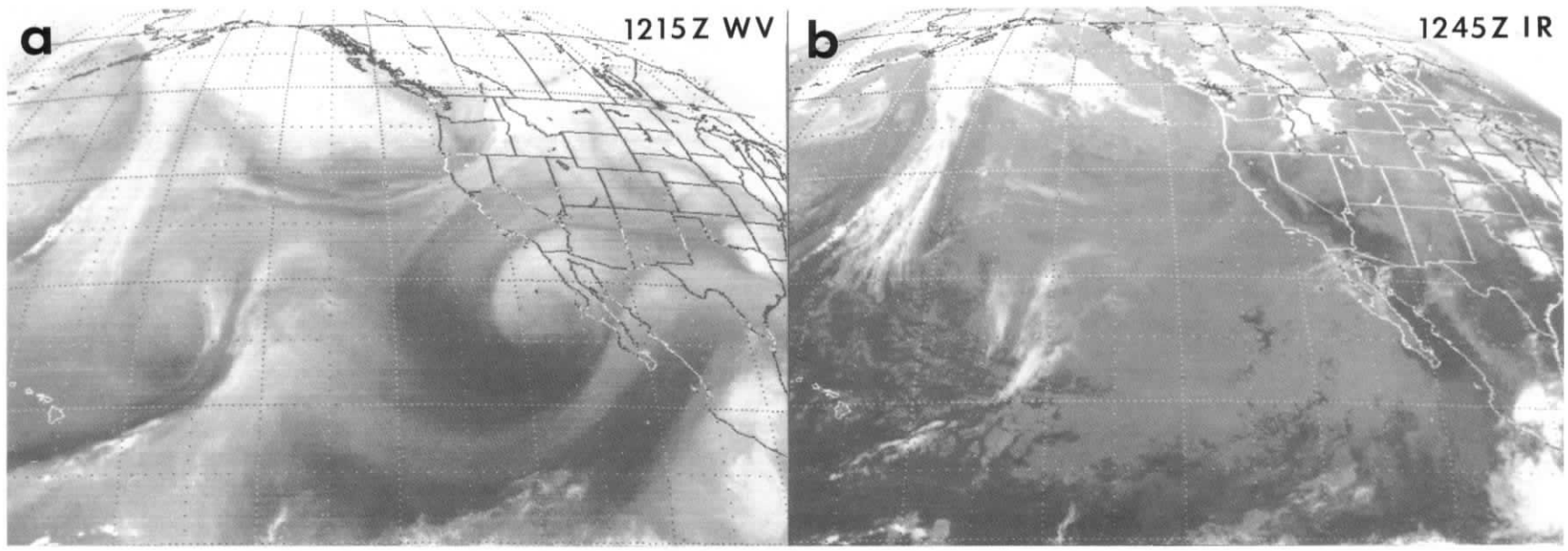

Figure 26 **WATER VAPOR - INFRARED IMAGE COMPARISON**
Fig. 26a. 6.7μm water vapor image, 1215Z 26 May 1982, GOES West,
Fig. 26b. 11.2μm infrared image, 1245Z 26 May 1982, GOES West.

3. COMPARISON - RADCOM RESULTS, IMAGE BRIGHTNESS, AND RADIOSONDE MOISTURE

a. Case Study - 26 May 1982

In this case, imagery from GOES West were compared to radiosonde data, and to RADCOM model brightness temperatures and weighting functions computed from the sounding data.

The 6.7μm water vapor image and an infrared image are shown in a large area view on **Figure 26**. A closer view, KB7 sector water vapor image, with cross section locations and selected measured image brightnesses is shown on **Figure 27**. Two dewpoint depression cross sections are shown on **Figure 28**. A "coastal" cross section extends from Port Hardy, British Columbia (YZT) to Mazatlan, Mexico (MZT). An "inland" section extends from Vernon, British Columbia (WVK) to Chihuahua, Mexico (CUU). Graphs of sounding data and computed weighting functions for selected stations are shown on **Figure 29**.

GENERAL DESCRIPTION

Circulation systems at the time of the imagery include "cold lows" centered over western Nebraska and south of Guadalupe Island. A southern branch of the jet stream crosses over Guaymas, Mexico (GYM) and El Paso, and extends over northern Texas. An open wave upper air trough extends along the west coast from northern California into British Columbia. A northern jet stream branch associated with this trough enters the west coast near Medford, and extends across the trough axis northeastward over Spokane (GEG), into central Canada. The northern trough has been "digging" in response to an amplifying ridge in the Gulf of Alaska; and, the ridge over central California and Nevada has been weakening and stretching in a northeast-southwest direction.

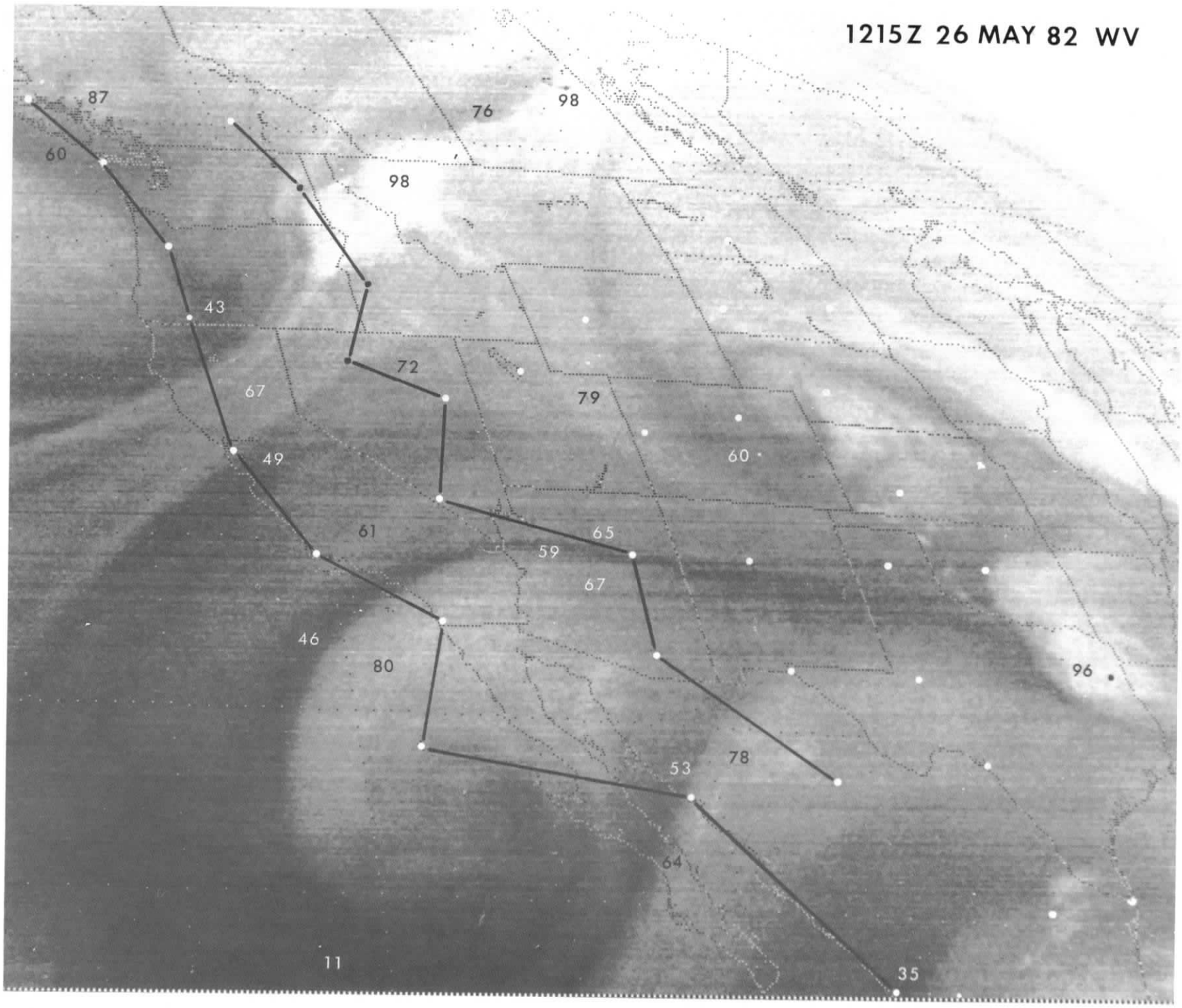

Figure 27 **WATER VAPOR IMAGE WITH CROSS SECTION LOCATIONS**
6.7μm water vapor image, 1215Z 26 May 1982, GOES West,
Digits: Image Brightness valid directly under the digit locations,
Dots: radiosonde sites, Connected Dots: cross section locations.

On the water vapor image of **Figure 27**, the warmest or darkest location is near the southern border of the image, indicated by an image brightness of 11. The coldest or lightest image brightness of 98 was measured at two locations: over western Montana and over south central Canada. Cloud top temperatures measured from infrared imagery at those locations were near -50°C.

CLOUD CONDITIONS ALONG THE CROSS SECTION

Of the 19 cross section sites, only 5 sites had middle or high cloud cover at 1200Z. There were middle clouds over Vernon (WVK), and both middle and high clouds at Spokane (GEG) and Boise (BOI). There were some mountain related middle clouds and a band of thin cirrus near Winnemucca (WMC), but the clouds did not appear to be directly over the site on IR imagery. The remaining sites of the "inland" cross section appeared to be cloud free, although there were cirrus in view of the ground observers at Ely and Chihuahua (CUU). Along the coastal cross section, Guadalupe (IGP) had clouds between 500mb and 400mb over stratocumulus; and Guaymas (GYM) had thin cirrus over the site. Of the remaining "coastal" cross section sites, Medford (MFR) was clear; and the others had low clouds.

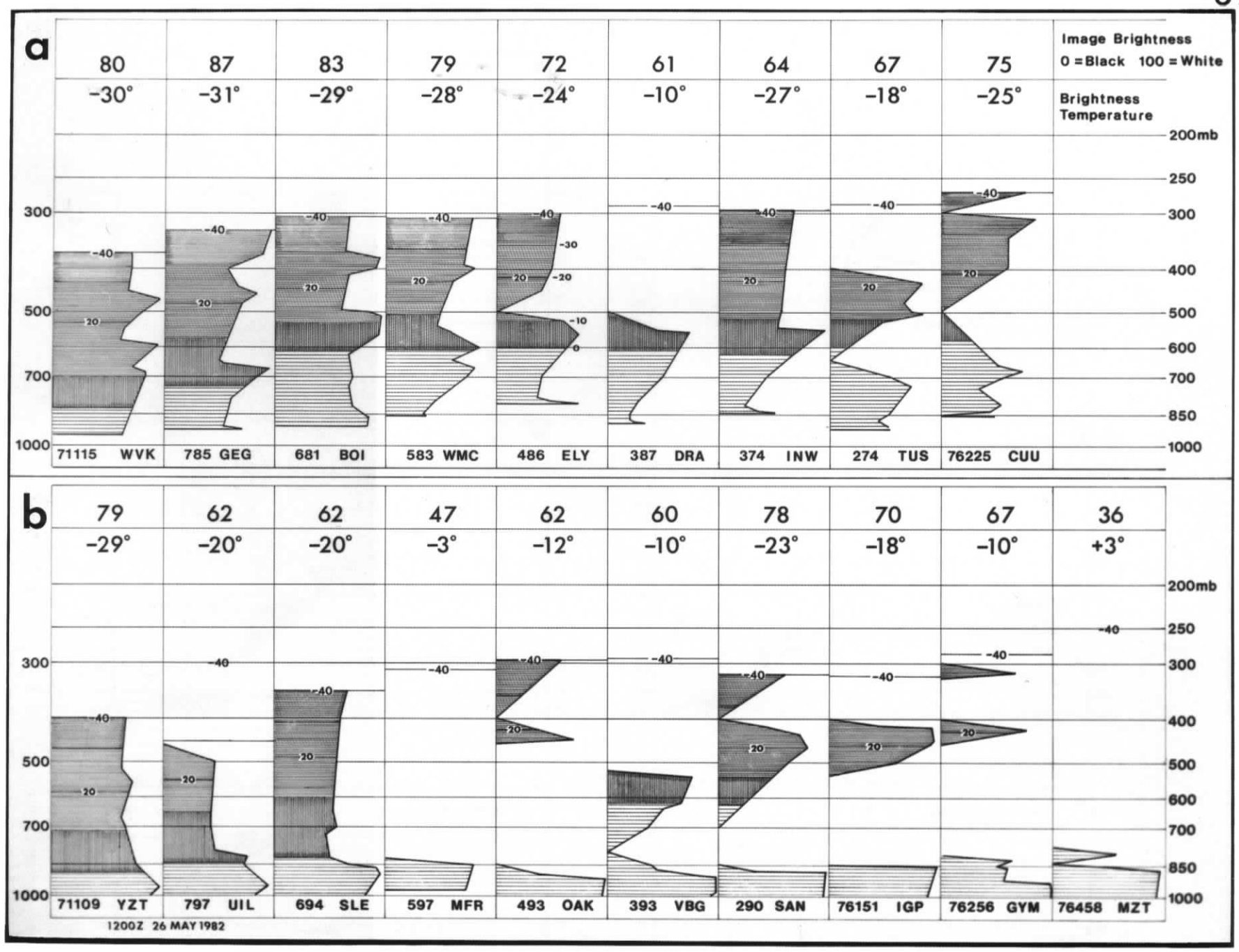

Figure 28 **INLAND AND COASTAL DEWPOINT DEPRESSION CROSS SECTIONS**
Fig. 28a. Inland cross section, Vernon, British Columbia to Chihuahua, Mexico.
Fig. 28b. Coastal cross section, Port Hardy, British Columbia to Mazatlan, Mexico.
Column shadings differ by 10°C air temperature intervals.

GENERAL COMPARISON - CROSS SECTION SOUNDINGS AND IMAGERY

Note that image brightness values plotted on **Figure 27** are valid directly under the digits. Image brightness values measured at the radiosonde sites are shown on **Figure 28** above brightness temperatures computed from the sounding data. Comparing the dewpoint depression plots on **Figure 28** with the imagery, the topographic concept is again generally valid. The two sites with the smallest measured image brightnesses are Mazatlan (MZT) and Medford (MFR). They also have the warmest computed brightness temperatures, and no dewpoint depressions less than 30°C in the middle or high troposphere. Two other sites, Vandenberg (VBG) and Desert Rock (DRA) have dewpoint depressions of 30°C or greater above 500mb. They have the 3rd and 4th darkest image brightnesses and relatively warm computed brightness temperatures of -10°C.

The 5 sites with the lightest image brightnesses also have the 5 coldest computed brightness temperatures. These are the 4 northernmost sites of the inland cross section and the northernmost site of the coastal section. Of these sites, there is more difference in the image brightnesses (range 79-87) than in the brightness temperatures (range -28°C to -31°C). Spokane and Boise with image brightnesses of 87 and 83 both had cirrus cloud cover. This would affect the measured image brightness, but is not accounted for in the computed brightness temperature.

The site with the 6th lightest image brightness was San Diego at 78. This is nearly as bright as Port Hardy (YZT) and Winnemucca(WMC), but the computed brightness temperature is -23°C. On the 1200Z IR image, there were thin cirrus and altostratus just southwest of San Diego and propagating toward the site. Its presence could not be determined by the surface observation because of a stratus overcast. Because of the proximity of the higher clouds and the fact that the image brightness measurement was taken west of the site, the clouds were likely a factor in the relatively cold image brightness, but wouldn't be a factor in the comparatively warmer brightness temperature computation.

An even greater puzzle involves the data at Winslow, Arizona (INW). The computed brightness temperature from the sounding data is -27°C, nearly as cold as those from the northern sites. However, the image brightness is only 64. We could assume that the radiosonde did not ascend through the narrow dark band located over Winslow on the image of **Figure 27**; however, note that the image brightnesses to the sides of the band are only in the mid to upper sixties range. It is possible that the humidity data in the sounding were incorrect, or that the radiosonde ascended through a very narrow band of moisture which was not resolved on the imagery. Such very; narrow bands do sometimes occur in such synoptic patterns. We would have expected the humidity at Winslow to have been similar to that of Tucson (TUS) with image brightness of 67 and BT = -18°C.

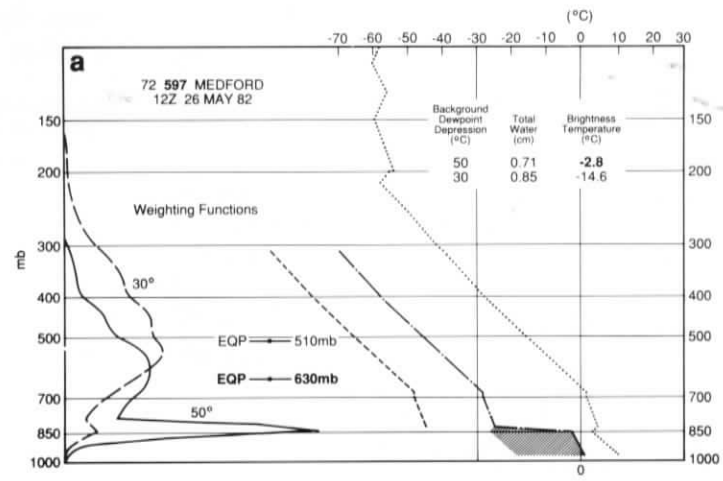
a
72 597 MEDFORD
12Z 26 MAY 82
Background Dewpoint Depression (°C)
Total Water (cm)
Brightness Temperature (°C)
50 0.71 -2.8
30 0.85 -14.6
Weighting Functions
30°
50°
EQP 510mb
EQP 630mb
mb
(°C)

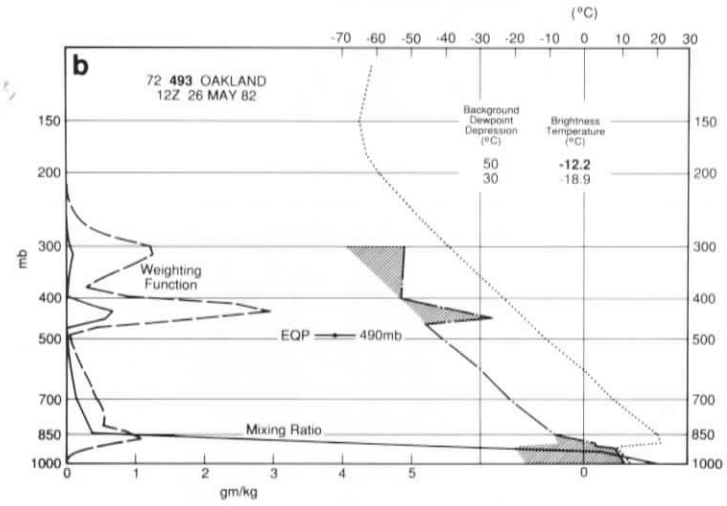
b
72 493 OAKLAND
12Z 26 MAY 82
Background Dewpoint Depression (°C)
Brightness Temperature (°C)
50 -12.2
30 -18.9
Weighting Function
EQP 490mb
Mixing Ratio
mb
gm/kg
(°C)

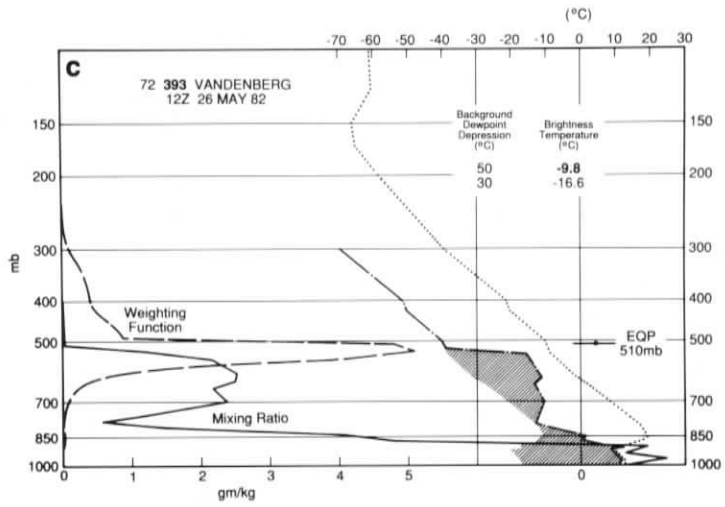
c
72 393 VANDENBERG
12Z 26 MAY 82
Background Dewpoint Depression (°C)
Brightness Temperature (°C)
50 -9.8
30 -16.6
Weighting Function
EQP 510mb
Mixing Ratio
mb
gm/kg
(°C)

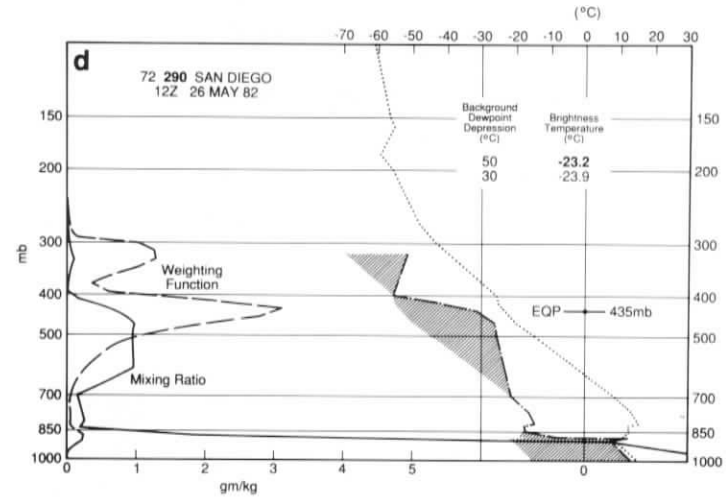
d
72 290 SAN DIEGO
12Z 26 MAY 82
Background Dewpoint Depression (°C)
Brightness Temperature (°C)
50 -23.2
30 -23.9
Weighting Function
EQP 435mb
Mixing Ratio
mb
gm/kg
(°C)

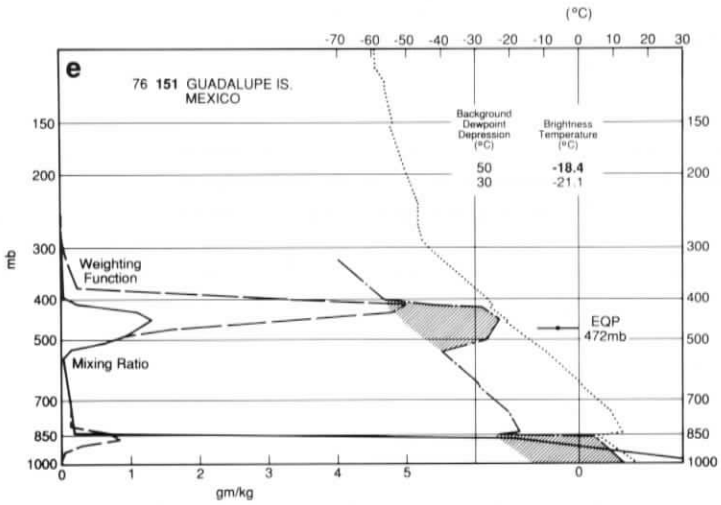
e
76 151 GUADALUPE IS. MEXICO
Background Dewpoint Depression (°C)
Brightness Temperature (°C)
50 -18.4
30 -21.1
Weighting Function
EQP 472mb
Mixing Ratio
mb
gm/kg
(°C)

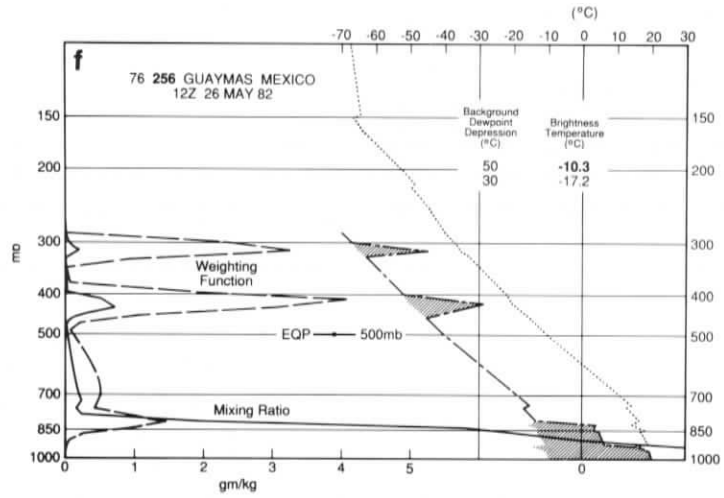
f
76 256 GUAYMAS MEXICO
12Z 26 MAY 82
Background Dewpoint Depression (°C)
Brightness Temperature (°C)
50 -10.3
30 -17.2
Weighting Function
EQP 500mb
Mixing Ratio
mb
gm/kg
(°C)

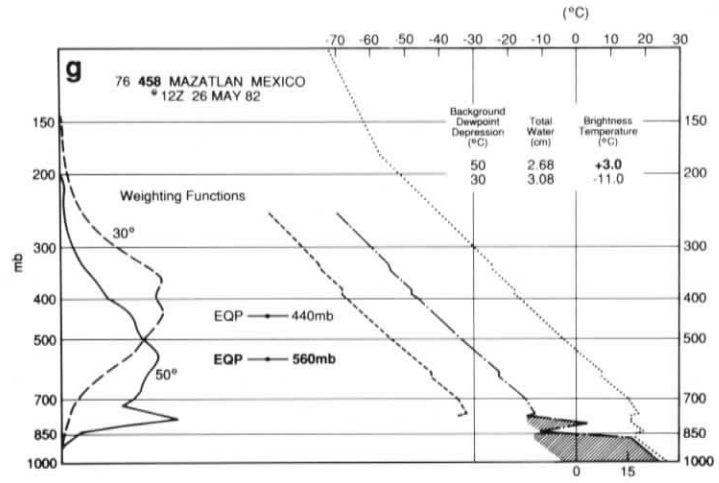
g
76 458 MAZATLAN MEXICO
*12Z 26 MAY 82
Background Dewpoint Depression (°C)
Total Water (cm)
Brightness Temperature (°C)
50 2.68 +3.0
30 3.08 -11.0
Weighting Functions
30°
50°
EQP 440mb
EQP 560mb
mb
(°C)

THE ORIGIN OF RADIATION REACHING THE SATELLITE - MOIST LAYERS

Along the coastal cross section, all sites except Port Hardy (YZT) and Salem (SLE) reported one or more layers of dewpoint depressions of 30°C. On **Figure 29**, detailed sounding data and RADCOM computed data are shown for 7 of the sites. On all of the graphs, two brightness temperatures are shown, and on the graphs for Medford and Mazatlan two weighting function plots are shown. As previously discussed, a 30°C dewpoint depression report implies 30°C or greater. On the graph for Medford on **Figure 29** the sounding is plotted with a dewpoint depression of 30° and with 50°C substituted at all levels at which 30° was reported. RADCOM data were computed for both soundings, and two weighting function curves are shown. With the sounding as reported, the computed brightness temperature is -14.6°C; and with 50° depressions, the brightness temperature is -2.8°C, a difference of 11.8°C. The weighting functions indicate, that when a 30°C dewpoint depression is used as reported, there is very little radiation contribution by the low level moist layer. At Mazatlan, where the air temperatures are warmer, the brightness temperature difference is 14°C. Through experimentation, we found that substituting 50° depressions in place of reported 30° depressions yielded the best correlations between computed brightness temperatures and imagery gray shades; therefore, use of 50° was adopted as standard procedure, and those brightness temperatures are considered to be the "correct" ones. The difference is most significant when no moisture is present in the middle and upper troposphere. Comparing the sites of **Figure 29**, note that the difference at San Diego with the dry air between 700 and 850mb, is only 0.7°C. Even with the deeper dry layer at Guadalupe, the difference is only 2.7°C.

Comparing the dry soundings at Medford and Mazatlan, use of the 50°C dewpoint depressions provides brightness temperatures that correlate reasonably well with the image brightnesses. It is useful to note that Medford had the least total water content (0.71 cm) of the cross section sites, and Mazatlan, with its warm nearly saturated air below 850mb, had the most (2.68 cm).

Considering some of the sites with moisture in layers, note (on **Figure 28**) that Vandenberg (VBG) and Desert Rock (DRA) both have computed brightness temperatures of -10°C and nearly the same image brightnesses. Soundings and computed weighting functions are shown for Vandenberg(VBG) on **Figure 29**. The top of the moist layer at Vandenberg was at 538mb with an air temperature of -9°C. Note that the weighting function peaks near the top of the moist layer, with little contribution from below. At Desert Rock, the top of the moist layer was at 551mb at -7°C.

The computed brightness temperature from the Guaymas, Mexico (GYM) data was also -10°C (as at VBG and DRA). However, note on **Figure 28** that the moisture distribution at GYM was significantly different from those at VBG and DRA. At GYM, dry conditions were reported between 800mb and 450mb, the layer in which significant moisture was present at VBG and DRA.

However, two higher layers of moisture above 450mb are present at GYM. The weighting function indicates 3 significant layers of contribution to the radiation reaching the satellite. Their combined effect provides a brightness temperature of -10°C, equal to the air temperature at 500mb, where the air is dry. At Vandenberg (VBG), a single weighting function peak is present near the top of the mid-tropospheric moist layer. This illustrates the complications of layered moisture with varied distributions producing similar brightness temperatures.

When the top of the moist layer is below 500mb, as at Vandenberg and Desert Rock, the brightness temperatures are similar to the air temperature at the top of the moist layer. However, with moist layers above 500mb, such as at San Diego, the brightness temperature is warmer than the corresponding temperature of the moist air. The moisture is translucent to the radiation, a part of which penetrates from below. This is also a factor at Guadalupe, where the air temperature at the top of the moist layer was -25°C at 418mb, and the computed brightness temperature was -18°C. These relationships can be seen by comparing the weighting functions and equivalent pressures of the sites. However, the brightness temperature computations do not include the effects of radiation from clouds. For example, the computed brightness temperatures at Guadalupe and Tucson are both -18°C with similar air temperatures near the tops of the moist layers. The image brightness at Guadalupe is 70 with middle clouds present. Tucson had clear skies and an image brightness of 67. Similar differences occur between Desert Rock which is clear and Guaymas with thin cirrus.

Figure 29

RADIOSONDE SOUNDINGS AND RADCOM COMPUTED DATA FOR SELECTED SITES

All graphs include: soundings, weighting functions, two brightness temperatures (using reported 30°C dewpoint depressions and using 50°C substitutions for 30°C reports - see text).

Graphs a and g: Dewpoint temperatures shown for both 30°C and 50°C dewpoint depressions;

Weighting functions and equivalent pressures shown for both 30°C and 50°C dewpoint depression soundings.

Graphs b, c, d, e, f: Weighting functions and equivalent pressures use 50°C dewpoint depressions substituted for 30°C reported depressions. Mixing Ratio is also plotted.

4. VARIED CHANNEL COMPARISON - POLAR ORBITING AND GOES SATELLITE IMAGERY

In this section, data of several different channels from polar orbiting satellites are shown and compared with GOES imagery, radiosonde data, and RADCOM computations. Imagery from the 6.7μm and 7.3μm channels, and the same polar orbiting satellite pass, are compared.

a. Case Study - 20 December 1983

In this case, a very cold, winter continental, environment is present. The effects of very cold air, and large temperature inversions, are illustrated.

On **Figure 30a**, a 6.7μm water vapor image from GOES East is valid at 1130Z 20 December 1983. The small numbers plotted on the image are image brightnesses. Two groups of white dots connected by black lines are the locations of two cross sections shown on **Figure 33**. Also shown on the GOES image, are two curved lines. These indicate the borders of imagery received from a southward pass of the polar orbiting satellite NOAA-7. Imagery from three channels taken during the NOAA-7 pass are shown on **Figure 30b**. The polar orbiting imagery are valid at 0929Z at the northern border, and at 0954Z at the southern border, generally two hours earlier than the GOES image. The images from NOAA-7, on **Figure 33b**, consist of an infrared "window" channel, 7.3μm water vapor, and 6.7μm water vapor. The images from each channel are divided into individual panels which are numbered one through five, from north to south, for reference purposes.

A higher resolution enhanced infrared image is shown on **Figure 31**. The image is from the same NOAA-7 pass as those images on **Figure 30b**; but, the area shown is limited to panels 2 and 3, and the width is slightly smaller. Selected radiosonde sites are shown on the image. Since the image was not gridded, the locations were estimated using terrain maps and gridded GOES imagery valid at the same time. A 1530Z visible GOES image is shown on **Figure 32**. The visible image is too late in time for adequate comparison to the water vapor images and radiosonde data; however, it can be used to identify patterns and features on the infrared images. Two dewpoint depression cross sections are shown on **Figure 33**. The longer section extends from Moosonee, Canada (YMO) to Belize (78583), on the east coast of the Yucatan Peninsula. The second cross section extends from International Falls (INL) to Apalachicola (AQQ). The cross section locations are shown on **Figure 34** which is a larger version of **Figure 30b.** Although the two westernmost cross sections identified on the IR panel of **Figure 34** will not be shown, it is useful to list the sites involved. Only two sites from the westernmost section appear on the image; they are Oklahoma City and Longview, Texas. The sites on the third section (counting from the east) are, from north to south: Huron (HON), Omaha (OMA), Topeka (TOP), Monett (UMN), Little Rock (LIT), Jackson (JAN), and Boothville (BVE). On **Figure 35**, soundings and weighting function graphs are shown for four selected sites.

The numbers shown on the NOAA-7 imagery of **Figure 34**, and above each column of the cross sections of **Figure 33**, are values of "brightness index", not the "image brightness" used for the GOES imagery.

"BRIGHTNESS INDEX" - EXPLANATION AND COMPARISON TO "IMAGE BRIGHTNESS"

As with the "image brightness" used with GOES imagery, the "brightness index" is a 0-100 scale representation of the gray shades. On a single image it provides a quantitative comparison of the gray shades. However, each channel of the polar orbiting satellite imagery uses a different conversion from signal to gray shades. The range of signal values from each channel were spread over a full range of gray shade to provide an optimum display of each channel. This is an advantage for viewing the imagery from each channel, but causes a problem in comparing imagery of different channels. For example, on **Figure 34**, the general gray shades of panel 2 (over southern Canada and the northern Great Lakes) appear darker on the water vapor channels than on the IR channel. This implies colder brightness temperatures on the IR, a possibility with large temperature inversions; but, it may not be valid.

Because of this problem, "brightness index" was developed to provide a better quantitative comparison of gray shades among all three channels. "Brightness Index" is not a direct measurement of brightness temperature, but its derivation is based upon the different conversions from signal to gray shades for each channel. It eliminates that difference. Since digital data were not available, "brightness index" was obtained by measuring the gray shades from individual images, converting them to signal counts, then converting the count values to a 100 digit scale. On the IR channel with its large signal range, all 100 "brightness index" values are possible. On the IR channel "brightness index" is equivalent. to "image brightness". Black is equal to zero and white is equal to 100. On the 7.3μm channel, "brightness index" values range from a minimum possible value of 28 to maximum possible value of 95. On the 6.7μm imagery, the range is 42-96. The utility and relative accuracy of the "brightness index" values can be better judged during the discussions of specific radiosonde sites and image patterns. As with the "image brightness", the "brightness index" provides a quantitative means to compare gray shades within a single channel. It also provides a better means to quantitatively compare gray shades from channel to channel. In this text, the use of "brightness index" is limited to this one case study. It will be abbreviated as "BI" when more convenient within the following discussion.

GENERAL DESCRIPTION - THE 20 DECEMBER 1983 CIRCULATION SYSTEMS

The case provides an example with very cold winter season continental air and strong temperature inversions, of both radiation and frontal types. A large surface high pressure system extended across the Great Lakes with 1043mb centers over northern Minnesota, and over southern Canada near Ottawa. The upper air systems included a closed low over the northern Hudson Bay with open troughs over the western United States and west of Mexico. A jet stream branch around the western U.S. trough merged with a branch across Mexico to form a wide west-southwesterly jet stream over the eastern United States. Upper air winds of greater than 100 knots were present from lower Michigan to Florida.

Over the eastern half of the United States, surface winds were of northerly component from the Great Lakes southward to a surface front extending from Belize to the western tip of Cuba to Key West and northeastward. Surface winds turned to southeasterly over the high plains.

Figure 30

IMAGE COMPARISON - COLD AIR REGIME

Fig. 30a. 6.7μm water vapor, 1130Z 20 December 1983, GOES East, Connected white dots are cross section locations.
Long curved black lines are boundaries of image area of NOAA-7 imagery shown on **Fig. 30b.**
Digits are Image Brightness measured from the GOES image.
Fig. 30b. NOAA-7 imagery valid time: 0929Z north border, 0954Z south border, 20 December 1983,
Left column: 11.1μm infrared,
Center column: 7.3 μm water vapor,
Right column: 6.7μm water vapor,
Gray shade conversions differ for each panel - see text.

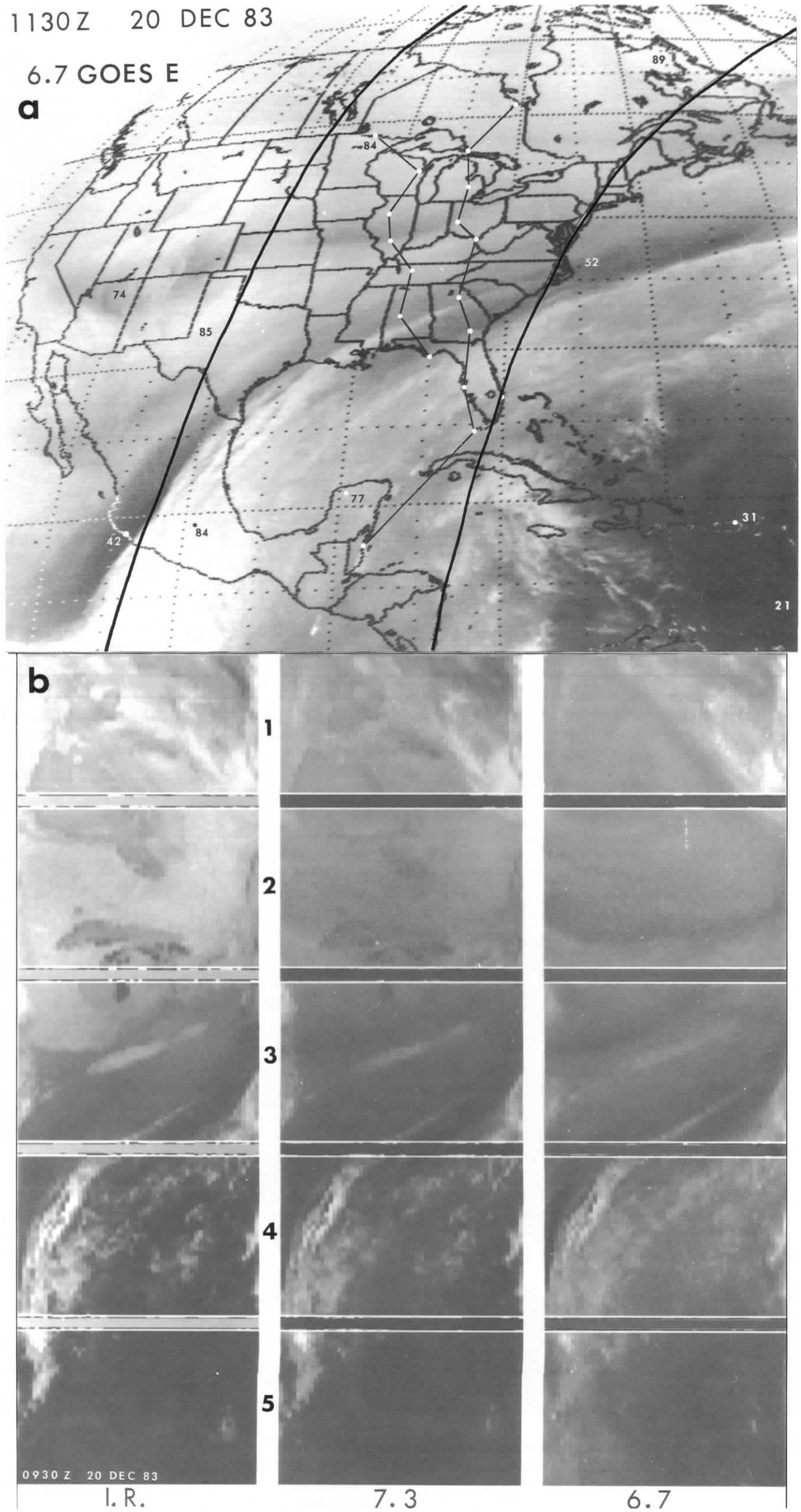
1130Z 20 DEC 83
6.7 GOES E
a
b
89
84
52
74
85
77
84
42
31
21
1
2
3
4
5
0930 Z 20 DEC 83
I.R.
7.3
6.7

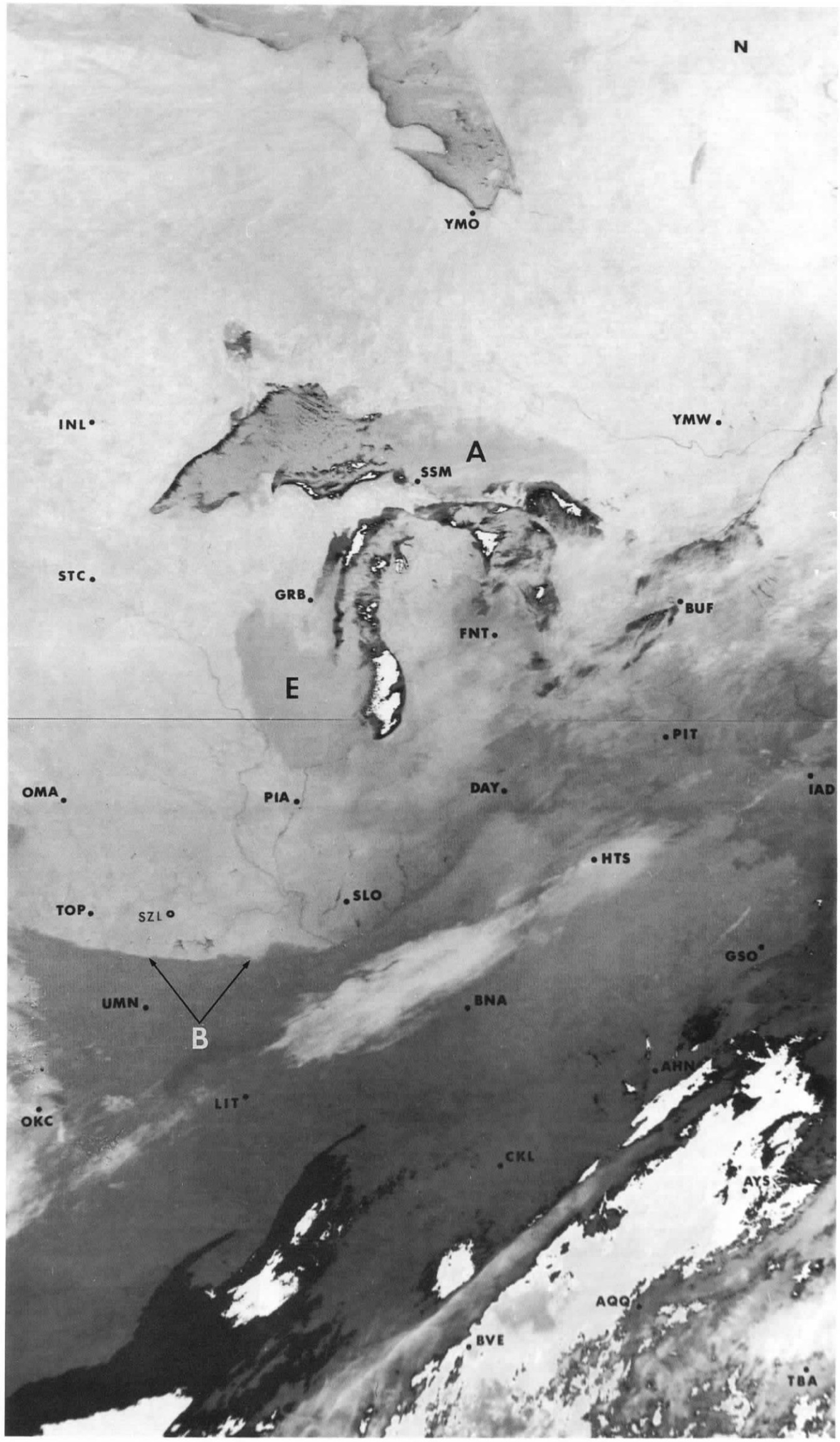

Figure 31 **HIGH RESOLUTION INFRARED IMAGE**
11.1μm infrared image, NOAA-7 orbiting satellite, 20 December 1983, 0934Z to 0945Z north to south borders. Gray shade - temperature conversion includes reversals. Reversals in shades at southern portions are not significant to discussion.

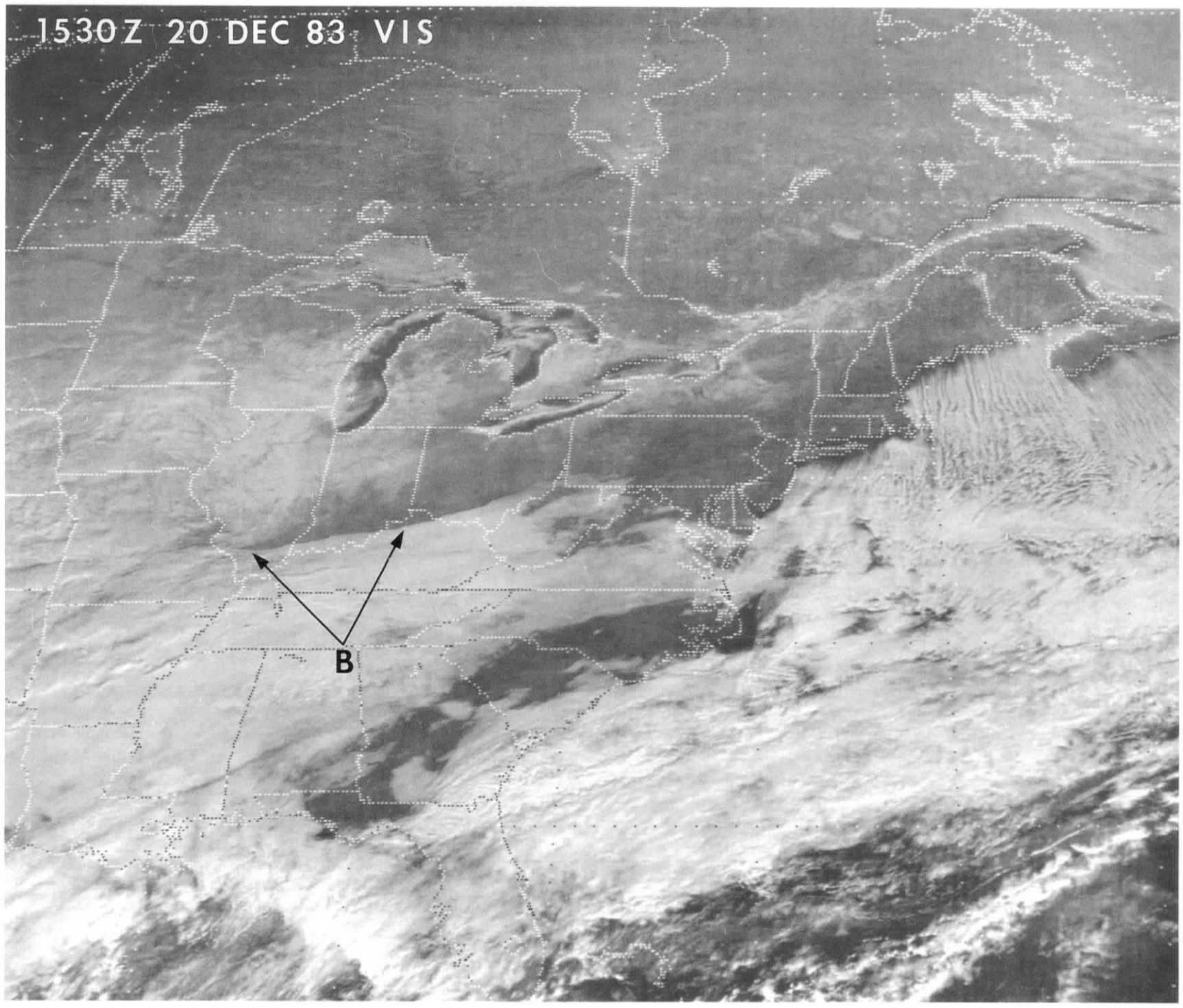

Figure 32 VISIBLE IMAGE
Visible image, 1530Z 20 December 1983, GOES East.

CLOUD CONDITIONS

Although the cloud conditions are too complex to adequately describe in words, we will discuss some of the patterns and features on **Figure 31**, and on the visible image. At 0930Z, a well defined cloud border, "B", extended from just south of Topeka, Kansas (TOP), across southern Missouri. This portion is very distinct on the IR imagery. The border continues across southern Illinois and Indiana to Dayton, Ohio (DAY). From there, it continues ragged and poorly defined over western Pennsylvania. During the time interval from 0930 to 1530Z, the western end of the border remained nearly stationary, although becoming overlain by higher clouds from the west; and, the eastern portion moved southward over the Ohio Valley and western Pennsylvania. There were two primary axes of maximum winds in the jet stream over the eastern United States. This border coincided with the northern one.

Generally, the region south of the boundary was covered with altostratus, stratus, and several streaks of cirrus. The region north of the boundary into east central Canada was generally clear with patches of low clouds, most of which were associated with Great Lakes moisture advection. The two largest areas of such low clouds are at A, east of Lake Superior (north of the low level ridge axis), and at E, over southern Wisconsin and northernmost Illinois in low level northeasterly flow. The cloud tops north of boundary "B" are lower but colder than those south of the boundary. On the enhanced IR image of **Figure 31**, the gray shade regions over Minnesota, and Quebec Province represent radiation temperatures primarily from cloud-free cold land surface. Infrared ground temperatures ranged between -30° and -45°C. The weather station at Nitchequon, Quebec, at "N" on the figure, reported ice crystals and surface temperature of -42°C (-44°F) at 1200Z.

South of the Kansas-to-Pennsylvania boundary over the United States, the altostratus tops tend to be higher and colder toward the northeast. They are lower and give way to stratus toward the south and west. Consider the areas on opposite sides of the distinct border over Missouri. On the central IR panel of **Figure 34**, a "brightness index" value of 50 is printed over Whiteman AFB, Missouri (SZL on **Figure 31**) on the clear side of the border. Whiteman reported clear with a surface air temperature of -22°C (-8°F) at both 0930 and 1200Z. The measured radiation temperature from GOES enhanced IR imagery was -24°C. The similarly measured IR temperature over southern Missouri near Monett (UMN) was -8°C. Cloud tops indicated by the Monett sounding were at 771mb with an air temperature of -7°C. The surface temperature at Monett was -15°C. At Huntington, West Virginia (HTS) the altostratus tops were at 632mb with an air temperature of -14°C. The cirrus tops over western Kentucky had a NOAA-7 IR "brightness index" of 51 - only slightly lighter than the 50 value for the land over Whiteman AFB, Missouri. The radiation temperature measured from enhanced IR imagery over the cirrus was -24°C. At Nashville (BNA) on the southern border of the cirrus, the top of the higher level moist layer was at 445mb with an air temperature of -27°C.

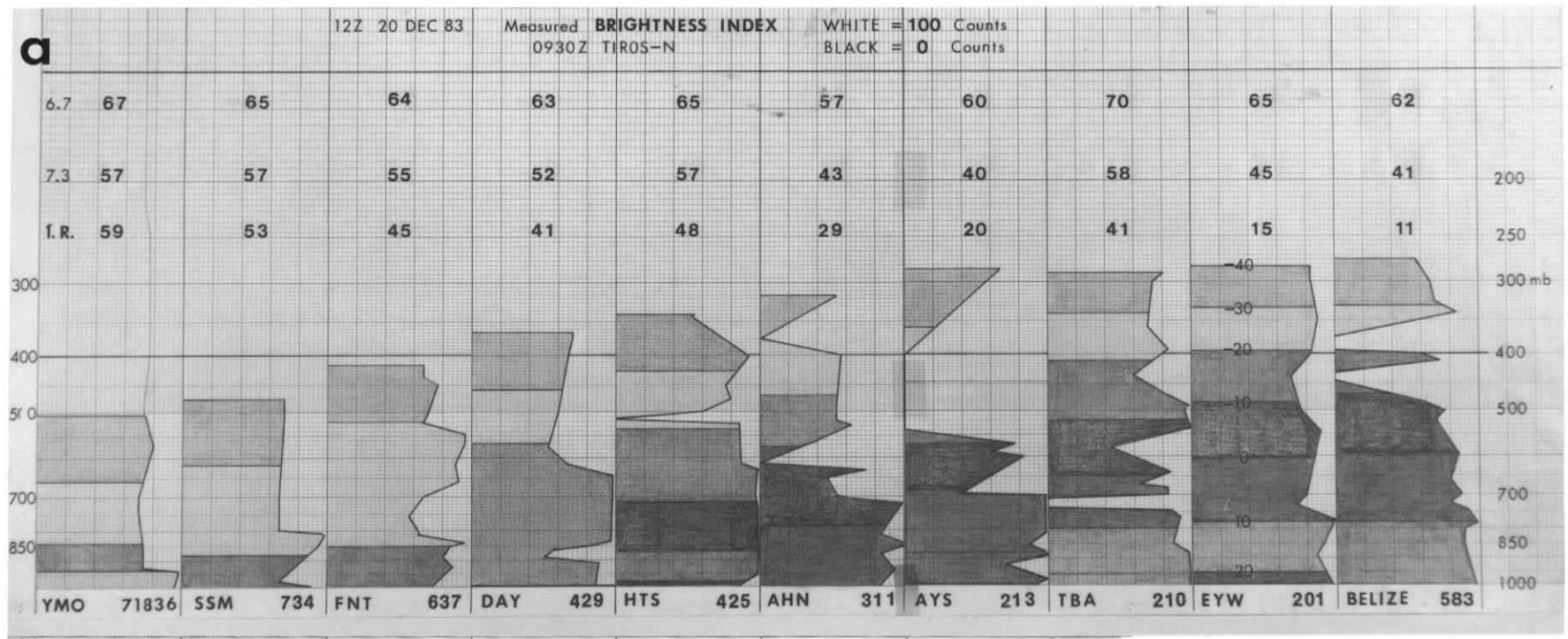

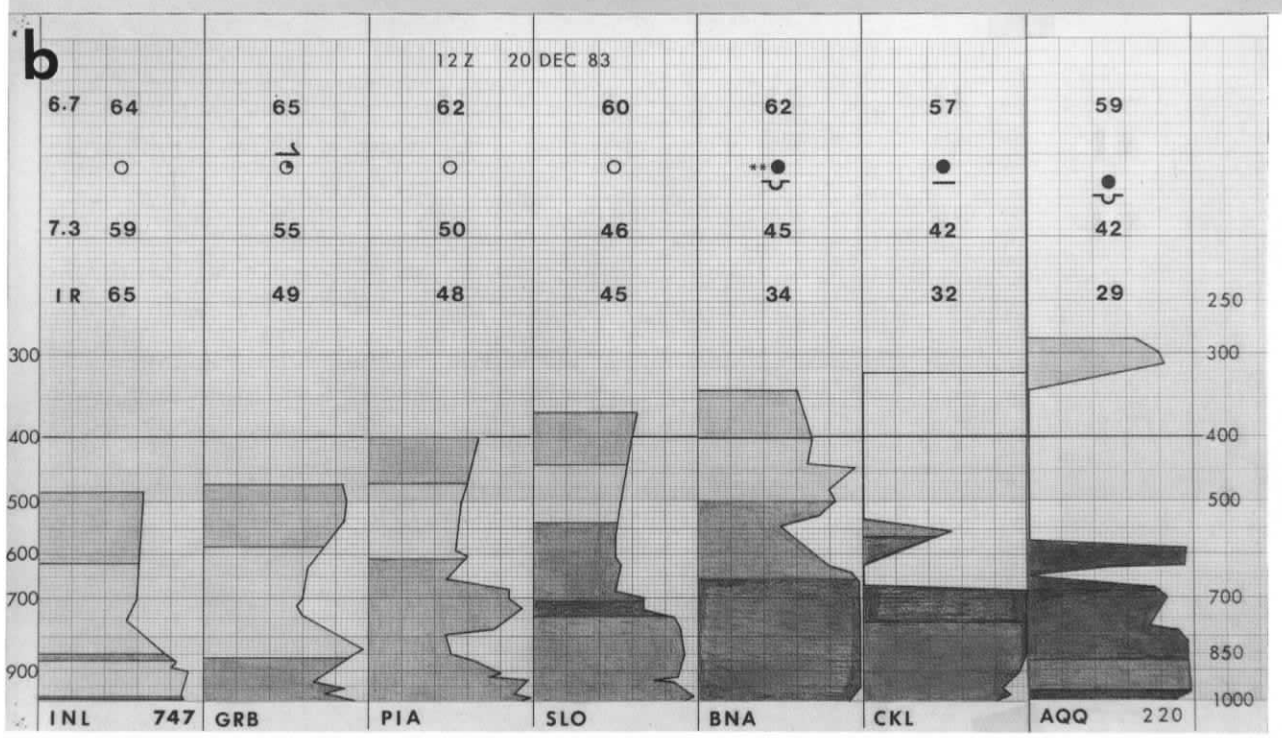

Figure 33

DEWPOINT DEPRESSION CROSS SECTIONS
Dewpoint depression data from 1200Z 20 December 1983 soundings.
Numbers at the tops of the columns are "Brightness Index" from the NOAA-7 satellite pass, valid times between 0937Z and 0948Z. Brightness indices (see text) are listed for 6.7μm, 7.3μm, and infrared (11.1μm) measurements.
Column shadings vary for 10°C air temperature intervals.

THE WATER VAPOR IMAGERY

Compare the IR, 7.3μm, and 6.7μm imagery from NOAA-7 on **Figure 34**. On the IR image, the borders of Hudson Bay, James Bay, the St. Lawrence River, parts of the great Lakes, and many cloud boundaries, are distinct. On the 7.3μm imagery, many of these features are less distinct or obscured, and some different features can be seen. Although many of the land or surface features can be seen, they are partially obscured by water vapor. On the 6.7μm image most of the surface and low cloud features are obscured. Even the cirrus band over Kentucky is not defined. The obscuration by water vapor is much greater in the 6.7μm band, with its large sensitivity to moisture absorption. The only surface feature discernable on the 6.7μm imagery is the shoreline of the St. Lawrence River near Seven Islands, Quebec which is identified by a white dot near the eastern border of panel two on **Figure 34**. The boundaries and features which appear on the 6.7μm imagery will be discussed after an examination of the radiosonde data.

RADIOSONDE DATA COMPARED TO IMAGERY

The two easternmost cross sections identified on the NOAA-7 IR image are displayed on **Figure 33**. Brightness Indices measured from the NOAA-7 images are printed above the dewpoint depression data for each radiosonde site.

On the eastern cross section, none of the sites are very dry from a relative humidity basis. Only Waycross (AYS) has a significant layer of 30°C depressions. Overall, Athens (AHN) is slightly drier above 700mb. On the 6.7μm image, the lightest brightness index of the cross section sites was 70 at Tampa (TBA) which had a high cloud overcast. At Key West, there were cumulus, towering cumulus, and cirrus in the vicinity, and a very deep moist layer. The Key West brightness index of 65 compared to Tampa at 70 is reasonable because of the difference in high clouds. However, the high clouds at Tampa produced a much larger difference in the 7.3μm brightness indices between Tampa and Key West. The largest BI difference is in the IR, in which considerable radiation penetrated between clouds at Key West and was not affected significantly by the deep moisture.

Comparing Athens and Waycross, notice that Waycross has more moisture between 300 and 400mb, and has the larger 6.7μm BI. Athens has more moisture between 400 and 500mb, and has the larger 7.3μm BI.

Huntington (HTS) has greater brightness indices for all three channels compared to Athens and Waycross. The cirrus band over Kentucky extended over Huntington at 0930Z and the sounding is very moist near 400mb at 1200Z, with some cirrus still present.

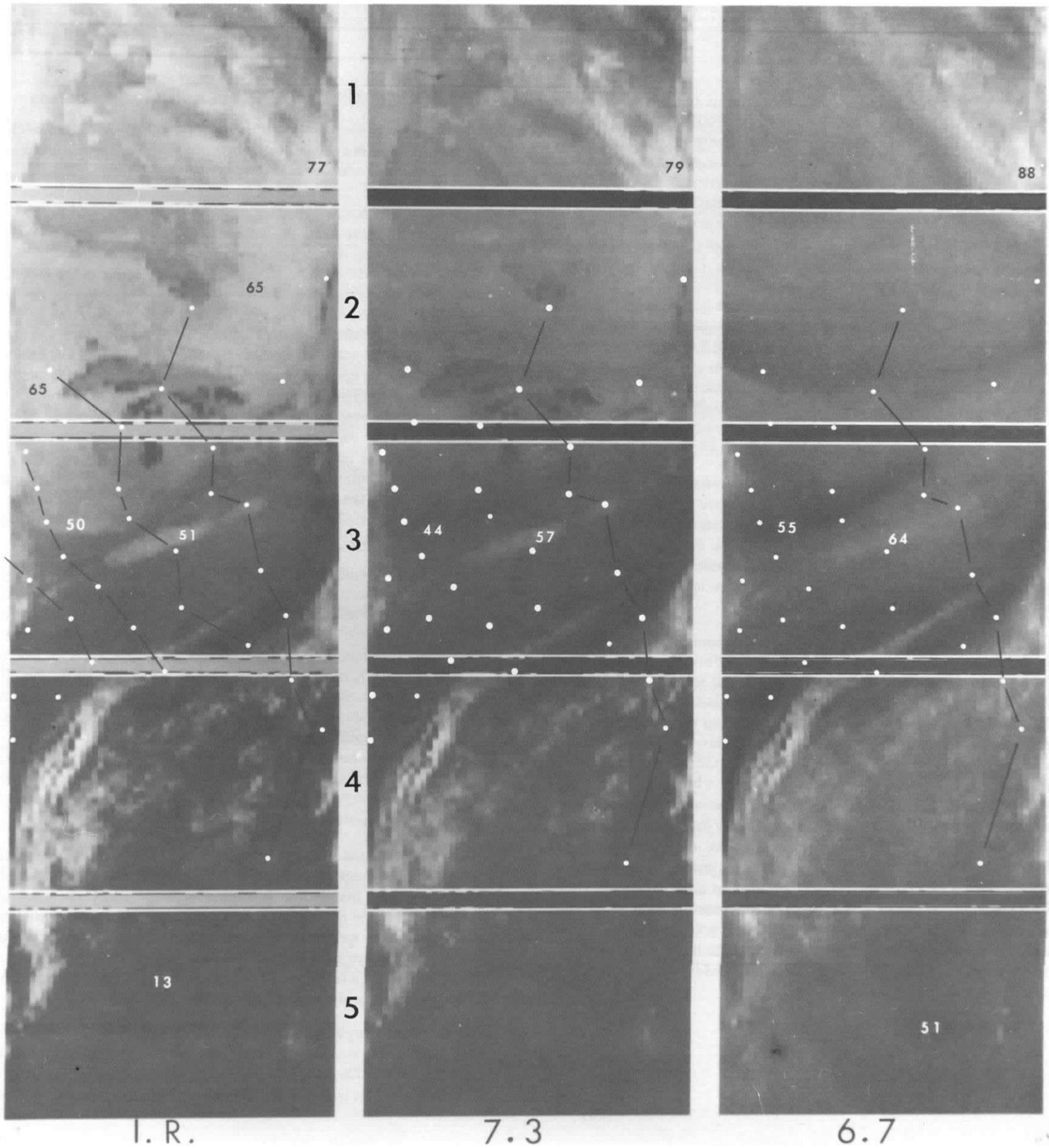

Figure 34 **NOAA-7 IMAGERY WITH RADIOSONDE SITE LOCATIONS**
Images are same as **Figure 30b**. White dots: radiosonde site locations (see text). Sites are connected as cross section locations on IR panels. The eastern cross section location is shown on 7.3μm and 6.7μm panels (sites on **Figure 33a**). Digits are Brightness Index.

THE EFFECTS OF VERY COLD AIR

On the eastern cross section, Moosonee (YMO) has the second lightest 6.7μm gray shade after Tampa (TBA) which had thin cirrus overcast over other layered cloudiness. International Falls (INL), the northernmost site on the second cross section, has the lightest gray shades - or largest "brightness indices" - of all sites on the 7.3μm and IR imagery. The northern sites have cold radiation temperatures because they are cold, not because their soundings have large moisture content. The driest, and overall coldest, sounding of those identified on the NOAA-7 imagery is from Seven Islands, Quebec which is on the shore of the St. Lawrence River and identified by a white dot near the eastern border of panel two on **Figure 34**. It is useful to compare data from Seven Islands to that from Key West (EYW), a southern site with clouds,but not overcast. Soundings and weighting function graphs for the two sites are shown on **Figure 35**,

and the two soundings were overlain on the same temperature scale on **Figure 7** of Section A. Although both sites are **relatively** humid, the total water content of the Seven Islands sounding is only 0.105 cm, compared to 4.61 cm at Key West. Comparing the weighting functions for 6.7μm radiation, the maximum radiation contribution from the moisture at Key West was near 300mb, and no radiation was contributed from air below 700mb. At Seven Islands the maximum contribution was from 500mb, and 7.2% of the radiation was contributed by the surface. The surface contribution did not produce significant warming to the net brightness temperature because of the cold surface air temperature of -27.7°C, but it did allow surface features to be detected on the 6.7μm imagery. Of all the sites identified on the imagery, Seven Islands produced the coldest computed 6.7μm brightness temperature of -36.2°C. It had the second lightest 6.7μm BI of 68 compared to 70 at Tampa with its cirrus overcast. In the 7.3μm band, 50% of the radiation at Seven Islands was contributed from the surface; however, because of the cold low level air and surface, the 7.3μm brightness temperature was only 6°C warmer than the 6.7μm BT. At Key West, the corresponding difference is 18.4°C.

At the northern sites, with their overall cold air and surface temperatures, there is less potential for brightness temperature differences. For example, at Seven Islands, the warmest air temperature in the sounding is -25°C, which should be the warmest brightness temperature possible. There is also less potential for gray shade differences on the 6.7μm imagery; and, we typically observe this uniformity on imagery as opposed to large contrasts at lower latitudes.

Although the humidity of the cold high latitude atmosphere has less effect on the brightness temperature, differences can be seen on 6.7μm imagery. The patterns and features tend to be lower in the atmosphere than those normally seen on 6.7μm imagery, when high clouds are not a factor. In this case, the high clouds over northern Labrador and norther Quebec have top temperatures between -50 and -60°C. They show vividly on the 6.7μm imagery. Otherwise the gray shades on the northern two panels of the 6.7μm imagery are relatively uniform. However, a boundary can be seen over the western tip of Lake Superior and extending eastward over Sault Saint Marie (SSM). The portion of the boundary just west of Lake Superior is most distinct. The moisture distributions at International Falls (INL) just north of the boundary, and St Cloud, just south of the boundary; are similar except that St Cloud has a moist layer between 600 and 700mb. Farther to the east, the moisture difference is apparently lower and less distinct, although radiosonde sites are not available for a good comparison. The boundary feature is associated to the stretching axis of a hyperbolic zone in the 850mb and 700mb wind fields.

THE EFFECTS OF LARGE TEMPERATURE INVERSIONS

Generally the presence of moisture in the atmosphere causes brightness temperatures of the water vapor channels to be cooler than those of the window infrared channels. This is not always the case, however, when large temperature inversions are present. The darker gray shades on the 7.3μm and 6.7μm northern panels of **Figure 34**, compared to the IR imagery, imply that the moisture may be causing warmer brightness temperatures.. Comparing the "brightness indices" for different channels at the northern sites indicates that this may be valid. At four of the radiosonde sites, the 7.3μm "brightness indices" are less than their corresponding IR brightness indices. At International Falls (INL) the 6.7μm BI is also less than the IR BI. Data graphs for International Falls are shown on **Figure 35**. Note that the computed brightness temperatures indicated the same trend as the "brightness indices". The 6.7μm and 7.3μm brightness temperatures are both warmer than the surface air temperature. A 17°C temperature inversion is present at the site. The air below 514mb is warmer than the surface air temperature, and that above is colder. The 7.3μm brightness temperature is the warmest, with 42 % of the 7.3μm radiation contributed by the surface. Forty-eight percent is contributed by air warmer than the surface, and only 10% from air colder than the surface. For 6.7μm radiation, 56 % was contributed by air warmer than the surface.

At Peoria (PIA) and Salem, Illinois (SLO), the 7.3μm brightness indices are similar to those of the IR, but significantly darker than the 6.7μm values. At these locations with their more moderate air temperatures, the inversion affects the 7.3μm radiation significantly; but with more moisture, has much less effect on the 6.7μm radiation. On the graph for Peoria on **Figure 35**, the 6.7μm weighting function can be seen to peak near 400mb in air colder than the surface. Although there is a significant moist layer at 700mb, it is in air warmer than the surface. The 7.3μm weighting function reaches a maximum value at 700mb in the relatively warm air. The 7.3μm brightness temperature was significantly affected by the inversion, only 1.2°C cooler than the surface air temperature. In the very dry cold air farther to the north, the inversion affects both the 7.3μm and 6.7μm brightness temperatures.

Generally, when the primary moist layer is near 700mb in an atmosphere with moderate temperatures, the 7.3μm brightness temperature is closer to the 6.7μm BT than to the IR brightness temperature. The presence of the large inversion at Peoria created an exception. In a very cold atmosphere the water vapor band brightness temperatures are similar to that of the IR, and all are cold, similar to Seven Islands in this case. If, under those conditions, a large inversion is present, the IR brightness temperature may be the coldest, as at International Falls in this case.

The next case study illustrates another condition where the 7.3μm brightness temperature is usually closer to the IR value, and much warmer than the 6.7μm value. This common situation involves high level moisture with a dry lower middle troposphere, with no significant inversion required.

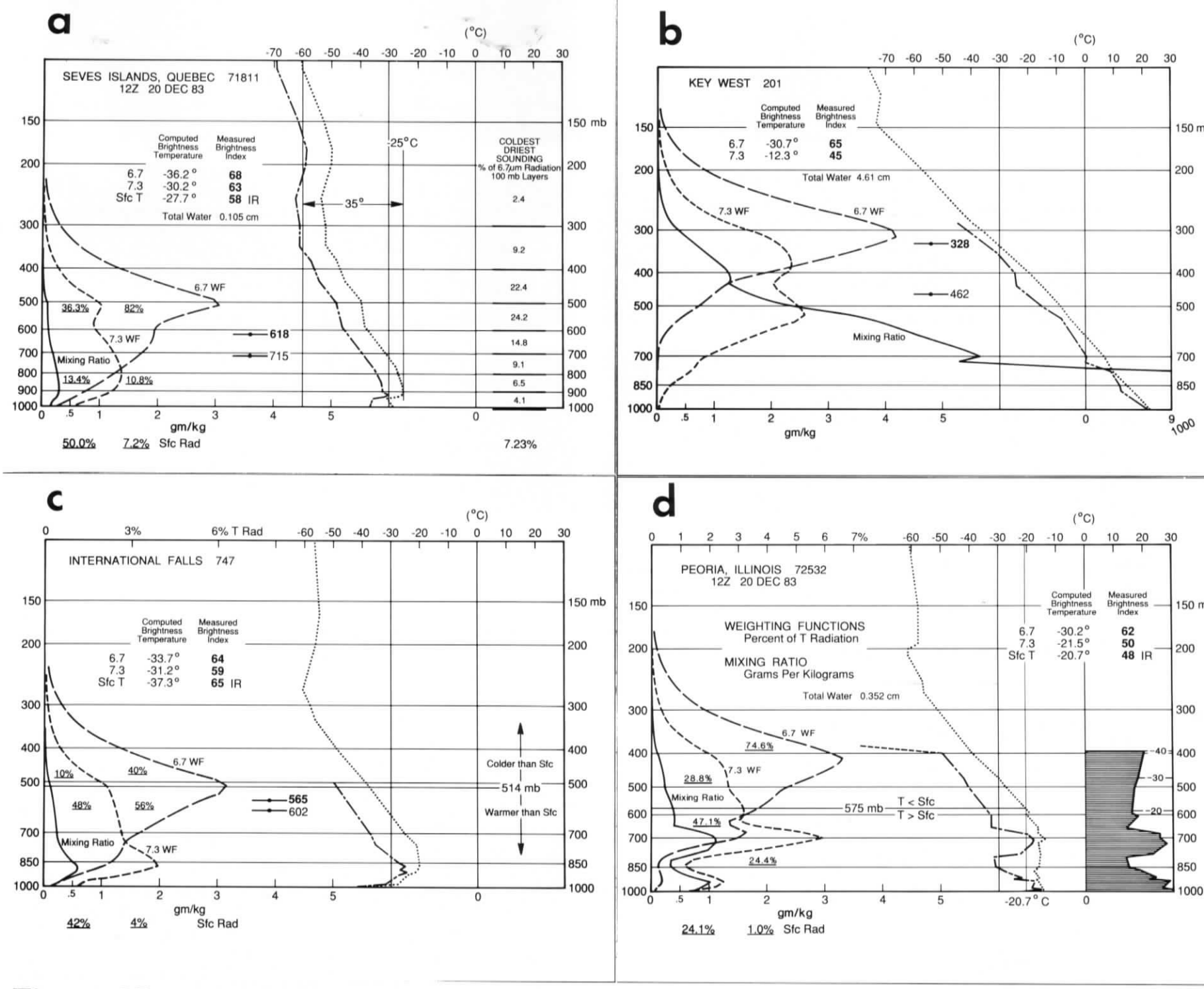

Figure 35 **PLOTS OF RADIOSONDE AND RADCOM DATA FOR SELECTED SITES**
All graphs include plots of air temperature, dewpoint temperature, weighting functions for both 6.7μm and 7.3μm data, and mixing ratio. A shaded dewpoint depression 30°C wide column is shown for Peoria (**Fig. 35d**).

Tables on Graphs:	Computed brightness temperatures and measured brightness indices are compared for both 6.7μm and 7.3μm data. Reported surface temperatures (Sfc T) are compared to "window" infrared brightness indices.
Equivalent Pressures:	Shown by horizontal lines with dots for graphs on **Fig. 35a, b, c**. Bold pressures are from 6.7μm data.
Surface Contribution to Radiation:	Percentages plotted below each graph on the left side, labeled "Sfc Rad". 7.3μm data to left of 6.7μm data. Surface contribution as a percent of the total radiation reaching the satellite. There were no surface contributions for Key West.
Layer Contributions:	**Fig. 35a**. Percentage contributions to total radiation by 100mb thick layers are shown on the right with the surface contribution repeated. Values for 6.7μm data.
	Figs. 35a, c, d. Percentage contributions to the total radiation are shown for air colder than and warmer than the surface air temperature are plotted inside the weighting function curves. Values on the left are for 7.3μm radiation, those at higher altitudes are contributions from colder air.

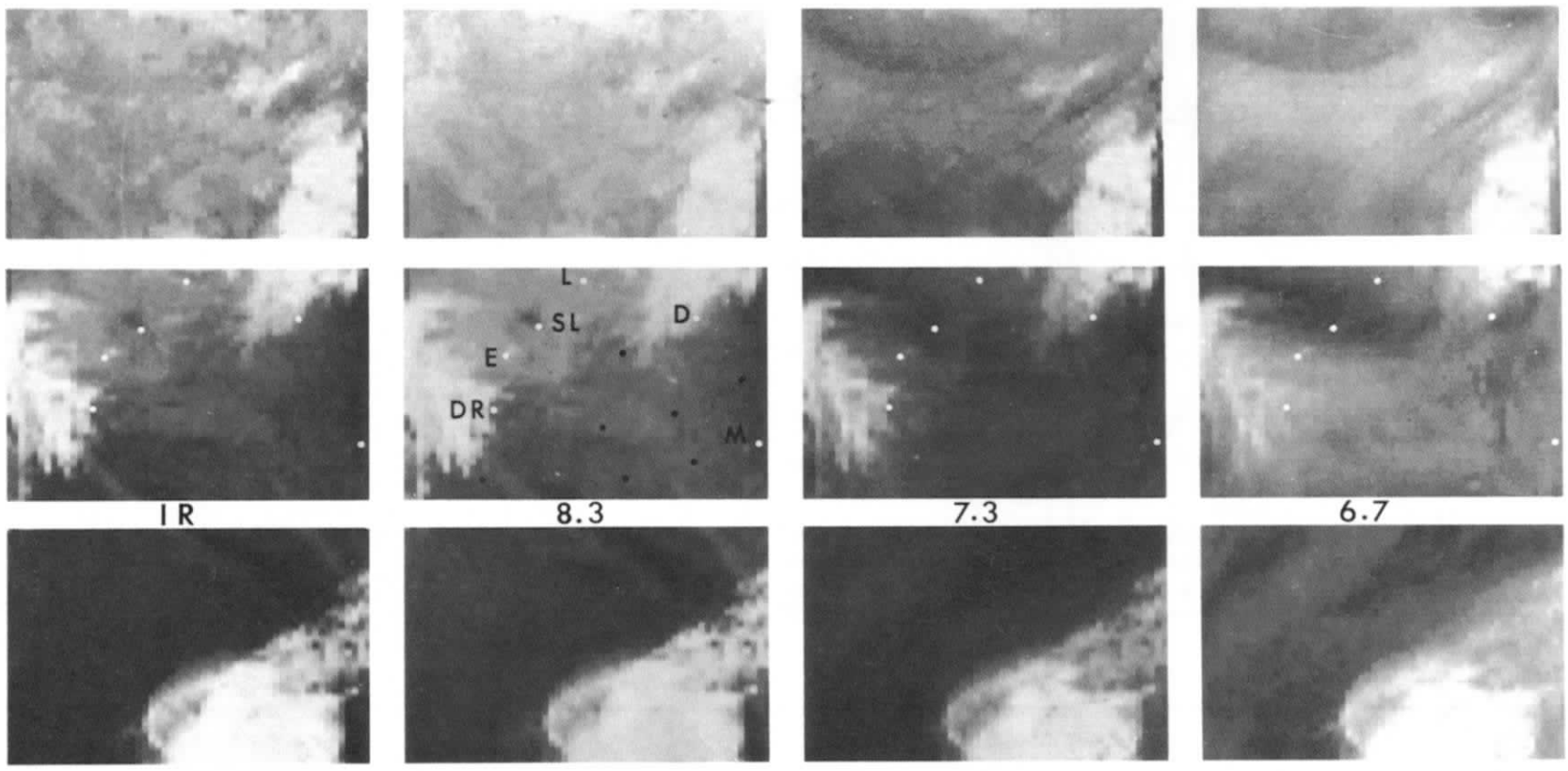

Figure 36 **MULTICHANNEL IMAGERY FROM NOAA-8**
Imagery from four channels are shown side by side with three panels each. Channels are from left to right: 11.1μm "window"infrared, 8.3μm water vapor, 7.3μm water vapor,and 6.7μm water vapor, 1035Z 19 October 1982. White dots on the center panels for each band indicate radiosonde sites. These are labeled on the 8.3μm panel as: DR: Desert Rock, Nevada; E: Ely, Nevada; SL: Salt Lake City, Utah; L: Lander, Wyoming; D: Denver, Colorado; and M: Midland, Texas.

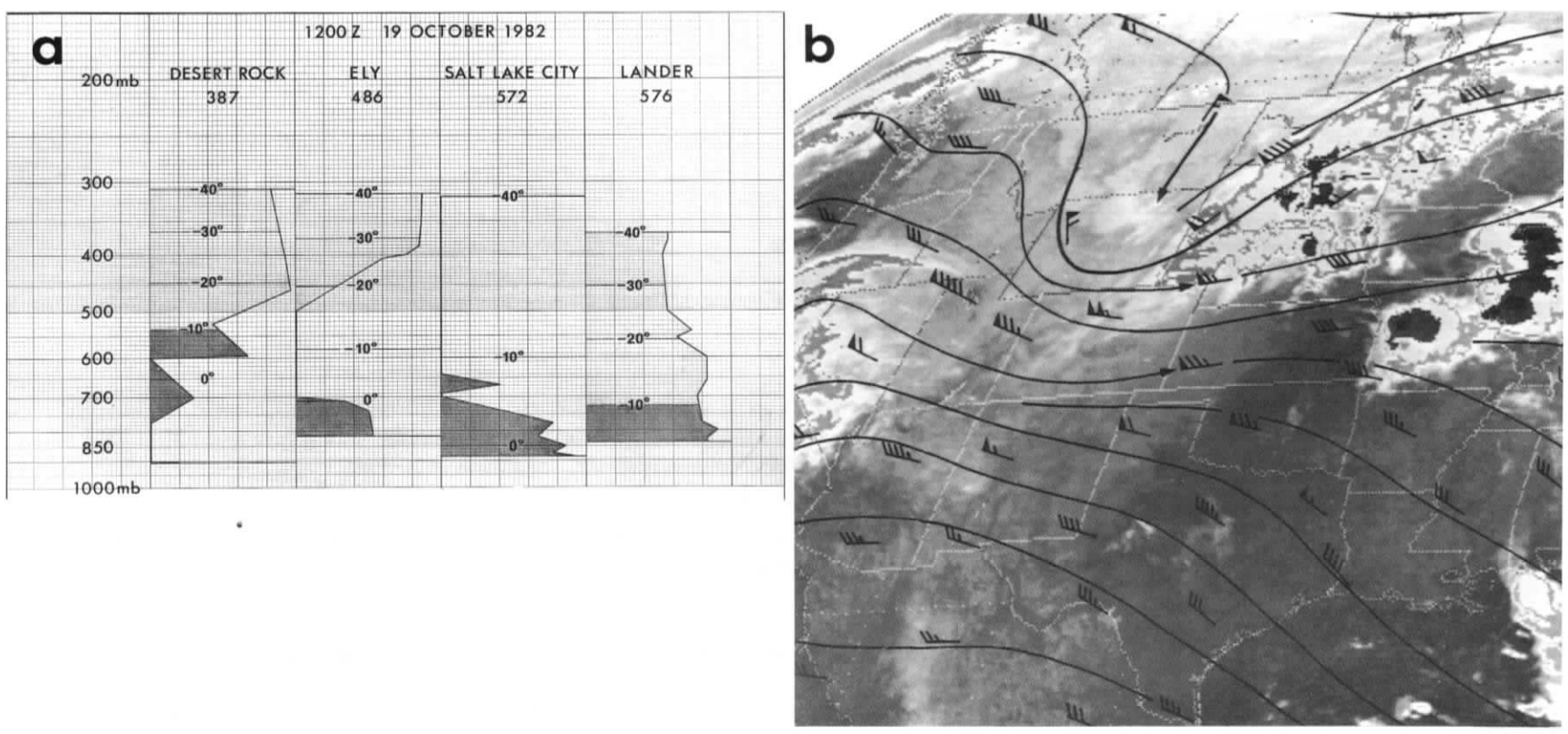

Figure 37 **DEWPOINT DEPRESSION CROSS SECTION AND 300mb ANALYSIS**
Fig. 37a. Dewpoint depression cross section from southwest (left) to northeast (right) along the western four white dots shown on **Figure 36**. Radiosonde data: 1200Z 19 October 1982.
Fig. 37b. Enhanced infrared image, GOES East, 1200Z 19 October 1982 with 300mb winds and streamlines.

b. Case Study - 19 October 1982

On **Figure 36** are imagery from four channels of the polar orbiting satellite NOAA-8, valid at 1035Z, 19 October 1982. The imagery are, from left to right, 11.1μm (window IR), 8.3μm water vapor, 7.3μm water vapor and 6.7μm water vapor. The 8.3μm water vapor band is less sensitive to moisture than 7.3μm, and in standard image format, appears very similar to the window IR imagery. Although the imagery are not gridded, selected radiosonde sites have been located on panel 2. Those with white dots are identified by letters on the 8.3μm image. A dewpoint depression cross section from Desert Rock, Nevada (DR) to Lander, Wyoming (L) is shown on **Figure 37a**. On **Figure 37b**, 300mb winds and streamlines are superimposed on a GOES East enhanced IR sector valid at 1200Z.

GENERAL DESCRIPTION

A jet stream branch entering western Canada is curved anticyclonically southward over eastern Montana and western Wyoming to northeastern Utah, where it merges with another branch over southern Oregon and northern Nevada. The pre-cyclogenetic "baroclinic leaf" cloud pattern extending from northeastern Colorado to northern Minnesota can be seen on Eastern parts of the top two panels of the NOAA-8 imagery. The radiosonde site labeled "D" is Denver which had the maximum 300mb wind speed within the area of the GOES East IR image on **Figure 37b**. The cold clouds on the western portion of panel 2 of the NOAA-8 imagery are over Nevada, California, and southern Oregon in advance of an upper trough west of California.

THE WATER VAPOR IMAGERY AND RADIOSONDE MOISTURE DISTRIBUTIONS

Near the axis of the jet stream branch over the western states, a band of cirrus extends downstream over southern Idaho to the northern border of Utah. South of there, the cold clouds dissipate at the ridge axis forming a ragged cloud border over Nevada. On the 6.7μm image, the ragged edge is not discernible, since the moisture continues downstream beyond the ridge axis where the clouds dissipate. The light gray shade over eastern Nevada gradually darkens eastward from there. Along the northern edge of this moist region, over Salt Lake City, there is a dark area on the 6.7μm imagery. On the 7.3μm image, the boundary between the dark and light region cannot be seen. The entire area is generally dark on the 7.3μ imagery.

On the cross section of **Figure 37a**, note that Desert Rock and Ely are very moist at high levels with dry air below that. The 6.7μm radiation is absorbed and radiated from the cold moisture above 500mb producing generally cold brightness temperatures and a light gray shade. Since there is little moisture in the lower middle troposphere, the 7.3μm radiation from warm low levels is able to reach the satellite. At Salt Lake City, the air is dry above 700mb, and the gray shades are dark on both 7.3μm and 6.7μm images. At Lander, the air is moderately humid through a deep layer. There is less difference between the 6.7μm and 7.3μm gray shades there.

The vertical moisture distribution downstream from the upper air ridge axis over eastern Nevada is very common for that synoptic situation. Also common is a relatively large brightness temperature difference between 7.3μm and 6.7μm channels. The 6.7μm is relatively cold or light gray on imagery, whereas the 7.3μm is relatively warm or dark. On this sample, the apparent difference is large because the entire 7.3μm image is slightly darker than the 6.7μm image. However, this effect caused by the different conversions from signal to gray shade is minor. Generally, 7.3μm brightness temperatures are warmer than those of 6.7μm, and the imagery should be overall darker.

A MOUNTAIN EFFECT ON WATER VAPOR IMAGERY

On the second panel of the 6.7μm image some dark irregular bands can be seen on the eastern part of the panel. These are related to the mountain ranges of New Mexico and southern Colorado. The pattern is unique to the 6.7μm image, and is not clouds or terrain. Such patterns are frequently observed on 6.7μm imagery associated to mountain ranges. When other water vapor channel imagery is available, as in this case, the patterns are most vivid on the 6.7μm imagery, or unique to the 6.7μm imagery. They consist of very large gray shade differences over very small horizontal distances, sometimes at single pixel intervals. They are usually not associated with mountain lee cirrus decks, or with mountain wave clouds which are usually at relatively low levels. It may be that the presence of such clouds would mask the water vapor features or make them less obvious.

Apparently there are significant localized vertical motions causing the top of the moist layer to descend to relatively low levels with dry air above. This could be compounded by adiabatic warming to account for such dark gray shades. We do not know the conditions causing the effect; but, since it is common and on the imagery of this case, it should be noted.

This page intentionally left blank

IMAGE GRAY SHADES - A GUIDE TO INTERPRETATION

This discussion of Part One concepts addresses the question: what do the image gray shades mean in regard to the vertical distributions of moisture in the atmosphere? It is intended especially for those persons who wish to read Part Two, but do not wish to read Part One.

Although both 6.7μm and 7.3μm bands were discussed and compared in Part One, only 6.7μm imagery was used in Part Two. Therefore, this section addresses only 6.7μm radiation and imagery.

a. Radiation Concepts

Infrared radiation, including that within the 6.7μm band, is emitted by the earth's surface and clouds. A part of this radiation emitted toward the satellite is absorbed and re-radiated by water vapor in the atmosphere above the cloud tops or earth's surface. Since the air temperature commonly varies very significantly in the vertical, the re-radiation by the moisture is at a different energy than the radiation arriving from below. In most cases, the moisture above the clouds or earth's surface is colder; and, the radiation emitted by the moisture is of lower energy than that arriving from below. Therefore, the net intensity of the radiation arriving at the satellite from the earth's surface or cloud tops is reduced by the re-radiation by water vapor in the path. It is this change, or reduction, that enables us to detect the presence of the moisture.

The amount of absorption of radiation by water vapor is dependent upon the amount of moisture within the radiation's path and the wavelength of the radiation. Most of the absorption by water vapor occurs at the lowest layers in the atmosphere where the largest amounts of moisture are present in the warmest and most dense air. Radiation in the "standard infrared" bands, or "window channels", is not easily absorbed by water vapor. Significant absorption does occur with very humid low level air. However, radiation in the 6.7μm band is very easily absorbed by water vapor; and, radiation from the earth's surface is not usually able to penetrate to the satellite.

Since radiation intensity in the infrared bands is highly correlated to the temperature of the emitting substance or objects, the radiation measurements may be converted to "brightness temperature" values. These temperature values are essentially the temperature that an object would have if it were radiating with near "black body" characteristics, and without significant absorption in the radiation's path to the measuring instrument. The "brightness temperature" values converted from satellite measurements in the "window" infrared bands have been reasonably well correlated to temperatures of the earth's surface, and to the cloud top temperatures of some types of cloudiness. The satellite measurements of 6.7μm radiation may also be converted to "brightness temperatures." If such a "brightness temperature" is compared to a corresponding "standard infrared brightness temperature", the difference may be attributed to the absorption and re-radiation by water vapor above the earth's surface or clouds.

b. 6.7μm Imagery

The satellite measurements of 6.7μm radiation may be converted to "brightness temperatures", or they may be converted to specific gray shades or colors and displayed in an array as imagery. When displayed as gray shades, the common convention, and that used exclusively in this presentation, is that lighter shades indicate colder "brightness temperatures" or lower energy measurements. Thus, an area of darker gray shades on an image indicates radiation arriving from a warmer source.

Radiation in the 6.7μm band commonly does not penetrate from the earth's surface to the satellite. Most of the radiation is absorbed and re-radiated by moisture in the atmosphere, or is radiated from clouds. Therefore, surface features are rarely observed on 6.7μm imagery. The exceptions occur most frequently over continents during the winter seasons, in cases where the air is very dry. In these situations, surface features of large temperature contrasts, such as shorelines and ice boundaries on lakes will be revealed on the imagery. Elsewhere, and during other seasons, high mountain terrain features are sometimes revealed, when the air is relatively dry in the middle and upper troposphere.

On a 6.7μm image, the lightest gray shades are contributed by high cold cloud tops; and, the darkest shades are observed over lower latitude areas when the air is very dry through a deep layer in the atmosphere.

c. Image Gray Shades And The "Topographic" Concept

Since atmospheric moisture, in typical concentrations, is translucent to 6.7μm radiation, the relationship between image gray shades and the vertical moisture distribution is very complex. The radiation measurement at the satellite provides a single scalar value that can be converted to a "brightness temperature" or an image gray shade. We know of no situation in which this single value provides totally accurate knowledge of the atmospheric moisture. Even if the measured "brightness temperature" were equal to the surface temperature, we would require additional knowledge to know that the entire atmosphere was extremely dry. However, if we lower our requirements for accuracy, and use additional information, the knowledge gained from the measurements can be increased to very useful levels.

"Moisture Topography"

We know of no simple accurate relationship between the image gray shades and the distribution of atmospheric moisture. Probably, the most useful simple concept is the "topographic" representation.

The "topographic" concept can be applied under the following conditions or assumptions. There are no clouds. Moisture is present at significant relative humidities upward to some specific altitude, above which the air is relatively dry. This moisture is not arranged in layers at altitudes above a threshold level. This threshold level and its variation will be discussed; however, for the present, consider it to be near 600mb. And, finally, the air temperature decreases upward without significant inversions within the troposphere. Under those conditions, as the top of the moist layer increases in altitude, the measured "brightness temperatures" decrease, or the image gray shades become lighter. Thus, using this concept, a water vapor image may be considered to represent a "moisture terrain", in which the light areas are "mountains of moisture" extending upward to high altitudes, and the dark areas are "valleys" where the dry air extends downward to the lowest levels. Of the simple generalizations between moisture content and image gray shades, the "topographic" representation is the most accurate and the most useful. We recommend the "topographic" concept as a "starting point" for estimating moisture distribution from water vapor imagery. Many of the primary exceptions can then be identified; and, many of those can be qualitatively resolved by applying additional information.

At least two other simplified concepts have been suggested for relating image gray shades and atmospheric moisture. One of these is that the gray shades are an indication of the amount of moisture within a specific layer in the upper middle troposphere - for example near 400mb. This can be used to some effectiveness as a part of the tropospheric concept. If very light gray shades are observed, and no middle or high clouds are present, the air is likely relatively moist in the upper middle troposphere. At the other extreme, where very dark gray shades are observed, the air in the upper middle troposphere is likely very dry. The concept is not useful for a large range of intermediate gray shades. A second simplified concept is that the gray shades represent the water content of the atmosphere. Over areas of non-mountainous terrain, most of the water content in the atmosphere is usually below 700mb. Commonly, these lower levels of the atmosphere are obscured on 6.7μm imagery by moisture above. Although 6.7μm measurements, or imagery, might be used in conjunction with other information to estimate water content, it would represent a relatively poor single source for this purpose.

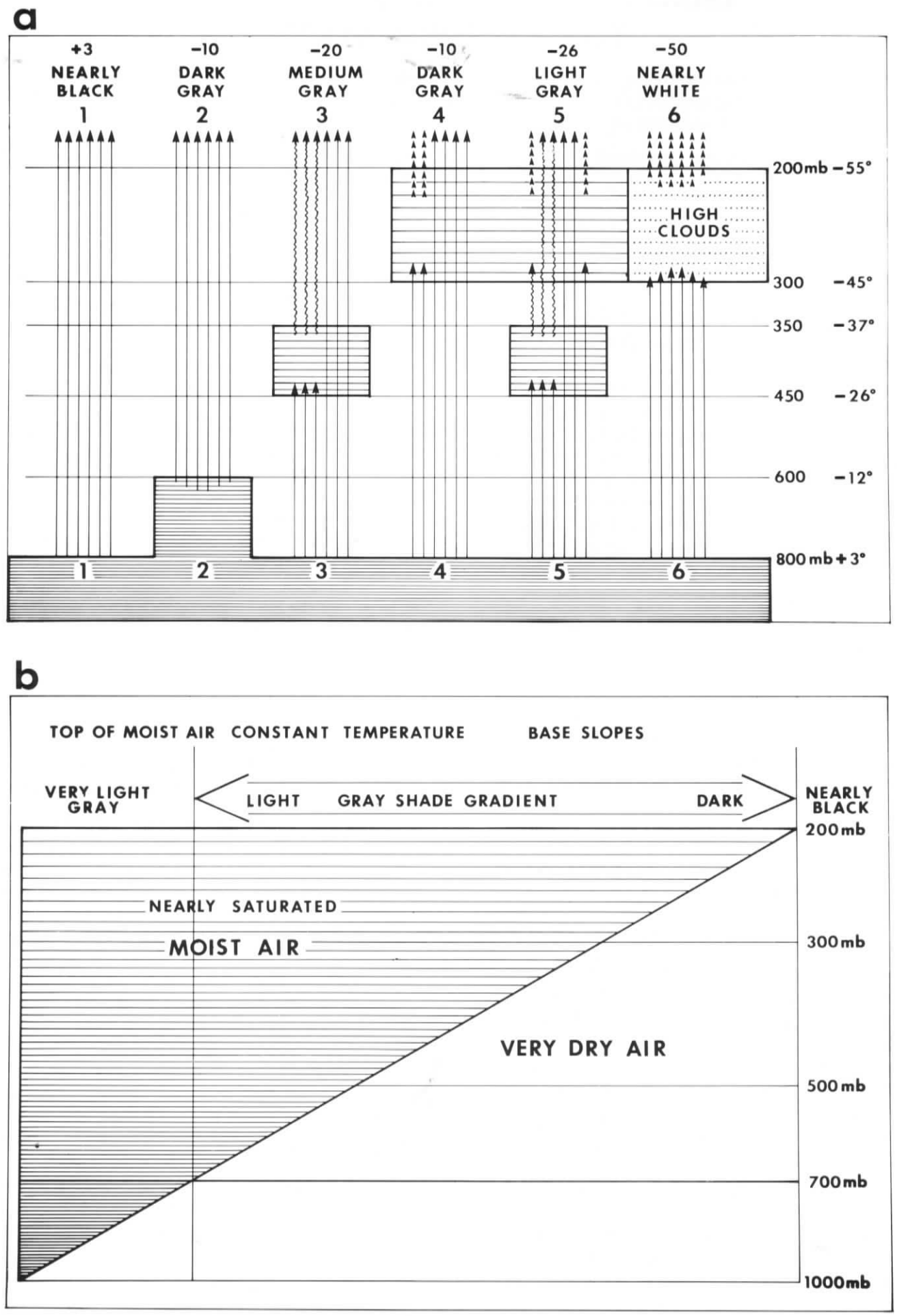

Figure 38 **LAYER MOISTURE EFFECTS ON 6.7μm RADIATION**
Drawings with logarithmic vertical scale of pressure. Representative air temperatures with labeled pressure surfaces are degrees Celsius. Numbers along the top of the **Fig. 38a** are brightness temperatures in degrees Celsius. Areas of horizontal hatching indicate moisture of single digit dewpoint depressions. The dotted area indicates high clouds.

The "Threshold" Level

We mentioned that much of the atmospheric moisture is translucent to 6.7μm radiation. If the moisture is present at sufficient mixing ratio and density, it becomes relatively opaque to the radiation. This is most likely to occur at lower altitudes where the warmer air holds more moisture, and the air pressure is larger. With an air temperature sounding such as the U.S. Standard Atmosphere, and moisture present at single digit dewpoint depressions, the moisture becomes relatively opaque to 6.7μm radiation at approximately 600mb and below. Under these conditions, any moisture with its top at or below this 600mb "threshold" level will produce a satellite measured "brightness temperature" equal to the air temperature near the top of the moist layer. If the depth of the moisture is increased, such that the top of the moisture is above the "threshold" level, the measured "brightness temperature" will be colder, but not truly representative of the air temperature at the top of the layer. The "threshold" level varies, primarily according to the air temperature. During the winter seasons or at high latitudes, it is likely to be below 700mb. During the summer seasons or at low latitudes, it may be between 400 and 500mb.

The "threshold" level is not only significant to quantitative measurements of "brightness temperature"; but, it is also important for qualitative interpretations of vertical moisture distribution. This is significant when moisture is present in finite depth layers above the "threshold" level. This complication of layered moisture represents one of the primary exceptions to the "topographic" concept, and may be illustrated by the drawings on **Figure 38.**

d. Primary Exceptions To The Topographic Concept

LAYERED MOISTURE CONDITIONS

Even when clouds are not a factor, and the air temperature decreases upward with an average lapse rate, the moisture is often concentrated in layers. When the layers are located above the "threshold" level, significant amounts of radiation pass through the layers from some warmer origin below. Although some of the radiation is absorbed and re-radiated by the moisture in the layer, the net radiation reaching the satellite is partly from the layer and partly from below. Thus, the "brightness temperature" is warmer than the air temperature in the layer.

Consider the drawing on **Figure 38a**. Areas of nearly saturated moist air are depicted on a vertical scale of pressure and temperature by hatched shading. Six different cases, or situations, are shown and numbered from left to right. The satellite measured "brightness temperatures" and qualitative descriptions of image gray shades are shown for each case at the top of the drawing.

In all cases, the air is considered to be nearly saturated below 800mb. In case #1, the air is very dry above 800mb. This would produce a very dark gray shade on imagery. Since the moisture is of high mixing ratio in dense air, most of the radiation reaching the satellite would originate from near the top of the moist air; and, the measured "brightness temperature" would be nearly identical to the air temperature at 800mb. In case #2, the depth of the moisture has been raised to 600mb. The image gray shade would be dark gray, noticeably lighter than that of case #1 on most image displays. The top of the moisture would be slightly translucent to the 6.7μm radiation; therefore, the "brightness temperature" would be slightly warmer than the air temperature at 600mb.

In case #3, a layer of moisture is also present in the upper middle troposphere between 450mb and 350mb. The image gray shade produced by case #3 would be significantly lighter than those of the first two cases. The "topographic" concept would be valid in regard to the gray shades. However, the "brightness temperature" would not be representative of the air temperature at the top of the upper middle tropospheric moist layer. A part of the radiation reaching the satellite would originate from the higher moist layer: but, another part would originate from the warmer lower level moisture and pass through the upper layer. The measured "brightness temperature" would be equal to the air temperature somewhere between the two layers of moisture, where the air is dry.

In case #4, an additional layer of moisture is present in the upper troposphere instead of the middle troposphere. Since this moisture is at low mixing ratio and at low density, a large amount of the radiation arriving from below passes through the high layer. Only a small portion of the radiation is absorbed and re-emitted at the low energy level of the very cold air. Therefore, the resulting "brightness temperature" is 13°C colder than that of the low moisture at 800mb, but not nearly as cold as the air temperatures between 300mb and 200mb. The image gray shade would be lighter than the very dry situation of case #1, but not as light as case #3. The dark gray shade produced by case #4 is equal to that of case #2. If such a dark gray shade is observed on imagery, it could result from a high layer of moisture above the boundary layer moisture, or from a moist top near 600mb with dry air above. The topographic concept is not valid with high moist layers present; and, the vertical moisture distribution cannot be estimated from the gray shades alone. However, the difference between case #2 and case #4 can often be determined by considering the moisture patterns on the imagery. For example, the dark gray shades may extend downstream from an area of high cirrus clouds, implying that the shades were produced by a high moist layer rather than moisture in the lower middle troposphere. A sequence of images may reveal that the area of dark gray shades remained from recently dissipated high clouds spreading from previously existing thunderstorms.

Case #6 illustrates the difference between high level clouds compared to high level saturated air. Although the density of the cloudiness is a factor, the high clouds will prevent most of the radiation from below to pass through. Most of the radiation reaching the satellite originates within the cloud layer; and, nearly white shades are observed on the imagery.

In case #5, an upper middle tropospheric moist layer is present under the high layer of case #4. Although the top of the moisture is not higher in case #5, lighter gray shades would be observed on the imagery, because the radiation arriving at the base of the higher layer is from a colder source than that of case #4. This concept is further illustrated on **Figure 38b**. The top of a large moist area is constant, but the vertical depth of the moisture varies from very deep on the left side to very shallow on the right. Although the air temperature at the top of the moist air is constant (by definition in this case), the gray shades on an image would range from very light gray to very dark. Consider the change from right to left. As the base of the moist layer is lowered, less of the radiation from the warm surface would be able to penetrate the moisture, and the gray shades would become lighter. However, once the base of the moisture reaches approximately 700mb, none of the radiation from below that level is able to penetrate the moisture above. Therefore, to the left of that point, the gray shades no longer vary, but are maintained at a very light gray shade.

In the case shown on **Figure 38b**, the amount of absorption accomplished by the moisture at any location would depend upon the amount of moisture. Since the air is nearly saturated in the moist region, the amount of moisture present would depend upon the air temperature. A vertical line is drawn through the point where the base intersects 700mb. To the left of that line, no radiation would reach the satellite from below 700mb; however, the radiation reaching the satellite would arrive from various levels of the moisture above 700mb. The radiation reaching the satellite would arrive from moisture in air at various temperatures; and, the resulting "brightness temperature" would not be representative of the air temperature at the top of the moisture. For an average mid-latitude air temperature sounding, the "brightness temperature" would be equal to the air temperature somewhere between 300mb and 400mb. If the air temperature sounding were warmer, the amount of moisture would be increased, contributing to more absorption by the moisture at high and middle levels. The level from which no radiation penetrates to the satellite would be raised in altitude; and, the brightness temperature would equal the air temperature at a higher altitude. Although the radiation reaching the satellite would be from higher levels, the brightness temperatures would not change significantly because the air temperatures are warmer at those higher levels. Therefore, the primary result of raising the air temperature of the sounding is to raise the "level of obscuration." At tropical latitudes, the sounding tends to be warmer below 200mb and colder above to a tropopause near -70°C and 100mb. The most significant difference on the water vapor imagery is that the lower layer obscured by mid and high level moisture is of greater vertical depth.

The situation illustrated on **Figure 38b**, violates the "topographic" concept, and is commonly observed in the atmosphere on the downstream sides of upper air ridges, on the equatorward side of the jet streams. The top of the moisture is not likely to be of constant temperature as shown, and the base will slope in a more irregular manner, often in the form of multiple moist layers. The situations are usually recognizable by the patterns on the imagery.

COLD AIR TEMPERATURES AND INVERSIONS

Whereas the range in air temperatures in a summer season or low latitude sounding may be near 100°C between the warmest and coldest levels, the range is much smaller during winter seasons at middle and high latitudes. During winter, especially on the poleward side of the jet stream or within an upper air trough environment, the warmest air in a sounding may be near -30°C and the coldest air near -50°C, producing temperature ranges near 20°C. For the cold sounding, the warmest origin from which radiation may be emitted is -30°C. With a normal image display, this "brightness temperature" would be light gray. No darker gray shades would be possible, since no warmer temperatures exist in the sounding. Therefore, during winter seasons at high latitudes, or at middle latitudes during cold weather regimes, the gray shades on a 6.7μm image range between light gray and nearly white. No dark shades are observed, although the atmosphere may be very dry. In fact, the driest atmospheric conditions are often observed within winter cold air regimes, with total precipitable water of less than one tenth of a centimeter relatively common over continental areas.

The mere coldness of the air does not violate the "topographic" concept. Relative humidity differences and various vertical distributions of moisture will exist and show on imagery as variations of gray shades. However, features at lower altitudes will be observed. Although the upper atmosphere may be relatively humid, the absolute humidity is low, and more radiation from low levels is able to penetrate to the satellite. Therefore, moisture patterns associated with lower level features, such as surface frontal zones, will appear on the 6.7μm imagery.

Also, common with the winter season cold air regimes are large temperature inversions, especially over continental areas. These do cause exceptions to the "topographic" concept. At higher latitudes, these large temperature inversions are maintained above the boundary layer during the daylight hours. Although enough radiation may penetrate to the satellite from the earth's surface to reveal surface orographic features, the 6.7μm radiation is sensitive enough to moisture such that most of the radiation reaching the satellite does originate from the atmospheric moisture. Since this moisture is often present within a relatively deep layer with air temperatures warmer than the surface, it is not uncommon for the 6.7μm "brightness temperature" to be warmer than the surface. With this situation, patterns of lower tropospheric moisture may be present on an image at similar gray shades as adjacent drier regions, or in some cases have darker gray shades than the drier areas.

Some similar violations to the "topographic" concept can occur in association with strong frontal inversions in addition to those with winter season cold air regimes. These are very difficult to detect, even using associated radiosonde data with thorough analyses. However, we believe they will not usually cause significant problems for general image interpretation.

e. Clouds

Although clouds are often ignored in discussions of water vapor imagery and radiation concepts, they are frequently significant to operational image interpretation. The following summary of cloud effects on 6.7μm water vapor imagery is based upon our empirical studies of imagery.

HIGH CLOUDS

Clouds with high altitude tops are the most likely to be explicitly observed on 6.7μm imagery. Therefore, the tops of deep convective cells and high cirrus decks are the most frequently observed. These can often be distinguished from surrounding moisture patterns by their nearly white gray shades, their well defined or ragged edges, and in some cases by the texture of the patterns. In some cases, high clouds cannot be distinguished from the adjacent moisture. This is most often true on the downwind sides of clouds, where the clouds are thinning and dissipating; or in situations where residual high cloudiness from previously active convective weather is dissipating with time. Generally, a significant gray shade change is present between clouds and moisture. However, with a moist environment, the change may be gradual and difficult to interpret.

CLOUDS UNDER HIGHER LEVEL MOISTURE

Clouds may be implicitly observed on water vapor imagery. This type of observation is most common with middle clouds located under layers of high level moisture. The clouds act as a cold radiation source relative to the surrounding clear areas. The radiation from the cloud tops produces an area of lighter gray shades within the higher level moisture pattern. Although the high level moist layer may be quite uniform, it will have a textured, cellular, or irregular gray shade pattern consistent with the pattern of cloudiness at a lower level. The patterns in the high level moisture may be mistaken for "moisture parcels" or differences in top height or relative humidity of the high moist layer. This can be a problem when "moisture parcels" are tracked to produce wind estimations. Sometimes this situation can be detected by observing significant differences in motion on time-lapse imagery; however, the best precaution is to compare the water vapor imagery with corresponding "window" infrared or visible imagery.

LOWER CLOUDS UNDER DRY AIR ALOFT

In cases with very dry air above clouds in the lower troposphere, the radiation from the clouds will reach the satellite affecting the gray shades or "brightness temperatures." However, in some of these cases, the cloud patterns cannot be distinguished on the water vapor imagery. This is especially true of stratified cloud patterns below the "threshold" level.

Stratocumulus And Low Level Altostratus

Patterns and cells within stratocumulus fields are rarely discernible on 6.7μm water vapor imagery, even with very dry conditions above, and cells with sufficient size to be resolved on the imagery. We believe there are two basic and related reasons for this. The clouds are usually below the "threshold" level where moisture at common relative humidities is nearly opaque to radiation. Secondly, relatively small and shallow vertical motion regimes are involved in the formations of the cloud patterns. Therefore, the radiation originating from the adjacent clear regions is of similar intensity as that from the cloud areas.

Cumuloform Clouds - Cold Trough Environment

Within an upper air trough environment, convective cells often expand and extend upward into the cold mid-tropospheric air. Since the associated tropopause is relatively low and indistinct, debris does not tend to spread and persist at the cloud tops. With relatively warm dry conditions prevalent above the clouds, the radiation from the cloud tops is able to penetrate to the satellite at 6.7μm, although the cloud tops are at relatively low altitudes compared to the clouds and moisture of the adjacent ridges. On 6.7μm imagery, the area of convective cells forms a relatively cold pattern, often with a cellular appearance. During later stages, moisture tends to accumulate aloft from dissipated cells; and, the residual moisture covers the areas among the active cells. The pattern on the image becomes more uniform, with individual cells obscured by the surrounding moisture. Since the cloud tops and residual moisture are in very cold air, the pattern on the image is often of equal gray shades, or even lighter, than the moisture of the adjacent ridges, which is in much higher and colder air. Such convective cells range in top height from 700mb to 400mb, from case to case; whereas the top of the moisture of the adjacent ridges is likely to be between 250mb and 150mb. This type of cellular moisture pattern is more likely over oceanic areas than over continents. The patterns are associated with the mid-tropospheric thermal trough portion of the overall cyclonic flow field. Therefore, they are likely on the western side of the axis of a "digging" trough, or moving along the left side of a speed maximum in the jet stream zone (Northern Hemisphere).

f. Gray Shade Interpretation - A Practical Guide

Generally, with 6.7μm imagery, the use of gray shades to determine the vertical distribution of moisture is very difficult. The degree of difficulty depends upon the atmospheric conditions and the accuracy desired. Even with 6.7μm data in the form of calibrated brightness temperatures, the problems are complex. However, in many cases, the gray shades and their patterns may provide useful information on moisture regimes and their relative vertical structures. The following outline is intended as a rough guide to estimating the vertical moisture distribution. Generally, the concepts apply to middle latitude, moderate season temperature regimes.

Condition A - Gray Shades - Very Light to Nearly White (lightest 10%)

Cirrus clouds are likely. The patterns are often recognizable by a textured appearance and relatively distinct edges with respect to surrounding slightly darker gray shades. Nearly white uniform patterns and poorly defined edges usually indicate cirrus cloud tops with moisture above.

Exceptions: Very cold winter season continental air - rare.
Nearly saturated upper tropospheric moisture at tropical latitudes - relatively common at low latitudes.

Condition B - Gray Shades - Light to Very Light (75-90% of white)

Significant moisture is present in the upper middle troposphere -typically with single digit dewpoint depressions through a layer of at least 100mb thickness, between 500 mb and 300mb. May be larger dewpoint depressions through a deeper layer. May be dry in the lower and lower middle troposphere.

Exceptions: Very cold winter season continental air - common in season.
Combinations of middle clouds and moist layers - common but often detectable by patterns and texture.

Condition C - Gray Shades - Very Dark to Nearly Black (lower 40% of shades)

The air is very dry in the middle and upper troposphere. Dry air probably extends down to 700mb - perhaps near the surface. Deep dry conditions most likely if the dark area is becoming darker with time or expanding in area. If the dark area has a well defined distinct boundary, the very dry conditions probably extend to lowest altitudes adjacent to the boundary.

Exceptions: The dark area is decreasing in size or becoming lighter with time - thin high moisture may be present.
Residual dark areas at tropical latitudes or summer season middle latitudes often have thin high moist layers.

Condition D - Medium Gray Shades (40 to 75% of whiteness scale)

The vertical location of the moisture cannot be determined. It cannot be reasonably well estimated from the gray shades alone, except that conditions A, B, and C can be considered very unlikely. Numerous combinations of moisture conditions and clouds may produce the medium gray shades. A moist layer in the upper troposphere with significant radiation penetrating from below may produce an identical gray shade as a layer or top of the moisture in the lower middle troposphere. The following techniques may help resolve the problem in many cases.

Pattern Recognition: The gray shades may be associated with a recognizable pattern that will enable the relative altitude to be estimated. (See Part Two)

Source Recognition: The moisture pattern may extend from some recognizable source, such as downstream from a cloud area or thunderstorm anvils. It may be residual from dissipated clouds recognized from other imagery.

Movement: The direction and speed of movement may be useful in estimating the vertical location, based upon known or suspected vertical differences in wind directions.

Partial or Past Upper Air Data: A past radiosonde report may be available within the same moisture pattern tracked from previous images.

This page intentionally left blank

PART TWO

PATTERNS AND FEATURES ON 6.7μm WATER VAPOR IMAGERY

In Part Two patterns and features observed on 6.7μm water vapor imagery are illustrated and discussed, and related to the associated circulation systems and atmospheric processes.

PART TWO - SECTION TITLES

SECTION A.	BASIC TYPES OF BOUNDARIES
SECTION B.	EVOLUTION OF FEATURES
SECTION C.	CYCLOGENESIS AND STORM EVOLUTION
SECTION D.	MOISTURE PATTERNS OF SPECIFIC CIRCULATION SYSTEMS AND FEATURES
SECTION E.	TROPICAL APPLICATIONS

INTRODUCTION TO PART TWO

Procedures and Objectives

Our overall objective was to enable persons to more correctly interpret water vapor imagery to recognize features and changes and their relationships to the circulation systems.

There are many potential applications of single channel water vapor imagery ranging between meteorological research and operational weather analysis and forecasting. Water vapor imagery and data can provide some of the quantitative types of information required to initialize forecast models. For example, winds may be estimated by tracking moisture parcels or features and assigning vertical locations to the motion vectors. Initial moisture fields may be improved over regions of sparse conventional upper air data.

It was our contention that water vapor imagery - which is available to many operational forecast offices - could be highly useful at a later stage of the decision making process. It may be applied in conjunction with forecast model output to refine forecasts, provide better aviation weather support, and as a primary source of information over oceanic and low latitude regions. We chose to pursue relationships and knowledge which could be applied to these tasks.

Priorities

In the process of relating imagery to the upper air circulation systems, the wind field was given a higher priority than the height field. On the upper air analyses shown in the following sections, streamlines are generally shown in place of or in addition to height contours. This selection is primarily a consequence of our objectives. However, we also found that many of the features on the imagery could be related more explicitly - or better - to the wind field rather than to the height field. And thirdly, significant regions of temperature and vorticity advection, which correlate to features of the water vapor imagery, were difficult to detect and observe using height contours; since they commonly develop in conjunction with relatively large supergradient or subgradient wind components.

In relating imagery to circulation systems, a higher priority was given to atmospheric events and processes rather than conditions, although both are addressed. We address questions such as: Does the water vapor imagery indicate that cyclogenesis is beginning, progressing, or being interrupted? Is an upper air low "cutting off" or "opening"? Is a blocking situation forming or breaking? If such processes or events can be reliably identified from the water vapor imagery, the atmospheric behavior can be compared to model output. Forecasts can then be confirmed, modified, or significantly changed.

Approaches

The approaches taken in our studies have some bearing upon the material presented here and the way in which it is presented. Two related, but different, approaches were used. The first approach was to study water vapor imagery with minimum discretion to the types of associated circulation systems. All imagery collected from NOAA GOES satellites from September 1981 through May 1988 were examined. Generally, imagery were available at six hourly intervals from at least one satellite; however, there were periods of no imagery and others with imagery at one hourly intervals. Images were viewed individually and in time-lapse motion. Because of the complex interactions among multiple circulation systems, each water vapor image is unique. Patterns can be complex and difficult to understand. However, we identified various categories of patterns and features which occurred relatively frequently and over most geographical regions. These were studied to determine their behavioral characteristics and their relationships to the circulation fields. Although cases were studied at various locations, the relationships to the wind and density fields were determined by selecting well defined cases over the United States upper air data network.

The second basic approach was to choose significant atmospheric events and features, such as mid-latitude and tropical cyclogenesis; identify cases and study the associated water vapor imagery. Of the water vapor image features and changes identified from this approach, many had been noted and studied from the other approach. Therefore, their circulation system relationships were known. Others had not been identified as significant using the first approach. These were then studied in regard to their associated circulation environments; however, we were not always successful in understanding the image feature or change. If the correlation is reliable and useful, it is presented without the understanding.

Overlaid Analyses

Since we found individual cases or samples to be unique in some ways, we chose not to study specific cases in great detail but, to study many examples in less detail. Analyses can be extensively refined by careful readjustment between vertical cross-sections and constant pressure surfaces. Generally, we did not refine the analyses to a high degree, but applied a moderate degree of refinement.

In the following sections, all analyses of conventional weather data are superimposed on the satellite imagery. Generally, the analyses are modified versions of operational analyses produced by the United States National Meteorological Center (NMC), although a few were produced directly from radiosonde data. The amount of modification varies considerably depending upon the purpose of the analysis and the form of the original NMC analysis.

Generally, analyses can be improved by using satellite imagery during the analysis process. Empirical relationships can be used to identify and adjust features of the analysis. We intentionally minimized this process. Imagery were used at times to interpolate features between data points or to extend features beyond the data field, but only after its relationship to the imagery had been established by other data on the same analysis.

Upper Air Analyses

Most of our analyses are modified versions of NMC Analyses. Radiosonde data were used to fill in missing data reports and check vertical changes. Streamlines were hand drawn to the wind reports. The wind speed field was not a factor in the streamline analysis process. The intention was to illustrate the wind directions. Isotachs and isotherms were re-analyzed to reduce the degree of smoothing in the original computer produced analyses. Continuity in time - especially hindsight - was a factor in the desmoothing process. Maintaining vertical balance in the density field was not a requirement for our purposes. Intermediate isopleths were added when useful to better define the data field; however, isotherms are routinely shown at 5°C intervals, and isotachs are shown at 20 knot intervals at 70 knots and greater values. On many analyses, axes of maximum winds are shown by series of arrows or arrowheads oriented parallel to the wind direction. These are not three dimensional jet stream core analyses, merely axes of maximum wind speed on the specific constant pressure surface. In some cases, arrowheads were placed end to end instead of parallel to the wind direction. Also, some jet stream core analyses are used. These exceptions are noted in captions or in the related discussion.

Surface Analyses

Fewer surface analyses are shown in the following sections, since their relationships to the 6.7μm imagery are generally implicit. All of those shown are modified versions of NMC operational analyses. Isobaric fields were used as originally analyzed or modified only slightly. Surface frontal positions were re-analyzed. Adjustments were primarily the consequence of hindsight and more time available for subjective analysis. Surface low pressure positions and central minimum pressure values were adjusted slightly by constructing storm tracks and pressure change curves.

Analyses were hand transferred from the original map projection to the satellite image map projections. Most analyses shown were completed during the research phase of our work.

SECTION A
BASIC TYPES OF BOUNDARIES

Perhaps the most important features on water vapor imagery are the boundaries between different moisture regimes. We found that understanding the boundaries was a key to understanding the overall moisture patterns.

From observations of water vapor imagery, we identified common types of boundaries, based upon their different characteristics and behavior on the imagery. The most prevalent and significant of these were then categorized into seven basic types, for the purpose of presentation here. In this section, the boundary types are defined and illustrated, with emphasis on their image characteristics and behavior. Although the circulation environment of the boundaries is used in the categorization scheme, specific applications and relationships to the wind and temperature fields are discussed more thoroughly in subsequent sections, in context with associated circulation systems and atmospheric processes.

Some of the boundaries observed on water vapor imagery are cloud edges or cloud system borders. These do not necessarily represent significant differences in moisture regimes across the borders. However, many cloud edges or cloud system borders are also boundaries of significantly different moisture regimes. This is especially true when the boundary appears "distinct" on the water vapor imagery - a large gray shade difference is present across a small horizontal distance.

In our discussion of boundaries, we shall begin with some overly simplified concepts; then, reinstate the complexity in the description of individual cases. Although horizontal temperature differences can be a factor, distinct boundaries or differences in gray shades on water vapor imagery usually represent a difference between moisture aloft on the cold light gray side and drier air aloft on the warm darker gray side. Consider the following four processes which may contribute to such differences in the upper air moisture fields:

[1] Moist air may rise over one region, without a significant change in the adjacent ambient conditions.

[2] The opposite may occur. Moist air may sink over an area - being replaced by dry air aloft - resulting in new dry upper air conditions adjacent to unchanged moist ambient conditions.

[3] A moisture boundary may result as a combination of the first two processes. Moist air may sink adjacent to an area of rising moist air.

[4] Horizontal deformation processes without significant vertical motions on the same scale may cause an initially gradual or indistinct moisture gradient to become well defined and distinct.

The fourth simplified process - involving the role of horizontal deformation - is usually associated with a hyperbolic circulation regime, or a "col" in the related wind field. The boundary forms, or becomes distinct, along the stretching axis of the hyperbolic region. We shall refer to such stretching axes as "deformation zones". When the associated circulation systems are moving, the hyperbolic field may not be present in the winds or air motions with respect to the earth, but be significant in the air motions with respect to the moving systems. In those cases, the "deformation zone" effects are present although not explicitly revealed in the wind fields.

Most significant boundaries observed on water vapor imagery involve a combination of the horizontal deformation process and one or more of the vertical motion processes. However, considering the effects individually is useful in understanding basic differences in the types of boundaries. Often, one of the vertical motion processes plays a dominant role to establish the specific characteristics of the particular boundary type.

TERMINOLOGY

On a water vapor image, gray shades may change gradually across a horizontal distance, or they may change abruptly forming a discontinuity of significantly different gray shades between adjacent image pixels. We have chosen the word "boundary" to apply to an interface between adjacent areas of different gray shades, where the interface appears relatively abrupt, as opposed to a gradual change across a large distance. On water vapor imagery, the "abruptness" of the interfaces, or the horizontal gray shade gradients, vary significantly. Choosing a threshold at which a gradient becomes a boundary is an arbitrary decision, and will remain so in this presentation. No quantitative definition was chosen, because of different requirements for various applications, and the variability of the image reproduction. However, it is necessary to describe such differences and their changes with time. Therefore, we have chosen some terminology to apply to different or changing conditions.

"Definition" We shall use the term "definition" to describe two aspects of boundary conditions. It is used to describe the "abruptness", the amount of gray shade gradient; and the regularity of the shape. For a boundary to be "well defined", it must be abrupt and of regular shape. Perturbations may be present, but they must be systematic in shape, as opposed to ragged. The gray shade differences involved need not be large; however, they must occur across a relatively small horizontal distance.

Distinctiveness The amount of gray shade difference across a boundary. A boundary would be very distinct, if the shades changed from near white to near black across the interface.

Some aspects of the use of "definition" and "distinctiveness" may be illustrated on the adjacent drawing, on which four graphs of gray shade differences and image distance are shown. For example, on the first graph, a boundary would appear well defined with only a 10% gray shade change, if it were a discontinuity; however, it would not appear distinct. If that change occurred over some finite distance, as in the second graph, it would appear both indistinct and poorly defined. A 30% gray shade change across that same distance would appear better defined, because of the larger gray shade difference; and, it would appear more distinct. And, finally as implied by the fourth graph, a large gray shade difference occurring as an interface, would appear both well defined and distinct.

Bands or Slots Such elongated zones of either dark or light gray shades have finite width; and, have *two* boundaries associated, one on each side. The term "band" is applied to both light and dark features, whereas the term "slot" is applied to only dark zones. Generally, the term "dark band" implies a narrower feature than the term "slot".

Edge We shall sometimes substitute the term "edge" to refer to a very poorly defined interface, when the gray shade differences occur over a long distance or are of irregular shape.

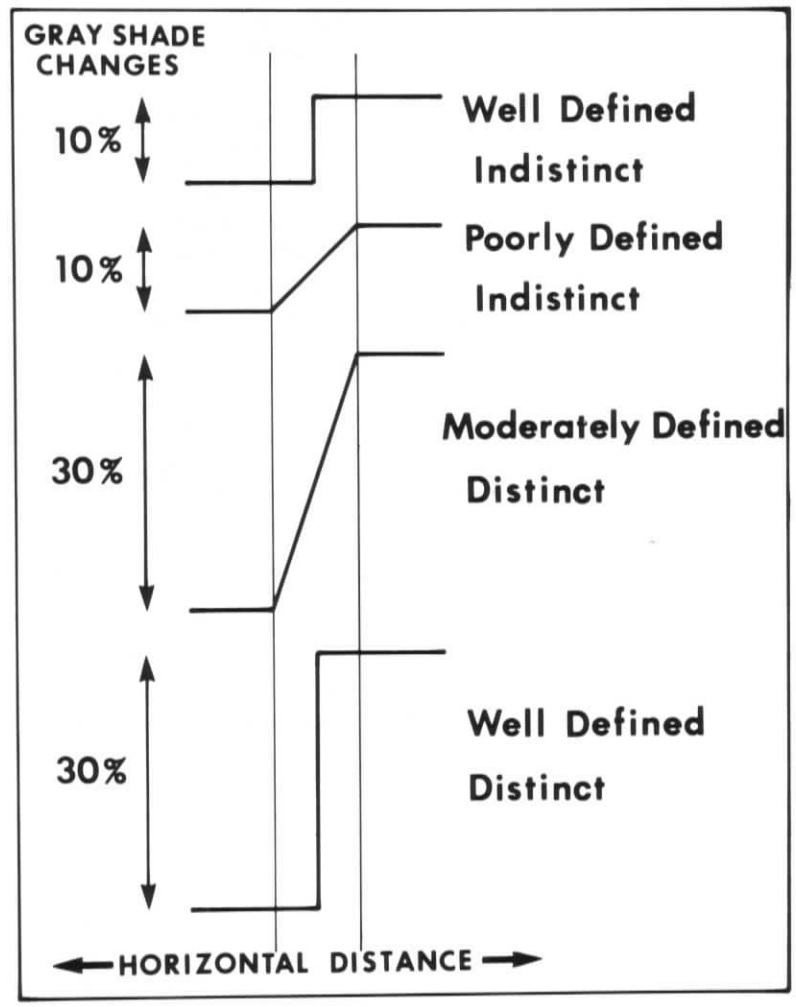

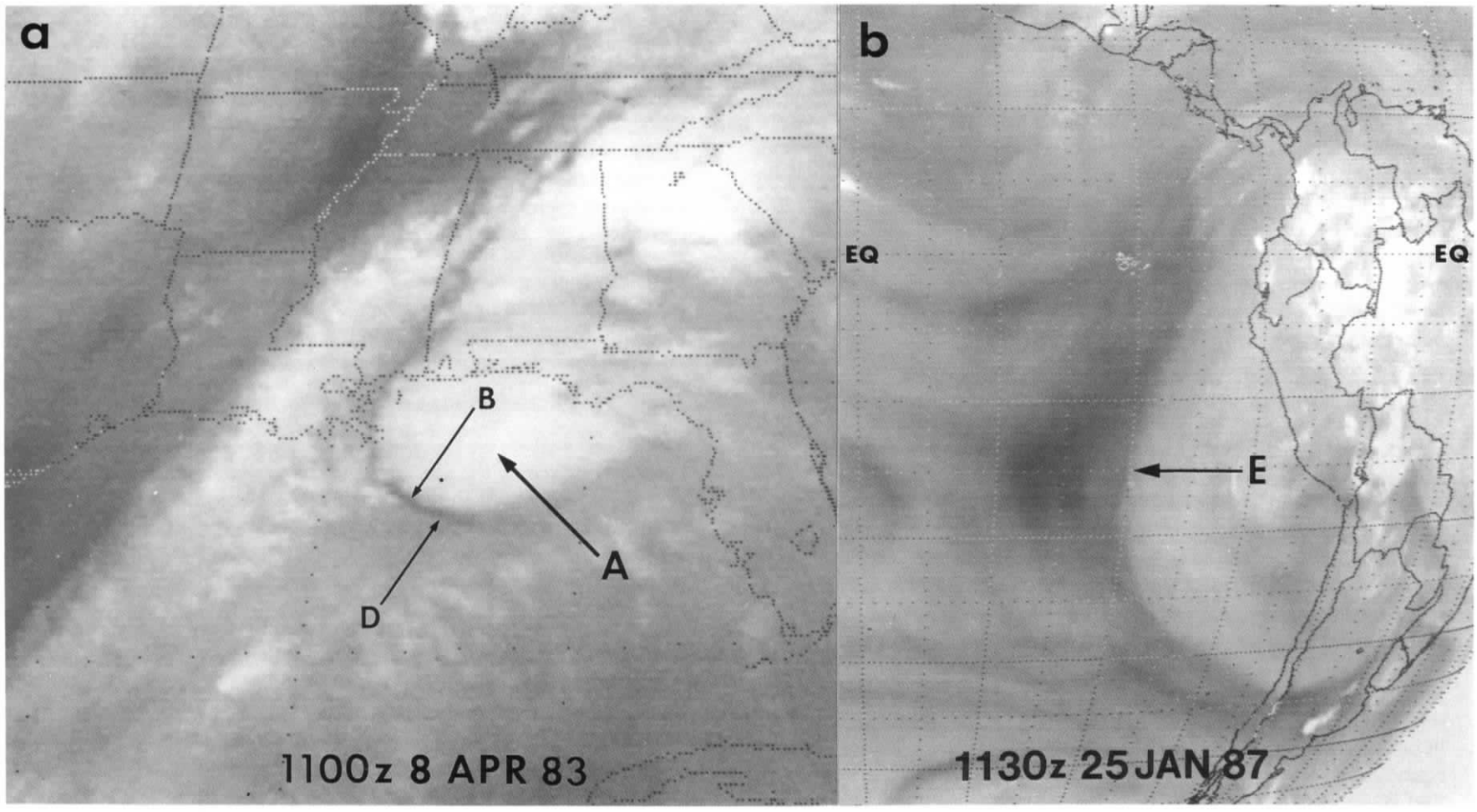

Figure 1 HEAD BLOCKING - CONVECTIVE AND CONTINENTAL SCALES
Fig. 1a. 6.7μm Image, 1100Z 8 April 1983, GOES East.
Fig. 1b. 6.7μm Image, 1130Z 25 January 1987, GOES Central.

1. HEAD BOUNDARIES

a. "Head Blocking" - A General Concept

One of the most common types of boundaries observed on water vapor imagery forms in response to moisture spreading in the upper atmosphere from areas of upward vertical motion. The spreading of the upper level moisture becomes "blocked" on one side, where it attempts to spread in the opposite direction to the ambient upper air wind field. Generally, a well defined boundary forms on the upstream side of the moisture regime produced by the upward vertical motion. We refer to this specific type of blocking process as "head blocking". The boundaries formed by this process occur at many different scales, and at various levels within the atmosphere. Those which occur in the lower troposphere are usually not observed on 6.7μm imagery.

An example of a boundary formed by "head blocking" at the convective scale is shown on **Figure 1a**. A thunderstorm complex is located at "A" over the Gulf of Mexico within a regime of strong upper air southwesterly winds. A well defined boundary is present at "B" on the upstream side of the cloud system, where the spreading upper air moisture and cloud anvil are "blocked" by the opposing flow. In this case, comparison with infrared imagery indicated that the boundary "B" on the water vapor image was nearly coincident with the edge of the cloud anvil. In some cases, the upper air moisture extends beyond the cloud edge; but, the coincidence of the cloud and moisture edges, as in this case, is common with "head blocking" associated with thunderstorms.

Note that a narrow dark area or band is present at "D" adjacent to the boundary "B". Such dark bands are commonly observed along the dry sides of boundaries formed by the "head blocking" process. We believe that this narrow dark zone, and similar ones with other cases, are caused by localized downward vertical motion in response to upper air convergence between the spreading high level moist air and the upstream ambient flow. Similar dark zones related to larger scale systems will be shown and discussed.

Another example of a boundary produced in a similar manner is shown on **Figure 1b**, at "E". In this second case, the feature and the circulation systems involved are of the continental scale. During this season of the year, thunderstorm activity over South America produces a huge upper level moist region. Although the convective clouds occur in diurnal cycles, the upper air moisture accumulates and attempts to spread away from the continent in all directions. When significantly strong high level westerly winds are present over the southeastern Pacific Ocean region, as in this case, a well defined boundary forms on the western side of the South American moisture regime. Generally, a col forms in the high level wind field between the moist easterly winds and the drier Pacific westerlies. Some of the moist air turns anticyclonically southward, and part turns cyclonically northward and across the equator.

The two boundaries shown on **Figure 1**, although of markedly different scales, are both cases in which the dominating process was moisture accumulating at high levels by upward vertical motion. The second process involved was that of upper air "blocking" or deformation between the spreading moist air and ambient air.

b. "Head Boundaries" of Synoptic Scale Systems

Although the "head" blocking patterns occur over a large range of scales, as demonstrated by **Figure 1**, we shall apply the term "head boundary" to systems of the synoptic scale. Two synoptic scale systems with head boundaries are present on the water vapor image of **Figure 2a** which is repeated on **Figure 2b** with a 300mb analysis superimposed. The case was chosen to illustrate the head boundary labeled "A". The presence of a second head boundary, at "B", was coincidental. Head boundary "A" is an excellent example, with many of the image characteristics common to head boundaries in general. We shall discuss those features first, then point out the significant relationships to the circulation systems.

Image Characteristics of Head Boundaries

Basically, a head boundary consists of a relatively well defined interface between an area of high clouds and cold upper level moisture on one side, and varied conditions on the drier side. As with convective scale and continental scale examples shown on **Figure 1**, the high level clouds and moisture tend to accumulate and spread from an area of upward vertical motions. The well defined head boundary forms on the "upstream" side of the spreading high level moisture, where that moisture is spreading toward, or "blocking", the ambient upper air winds. Note on **Figure 2a**, that the head boundary "A" is very well defined from point "C" over Lake Superior southward along the western side of the cold clouds and moisture, and including that part over the Gulf of Mexico. However, the distinctiveness of the boundary varies along that same length. The difference in distinctiveness is related to varied conditions along the dry side of the boundary; whereas, the conditions on the cold side are relatively uniform. The uniformity on the moist side and variability on the dry side is an important common characteristic of head boundaries. That portion of the head boundary over Texas and the Gulf of Mexico is relatively distinct, because there is a narrow dark area or band present on the dry side of the head boundary. That dark band is indicated at "D". From the perspective of the dark band, the northeast side, formed by the head boundary, is both distinct and well defined. The opposite side of the dark band, generally toward the southwest, is poorly defined; the edge consists of a gradual change to lighter gray shades. Narrow dark bands of this type are often observed along head boundaries or portions of head boundaries. Generally, the darkest or driest part of the band is directly adjacent to the head boundary; and, the side opposite to the head boundary is poorly defined, either gradual or irregular, or a combination of both.

Before continuing, we must point out that a part of this appearance on water vapor imagery is caused by an optical illusion. When two areas of different gray shades are located adjacent to each other with a sharp or discontinuous interface, a gradient will appear to be present in each gray shade directly adjacent to the interface, even though each of the shades is uniform. This illusion is more apparent on the darker side of the interface, where the gray shades appear to be darkest directly adjacent to the interface. Also, the effect is greater when the gray shade difference across the interface is relatively small; therefore, covering the lighter side with a piece of white paper will usually reveal the illusion. This illusion can be observed under controlled conditions by viewing a photographic step-wedge, such as those often present across the tops of many satellite images. Although each gray shade in the steps is of constant gray shade, each will appear to have a slight gradient within it. We have taken this problem into account in our descriptions of the imagery in this case, and elsewhere within the text.

In regard to the narrow dark bands often observed directly adjacent to head boundaries, we have viewed these in many cases, often using both water vapor and other satellite imagery in time-lapse motion, and in some cases additionally in time-lapse motion from camera systems looking upward from the ground. These observations indicated that an area of downward vertical motion is common along the head boundaries. Although this downward vertical motion, or sinking zone, may extend for long distances along the boundary, the effect is very localized in the direction orthogonal to the boundary, and in vertical depth. We believe that localized downward vertical motion is present, and that it is caused by upper level convergence between the ambient upstream flow and the "blocking" flow from the moist side. There were also indications that a localized zone of upward vertical motion may be present along the boundaries above the level of maximum convergence; however, in regard to water vapor imagery interpretation, we are concerned with the sinking portion related to the dark zones. Radiosonde observations indicated that the narrow dry zones are variable in depth, but are usually confined to the upper troposphere, generally above 500mb. This relatively shallow upper air depth of the dark zones adjacent to head boundaries is not true of some of the other types of dark zones or slots that will be discussed with subsequent topics.

Note on **Figure 2a**, that the distinctiveness of the head boundary varies significantly along the northwest portion, to the north of Texas. This type of variation, caused by different conditions on the upstream drier side, is common with head boundaries; and, especially those which have persisted for a relatively long period, as in the case shown.

Upper Air Analysis Features Related to Head Boundaries

The 300mb analysis on **Figure 2b** contains streamlines, isotachs, and arrowheads indicating the axes of maximum winds with speeds of 70 knots or greater. Note that the arrowheads have been placed parallel to the wind directions rather than parallel to the axes of maximum winds. This standard procedure will be used with most upper air analyses in this presentation. The exceptions will be noted.

In the case shown here, the upper air system is associated with a "warm core" tropical cyclone centered near the southern coast of Louisiana. The system had been present for several days and nearly stationary. Consider the large cold upper air moisture regime on the eastern side of the head boundary"A". A part of that regime is associated with cyclonically curved flow at 300mb, and an even larger portion is associated with anticyclonically curved flow. As the upper air cyclone closed, the upper air ridge "built back" around the northern side of the low. The moisture accumulated at high levels from the upward vertical motions, moved westward within the upper level easterly wind regime between the ridge and the cyclone. Where this moisture encountered the upstream opposing westerlies, a "blocking" effect formed. A part of the moisture turned anticyclonically northward around the "build-back" ridge, and another part turned southward around the upper air cyclone. This division or "split" in the moist side flow is centered over central Texas on the 300mb streamline pattern shown. A similar "split" in the flow occurred in the drier air approaching within the upstream westerly winds. That "split" in the upper air streamlines is located over northwest Texas and eastern New Mexico. Together, these flow patterns form a col in the 300mb streamlines. Note the asymmetry of the col pattern, relating to the fact that the "splits" in the opposite sides of the col are not aligned. This condition is common; and, the systematic variations in such asymmetry are related to the evolutions of systems. This will be addressed in later sections. Of significance here, is the fact that the head boundary is located along the stretching axis of the col, which we shall refer to as a "deformation zone". The upper air winds along the boundary in the col region are very light at the level of the boundary. North and south of the col region, the wind speeds increase, in opposite directions, and the streamlines are nearly parallel to those portions of the head boundary.

The foregoing relationships between head boundaries and their associated upper air wind fields are common with the mature stages of storm systems within an environment of upper air westerlies. In those cases, the systems are stationary or slowly moving with a closed upper air cyclone and a significant region of upper air easterly winds on its poleward side. The head boundary is formed between the easterly winds and the upstream westerlies and is likely to be nearly stationary in that region. In such cases, there are likely to be two jet stream branches associated with the head boundary. One will be along the equatorward end of the head boundary; but, the axis of maximum winds of this branch will not coincide with the head boundary itself. The axis is likely to be parallel to a part of the head boundary, but on the dry air side. In this case, such a branch is present over northeastern Mexico and the Gulf of Mexico. A second jet stream branch is likely along the poleward end of the head boundary; and, the axis of maximum winds of that branch is likely to coincide with a portion of the head boundary. Although these jet stream branches along the poleward end are more common, none is present in the case shown here. In this case, a jet stream branch had been present along that portion extending southeastward from point "C"; however it has dissipated in response to changes in the mid-tropospheric thermal field. This type of change with time will be illustrated and discussed primarily in Sections B and D.

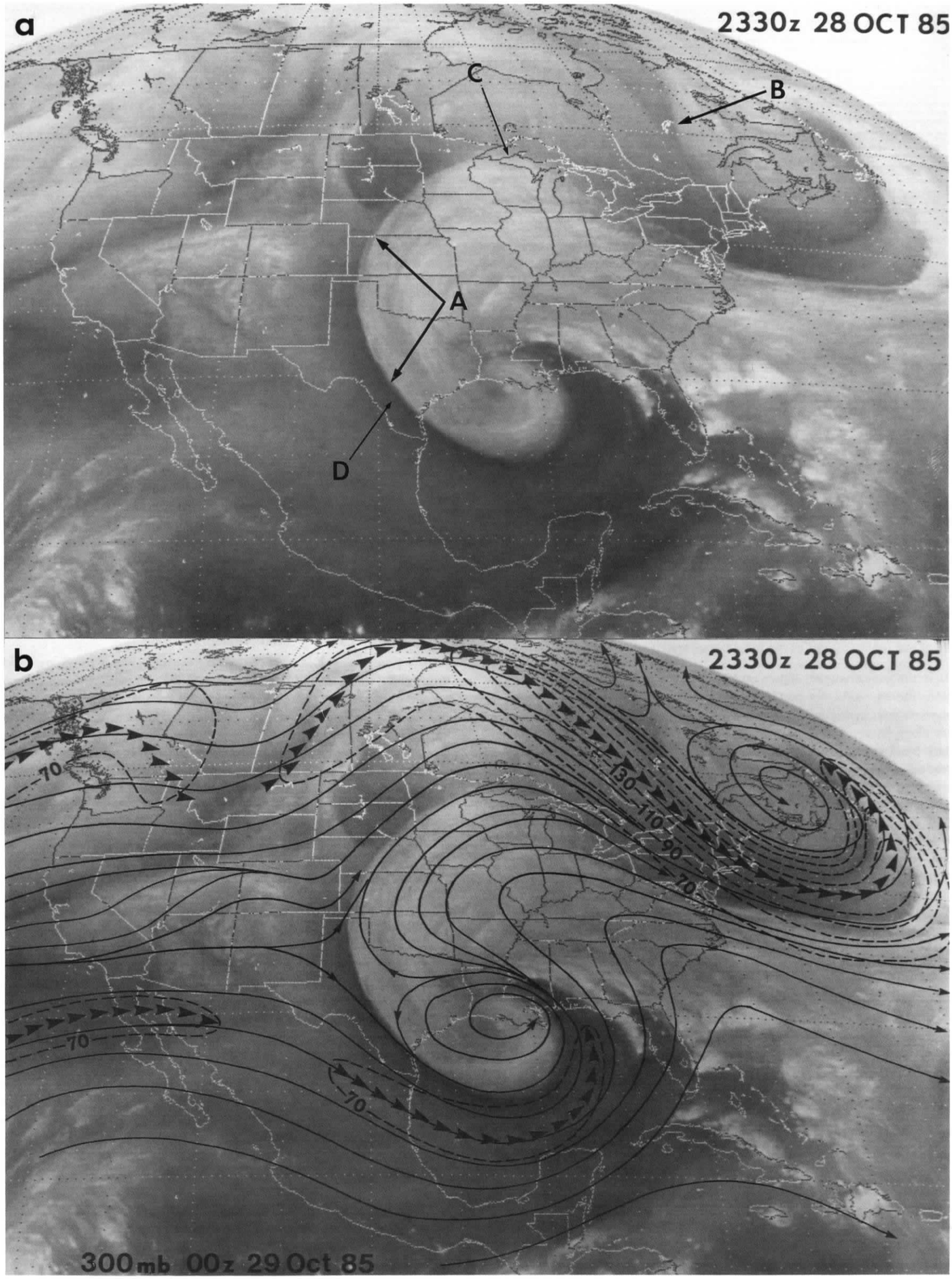

Figure 2 HEAD BOUNDARY - CLASSICAL EXAMPLE

Fig. 2a. 6.7μm Image, 2330Z 28 October 1985, GOES Central.

Fig. 2b. Same Image with 300mb Analysis, 0000Z 29 October 1985. Thin solid lines - streamlines. Arrowheads - axes of 300mb maximum wind speeds. Dashed lines - isotachs in knots.

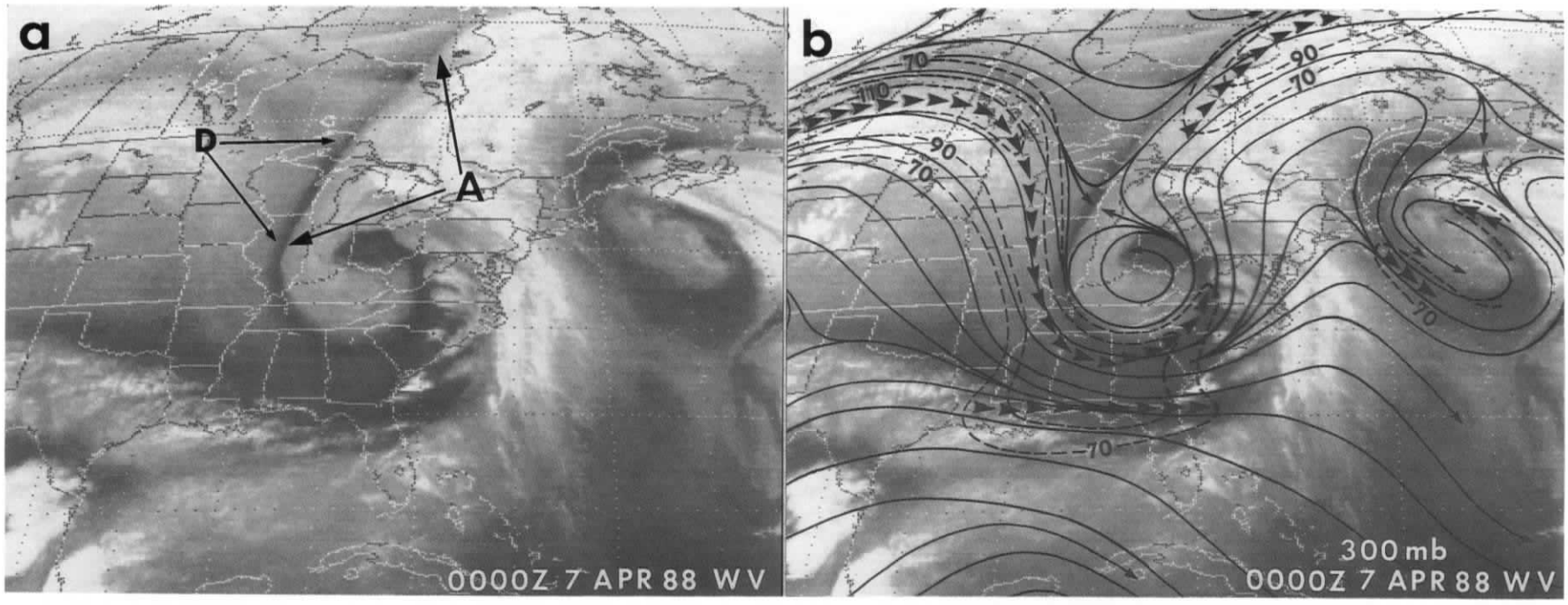

Figure 3

SYNOPTIC SCALE HEAD BOUNDARY
Fig. 3a. 6.7μm Image, 0000Z 7 April 1988, GOES East.
Fig. 3b. Same Image with 300mb Analysis. Solid lines - streamlines. Dashed lines - isotach in knots. Arrowheads - Axes of 300mb maximum wind speeds.

Another example of a head boundary is shown on **Figure 3**. The head boundary is indicated at "A" on **Figure 3a**, and the image is repeated with a 300mb analysis on **Figure 3b**. The associated weather system, in this case, is a winter storm system. However, the basic relationships between the head boundary and the upper air wind field are similar to those of the last case. The head boundary is located along the stretching axis of a col in the 300mb wind field, and is nearly parallel to the wind directions to the north and south of the col. In this case, a jet stream branch is present along the poleward end of the head boundary.

As in the previous case, shown on **Figure 2**, there is a narrow dark band along the west side of a portion of the head boundary. The band is even more obvious in this case, because there is a relatively well defined boundary along its western side, indicated by "D". The upstream edge of the dark band in the previous case consisted of a gray shade gradient with gradual change to lighter shades. That gradual or irregular type of upstream edge to the dark bands adjacent to head boundaries is more commonly observed than the well defined type present in this case at "D". The very narrow width of the dark band between "D" and "A" is common with head boundaries. That fact that very narrow dark bands, such as this one, remain present for long periods of time (often 24 hours or longer) suggests that the dry air is not merely residual, and that localized downward vertical motion may be maintaining the feature. This is also implied by observing water vapor imagery in one hourly time-lapse motion. Usually, small moisture parcels approaching the dark band from the western side disappear at the western edge of the dark band, suggesting downward vertical motion there.

Head boundaries vary significantly in their shapes, and in their relationships to specific wind field features, especially during the earlier phases of system development. The boundaries, and their changes with time are very useful in applications of water vapor imagery to analysis and forecasting. Many examples will be shown in the following sections; and, the variations and applications will be discussed.

2. BOUNDARIES ON THE FORWARD SIDES OF UPPER AIR TROUGHS

Since the boundaries on the forward sides of upper air troughs are often very significant to the forecasting of weather conditions and their changes with time, we have included these as a special category. Within this category, we have identified three basic types of boundaries. Two of these, referred to as "dry surge boundaries" and "baroclinic leaf boundaries" are unique types of boundaries, and would be designated as basic types of boundaries with specific image characteristics and relationships to the upper air wind field. However, since they both occur on the forward sides of upper air troughs in the westerlies, it is useful to discuss them together. Since these are not the only types of boundaries found on the forward sides of troughs, we have designated a third type common to that location. This has been designated a "parallel jet stream" type. Therefore, three types of boundaries on the forward sides of troughs will be illustrated and compared. This special grouping of boundary types is of additional value, because boundaries on the forward sides of upper air troughs often occur in combinations, or are present in a stage of transition between different types.

Before proceeding, it is useful to comment on the use of the "parallel jet stream" designation. Jet streams occur in other locations in addition to the forward sides of troughs. Many of those have moisture boundaries parallel to, or coincident with, their axes of maximum winds. However, the variability of these types, and their specific relationships to the associated wind fields, is large. For that reason, we did not categorize basic boundaries in regard to the jet stream relationships, except on the forward sides of troughs. Jet stream relationships to water vapor image features will be illustrated and discussed specifically in Section D, and in many other topics in context with other subjects. Although the relationships of jet stream conditions and water vapor imagery is often one of the first questions raised, the variability and complexity of the subject, requires that it be addressed near the end of this presentation.

To the subject designation, boundaries on the forward sides of upper air troughs, we shall add the condition that the upper air winds are westerlies. Therefore, the boundaries involved are most frequently on the eastern sides of the troughs, or in some cases, the northeast or southeast sides. As implied, the troughs involved are not stationary, but moving, and with some eastward component of direction. Image features related to stationary systems, and those within upper air easterly winds will be discussed with other topics.

A common characteristic of moisture boundaries on the forward sides of upper air troughs is that they are often very distinct. There are two reasons for this. High clouds are often present along the moist sides of the boundaries. This causes the gray shades on the moist sides to be very light, because the clouds prevent radiation from lower warm sources to penetrate to the satellite. Secondly, vertically deep dry areas, or "slots" are often present along the drier upstream sides of the boundaries. These dry zones tend to be deeper (extend downward to lower levels) than those usually associated with head boundaries. Generally, they are also wider than the dry bands or zones adjacent to head boundaries. Therefore, the image gray shades to the rear of the boundaries are often very dark; and, a large contrast of gray shades will be present across the boundary. Although some boundaries on the forward sides of troughs are very well defined, they are generally not as well defined as head boundaries. There is more variability in the vertical slopes and in cloud conditions with boundaries on the forward sides of troughs than with head boundaries.

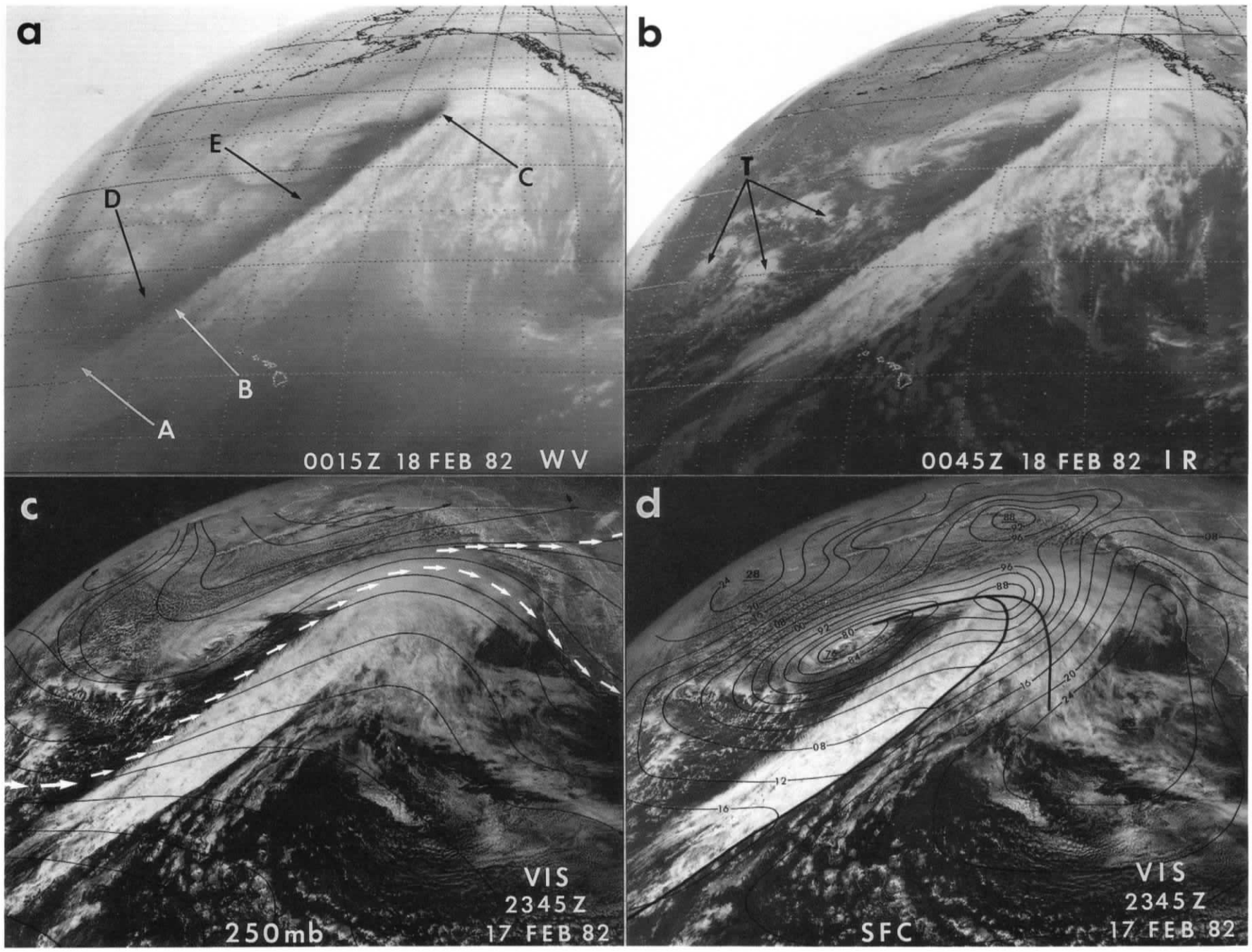

Figure 4 **PARALLEL JET STREAM BOUNDARY**

Fig. 4a. 6.7μm Image, 0015Z 18 February 1982, GOES West. **Fig. 4b.** 11.2μm Infrared image, 0045Z 18 February 1982. **Fig. 4c.** Visible Image, 2345Z 17 February 1982 with 250mb analysis. Black lines - streamlines. White arrows - Axes of 250mb maximum wind speeds. **Fig. 4d.** Same visible image with surface isobars and frontal locations.

a. Parallel Jet Stream Boundaries

Although the boundaries on the forward sides of upper air troughs often occur in combinations, or in transition from one type to another, they also occur primarily as a single type. Of those single types, the most common is the parallel jet stream type. With these cases, the jet stream axis of maximum winds is most likely to be nearly coincident with the moisture boundary. The second most common condition is that the axis of maximum winds will be parallel to the moisture boundary, but on the dry side. In some cases, primarily during the "slotted phase" of winter storm evolutions, two separate levels of maximum winds will be involved with the jet stream structure. In those cases, the higher level axis of maximum winds is likely to be on the moist side of the boundary; and, the lower level axis is likely to be within the "dry slot" and parallel to the boundary.

An example of a boundary with a parallel jet stream is shown on **Figure 4** with water vapor, infrared, and visible imagery. The visible image is shown twice with 250mb and surface analyses superimposed. Although all images on the figure are of the same scale, the area of view of the visible images is farther to the east than that of the water vapor and infrared images. Note that the water vapor image is also shown on **Figure 63b** in Section D with the 250mb analysis superimposed. There, the jet stream conditions and relationships to the image are discussed in detail. The weather system, shown on **Figure 4**, over the northeastern Pacific Ocean includes a vertically deep cold frontal zone in advance of the upper air trough. Cloud conditions within the frontal zone consisted primarily of multiple layers ranging from fractostratus to cirrostratus. The primary moisture boundary in advance of the upper air trough, designated "A-B-C" on the water vapor image, coincided with the cirrus cloud edge seen on the infrared and visible images, except along the southwestern end where the clouds along the upstream side of the frontal zone are at middle and lower levels. The 250mb axis of maximum winds, indicated by white arrows on **Figure 4c**, is near and parallel to that portion of the moisture boundary from "B" to "C". Along the "A-B" portion of the boundary, the 250mb axis of maximum winds is not parallel to the boundary, but approaches from the west at an angle, becoming parallel at "B". Although the axis of maximum winds is parallel to the moisture and cloud boundary from "B" to "C", the wind directions are not. At the southwestern end of the boundary, from "A" to "B", the 250mb streamlines cross the boundary at relatively large angles. Northeastward along the boundary from "B" to "C", the crossing angle between the streamlines and the boundary decreases, such that the streamlines are nearly parallel to the boundary, and to the axis of maximum winds, at "C". This particular configuration of the axis of maximum winds, the wind directions, and the boundary, is very common with boundaries on the forward sides of upper air troughs.

With boundaries on the forward sides of upper air troughs, there is usually a dark zone of elongated shape on the water vapor imagery, along the rear side of that portion of the boundary which is parallel to the jet stream. These elongated dark zones of dry air in the middle and upper troposphere are generally parallel to the primary moisture boundary and the associated axis of maximum winds. The shapes of the dark zones are dependent upon both the primary moisture boundary on the downstream side, and a second boundary along the upstream side. The variations of such dark zones are largely influenced by the differences of the boundary conditions on the upstream side and the moisture regimes present there. Consider the dark zone to the rear of boundary "B-C" on **Figure 4a**. That portion of the dark zone to the northeast of point "E" is wider and darker than the portion to the southwest of "E". The

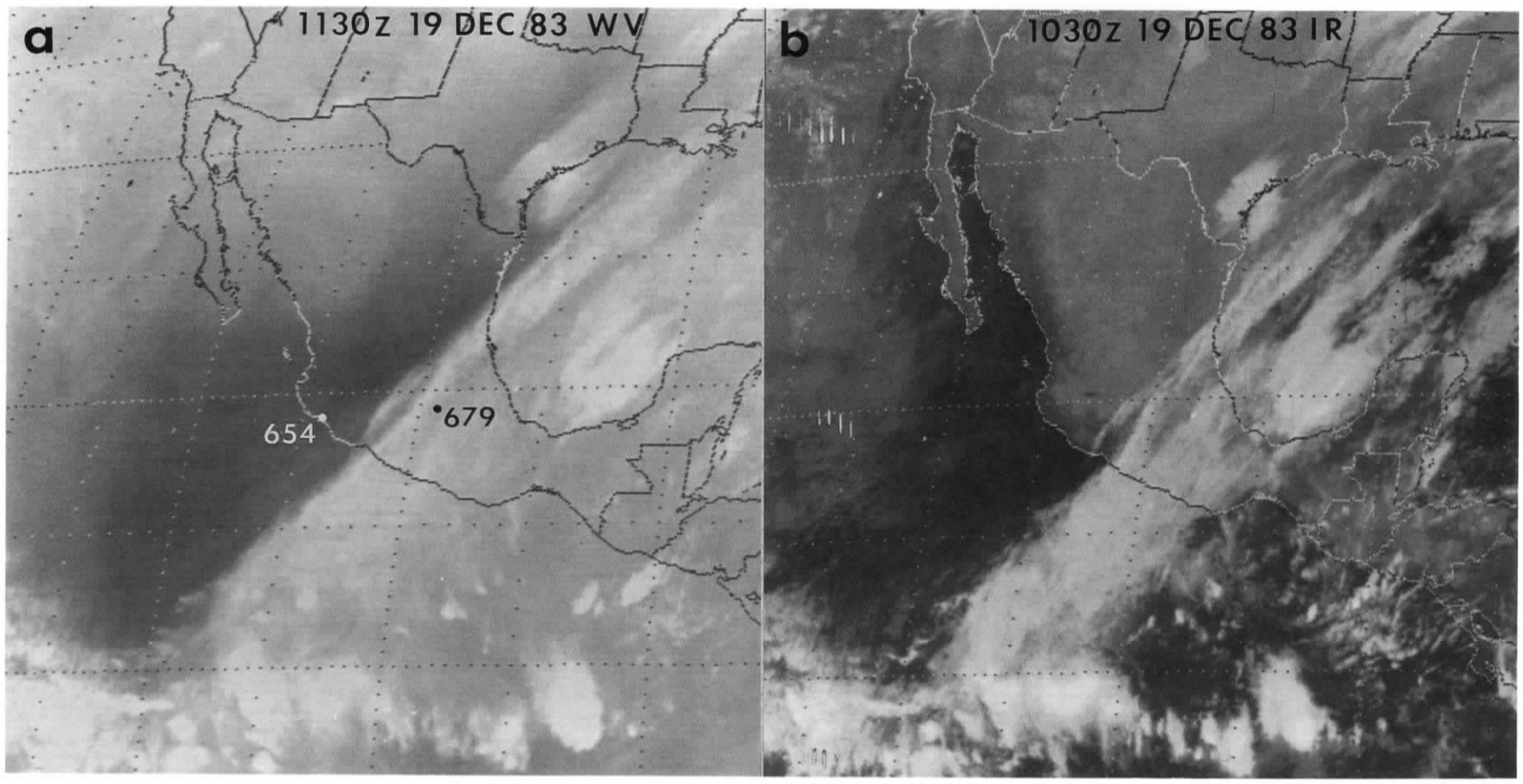

Figure 5

PARALLEL JET STREAM BOUNDARY - ITCZ "FLARE-UP" SYSTEM
Fig. 5a. 6.7μm Image, 1130Z 19 December 1983, GOES East. Radiosonde Sites: 654 = Manzanillo, 679 = Mexico City.
Fig. 5b. 11.2μm Infrared Image, 1030Z 19 December 1983, GOES East.

northeastern part is an example of a classical "dry slot" as the term is generally applied to winter storm systems. The clouds and upper air moisture forming the upstream side of the dry slot - the northwestern side - is a part of the "head" portion of the storm pattern. This portion has "built back" around the northern side of the storm system from the downstream side; or, has fallen back in a relative motion sense, as the portion along the jet stream zone moved more rapidly. These processes, both of which were involved in this case, will be discussed in subsequent sections. Generally the dark zones of the "dry slot" category are vertically deep with dry air extending downward to near the surface. The depth in this case is implied by the absence of even low clouds in the dry slot area on the infrared and visible images. That part of the dry zone between "D and E" is not as wide as the "dry slot" portion, and the upstream boundary along the rear side of that part is poorly defined and less distinct compared to the northwest side of the "dry slot". Note on the infrared image, the large area of convective cloudiness identified by "T". Such clouds are common over oceans within upper air troughs on the left sides of the jet stream (right side - Southern Hemisphere). Cold air is present in the middle troposphere and the tropopause is relatively low and indistinct. Although the cirrus debris from the convective cloud clusters does not persist and merge with that of adjacent clusters, moisture does accumulate at high levels. In this case, that moisture produced by the convective clouds moved eastward over the drier mid-tropospheric air and formed the rear side boundary of the dry zone between "D" and "E". This illustrates one of the ways by which the dark zones vary along the forward sides of upper air troughs.

Another boundary of the "parallel jet stream" type is illustrated on **Figure 5**. Unlike the last case, with its vertically deep cold frontal zone and moderately strong surface front, the boundary of this case is primarily a feature of the upper atmosphere. The cloud system shown on **Figure 5b** is of the category we have referred to as "flare-ups" or "ITCZ flare-ups". The condition occurs when moisture accumulated aloft from low latitude convective weather moves poleward in advance of an upper air trough in the westerlies. Often, the convective weather involved is associated with the ITCZ. When the associated trough is forced equatorward by the system upstream, or "digs" equatorward with a significant jet stream present on the upstream side of the trough, a distinct boundary is formed and high clouds form very rapidly along the moist side of the boundary. The term "flare-up" originated from the appearance of the rapid cloud formations when viewed on infrared and visible imagery in time-lapse motion. Such systems vary significantly in their vertical depth.

In the case shown on **Figure 5**, the upper air trough does not have a strong "digging" jet stream branch on its upstream side. Rather, the trough has been forced southward and eastward by another system farther to the northwest. The winds on the upstream side of the dark region have rotated anticyclonically with time, increasing the equatorward component of the flow over a relatively wide area. A jet stream branch has formed on the forward side of the trough parallel to the boundary. In this case, the jet stream branch is relatively high and shallow, of the "subtropical" structure more common during the summer half of the year. At Mexico City (679) the maximum wind was reported at 202mb at 225° and 90 knots. The wind speed was only 30 knots at 400mb. In conjunction with this, the moisture was high level and the clouds were primarily high cirrus. At Mexico City, dewpoint depressions of less than 5°C were reported at 361mb and above; whereas, a dry layer with 30°C depressions was present from 600 to 400mb. Farther to the west, at Manzanillo (654) under the dark area, 30°C dewpoint depressions were reported at 710mb and above. Although the dark area on the dry side of the boundary is oriented generally northeast-southwest, it is not a well defined "slot" shape, as is more common to the rear side of parallel jet stream boundaries. This shape could present a problem in correctly interpreting the boundary as a parallel jet stream type. However, there are three reasons to do so. Most "ITCZ flare-up" boundaries have a jet stream parallel to the moist boundary or cloud edge. Most straight boundaries (great circle) with southwest-northeast orientation on the east side of a trough have a parallel jet stream branch. And thirdly, when a question arises, the changes with time from a sequence of images should be considered. The image shown on **Figure 5** was at an early stage of the boundary formation. The dark region to the rear of the boundary was becoming more elongated in an orientation parallel to the boundary. Twelve hours after the image shown, and for 24 hours after that, the boundary remained will defined and distinct; and, the dark region had formed a well defined slot shape, with its rear side better defined and parallel to the forward side. We intentionally used the early image to illustrate the exception and address the subject.

In both cases of parallel jet stream boundaries shown here, the shapes of the boundaries were nearly straight, or nearly a "great circle" on the earth's surface. Other boundaries of this type may be concave from the moist side perspective, or slightly convex. Many additional cases will be shown and discussed in subsequent sections, and those of different shapes will be included.

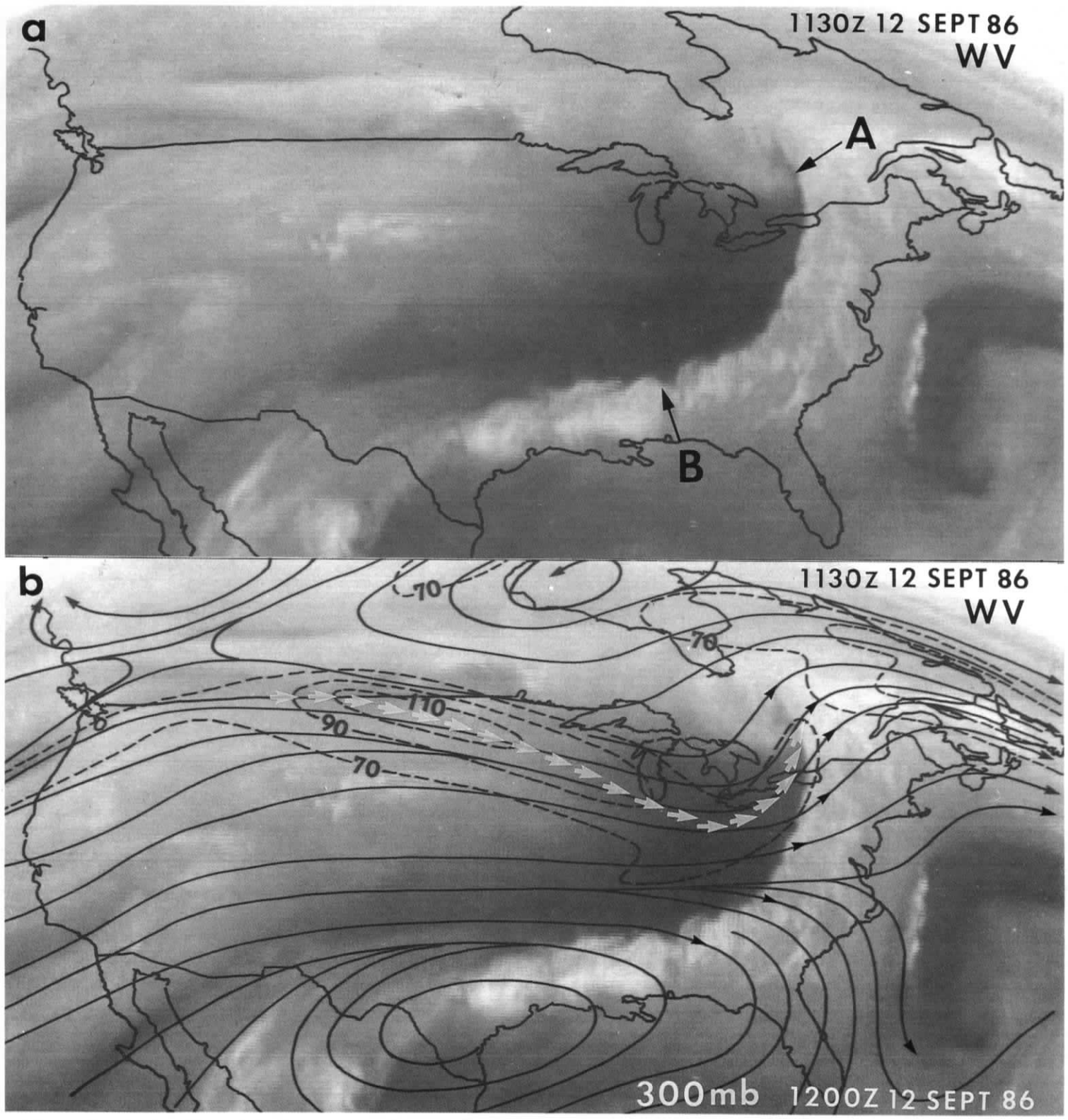

Figure 6

DRY SURGE BOUNDARY
Fig. 6a. 6.7μm Image, 1130Z 12 September 1986, GOES Central.
Fig. 6b. Same Image with 300mb analysis, 1200Z 12 September 1986. Solid black lines - streamlines. Dashed black lines - isotachs in knots. White arrows - axes of 300mb maximum wind speeds.

b. Dry Surge Boundaries

A second type of boundary found on the forward sides of upper air troughs is referred to as a "dry surge" boundary. On **Figure 6**, an example of a "dry surge" boundary is present from "A" to "B". The water vapor image is repeated with a 300mb analysis superimposed.

Image Features

The boundary, "A-B", is curved concave toward the upstream western side. Although not determined by the single image, the boundary is moving rapidly eastward. The central portion of this boundary moved at an average speed of nearly 50 knots during the 12 hour period between 0530Z and 1730Z. Portions of the boundary to the north and south of the central portion did not move as rapidly. This differential speed of movement was the primary factor contributing to the curved shape of the boundary. Note that the dark region on the upstream dry side of the "dry surge" boundary is not an elongated zone parallel to the boundary. Instead, it is a wide area. On the western side of this area, the image gray shades lighten gradually toward the west. Commonly, the western upstream sides of dark areas to the rear of "dry surge" boundaries are poorly defined. They tend to lighten gradually, be irregular in shape, or both. Any relatively large features on the upstream sides of such dark areas tend to be oriented toward the boundary, rather than parallel to it. The curvature, rapid speed of movement, and wide dark areas on the rear sides, are common aspects of "dry surge" boundaries.

Relationships to the Wind Field

The primary jet stream zone associated with the boundary is not parallel to the boundary. It is upstream from the boundary and oriented toward the boundary. The 300mb winds are across the boundary in a difluent pattern with relatively large crossing angles. This is common with "dry surge" boundaries. Also common is the fact that the upper air circulation systems directly associated with the boundary are of the "open" type. The streamlines are across the trough and ridge axes. This correlates to the rapid speed of movement and to the fact that the image gray shades on the rear side of the dark area lighten gradually in the upstream direction.

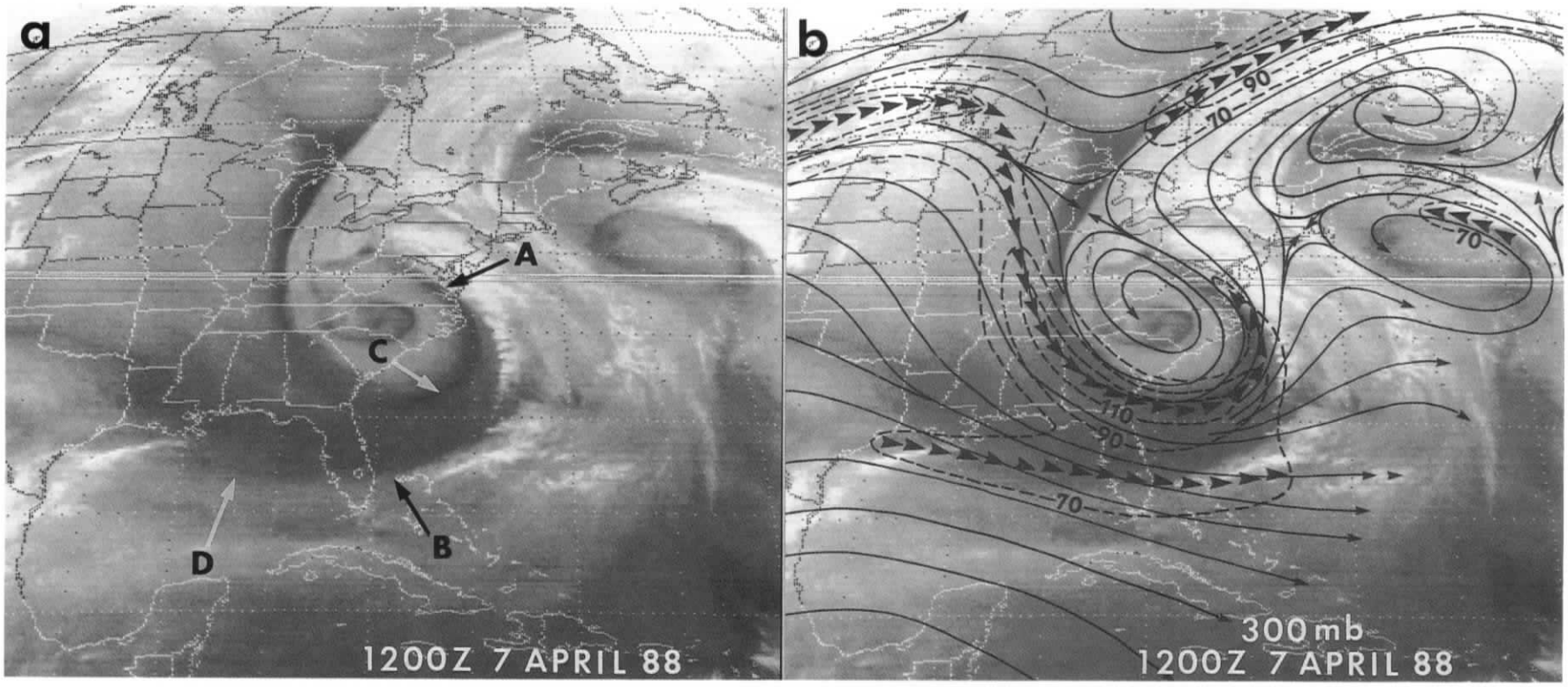

Figure 7

DRY SURGE BOUNDARY - SPECIAL DUAL JET TYPE
Fig. 7a. 6.7μm Image, 1200Z 7 April 1988, GOES East.
Fig. 7b. Same image with 300mb analysis, 1200Z 7 April 1988. Solid black lines - streamlines. Dashed black lines - isotachs in knots. Black arrowheads - axes of 300mb maximum wind speeds.

Boundaries on the forward sides of upper air troughs may be primarily of the "dry surge" type, or primarily of the "parallel jet" type, or some combination of the two types. The combinations often occur when the boundary is in transition from one type to the other. For example, during the cyclogenesis process, the boundary on the forward part of the associated trough is likely to be changing from a "dry surge" type to a "parallel jet" type. As a portion of the trough closes and decelerates, the boundary in advance of that portion is a "parallel jet" type; whereas, another portion - or perhaps all - of the boundary equatorward of there is likely to be a "dry surge" type. Therefore, during the transition phase, at a given time, part of the associated boundary will be of the "dry surge" type, and the part poleward of there will have a parallel jet stream. We might consider the boundary as a combination of two types; or, during the earlier stages, when the "dry surge" portion dominates, we may consider the boundary as primarily a "dry surge" boundary with a jet stream axis parallel to its poleward end. An opposite type of change often occurs when a "cut-off" low opens and accelerates eastward.

Another type of combination often occurs when a boundary on the forward side of a trough has two jet stream branches on the upstream side. An example of this special type of combination is shown on **Figure 7**. The water vapor image and 300mb analysis are 12 hours after those of **Figure 3**. The system over the eastern Unites States has completed its cyclogenesis phase; and, the closed upper air low is moving southeastward in conjunction with the "open" upstream ridge and the "blocking" pattern formed east of New England. The boundary on the eastern side of the low and its trough to the south is indicated from "A" to "B". This boundary has high cold moisture and clouds on its eastern side. It may be considered primarily as a "dry surge" boundary, although there is a jet stream axis parallel to its northern end, primarily that portion over Virginia. However, the jet stream branch has another moisture boundary parallel to it at "C", with a narrow darker slot on its cyclonic side. Boundary"C" merges with the northern part of boundary "A-B"; therefore, northwest of there, the jet stream axis is parallel to both boundaries. Farther to the south, there is another jet stream branch at "D". This axis of maximum winds is parallel to the western extension of boundary "A-B". The southern jet stream branch does not curve northward with boundary "A-B". It extends across the base of the ridge with decreasing wind speeds. Therefore, boundary "A-B-D" is parallel to jet stream branches at both ends, but has a "dry surge" portion between the two jet stream branches.

This special combination of boundaries and jet streams illustrated on **Figure 7** is relatively common. It often develops when cyclogenesis occurs on the forward side of an upper air trough, but not at the base of the trough. In those cases, a jet stream branch crosses the trough initiating the cyclogenesis and often resulting in two jet stream branches on the south or southeast sides of the developing system (Northern Hemisphere). Other cases are shown in Sections B and C with sequential images and analyses.

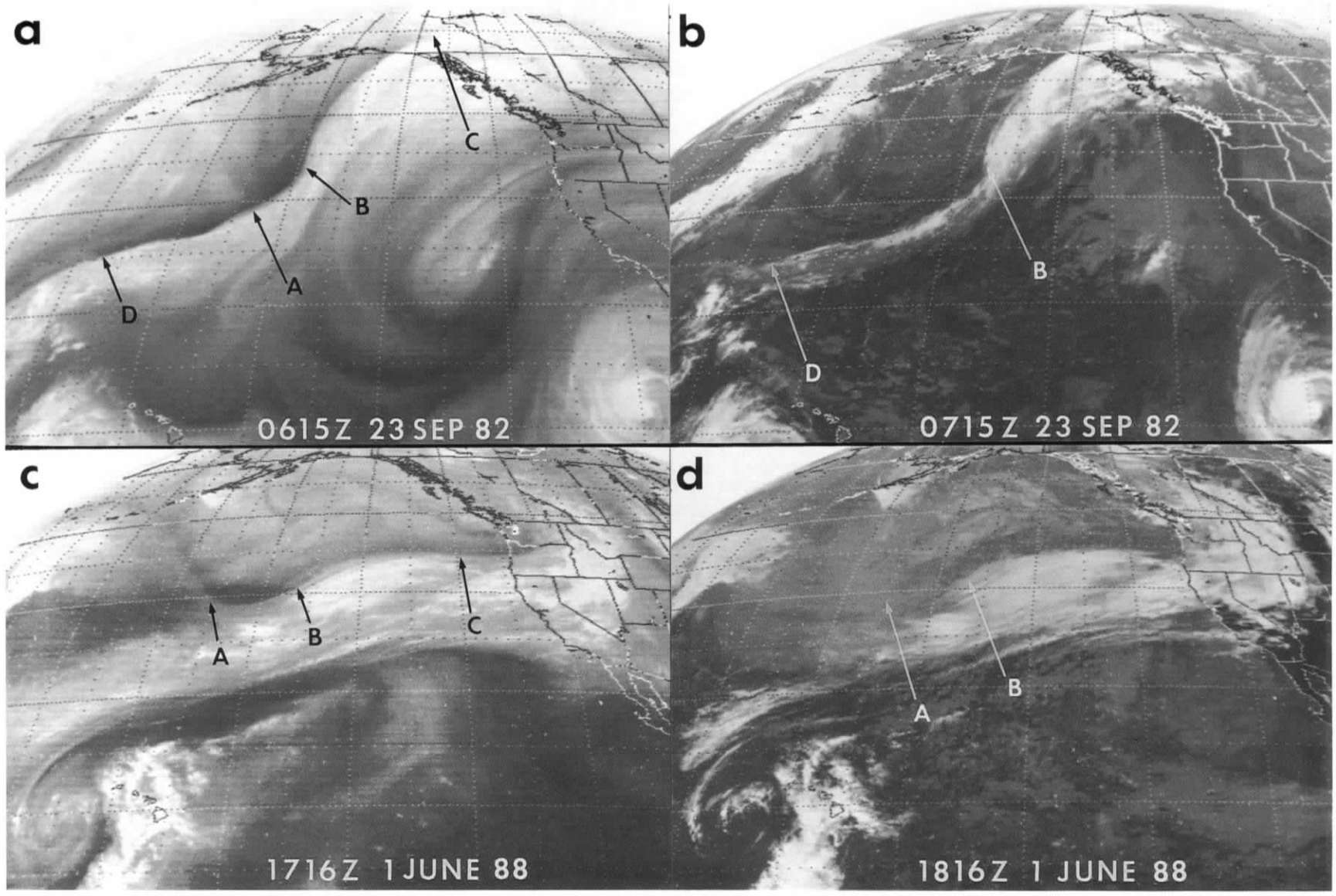

Figure 8 BAROCLINIC LEAF MOISTURE BOUNDARIES - TWO EXAMPLES

Fig. 8a. 6.7μm Image, 0615Z 23 September 1982, GOES West.
Fig. 8b. 11.2μm Infrared Image, 0715Z 23 September 1982, GOES West.
Fig. 8c. 6.7μm Image, 1716Z 1 June 1988, GOES West.
Fig. 8d. 11.2μm Infrared Image, 1816Z 1 June 1988, GOES West.

c. "Baroclinic Leaf" Boundaries

The term "baroclinic leaf" has been used [Weldon, 1979] to describe the type of cloud system which is frequently present, prior to, and during the early phases of cyclogenesis in the westerlies. On water vapor imagery, the baroclinic leaf system represents a special type of boundary on the forward sides of upper level troughs. Two examples are shown on **Figure 8**. Water vapor and infrared images are shown for each case, with the infrared images valid one hour later than the water vapor images.

The moisture boundaries associated with baroclinic leaf systems generally coincide closely with the upstream borders of the cold high clouds of the leaf pattern, but extend beyond the ends of the cloud border. Leaf boundaries usually form a low amplitude "S" shape; and, the portions on opposite sides of the inflection point have different characteristics. The convex portion is similar to a head boundary. A cirrus cloud shield is commonly present on the light gray "moist" side. Conditions may vary along the side opposite to the boundary. The boundary is usually very well defined with a very narrow dark band adjacent to the moist side; however, in many cases, the boundary may not be distinct - with large gray shade differences across the boundary. In the case shown here on **Figures 8a** and **b**, the convex portion of the boundary, labeled "B-C", is relatively distinct, in addition to being well defined. The concave portions of baroclinic leaf boundaries - labeled "A-B" in the cases shown - are similar to dry surge boundaries. Generally, a relatively wide dark or dry zone is present to the rear of that portion. Mid and upper tropospheric wind directions are typically across the concave portion of the boundaries, and nearly parallel to the convex portions.

In the case shown on **Figures 8a** and **8b**, the boundary is oriented southwest to northeast. The cold clouds are primarily in advance of the convex portion of the boundary; however, a narrow band of cirrus extends southwestward to "D". In many cases, the cloud boundaries become gradually warmer in top temperatures in the upstream direction away from the inflection point. In the case shown on **Figures 8c** and **8d**, cold clouds are present along the convex portion of the boundary. Along the concave portion, cold clouds are not coincident with the moisture boundary. In the second case, the upper air trough is of lesser amplitude. At point "A" in both cases, jet stream branches from the northwest merge with the leaf boundaries. Varied features are present to the southwest of there, depending upon the different circulation environments.

Baroclinic leaf boundaries are commonly undergoing rapid transition. Usually the amplitude of the boundary increases with time. The cold cloud region adjacent to the convex portion usually becomes wider, and that adjacent to the concave portion becomes narrower. The evolution of features on the water vapor imagery will be illustrated in section C under the topic of "cyclogenesis and storm evolution". Other examples of baroclinic leaf boundaries and cloud systems will be shown in sections "B" and "D".

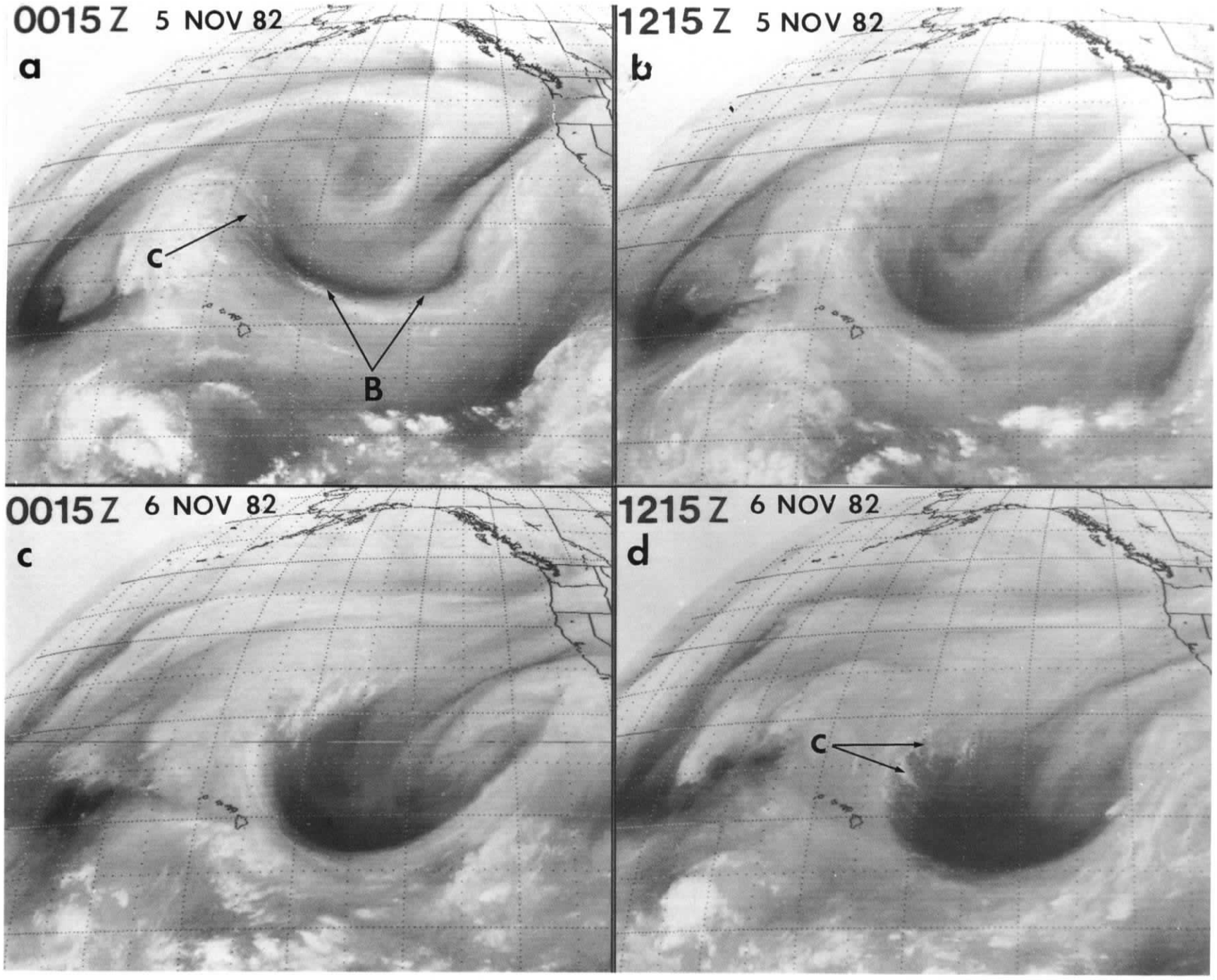

Figure 9 **BASE SURGE BOUNDARY - DIRECT TYPE**
Sequence of 6.7μm images at 12-hour intervals. GOES West.
Fig. 9a. 0015Z 5 November 1982. **Fig. 9b.** 1215Z 5 November 1982.
Fig. 9c. 0015Z 6 November 1982. **Fig. 9d.** 1215Z 6 November 1982.

3. BASE SURGE BOUNDARIES

The dominating process contributing to this type of boundary is synoptic scale sinking on the dry side. Conditions on the moist side vary.

A time sequence of water vapor images, at 12-hour intervals, is shown on **Figure 9**. At the initial time, on **Figure 9a**, the boundary feature at "B" east of the Hawaiian Islands is concave to the north with a relatively narrow dark band along the north side. During the sequence of images, the upper air ridge north of Hawaii "builds", and the northerly component flow on the east side of the ridge increases. A region of darkening on the image, or drying aloft apparently from sinking air, forms north of the boundary; and "surges" southward. The boundary also accelerates southward in advance of the sinking region, and becomes more distinct. During the last 12 hours of the period, between **Figures 9c** and **9d**, the boundary decelerates in its southward motion and becomes irregular. In this case, the boundary reached its southernmost location at approximately the time of **Figure 9d**. We use the term "surge" to describe this type of significant, but temporary motion. The feature accelerates, then decelerates, significantly as it changes position and shape.

By our definition, the base surge boundary includes the "surge" process; therefore, it is necessary to view a sequence of images for accurate identification. It also requires the presence of the synoptic scale dark or dry region on the rear poleward side. If a boundary, viewed on a single still water vapor image, is curved concave to the poleward side, and has a relatively wide dark region on the poleward side; it has likely formed by the base surge process. However, there are exceptions. Similar patterns may occur by interactions of circulation systems involving a region of residual dry air aloft; and, some upper air cyclonic circulation systems can produce a similar pattern. Usually, the distinction between these and base surge boundaries, can be identified on the imagery by comparing the locations and configurations of surrounding features relative to the boundary. Also, the boundaries formed by these other methods tend to be less distinct.

In the case shown here, note on **Figure 9a**, that the boundary "B" does not yet have a large dark region along its poleward side. The boundary would not be identified as a base surge boundary at the time of the first image. However, the base surge process has just begun; and, by the second image, some darkening has begun, and the boundary has moved southward approximately 3° of latitude. By the 3rd and 4th images, a large dark region has formed, and the boundary has "surged" southward. Identification of the feature as a base surge boundary would have been likely by the second image time, and definite by the third image.

Base surge boundaries are primarily features of the middle to upper middle troposphere - commonly observed in the humidity and wind fields between 600mb and 300mb. Although some of the surge boundaries include a surface frontal zone, most do not. With many of the strong very distinct cases, the boundary extends upward to 250mb or 200mb; however, in many other cases high level winds and moisture features are not consistent with those of the middle level boundary and its adjacent dark region.

Other examples of base surge boundaries will be shown in Sections B and D in relation to their upper air circulation systems, and in Section E wherein they will be applied to tropical weather systems and their changes.

There are many types of upper air circulation system changes which contribute to base surge events. All of these involve the increase of the equatorward component of the winds on the eastern sides of upper air ridge systems. Although we will illustrate several of the circulation changes in subsequent sections; several of the most commonly observed types are listed as follows:

[1] An upper air ridge amplifies in conjunction with cyclogenesis on the upstream side of the ridge. Two common types of changes may occur on the downstream side of the ridge:

- 1a. The upper air winds rotate anticyclonically with time, causing a sudden increase in the equatorward flow, without a jet stream branch extending equatorward. The amplified ridge remains in an "open" configuration.
- 1b. The jet stream branch on the downstream side of the ridge"hooks" anticyclonically and extends equatorward. The ridge changes to a "closed" type of configuration with flow around the periphery, instead of across the axis, as in an "open" mode.

[2] Ridges within two branches of westerlies move into phase. Usually, a ridge in the poleward side branch overtakes a slower moving ridge in the equatorward side branch. With the ridges in phase, the winds on the forward sides of both ridges rotate anticyclonically, contributing an equatorward surge in the flow.

[3] On the western side of a "blocking" circulation regime, a newly formed speed maximum in the jet stream zone surges eastward toward the "block". As the speed maximum approaches the area where the flow splits into two branches, an equatorward surge of flow occurs in the equatorward branch. In the Northern Hemisphere, this surge occurs in the southwest quadrant of the blocking pattern.

In the case shown on **Figure 9**, an upper air ridge north of the Hawaiian Islands amplified. This had already begun at the time of the first image. Note the cirrus cloud elements at "C" on **Figure 9a**. If extended downstream, they would be approximately parallel to the boundary "B". On subsequent images, the cirrus elements become rotated and extend across a part of the newly formed dark area. On **Figure 9d**, the cirrus elements at "C" would extend across the boundary at significant angles in the equatorward direction. In other cases, we will show the related upper air analyses over the North American radiosonde network.

Base surge events and their base surge boundaries can be categorized into two types that are significant to tropical system applications. These are "direct" and "indirect". They will be outlined and illustrated in the summary of this section; and, examples of each type are shown in later sections. The case shown on **Figure 9** is a "direct" type, in which a boundary with a parallel jet stream was initially present before changing to a base surge boundary.

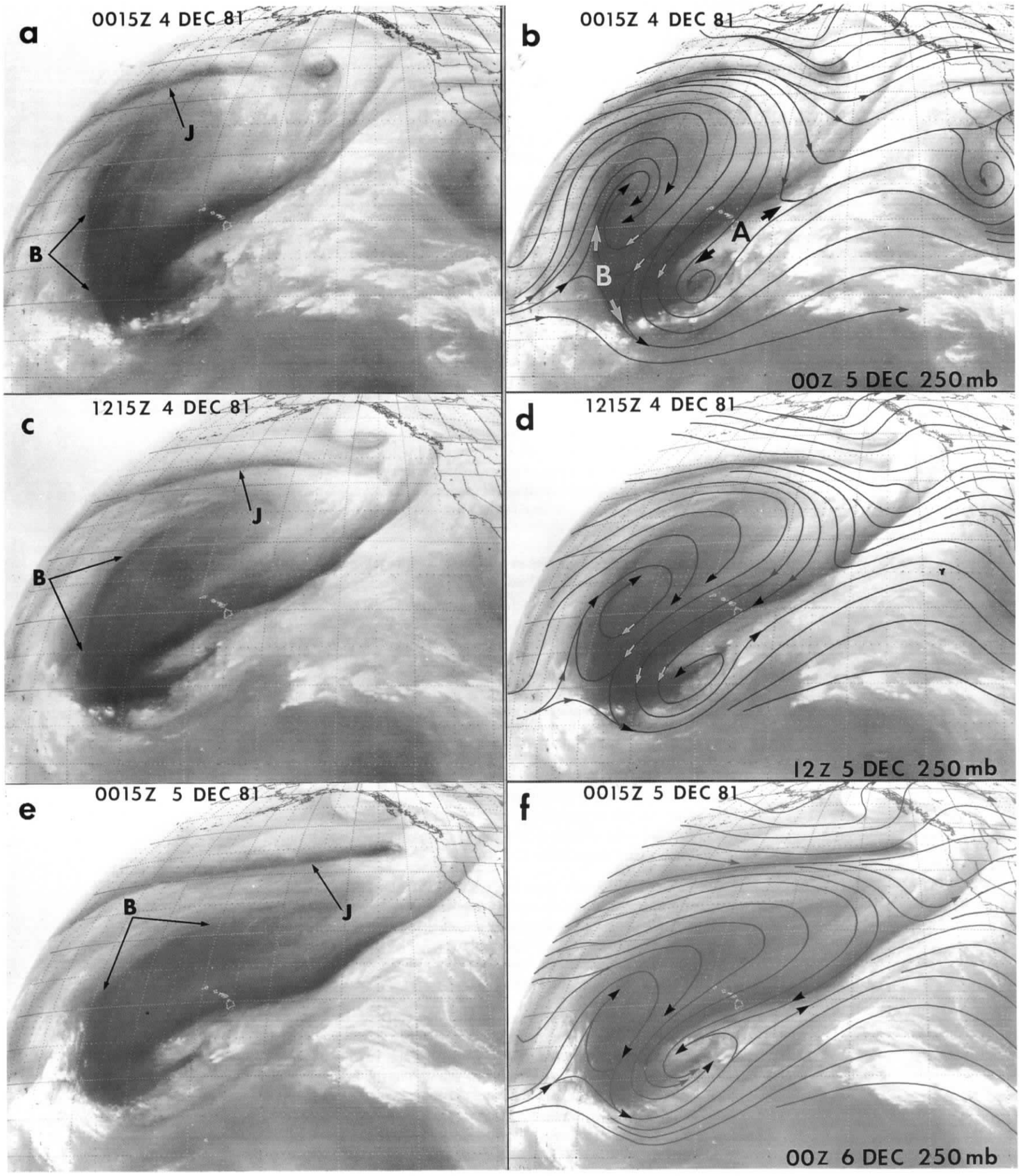

Figure 10 **INSIDE BOUNDARY**

Sequence of three 6.7μm images at 12-hour intervals, repeated with 250mb streamline analyses.
Fig. 10a. 0015Z 4 December 1981 with 0000Z 250mb analysis on **Fig. 10b.**
Fig. 10c. 1215Z 4 December 1981 with 1200Z 250mb analysis on **Fig. 10d.**
Fig. 10e. 0015Z 5 December 1981 with 0000Z 250mb analysis on **Fig. 10f.**

4. INSIDE BLOCKING -"INSIDE" BOUNDARIES

As in the case of base surge boundaries, active synoptic scale sinking is a primary contribution to the formation of "inside" boundaries. A second equal contribution is that of "blocking" or horizontal deformation, as in the case of head boundaries.

Inside blocking occurs as a result of upper air anticyclogenesis - or the formation of a closed anticyclone. As the upper air high pressure system closes, the newly formed easterly winds on its equatorward side form a "col" or hyperbolic region in opposition with the upstream westerlies. The inside boundary forms along the deformation zone, or stretching axis of the col. Generally, the air approaching the deformation zone from the east has undergone synoptic scale sinking during the anticyclogenesis process, or is actively sinking; and is dry in the middle and upper troposphere. Usually, the air approaching the deformation zone from the west is moist aloft, and a well defined distinct boundary is observed on the water vapor imagery. In many cases, cirrus clouds are present along the west side of the boundary for a large portion of its extent. Whereas, the primary blocking effect with head boundaries is contributed by rising moisture within its blocking easterlies; the primary contribution to inside blocking is by sinking air and drying aloft on its eastern blocking side.

An inside boundary is illustrated on **Figure 10**. Water vapor images are shown at 12-hour intervals in the left column. The same images are repeated in the right column with 250mb streamline analyses superimposed. (Note that the streamlines associated with the anticyclone spiral inward. A discussion is located in the boxed area on this page.)

On **Figure 10b**, two col regions have been identified. The col region "A" is associated with the closed cyclone southwest of the Hawaiian Islands. The moisture boundary parallel to the stretching axis of col "A" was a "head" boundary which formed when the low closed and a small synoptic scale ridge began to build on the northeast side of the low. This smaller ridge has been depressed by the large anticyclone and the northerly component flow on its eastern side. Note that during the sequence of images, the stretching axis of col "A" rotated anticyclonically with time. This is common when the large ridge or anticyclone "rolls over" onto the poleward side of the trough. The concept will be discussed in the following sections.

Col region "B" formed as the anticyclone closed. The boundary along its stretching axis is referred to as an "inside" boundary. The reason for the term "inside" can be explained by its evolution during the sequence of images. Note that the boundary extends northeastward within the anticyclonic wind field, and becomes nearly parallel to the jet stream boundary "J". If the jet stream axis is considered to represent the poleward border of the anticyclone, the boundary "B" extends with time on the "inside" of the anticyclonic circulation with respect to the primary jet stream axis. Since this type of evolution of such boundaries was common, the name "inside" was chosen.

The dark region of drier middle tropospheric air initially formed on the eastern side of the boundary, also moves anticyclonically. In some cases, when the warm core anticyclone is relatively large and slow moving, the associated dark regions move completely around the high center, while becoming elongated. This may result in an inward spiral pattern of adjacent moist and dry zones about the anticyclonic circulation. In this case, the anticyclone became elongated eastward along the southern side of the strong jet stream zone.

Inside boundaries vary in their vertical extent and orientation. Often the associated col regions are in the wind field between 500mb and 250mb. However, during the summer season over the United States, inside boundaries may relate well to the 200mb winds, but poorly at 500mb.

In the case shown here, a closed cyclone was present at the base of the trough, to the south of the closed anticyclone. The presence of the closed low is common with inside boundaries; however, in some cases the trough remains open. When the anticyclone moves, expands, or extends eastward (as in this case), a closed low usually forms, or the equatorward end of the trough changes to a narrow cyclonic shear zone. The term "inside" describes that part of the boundary poleward of the col in the wind field, that extends "inside" the circulation of the anticyclone. In most cases, that part of the boundary on the equatorward side of the col is also well defined and has a jet stream branch associated. However, in some cases, only the poleward portions of the inside boundaries are well defined. Such inside boundaries may appear on the imagery as the poleward half of a crescent shaped dark area and related boundary. Two common types occur. In one type, the trough is present only as a cyclonic shear zone. The second type occurs at low latitudes where the easterlies extend to the equator. Many examples of inside boundaries will be shown in following sections.

Anticyclonic Inflow With Warm Core Anticyclones

On the upper tropospheric analyses shown in the following sections, streamlines associated with closed upper air anticyclones are shown spiraling inward. Although we do not consider this phenomenon significant to any of the main concepts being illustrated, it may cause a distraction in the communication process. Such streamline patterns are common to warm core upper air anticyclones and are generally present from 250mb to 400mb and often at 500mb. The streamlines were carefully drawn to the upper air wind reports without the use of any preconceived conceptual model. Although we have not investigated this empirical relationship in detail, we have given it some attention. The conditions involved vary from case to case. Weak supergradient wind conditions are sometimes present over a large portion of the anticyclonic flow field. In other cases, significant supergradient winds are concentrated in one quadrant of the anticyclone, with the remaining wind directions nearly parallel to the height contours. This is sufficient to cause a net inflow of the streamline field. In some cases, the supergradient conditions can be observed to rotate around the anticyclone with time in conjunction with certain features on the water vapor imagery.

On satellite imagery, certain cloud and moisture features associated with upper air anticyclones and ridges can be observed to "hook inward". They may be anticyclonically curved bands oriented across the height contours and wind directions or features that move anticyclonically inward with time. Such features are not necessarily related to the inward spiraling streamline conditions. They can be related to anticyclonic horizontal shear, and to trajectories associated to a moving anticyclonic circulation system.

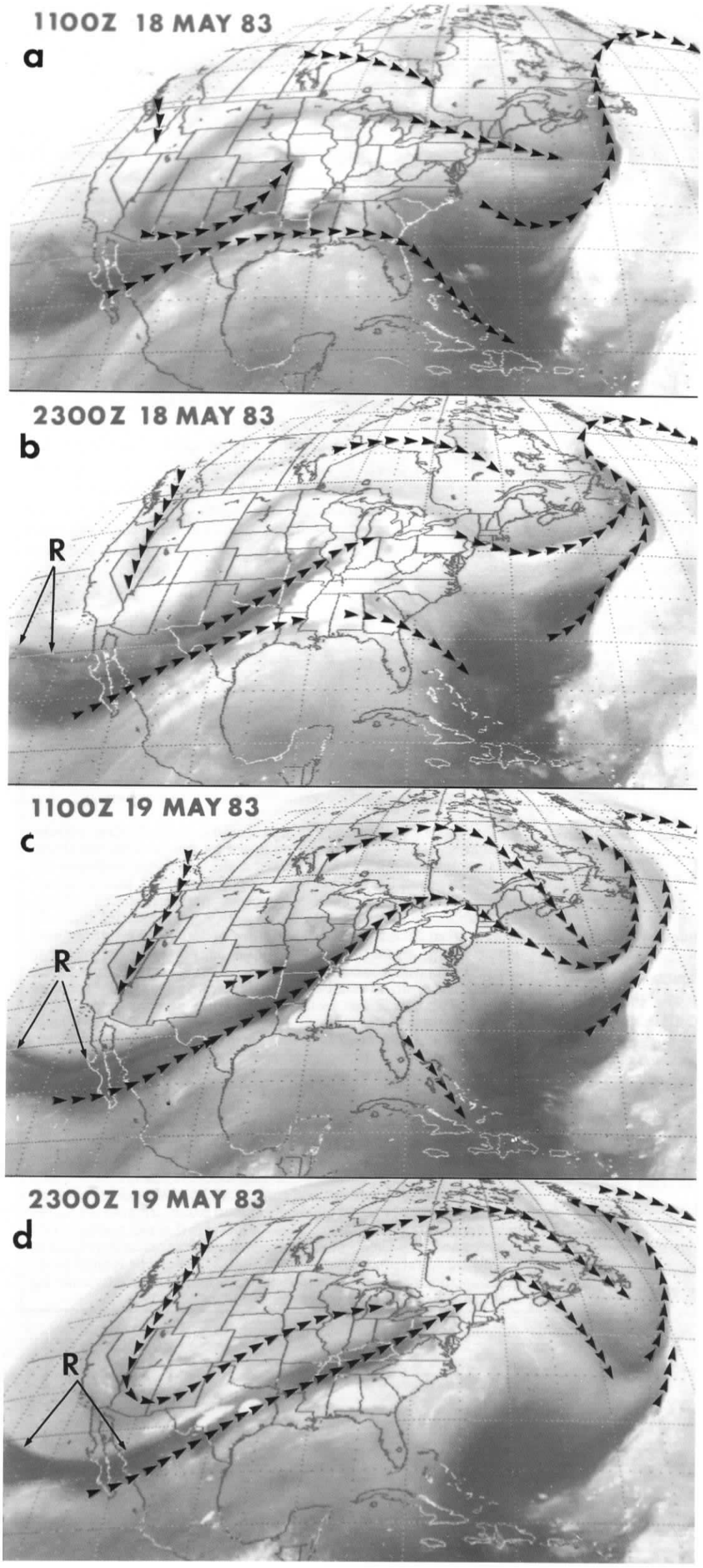

Figure 11

BOUNDARY CHANGES AND EVOLUTION
Sequence of four 6.7μm images at 12-hour intervals, from GOES East.
Fig. 11a. 1100Z 18 May 1983.
Fig. 11b. 2300Z 18 May 1983.
Fig. 11c. 1100Z 19 May 1983.
Fig. 11d. 2300Z 19 May 1983.
Black arrowheads indicate axes of maximum 300mb winds with speeds of 70 knots or greater.

5. RETURN MOISTURE AND RESIDUAL EFFECTS

a. Introduction

Features on water vapor imagery, such as boundaries, are transient. They are formed, exist for some period, then are either actively destroyed, or allowed to dissipate gradually. Once a moisture boundary has formed, it may be destroyed as quickly as it formed; or, in the absence of synoptic scale vertical motions or mixing effects, it may persist. When boundaries persist, they may remain as "residual" features after the circulation and thermal field systems related to their formation are no longer present. Since many features on an image are undergoing change with time, and others remain as residual features produced by some earlier circulation system, it is often difficult to interpret a single water vapor image. The task is easier and more accurately accomplished when a sequence of previous images are used, or when images are viewed in time-lapse motion.

Figure 11, on the facing page, includes four images at 12-hour intervals with 300mb axes of maximum winds superimposed. The figure is repeated on the following page with sharper image reproduction and with the axes of maximum winds omitted. Note that the same sequence of images is also shown as **Figure 74** with the discussion of jet streams in Section D. Also, a similar sequence of four images with 300mb analyses superimposed, valid just prior to this set, is shown as **Figure 71.** Here, as **Figure 11**, the sequence will be used for two purposes: (1) to provide an example of a "return moisture" boundary during its formative stages, and (2) to introduce the subjects of boundary changes with time and residual effects. Although streamline analyses are not shown on **Figure 11**, the third image of the sequence (**Figure 11c**) is also shown in Part One, **Figure 18**, as an enlarged view with and without a 300mb analysis superimposed.

The primary circulation systems and changes occurring during the 36-hour period are as follows. At the time of the first image, **Figure 11a**, a large upper air cyclone is present over the central United States. At 500mb and 300mb, the closed low is centered over northern Kansas, with a trough extending southwestward to the southeastern corner of Arizona. During the period shown, a large slow moving ridge over the northeastern Pacific Ocean amplified significantly; and, caused the jet stream branch on its eastern side to extend southward from western Canada to southern Nevada. The 300mb axis of maximum winds associated with this jet stream branch is shown on the images by arrowheads. As the jet stream over the western states extended southward, a cold trough along its eastern side also moved southward. This weakened the ridge on the western side of the central U.S. cyclone and caused the winds to rotate cyclonically with time on the west side of the cyclone. The low opened and accelerated northeastward as it did so. By the last image time, the original cyclone has opened in the upper air wind fields, and can be identified by a 500mb vorticity maximum centered at the intersection of Lakes Superior, Michigan, and Huron. A new low has closed at the base of the "digging" trough, and is centered over northern Arizona at 500mb.

b. A "Return Moisture" Boundary

General Concept

Upward vertical motion occurs within wind regimes of all directions; however, when jet streams are perturbed at relatively large amplitudes with large meridional components in the upper air flow, much of the upward vertical motion occurs on the upstream sides of upper air ridges. Therefore, the moisture accumulated aloft moves poleward. Often such moisture accumulated at middle and upper levels will be "returned" equatorward as "residual" moisture, relatively unaffected by large scale vertical motions. This moisture may flow equatorward around the eastern side of an upper air ridge. This is most common when the jet stream around the ridge is in a "channeled" configuration (wind directions are nearly parallel to the isotherms and vorticity isopleths). Such ridges are usually in a "closed" circulation mode and nearly stationary; the jet stream tends to "hook" around the ridge and extend equatorward; and, the moisture is able to move equatorward for long distances without synoptic scale downward motion. Such situations produce the most significant return moisture effects.

In many cases, a well defined boundary forms on the forward sides of the return moisture regime. These "return moisture" boundaries move with an equatorward component, with the primary upper air moisture on the rear or poleward sides. Those "return moisture" boundaries that move directly equatorward are often of curved shape and convex toward the equatorward direction. These curved types are usually relatively free of high cloudiness on their moist sides. Those boundaries that move with an eastward component - in addition to equatorward - are often nearly straight and commonly have considerable high cloudiness on the moist sides.

Although the characteristics of return moisture boundaries vary, horizontal deformation appears to be the primary contribution to their formation. Generally, significant synoptic scale vertical motions are not evident, on either sides of such boundaries. While the boundaries are moving rapidly, the streamlines of the upper air wind fields cross the boundaries in a diffluent pattern from the rear to the forward sides. After the boundaries have slowed or become stationary, a col is usually present in the upper air wind fields.

Example on Figure 11

On the image sequence of **Figure 11**, a return moisture boundary formed along the western part of the images, and is labeled "R". The boundary became identifiable between the times of **Figures 11a** and **11b**. It moved equatorward, and became better defined during the last 24 hours of the sequence. In this case, the high level moist air flowed southward around the Pacific ridge on the right side of the "digging" jet stream. A part of that moist air turned cyclonically around the southern side of the "digging" trough, and moved over the southwestern U.S. and northern Mexico. In this case, the return moisture boundary became very well defined, and also relatively distinct. The distinctiveness was related to the relatively dry conditions present in advance of the boundary. In other cases, when conditions are not as dry in advance of return moisture boundaries, the boundary will be less distinct with only a narrow dark band in advance of the boundary. Such a narrow band is also present in this case, in addition to the wider dark region. This narrow band is evident on **Figure 11b**, and most vivid on **Figure 11c**, just in advance of the boundary "R"

The related 300mb wind field with difluent flow across the boundary can be viewed on **Figure 18** of Part One, if desired. The analysis is valid for the third image time of the sequence. In this case, a col had likely formed by the last image time; however, upper air data over the area were not of sufficient density to properly analyze the col with respect to the boundary. Other examples of "return moisture" boundaries are shown on **Figures 25, 29, 57,** and **87.**

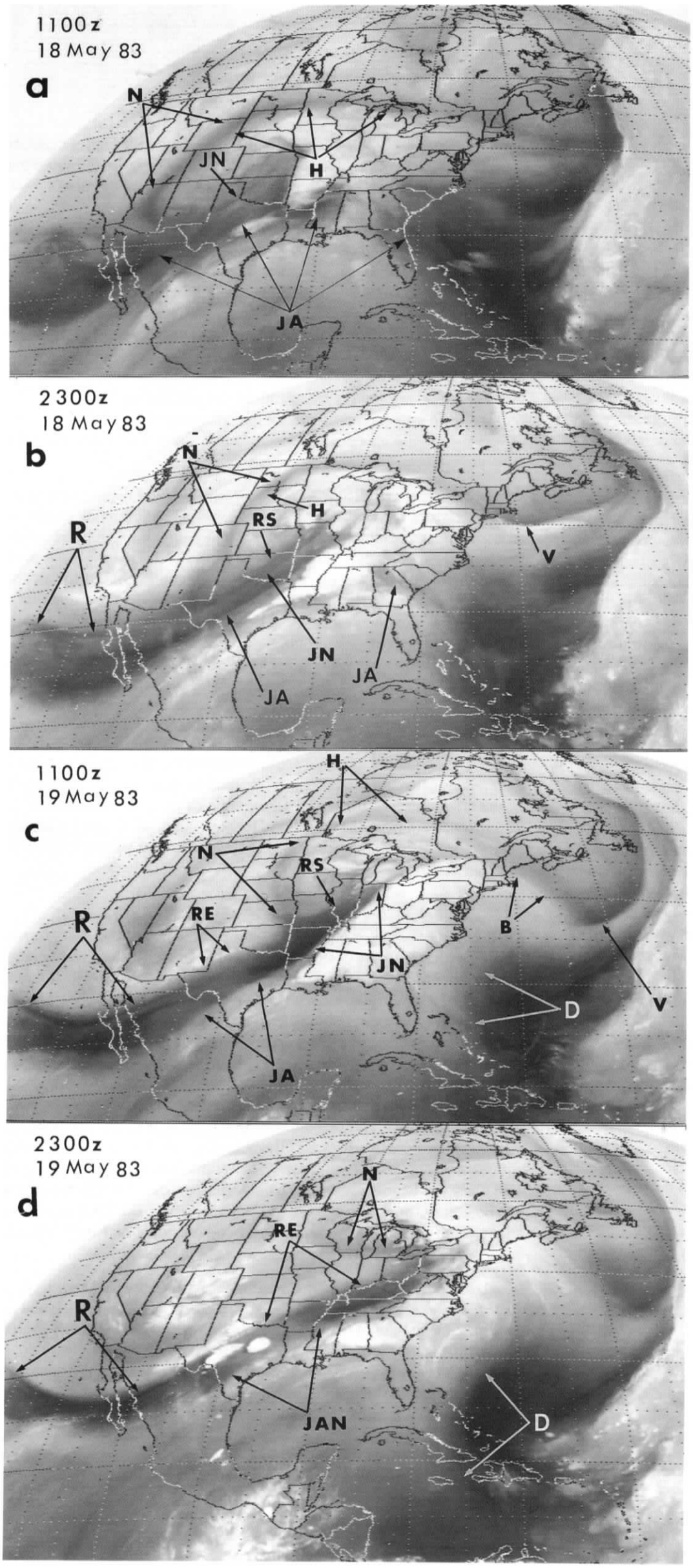

Figure 11 **Repeated**

BOUNDARY CHANGES AND EVOLUTION
(Without axes of maximum winds).

c. Boundary Changes and Residual Effects

In addition to the return moisture boundary, a number of other boundaries are present on the sequence of images on **Figure 11**. Some of these form during the sequence and others dissipate. Here we will merely draw attention to some boundaries and their changes. To prevent obscuration of features, axes of maximum winds are omitted from **Figure 11 - Repeated**. For references to jet stream axes, see the initial version of **Figure 11** on page 76.

Consider boundaries labeled "H" and "N" and the elongated dark zone between them on the first image. The elongated dark zone extends from Arizona to Minnesota, and eastward across the Great Lakes to the Atlantic Ocean. Boundary "H" along the equatorward side of this dark zone is a "head" boundary that formed when the central U.S. cyclone developed. Moisture from the ridge on the downstream side of the developing low has spread, partly westward around the low to eastern Arizona, and partly eastward along the southern side of boundary "H" to the Atlantic Ocean. A jet stream axis is present along boundary "H" from Lake Huron eastward. West of that portion, the dark zone is bounded on its poleward side by boundary "N". The moisture on the northwest side of boundary "N" originated from the ridge that was initially on the upstream side of the developing low. As the low closed, a part of that moisture spread southward along the western side of the low, and a part moved eastward as the northern portion of the upstream ridge "rolled over" the poleward side of the low into central Canada. A jet stream axis had been present along the western part of boundary "N" prior to the time of **Figure 11a**. This jet axis was oriented NE to SW. (See **Figures 71c** and **71d**.) Although the winds have decreased significantly during the 24 hours prior to **Figure 11a**, the dark zone and boundaries "N" and "H" remain relatively well defined over Arizona, Utah, and Wyoming.

Consider the evolution of the dark zone and its two boundaries during the sequence of images. The low has already begun to open at the time of the first image. Upper air winds, that were parallel to the boundary "N" from Wyoming to Arizona prior to the sequence, have rotated to cross the boundary from its northwest side to its southeast side. As the jet stream extends southward over the western states with its related cold trough "digging" southward along its eastern side, the thermal ridge along the west side of boundary "N" weakens; and, the upper air winds between the "digging" trough and the low rotate cyclonically with time. The winds cross that portion of boundaries "N" and "H" at increasingly larger angles as the low opens and accelerates northeastward. Although boundaries "N" and "H" lose definition and become less distinct with time, parts of them remain as residual features. By the second image time, they were no longer identifiable in the wind and thermal fields, although they were identifiable in the 500mb vorticity pattern through the third image time. Note that part of the boundary "N" which was on the western side of the low on the first image has rotated onto the south side of the remaining vorticity maximum by the last image time.

At the time of the first image, two jet axes were present along the southeastern side of the low. One of these, was along boundary "JA". This axis of maximum winds curved anticyclonically from Mexico to northern Florida around a ridge over the Gulf of Mexico. That ridge is separated from the ridge over the eastern U.S. on the east side of the low. Although the streamlines of the U.S. and Gulf ridges merge as anticyclonic curvature patterns, they are separated in the vorticity and thermal fields by the jet stream "JA". A second jet stream axis was along boundary "JN", extending from southeastern Arizona to northwestern Missouri. The jet axis along "JN" had previously extended around the western side of the low; and, was associated with the baroclinic zone between the cold thermal trough of the low and the thermal ridge extending from upstream around the southern side of the low. By the second image time, the double jet structure is still identifiable in the wind speed and vorticity fields over Texas. However, during the night between **Figures 11b** and **11c**, a large area of deep convective weather formed along the eastern side of the opening trough. The ridge over the Gulf of Mexico merged with the intensifying ridge over the eastern United States, and a "break" occurred in the jet stream branch along "JA". The western part of jet stream "JA" merged with stream "JN" and formed a long jet stream from the southern tip of the Baja Peninsula to Lake Huron. This is evident in the merger of the moisture patterns from the Gulf of Mexico over the eastern U.S. The vorticity and thermal patterns of the eastern U.S. and Gulf ridges have merged at mid-tropospheric levels.

By the third image time, the newly combined boundaries "JA" and "JN" have become better defined, and increased in distinctiveness as the area along their rear sides became darker with time from Texas to Indiana. These changes observed on the imagery are characteristic of situations in which "cut-off" lows open and accelerate eastward (or northeastward in this case). As the cold trough moved southward on the west side of the low, the thermal ridge between the low and the trough weakened, and the winds rotated cyclonically with time across the isotherms. The baroclinic zone on the west side of the low weakened and that on the south side, or southeast side of the trailing trough, intensified. As cold advection in the middle troposphere increased there, sinking occurred and was revealed by darkening with time on the water vapor imagery. The jet stream wind speeds increased on the southern side of the low in advance of the cold advection region.

In this case, with the "digging" jet stream "hooking" around the slow moving Pacific ridge, the north to south jet stream did not progress eastward during the opening process. As a result, some of the return moisture moved cyclonically around the base of the digging trough; and, by the time of **Figure 11c**, this has formed a new boundary "RE" on the northwest side of boundary "JA". The moist air on the northwest side of "RE" is moving rapidly northeastward along the poleward side of jet stream "JA" and is extending the return moisture boundary northeastward. That moisture is associated with warmer air of the Pacific ridge, and produces two complicating effects. At the time of **Figure 11c**, the wind speeds are increasing with time along the north side of boundary "RE", between the warmer air of the return moisture from the Pacific and the colder air moving southward on the left side of the "digging" jet stream. By the last image time, a new axis of maximum winds has formed, with 300mb wind speeds of greater than 70 knots from Arizona to Lake Michigan. This accelerated the rotation of boundary "N". The second significant effect is that the warmer air along the equatorward side of the new jet axis is decreasing the baroclinity of the original jet stream "JAN". In conjunction with this change, boundary "JAN" has lost both definition and distinctiveness between the last two image times.

Several other boundaries are present on the image sequence. The boundary labeled "RS" on **Figure 11b** is a type of return moisture boundary. In this case the moisture moved around the low in cyclonic flow, and forms the rear of the slot adjacent to boundary "JN". Since such boundaries are a part of the cyclonic storm structure, we usually do not specifically identify them as "return moisture" boundaries. On that same second image, another boundary is identified at "V". This boundary is a part of the eastern extension of the original "head" boundary; however, it has become better defined and more distinct between the first two image times. As the northern part of the upstream ridge "rolled over" the low into Ontario Province, two significant changes occurred. The warm air of the Canadian ridge merged with that of the U.S. ridge on the northeast side of the low. That part of boundary "H" across the Great Lakes became poorly defined and indistinct, showing only as a high cloud edge. The jet stream winds, that had been present along that part of boundary "H", decreased significantly. Secondly, as the two ridges over the eastern United States and Canada moved into phase and merged, the northerly components of the winds along the eastern sides of both ridges increased. This common change with ridges moving into phase, caused the eastern end of boundary "H" to accelerate equatorward and become better defined and distinct. That part of the boundary at "V" continued to accelerate southeastward, aided by the fact that jet stream "JN" intensified and broke across the ridge between the times of **Figures 11b** and **11c**. This increased the northwesterly wind speeds along the jet stream at "B". A "base surge" boundary began to form at "V" with darkening with time on its poleward side; however, that formation did not continue because of changes to the west. And, finally, as the ridge intensified over the east coast of the U.S., anticyclogenesis occurred; and, an "inside boundary" began to form at "D".

The foregoing discussion of boundary changes was intended to introduce the subject. As boundaries form and dissipate, changes in their definition and distinctiveness are often important keys to the interpretation of imagery. Such changes will be shown and discussed in detail in the subsequent sections, with illustrations of the related wind and temperature fields.

6. SUMMARY - BOUNDARIES

Seven common types of boundaries were illustrated and described in this section. For summary purposes, they may be arranged as follows:

Blocking Situations:	**Head Boundaries**
	Inside Boundaries
Surge Conditions:	**Dry Surge Boundaries**
	Base Surge Boundaries
Special Types:	**Parallel Jet Stream Boundaries**
	Baroclinic Leaf Boundaries
	Return Moisture Boundaries

On the drawings shown in this section, shaded areas indicate cold light gray patterns on the imagery, with very moist conditions in the upper troposphere, and perhaps cirrus clouds. The streamlines represent the upper troposphere, typically 300mb or 250mb depending on the latitude and season of the year. Arrowheads indicate axes of maximum winds at these levels, and usually imply jet stream axes.

a. Summary - Blocking Boundaries

Common Aspects of HEAD BOUNDARIES and INSIDE BOUNDARIES

Both types are usually curved convex toward the upstream side.

Both types are nearly stationary or slowly moving.

Both types are commonly well defined.

Both form in response to the development of a zone of upper air easterly winds or winds opposing the ambient upper air wind directions. At mature stages, the boundaries usually extend along the stretching axis of a col in the upper air wind field, between the area of easterly flow and the upstream westerlies.

The upstream westerlies split into two branches around the poleward and equatorward sides of the blocking boundaries (An exception to this occurs at low latitudes, and will be discussed in Section E.)

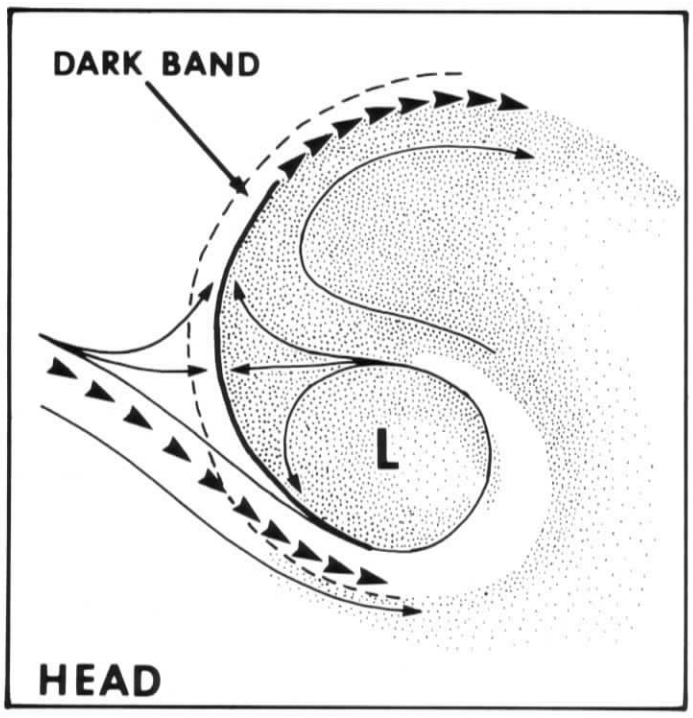

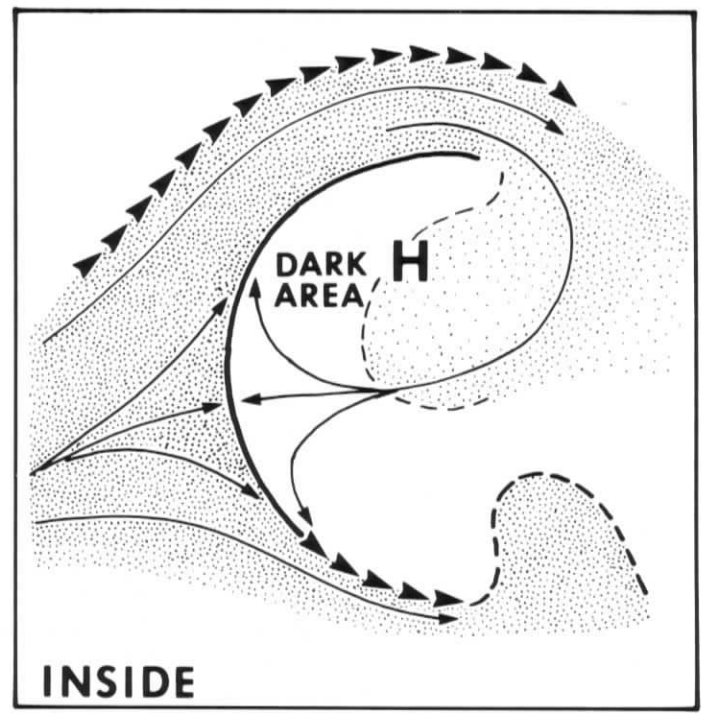

Specific Characteristics of HEAD BOUNDARIES

Synoptic scale upward vertical motion on the downstream blocking side is a primary factor in the boundary's formation. The downstream side is moist at high levels, often with cirrus clouds.

The boundaries commonly form when a downstream ridge "builds back" around the poleward side of a closing upper air low. The event is usually associated with cyclogenesis, including the formation of a new surface low center.

Although well defined, the boundaries may not be distinct.

A very narrow dark zone is likely along all or part of the boundary; however, conditions along the upstream dry sides vary among cases, and along the length of most single boundaries.

Specific Characteristics of INSIDE BOUNDARIES

The primary blocking side - the downstream side - is dry. Synoptic scale downward vertical motion on the downstream blocking side is a primary factor.

The boundaries form when an upper air anticyclone closes, and upper air easterly winds develop on its equatorward side. The anticyclogenesis is often associated to an upstream ridge "rolling over" a portion of its adjacent downstream trough.

A wide dark region is common on the downstream dry side.

The boundaries are often distinct and well defined. Although conditions vary on the upstream moist sides, high clouds and very moist conditions are very common.

b. Summary - Surge Boundaries

Common Aspects of DRY SURGE BOUNDARIES and BASE SURGE BOUNDARIES

Both types are concave toward their upstream or rear sides.

Both move very rapidly while forming.

Synoptic scale downward vertical motion on the upstream side is a primary factor in the formation of both types. Large dark regions form on the upstream or rear sides, usually as the boundaries accelerate.

Both are associated with "open wave" upper air wind systems, rather than "closed" circulation environments, and are oriented across the upper air flow.

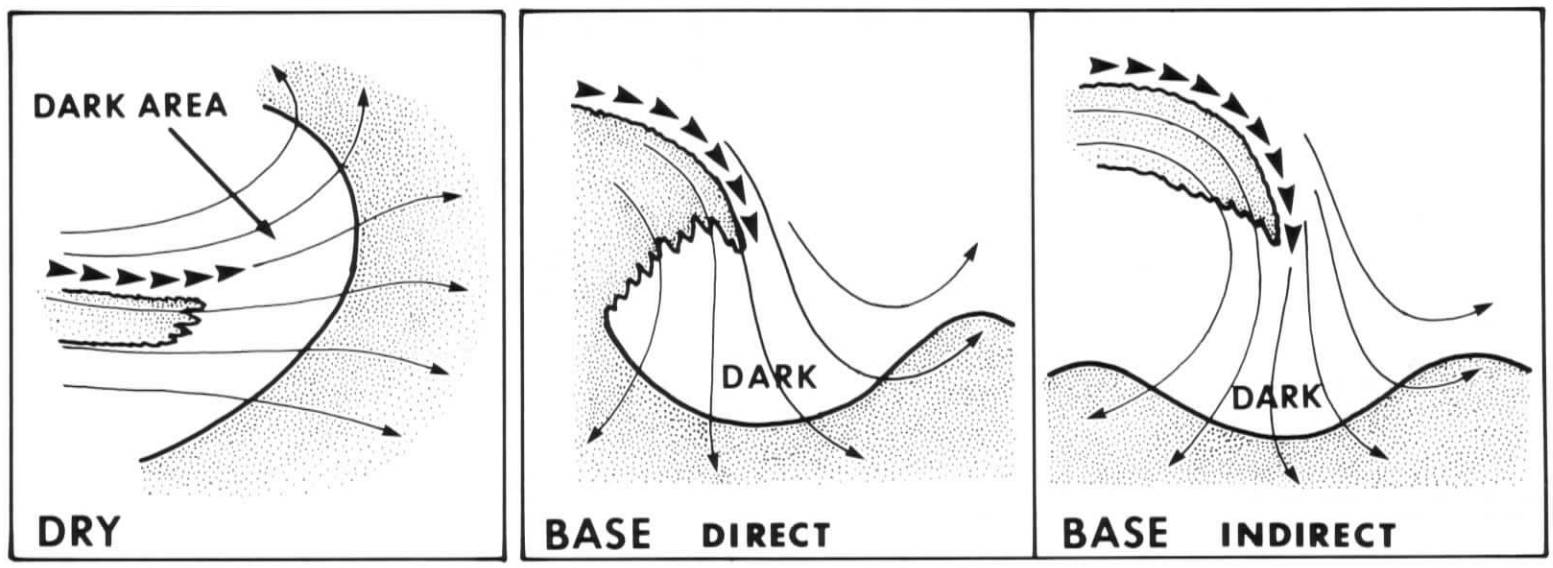

Specific Characteristics of DRY SURGE BOUNDARIES

Usually move eastward with a wide dark region on the upstream western side.

The primary jet stream associated with the boundary is likely to be upstream from the boundary, and oriented toward the boundary. A jet stream branch is not likely to be coincident with or parallel to the boundary.

The boundaries are usually very distinct, since high clouds and abundant high level moisture are commonly present on the forward sides adjacent to the wide dark areas.

Definition of the boundaries varies because convective weather tends to form retrogressively near the boundary locations, and the boundaries sometimes slope eastward with increasing heights.

Specific Characteristics of BASE SURGE BOUNDARIES

Usually move equatorward with a wide dark region on the upstream poleward side.

The boundaries form in response to a sudden increase of the equatorward components of the winds on the eastern side of an upper air ridge, or the western side of a trough.

The boundaries are usually well defined but the distinctiveness varies greatly because of variable conditions on the moist sides.

Two Types Of Base Surge Processes:

Direct. A boundary is initially present, but not moving rapidly, and usually with only a very narrow dark zone along its poleward side. The boundary extends westward onto the eastern side of the upper air ridge which causes the base surge. That ridge is within the same branch of westerlies as the initial boundary. With this type of process, a jet stream branch is likely parallel to the initial boundary; and, it may remain present along the eastern end of the boundary after the base surge process occurs.

Indirect. Initially, a boundary is often not present until a new dark region begins to form and surge equatorward. The upper air ridge related to the base surge is not within the same wind regime where the base surge boundary forms. The ridge is usually a part of a jet stream branch, or a separate branch of westerlies located poleward of the surge boundary wind field. An initial jet stream branch is not likely along the surge boundary, although a separate jet stream branch may extend equatorward into the dry region at the rear side of the base surge boundary.

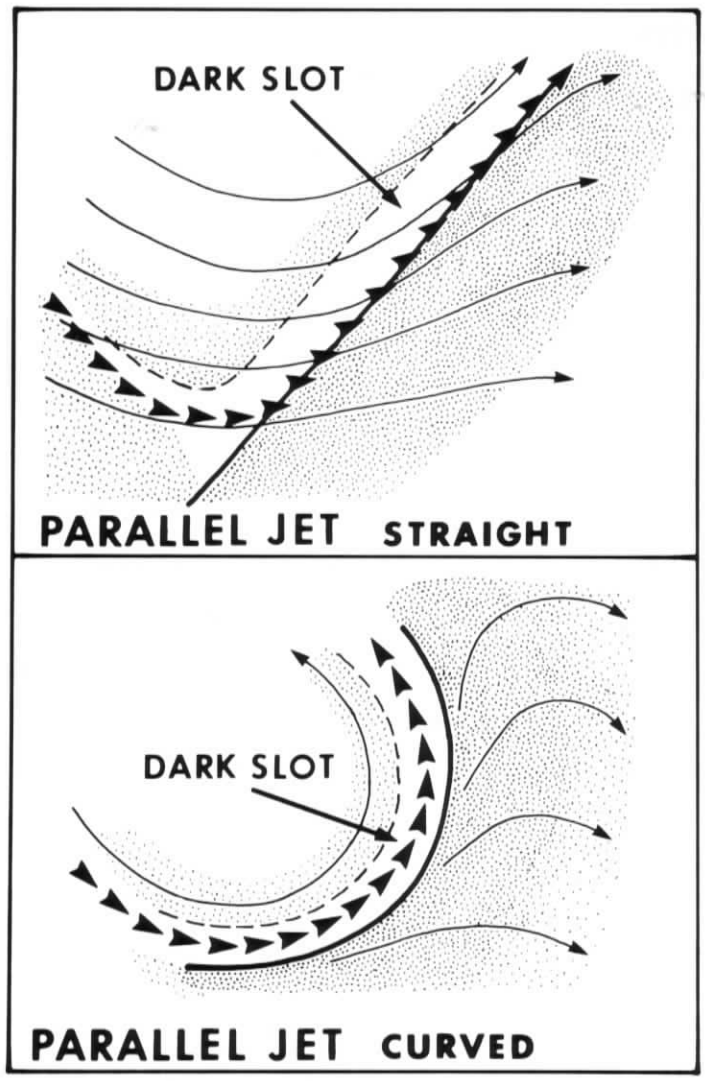

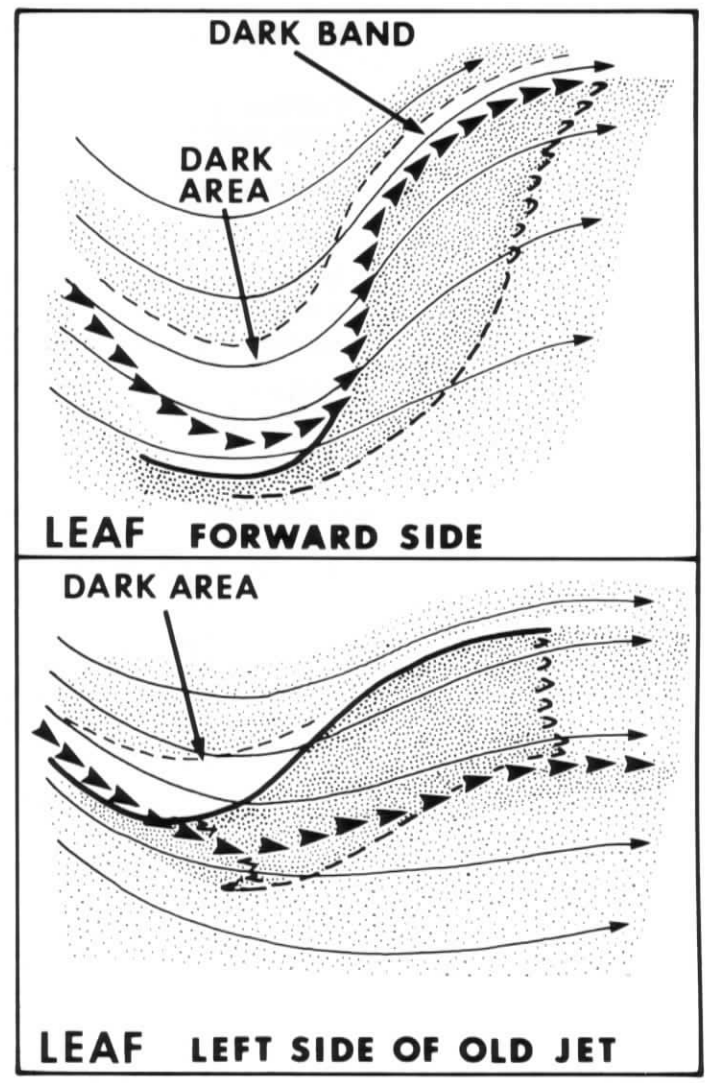

c. Summary - Special Boundary Types

PARALLEL JET STREAM BOUNDARIES

Although boundaries that are parallel to, or coincident with, jet stream axes occur at many locations with respect to the circulation environment, those on the forward sides of upper air troughs were chosen as a special type, because their image characteristics and relationships to the wind field were consistent. Boundaries along the poleward sides of upper air ridges are very consistent in features and wind field relationships; however, they are addressed here as a portion of "head" boundaries, or as a downstream extension of "head" boundaries.

Characteristics of PARALLEL JET STREAM BOUNDARIES on the forward sides of upper air troughs

The shapes of these boundaries range from nearly straight (great circle) to significant curvature with the jet stream axis curved cyclonically around a closed upper air cyclone. These are curved concave toward the trough side. Those that are curved with any significant degree of convex curvature toward the trough side, are usually a part of a "baroclinic leaf" type of boundary (see next topic).

An elongated dark zone, or dry slot, is usually present along the upstream dry side of the boundary. The upstream edge, on the trough side of the elongated dark zone, is likely to be less well defined than the primary boundary on the opposite side; but, the overall shape of the edge is likely to be parallel to the primary boundary.

Since high clouds are usually present on the moist side of the boundary, the parallel jet stream boundaries are usually distinct.

Although the jet stream axis is parallel or coincident with the boundary, the associated upper air winds are generally oriented across the boundary, at larger angles near the equatorward end, and at very small angles near the poleward end. The average crossing angles are usually smaller than those with "dry surge" boundaries. With boundaries curved around an upper air low or "closed" type of high amplitude trough, the upper tropospheric winds are usually nearly parallel to the boundary, or with very small crossing angles.

BAROCLINIC LEAF BOUNDARIES

This is another special boundary type that is located on the forward sides of upper air troughs in the westerlies. Many of the baroclinic leaf cloud systems associated with this type of boundary evolve to winter storm systems with surface cyclogenesis.

Characteristics of BAROCLINIC LEAF BOUNDARIES

Usually have a low amplitude "S" shape, with an inflection point at the intersection of the concave and convex portions.

The convex portion, along the poleward end of the boundary, has characteristics similar to those of "head" boundaries. A very narrow dark region is likely to be present on the rear side of this portion of the boundary, which is likely to be decelerating its speed of movement.

Whereas the convex portion is likely to be very well defined, and becoming less distinct with time, the concave portion is likely to be distinct and remaining so. The concave portion is not likely to be as well defined as the convex portion. Deep convective weather is likely to form just to the rear of the concave portion of the boundary; thus, reforming the boundary to the rear of its initial position, and contributing to poorly defined boundary shapes during periods of reformation. This concave part of the boundary is likely to be accelerating eastward, thereby increasing the amplitude of the "S" shape.

Leaf boundaries on the forward sides of upper air troughs are likely to have a jet stream axis coincident with its length. Other leaf boundaries which form to the left of the original jet stream position, such as a short wave moving across a trough, do not have a jet axis coincident with the boundary. An example is discussed in Section D.

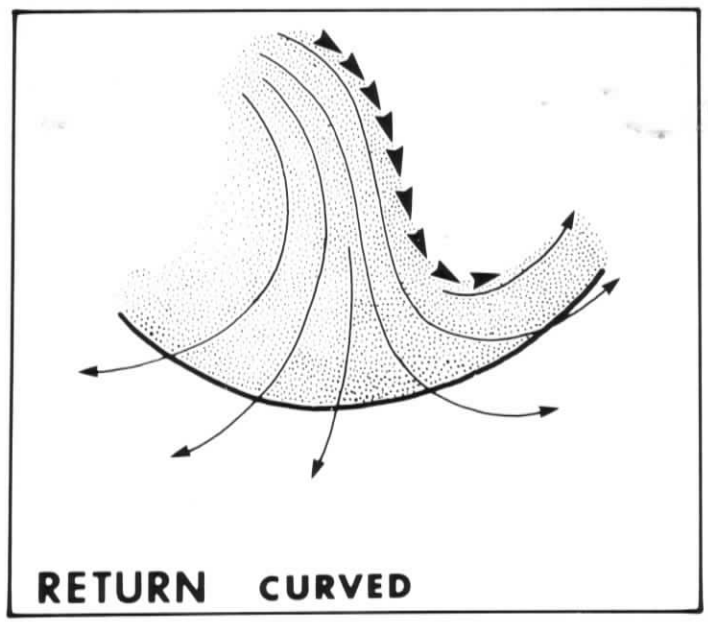

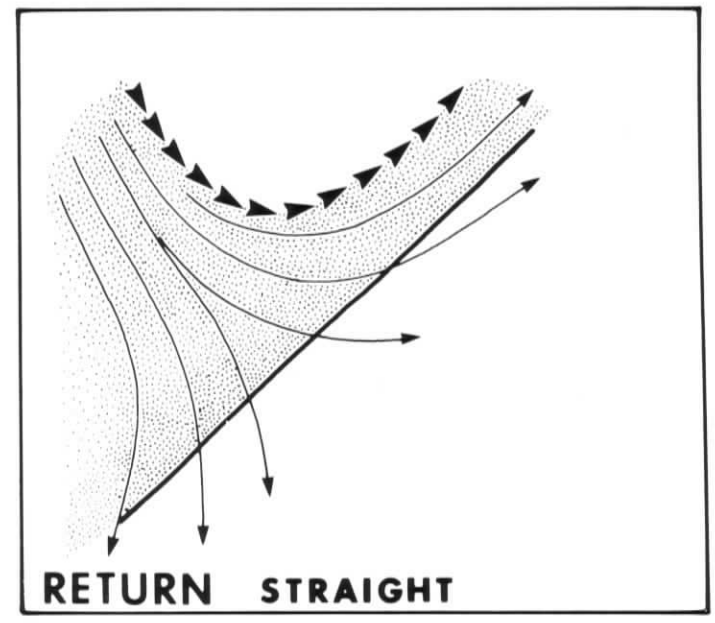

RETURN MOISTURE BOUNDARIES

These boundaries, during their initial stages, constitute a special type of boundary on the rear side of an upper air trough, or on the forward side of an upper air ridge. Moisture accumulated at high levels on the upstream side of an upper air ridge moves across the ridge, and turns equatorward. Return moisture boundaries form on the forward side of this moisture as it moves equatorward.

Characteristics of RETURN MOISTURE BOUNDARIES

The boundaries move equatorward with upper air moisture on the rear or poleward sides.

The boundaries are often very well defined during their acceleration phases; but, the distinctiveness varies considerably, dependent upon the moisture environment in advance of the boundary.

Horizontal deformation is a significant factor in the boundary formations, with localized downward vertical motion along a long narrow zone just in advance of the boundaries.

The associated upper air winds usually cross the boundaries in a diffluent pattern during their movement, with a col forming after becoming stationary.

Those moving directly equatorward are usually curved with very little high cloudiness within the moist region to the rear of the boundary. Straight boundaries move with an easterly and equatorward component. High cold clouds are usually present to the rear of the straight types.

d. Some General Observations in Regard to Boundaries

Orientations with Respect to the Upper Air Winds

In "open wave" upper air circulation environments, the moisture boundaries tend to be oriented across the flow. In these situations, in which the upper air streamlines are oriented across the ridge and trough axes, the circulation systems and the moisture boundaries are moving significantly.

In "closed" upper air circulation environments, the moisture boundaries tend to be oriented parallel to the flow or through the stretching axes of cols in the wind field. In these situations, the upper air flow is oriented around anticyclones and cyclones, or elongated ridges and troughs; and, both the systems and the moisture boundaries are nearly stationary or moving very slowly.

Boundary Distinctiveness and Its Changes with Time

There are better correlations between the change of distinctiveness of boundaries and changes in the circulation conditions, than between the conditions themselves. For example, specific types of changes in boundary conditions are empirically well correlated to atmospheric changes, such as cyclogenesis or the opening of a cut-off upper air low. The correlations are not as great between particular boundary conditions at a specific time and the existing circulation systems.

The subjects of changing conditions with time are addressed in all of the remaining sections, and specifically in the next section.

e. Reference List - Examples of Boundaries

Examples of various types of boundaries are present on many figures. Figure numbers are listed below. Bold numbers indicate that the boundary is a topic of discussion in the accompanying text.

Head	**1**, **2**, **3**, 4, 7, **10**, **11a**,**b**, **13**, **14**, **15**, 29, 37, **41**, **42**, 43, **44**, 45, 47e,f,g, **56c**,**d**, **62**, **66c**,**d**, **67**, **68**, **69c**,**d**, **75b**, 90
Inside	**10**, **11d**, **20**, **21**, **22**, **24**, **25**, **35**, **37**, **57**, 61, **66a**,**b**, **67**, **68**, **74d**, **79**, **80**, **84**, **85a**, **86e**
Dry Surge	**6**, **7**, **12e**, 37, 61a,b, 62a,b, **64a**,**b**, 69c,d
Base Surge	
Direct	**9c**,**d**, **18**, **19**, **64a**,**b**, **70**, **83**, **86d**
Indirect	**16**, **17**, 77, **81**, **82**, **86b**,**c**, **89**
Parallel Jet	**4**, **5**, **11**, **63**, **64c**,**d**
Leaf	**8**, **38**, **39**, **40**, **41**, **49a**,**b**,**c**, **65**
Return	**11c**,**d**, **25**, 29, **57**, 74c,d, **87c**,**d**,**e**

This page intentionally left blank

SECTION B

EVOLUTION OF FEATURES

In this section, we shall discuss some of the common changes with time of features observed on water vapor imagery. Sequences of imagery are used along with selected upper air analyses to illustrate the formation, evolution, and dissipation of image features, including many of the boundary types introduced in Section A. Emphasis has been given to features which are explicitly observed on water vapor imagery and difficult to observe on visible and standard infrared imagery.

1. "DARK" REGIONS AND "DARKENING" WITH TIME

An area of "darker" gray shades on water vapor imagery is an area from which radiation arrives at the satellite from a warmer source. Generally, on 6.7μm imagery, a darker area is associated with relatively drier air in the middle and upper troposphere. However, as pointed out in Part One, layered conditions and temperature differences may produce exceptions; and, often introduce complications, even when dry air aloft is the primary contribution.

In the particular cases chosen for this section, the significant presence of dry air aloft, or drying with time, were primary factors. Upper air radiosonde data were used to confirm specific conditions. However, in general, we shall use the term "dark" instead of "warm" or "dry", since layered conditions and temperature differences may be contributing factors.

During the winter seasons at higher latitudes - especially over continents - dark regions may be absent on water vapor images. Although the atmosphere can be very dry, the cold temperatures contribute to light gray shades. Elsewhere, and during other seasons, dark areas and features are common, ranging from single pixel sizes at the lee of mountains to very large regions over the subtropical latitudes. The large subtropical dark regions are more prevalent in the winter hemispheres.

Generally, the dark areas are associated with dry conditions in the middle and upper troposphere. Once an area aloft has become dry, it tends to remain so until replaced by moist air. This can occur by the convergence of adjacent moisture regimes, or by "moistening" by smaller scale mixing processes such as convective weather. If no "moistening" process occurs immediately, the residual dry air aloft will move and evolve with the associated wind fields. Thus, the dark regions may evolve into a variety of shapes and be present in a variety of different types of wind regimes. This residual evolution of dry and moist areas aloft, causes difficulty in relating the dark areas on imagery to specific types of circulation systems. If generalizations must be made in this regard, we found the following to be the best correlations. Dark regions tend to be associated with middle tropospheric thermal troughs and light areas with thermal ridges. The levels of temperature fields referred to here range from 600mb to 400mb, and upward to 300mb over low latitudes and during summer seasons. The generalization could be made, substituting height field troughs and ridges at those similar levels, but the correlation decreases significantly. This relationship is useful only in cases of open moving systems.

Another generalization is that dark regions are more prevalent in equatorward upper air flow, and light regions in poleward upper air flow.
Fortunately, there are better correlations for specific types of "synoptic situations" - specific circulation system types at specific phases of their evolution. Relatively useful relationships were also found in regard to "changes with time". The formation and demise of synoptic scale dark regions can be related to specific circulation features and their changes.

Numerous examples of darkening with time were observed on successive water vapor images; and, in many cases, viewed on time lapse motion at one hour intervals. In cases over the continental data network, radiosonde data were used to confirm vertical moisture distributions and their changes with time.

Although we did not have measurements of vertical motion, we conclude that darkening with time on 6.7μm water vapor imagery generally implies active sinking - or downward vertical motion in progress. There are exceptions and complications. For example, some observed darkening can be caused by the dissipation of layered clouds or numerous small convective cloud elements. Such clouds can dissipate by mixing or by radiational effects. We believe that such cloud dissipation effects, and radiational warming effects, are relatively minor contributions in general; or, when they are not minor, they can usually be detected. However, in our case analyses relating darkening with circulation features, we excluded those cases in which cloud and radiation effects appeared to have any significant role in the gray shade changes.

There are two ways in which darkening with time can be observed on water vapor imagery. One method is to observe the changes of a dark area on successive images. A dark region may form within a larger region of generally lighter gray shades; or, a dark region may become larger in area, become darker in gray shades, or both. Such changes, when significant, can be observed by comparing successive still images. However, relatively uniform production of imagery is necessary.

By the first method, changes in gray shades are observed following the system in time, as it moves. The second method is to observe the gray shade changes of individual moisture parcels or elements in motion. Using imagery in one-hour time lapse motion, small moisture elements can be observed becoming darker in time as they approach a dark region. This darkening with time following the individual parcels - is very difficult to observe by comparing successive still images. It is relatively easy to observe when imagery are viewed in time-lapse motion. It is also not necessarily indicative of downward vertical motion. Evidence in some cases indicated that horizontal moisture divergence was a significant factor in parcel darkening. In other cases, cloud element dissipations - both at and below - the primary moist layer were factors.

When moisture is warming by downward vertical motion, it is most explicitly viewed by water vapor imagery in time-lapse motion. There are cases in which dark areas are changing little with time as they propagate, yet parcel darkening can be observed along the upstream edge of the area. However, most dark regions observed on water vapor imagery are undergoing changes with time as they move. Therefore, significant parcel darkening and the associated downward vertical motions can usually be implied by comparing successive still images. Although more frequent imagery is desirable, images at 6-hour intervals are usually adequate for observing significant events of synoptic scale darkening.

We have identified several common types of area darkening, and related them to associated circulation features and changes. The following cases illustrate some of those types. Other cases are included with other primary subject materials of later sections.

a. Darkening With Time in Westerly Wind Regimes

Dry Surge Darkening

On **Figure 12**, water vapor images are shown at 12-hour intervals, and are repeated with 500mb streamlines and isotherms. Black arrowheads indicate jet stream axes, derived from maximum wind analyses (not 500mb winds). The primary jet stream branch was the southern one shown, with wind speeds in the core generally between 130 and 150 knots. The level of maximum winds was slightly below 200mb along those portions of the core over the dry regions, and near 150mb along the eastern portion with high level moisture and clouds.

In this case, at the initial time, conditions were relatively dry with the darkest area over northwestern Mexico. During the 24 hour period, this region becomes darker with time as it moves eastward. Because of the contrast in gray shades with the cold top convective cloudiness on the later images, the darkening appears greater than actually occurred. On **Figure 12a**, within the dry region over northwestern Mexico, the minimum measured "**image brightness**" * was over the Gulf of California with a value of 33 indicated by a white dot. On **Figure 12c**, the measured "image brightness" was 15 at the white dot over southern Mississippi. The darkest area was slightly southwest of there but couldn't be measured because of the map grid. Generally, the 24 hour darkening was between 15 and 20 points on the 0-100 scale, which was significant.

In this case, the darkening region is within the jet stream zone with upper air cyclonically curved flow. Note, that it is associated with 500mb cold advection, which increased and became more concentrated in area during the sequence of images. The 500mb wind speeds within the darkening region were between 40 and 65 knots.

We refer to this type of darkening with time in the westerlies as "dry surge" darkening. The darkening is often associated with the accelerated phase of a short wave system in the westerlies. Generally the maximum darkening occurs under, or slightly to the cyclonic side of the jet core. Significant 500mb cold advection is commonly present. When the darkening with time is associated with the formation of a new dark region, the 500mb cold advection generally begins or becomes significantly greater in magnitude during the same period. Prior to the darkening, a strong baroclinic zone may be present but the winds are parallel to the isotherms. The 500mb winds in the darkening region are usually either parallel to the height contours or crossing toward higher heights. Wind speeds often decrease from upstream into the dark region. In the case shown, at the time of **Figure 12e**, 500mb wind speeds were 40 knots in west central Alabama, 55 knots in central Mississippi, and 75 knots over northeastern Texas.

* "Image Brightness" is a quantitative indication of image gray shades using a scale of 0-100 (black = 0, white = 100). The data are derived from densitometer measurements of image gray shades, and are normalized to account for differences in image reproduction. The concept is applied extensively in Part One, Section C, and is introduced on page 28.

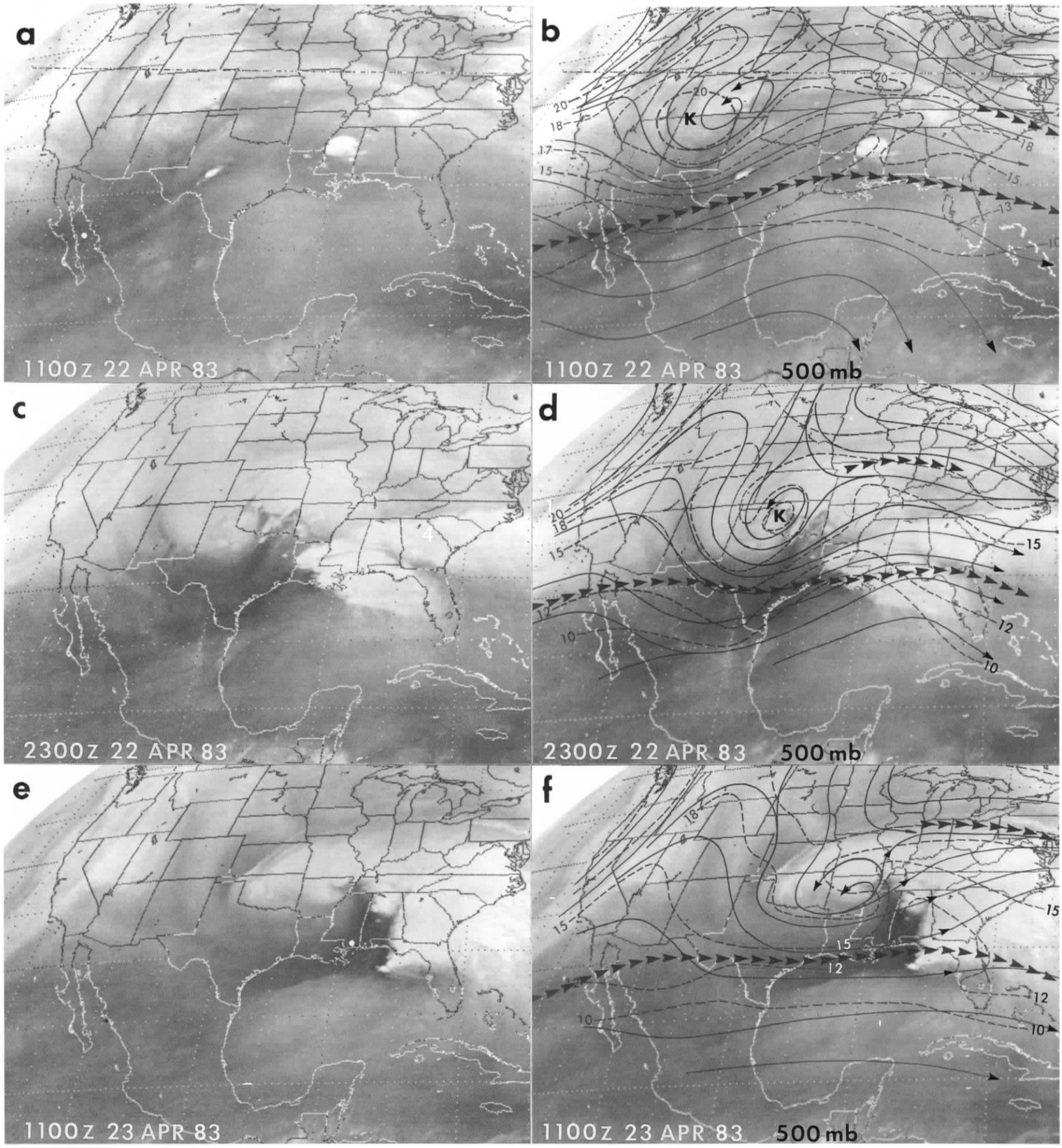

Figure 12 **DARKENING WITH TIME - DRY SURGE EASTWARD**

Sequence of three 6.7μm images at 12-hour intervals on the left column. Same images are repeated on the right column with analyses: solid lines - 500mb streamlines, dashed lines - 500mb isotherms labeled in degrees Celsius, black arrowheads - jet stream axes from maximum wind analyses. Upper air data are valid one hour after the images.

Figures 12a and **12b**. 1100Z 22 April 1983 GOES East.

Figures 12c and **12d**. 2300Z 22 April 1983 GOES East.

Figures 12e and **12f**. 1100Z 23 April 1983 GOES East.

Head Darkening

On **Figure 13**, as in the last case, imagery are shown at 12-hour intervals with and without 500mb streamlines and isotherms. On **Figure 14**, close-up views are valid 6 hours prior and 6 hours after the sequence on **Figure 13**.

On **Figure 13a**, a small dark region is present over the northern border of Minnesota at "D". This area is enlarged on **Figure 15b**, on a close-up sector, although the gray shade display is different. The dark region, "D", is on the "dry" side of the head boundary associated with the closed low over north central Iowa. A surface low with the system is centered over east-central Iowa with a minimum pressure of 994mb at 1200Z. Note on **Figure 13b**, that the region of cyclonic curvature in the 500mb winds is dominated by relatively warmer air. The thermal trough is narrow, extending from Kansas to eastern Wisconsin.

As previously discussed, head boundaries generally do not have wide dark zones along their "dry" sides. The formation of a dark area adjacent to the head boundary of a storm system is an indication that the trough on the dry side of the boundary may be intensifying.

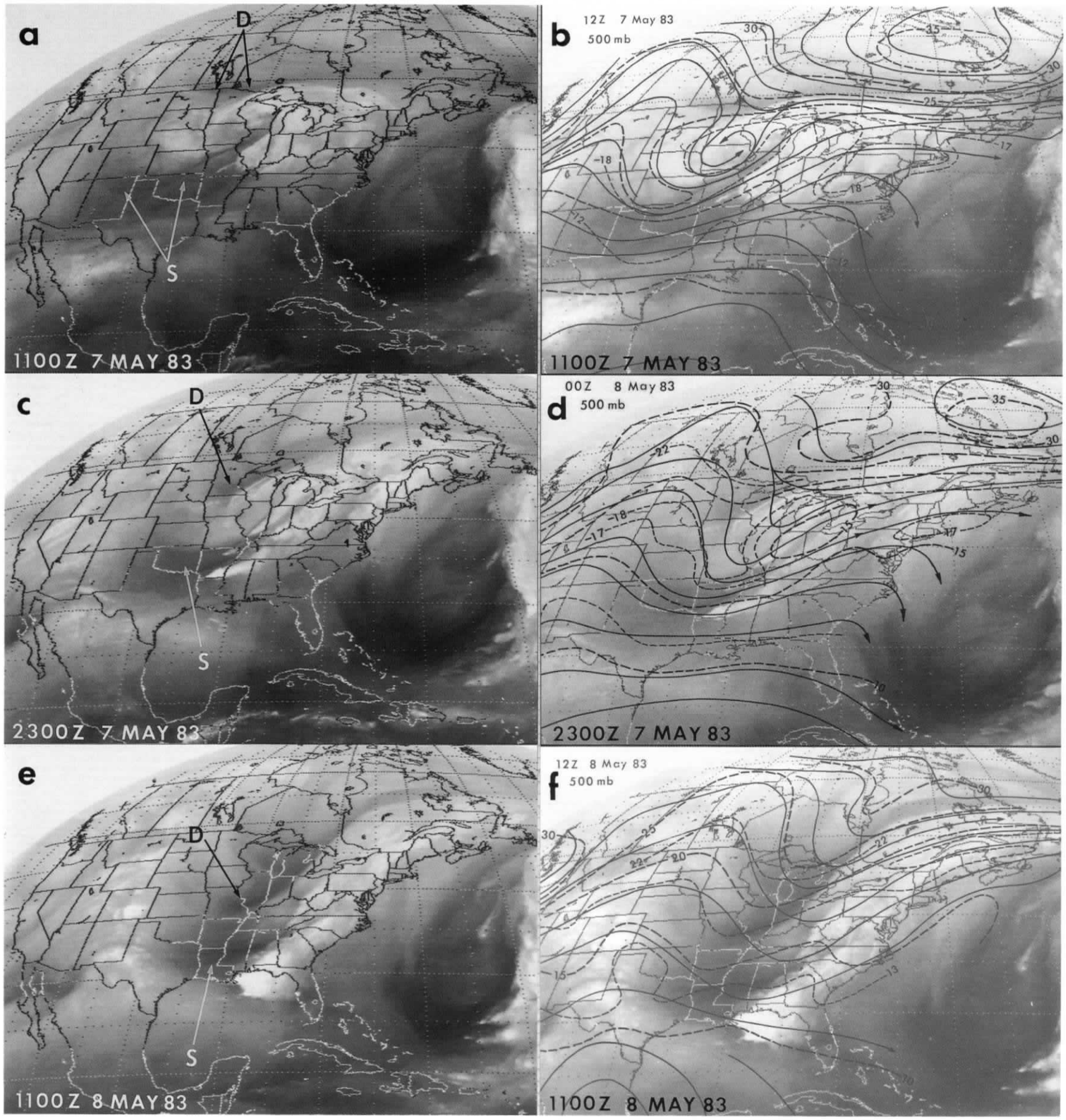

Figure 13 **HEAD DARKENING**
Sequence of three 6.7μm images at 12-hour intervals on the left column. Same GOES East images on the right column with 500mb streamlines (solid) and 500mb isotherms (dashed) labeled in degrees Celsius. Analyses valid one hour later than respective images.
Figures 13a-13b. 1100Z 7 May 1983. **Figures 13c-13d.** 2300Z 7 May 1983. **Figures 13e-13f.** 1100Z 8 May 1983.

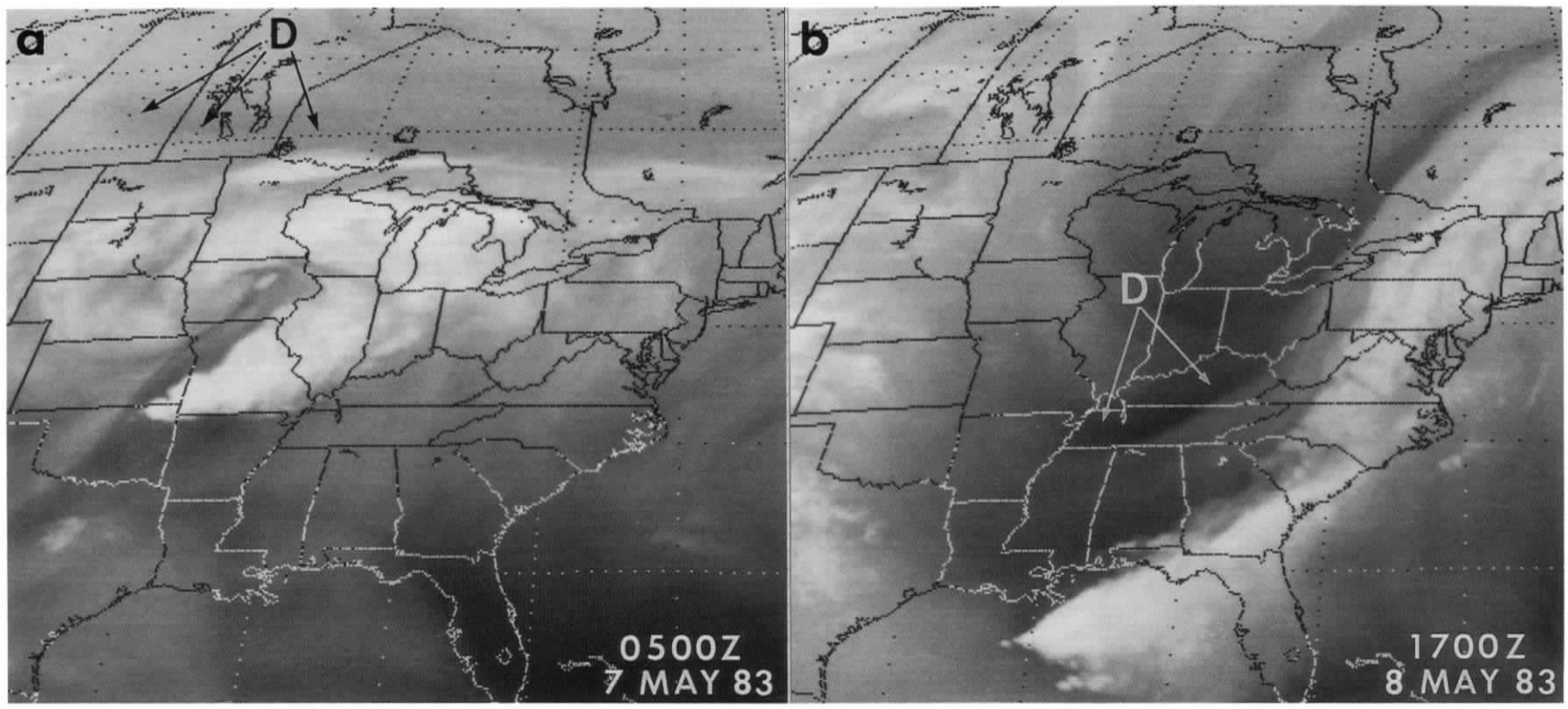

Figure 14 **CHANGES DURING THE HEAD DARKENING EVENT**
6.7μm images valid six hours before and after the sequence of **Fig. 13**. **Fig. 14a**. 0500Z 7 May 1983. **Fig. 14b**. 1700Z 8 May 1983.

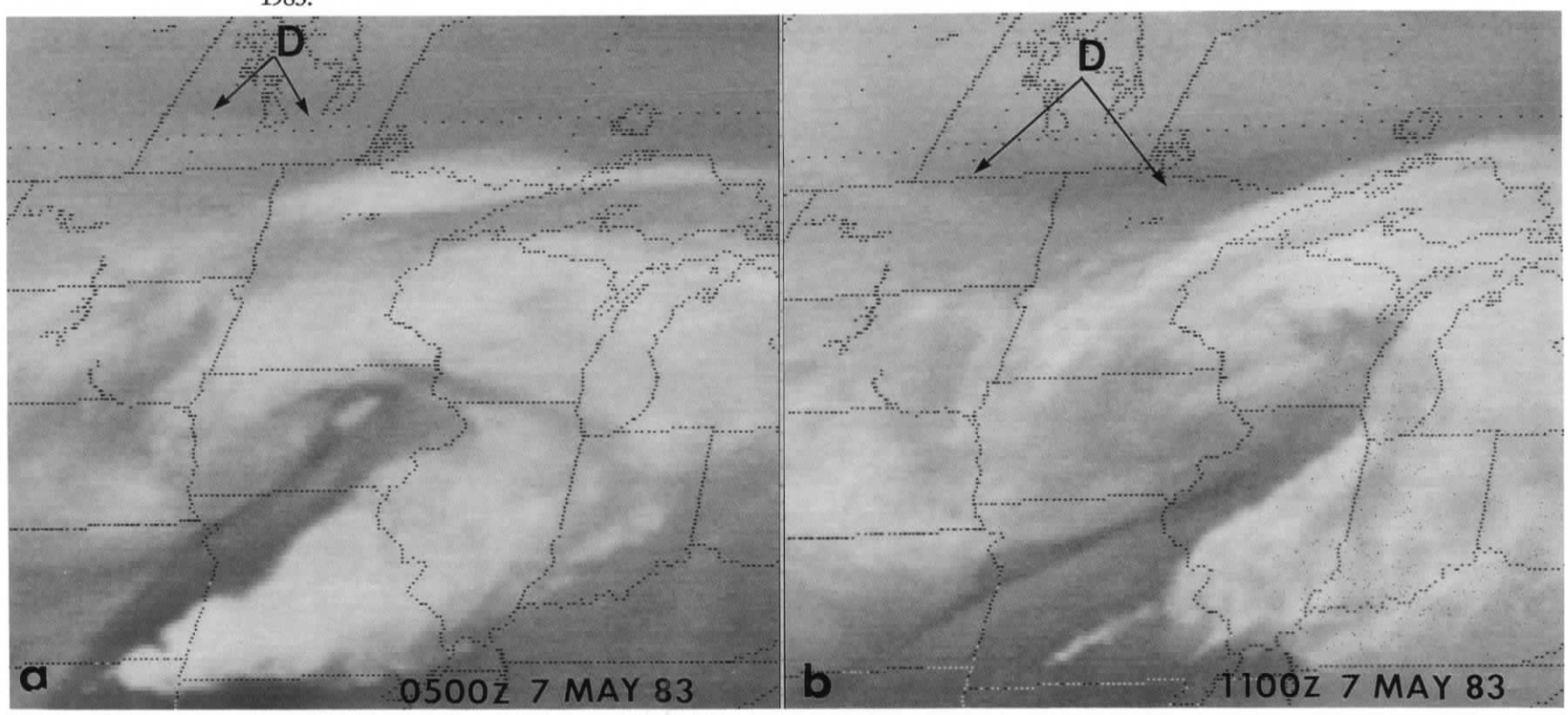

Figure 15 **EARLY DETECTION OF HEAD DARKENING - CLOSE- UP IMAGES**
Close-up view 6.7μm images, 7 May 1983. **Fig. 15a**. 0500Z (same time as **14a**). **Fig. 15b**. 1100Z (same time as **13a** and **13b**).

Commonly, during the evolution of a storm system, the colder mid-tropospheric air approaches from around the equatorward side of the upper air low or vorticity maximum. The primary dark region is in the dry surge position, often evolving to a "slot" configuration. In this case, at the time of **Figures 13a** and **13b**, the primary dark area is southwest of the storm system, at "S", but is no longer darkening.

Twelve hours later, on **Figure 13c**, head darkening has become significant. Not only has the dark region "D" become larger, but the head boundary has changed from a convex curvature to straight. The southern dark region has become smaller. On the 500mb analysis, **Figure 13d**, cold advection is minimal in the vicinity of the southern dark area, but has become significant at the head region. The previously closed low has opened to a trough. By this time, the surface low pressure system has become elongated with a minimum pressure of 1002mb near the northeast corner of Indiana.

By **Figure 13e**, some renewed darkening has occurred with the southern dark area; but, the head darkening has dominated. At this time, no surface low center is identifiable. The minimum pressure along the elongated surface trough was 1004mb.

During the 24 hours of the image sequence on **Figure 13**, the continued evolution of the storm system was halted. The surface low stopped deepening and filled. The associated upper air low opened as the primary region of mid-tropospheric cold advection changed from the slot position to the head position. At the initial time, in this case, there were three jet stream branches across the upstream ridge: one over Mexico, another over Canada, and the strongest from Colorado to Oklahoma to central Illinois. The open western end of the Canadian trough intensified with more northerly flow across the northern portion of the ridge. The primary cold advection then occurred at the head position of the central U.S. storm. By the last image time, the flow over the ridge was more equally distributed. Although three jet branches remained, the central branch had become the weakest of the three.

Water vapor imagery can be a valuable tool for early detection and observation of this type of event. It may be used to verify or refine model forecasts over continental data networks, or to recognize the events elsewhere.

On **Figure 15**, close-up images are shown at the time of **Figure 13a**, and 6 hours earlier. The new darkening at "D" would have been difficult to detect on still imagery prior to the 1100Z image. By 1100Z, it should have been identified; however, the question of its significance would arise. Had the forecast models indicated the change and opening of the low, the observation of area "D" on the water vapor imagery would provide early confirmation. If no such changes were indicated by the computer forecasts, area "D" should be considered as a potential model error, and observed carefully. If the area continues to darken and expand, and the head boundary changes shape from convex to concave, the event has become significant. Interruption of the storm evolution is likely.

Another example of early indication of head darkening was shown by **Figures 3a** and **7a**. Although the head boundary had remained convex at the time of **Figure 7a**, its shape reversed shortly afterward.

b. Base Darkening

Base darkening occurs during the formative phase of base surge boundaries. However, the boundaries can remain as distinct features after the darkening has ceased. Although distinct base surge boundaries are usually associated with base darkening, this is not always the case. In some cases, the darkening occurs without a distinct or well defined boundary.

An excellent example of base darkening was shown on **Figure 9**, associated with the example of a base surge boundary over the Pacific Ocean. However, little data were available to relate the imagery to the circulation systems.

As with base surge boundaries, base darkening is associated with an increase in the equatorward component of upper air flow. Although there are several ways in which this occurs, it is often associated with the amplification of an upper air ridge system. We shall illustrate several of the types. A significant difference in those types involves the presence, or absence, of an initial boundary; and, whether that boundary is associated with a significant axis of maximum winds. The Pacific case of **Figure 9** did include an initial boundary with a jet stream branch associated; the following case did not.

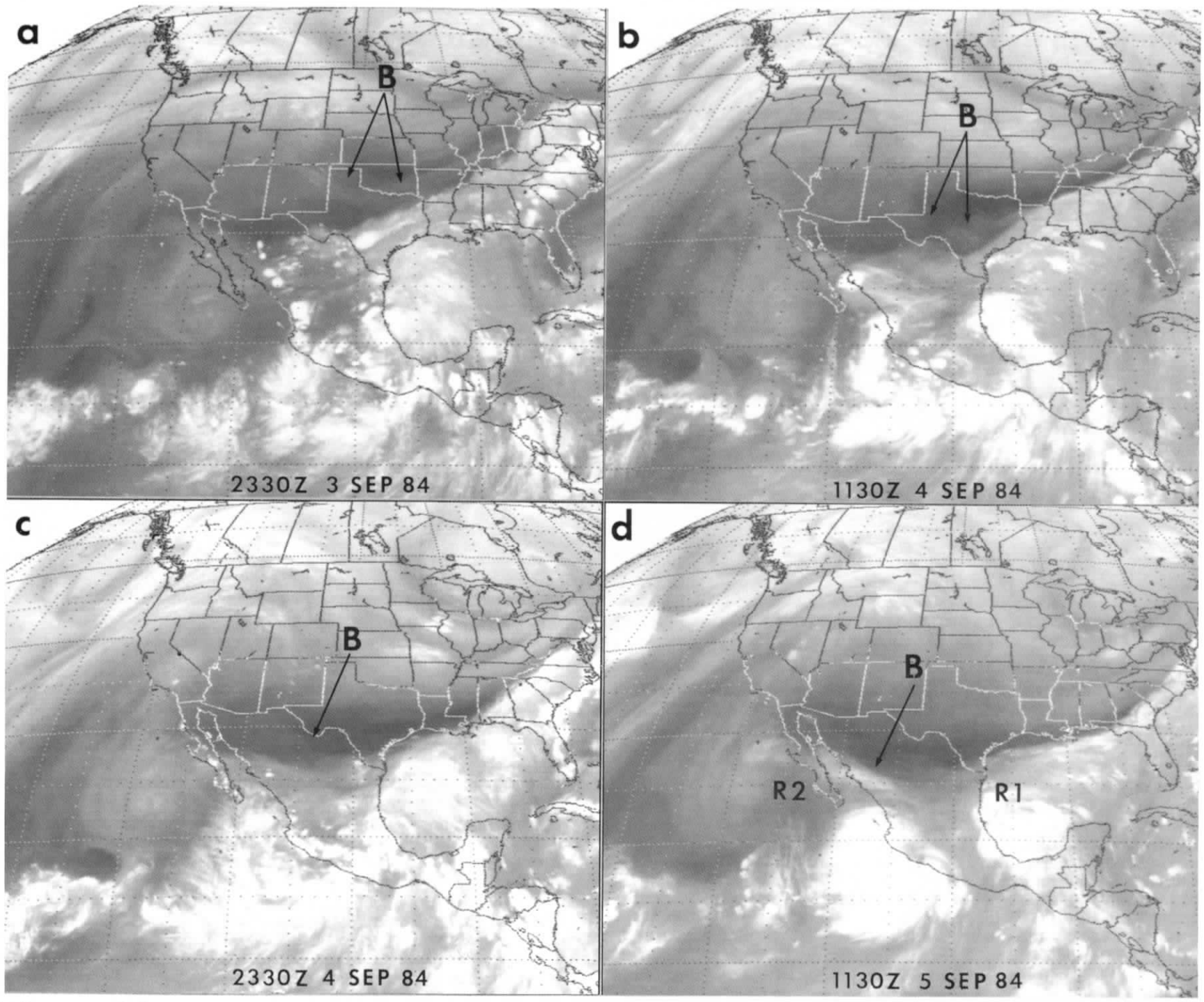

Figure 16 **BASE DARKENING - INDIRECT TYPE**
Sequence of four 6.7μm GOES Central images at 12 hour intervals. Labels "R2" and "R1" are referenced in Section E text.
Fig. 16a. 2330Z 3 September 1984. **Fig. 16b.** 1130Z 4 September 1984.
Fig. 16c. 2330Z 4 September 1984. **Fig. 16d.** 1130Z 5 September 1984.

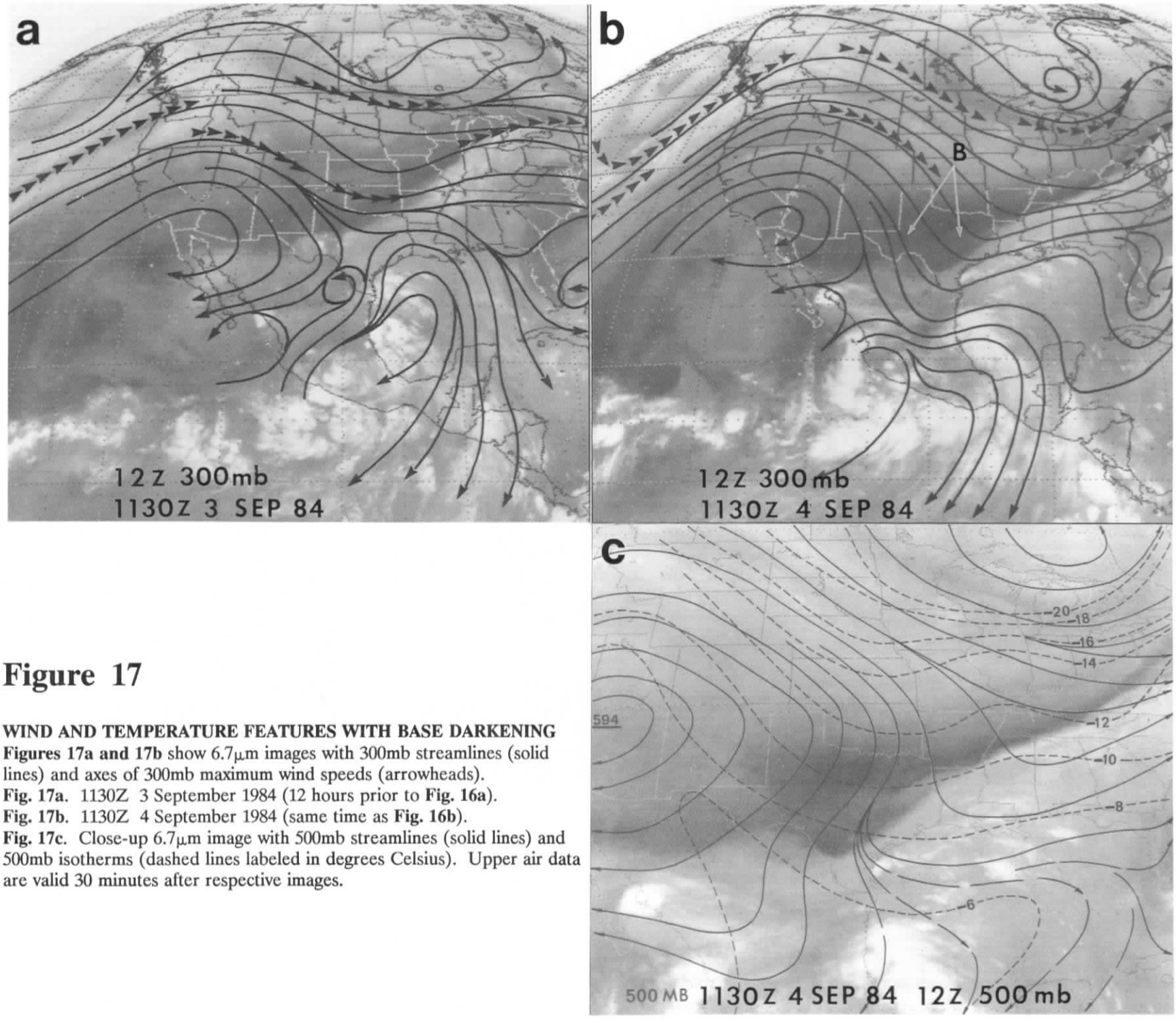

Figure 17

WIND AND TEMPERATURE FEATURES WITH BASE DARKENING
Figures 17a and 17b show 6.7μm images with 300mb streamlines (solid lines) and axes of 300mb maximum wind speeds (arrowheads).
Fig. 17a. 1130Z 3 September 1984 (12 hours prior to **Fig. 16a**).
Fig. 17b. 1130Z 4 September 1984 (same time as **Fig. 16b**).
Fig. 17c. Close-up 6.7μm image with 500mb streamlines (solid lines) and 500mb isotherms (dashed lines labeled in degrees Celsius). Upper air data are valid 30 minutes after respective images.

On **Figure 16**, four water vapor images are shown at 12-hour intervals. On the first image, a small dark region has formed at "B" over Oklahoma and northern Texas. At that time, a residual dark region was already present farther to the south - an elongated irregular region over northern Mexico and central Texas. A moderately distinct, but irregular boundary is present along the southern side. With time, the northern dark region can be observed to increase in size and move southward, merging with the elongated southern dark area.

By the last image, **Figure 16d**, a relatively wide dark region is present across northern Mexico and southern Texas. The boundary along the southern side of the dark area has become better defined, and formed a concave shape - from the moist side perspective. Although some thin cirrus and middle cloudiness were present on the moist side of the boundary, their patterns were irregular. The boundary was primarily defined by the difference in moisture regimes.

On **Figures 17a** and **17b**, 300mb analyses are shown on water vapor images valid 12 hours before and after the first image of **Figure 16**, a 24-hour period when the base surge was first detectible and expanded to significant size. During the period between analyses, the upper air ridge over the western United States amplified; and, the winds on its eastern side changed to a more northerly component. The ridge amplified while moving eastward slowly; whereas, the center of the anticyclone remained nearly stationary. On **Figure 17c**, a 500mb analysis valid at the time of the second 300mb analysis, is shown on a close-up water vapor sector. A region of maximum anticyclonic curvature in the 500mb streamlines is present along the northern edge of the dark zone, which is located within a region of cold air advection. The 500mb wind speeds over northern Texas and Oklahoma were between 15 and 20 knots. The advection was relatively weak although the streamlines crossed the isotherms at large angles.

In this case, the base darkening produced a new base surge boundary that moved southward and merged with a residual moisture boundary over northern Mexico. Although the case was complicated, we would consider this an "indirect" type of base surge event. The final merged base surge boundary was not a part of the ridge system which amplified to cause the base surge. There was no jet stream branch along the new boundary or the residual boundary. A base surge event of the "direct" type is shown in the next case.

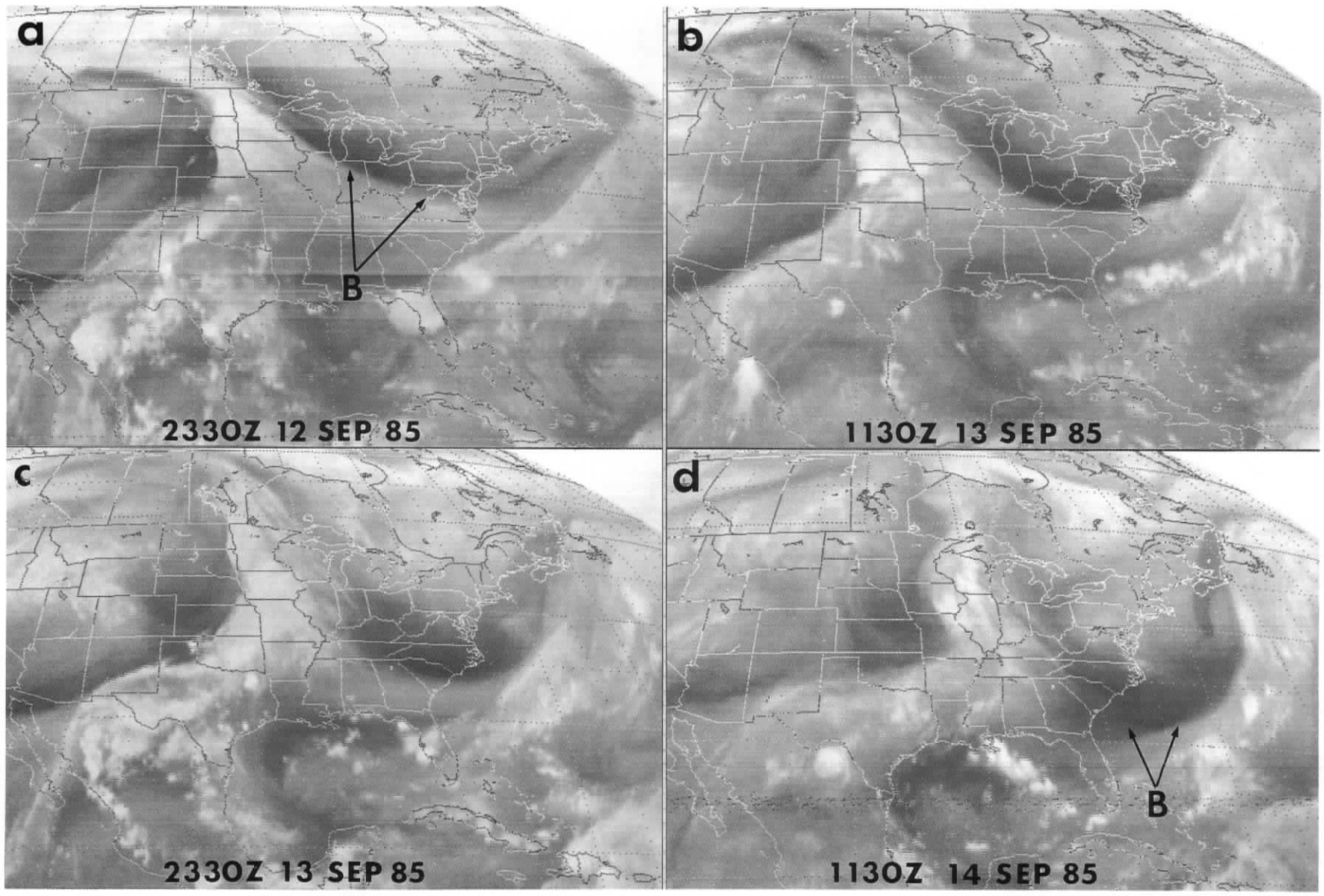

Figure 18 **BASE SURGE DARKENING - DIRECT TYPE**
Sequence of four 6.7μm GOES Central images at 12-hour intervals.
Fig. 18a. 2330Z 12 September 1985. **Fig. 18b.** 1130Z 13 September 1985.
Fig. 18c. 2330Z 13 September 1985. **Fig. 18d.** 1130Z 14 September 1985.

On **Figure 18**, water vapor images are shown at 12 hour intervals. The boundary, initially present at "B", changed to a base surge boundary. During the 36 hour period, a wide dark area formed on the north side of the boundary which accelerated south-southeastward. On **Figure 19**, analyses are shown on the first and third images of **Figure 18**. The fourth image time was not used because the boundary and its adjacent dark area had moved east of the radiosonde network.

At the first image time, the dark area on the northern side of boundary "B" is relatively narrow, although it has begun to widen over the Michigan to Ohio area. Note on the 300mb analysis of **Figure 19a**, that the axis of maximum winds is nearly coincident with the boundary from Wisconsin eastward. During the following 24 hour period, the upper air ridge, "R", at the upstream end of the jet stream branch, amplified significantly. The winds along the boundary to the east of ridge "R" rotated anticyclonically with time. Base darkening occurred, and the boundary surged equatorward. By the last image time, a wide dark area is present along the northern side of the boundary. A "direct" type of base surge process occurred.

At the first image time, the jet stream branch along boundary "B" was of the "channeled" configuration with wind speeds of greater than 110 knots from northern Virginia eastward. Speeds of greater than 90 knots were present from Lake Michigan eastward at 300mb. With the "channeled" structure, the axis of 300mb maximum winds is parallel to the wind directions and to the boundary. On **Figure 19c**, a 500mb analysis is shown on an enlarged image sector with a lighter gray shade display. Note that the streamlines are nearly parallel to the isotherms along the boundary and strong wind zone. Similarly, the streamlines were nearly parallel to the 500mb vorticity isopleths (not shown). Such moisture boundaries, with concave curvature in the poleward direction and a relatively narrow dark zone along their drier side, usually have a jet stream branch coincident with them; and, the jet stream is usually of the "channeled" configuration.

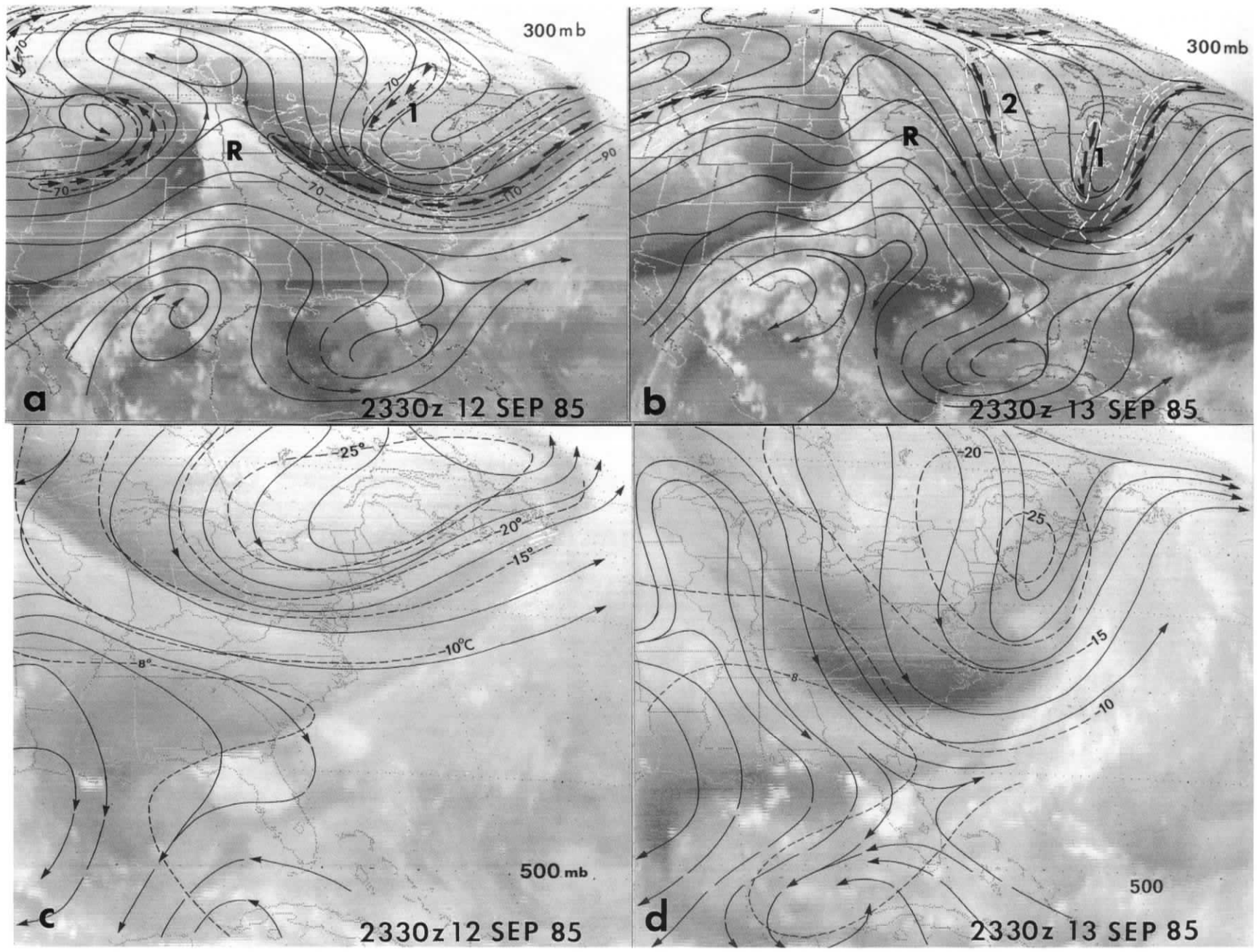

Figure 19 **UPPER AIR FEATURE CHANGES - WIND AND THERMAL FIELDS**

Figures 19a and 19b. Same 6.7μm images as 1st and 3rd times of **Figure 18**, with 300mb streamlines (thin solid lines), 300mb isotachs (short dashed lines labeled in knots), and axes of maximum 300mb wind speeds (black arrows). **Figures 19c and 19d.** Close-up 6.7μm images valid at the same times as images **19a** and**19b**. Solid lines - 500mb streamlines, dashed lines - 500mb isotherms (°C).

As ridge "R" amplified and opened, the upper air winds on the east side of the ridge rotated to more northerly components. Analyses are shown 24 hours after the first image time on **Figures 19b** and **19d**. The 300mb wind speeds have decreased significantly along that part of the boundary moving southward, and the streamlines are oriented across the boundary with an equatorward component. At 500mb, the streamlines are no longer parallel to the isotherms. They cross with cold advection components within the new dark area, and along that portion of the boundary on the equatorward side of the dark area. Such changes are typical when a boundary similar to this one at its initial time develops a wide dark area along its poleward side and surges equatorward. (Note that the speed maximum labeled "2" on **Figure 19b** was a new branch that broke southward through the west-to-east oriented Canadian ridge, as ridge "R" intensified and opened. It was not a part of the jet stream branch along boundary "B".)

This case illustrated a "direct" type of base surge event. In regard to image interpretation, it is useful to be able to distinguish between those types of boundaries present at the beginning and end of the period shown. Both have a similar orientation concave toward the poleward side. That with the narrow dark zone along its poleward side had a jet stream branch coincident with the boundary. After such a boundary develops a wide dark zone and surges equatorward, a coincident jet stream branch is no longer likely, except along the eastern end of the boundary. Interpretation can be improved by observing the changes with time of the dark zones, and the movement of the boundaries, rather than relying on the characteristics on a single image.

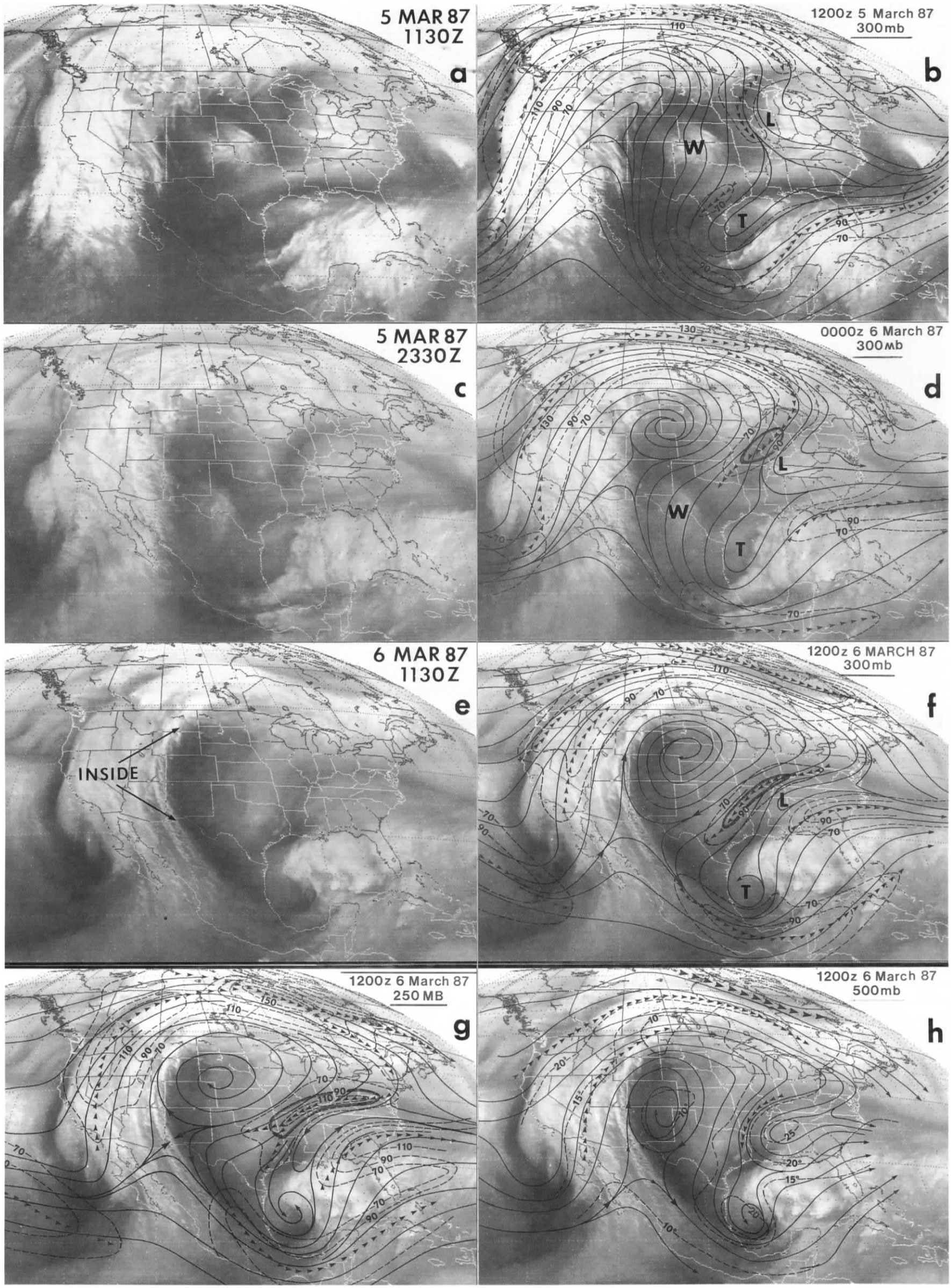
5 MAR 87
1130Z
a
1200z 5 March 87
300mb
b
W
L
T
5 MAR 87
2330Z
c
0000z 6 March 87
300mb
d
W
L
T
6 MAR 87
1130Z
e
INSIDE
1200z 6 MARCH 87
300mb
f
L
T
1200z 6 March 87
250 MB
g
1200z 6 March 87
500mb
h

2. ANTICYCLOGENESIS - INSIDE BOUNDARY EVOLUTION

a. Blocking System - Spring Season

On **Figure 20**, three water vapor images are shown at 12-hour intervals (a,c,e), and repeated with 300mb analyses superimposed (b,d,f). The last image of the sequence (**Figure 20e**) is also shown with 250mb and 500mb analyses superimposed (g,h). An enlarged view of that image is repeated on this page with selected radiosonde site locations. Finally, an image valid 12 hours after the **Figure 20** sequence is shown on **Figure 21** with and without a 300mb analysis, and on **Figure 22** with 500mb vorticity and temperature analyses.

Inside Boundary Formation and Characteristics

At the initial time, a large upper air ridge is present over the western United States and northwestern Mexico. Although the ridge is of very large amplitude, it is not closed on any of the standard upper air pressure surfaces. On the eastern side of the ridge, there are three synoptic scale systems. These are revealed on the 300mb analysis by a trough over the western Gulf of Mexico, at "T", a short wave perturbation over parts of Kansas, Oklahoma, and northwestern Texas, at "W", and a trough and speed maximum over the Lake Michigan area, at "L". This latter system has been intensifying during the past 12 hours as it moved southward, and has developed a closed cyclone in the surface and 850mb wind fields. At the surface, a closed low is centered over central Illinois, with a trough extending southwestward to the Texas panhandle.

The region between the ridge axis, and the jet stream axis off the west coast and over Canada, is very moist with considerable cold top clouds. The eastern edge of this moisture, which generally coincides with the 300mb ridge axis, is very irregular with ragged cirrus cloudiness along much of the edge. Such a pattern is indicative of an open ridge wind system.

By the second image time, an upper air anticyclone has closed in the 300mb wind field, and is centered over western Nebraska. A closed center is also present at 250mb, but not at 500mb or below. The easterly wind speeds on the southern side of the closed center range between 10 and 15 knots.

A stronger jet stream speed maximum has "hooked" around the upper air ridge over the Great Lakes, and extends over eastern Oklahoma. The small short wave system, "W", has moved to western Texas. Although the region of upper air moisture and high clouds are present, the system cannot be identified in the curvature of the 300mb winds. It is revealed in the wind and temperature fields at 500mb and 700mb. To the north of that small system, new image darkening has occurred. The dark region is over the Texas panhandle and parts of New Mexico and Colorado on **Figure 20c**. The surface low over Illinois has moved slowly southward and weakened. The associated system aloft, "L", has closed at 700mb, but is open at 500mb and above.

During the next 12 hours, the speed maximum has continued to "hook" around the anticyclone. By the third image time, a large region of relatively strong northeasterly and easterly flow has formed on the southern side of the anticyclone. The third image is repeated with radiosonde site locations. At Stephenville (S) in north central Texas, the maximum wind reported was 055°/99 knots at 216mb. Directly south of the anticyclone center, the maximum easterly winds are near 300mb and range from 13 knots at North Platte, Nebraska (NP), 41 knots at Dodge City (DC), 43 knots at Amarillo (A), 47 knots at Midland (M), to 57 knots at Del Rio (DR). The eastern side of the primary high moisture and cloud region has changed from a ragged edge to a relatively well defined and distinct "inside" boundary. Col zones associated with the boundary are present in the wind field from 700mb to 250mb. At 300mb and 250mb, the moisture boundary is located along the deformation zones - stretching axes - of the cols, and is nearly parallel to the winds to the north and south. At 500mb, the deformation zone in the wind field is near the boundary, but oriented at a slightly different angle; and, the streamlines cross the boundary along its northern end.

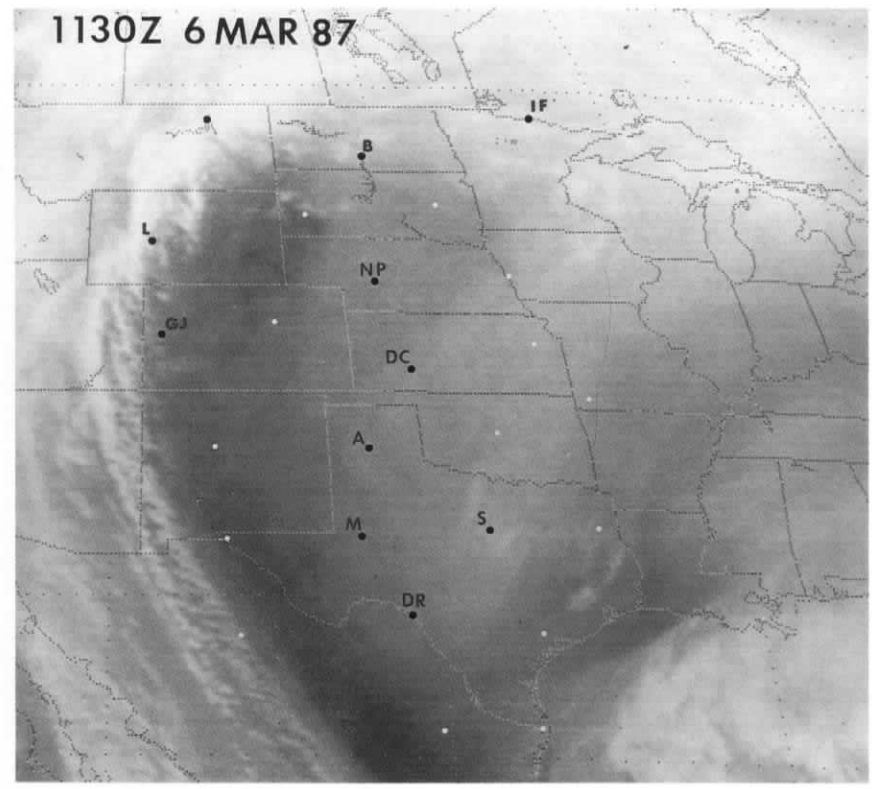

RADIOSONDE SITE LOCATIONS
6.7μm image, 1130Z 6 March 1987 (Same time as Figure 20e).

Along the eastern side of the boundary, a relatively wide dark region has formed extending from Mexico to Wyoming. Radiosonde sites within that zone reported 30°C dewpoint depressions from near 800mb upward to the -40°C air temperature. South of the anticyclone center, on the eastern edge of the dark zone, the gray shades lighten gradually toward the east. Sounding sites directly south of the center reported 30°C dewpoint depressions from the boundary layer to 400mb with generally double digit depressions above. Farther to the east, the base of the high level moisture was lower. At Stephenville, Texas, where cirrus clouds were present at the time of **Figure 20e**, 30°C dew point depressions were reported from 500mb to 800mb. Above that, depressions decreased to 2.4°C at 321mb where the air temperature was -40°C. North of the anticyclone center, over the Dakotas, a moist layer was present at mid-troposphere levels between 400 and 500mb.

The moisture that rotated around the southern side of the anticyclone within the newly formed easterly winds was primarily located at high altitudes. The variation of image gray shades of this moisture pattern is dependent upon the thickness of the moist layer and the relative humidities, rather than the height variations of the top of the moist layer. Generally, within such patterns, areas of lighter gray shades are areas of greater thickness and relative humidity. Less radiation from the lower level warmer origins passes through such areas. The darker portions of the pattern are areas of relatively thin moist layers at similar altitudes. More radiation from the warmer sources below is able to pass through the layer. Some areas of cirrus clouds may be formed within the upper tropospheric moisture. These usually have the lightest gray shades, such as near Stephenville, Texas (S) in this case. These upper air moisture conditions and related image patterns are very common for cases of upper air anticyclogenesis; and, the moisture moving around the anticyclone at the rear of the dark region is likely to be at high altitudes, although the gray shades range from light to dark gray.

Figure 20

INSIDE BOUNDARY FORMATION
Sequence of three 6.7μm GOES Central images (**a,c,e**) repeated with 300mb analyses (**b,d,f**). The last image is also repeated with 250mb and 500mb analyses (**g,h**). Images times are: 1130Z 5 March 1987 (**a,b**) 2330Z 5 March 1987 (**c,d**) 1130Z 6 March (**e,f,g,h**). Analyses are valid 30 minutes after images. Solid black lines - streamlines. Black arrows - axes of maximum wind speeds for respective pressure surfaces. Dashed black lines - isotachs (knots) except on **Fig. 20h** - 500mb isotherms (°C). Ninety knot isotachs over eastern U.S. are widened.

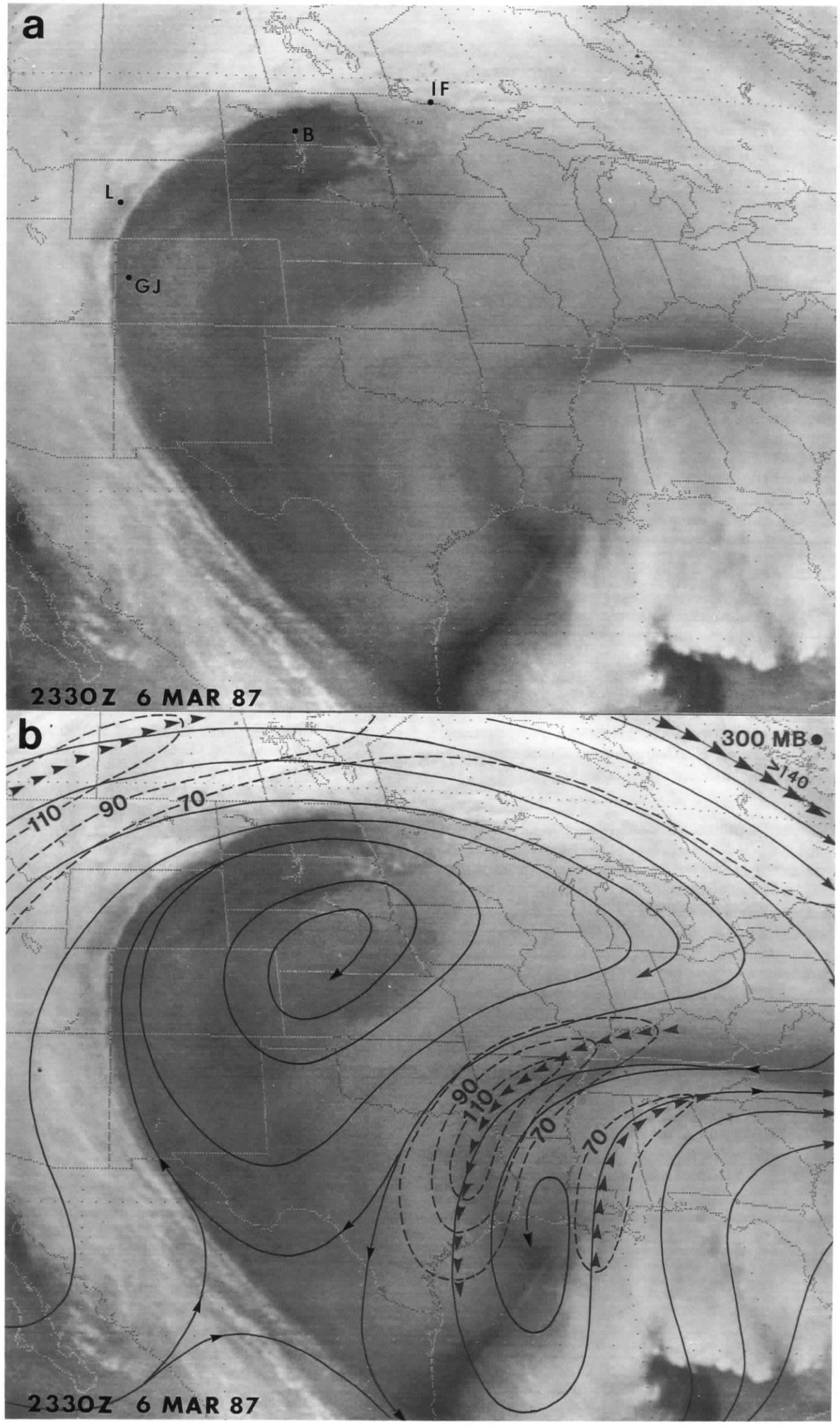

Figure 21 **WELL DEFINED INSIDE BOUNDARY - MATURE PHASE**

Fig. 21a. 6.7μm close-up image, 2330Z 6 March 1987, GOES Central.

Fig. 21b. Same image with 300mb is streamlines (solid black lines), 300mb isotachs (dashed black lines), and axes of 300mb maximum wind speeds (arrowheads). Analysis valid: 0000Z 7 March 1987.

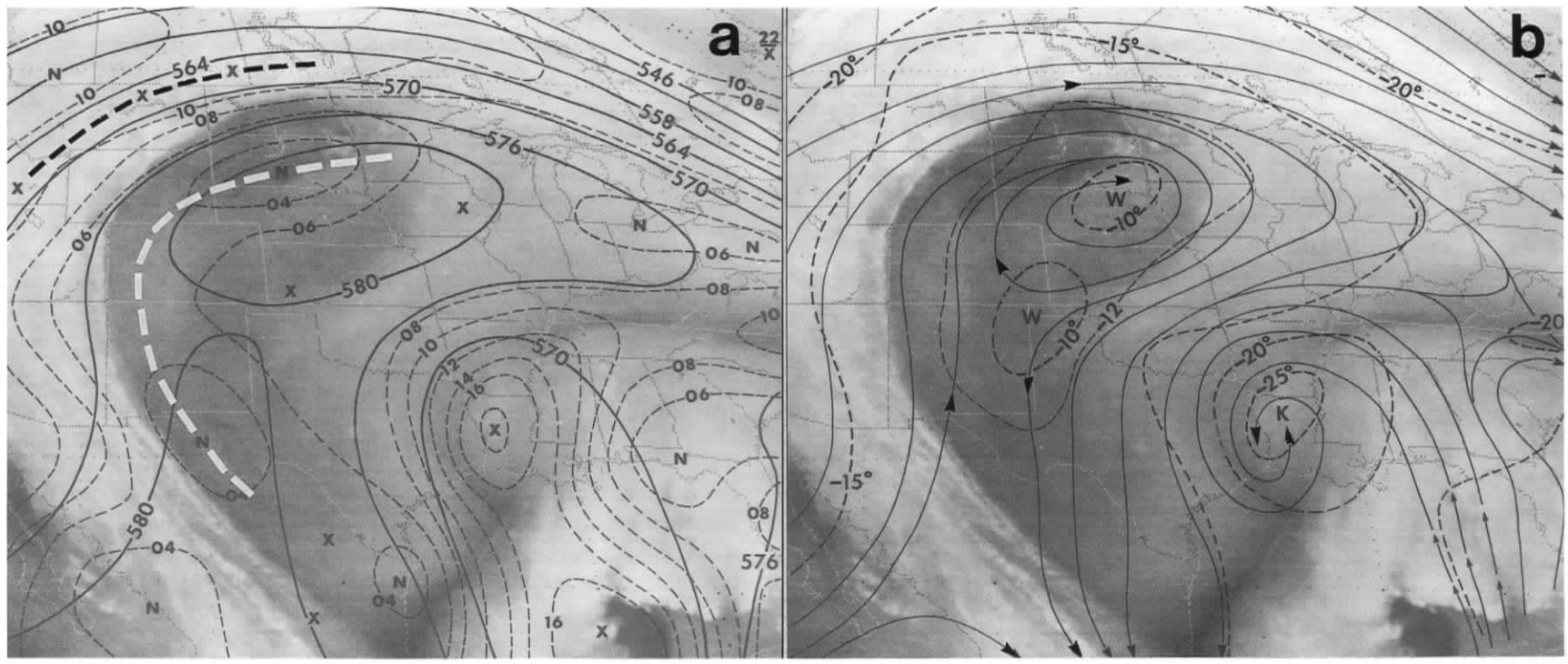

Figure 22 **MID-TROPOSPHERIC WIND AND THERMAL FEATURES**
500mb analyses (0000Z 7 March 1987) on 6.7μm close-up image (2330Z 6 March 1987).
Fig. 22a. 500mb height contours (solid black lines) 500mb vorticity isopleths (dashed black lines). Heavy dashed lines: black = lobe of maximum vorticity, white = lobe of minimum vorticity.
Fig. 22b. 500mb streamlines (solid black lines), 500mb isotherms (dashed black lines - °C) W = warm K = cold.

On **Figure 21**, a close-up water vapor image is valid 12 hours after the last image of **Figure 20**. By this time, the inside boundary has become even better defined. A well defined cirrus cloud band is coincident with a large part of the moisture boundary. However, the boundary has become slightly less distinct south of Wyoming; since high level moisture, moving around the anticyclone within the upper air easterlies, has extended over much of the dark region adjacent to the boundary. A part of the boundary from Wyoming northeastward has remained distinct, where the air of the dark region has remained dry through a deep layer and extended northeastward over the Dakotas. Radiosonde sites within the remaining dry region reported 30°C dewpoint depressions from 850mb upward. Four of the sites reported no depression less than 18°C in their entire soundings.

The distinct portion of the boundary has also extended around to the north side of the anticyclone "inside" the position of the main Canadian jet stream axis. In several cases over the United States data network, in which inside boundaries extended around the poleward side of the anticyclone, the boundaries were associated with separate mid-tropospheric speed maxima and 500mb vorticity gradients. In this case, there were four radiosonde sites near that portion of the boundary adjacent to the remaining dark region. Of these, three reported double speed maxima aloft. At International Falls, Minnesota (IF), maximum winds were 59 knots at 410mb and 50 knots at 250mb. At Bismarck, North Dakota (B), maxima were 59 knots at 500mb and 64 knots at 291mb. At Lander, Wyoming (L), maxima were 85 knots at 371mb and 65 knots at 228mb. The fourth site, Grand Junction, Colorado (GJ), reported a single maximum wind of 64 knots at 320mb. The NMC LFM 500mb vorticity analysis is shown superimposed on the water vapor image on **Figure 22a.** A lobe of minimum (anticyclonic) vorticity extends along the dry side of the border, with a lobe of maximum vorticity on the moist side. The vorticity minimum over South Dakota was over western Colorado 12 hours prior to the time shown. As in other observed cases, the vorticity minimum and gradient along the border became well defined as the inside boundary developed.

After the time shown here, the dark region moved rapidly eastward over the Great Lakes, reaching northern Lake Huron in 12 hours. The boundary became less distinct, and the gray shades of the dark region lightened. In this case, the Pacific jet stream broke through the southern ridge over Mexico, and the upper air low over the Gulf of Mexico moved northeastward over the southeastern United States and merged with the low shown over southern Louisiana on **Figure 22**. The merged cyclonic systems then became open to the west, and the anticyclone on the north side became open to the east.

In blocking situations with anticyclogenesis and inside boundary formations, the primary dark region tends to form on the south side of the closing anticyclone (usually the southwest quadrant as the boundary forms). The dry region then moves northward as the border extends. If the primary jet stream approaching the west side of the block is zonal, the block tends to hold. The anticyclone remains nearly stationary and the dark region is likely to spiral around the anticyclone and remain relatively dry or dark on the imagery.

When the main jet stream to the west of the block is oriented southwest to northeast or rotates to that orientation, the anticyclone is likely to open, and the dark region will lighten relatively rapidly. The inside boundary becomes indistinct before it can rotate around the anticyclone.

In the case shown here, the Pacific jet stream was oriented northwest to southeast. The anticyclone remained closed while the dark zone moved to its north side, then opened to the east when the jet stream broke through the southern ridge over Mexico, after the series of images shown here.

The formation of inside boundaries has been related to warm core anticyclogenesis, specifically to the closing of the anticyclone in the upper air streamlines. In this case, at the second image time, a closed anticyclone was present in the 250mb and 300mb wind fields prior to the formation of a distinct inside border. In other cases, inside boundaries were observed to form prior to the closing of an anticyclone. Generally, in such cases, the systems were moving during the formation process and a significant anticyclonic vorticity center had developed. Relative motions of the air were likely a factor in the blocking effect. However, the primary conditions affecting the border formations are the development of upper level easterly winds, their strength, and vertical depth. Our observations indicate that the easterlies initially develop in a shallow layer and increase in vertical depth with time, especially downward. If the initial easterlies are formed below the level of cirrus clouds in the upstream westerlies, ragged cirrus can extend over the boundary already distinctly observed in the moisture. This type of situation has been observed frequently using short interval time-lapse motion. In some cases, the boundaries formed and dissipated without affecting the cirrus level. Although exceptions and complications occur, the relationship between inside boundary formation and upper air anticyclogenesis is generally a reliable one.

Vertical Variations and Vertical Phase Differences

As pointed out, inside moisture boundaries vary vertically during the evolution of a single system and from case to case, depending upon the vertical location and depth of the "blocking" easterly winds. Conditions can also vary vertically along different portions of the border.

Variations from case to case depend upon the type of jet streams and systems involved. In the case shown here during the spring season, the primary jet stream over the eastern Pacific Ocean was south of 30°N and involved in the system development. Although the anticyclone was closed at 500mb, and the col was present in the 700mb wind field; the inside boundary was best associated with the wind fields at 250mb and 300mb. During the summer season over the United States data network, inside boundaries are often best related to the wind fields at 250mb and 200mb. During the winter, the relationships are often best at 300mb and 500mb. Overall, we found the best relationship from case to case and over all seasons to be at 300mb. This generalization applies specifically to inside boundary systems.

Atmospheric systems often become vertically out of phase, especially during rapidly changing situations, such as anticyclogenesis or cyclogenesis. When this occurs, the patterns on water vapor imagery may reveal the upper tropospheric circulation patterns and "hide" different patterns at middle levels. In other situations, when little moisture has been accumulated at high levels, the water vapor imagery may reveal conditions at middle levels; whereas, the different high level conditions are not apparent. Consider, in the case here, conditions over the eastern United States, where the cyclonic system labeled "L" moved southward adjacent to the "hooking" jet stream branch.

At the third image time of this series, shown on **Figure 20e**, a moist area was present over the southeastern United States. On the left column of **Figure 23**, the image of **Figure 20e** is repeated, along with the 250mb, 300mb, and 500mb analyses shown as **Figures 20g, f,** and **h**. On the right side of **Figure 23**, a close-up view of the eastern United States is shown with upper air wind reports. The moist area over the southeastern United States is bounded on its western and northern sides by an elongated dark zone which curves from Louisiana northward across Arkansas, then along the Ohio River Valley and across the Delaware coast. The moist area is generally free of clouds, except for some patches of middle clouds (tops near 500mb) over Mississippi and Alabama. Some high clouds extend from the south over the coastal regions. Comparing the image with the three upper air analyses, the moisture pattern of relatively uniform gray shades over the southeastern United States appears best related to the 500mb wind field. At 500mb, the cyclone centered over northeastern Mississippi has retained its circular shape. However, at 300mb and 250mb, the trough has become elongated into a cyclonic shear zone between the ridge extending across the Great Lakes and an intensifying southern ridge building northward rapidly in conjunction with cyclogenesis over the Gulf of Mexico.

Consider the western and northern sides of the moist area. The jet stream axis on that side of the trough is curved adjacent to the dark zone from southern Ohio to southwestern Arkansas, with levels of maximum winds between 250mb and 200mb. From southwestern Arkansas into northeastern Texas, the jet stream splits into two branches. A high level branch extends westward across northern Texas; and, a lower level branch extends southwestward to the southern Texas coast on the western side of the Gulf of Mexico cyclone. Both branches are evident on the 250mb analysis. Neither jet stream branch curves cyclonically around the southeastern U.S. low. However, the flow at 500mb does. On the south quadrant of the low, "L", the 500mb streamlines curve cyclonically around the low. At Bootheville in southeastern Louisiana, the 500mb wind was 275°/9 knots. However, the 300mb wind at Bootheville was 220°/60 knots, and the maximum wind was 200°/80 knots at 262mb. The upper tropospheric ridge has intensified rapidly in response to the cyclogenesis in the Gulf of Mexico; and the jet stream branch along the poleward side of that ridge has moved northward with increased wind speeds. Although the middle and upper tropospheric ridges are in phase over Georgia and South Carolina, the western part of the upper tropospheric ridge has built northward over the southern portion of the middle tropospheric cyclone, "L". On the close-up water vapor image of **Figure 23**, an indistinct boundary with slightly lighter gray shades to the southern side is labeled "JS". To the south of that boundary, layers of high level moisture have moved rapidly northeastward over the middle level moist layers associated with the southeast U.S. system. To the north of that boundary, moisture is concentrated at or below 500mb with relatively drier conditions above. The boundary "JS" is apparently nearly coincident with the jet stream axis associated with the building southern ridge. Maximum reported winds at sites near the boundary are between 300mb and 250mb with wind speeds increasing from 83 knots at Centreville, Alabama (C); 103 knots at Athens, Georgia (A); and 112 knots at Cape Hatteras (H).

Although the vertical phase differences were relatively significant only on the southwest and south sides of the 500mb low center in this case, we found the imagery difficult to interpret using only the single image of **Figures 20e** or **23**. The indistinct boundary "JS", moving northward over the southeastern United States, is easier to detect using imagery in time-lapse motion. Without the detection of boundary "JS", the narrowing of the upper tropospheric trough between the two opposing jet streams would have been difficult to interpret. If boundary "JS" were detected, and related to the northward movement of the anticyclonic flow of the southern ridge; we may have guessed that the region of cyclonic flow had also narrowed and elongated at 500mb; however, it did not.

This case illustrates some of the types of problems of interpreting water vapor imagery when atmospheric systems become out of phase in the vertical. In other cases, the vertical phase differences can be significantly greater. Often the problems can be minimized by careful examinations of imagery in sequence, or by using imagery in time-lapse motion whereby parcel motions can be observed and pattern evolutions are more evident.

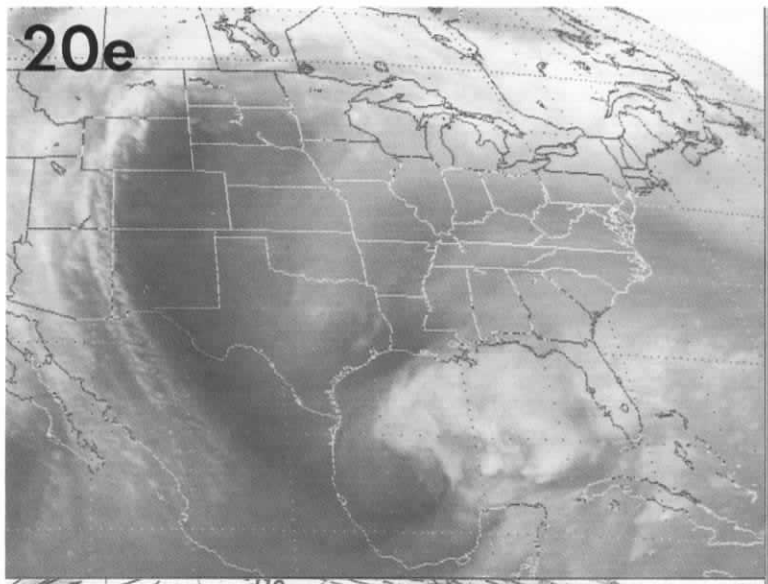

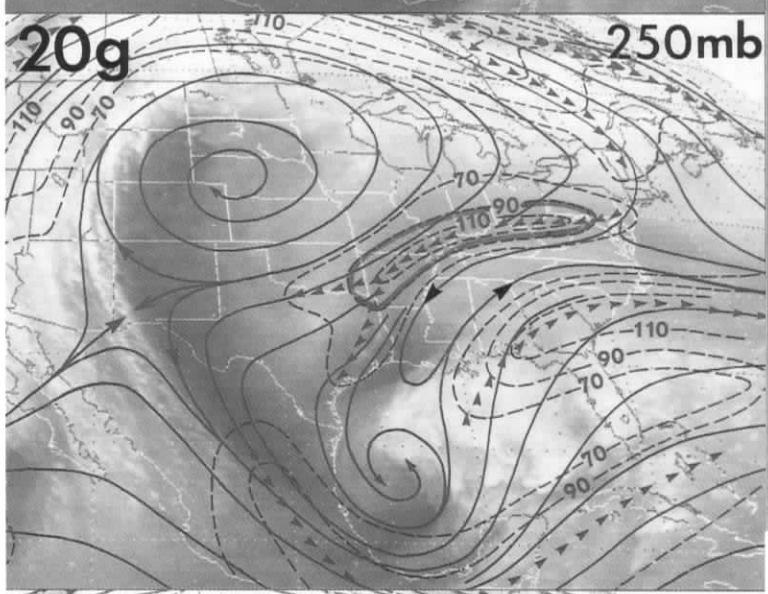

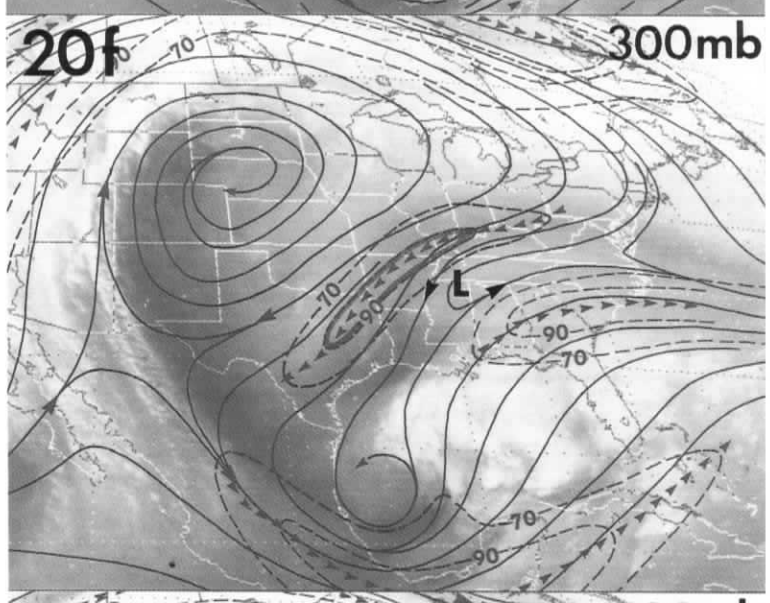

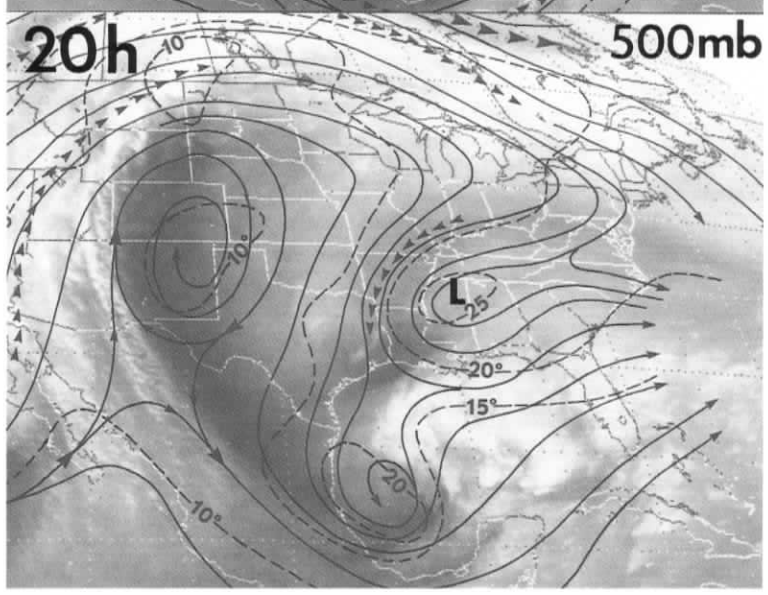

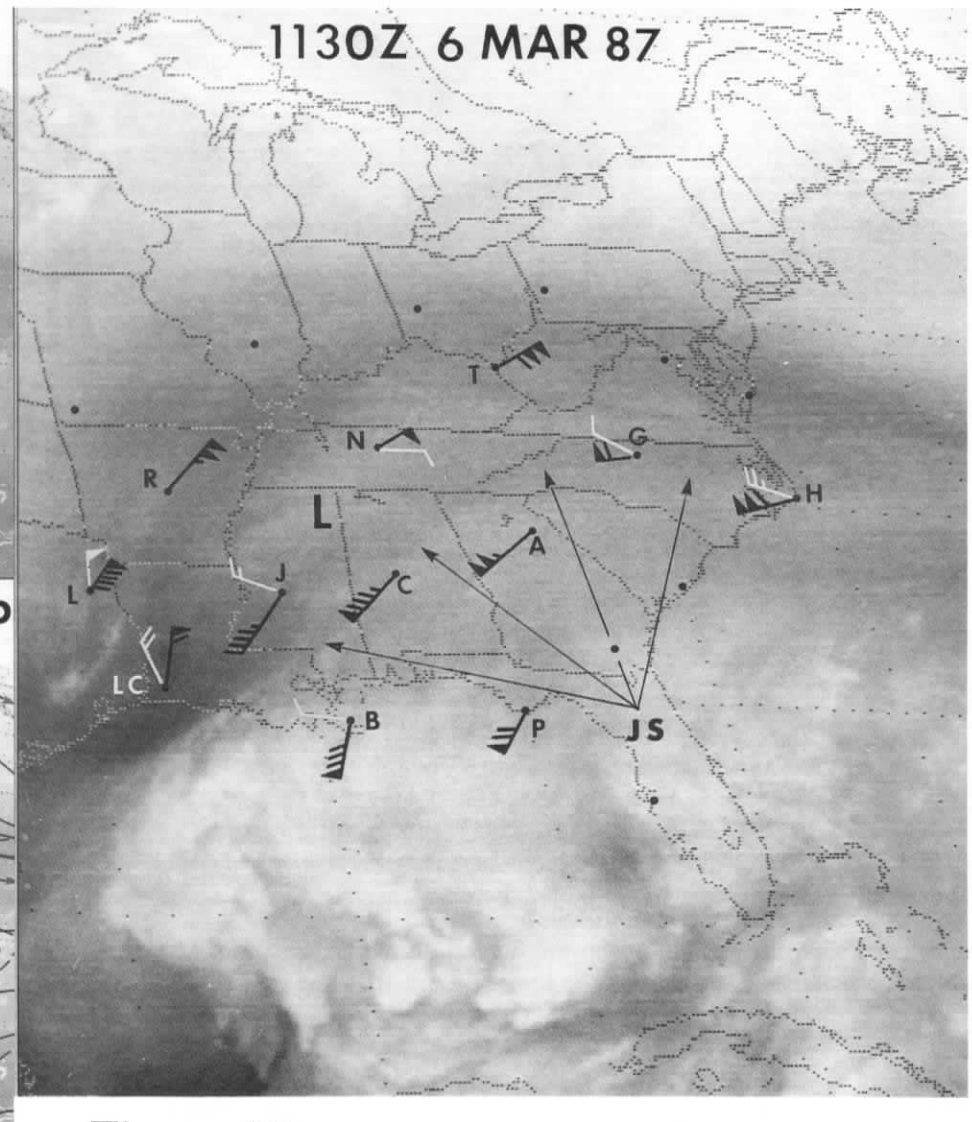

Figure 23 VERTICAL VARIATIONS

The same 6.7μm Water Vapor image, 1130Z 06 March 1987, GOES Central is shown with varied upper air analyses and radiosonde data from 1200Z 06 March 1987, the third image time of the series.

Left Column Images

Figures 20e, g, f, h are repeated with a smaller geographical area. The 250mb, 300mb, and 500mb analyses are superimposed on the same image shown at the top of the column.

Right Column Image

A close-up area of **Figure 20e** is shown with upper air wind reports from 12 radiosonde sites listed below.

Black Symbols: Maximum winds (altitudes listed below)

White Symbols: 500mb (shown for sites with 15° or greater directional difference between max winds and 500mb winds)

Site Identification and Altitudes of Maximum Wind Reports

Little Rock	(R)	225 mb	Huntington	(T)	250 mb
Longview	(L)	210 mb	Nashville	(N)	29,000 ft
Lake Charles	(LC)	33,000 ft	Centreville	(C)	287 mb
Jackson	(J)	30,000 ft	Athens	(A)	268 mb
Boothville	(B)	262 mb	Greensboro	(G)	302 mb
Apalachicola	(P)	270mb	Cape Hatteras	(H)	264 mb

b. Moving System - Winter Season

On **Figure 24**, water vapor images are shown at 12-hour intervals; and, the first and last images of the sequence are repeated with 500mb streamlines superimposed. On the first image, an inside boundary is present at "B", extending from near the tip of the Baja Peninsula to the northeastern corner of Arizona. During the 12 hour period prior to the first image, the moisture pattern over the Baja Peninsula was moving eastward. Its eastern edge was decelerating and becoming more distinct. By 1200Z, near the time of the first image, an anticyclone had closed in the wind fields at 300mb, 400mb and 500mb. At 1730Z, six hours after the first image, the boundary had remained nearly stationary at its southern end, and moved very slowly eastward at the northern end. It had also attained its most well defined and distinct appearance. After that time, the boundary accelerated eastward. It began to lose definition and become less distinct. Already, by the second image time on **Figure 24b**, the gray shades of the dark area on the east side of the boundary have lightened slightly, and the boundary has become slightly irregular with ragged cirrus present. The decreases of definition and distinctiveness continued during the remainder of the sequence as the boundary moved eastward.

In this mid winter case, the 500mb wind field was best associated with the water vapor image patterns. At the time of the first image (see **Figure 24e**), the anticyclone was closed in the 500mb wind field; and, the related col over northwestern Mexico was associated with the inside boundary. A second col region over eastern Texas formed as the cyclone closed. The closed systems and their associated cols were also present in the 300mb wind field. In this case, as the boundary accelerated eastward during the sequence of images, the anticyclone opened to a ridge first, then the cyclone opened. By the time of the fourth image, the 500mb wind field has "opened". At that time, a small low was still closed in the 300mb winds; but, the high had opened.

Notice on **Figure 24f**, that the 500mb streamlines do not appear well related to the image patterns. Although the inside boundary has lost definition and distinctiveness, it still remains as a residual feature. During this case, of the four radiosonde times shown, the inside boundary was well associated with a col in the wind fields only at the first image time, when the boundary had just formed and become nearly stationary. After the first image time, the "model" relationships between the boundary and the upper air streamline fields were no longer present. This change is normal, and should be recognized on a sequence of imagery by the acceleration of the boundary, and its loss of distinctiveness and definition. However, this case illustrates that care must be taken when interpreting water vapor imagery in regard to the related wind field features. With the "blocking regime" boundaries, including both "inside" and "head" boundaries, the associated cols and closed circulation systems are likely to be present and well related to the imagery, when the boundaries are nearly stationary. The boundaries will form and become more distinct while they are still moving and decelerating. During later stages, when the associated wind field systems "open", the inside boundaries will accelerate and lose definition and distinctiveness. However, this loss occurs over a finite time period. The boundaries remain as residual features, and may be misinterpreted on a single still image.

Figure 24

INSIDE BOUNDARY - MOVING SYSTEMS DURING WINTER SEASON
Sequence of four 6.7μm images at 12-hour intervals (**a,b,c,d**) with 500mb streamlines superimposed on the first and last images of the sequence (**e,f**). Image times: 1130Z 30 January 1986 (**a,e**), 2330Z 30 January 1986 (**b**), 1130Z 31 January 1986 (**c**), 2330Z 31 January 1986 (**d,f**). Images are from GOES Central; 500mb data are valid 30 minutes after respective image times.

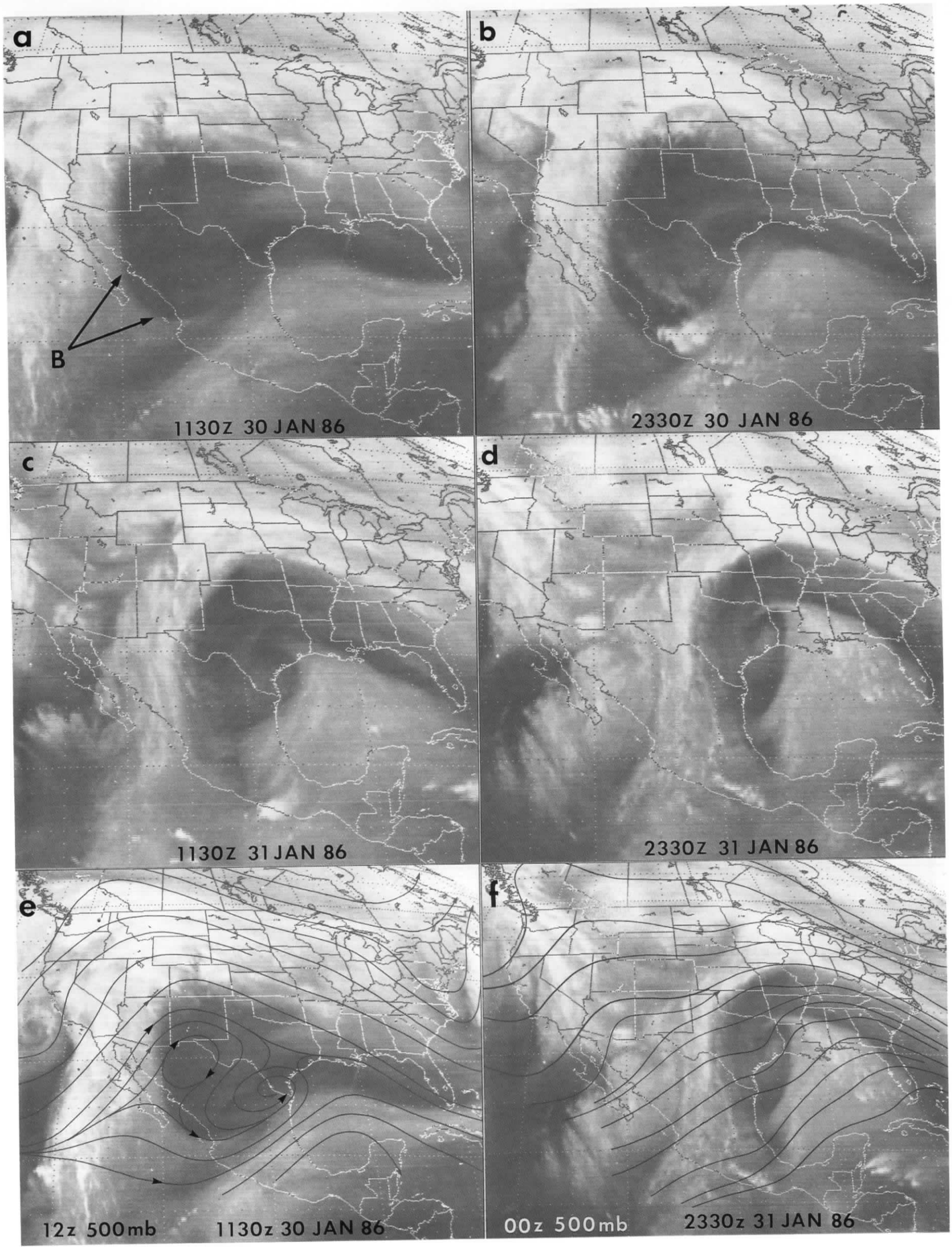
a
B
1130Z 30 JAN 86
b
2330Z 30 JAN 86
c
1130Z 31 JAN 86
d
2330Z 31 JAN 86
e
12z 500mb
1130z 30 JAN 86
f
00z 500mb
2330z 31 JAN 86

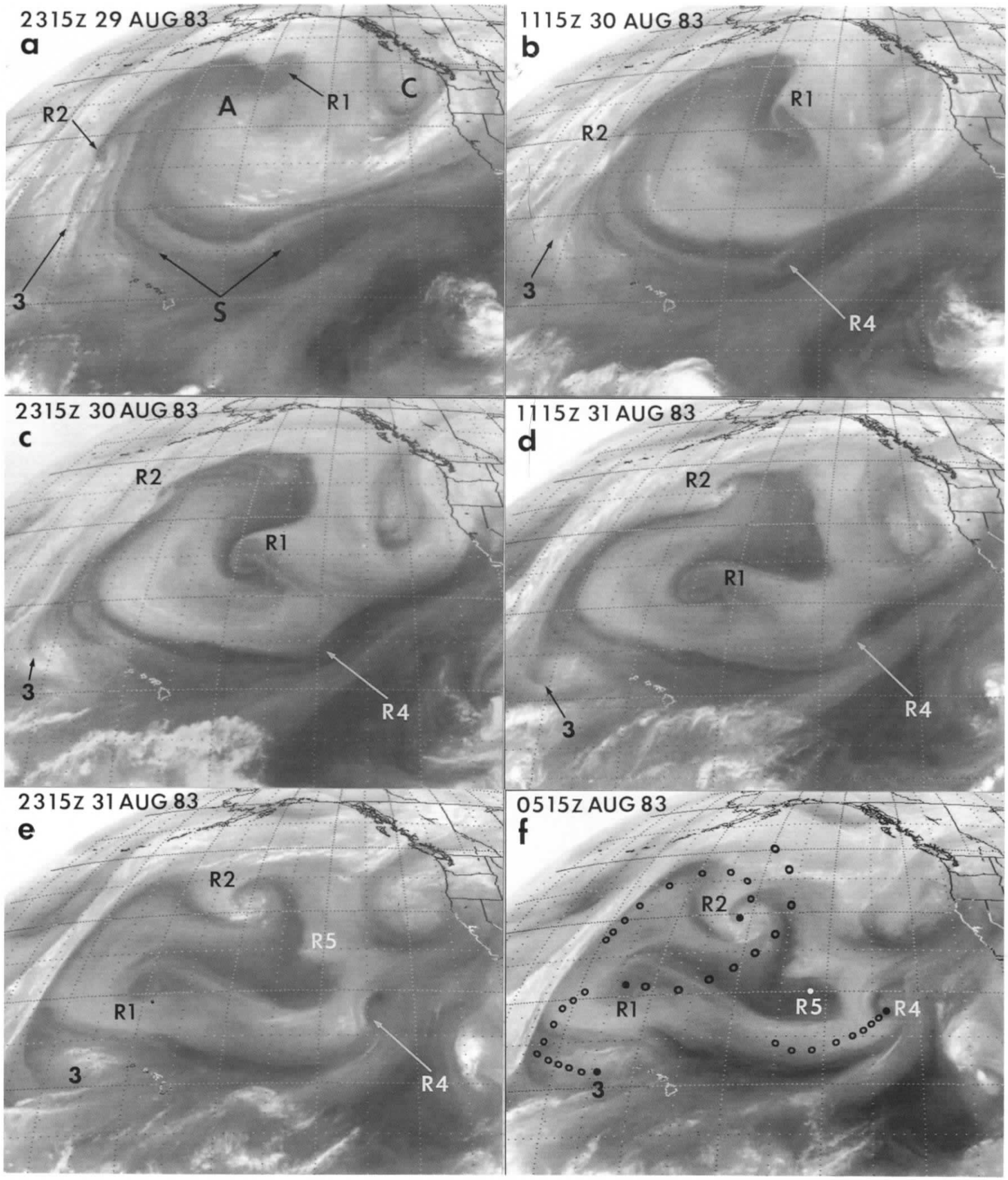

Figure 25 **INSIDE PERTURBATIONS**
Sequence of five 6.7μm GOES West images at 12-hour intervals (**a,b,c,d,e**). On **Fig. 25f**, a 6.7μm image valid 6 hours after the sequence includes 6-hourly positions of features (circles) with the last position - valid at the image time - as a solid dot. Image times and dates are labeled on the figure.

c. Inside Perturbations - Reverse Image Patterns

Inside boundaries commonly extend through a col in the upper air winds. The flow at both ends tends to be nearly parallel to the boundary, but of opposite directions. There is commonly a jet stream branch along the equatorward end. This speed maximum is usually present prior to the anticyclogenesis and boundary formation. It is likely to originate as a part of the jet stream that extended over the original amplifying ridge. As discussed, a separate mid-tropospheric speed maximum and vorticity gradient is likely to form along the poleward end of the boundary. One significance of this "inside" speed maximum is that perturbations sometimes form along that portion of the boundary. When they do, they are commonly independent or out of phase with perturbations which may also be occurring along the main jet stream along the poleward side of the same moist zone. Also, they tend to have unusual moisture, clouds, and weather patterns; since the upper level moist air is on the left side (Northern Hemisphere) of the perturbed boundary.

On **Figure 25 a-e**, five images are shown at 12-hour intervals. **Figure 25f** is valid 6 hours after the 5th image, and is used to show the tracks of the individual systems discussed. At the first image time, a large upper air anticyclone had already formed over the northeastern Pacific Ocean. It was centered near "A" on the 250mb wind analysis form aircraft reports. The trough to the east of the anticyclone has formed a closed center at "C". An inside boundary had formed on the western side of the anticyclone, and has rotated around the northern side. A large region of high level moisture has rotated around the anticyclone, and is bounded on the south side by a cyclonic shear zone at "S".

At the initial image time, two perturbations have formed along the inside boundary at "R1" and "R2"; and, a third is forming at "3". The primary col region on the west side of the anticyclone is located between systems "R2" and "3". Those systems are, therefore, in motion fields of opposite directions. Also, their moisture patterns evolve in different ways. System "R2" moves initially toward the NNE around the poleward side of the anticyclone. Note that "3" moved in the opposite direction, before turning toward the southeast. System "R2" moves along its boundary with the moist side to the left with respect to the direction of movement. We refer to the moisture patterns involved with such systems as "reverse image".

The "reverse image" configuration is most significant during the early stages of the system evolution, while the system is "open" and moving. Consider system "R2" during the first 36 hours of the sequence. At the time of **Figure 25d**, it was moving nearly eastward. Prior to that time, it moved northeastward. The pattern rotated cyclonically as the system moved, but without a closed wind field (opposing winds were not present on the system's left side). The rotation would be revealed as a maximum of cyclonic vorticity with an open trough. In this case, the system formed on the western side of a closed high and moved northeastward, then eastward around the northern side of the high. Such systems usually form on a moisture boundary directly in advance of the upstream trough, with dry air to the west and moist air to the east. In those typical cases, the moist air rotates back around the forward side of the vorticity maximum onto its left side, then "falls back" on the left side with respect to the drier air moving more rapidly on the right side of the vorticity maximum. In this case, the perturbation formed on an inside boundary, with the moist air to the west and the dry air to the east. The dry air in advance of the cyclonic vorticity maximum "fell back" around the left side, as the moist air advanced on the right side of the vorticity maximum. Thus, at the fourth image time, **Figure 25d**, the system is moving eastward, with dry air falling back on its northern side, and moist air moving more rapidly on its southern side - a reverse moisture configuration for a typical open wave system in the westerlies. This often results in clouds and weather on the rear side of the vorticity maximum with clear skies on the forward side. With system "R2", convective clouds developed on the moist southern side prior to **Figure 25d**. This "reverse image" character is common with perturbations which develop along inside boundaries on the poleward side of the associated cols; and along the eastern ends of "return moisture" boundaries, where the perturbations move eastward with moist air to the north and dry air to the south (see system "R4"). In this case, system 3 formed along the inside boundary, but on the equatorward side of the col. It moved initially with the moist air on the right; and, its moisture pattern evolution was the more typical type.

System "R1" also formed along the inside boundary on the poleward side of the col. Note on the first image, that the primary upper air moisture has formed a "cusp" shape to the rear of the cyclonic vorticity maximum of "R1". Systems "R1" and "R2" moved in anticyclonic shaped paths about the primary anticyclone center which retrograded slowly westward during the 48 hour period. System "R5", forming at the end of the period, is also on the inside boundary and a reverse image type.

System "R4" formed at the southwest end of a narrow trough, just east of where the trough changed to a cyclonic shear zone along its western extension. Two moisture boundaries are involved with this perturbation, one on each side of the trough. The northern boundary is a "return moisture" boundary, similar to the one shown on **Figure 11** of Section A. With respect to the northern "return moisture" boundary, system "R4" has a "reverse image" configuration. The return moisture moved southward on the rear side of system "R4" as it moved eastward. An area of cirrus and middle clouds formed on the rear side of the vorticity maximum within the moist air from the northern moisture regime.

On **Figure 26**, a water vapor image is shown with and without a 500mb analysis. The perturbation over the high plains was a reverse image type since it formed along a boundary with the primary moist side to the left. A well defined moist boundary, originating from an inside boundary, had become poorly defined by the time the perturbation formed. However, the primary moisture was still to the west with drier air to the east. At the time of the image, the 500mb vorticity maximum was centered over eastern Colorado, and moving slowly northeastward. The ridge portion of the system is primarily warm and dry, in advance of a cool moist trough. At Topeka, Kansas, the 500mb temperature was -02°C with a 30°C dewpoint depression. To the southwest, at Dodge City, Kansas, the 500mb temperature was -07°C with a 3°C dewpoint depression.

In many cases, with upper air reverse image systems, no significant clouds or weather occur. In other cases, such as when a vertically deep frontal trough moves onto the west side of an existing blocking regime, significant precipitation and clouds may occur in association with a reverse image perturbation. In such cases, the surface frontal zone moves under the upper inside border. A wave-like feature along the surface front has precipitation on its rear side, with a weather break on the forward side.

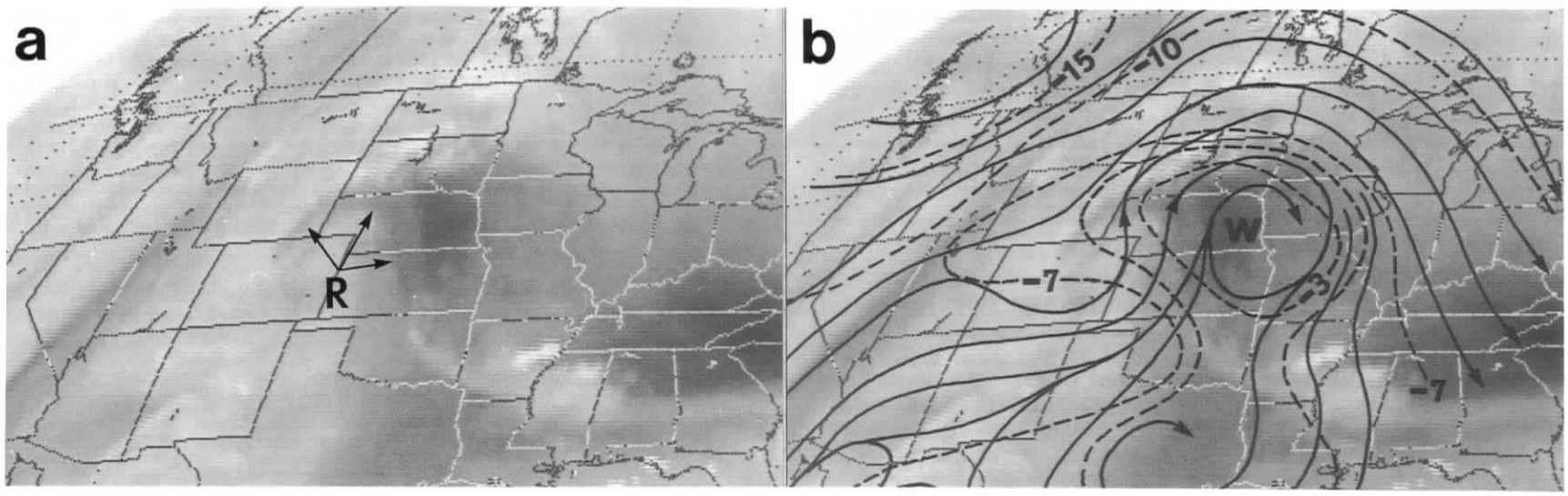

Figure 26 **INSIDE PERTURBATION WITH 500mb ANALYSIS**
Fig. 26a. 6.7μm image, 1131Z 26 July 1983, GOES East. **Fig. 26b.** Same image with 1200Z 26 July 1983 500mb streamlines (solid lines) and isotherms (dashed lines °C) "W" indicates warm thermal feature.

a. Overview - "Blocking Regimes" and System Evolutions

Within an area of predominantly westerly upper air winds, an area of easterly winds may develop. On the western side of the area of easterly winds, a col pattern is formed in the wind field,where the upstream westerlies become "blocked" and split into two branches. Since such areas of easterly winds are limited in area and temporary in time, we refer to the general situation as a "blocking regime." Basically, blocking regimes occur in the upper air wind fields where warm air in the middle troposphere is present on the poleward side of cold air; and, some form of upper air ridge or anticyclone is present on the poleward side of a trough or cyclone. However, there are different combinations, and various ways in which the situations may develop. These differences are associated with different types of cloud and moisture patterns, and their changes with time. We have already discussed two basic types of moisture boundaries, in which blocking was significant to their formation. These were "head" and "inside" boundaries. In this regard, blocking regime formations may be categorized into two basic types, in which either a "head" boundary or an "inside" boundary is the primary feature of the associated water vapor imagery.

(1) Two Basic Types of Blocking Regime Formations

Anticyclogenesis With Inside Boundary Formation
(See Drawings 1a and 1c on page 105)

The easterlies result from anticyclogenesis. The trough on the equatorward side of the anticyclone moves westward into that position from the trough originally on the eastern side of the developing ridge. The easterly wind regime is primarily dry in the middle troposphere, resulting from downward vertical motion during the anticyclogenesis process. An "inside" moisture boundary forms on the western side of the easterlies. In the mature stage, the upper air high is closed, but not "cut-off" from the upstream westerlies. The trough on its equatorward side remains open to the east. In this basic configuration, shown on **drawing 1a**, a distinct dark area is usually observed on water vapor imagery along the eastern side of the inside boundary. Those dark areas usually have a rounded shape on the equatorward end, and a cusp-like pointed shape at the poleward end. Examples are present on **Figure 29** over the Pacific Ocean on images T-2 and T-3. Other examples at tropical latitudes are shown in Section E on **Figures 85a** and **88d**. Frequently, with inside blocking regimes, a closed cyclone forms in the trough to the equatorward side of the anticyclone. This common alternative configuration is shown on Drawing 1c on page 105. In such cases the distinct dark area on the water vapor imagery is likely to have an overall crescent shape, with pointed cusp shapes on both the north and south ends.

Cyclogenesis With Head Boundary Formation
(See Drawing 1b on page 105)

The easterlies result from cyclogenesis. The ridge on the poleward side "builds back" from the ridge originally on the eastern side of the developing trough. The easterly wind regime is primarily moist in the middle and upper troposphere, resulting from upward vertical motions. A "head" moisture boundary forms on the western side of the easterly wind regime. In the mature stages, the cyclone is closed, but not "cut-off" from the upstream westerlies. The ridge on its poleward side remains open to the east.

Blocking regimes vary significantly in the size of the related circulation systems, and in duration. When they are large and persistent, they are often considered as "blocks" within the westerly long wave patterns. Such large and persistent blocking regimes usually involve combinations of cyclogenesis and anticyclogenesis, and the associated "head" and "inside" boundaries. There are often two branches of easterly winds. These commonly merge in the upper troposphere to form one relatively wide region of easterlies, although those associated with the anticyclone usually occupy a layer of higher altitudes than those with the cyclone. Within the wide zone of easterlies, dual structure is likely in the wind speed, temperature, and vorticity fields.

There are various blocking regime combinations and complex system evolutions; however, we have observed two common types. In some cases, these evolve through complete cycles. The two types of cycles are illustrated by two sequences of drawings on page 105, labeled 2a-f and 3a-f. Note that the streamlines and axes of maximum winds (arrowheads) are intended to represent a pressure surface in the upper troposphere, typically 300mb at middle latitudes, or 250mb during summer seasons or at lower latitudes. The shaded areas represent commonly associated patterns of cold moisture depicted as very light gray on standard water vapor imagery. The darker shading on the drawings indicate areas likely to have high cold cloud tops and nearly white shades on the water vapor imagery. The shading has been intentionally omitted from drawings 2f and 3f, because of the large variability of patterns and sequences of events during the "opening" stages of the system evolutions.

(2) Two Common Types of Evolution of Large Blocking Regimes

The Roll-Over Evolution (See Drawings 2a-f)

2a. Cyclogenesis has begun along the eastern side of an open upper air trough. The primary jet stream branch is on the upstream side of the western ridge ("W").

2b. The high cloud and moisture boundary on the eastern side of the trough has formed a "cusp" shape as cyclogenesis proceeds. In conjunction, a break has occurred in the jet stream axis along the eastern side of the trough. The western ridge has begun to "roll-over" (forming a positive tilt configuration) in response to the strong jet stream on its northwestern side. The northern portion of the trough has accelerated eastward; whereas, the southern portion has slowed and formed a closed upper air cyclone. A distinct head boundary has formed along the stretching axis of the new col in the wind field.

2c. As the trough narrows and weakens between the two merging ridges "E2" and "W1", a break has occurred in the jet stream axis along the western side of the trough; and, the closed low has become "cut-off". As the upstream ridge "W1" continued to "roll-over", and the northern open portion of the trough moved eastward, the head boundary has rotated anticyclonically.

2d. Mature Stage. Anticyclogenesis has occurred in the "W1" position, forming a wide zone of easterly winds with a blocking inside boundary along the stretching axis of the new col. A new dark area has formed to the north of the "cut-off" low, where the easterly winds turn northward around the new upper air anticyclone. The head boundary has continued to rotate anticyclonically; and, the trough along the western end of that boundary has narrowed and weakened between the merging warm air regimes of ridges "W1" and "E2". Note that the low is "cut-off", whereas the anticyclone is closed, but not "cut-off".

2e. The anticyclone has opened; and, ridge "W1" is merging with ridge "E2". The head boundary continued to rotate and remains as a residual feature, although the western end has lost definition where the flow around the cyclone has begun to extend northward around the western side of ridge "W1". The jet stream branch along the northwest sides of ridges "W1" and "W2" has broken; and, a new jet branch is breaking across ridge "W2" in response to a new ridge amplification farther to the west.

2f. In response to the new western jet stream branch, the closed low has opened. Ridge "W1" originally a part of the upstream ridge, has now merged with the remaining downstream ridge "E2". The cycle has been completed. Although the resulting systems are open and moving, parts of the inside and head boundaries may remain on the water vapor imagery as residual features. The character and behavior of those residual boundaries varies considerably from case to case, depending upon the sequence of events during the opening phase.

The Build-Back Evolution (See Drawings 3a-f)

3a. Cyclogenesis has begun along the eastern side of an open upper air trough. The primary jet stream branch is along the eastern side of the upstream ridge, contributing to a negative tilt of the trough.

3b. In conjunction with the cyclogenesis process, the eastern ridge has begun to "build back" to the northern side of part of the trough. The high cloud and moisture boundary along the eastern side of the trough has formed a "cusp" shape; and, the jet stream branch along the boundary has broken near the point of the cusp. That part of the boundary to the northeast of the cusp point has the characteristics of a head boundary.

3c. An upper air closed low has formed; and, the distinct head boundary extends along the stretching axis of the related col in the wind field. The eastern ridge has begun to break into two parts, as anticyclogenesis is beginning at the build-back portion at "E2".

3d. Mature Stage. Anticyclogenesis has occurred at "E2". As the new region of easterly winds formed, a new dark region formed in the anticyclonic easterlies; and, a new inside boundary formed along the stretching axis of the newly formed col in the wind field. Often is such cases, as the winds rotate anticyclonically with time along the east side of "E2", a new closed low is formed in the trough to the east of ridge "E1". This results in the classical "omega" configuration in the upper air circulation systems. However, the dominant feature on associated water vapor imagery is usually the new inside boundary. Note that the anticyclone is "cut-off" from the primary jet stream zones, and the first cyclone to its southwest is closed, but not "cut-off". The newly formed eastern cyclone has become "cut-off" soon after its formation. The conditions shown are the most common.

3e. The anticyclone at "E2" has continued to drift westward after its formation; whereas, the cyclone to its south has moved slightly eastward. In response, the head and inside boundaries have continued to rotate cyclonically with time. The jet stream branch on the southern side of the first low has begun to break across ridge "E1"; and, the jet stream associated with the western ridge has begun to break, with a new branch beginning to extend northeastward.

3f. The cycle becomes completed as the western jet stream extends to the north of system "E2". The anticyclone has opened to the west. The remaining southern jet stream branch has broken across ridge "E1", merging the two cyclones; and, the jet stream branch around the eastern side of "E2" has turned southward around the two opening lows. The head and inside boundaries may remain as residual features; however, the variability from case to case is even greater than during the opening phase of "roll-over" cycles. This subject will be addressed with individual cases.

An example of a "roll-over" evolution follows as the next case study. The last case study of Section B illustrates a "build-back" evolution blocking regime during its mature stages. Other combination blocking regimes are illustrated in Section D.

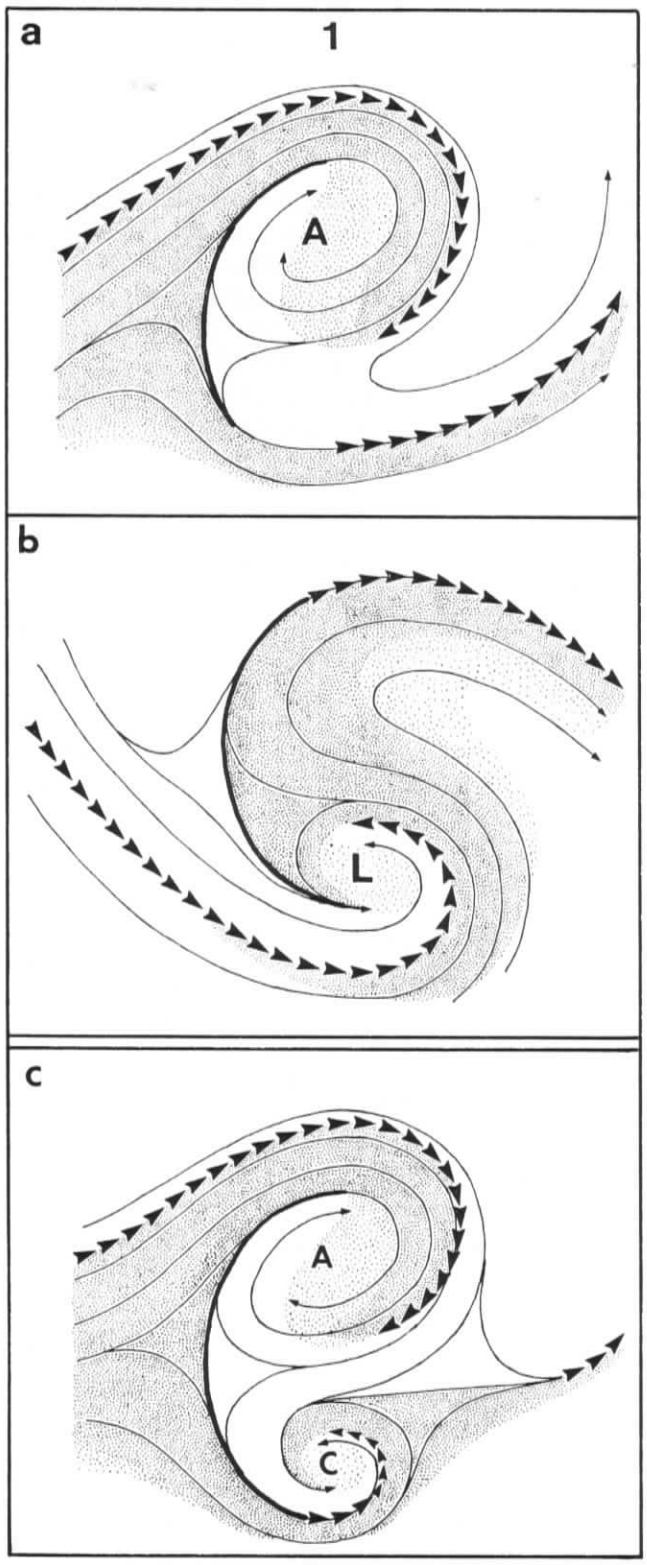

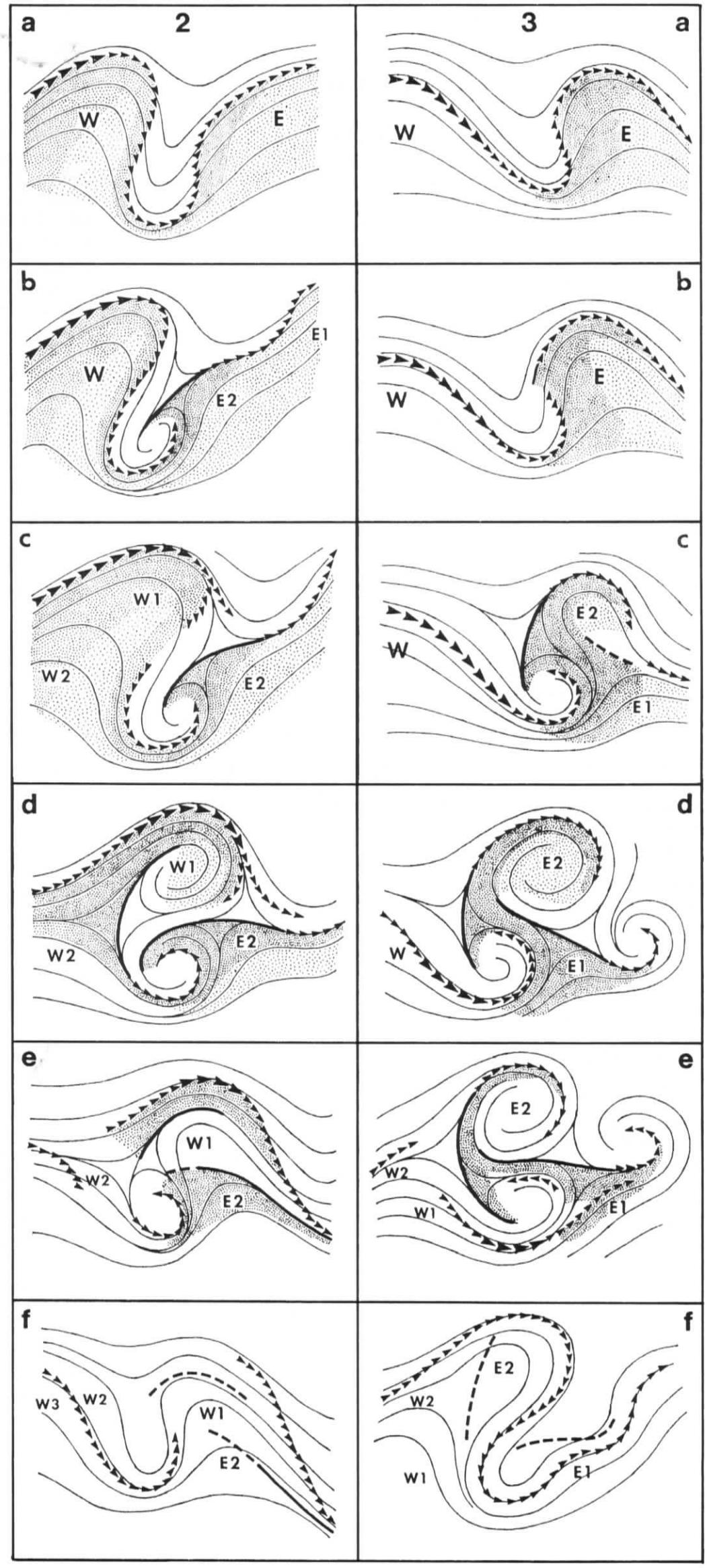

1a. Inside Boundary Formed from Anticyclogenesis

1b. Head Boundary Formed from Cyclogenesis

1c. Inside Boundary and Anticyclone with Closed Cyclone Formed in the Equatorward Side Trough

2. Roll-Over Evolution - Time Sequence

3. Build-Back Evolution - Time Sequence

Streamlines: Typically 300mb Wind Field (250mb for summer season or low latitudes)

Arrowheads: Axes of Maximum Winds on the same pressure surface as the streamlines

Shading: Areas of very cold moisture on water vapor imagery; darker shading indicates patterns of high cold cloud tops.

b. Introduction to the Case Study

In the following case study, a blocking regime forms and undergoes a "roll-over" type of evolution. A complete cycle is achieved within a 4 day period without major interruptions or complications. However, there are variations from other cases and complications, as is always the case with real atmospheric events. With blocking regimes, the relative sizes of the cyclones and anticyclones vary. In this case, the cyclone is large and strong. The anticyclone was relatively small in area, and its "closed" phase was of short duration. However, the primary boundaries on the water vapor imagery were of common types and evolution. A basic objective in showing the case, is to illustrate the primary boundary evolutions and their relationships to the evolving circulation systems. However, many of the smaller scale features and variations are also of types commonly observed. Therefore, we shall also address those. Furthermore, when showing real imagery, many complicating features, perhaps very unique in character, will be present. In many cases, we must address these, simply because they are there. A slightly complicated set of images is required. We must explain those prior to discussing the case.

(1) Imagery and Analyses

On **Figures 29** and **35**, a series of l6 large area images are shown. The images are in sequence at 6-hour intervals, except for a 12-hour interval between the first two images. For convenience in comparison with other figures, the images are identified by time-dates, and by "synoptic times" labeled "T-0" through "T-16". At "synoptic time" "T-6", no 1130Z water vapor image was available; therefore, a 1200Z infrared image has been substituted. Radiosonde data were available for only even numbered "synoptic times" at 12 hour intervals. Selected wind and thermal field features are shown on the even numbered images valid at 1130Z and 2330Z. A large area water vapor image for synoptic time "T-1" was intentionally omitted in order to show the previous time with upper air data; however, a close-up view of time "T-1" is shown as **Figure 30c**. Note that **Figure 29**, showing large area views for times "T-0" through "T-8", is repeated as **Figure 33**.

Large scale features and changes are discussed in time sequence using the large area views of **Figures 29, 33**, and **35**. However, some detailed features, are not adequately shown on the large area images. Therefore, close-up views of selected images are introduced as required.

(2) Image Patterns Near the Mature Phase of the "Roll-Over" Cycle

On **Figure 27**, a water vapor image is shown valid at "synoptic time" "T-9" which we regard as the mid point of the "roll-over" cycle. A water vapor image valid six hours later at time "T-10" is shown on **Figure 28a** with a 300mb analysis superimposed. The water vapor image, valid at 1130Z, is adjacent to an infrared image, valid at 1200Z with a 500mb analysis. Streamlines are shown for both analyses, with 300mb axes of maximum winds and isotachs, and 500mb isotherms.

Consider the various boundaries and features on **Figure 27**. The overall pattern implies the presence of the upper air cyclone centered near San Diego. However, there are numerous boundaries, with related dark bands. Given only the single water vapor image of **Figure 27**, we might ask: to what extent and success can we interpret the various image features in regard to the upper air wind and thermal fields? This depends greatly on the skill of the observer. An experienced observer is likely to recognize the presence of the cyclone, and the fact that it has been "cut-off" by a "roll-over" process. The existence of a jet stream axis along boundary "U2" should be recognized, although it is indistinct and difficult to locate along its eastern extension over Canada. However, the very light moisture pattern along its southern side extends across the northern side of the low with a relatively continuous pattern, implying that the upstream ridge has "rolled over" the closed low. Prior to the "roll-over" event, a jet stream extended from boundary "U2", around the ridge, to the western side of the low. During the "roll-over" process a "break" occurs in this jet stream zone on the northern side of the low; thus, the low has become "cut-off" from the primary jet stream zone over Canada. However, a branch of the jet stream is likely remaining around some part of the cyclone. If that branch is present, it is likely along boundary "B". The dark slot along the eastern side of "B" extends completely around the low to location "S". Since the overall moisture pattern of the low is well defined with active convective cloudiness present, a jet stream branch is very likely, at least around its southern quadrant. A significant question is: how far does that branch extend around the western side of the low? The fact that boundary "B" is well defined and distinct on the western side of the low is an indication of a jet axis there, but not a highly reliable one. It is necessary to observe the moisture pattern on the opposite side of the dark slot from boundary "B", labeled boundary "H" in this case. Boundary "H" is a "head" boundary formed during the cyclogenesis phase of the "cut-off" low. Note that a strong jet stream branch does extend along boundary "B" from Oregon southward. A reliable interpretation of that jet stream's presence, from the single image, is not likely. We shall address the subject with the sequence of images.

The presence of another jet stream branch is implied along boundary "A". That part of the boundary west of Mexico has a relatively narrow dark zone along its northern side; and, cirrus cloud features suggest a zone of maximum winds. The related axis of maximum winds is shown on **Figure 28a**. The jet stream axis extended westward, beyond the arrowheads, at altitudes above 300mb. However, boundary "A" extends as a continuous feature across the coast of Mexico and northward to Wyoming; and, there are no strong winds related to the portion over the United States at "AR". Also, there are no strong winds along boundary "A2" which lies along the stretching axis of a col in the 300mb wind field. The understanding and interpretation of the boundary features are more easily achieved by viewing their evolution on a sequence of imagery. Prior to discussing the evolution of systems, we may compare the analyses on **Figure 28**. The anticyclone present at 300mb to the northeast of the cyclone has just closed within the past 12 hours prior to the analysis. At 300mb, the upper air cyclone is elongated northeastward from its center, and there are two zones of maximum wind speeds within the easterly winds. One is over Nevada, where the jet stream branch curves cyclonically around the low. The other is over Montana where the streamlines change from cyclonic to anticyclonic curvature. These represent the two branches of easterly winds involved in the blocking regime. At 500mb, only the southern branch of easterlies is present; however, a double thermal gradient is present. We shall address this vertical structure in the following discussion of the system evolution.

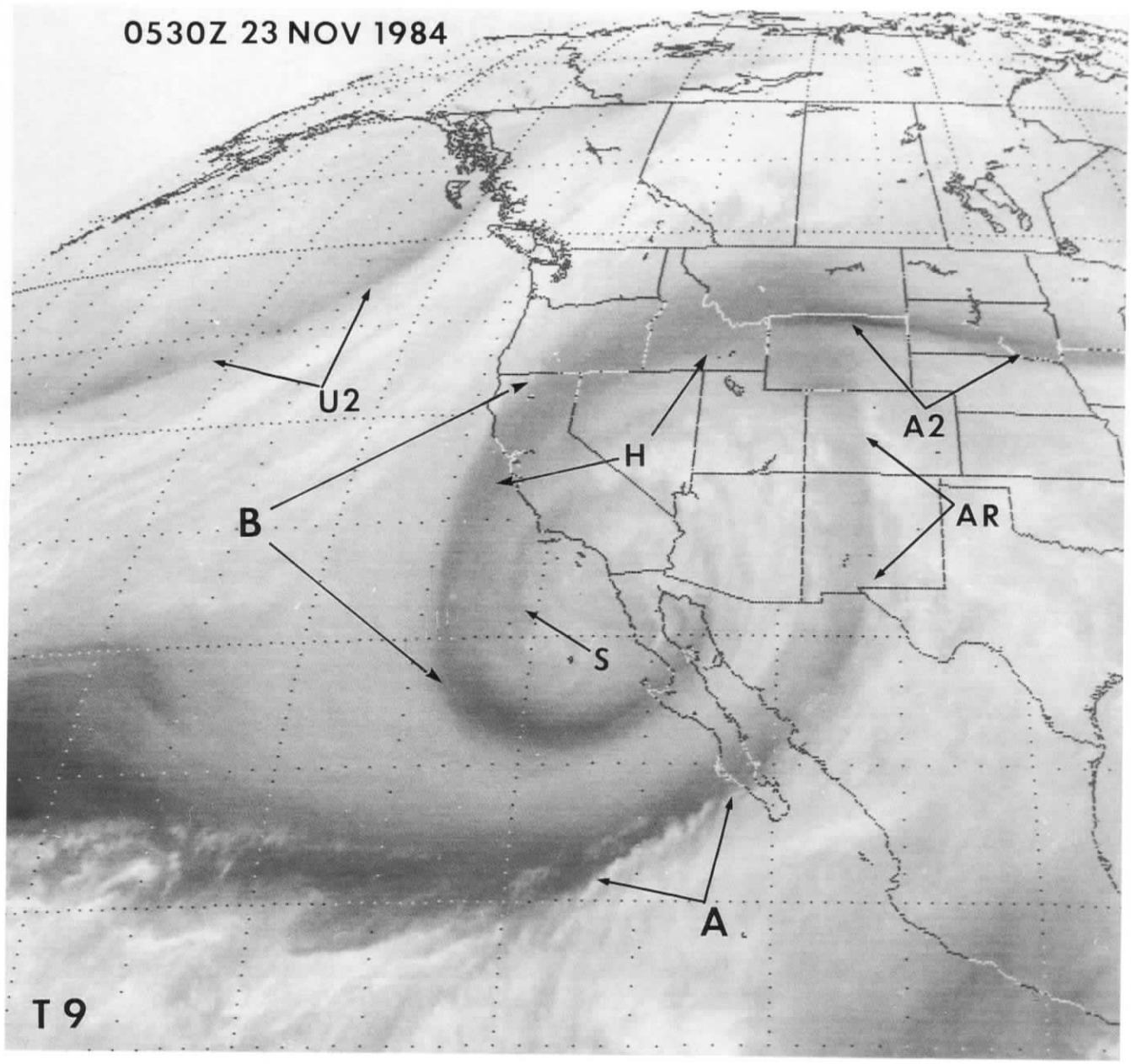

Figure 27 **MATURE PHASE - ROLL- OVER CYCLE**
6.7μm image, 0530Z 23 November 1984, GOES Central, Time **T-9**.

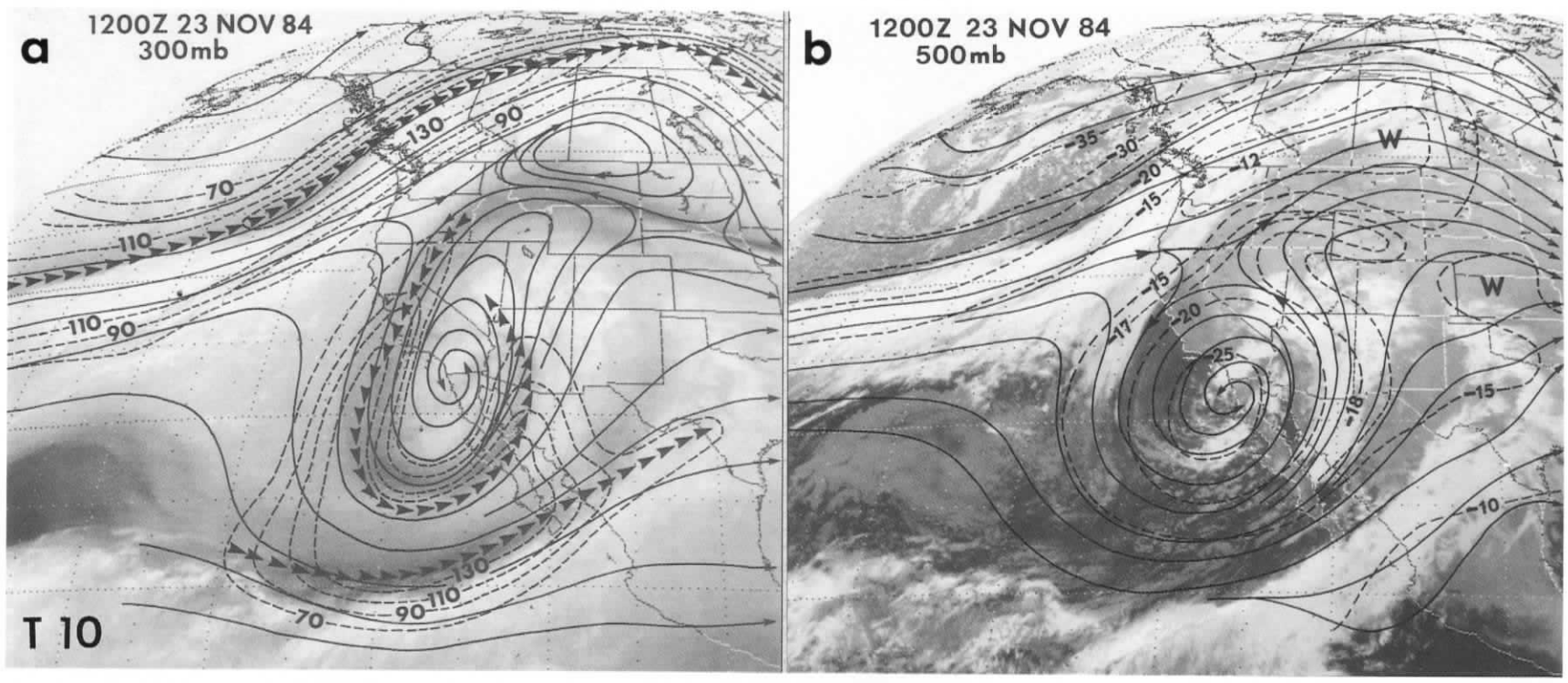

Figure 28 **MATURE PHASE - UPPER AIR ANALYSES - TIME T-10**
Fig. 28a. 6.7μm 1130Z 23 November 1984, GOES Central with 300mb analyses, 1200Z 23 November 1984. Streamlines - solid lines. Isotachs - dashed lines (knots). Axes of maximum 300mb wind speeds (arrowheads).
Fig. 28b. 11.2μm infrared image, 1200Z 23 November 1984, GOES Central with 500mb analysis. Streamlines - solid lines. Isotherms - dashed lines (°C). "W" indicates warm.

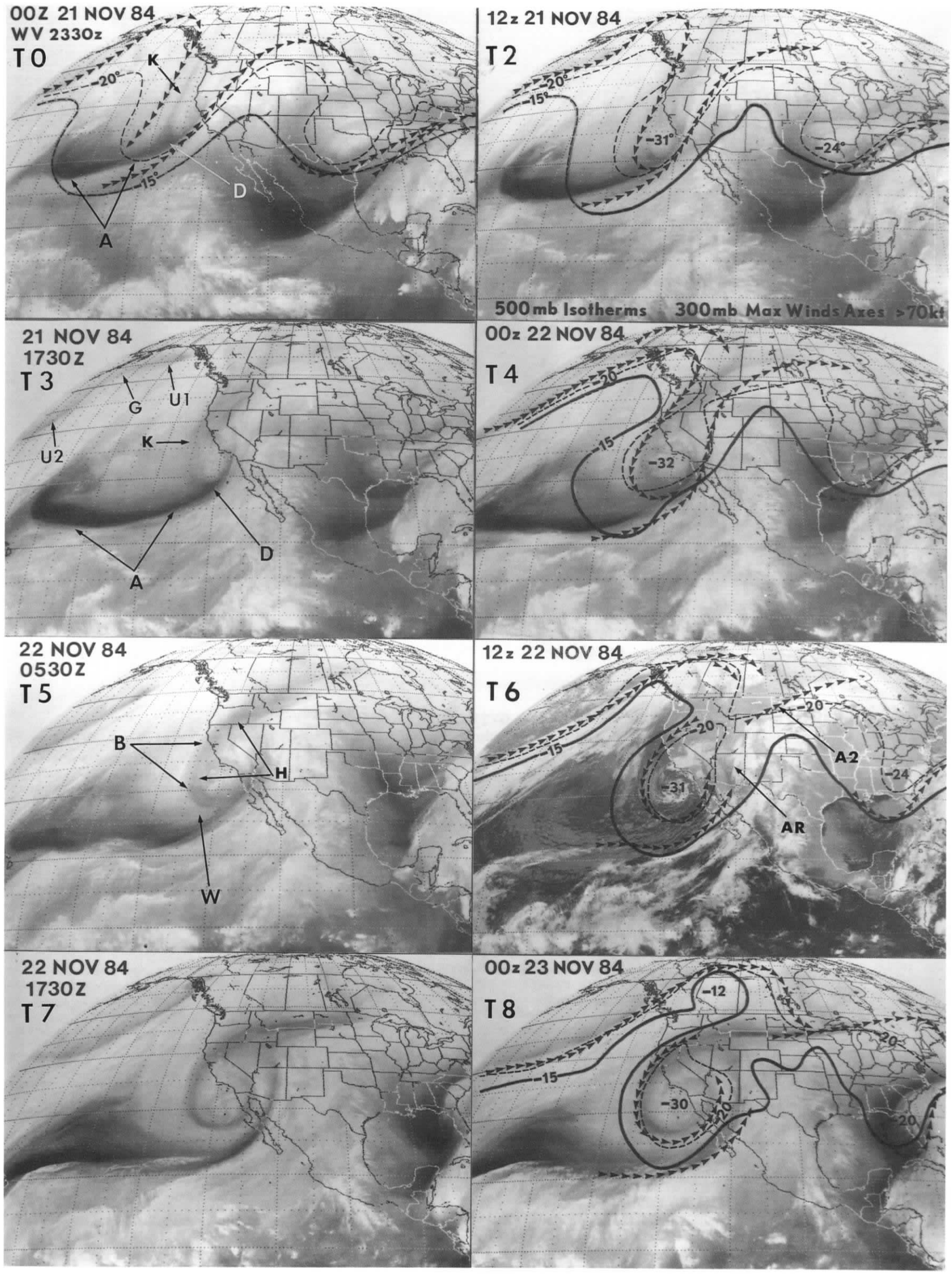
00Z 21 NOV 84
WV 2330z
T0
K
-20°
-15°
D
A
12z 21 NOV 84
T2
-20°
-15°
-31°
-24°
500mb Isotherms
300mb Max Winds Axes >70kt
21 NOV 84
1730Z
T3
G
U1
U2
K
D
A
00z 22 NOV 84
T4
-20
-15
-32
22 NOV 84
0530Z
T5
B
H
W
12z 22 NOV 84
T6
-20
-20
-15
-31
A2
-24
AR
22 NOV 84
1730Z
T7
00z 23 NOV 84
T8
-12
-20
-15
-30
-20
-20

c. System Evolution - "Roll-Over" Cycle

At the radiosonde times of **Figures 29** and **35**, 300mb axes of maximum winds are shown as arrowheads placed end to end. They are not parallel to the winds as is our standard procedure for most analyses. Also shown are the -15°C 500mb isotherms as wide solid lines, and the -20°C 500mb isotherms as dashed lines. Maximum and minimum values of 500mb temperatures are shown where closed thermal highs and thermal lows appeared on the analysis.

(1) Large Area Sequence - Times T-0 to T-4

Time T-0 - 00Z 21 November 1984

At the time of the first image, an open upper air trough extended from western Canada southward across the Oregon coast to a position west of San Francisco. A 500mb vorticity maximum was analyzed at that location. From there, the trough extended southwestward parallel to moisture boundary "A". An associated surface trough and frontal zone extended from northern Idaho, across western Nevada, and across the coast of southern California.

The upstream ridge west of the trough had been amplifying. The jet stream on the forward side of that ridge rotated clockwise and extended equatorward, as the ridge amplified. In response to this, the trough had been "digging" southward and increasing in amplitude. Moisture boundary "A" had become more distinct, and moved southward. Although the dark zone along the northern side of that boundary had been darkening with time, it remained relatively narrow except on the western end, where a closed anticyclone formed at the southwestern end of the overall ridge pattern. (See inside boundary - times T-2 and T-3). The axis of maximum winds along the forward side of the trough is shown along the eastern part of boundary "A". A jet stream axis was also present farther to the west, but wind speeds greater than 70 knots were above 300mb.

Time T-2 - 12Z 21 November 1984

By the second radiosonde time, the upstream ridge has moved over northwestern Canada. A closed low has nearly formed at 500mb. If so, the center is near San Francisco with a col region over Oregon; and, the easterly winds occupy only a very small region over northern California. On the water vapor imagery, a narrow dark band has formed over Oregon and Washington where the stretching axis of the col or the "deformation zone" is forming.

A surface low with a 1010mb central pressure is present over southwestern Nevada, with a cold frontal zone extending across the southern California coast near Los Angeles.

Time T-4 - 00Z 22 November 1984

By this time, a closed low has formed from 700mb through 500mb. The deformation zone through the stretching axis of the col in the 500mb wind field is oriented southwest to northeast across southeastern Oregon to central Idaho. This feature has rotated slightly anticyclonically during the past 12 hours. In the middle troposphere, warmer air from the downstream ridge has moved, or "built" back on the northern and northeastern sides of the low. This is evident by the change in the -20°C isotherm on **Figures T-2** and **T-4** of **Figure 29**. Within the middle troposphere, from 700mb through 500mb, easterly winds have developed on the northern side of the new low. In the upper troposphere, at 300mb and above, a true closed cyclone has not formed, although the trough has narrowed to a cyclonic shear zone from northern California to central Idaho. Between times T-2 and T-4, the 300mb axis of maximum winds on the eastern side of the developing low has rotated counterclockwise. The southern part of that jet stream branch has moved eastward to northwestern Mexico, whereas the part over Idaho remained nearly stationary, contributing to the rotation. This change, combined with the fact that the axis of maximum winds around the upstream ridge moved eastward over Oregon, resulted in a more rounded shape of the axes of maximum winds around the developing low. However, at 300mb and above, the winds of easterly component on the poleward side of the low are contributed by flow around the upstream ridge. At high levels, no area of easterly winds has "built-back" to the northern side of the low from the eastern side. Such easterlies have developed at middle tropospheric levels.

As cyclogenesis is occurring, the upstream western ridge has "rolled-over" to the poleward side of the new low. By time T-4, the -20°C 500mb isotherm has moved eastward over western Canada and parts of Washington and Oregon. The thermal trough has narrowed over eastern Oregon, where the -20°C isotherms from the two ridges have nearly merged. Generally, in cases such as this, in which the upstream ridge has "rolled over" to such an extent during the early phase of cyclogenesis; the new closed low would have already become "cut-off" from the upstream jet branch. A break would have occurred in the jet stream branch extending around the upstream ridge to the circulation of the low. However, in this case, one of the significant complications has developed. A strong storm development has occurred on the western side of the upstream ridge over the Pacific Ocean. Consider the image at time T-3. In response to the Pacific Ocean cyclogenesis, a new short wave ridge has formed at position "G"; and, a new jet stream speed maximum has developed along segment "U1" of the moisture boundary. By time T-4, the new speed maximum along boundary "U1" has caused the jet stream to "break across" the initial short wave ridge moving into western Canada. Two axes of maximum winds are present at 300mb over western Canada. The newer of the two is the southern branch that extends around the low off California. We will address changes related to this complication within the following discussion of close-up images.

We now direct your attention to the close-up images of **Figures 30** and **31**, and the related text on facing pages. Features labeled "K" and "D" here will be addressed, along with the changing patterns to the northeast side of the developing low. Discussion of large scale changes will be resumed with time T-5.

Figure 29

SEQUENCE OF IMAGES - LARGE AREA VIEW - TIMES T-0 - T-8
Image times are numbered at 6-hour intervals beginning with **T-0**, 2330Z 20 November 1984. Images for even numbered times are 30 minutes prior to radiosonde times, include analysis features, and are labeled by their radiosonde time. Images at odd numbered times are labeled by their image times. The image for time **T-1** is not shown here (see **Figure 30**). An infrared image is substituted for the 6.7μm image at time **T-6**. Analysis data overlain include: axes of 300mb maximum wind speeds with speeds of 70 knots or greater (arrowheads). 500mb isotherms -15°C (wide solid line) -20°C (thin dashed line). Maximum and minimum 500mb temperatures associated with thermal lows and thermal highs.

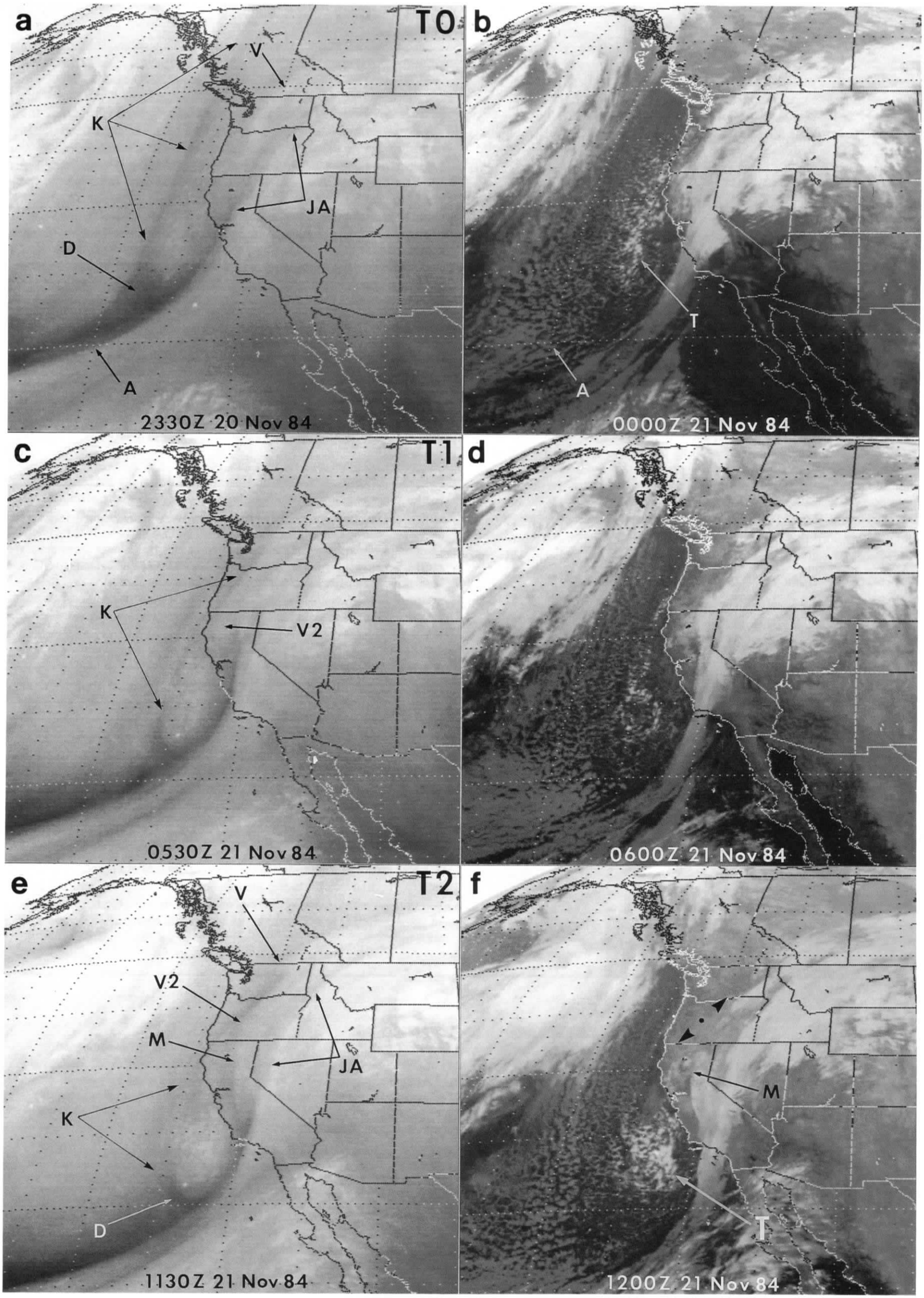
a
T0
V
K
JA
D
A
2330Z 20 Nov 84
b
T
A
0000Z 21 Nov 84
c
T1
K
V2
0530Z 21 Nov 84
d
0600Z 21 Nov 84
e
T2
V
V2
M
JA
K
D
1130Z 21 Nov 84
f
M
T
1200Z 21 Nov 84

(2) Close-up Images - Synoptic Times T-0 to T-5

Dark Band "K"

In Section A on boundaries, we discussed boundaries on the forward sides of upper air troughs as a primary category. We did not include such a category on the rear sides of troughs, since boundaries in that position are less consistent in regard to image features and their relationships to the related wind fields. However, there are some specific types of boundaries and features on the forward sides of ridges (rear sides of troughs) which are common and consistent. One of these is present in this case, and is labeled "K" on the images of **Figure 30**. Dark band features of this type are often observed in large amplitude long wave situations, and often when the upstream ridge is in the process of "rolling over" the downstream trough, as in this case. With the upstream ridge in the "roll-over" mode, the dark bands are usually rotating anticyclonically with time. Generally, the bands are relatively narrow and well defined, but indistinct. They may easily be overlooked, especially on still imagery. The "K-bands" tend to be parallel to the 500mb isotherms between the trough and the upstream ridge, and usually along the eastern side of the associated jet stream axis. They apparently divide the moisture regimes of the trough and the upstream ridge. The moisture in the trough is usually within cold mid-tropospheric air. Although the moisture of the ridge usually extends higher into very cold upper tropospheric air, the related gray shades are not representative of those very cold temperatures. Therefore, the gray shades on opposite sides of the dark bands are often similar. By our own definition, a band has finite width and includes two boundaries. With the "K-bands", both boundaries are often indistinct; however, the boundary along the western side - adjacent to the upstream ridge - is likely to be more distinct and better defined than the one along the eastern side.

At time "T-0", on the water vapor image of **Figure 30a**, the dark band "K" is indistinct but relatively well defined - especially along its western border. That portion between the arrows is east of the axes of maximum winds at 300mb and 250mb, based upon aircraft reports. At the southern end, "K" merges with a dark triangular or delta feature,"D". During the time period between "T-0" and "T-2", feature "K" became indistinct. By time "T-2", it is present only as an interface between the texture of the moisture patterns. We do not know the reason for this change in character of the feature "K". The jet stream and the mid-tropospheric temperature gradients between the trough and ridge have remained significant; although there may have been some weakening. The change could also have been caused by a vertical phase difference, such as the higher level moisture on the west side partially overlaying the eastern moisture. An interface is identifiable at time "T-2", largely because of the texture and gray shades on the trough side. Note on the infrared images, that a region of cold topped convective cells are present in the trough environment, at "T". Such cells are common under cold mid-tropospheric troughs over oceans, especially when the colder mid-tropospheric air is moving toward warmer sea surface temperatures. The colder cells are not under the center of the trough, but under the colder air of the thermal trough. On the images shown, this is initially elongated along the west side of the trough, then moves to the southwest side of the forming low and becomes more circular in shape. The radiation from the cold cloud tops causes a cellular pattern in the water vapor imagery, and the moisture spreading from the non-persisting tops causes the trough pattern to moisten with time. Although that moisture is lower, it appears even colder than the moisture of the ridge to the west. The ridge moisture extends into high cold air, and has a more uniform appearance.

Note on **Figure 31**, that the dark band "K" became even less distinct at time T-3. However, by time T-4, a boundary along the western side of the dark band appears to be reforming at "B". We shall discuss this change, but after addressing some related features.

The "Build-Back" Ridge and Related Image Features

An upper air low can be formed, in effect by default, by the process of an upstream ridge "rolling over" a portion of the trough and merging with the downstream ridge. Lows formed by this pure "cutting-off" process commonly do not have significant clouds and precipitation associated; and, surface cyclogenesis is usually not involved. With the more common "cyclogenesis" process, involving both the formation of a new surface low, and the closing of an upper air cyclone, a thermal ridge in the lower middle troposphere "builds back" around the trough from the downstream side. Usually, this "build-back" process begins in the lower middle troposphere, and extends vertically upward with time, either in two or more discrete steps, or as a relatively continuous process. As the "build-back" process occurs, the upper air easterly winds develop between the cool air of the trough and the warmer air of the "build-back" thermal ridge. In some cases, especially when the primary jet stream branch involved is on the upstream side of the trough, with a negative "tilt" orientation of the short wave features, the process of forming the upper air closed low is dominated by the "build-back" ridge rotating around a portion of the trough from the downstream side. In other more common cases, the low becomes closed partly from the "build-back" thermal ridge, and partly by the warmer air of the upstream ridge "rolling over". With cyclone developments, the roles of the two ridges are significantly related to the configuration of clouds and precipitation, to the jet stream wind fields, and to the subsequent evolution of those features. Water vapor imagery has proved to be a valuable aid for observing the ridge developments, particularly the role of the upstream ridge where clouds are often absent. This subject will be discussed in Section C on cyclogenesis; however, the concepts are necessary in discussing some of the image and analysis features of this case.

Consider the image features on the eastern side of the developing low in this case. At time T-0, **Figure 30a**, the jet stream branch along the forward side of the trough extended along boundary"A", and northeastward along that part of the boundary labeled "JA". Note that another moisture boundary is present at "V" to the northwest of "JA". A cyclogenesis process had begun prior to the time of the first image, resulting in a moisture boundary "building back" to the left of the jet stream axis. That process did not proceed, nor did a second attempt, indicated by a wave shape feature labeled "V2"; since the primary cold mid-tropospheric air was driven southward by the strong jet stream zone on the west side of the narrowing trough. However the features are present as complications on the imagery, and in the wind and thermal fields to the north of the cyclone that does develop.

By time T-2, the trough has become very narrow from northern California across Oregon. A cyclone is beginning to close between 700mb and 500mb. The deformation zone through the stretching axis of the forming col region is located near the narrow dark band across Oregon, indicated by opposing arrows on the infrared image. A new area of middle level moisture and clouds is building back from the jet stream zone, at "M". There are no indications on the water vapor imagery that cold air is breaking across the trough to the southwest parts of perturbations "V" or "V2". There are such indications to the southwest of "M". One of these involves the evolution of the cold mid-tropospheric air indicated by the clouds at "T"; and, the other is the presence of the triangular dark area at "D", which is the next topic of discussion. Another indication is that boundary "M" has not merely fallen back with respect to the jet stream zone; but, by time T-2, it is moving back with respect to the ground.

By time T-3, the moisture boundary "M" has built-back over central California, and changed from a convex curved shape to a "cusp" shape, with the apex or point of the cusp at "P1". Another cusp has formed on the higher level moisture boundary associated with the jet stream axis. The apex of that higher feature is at "P2". Cusp formations associated with cyclogenesis are discussed more extensively in Section C. In this case, the cusp point "P2" formed on boundary "JA" which had been coincident with the jet stream axis. Generally, as a cusp forms on a boundary related to the jet stream axis during cyclogenesis, the jet stream winds become vertically shallow and weaken rapidly near the region where the boundary becomes increasingly convex and forms the point of the cusp. A "break" forms in the jet stream zone near the point of the cusp; and, the remaining two branches may be connected by an axis of maximum winds across the ridge to the east of the point of the cusp.

At the next radiosonde time, T-4, the 300mb axis of maximum winds no longer follows along boundary "JA". On **Figure 31c**, axes of maximum 300mb winds with speeds greater than 90 knots are shown in the area where the "break" is in progress.

Wind speeds were 115 knots over southern Nevada, 70-75 knots over northeastern Nevada and southern Idaho, and greater than 90 knots over Montana. During the 6 hours between times T-3 and T-4, the point of the higher cusp at "P2" did not move westward, but remained nearly stationary. However, the angle of the cusp became slightly smaller, as portions of the boundary to the north and south of the point rotated in opposite directions.

By time T-4, the lower level cusp point, "P1", has moved westward off the California coast in conjunction with the new easterly winds in the middle troposphere. A warm ridge has built back around the newly formed low in the middle troposphere. The 500mb winds have changed from southwesterly to south-southeasterly over Nevada during the prior 12 hours. During that period between times T-2 and T-4, the temperatures warmed at Oakland, near San Francisco, by 5°C at 500mb and 6°C at 700mb. At time T-4 a moisture boundary labeled "H" extends northeastward from point "P1". Boundary "H" is a middle tropospheric "head" boundary along the northwestern edge of the warm air that built back around the northern side of the new low. Recall that the low had not yet closed at 300mb and higher. Cusp "P2" has remained nearly stationary over northwestern Nevada; the higher level moisture has not moved westward. As the upstream ridge continued to "roll over", the dark band "K" is across Washington and Oregon; and, a portion of the boundary "B" along the west side of the dark band has moved adjacent to the "head" boundary "H".

◄ Figure 30

CLOSE-UP VIEWS - TIMES T-0, T-1, T- 2
Water vapor and infrared image pairs at 6-hour intervals - from GOES Central.

T-0. Fig. 30a. 6.7μm image, 2330Z 20 November 1984.
Fig. 30b. IR image, 0000Z 21 November 1984.
T-1. Fig. 30c. 6.7μm image, 0530Z 21 November 1984.
Fig. 30d. IR image, 0600Z 21 November 1984.
T-2. Fig. 30e. 6.7μm, 1130Z 21 November 1984.
Fig. 30f. IR image, 1200Z 21 November 1984.

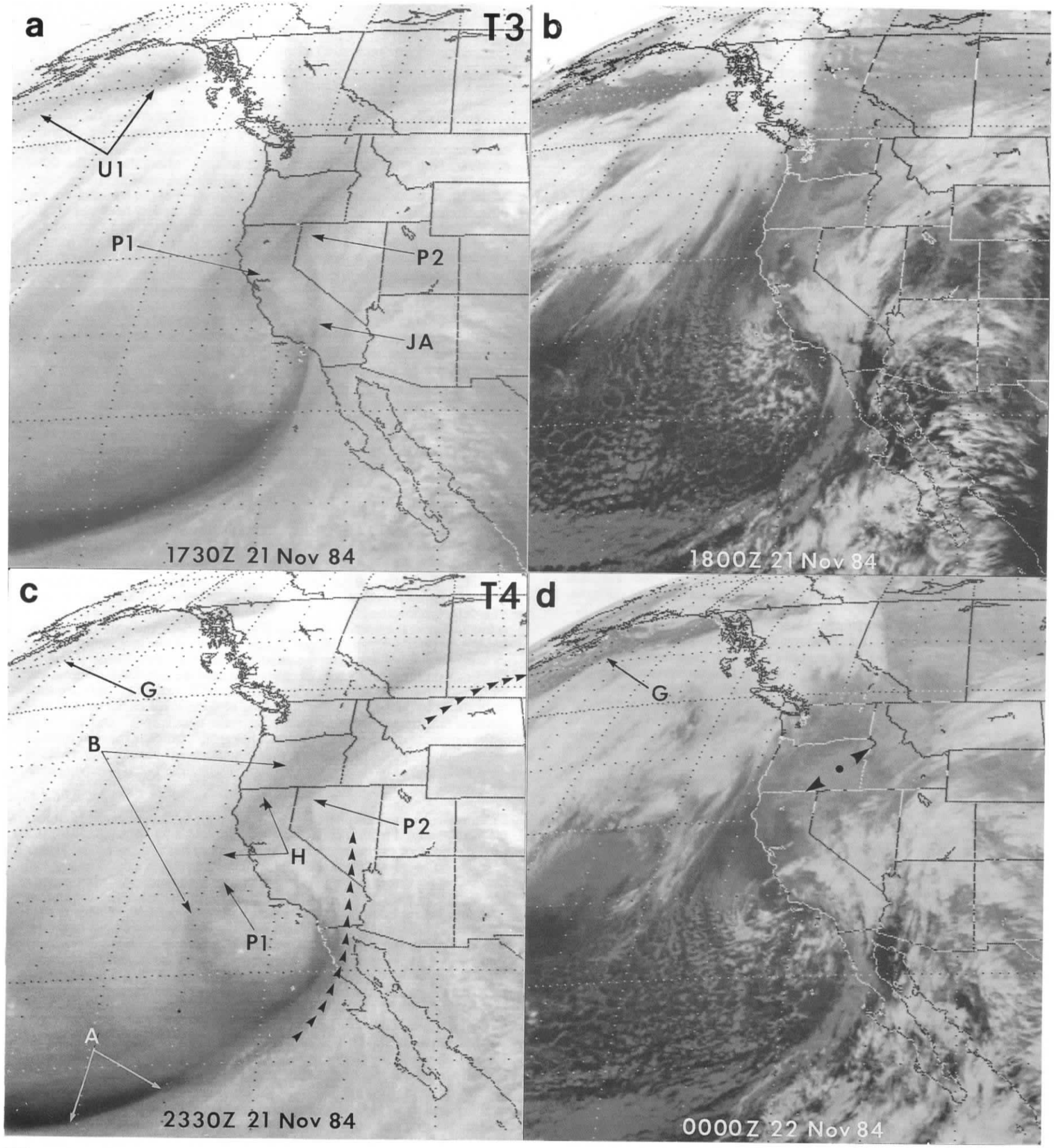

Figure 31 **CLOSE-UP VIEW - TIMES T-3, T-4**

Water vapor and infrared image pairs at 6-hour intervals - GOES Central.

T-3. **Fig. 31a.** 6.7μm image, 1730Z 21 November 1984. **Fig. 31b.** IR image, 1800Z 21 November 1984.

T-4. **Fig. 31c.** 6.7μm image, 2330Z 21 November 1984. **Fig. 31d.** IR image, 0000Z 22 November 1984.

Figure 32 **WEDGING FROM DRY DELTA - MODEL AND IMAGE EXAMPLE**

Fig. 32 a-b-c. Large scale drawings - dry delta situation. **Fig. 32 d-e-f.** Close-up drawings - wedging.
Fig. 32g. Close-up image 6.7μm GOES Central 0530Z 22 November 1984 - Time **T-5.**

The "Dry Delta" and "Moist Wedge" Features

A triangular shaped dark region is identified on **Figure 30a** at "D". Such features have been observed in specific situations on water vapor imagery; and, their recognition can provide some useful information.

The delta features are commonly present during the pre-cyclogenetic and early phase of cyclogenesis. **Such dark delta features are often observed in cases where development occurs along the forward side of an upper air trough, but not at the base of the trough.** Such developments are generally associated with a jet stream branch extending across the trough from the upstream ridge. Consider the drawings on **Figure 32, a,b,c.** The schematic of three drawings represents a jet stream branching across the trough with a "roll-over" process. The temperature references indicate mid-tropospheric air temperatures. At the initial time, a cold trough is shown between two warm ridges. Then, at the second time, the northern portion of the upstream ridge "rolls over", extending the jet stream branch across the trough. Commonly, during the early stages of this process, the jet stream on the east side of the ridge changes character. The axis of maximum winds shifts significantly to the right - looking downstream. It is not parallel to the wind directions. This "NVA" type of structure (See Section D3) increases, sometimes until the axis of maximum winds is nearly across the flow, then the wind speeds decrease and the jet "breaks" in that area, forming two branches. This break is indicated on **Figure 32b**. As the northern branch extends across the trough, the warm mid-tropospheric air on the right side of the jet approaches the warm air on the downstream side of the trough. That portion of the trough becomes narrow, and usually, the thermal gradients weaken. This is represented on **Figure 32c**. At location "D" on that drawing, the jet branch across the trough has approached, or is nearly intersecting, the jet stream along the forward side of the trough. That location also represents a division point of significantly different character of the trough itself. To the north of "D", the trough is wide with cold air. To the south the trough has become narrow between the two warm air ridge regimes, and usually the temperatures have moderated significantly along that narrow portion. Conditions along that narrow portion vary from case to case. It may consist of a cyclonic shear zone or a weak open trough with diffluent flow across the feature. Also at point "D" is the location where the dark delta features are observed on water vapor imagery.

The drawing of **Figure 32d** represents a close-up view at the "D" location as it might appear at the time of **Figure 32c**. Since the southern portion of the trough has become elongated to a narrow boundary-like feature between the two ridge regimes, a dark delta shaped feature is formed by three primary boundaries. Often these boundaries are not straight. Side "A" is slightly concave from the moist side perspective, and is formed by the downstream ridge baroclinic zone. Usually a significant jet stream axis is present along that boundary, although it may have weakened along its southwestward extension. Side "C" is usually convex toward the dark area, and is formed by the cold mid-tropospheric air of the trough, which has been sustained, or may have become even colder as cold air was advected from the cold side of the branching jet stream. Side "B" is also convex, and formed by the upstream ridge moisture regime. That side is likely to be the most variable with time, and may be diffuse when viewed closely, as the flow is likely crossing the boundary from the moist side toward the dry side. The moisture to the west of side "B" may be relatively high, sometimes with relatively drier air in the lower middle troposphere.

The drawings of **Figures 32d,e**, and **f**, represent a change with time in the "dry delta" features. We have referred to this type of change as "warm wedging", or "moist wedging" as it appears on the water vapor imagery. A jet stream, branching across the trough, is present between the cold air tothe north of boundary "C" and the warm air of the upstream ridge, to the west of boundary "B". Initially, this jet stream branch does not merge with the jet stream on the forward side of the trough, along boundary "A". In many cases, after a "dry delta" is formed, the jet stream branching across the trough will rotate cyclonically around the northern part of the trough; but, it will not merge with the jet stream along "A". Instead it will rotate onto the left side of jet stream "A". A wedge shaped area of warmer mid-tropospheric air from the upstream ridge is "driven" between the cooler air to the left of jet stream "A" and the colder air of the trough farther to the north. This "wedging" process often results in a double baroclinic zone and a dual jet stream structure on the southern and sometimes eastern quadrants of developing cyclones. It also may result in double zones of clouds and precipitation, such as a new zone of severe convective weather breaking out to the rear of the original dry slot over the central or eastern United States. The process is not often revealed on visible or infrared imagery, but can be recognized early on water vapor imagery by the presence of a "dry delta" and its subsequent evolution. The drawings of **Figure 32** illustrate the evolution. Boundary "B" becomes increasingly curved with time - convex from the moist side - as indicated by the dashed lines of **Figure 32e**. The boundary "B" changes to a cusp shape. However, in this case, the point of the cusp is accelerating downstream, rather than falling back and reversing direction as those discussed in the "build-back" process. Therefore, we use the term "wedge", and the term "moist wedging" as the change is observed on imagery. The dark delta shaped area changes to a "Y" shape, as the moist air "wedges" into the dry area. The branch of maximum winds associated with the "wedging" rotates or moves to the left side of the original jet stream branch along boundary "A". In many cases of cyclogenesis, when "wedging" occurs, two jet stream branches are present on the southeastern quadrant of the new upper air low. Sometimes both branches will persist; and, in other cases, the wind speeds along the original equatorward branch will decrease rapidly as warm air from the upstream ridge is extended along its left side.

On the sequence of water vapor images of **Figure 30**, the dry delta feature, "D", persisted, but with small scale changes in shape and distinctiveness. At the times on **Figure 31**, the feature became even less distinct. Although the jet stream from the upstream ridge along dark band "K" and boundary "B" had not extended around the developing low or merged with the jet branch along boundary "A", winds at the leading end of the branch did cross the west side of the dry delta from the upstream ridge side. Apparently, as the dry delta became less distinct, the flow across its western border continued without local downward vertical motion required to maintain the dry conditions. This change and the loss of distinctiveness of the dark band "K" were likely related to a weakening of the jet stream zone on the western side of the trough. However, at time T-4, this jet stream zone is beginning to strengthen significantly, as the new jet stream speed maximum that formed along boundary "U1" (over the Gulf of Alaska) broke across the ridge. That speed maximum has begun to move southward on the east side of the ridge, and is along the northwestern quadrant of the new low by time T-4. Boundary "B" is again becoming distinct, and the dark zone along its eastern side is becoming darker. At time T-4, this darker zone, along with a lighter area to the west of boundary "B", are moving southward on the western side of the low.

Just after time T-4, as boundary "B" increased in distinctiveness and definition, a "moist wedge" feature developed rapidly. A close-up water vapor image for time T-5 is shown on **Figure 32g**. The newly formed wedge shape is labeled "W". The new jet stream speed maximum has reached the western side of the low, and is beginning to rotate cyclonically into a position to the left of the original jet stream along boundary "A".

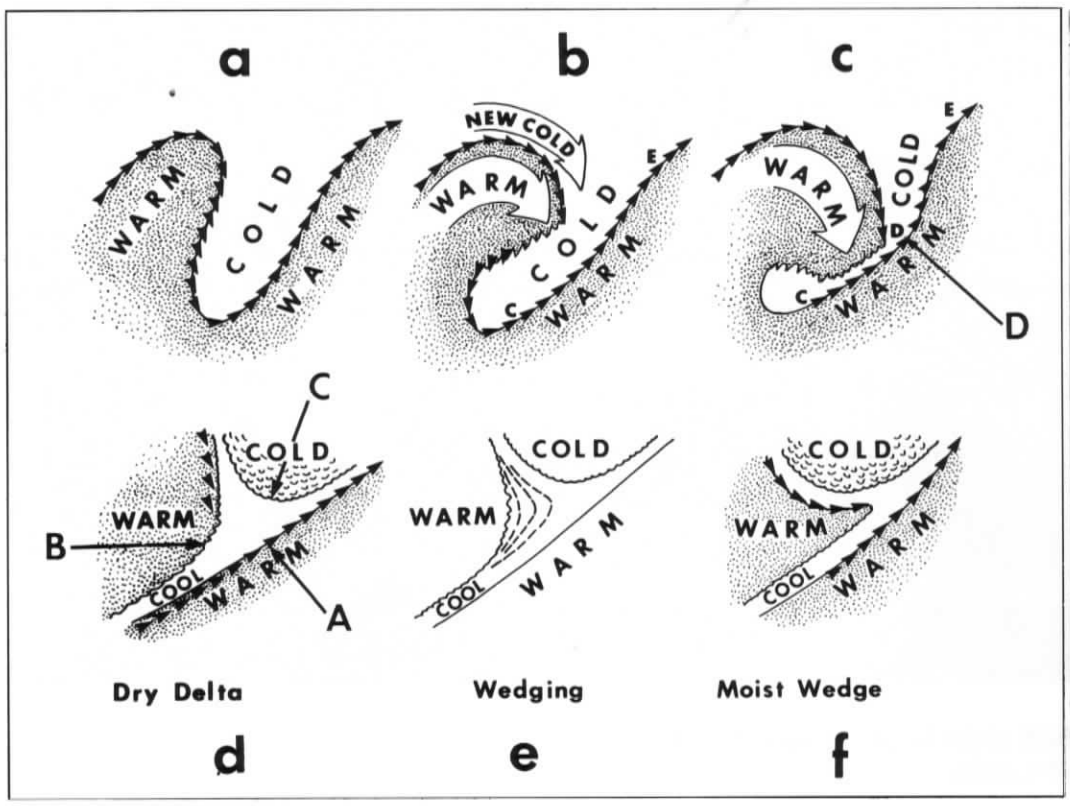

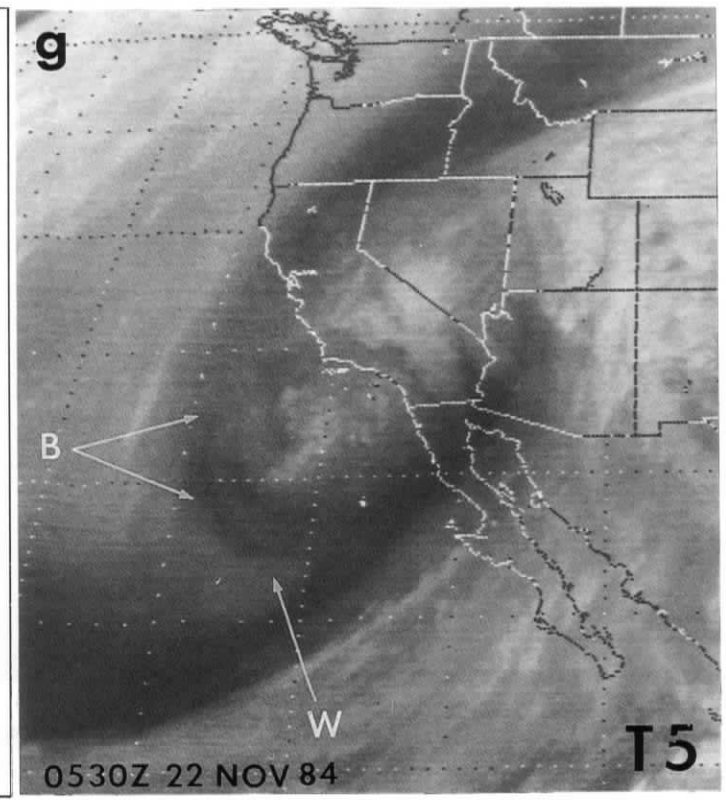

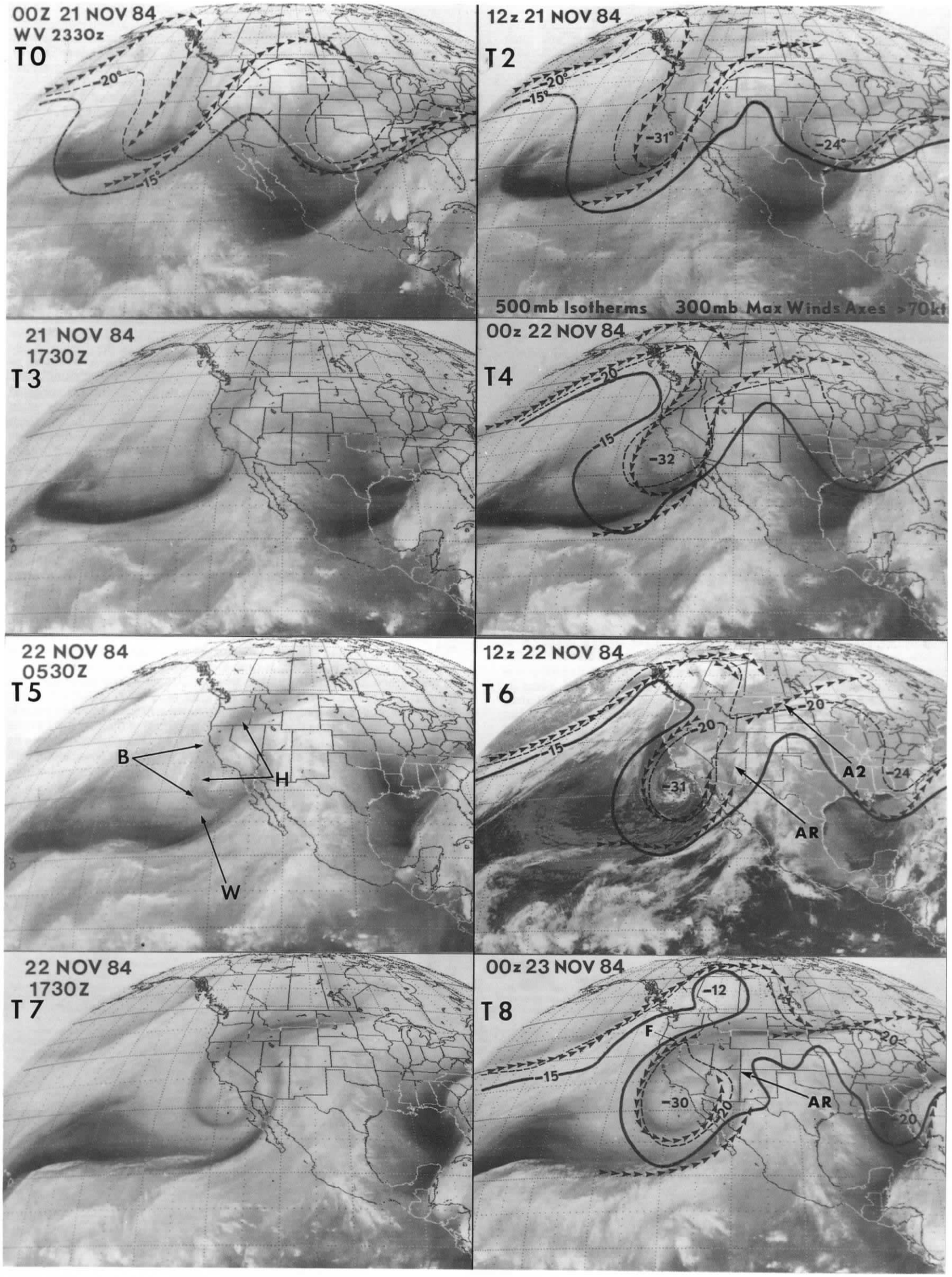

Figure 33 SEQUENCE OF IMAGES - LARGE AREA VIEW - TIMES T-0 - T-8
Fig. 29 REPEATED - See **Fig. 29** Caption.

(3) Large Area Sequence - Times T-5 to T-16

Time T-5 - 0530Z 22 November 1984

The close-up view of **Figure 32** was valid at time T-5. On the large area view on **Figure 33**, valid at that time, the moist wedge feature is again labeled "W". In this case, the change from the dry delta shape to the moist wedge shape occurred very rapidly. This rapid change was caused by the darkening at the southern end of boundary "B", as the jet stream speed maximum moved southward onto the western side of the new closed low. Large area views for times T-0 through T-8 were shown on **Figure 29**, and are repeated here as **Figure 33**.

Time T-6 - 12Z 22 November 1984

The 1130Z water vapor image was not received north of 30° latitude. Therefore, an infrared image has been substituted. Water vapor features must be interpolated between the T-5 and T-7 synoptic times; however, the analysis features are shown on the 1200Z infrared image.

The upstream ridge has continued to "roll-over" into western Canada; and, the jet stream over that ridge no longer extends to the branch around the western side of the low. The low has become "cut-off" from the primary polar jet stream zone. The deformation zone through the col has remained over southern Idaho, but has continued to rotate anticyclonically. Near the col position, and to the northeast of there, the trough has narrowed and warmed, as the warmer air of the upstream ridge has moved toward that of the downstream ridge. Note that the -20 °C isotherms form a hyperbolic pattern. The temperature gradients between that portion of the trough and the upstream ridge have decreased; and, the jet stream wind speeds have decreased, forming the "break" in the jet stream. The strong northerly winds on the eastern side of the Canadian ridge have depressed the trough southward. This "dump-over" effect has caused the axis of maximum winds on the southern side of the trough, at "A2", to straighten and move southward. Whereas the 500mb temperatures over Washington, Oregon, and Idaho have become warmer during the past 12 hours, those over eastern Montana, North Dakota, and northern Minnesota have cooled.

On the eastern side of the "cut-off" low, the jet stream wind speeds have decreased since time T-4. The situation there is somewhat complicated, and not directly correlated to the fact that the low has become "cut-off". A "break" has occurred in the jet stream over Utah and Arizona, where a relatively well defined cirrus cloud edge has persisted at "AR". There were, in this case, two processes involved. The initial "break" in the jet stream occurred in conjunction with the higher level cusp formation which is commonly associated with cyclogenesis. Typically, in such cases, the jet stream branch south of the cusp apex (point "P2" in this case) remains relatively strong and rotates cyclonically around the northern side of the low. In those cases, high level moisture at the cusp region also extends westward around the low in advance of the rotating speed maximum. In cyclogenesis cases, in which the upstream ridge "rolls over", and does so early in the cyclogenesis process; the cusp does not hook cyclonically around the low. The jet branch south of the cusp does not rotate cyclonically. In this case, the cusp point "P2" formed over Nevada, then moved or reformed eastward, reaching a position near Salt Lake City, Utah by time T-7. Furthermore, the jet stream "break" extended southward. This is related to a second set of events occurring in this case, and is less common.

Consider the southeastern quadrant of the low. At time T-5, the moist wedge feature had formed. The upstream ridge moisture, forming the wedge "W", cannot be observed directly on the infrared image at time T-6; but, notice that the moisture has rotated around the southern side of the low over western Arizona and southern Nevada by time T-7. A dry slot on the inside of that moisture has rotated over southeastern California. On the infrared image at time T-6, this evolution is indicated by the dual jet stream structure on the southeastern quadrant of the low. By that time, the -20°C isotherm has remained nearly stationary over southeastern Nevada and the California-Arizona border; whereas, the -15°C isotherm has moved eastward to central New Mexico. The systems related to this are of subsynoptic scale. Note at time T-7, that both dry slots are located between San Diego and Tucson radiosonde sites. Although such subsynoptic scale structure is difficult to analyze in the standard upper air network, experience with similar, but larger scale, events implies that a retrogression of the mid-tropospheric temperature gradient would be likely on the eastern side of the low. Generally mid-tropospheric warming occurs between the two axes of maximum winds, resulting in a decrease with time of the eastern gradient, while maintaining or strengthening the western one. In conjunction, the winds speeds of the eastern jet stream branch tend to decrease rapidly with time. This process likely contributed to the southward extension of the jet stream "break" in this case. Although the wind speeds and thermal gradient decreased, a residual boundary in the moisture and clouds remained, at "AR".

Time T-8 - 00Z 23 November 1984

By time T-8, the inside dry slot, adjacent to boundary "B", has rotated around to the northern side of the low, and extends across the California coast near Vandenberg. The leading moisture from the upstream ridge, initially identified as the moist wedge "W", has rotated around the low to the northwest quadrant; and, a double jet stream structure is present on the southeast quadrant of the low. The jet stream winds have increased again over Arizona. Although the southern outside jet branch has moved eastward and weakened, the inside branch has rotated to the northeast side of the low over Arizona. In conjunction with this, the 500mb temperatures have warmed over northern Nevada and northern Utah as a new thermal ridge built back on the northeast side of the low. This temporary "build-back" effect has caused the thermal trough on the northern side of the low to rotate northwestward over southeastern Oregon, at "F". That thermal trough remains form the cold air of the original open trough, in which the cyclogenesis occurred. The two remaining wide portions consist of the closed "cut-off" low and the open trough over central Canada. Between those portions, the system has narrowed between the merging ridges, and consists of an elongated col in the wind field and a thermal trough in the mid-tropospheric temperature field. The thermal trough and the stretching axis of the col have rotated clockwise, as the eastern end moved southward in response to the northerly flow on the eastern side of the "roll-over" ridge. That type of rotation of the wind and thermal features and the related moisture boundaries is common during the "roll-over" evolution. In this case, the rotation has accelerated by the west end of the narrow thermal trough moving northward. This complication was caused by the new jet stream branch rotating around the low and causing a new "build-back" ridge process on the northern side of the "cut-off" low. Boundary "A2" has rotated clockwise, and the wind speeds of the related jet stream branch are weakening as the warmer air of the two ridges are beginning to merge and the trough temperatures are warming. Boundary "AR" is still relatively well defined, but is obscured by its position directly along the eastern borders of Utah and Arizona. The boundary has become residual, as the associated wind speeds and temperature gradients have decreased significantly.

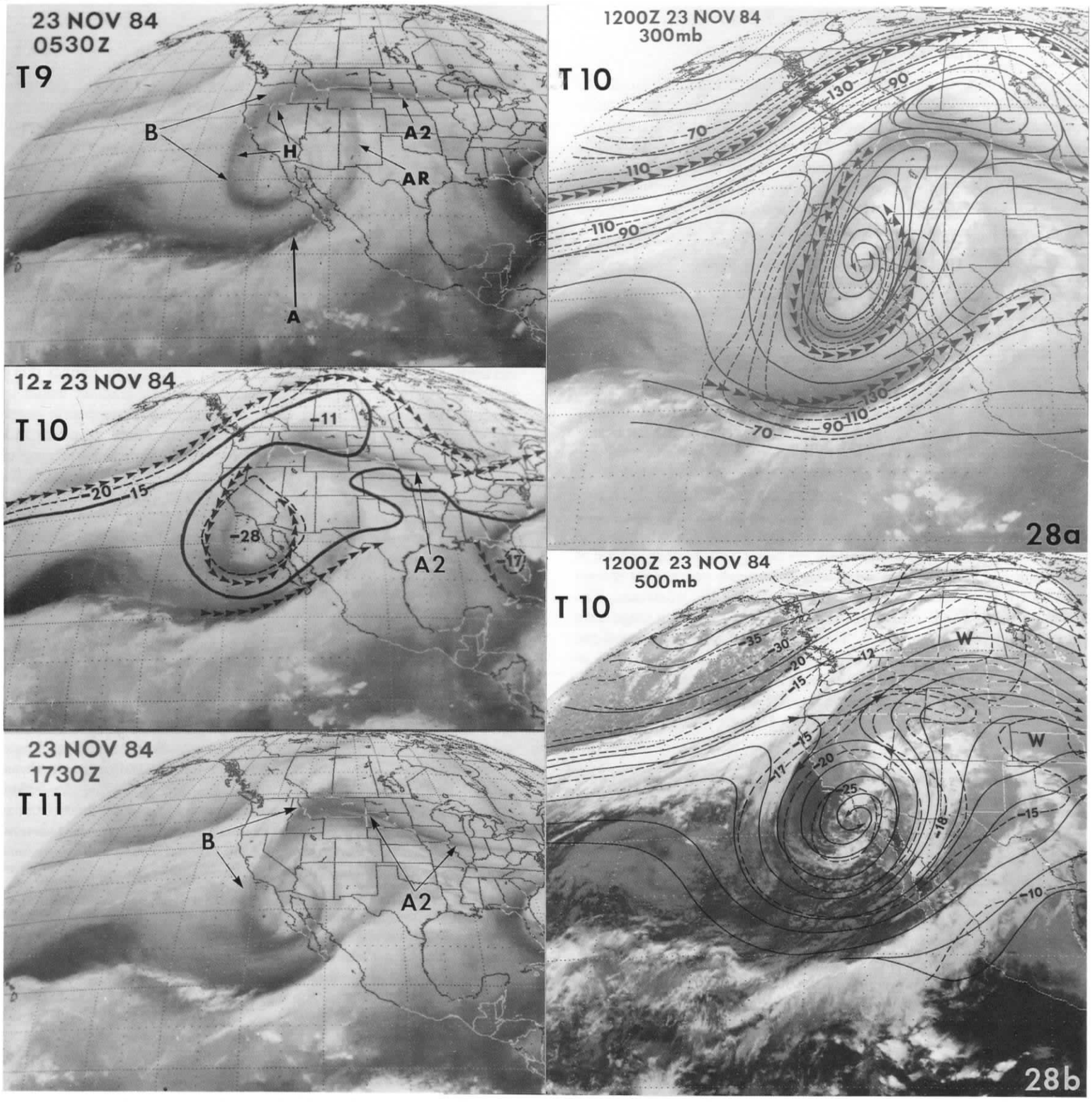

Figure 34

LARGE AREA VIEWS - TIMES T-9, T-10, T-11.
On **T-10**: 6.7μm image - 1130Z 23 November 1984 with 1200Z axes of maximum 300mb winds and 500mb isotherms (-15°C bold, - 20°C thin dashed), 500mb temperatures -11°C thermal high, -28°C thermal low.

MATURE PHASE - UPPER AIR ANALYSES - TIME T-10
Fig. 28a. 6.7μm 1130Z 23 November 1984, 300mb analysis.
Fig. 28b. Infrared image, 1200Z 23 November 1984, 500mb analysis.

Times T-9 and T-10 - 0530Z - 1200Z 23 November 1984

In the introduction to the case study, a close-up image valid at time T-9 was shown on **Figure 27**. Images with 300mb and 500mb analyses were shown on **Figure 28** for time T-10. Now that the evolution of the circulation systems and image features has been illustrated, the features present at the mature stage of the "roll-over" cycle can be more easily understood. For convenience, the **Figure 28** analyses and large area views for times T-9, T- 10, and T-11 have been placed together here as **Figure 34**.

The overall larger scale features present at time T-10 are typical of the blocking regime phase for this type of "roll-over" cycle. An upper air anticyclone has closed on the poleward side of a "cut-off" cyclone, and is beginning to merge with that portion of the downstream ridge on the east side of the closed low. The part of the trough between the two ridges has narrowed and weakened, and extends through a col region. The stretching axis, or deformation zone, of that col has rotated anticyclonically with time, and is revealed on the water vapor imagery as a narrow dark band along boundary "A2".

As with all cases, smaller scale features and complications are present. Although none of these are individually uncommon, they have occurred in a set unique to this case. Many of the complications involved in this case may be attributed to the second speed maximum that formed along the jet stream of the upstream ridge over the Gulf of Alaska. When that speed maximum formed in response to cyclogenesis south of the Aleutian Islands, the leading portion of the upstream ridge had already begun to "roll over" the developing low. The new speed maximum then broke across the ridge between times T-3 and T-4, and reached the western side of the low by time T-5. This event delayed the cutting off process of the low, and reintensified the low. Thus, by the mature stage at time T-10, the cyclone is relatively large compared to the anticyclone, and has a much stronger jet stream branch on its west side along boundary "B" than would be common for such blocking regimes. The new speed maximum contributed to the double jet stream structure on the southeastern quadrant of the low and the residual boundary labeled "AR" on the image of time T-9. Note that boundary "AR" became significantly less distinct and poorly defined by time T-10, although a clear zone remains between two cloud systems (see the infrared image of **Figure 34**). The new speed maximum also contributed to a complex vertical structure of the circulation systems. Recall that there were two cusp features at different levels formed by time T-3. By time T-4, the lower level and western cusp (point P1) was associated with a thermal ridge "building back" in the middle troposphere, to the northern side of the new low. The low had not closed at 300mb and above; but, a cusp with its point at "P2" had formed on the higher level moisture boundary, and the jet stream break had begun. Commonly, in many cases of cyclogenesis, the "build-back" process occurs in two discrete steps at two levels. The second, higher level, cusp formation follows the evolution of the first one, by "building back" around the low. The cyclone then becomes closed by the "build-back" process at the upper tropospheric levels, in addition to the middle levels. In this case, after the higher cusp formed, the new speed maximum hooked over the upstream ridge; and, the apex of the cusp at point "P2" remained stationary. It then moved eastward, instead of rotating around the new cyclone. That high level ridge never did rotate around the low, although a weaker smaller high level ridge did "build back" around with the moist wedge of the second speed maximum. Consider the results at time T-10. The details must be viewed on the analyses of **Figure 34**. At 300mb, a jet stream axis, with winds of 70 knots or greater, extends around the low to southeastern Nevada, and continues around the low over Nevada at lesser speeds, as a branch of maximum winds in the easterlies. However, the 300mb "cyclone" is elongated northward; and a second zone of maximum easterly wind speeds is present over Montana. The northern branch of easterly winds formed when the anticyclone closed. The southern speed maximum in the easterlies formed between times T-6 and T-7 as the moist wedge rotated around the low with the new speed maximum. The trough had remained open at 300mb and above prior to that time. Easterly winds were present to the north of the low prior to that time, but they were the result of flow coming around the upstream ridge, which had "rolled over" to an east-west orientation. At 500mb, the cyclone has a rounded shape, and the easterly winds do not extend north of central Nevada. In the middle troposphere, a ridge had built back around the low by time T-4, with the original cyclogenesis process. Thus, at 500mb, a ridge was present to the north of the low in both the wind and thermal fields; and this ridge was strengthened by a second "build-back" process, as the second speed maximum rotated around the low. At 500mb, by time T-10, the ridges have already merged in the wind field. However, they remain separate in the thermal field. The original thermal trough, that had become narrowed between the "build-back" ridge and the "roll-over" ridge, is still present over western Nevada, southern Idaho, and Wyoming. The new "build-back" thermal ridge is present from Colorado across northern Utah. The result is a double thermal structure on the northern side of the low, that corresponds to the double speed maxima in the easterly winds at 300mb.

Consider the features on the water vapor images of times T-9 and T-10. Boundary A2 was originally a part of boundary "A". When the high level cusp point "P2" formed and the break occurred in the jet stream on the forward side of the trough, the segment labeled "A2" separated the downstream ridge from the northern part of the trough. As the upstream ridge "rolled over", the moisture from that ridge narrowed the trough adjacent to boundary "A2", and caused the boundary to rotate anticyclonically with time. As the thermal trough narrowed and weakened, the jet stream wind speeds decreased. By time T-10, boundary "A2" lies along the deformation zone of a col in the 300mb wind field, separating the streamline fields of the two ridges. An axis of maximum winds is still present along the eastern end of "A2" from Illinois eastward.

Boundary "H" is a head boundary formed by the moisture of the "build-back" ridges. That moisture is present in the upper troposphere at this time as a result of the second vertically deeper "build-back" ridge process. At time T-9, boundary "B" is well defined and distinct, with the strong jet stream branch present from Oregon southward around the cyclone. From the imagery alone, even in sequence showing the evolution of features, we would not have determined the strength of that jet stream branch at time T-10. We would have expected it to have weakened more than it did, especially along the northwest quadrant of the low. Such jet stream branches on the west side of closed lows, and their image features, will be addressed in detail in Section D. There are indications that the branch is weakening with time. Boundary "B" became less distinct between times T-9 and T-10, as high level moisture moving around the north side of the low has overlain the dark slot east of the boundary. Such higher level moisture moving around the low is usually an indication that warmer mid-tropospheric air of the "build-back" ridge is also moving around the low. This usually weakens the temperature gradients associated with the jet stream branch, and results in a decrease in the wind speeds. The jet stream branch is weakening, but not as rapidly as we would have estimated.

When anticyclogenesis occurs, an inside boundary usually forms. At time T-10, the anticyclone had just formed in the 300mb field. Previous to that time, the flow around the ridge had turned southward to the west side of the low. At time T-10, the easterly winds split into two branches at the new formed col over northern Idaho. A part of that flow still turns southward to the west of the low, and a new branch turns northward around the new high. Portions of the drier air from the new darkening area are moving into both branches. This is causing the northern end of boundary "B" to become better defined and more distinct, and to extend northward with the dry air turning anticyclonically. Boundary "B" is not an inside boundary; however, a new inside boundary is forming as a northern extension of boundary "B". This type of boundary modification is common when anticyclogenesis occurs after the cyclogenesis with the "roll-over" evolution blocking regimes. By time T-11, just 6 hours later, the dark area over Montana has become larger; and, the inside boundary on its west side has become much more obvious on the image.

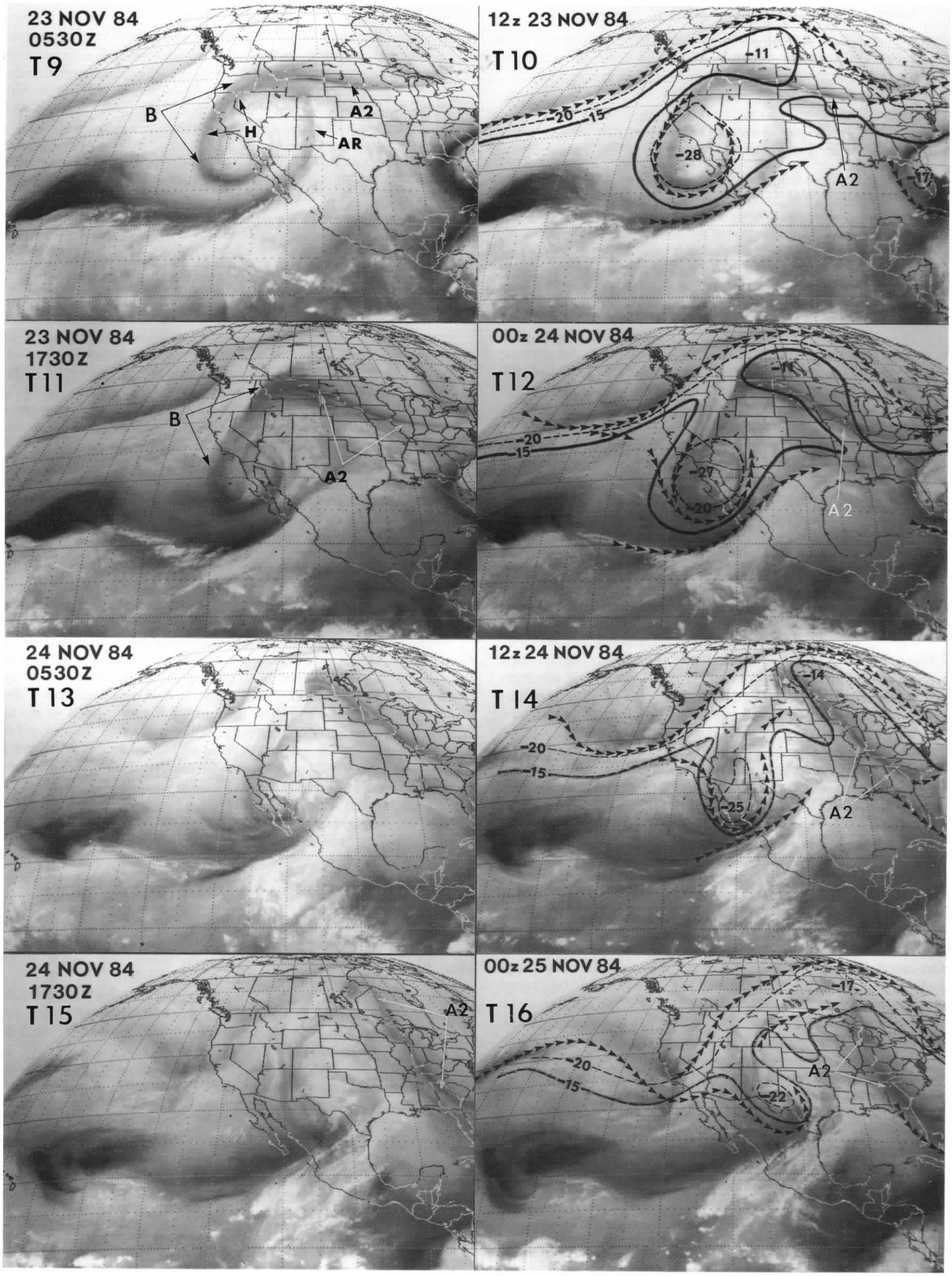
23 NOV 84
0530Z
T9
B
H
A2
AR
12z 23 NOV 84
T10
-11
-20
-15
-28
A2
-17
23 NOV 84
1730Z
T11
B
A2
00z 24 NOV 84
T12
-11
-20
-15
-27
-20
A2
24 NOV 84
0530Z
T13
12z 24 NOV 84
T14
-14
-20
-15
-25
A2
24 NOV 84
1730Z
T15
A2
00z 25 NOV 84
T16
-17
-20
-15
-22
A2

Time T-12 - 00Z 24 November 1984

The "roll-over" process has continued, although complicated by new short wave features. The thermal trough along boundary "A2" has weakened at 500mb; and, the -15°C isotherms of the two ridges have merged over the Iowa-Missouri area. The col is still present in the 300mb wind field with the stretching axis across central Iowa. The closed anticyclone at 300mb has moved eastward to Minnesota; and, the western part of boundary "A2" has become residual. Southerly winds from the east side of the closed low now extend northward into Canada on the western side of the anticyclone. The jet stream winds along the northern part of boundary "B" have weakened rapidly; and, the upstream ridge over the northwestern United States is beginning to merge with the "head" ridge which had built back on the north side of the low. The trough that extended northward from the low in the 300mb wind field and the 500mb thermal field has weakened between the merging ridges; but, a part remains moving northward into Montana at the southern end of the remaining inside boundary.

The jet stream zone along boundary "U2" over the Pacific Ocean is rotating clockwise with time; and, the blocking regime is beginning to open. The primary low has moved slowly eastward, and is still closed in the wind fields from 500mb through 200mb. However, a jet stream branch is breaking across the ridge just west of southern California and merging with the original axis of maximum winds across Nevada and southern California. At 300mb, the primary jet branch is the eastern one from Nevada. The 300mb wind at San Diego was north at 145 knots. At 200mb the branch across the ridge has become the primary one.

Time T-14 - 12Z 24 November 1984

The eastern thermal ridges have merged at 500mb. At 300mb a separate anticyclonic center is still present, and is now over northern Indiana with a deformation zone over Illinois and Kentucky. On the water vapor image, boundary "A2" has been maintained. Note that it has rotated more than 90° from its original southwest to northeast orientation. The trough over the Pacific Ocean on the western side of the upstream ridge has moved eastward to a position off the northwestern coast of the United States. It has been "digging" southward, as the ridge on its upstream side built northward. The low over northwestern Mexico is still closed at 500mb, but has opened at higher levels. It is no longer "cut-off" as the jet stream branch has now become established across the ridge over southern California.

As the low opened and moved eastward, a new thermal ridge has developed in advance of the trough and extends over eastern Colorado. A new speed maximum has formed over southeastern Wyoming and northwestern South Dakota.

Time T-16 - 00Z 25 November 1984

The low has now opened in the wind fields from 500mb through 200mb, although the amplitude remains large. The cold air of the low is merging with the cold air of the upstream trough, nearly completing the "roll-over" cycle. The northern portion of the trough which was previously connected to the low, is now over Newfoundland. A broad, but complex, ridge now separates the two features. Boundary "A2" still exists, primarily as a residual upper air feature. The deformation zone in the form of a col in the wind field is no longer present, although a double ridge structure does remain in the winds from 300mb through 200mb over the eastern states.

◄ **Figure 35**

SEQUENCE OF IMAGES - LARGE AREA VIEW - TIMES T-9 - T-16
6.7μm images at 6-hour intervals beginning with time **T-9** = 0530Z 23 November 1984. Even numbered images are valid 30 minutes prior to radiosonde times, include analysis features, and are labeled by their radiosonde time. Images at odd numbered times are labeled by their image times. Overlain analyses features include: axes of maximum 300mb wind speeds with speeds at 70 knots or greater (arrowheads), 500mb isothems: -15°C (wide solid lines) -20°C (thin dashed lines), maximum and minimum 500mb temperatures associated with thermal low and thermal highs.

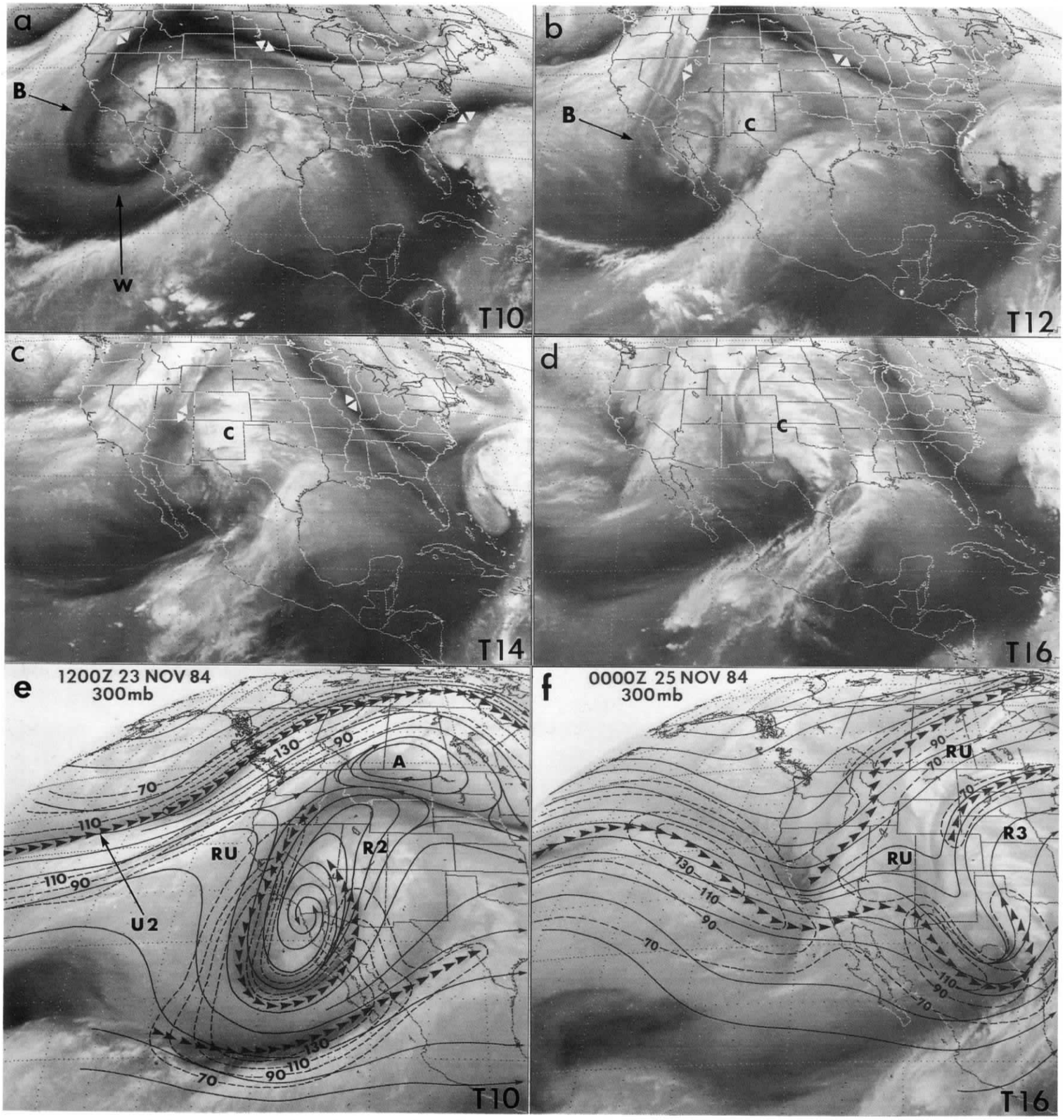

Figure 36

OPENING OF THE CUT-OFF LOW

Fig. 36 a- b-c-d. Sequence of 6.7μm images at 12-hour intervals for times **T-10, T-12, T-14, T-16.** Opposing white arrowheads indicate centers of cols in 300mb wind field.

Fig. 36e. (**Figure 28a** REPEATED) 6.7μm image, 1130Z 23 November 1984, with 1200Z 300mb analysis (streamlines, isotachs, axes of maximum winds).

Fig. 36f. 6.7μm image 2330Z 24 November 1984, GOES Central, with 0000Z 25 November 1984 300mb analysis (streamlines, isotachs, axes of maximum winds).

Water vapor images with 300mb analyses are at the same times as the first and last images of the sequence. The areas of view and gray shade conversions differ.

d. Moisture Pattern Changes Related to the Opening of the Cut-Off Low

On **Figure 36 a,b,c,d**, the four water vapor images, at 12-hour intervals, are close-up sectors valid at synoptic times T-10, T-12, T-14, and T-16. A different gray shade conversion has been used to enhance the darker features. Pairs of white triangles indicate the centers of cols in the 300mb wind fields.

During the 36-hour period shown, the "cut-off", low centered near San Diego on the first image, opened and accelerated eastward to southwestern Texas. By the time of the second image, boundary "B" has become poorly defined and indistinct. Moist air - primarily from the west - has merged across the dry slot, and multiple bands of cirrus extend along the boundary position. New darkening with time has occurred on the south side of the low; and, there is no well defined moisture boundary on the upstream side of this new dark region. The diffuse edge there implies open westerlies. Note that the moist band (W) along the right side of boundary "B" has become significantly darker on the south side of the low, although it is still identifiable as a faint pattern. The new dark region is within the jet stream zone at the base of the trough, and is of the "dry surge" type.

By the third image time, the opening low has moved eastward over northwestern Mexico; but, the dark area on the southern side of the low has not advanced, and has decreased in area. This is likely a result of temporary moistening aloft by convective clouds over the Mexican mountains. By the time of the last image, a better defined dark region is present over northeastern Mexico.

Images for the first and last times (T10 and T-16) are shown with 300mb analyses as **Figures 36e** and **f**. The first analysis, for time T-10, is the same one shown on **Figure 28a**. It is repeated here for easier comparison. The first image and analysis are valid near the mature stage of the blocking regime. The large scale systems had become nearly stationary; and, the circulation systems were in a "closed" mode. Note that the 300mb streamlines tend to be nearly parallel to the moisture boundaries. By the last image and analysis time, the circulations have changed to an "open" mode. Generally, the streamlines are across the moisture boundaries. In this case, the blocking regime did not persist. Just as it reached the mature stage, rapid changes were occurring in the upstream jet stream zones over the Pacific Ocean. At time T-10, the jet stream branch along boundary "U2" over the Pacific Ocean was still southwesterly with winds generally parallel to the boundary. However, a new ridge, to the west of the image area shown on **Figure 36**, was building rapidly. The jet stream along the western part of boundary "U2" on **Figure 36e**, then rotated anticyclonically on the eastern side of the building ridge, causing the trough to the north of "U2" to amplify and "dig" southeastward. In response to this, ridge "RU" changed to an "open" mode; and, a new jet stream broke across to merge with the flow around the "cut-off" low. As that occurred, the low opened and accelerated eastward.

Often, when "cut-off" lows open, and also accelerate downstream, several events occur. A new "dry surge" darkening occurs on the water vapor imagery at the base of the trough; a new area of clouds and precipitation forms in advance of the opening low; and, a new cyclogenetic process begins. A new "build-back" ridge forms, and a new surface low begins to form. These events occurred in the case shown. Note on the sequence of images of **Figure 36**, that a new region of cold clouds formed (at "C") on the eastern side of the opening low, and "fell back" to the northern side by the last image time. The new "build-back" ridge at 300mb, associated with that development, is identified as "R3" on **Figure 36f**. A new jet stream branch formed in conjunction with the new "build-back" ridge. It is present from northern Colorado across the Dakotas, where the residual boundary "B" became better defined again between times T-14 and T-16.

Although details vary from case to case, the changes observed on the water vapor imagery as this cut-off low opened are representative of other cases. Generally, as a cut-off low opens, the dark region around the western or upstream side of the cyclonic circulation lightens or disappears, and the upstream boundary becomes poorly defined as well as indistinct. This results from upstream winds beginning to cross the boundary. Sometimes during the cut-off phase of a low, the dark slot around the western side can become lighter by moisture coming around the north side of the low. This causes the western boundary to become less distinct, but is not a sign of opening. Such a lightening occurred during this case between times T-9 and T-10. Usually, when the opening begins, the western boundary becomes irregular as well as less distinct.

Also during the opening process, new darkening at the base of the trough is common; however, there is more variability in this aspect. Darkening at the base of the trough is more common when opening lows accelerate eastward during the opening process. If water vapor imagery are to be used alone to provide an early indication of the opening process, it is important to concentrate on the "changes with time" of the significant features. Boundaries may persist as residual features well into the opening phase. Lows which move out slowly, tend to remain closed for 24 hours or more after they are no longer "cut-off".

e. Summary and Perspective

In the case shown, a combination type of blocking regime formed while undergoing a "roll-over" system evolution. As is typical of such blocking regimes during the mature phase, two closed upper air circulation systems were present with two col regions associated with primary boundaries in the water vapor imagery. A closed anticyclone formed on the poleward side of a closed, and "cut-off" cyclone. During the formative stages of the "roll-over" cycle, a well defined boundary (labeled "B" in this case) formed on the western side of the cyclone. Although the shape of the boundary was concave toward the east, similar to the shape of an "inside" boundary, that shape was caused by the upstream ridge "rolling over" the northern side of the closed cyclone. A "head" boundary formed along the eastern side of boundary "B", contributing to a distinct dry slot between the two boundaries. The northeastern extension of the head boundary merged with the jet stream zone along the northern side of the downstream ridge (boundary "A2" in this case). The "head" boundary and its eastward extension were along the stretching axis a col zone formed as the cyclone closed. When the anticyclone formed, a new col region formed, and an "inside" boundary formed as a northward extension of boundary "B". During the "roll-over" evolution, the col regions and their associated moisture boundaries rotated anticyclonically with time.

There were several significant complications involved in the case. Since the cyclogenesis occurred in response to a jet stream branching across the trough, rather than a speed maximum coming around the base of the trough near the original jet stream position, two jet stream branches were involved in the cyclogenesis process. Although this is not an uncommon type of cyclogenesis process, it does result in the special condition of having two jet stream branches on the upstream side of the closing cyclone. The case was further complicated by a new speed maximum entering the circulation of the cyclone around the "roll-over" upstream ridge. This contributed to the "moist wedging" event that created a double baroclinic structure on the southeast quadrant of the closed low, a delay in the "cutting off" process, and a complicated vertical structure to the north of the closed low.

Relative to the sizes of the systems involved, the blocking regime was of short duration. However, the "roll-over" cycle was completed as the anticyclone merged with the downstream ridge, and the cyclone opened to the next upstream trough.

The next case illustrates another combination type of blocking regime, involving both a closed cyclone and a closed anticyclone; however, the systems undergo a "build-back" type of system evolution. The pattern formed by the primary moisture boundaries is significantly different.

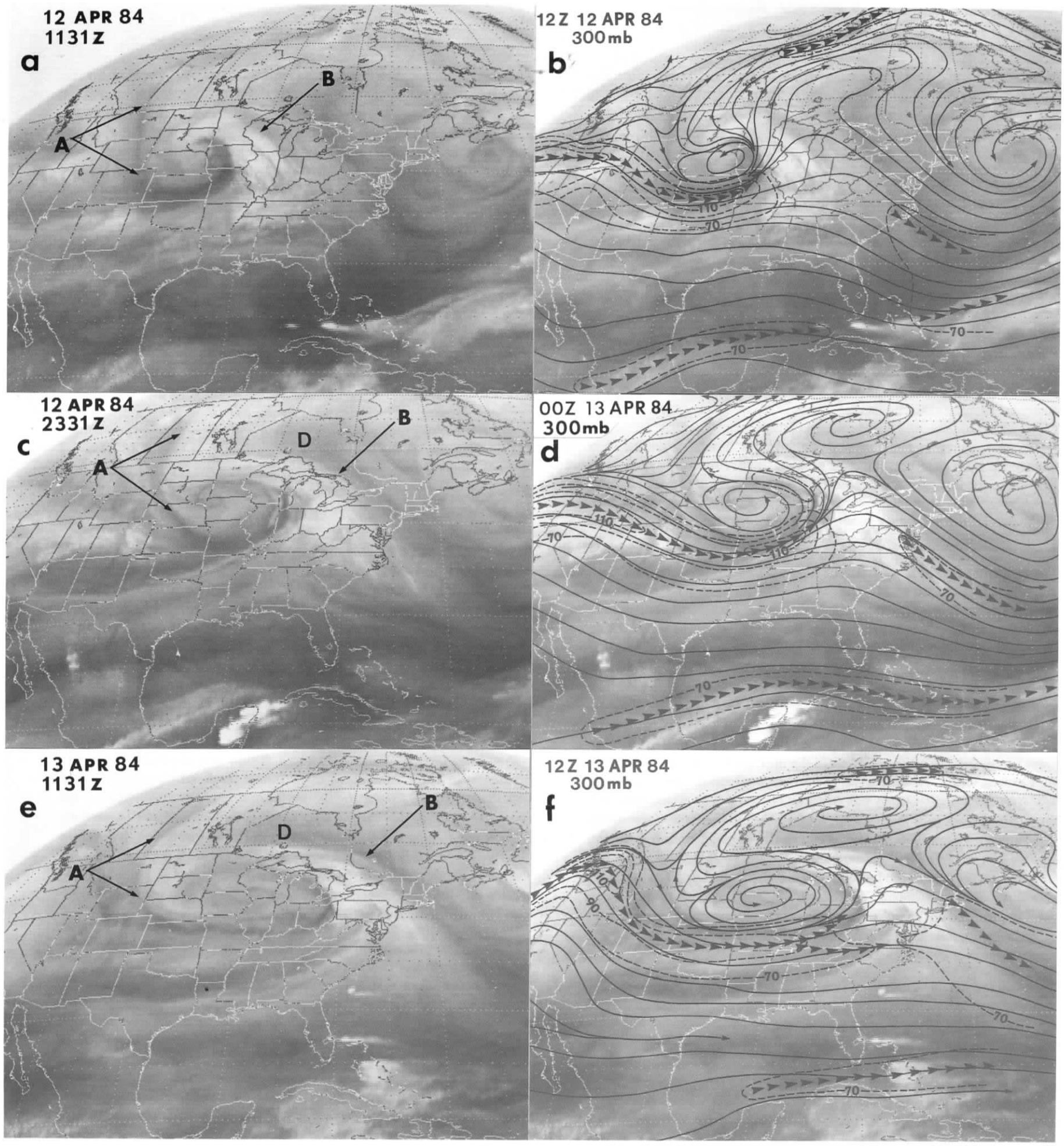

Figure 37 **BLOCKING REGIME WITH A BUILD BACK EVOLUTION**

Sequence of three 6.7μm images at 12-hour intervals. The GOES East images are repeated with 300mb analyses.

Fig. 37a. 1131Z 12 April 1984 image. **Fig. 37b.** Same image with 300mb analysis, 1200Z 12 April 1984.

Fig. 37c. 2331Z 12 April 1984 image. **Fig. 37d.** Same image with 300mb analysis, 0000Z 13 April 1984.

Fig. 37e. 1131Z 13 April 1984 image. **Fig. 37f.** Same image with 300mb analysis, 1200Z 13 April 1984.

Analyses: 300mb streamlines (solid lines) 300mb isotachs (dashed lines - knots). Axes of maximum 300mb wind speeds (where speeds are 70 knots or greater - arrowheads).

4. A COMBINATION BLOCKING REGIME WITH A "BUILD-BACK" EVOLUTION

On **Figure 37**, three water vapor images are shown at 12-hour intervals, and repeated with 300mb analyses superimposed. In this case, only a 24-hour period is illustrated. The circulation systems involved did not complete a full "build-back" cycle. However, they did evolve to the mature stage. Consider the changes leading to the mature stage.

12Z 12 April 1984

The upper air cyclone centered over eastern Nebraska at the time of the first image, had closed 12 hours prior to the time shown. The jet stream zone entering the northwestern coast of the United States was oriented generally west to east with only short wave perturbations. A new speed maximum formed on the eastern end of that jet stream branch, and accelerated eastward into the large ridge over the central United States and Canada. At the beginning of the cyclogenesis process, a portion of the ridge was already on the northeastern quadrant of the developing low, having "fallen back" relative to the rapidly moving short wave trough. Therefore, the new "build-back" ridge associated with the cyclogenesis process formed on the northeastern side of the short wave trough, and rapidly "built back" to the northern side of the newly closed low. The resulting "head boundary" labeled "A", has formed in a south-north orientation, and extends through the stretching axis of the newly formed col in the 300mb wind field.

In this case, the upstream jet stream has maintained its zonal orientation; and is not "rolling over" the position of the new low. Relatively weak short wave systems move across western Canada toward the blocking "head" boundary. Although a dark band is present along the western side of the "head" boundary, it is relatively narrow and indistinct, with variable moisture conditions along its upstream side. The "head" boundary is the primary blocking boundary associated with the new area of upper air easterly winds.

Already by the time of the first image, anticyclogenesis is beginning within the Canadian portion of the downstream ridge. The westerly winds across the ridge axis have begun to divide into two branches, as wind speeds have decreased significantly over the Great Lakes area. In conjunction with this double ridge structure, the 300mb streamlines on the northeastern quadrant of the closed low are significantly difluent. The high clouds in that area are formed in bands across the difluent flow pattern, and are undergoing significant deformation - stretching laterally as they move toward the northeast and decelerate. The northeastern edge of the cirrus clouds has become well defined at "B", implying the new deformation zone in the relative motions of the associated upper air winds.

00Z 13 April 1984

By the second image time, anticyclogenesis has occurred. A new dark area has formed at "D". The new moisture boundary along the southern side of that dark area has merged with the high cloud boundary to form a new primary boundary "B". As the anticyclone closed, a new col region formed in the 300mb streamlines, and the ridge has divided into two parts. A closed high is present to the north of the col; and, an open ridge remains to the south of the col. Boundary "B" may be considered as two parts. That part to the northwest of the col extends between the newly closed high and the closed low. That part to the southeast of the col lies along the eastern side of the open ridge. Commonly, during the anticyclogenesis phase, a new jet stream branch forms along this portion of the new boundary; or, a jet stream branch present along the forward side of the open ridge intensifies. This occurs in conjunction with cold advection to the southeast side of the closing high, where the winds tend to rotate anticyclonically with time. It is also common for a new closed low to form in the trough to the southeast of the newly closed high. The resulting set of circulation systems form an "omega" shape; and such blocking situations are referred to as "omega blocks". In this case, a closed cyclone was already present prior to the anticyclogenesis. However, the baroclinic zone intensified between the cyclone and the open ridge.

12Z 13 April 1984

By the third image time, the closed cyclone over the central United States has remained nearly stationary, but increased in size. The dark region "D" has moved westward. The western end of boundary "B" has extended westward; and, the region of easterly winds on the southern side of the anticyclone has extended westward. Thus, the two branches of upper air easterly winds, created by the cyclogenesis and by the anticyclogenesis have merged in the streamline pattern. The two branches of easterlies form a wide area of east winds between the closed "cut-off" high and the closed low. Note that the head boundary had moved eastward over Montana between the first and second image times; however, it has moved back toward the west in response to the strengthened easterlies.

At the mature stage of the blocking regime, a closed high is present on the poleward side of a closed low. In this case, with the "build-back" evolution, the high has become "cut-off" from the primary jet stream zone; whereas, the low is closed - but not "cut-off". The anticyclogenesis occurred within a part of the downstream ridge that built back to the poleward side of the low. The primary boundaries consisted of a "head" boundary formed with the cyclogenesis, then an "inside" boundary formed with the anticyclogenesis. Both boundaries and their related cols rotated cyclonically with time.

In the case shown, the systems did not complete a full "build-back" cycle. Had they done so, the high would have opened to the next upstream ridge, and the low would have opened to the northeast to the downstream trough. Instead, the initially warm temperatures of the anticyclone cooled significantly with time; and, the upstream jet stream did not branch around the poleward side of the high. The high elongated and weakened on the north side of the cyclone.

However, the systems did complete the first half of the cycle and formed the mature phase set of systems and water vapor features. Note that the "omega" pattern formed by the set of upper air circulation systems is usually not obvious on water vapor imagery. With the "omega block" type of blocking regimes, the dominating feature on the water vapor imagery is often the "inside" boundary separating the closed high and the open ridge to its equatorward side. Often, the clouds associated with the open ridge form a triangular pattern with an apex to the north or northwest. This apex forms when the two areas of easterlies merge between the closed high and the closed low. Additional examples of "build-back" blocking regimes will be illustrated and discussed in Section D.

This page intentionally left blank

SECTION C

CYCLOGENESIS AND STORM EVOLUTION

We have already shown several cases of cyclogenesis in context with other subjects; and, we shall refer to some characteristics of those. In general, the term "cyclogenesis" could be applied to the development of a large variety of circulation systems with closed lows in the pressure field and closed cyclones in the wind field. For example, upper air cyclones often develop without extending their closed wind and thermal fields into the lower atmosphere. Old weakening surface frontal zones break down into numerous small eddies with closed lows and cyclonic vortices within the boundary layer. Many types of orographically related low pressure systems form within the boundary layer at various horizontal scales. We shall exclude those types of development from this discussion.

In this section, we shall illustrate the development and evolution of vertically deep systems which include the development and propagation of a surface low pressure center. Basically, the subject of concern is "winter storm" development and evolution, although such systems occur during all seasons of the year. The subject of tropical cyclogenesis will be addressed briefly in Section E, in regard to system interactions and water vapor image applications.

Since this subject cannot be adequately presented superficially, we have carefully selected three cases with characteristics common to many others, in regard to water vapor image relationships.

1. A BASIC STORM SYSTEM DEVELOPMENT AND EVOLUTION

After studying hundreds of storm developments using satellite imagery and related "conventional" data, we have concluded that each was significantly unique. It is very difficult to choose an "average" or "typical" case. However, the case shown here had many characteristics common to other cases. Also, it was "permitted" to evolve to a mature stage without some form of synoptic scale "interruption" and to do so primarily over the United States data network.

The development occurred on the forward side of a relatively high amplitude upper air trough; and, the surface cyclogenesis occurred within a previously existing surface frontal zone. From a surface analysis perspective, the development was of the "frontal wave" type. As is often the case with such developments within an existing surface frontal zone, the associated speed maximum of the upstream jet stream moved to the right of the previously existing downstream jet stream location - a "digging" situation. Therefore, a vertically deep warm frontal zone was initially present and a single downstream jet stream intensified with the building upper air ridge. The surface cyclogenesis was of moderate strength with respect to both the amount and rate of deepening. The surface low pressure center deepened 14mb during a 30 hour period to a minimum central pressure of 995mb.

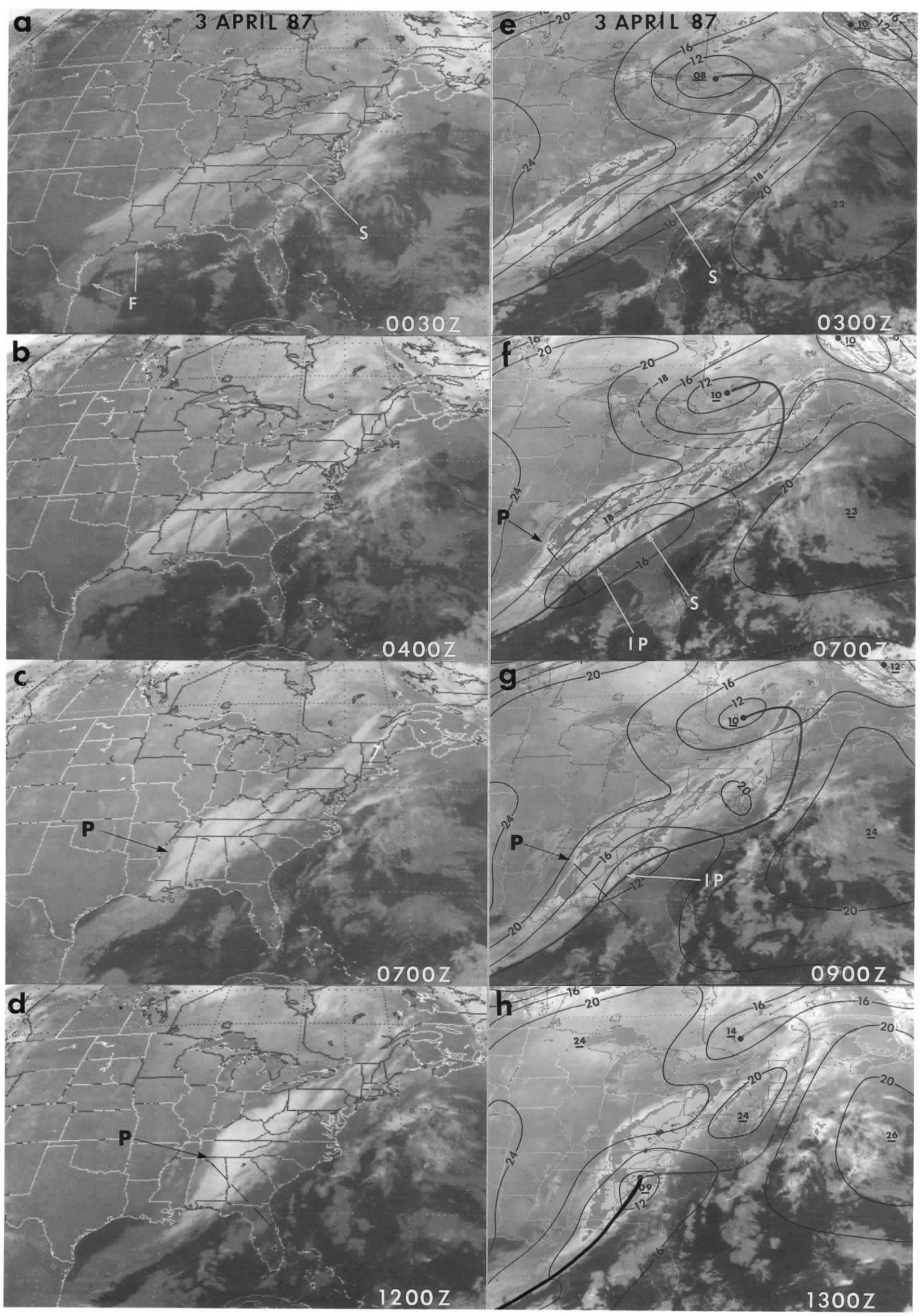

Figure 38

BAROCLINIC LEAF FORMATION - INFRARED IMAGES
Two sequences of images are shown. Both sets are 11.2μm infrared data. All times labeled on images are for 03 April 1987. **Left Column**. Sequence of infrared images with "Z" curve gray shade conversion. **Right Column**. Sequence of enhanced infrared images ("MB" curve gray shade conversion) with surface analyses superimposed. On the 0700Z image, the surface analysis is valid at 0600Z; and on the 1300Z image, the surface analysis is valid at 1200Z. Frontal positions (heavy solid lines) were interpolated to positions at the image times. Thin solid lines are isobars, at 4mb intervals.

a. The Formation of a "Baroclinic Leaf" Cloud System

The term "baroclinic leaf" was introduced by Weldon (1979) to describe pre-cyclogenetic cloud patterns on infrared and visible imagery. Two examples of "baroclinic leaf" cloud systems were shown on **Figure 8**. They were related to the specific "S" shaped type of boundaries observed on the forward sides of upper air troughs. We shall use the terminology and related concepts here in discussions of the pre-cyclogenetic and early cyclogenesis phases of development. It is not necessary for the reader to be familiar with those concepts, as those required will be provided in this discussion. The development of the "baroclinic leaf" cloud system is shown by infrared imagery prior to the discussion of water vapor images.

On **Figure 38**, sequences of infrared imagery and enhanced infrared imagery are shown for comparison and to illustrate the cloud pattern evolution. Surface analyses are superimposed on the enhanced infrared images. The analyses valid at 0600 and 1200Z are shown on images valid at 0700 and 1300Z, respectively. Frontal and trough positions were interpolated to the image times.

Consider the standard infrared images in the left column of **Figure 38**. At 0000Z, near the time of **Figure 38a**, a well defined surface frontal zone extended from New York City to New Orleans off the Louisiana coast and parallel to the Texas coastline at "F". The minimum observed surface pressure along the frontal trough was 1011mb over northern North Carolina, at "S". A relatively wide zone of cloudiness was present on the cold side of the surface frontal position. Although the cloud top temperatures and heights varied considerably in this zone, a relatively well defined band of cirrus was present along the western edge. This western boundary of the cloud zone coincided with the axis of the jet stream. Precipitation was reported within a long narrow band extending from eastern Pennsylvania to Louisiana, primarily along the central portion of the cloud zone.

Note on the 0030Z image, that the rear boundary of the cloud zone is slightly curved. There are two concave portions separated by a short convex portion centered over southeastern Missouri. This change in curvature is a sign of potential development; however, it might be a result of a transient short wave feature in the upper troposphere. The curvature is of low amplitude and the convex portion is short. Such features are often observed along jet stream related cloud borders on time lapse imagery. They tend to move rapidly with little change in amplitude and no apparent significant influences on middle or lower tropospheric conditions. Or, it could be the first sign of development. Other conditions on the 0030Z image imply that no "leaf" system has formed. The cold cirrus portion of the cloud tops is too narrow. The general top structure is too irregular and generally too warm. The cloud system is indicative of a vertically deep frontal zone with a parallel jet stream associated, although it does display potential development characteristics because of the convex curvature of the western boundary.

By 0400Z, **Figure 38b**, the general cloud tops have become colder, primarily in the form of cirrus bands parallel to the frontal zone. Such widening of the cold cloud tops and the fact that it is limited to a part of the overall length of the frontal zone is an indication of "leaf" formation. Another indication is that a break in the cirrus boundary has occurred - in this case over western Pennsylvania. However, the cloud top structure in the form of long cirrus bands is not typical of "leaf" cloud systems and the rear border of the cloud system has not maintained or increased its amplitude. In fact, the amplitude decreased as the small convex portion moved rapidly northeastward and dampened. Overall, the indications are in the direction of development. If the changes between the 0030 and 0400Z images continue, a baroclinic leaf cloud system is likely in the next three to six hours. On the 0300Z surface analysis, the minimum observed pressure was over western South Carolina at 1014mb. Since no clearly defined "leaf" cloud system was present, this should not be considered as the incipient low center of the expected development.

By 0730Z, the infrared image features indicate a "baroclinic leaf" formation or a baroclinic leaf phase of development. The cold cirrus cloud tops have formed a more uniform structure, and the rear border has become curved with greater amplitude and a "synoptic scale" wavelength. The convex portion extends from northern Mississippi to southern Indiana in comparison to the very short portion on the 0030Z image. Furthermore, the improved top structure is along that portion of the frontal zone at the inflection point "P" and the immediate downstream convex portion. The fact that the "leaf" system is in an early stage is indicated by the lack of a well defined break in the cirrus clouds in the downstream direction--northeastward in this case. The cirrus along the rear boundary begins to dissipate over northeastern Ohio, but there is no well defined "break" or end. Two other major bands of cirrus extend over Pennsylvania to Quebec Province. Generally, with well defined "leaf" systems, the frontal zone cloud band poleward of the "leaf" becomes narrower, or its cloud tops become warmer, or both changes occur. This results in a well defined downstream end to the cold cloud pattern of the "leaf". By 1200Z, **Figure 38d**, a break at the downstream end of the leaf pattern is more evident. The "leaf" cloud pattern has become distinct. At that time, in comparison to other cases in general, the "leaf" pattern is a relatively well defined one, but smaller than average.

Surface analyses are shown on the enhanced infrared images of the right column of **Figure 38**. Based upon the cloud conditions shown on the standard infrared images, we concluded that the "leaf" cloud system formed between 0400 and 0730Z. The 0600Z analysis is shown on the 0700Z image of **Figure 38f** with the frontal position adjusted for the time difference and small map grid error, and smoothed of sub-synoptic scale perturbations. At 0600Z, the minimum surface pressure reported along the frontal trough was 1013.1mb over northeastern Georgia. However, there was no well defined surface low center indicated in either the pressure or wind fields at that time. According to the "baroclinic leaf" model, no well defined surface center should be present during the early "leaf" stage, such as the pattern on the 0700Z image. A rule has been developed to locate the "incipient position" - the location with respect to the cloud pattern where the surface low will form as the system propagates. In some cases, there will be several weak low centers along the frontal trough. The rule helps establish which one of those is likely to persist and develop. To apply the rule, mark the inflection point along the rear border of the cloud system (in this case at point "P"). Draw a line through the inflection point perpendicular to the forward boundary of the cloud pattern. (If the forward border is irregular or distinct only along the equatorward end, use the general long axis of the leaf pattern instead.) The "incipient position" will be along the forward edge of the leaf pattern, approximately two degrees of latitude poleward of where the line intersects the edge. In this case, using the 0700Z image, the "incipient position" would be on the Alabama-Florida border where the front and cloud edge crosses it. Once the position has been established, low cloud features should be examined for evidence of a center. A small clear zone may be present if general low cloud cover prevails. In this case, there are no indications in the low clouds near that point. There is also no low center.

At 0900Z, the minimum pressure along the trough was 1010.9mb reported at Athens, Georgia. However, pressures ranged from 1011 to 1011.5mb along the trough axis from northeastern Georgia to southeastern Alabama. There were no indications in the wind field of a single well defined center. Applying the inflection point rule with the cloud pattern would imply an incipient position in west central Georgia, near Columbus. The surface frontal zone has become curved. Although it has moved as a cold front over the Virginia to New England area, and over the Gulf of Mexico, it has remained nearly stationary over the South Carolina to southeastern Alabama portion.

Since the cloud pattern evolution implied development, and surface cyclogenesis may be anticipated, it is useful to extrapolate the incipient positions implied by the "leaf" cloud patterns. Such extrapolation, using the 0700 and 0900Z positions, indicates a 1200Z position on the South Carolina border northeast of Athens, Georgia. This provides a guess of where the surface low center will be located if it has formed by 1200Z.

The surface analysis valid at 1200Z has been superimposed on the 1300Z enhanced infrared image of **Figure 38h**. For convenience and comparison, this same image and analysis is also shown on **Figures 39** and **40**. Consider **Figure 39**, where the 1200Z surface and 850mb analyses on enhanced infrared images are shown adjacent to close-up water vapor and visible images.

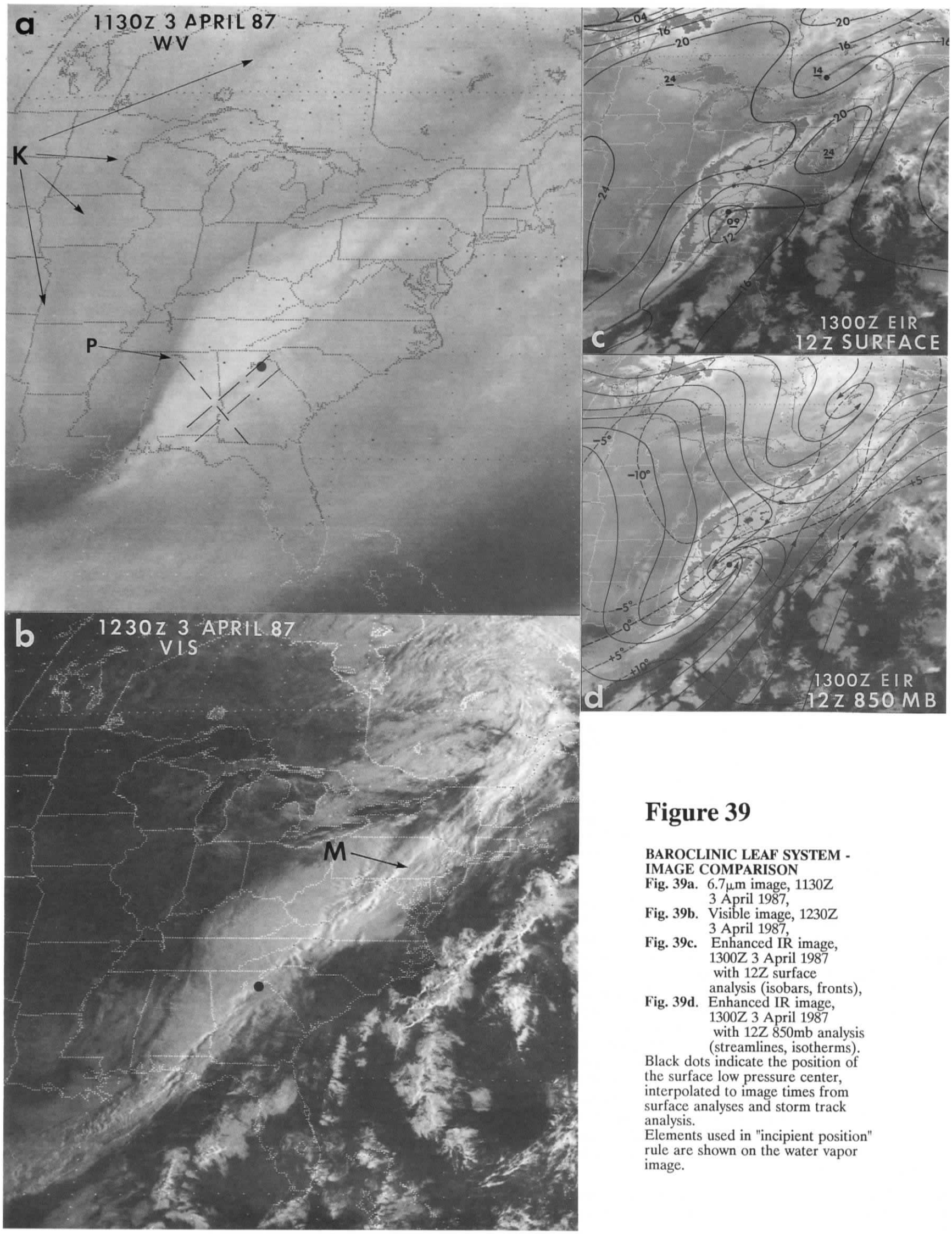

Figure 39

BAROCLINIC LEAF SYSTEM - IMAGE COMPARISON

Fig. 39a. 6.7μm image, 1130Z 3 April 1987,

Fig. 39b. Visible image, 1230Z 3 April 1987,

Fig. 39c. Enhanced IR image, 1300Z 3 April 1987 with 12Z surface analysis (isobars, fronts),

Fig. 39d. Enhanced IR image, 1300Z 3 April 1987 with 12Z 850mb analysis (streamlines, isotherms).

Black dots indicate the position of the surface low pressure center, interpolated to image times from surface analyses and storm track analysis.

Elements used in "incipient position" rule are shown on the water vapor image.

Prior to 1200Z, no well defined low pressure system had been present along the surface frontal trough. By 1200Z, a low pressure system had formed with relatively well defined patterns in both the surface wind and pressure fields. The minimum surface pressure along the frontal trough was 1009.6mb at Athens, Georgia, where the wind was 5 knots from the southwest. The new low center has been analyzed near Athens, and is indicated by a black dot on each of the images of **Figure 39**. Because of the relatively weak conditions at this early stage, and the density of the surface observing sites, the exact location of the surface low center cannot be determined, even with careful post-analysis techniques. The incipient position may be determined from the satellite imagery; however, at the image times near 1200Z, there are alternative solutions to the rule. An additional line of cold high cloud tops is present in advance of the general cloud top area of the "leaf" pattern. This was caused by convective clouds formed in lines along the eastern side of the surface frontal trough. Therefore, the analyst has a choice to determine which cold cloud edge is used for the incipient position technique. The two edges are indicated by lines "A" and "B" on the water vapor image of **Figure 39a**. In such cases, with alternative features on the satellite imagery, the feature best related to the axis of the surface frontal trough should be used. This may be known, based upon continuity and prior surface data. If not, our experience indicates that the rear - or western - feature should be chosen. In this case, the western feature would be along line "A" on the water vapor image, the line drawn along the edge of the primary "leaf" pattern, as opposed to the convective cloud tops in advance of the "leaf". Use of line "A" with the 1130Z water vapor image produce an incipient position just southwest of the analyzed position. Using the 1200Z infrared image would yield an incipient position very near Athens, Georgia. In this case, the location of the inflection point using the infrared image would produce the same result as using a water vapor image for the same time. However, in many cases, inflection points are more reliably determined from the water vapor imagery. Small perturbations along the rear boundary affect the cloud edge more than the moisture boundary. Therefore, use of the water vapor image provides better synoptic scale consistency. Particular care must be taken, when enhanced infrared imagery are used for locating the inflection points. False boundaries can be created because of reversals in the gray shade variations with temperature. In this case, had line "B" been used to determine the incipient position, the difference would have been only about 40 nautical miles.

b. The "Baroclinic Leaf" System and Related Analyses

Low Level Conditions

We stated that it is not usual for the surface frontal zone to be significantly curved or "waved" during the "baroclinic leaf" phase. In this case, the surface front has become significantly curved by 1200Z, although the surface low has just formed, and the cloud pattern is a well defined "leaf" system. This unusual amount of curvature was apparently related to the location of the "leaf" development in association to the Appalachian Mountains. The "leaf" system formed between 0300 and 0700Z. At the beginning of that period, the surface front had already crossed the mountains. A relatively large region of low level cold air was present over the low lands, east of the mountains, from North Carolina to New York. As the "leaf" formed, the cloud pattern rotated cyclonically. The rear border of the cirrus remained near the southwestern corner of Ohio between 0000 and 1200Z. North of there, the border moved northwestward from near Pittsburgh to near Buffalo. The upper air baroclinic zone also rotated. The maximum wind at Buffalo increased and that at Pittsburgh decreased during the 12-hour period. At both stations, air temperatures warmed between 400mb and 700mb. However, this rotation or retrogression of the baroclinic zone was limited to the middle troposphere. At low levels, the cold air was apparently blocked by the terrain and continued to push southward in the boundary layer - into North Carolina.

At 1200Z, the surface front passed Cape Hatteras. On the visible image at 1230Z, low clouds are present over most of Virginia; however, the cloud edge (at "M") that represents the eastern border of the "leaf" pattern, extends from the low center northeastward across Pennsylvania. This cloud border is related better to the stretching axis of the col in the 850mb wind field - **Figure 39d**. The cold air was very shallow over most of the area east of the mountains. The temperature inversion was below 850mb at the Hatteras, Greensboro, and Wallops Island radiosonde sites. At Washington Dulles, a 5°C inversion extended from 768mb to 870mb. The 850mb winds were calm, whereas the winds were 005°/12 kts at 4000 feet and 195°/19 kts at 6000 feet. The curvature of the frontal zone was related to very shallow cold air which had crossed the mountains prior to the "leaf" development. In the Virginia-West Virginia-Ohio area, the distance between the jet stream axis and the 850mb frontal zone is similar at 1200Z to that at 0000Z.

There was, however, a retrogression of the surface trough over northeastern Georgia, as the "leaf" developed and the surface low formed. Based upon observations of other cases, this lowering of pressure near the eastern edge of the developing leaf would likely have extended farther to the northeast. However, in this case, it was likely prevented by the cold air blocked on the east side of the mountains.

"Leaf" Characteristics - Water Vapor Imagery

On the water vapor image, the "leaf" appears as a very cold pattern, primarily because of radiation originated from high cold cloud tops. Recall from the sequence of infrared images on **Figure 38**, that a cold and relatively uniform cirrostratus cloud deck formed as the "leaf" pattern developed. Although the formation of this pattern occurred during the night, such cloud patterns are usually thick, such as to appear opaque on visible imagery. We refer to that part of the cloud pattern which is both opaque on the visible imagery **and** cold on the infrared imagery as the "**cold cloud shield**". Observations of other cases have indicated that, as the "cold cloud shield" forms, a new colder tropopause forms - usually below the original tropopause that was present prior to the cloud formation. We refer to this newer colder tropopause as the "cold cap". In this case, the "cold cap" tropopause associated with the "cold cloud shield" was located between 300mb and 250mb. Of the radiosonde sites under the "cold cloud shield", the "cold cap" tropopause was most distinct at Huntington, West Virginia, where the air temperature decreased upward to -61.7°C at 262mb, then warmed to -50.7°C at 225mb. Above that, the temperature warmed gradually upward to -48.3°C at 150mb, then cooled to a second tropopause of -60°C at 84mb. Of the standard level analyses shown on **Figure 40**, the "cold cap" thermal field is best defined at 300mb, where a distinct thermal trough has formed directly over the cold cloud pattern of the "leaf" system.

On the water vapor image, the pattern of the "leaf" system is revealed primarily by the "cold cloud shield". Consider the eastern and western borders of that pattern. The eastern border is relatively indistinct and poorly defined in comparison to the western one. As is usually the case with "leaf" systems, the radiosonde moisture data indicated little difference in upper air moisture conditions within the "leaf" pattern of clouds and over the adjacent area on the eastern side of the "leaf" pattern. Radiosonde stations over both of those areas reported upper tropospheric moisture conditions of single digit dewpoint depressions. Thus, the downstream borders of "baroclinic leaf" systems are usually revealed only as an edge of the "cold cloud shield", rather than as a significant difference of upper air moisture conditions. However, on the upstream, or western, sides of "leaf" systems, a relatively distinct and well defined boundary is usually present. As in this case, that boundary is usually associated with both a cloud edge, and a difference in upper tropospheric moisture conditions, with drier air on the upstream or western side. The "S" shape of the upstream boundaries of "leaf" systems is of special significance. During the "leaf" phase of system development, the boundary consists of convex and concave portions separated by an inflection point. We shall consider the two portions of the boundary separately, in regard to their relationships to the upper air analyses.

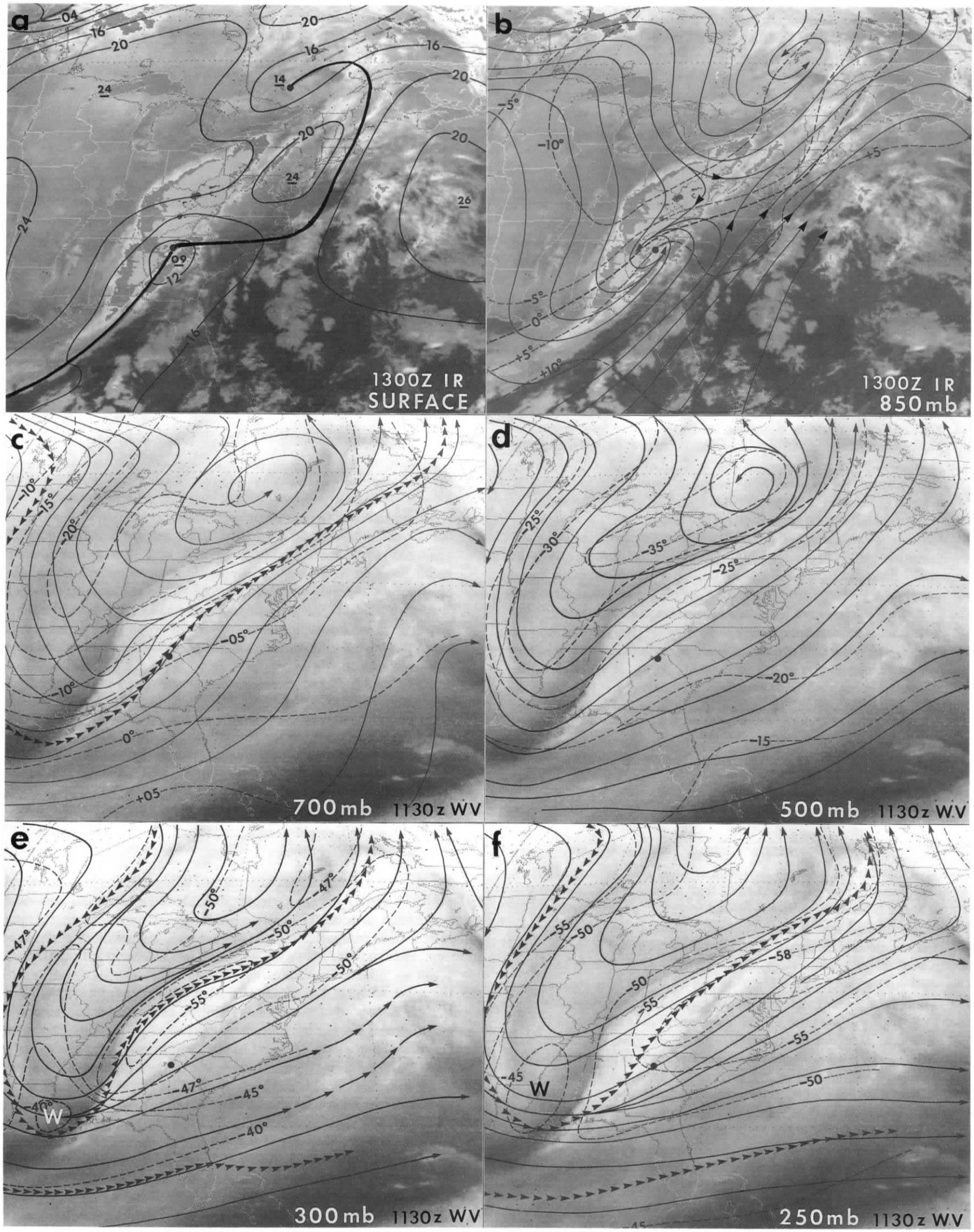

Figure 40

SURFACE AND UPPER AIR ANALYSES - BAROCLINIC LEAF PHASE
Analyses: 1200Z 3 April 1987. Surface and 850mb analyses on 1300Z 3 April 1987 enhanced infrared images. The 700mb, 500mb, 300mb, and 250mb analyses on 1130Z 3 April 1987 6.7μm Water Vapor images. Surface analysis: isobars (thin lines) frontal location (bold lines). Upper air analyses: streamlines (thin solid lines) isotherms (dashed lines). Series of arrowheads indicate axes of maximum wind speeds for the altitude of the specific pressure surface of the analysis. "W" = warm. "K" = cold.

The Convex Boundary of the "Leaf"

Generally, the convex portions of "baroclinic leaf" boundaries have characteristics similar to those of "head" boundaries on water vapor imagery. The boundary is likely to be very well defined, but may be indistinct; or, becoming less distinct with time. An elongated dark zone adjacent to the boundary is likely to be narrowing with time. It may change to a narrow dark band and persist, or it may disappear entirely. Usually, cirrus clouds are present along the moist side of the convex boundary. The moisture boundary may be coincident with the cloud edge, as in this case, or the moisture may extend beyond the cloud edge and remain better defined than the associated cloud edge.

On **Figure 40**, the surface and 850mb analyses are shown on the 1300Z enhanced infrared image, for comparison with other upper air analyses superimposed on the 1130Z water vapor image. It is common that the wind directions at levels near the jet stream core are parallel to the convex portions of "leaf" boundaries. In this case, note that the 500mb and 300mb streamlines are parallel to the convex part of the boundary. Our analysis of radiosonde data indicates that the convex portion of the moisture boundary was coincident with the jet stream axis, with maximum winds along that segment of the jet stream located between 350mb and 310mb. Since the 300mb pressure surface was the nearest standard surface to the jet stream core, the axis of maximum winds on the 300mb analysis is near to the convex part of the moisture boundary, but along the moist side.

The Concave Boundary of the "Leaf"

The concave portion of the "leaf" boundary is likely to have characteristics similar to those of "dry surge" boundaries. Usually a dark area of synoptic scale width is present on the upstream side of the concave portion. Usually, during the evolution of the "leaf" system, this dark area is likely to remain as a significant feature on the water vapor imagery, although it may change shape. In the case shown here, the darkest gray shades are over the Gulf of Mexico; however, the dark region extends over eastern Mississippi and western Alabama. At Jackson, Mississippi, 30°C dewpoint depressions were reported from 770mb upward to 400mb where the air temperature had reached -40°C.

Whereas the upper air streamlines were generally parallel to the convex portion of the boundary, they cross the concave portion at significantly large angles. Near the concave part of the boundary, cold air advection is present at standard pressure surface analyses from 850mb through 400mb. At 300mb, 250mb, and 200mb, the temperature gradient is reversed, and warm advection is present. At Centreville, Alabama, the wind directions backed with height from 005° at 850mb to 210° at 400mb. They veered from 210° at 330mb to 270° at 100mb. On that portion of the "leaf" south of the inflection point where the upper air streamlines crossed the cloud pattern, the high cloud tops sloped upward to the east. Over the northern portion of the "leaf", where the upper air winds are parallel to the "leaf" orientation, the cirrus tops are more uniform across the pattern.

Generally the upper air winds cross the concave portion of the rear border, even near the level of the temperature gradient reversal, where the wind directions have their largest southerly component - in this case between 400 and 350mb. On the standard level analyses shown on **Figure 40**, the minimum crossing angles are at 300mb. During the cyclogenesis phase of development, the concave portions of leaf boundaries usually surge forward rapidly; whereas, the convex portions move slowly or reverse their eastward propagation and move - or build - back to the west. Based upon observations on time-lapse imagery, we have referred to the region just in advance of the surging concave boundaries, as the "destabilization zone" of cyclogenetic storm patterns. Intense convective weather is common in this zone, even at night and during the cold winter seasons, with cells embedded in general cloud cover. Very heavy snowfall rates with accompanying thunder are common in this zone. It is also common that lines of convective cells move rapidly - often more rapidly than the low level frontal zone. During the second phase of cyclogenesis, the low level frontal zone is likely to "fall back" from under the middle and high clouds; and, it is common for new convective cells to form at the low level frontal position behind the original ones. Sometimes this reformation to the rear is a continuous process, and with other cases, it occurs in discrete steps with periods of several hours before reformation.

General Analyses and Image Features

In this case, the upper air trough was of very large amplitude. Note on **Figures 40e** and **f**, that a large amplitude ridge is located to the west of the trough, with a jet stream of generally northerly winds between the ridge and trough. On the water vapor image, a dark band is present parallel to the jet stream. This feature is indicated by arrows and labeled "K" on **Figure 39a**. Even on our original images, the feature is very indistinct at the 1130Z time. The dark band is similar to the "K" band shown over the Pacific Ocean on **Figure 30**. As in that case, this dark band is parallel to the jet stream on the western side of a large amplitude trough, and represents an interface between the upper air moisture of the trough and that of the upstream ridge. We shall apply the relationship of dark band "K" to other image features, during the cyclogenesis phases of the storm system. At the time of **Figures 39** and **40**, the only radiosonde site within the dark band was Monett, Missouri. There, 30°C dewpoint depressions were reported from 447mb to 396mb at the -40°C air temperature limit. This dry air at high levels is in agreement with observations of other features of this specific type.

With respect to the adjacent upper air ridges, the trough is very cold at 500mb and relatively warm at 250mb. The 300mb surface is nearer to the reversal of the temperature gradient. Although the trough is significantly warmer than the "cold cap" region over the "leaf", the thermal field within the trough is complicated, with a pattern of weak gradients. As at 250mb, the warmest air at 300mb is near the base of the trough. The closed -40°C isotherm area over Louisiana had just formed during the previous 12 hours as the "leaf" formed and the darkening began on the water vapor imagery to the rear of the concave boundary of the clouds.

c. The Cyclogenesis Phase of the Storm Evolution

"Leaf" to "Comma" Evolution with "Cusp" Formation

By "cyclogenesis phase", we refer to the period during which the pressure decreases at the center of a surface low or cyclone. This is a period of rapid changes with time, both in the system structure, and in the patterns and features on satellite imagery.

In the case shown here, the pressure had decreased along a segment of the surface trough adjacent to the forming "baroclinic leaf" cloud system. However, no well defined cyclone or low pressure center had formed along that trough prior to the 1200Z analysis. At 1200Z, with the cloud pattern in a well defined "leaf" pattern, a new low pressure system had formed. Although this constitutes the beginning of the "cyclogenesis phase", significant precipitation has already occurred during the "leaf" formation phase. New snow has accumulated to depths greater than 12 inches in the mountains of eastern Tennessee and western North Carolina. Generally, during the early part of the cyclogenesis phase, the "leaf" cloud pattern changes to a "comma" shape. The rear, or upstream, boundary of the "cold cloud shield" amplifies; as the degree of curvature increases. In many cases, the curvature of the convex segment increases more than that of the concave segment. The "cold cloud shield" adjacent to the convex part of the boundary becomes wider with time, as that adjacent to the concave part narrows. As these changes occur, the shape of the "cold cloud shield" approaches that of the comma punctuation mark (Northern Hemisphere cases). Also, during that period of time, the upper air ridge amplifies and begins to "build back", and the new surface low intensifies. This intensification involves the consolidation of the pressure gradient into a circular pattern of larger intensities; and, usually, a reduction of the pressure at the center of the low. Also, during the period, the low pressure center "falls back" from its initial location near the forward edge of the "leaf" system, toward the rear boundary to the equatorward side of the inflection point. Therefore, during the period, the surface low pressure center is located under the "cold cloud shield" or the "leaf" system. Note, that the surface center is not moving back with respect to the earth. It is being overtaken by the more rapidly moving cloud pattern and related upper air system.

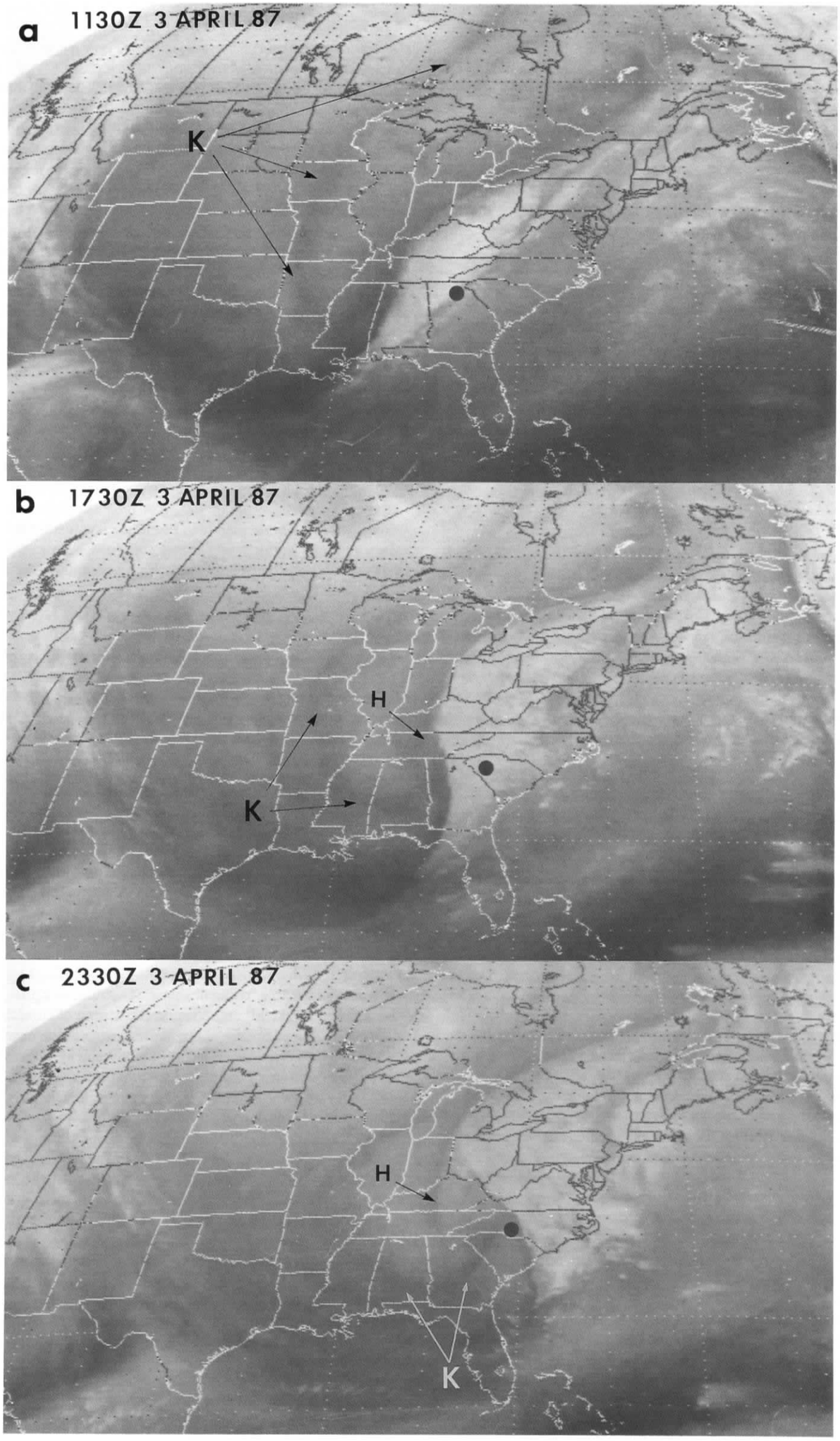

Figure 41

FIRST SEQUENCE OF WATER VAPOR IMAGES - 3 APRIL 1987
Sequence of three GOES East 6.7μm images from 3 April 1987 - 1130Z - 1730Z - 2330Z. Black dots indicate positions of the surface low pressure center, interpolated to image times from surface analyses and storm track analysis.

Usually near the same time that the surface low pressure center nears the rear boundary of the "cold cloud shield", a significant change in the pattern of the cloud system occurs. Commonly, the shape of the "cold cloud shield" does not reach a true punctuation mark comma shape. Before that amount of amplification occurs, a "cusp" pattern forms at the rear of the cold cloud pattern. The concave and convex segments of the rear boundary are initially separated by an inflection point. A "cusp" has formed when this separation occurs as a discontinuity or an apex. Actually, the apex forms slightly to the poleward side of the inflection point, where a region of maximum convex curvature amplifies rapidly to form a corner or apex. The cusp formation is a significant stage in the evolution of the cloud pattern, since it can be related to important changes in the surface pressure and upper air wind fields. There are several different ways in which cusp patterns form during cyclogenesis. Consider the following drawings, on which the shaded areas represent "cold cloud shield" (CCS) patterns.

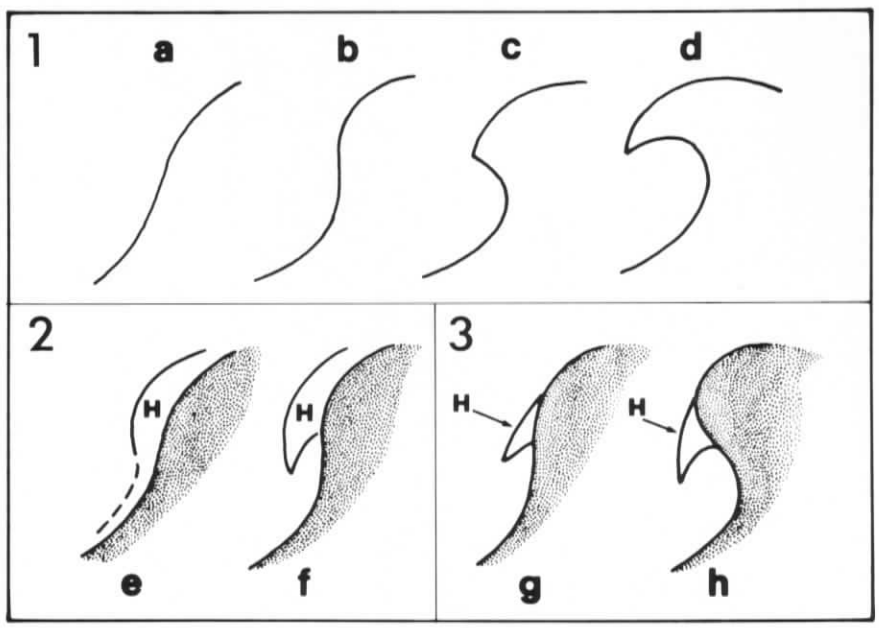

1 Amplification of CCS Boundary

The apex formation is observed directly on the rear boundary of the "cold cloud shield" just poleward of the inflection point location. As the apex forms, a break occurs in the jet stream.

2 Dual Leaf Pattern

A "head" region of cold clouds forms to the left of the jet axis (tops not as high or cold as those of CCS). A dry slot forms under the jet axis, producing an apex on the upstream end of the "head" cloud pattern.

3 Emerging Head

A middle cloud pattern (with convex edge or apex already formed) emerges or "falls-back" from under the "cold cloud shield".

The first sequence (a-d) represents the most basic type of cusp formation. The boundary of the "cold cloud shield" amplifies. However, the 2nd and 3rd types illustrated are more common. We consider the pattern to have reached the "cusp stage" when the apex is well defined on the imagery, and the angle formed by the two boundary segments is 90° or less. For the 2nd and 3rd types of evolution, the apex must be two degrees of latitude distance from the boundary of the "cold cloud shield" before the "cusp stage" is attained. In both second types of formation, a subsequent apex formation forms on the CCS boundary, and moves back over the initial head pattern - or merges with that pattern.

When the "cusp stage" has occurred in the cloud or moisture patterns, the following two image interpretations may be made: (1) a break has formed within the jet stream zone on the eastern side of the trough, and (2) the surface low center is located near the rear boundary of the "cold cloud shield". Features often present on water vapor imagery may be used to estimate the location of the center along the cloud boundary.

Consider the sequence of water vapor images on **Figure 41**. At the time of the first image, the cyclogenesis phase of the storm evolution had begun. A new surface low pressure system has formed on the frontal trough zone; and, the surface pressure is decreasing. A well defined "leaf" pattern has formed; and, the rear boundary of the "cold cloud shield" is amplifying. Once a well defined "leaf" pattern is recognized on the imagery, it is rare that any features related directly to the surface low pressure center can be observed - including use of visible and infrared images. Although the incipient position rule may be applied, it does not provide information in regard to the timing of the surface low formation, or when it will begin to "fall back" under the cold cloud shield. For cases in which no surface data are available for use in conjunction with the satellite imagery, we have developed the following rules. The surface low is likely to have formed, and be present near the incipient position, when the maximum width across the "cold cloud shield" is equal to twice the width at the inflection point location (using a line perpendicular to the forward edge of the "cold cloud shield"). The low center is likely to begin deepening, and "falling back" after that degree of amplification has been attained. Often, after the surface low has formed, and has fallen back under the "cold cloud shield", the forward edge of the cloud shield will become poorly defined or ragged. This can also be used as a sign that the low is under the "cold cloud shield", instead of near the forward edge.

During the first part of the cyclogenesis phase, while the surface low is "falling back" under the "cold cloud shield", we are aware of no way of determining its exact location from satellite imagery. Once the "cusp stage" is attained, a new interpretation rule is available for locating the surface center. Note on **Figure 41b**, that the rear boundary of the "leaf" pattern has amplified, and that the surface low pressure center (indicated by the black dot) has "fallen back" under the "cold cloud shield". During the last six hours of the sequence, between **Figures 41b** and **41c**, the surface low center has moved northeastward into North Carolina; but, the rear boundary of the "cold cloud shield" has moved more rapidly. The surface low center has fallen back relative to the cirrus cloud boundary; and, has emerged on the southwest side of the "cold cloud shield". In this case, the cusp stage has been attained at approximately 2000Z. After that time, the surface low center is likely to be near the rear boundary of the "cold cloud shield", and **very near** to the location where the axis of the jet stream intersects that boundary. In many cases, there will be no cloud features to locate that jet stream axis. If a dark band, referred to in a prior case as a "K band" is present on the water vapor imagery, it is likely to intersect the rear boundary of the "cold cloud shield". This intersection is likely to be of a relatively large angle at this early stage of the system evolution. A relatively reliable empirically derived rule is that the surface low center is likely to be near the cloud edge at a distance of one degree of latitude in the equatorward direction from the intersection. This rule is applicable after the cusp stage has been attained. If the high edge of the "cold cloud shield" has moved very rapidly, another cloud boundary of middle cloud tops is likely to be observed on visible or infrared imagery parallel to the frontal zone and behind the higher cloud edge. If so, this lower rear edge should be used with the intersection rule, instead of the edge of the "cold cloud shield".

In the case shown here, a dark band has been identified and labeled "K" on the water vapor image shown here as **Figure 41a**, and previously as **Figure 39a**. During the sequence of images, the band "K" extends eastward across the southeastern states, around the equatorward side of the newly forming upper air low. The northern end of "K" also moves eastward, whereas the central part remained nearly stationary over Missouri and Arkansas. As a result, the band "K" has formed a circular pattern during the period. It also intersects the "cold cloud shield" "A" near the northern border of North Carolina on **Figure 41c**. The image is valid after the "cusp stage" was reached at 2000Z; therefore, the intersection rule can be used. This would estimate the location of the surface low to be approximately 60 nautical miles to the northeast of its analyzed position. In this case, the rear edge of the "cold cloud shield" has moved very rapidly, and moved in advance of a middle cloud edge. The middle cloud edge cannot be seen on the water vapor image. Had that middle cloud edge been used for the intersection rule, the estimated position of the surface low center would have been just south of the analyzed position. The middle cloud edge will be addressed in our discussion of **Figure 42**, and the cusp formation. Prior to addressing the cusp formation, we must emphasize the value of the water vapor imagery for application of the intersection rule. The water vapor image may be used to provide the location of a dark band, "K", and combined with infrared or visible imagery, if available, to locate the rear cloud boundary.

On the 2330Z water vapor image, a new boundary "H" can be seen over eastern Indiana, extending southward across Kentucky and Tennessee. This feature consists of a narrow dark band along the western boundary of a region of clouds with middle tropospheric tops. The cloud top temperatures measured on the 0000Z infrared image range from an average of -25°C over Tennessee and Kentucky to -33°C on the colder portion over southwestern Ohio. The heights of the cloud tops are estimated to be just above 500mb. In hindsight, this feature and related middle cloud tops can be seen on the 1730Z water vapor image. A short segment is present over central Kentucky and Tennessee. At this earlier time, the feature is of such small size that it would be difficult - in real time analysis - to be sure that it was not some transient small scale feature. It was, in fact, the beginning of the cusp feature associated with the newly forming "head" boundary. In this case, it is of the type in which the middle cloud cusp emerges from under the rear of the cirrus boundary. Because of the prevalence of small transient feature along the rear boundaries of developing storm systems, it is necessary in operational applications of imagery to wait until the feature emerges approximately two degrees of latitude distance before identifying it as the cusp stage. The identification can be made earlier or with greater confidence, if the feature is emerging between the inflection point and the region of maximum convex curvature on the cold cloud boundary. This is the most common location. Viewing the imagery in time-lapse motion is also helpful.

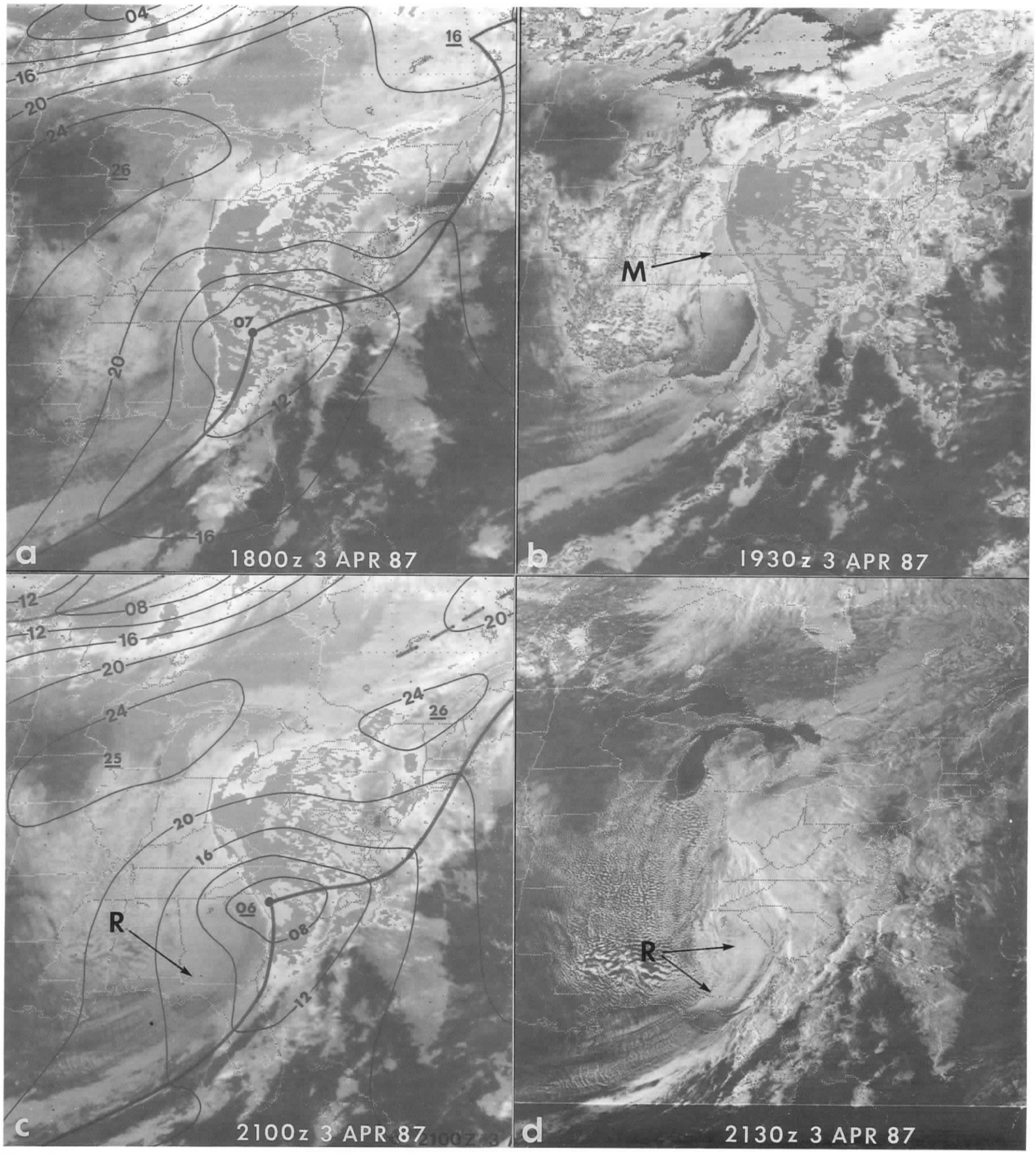

Figure 42

CUSP FORMATION AND DETECTION
Enhanced infrared and visible images from GOES East, 3 April 1987. **Figures 42a** and **42c**. Surface analyses are superimposed on 1800Z and 2100Z enhanced infrared images ("MB" curve gray shade conversion). **Fig. 42b**. A special gray shade conversion is displayed on the 1930Z enhanced infrared image. **Fig. 42d**. 2130Z visible image is shown.

On **Figure 42a** and **42c**, surface analyses are superimposed on enhanced infrared images valid at 1800 and 2100Z. Although the protruding middle cloud feature was detectable on the 1730Z water vapor image, it is very difficult to find on the two images with the surface analyses. On **Figure 42b**, a different infrared enhancement is used on an image valid at 1930Z. On this image, the emerging middle clouds are vividly displayed at "M". The infrared measured top temperatures at that time ranged from -18°C to -23°C. By 0000Z, the middle cloud tops had become generally colder, and likely higher.

In this case, the middle cloud cusp had emerged a distance of two degrees of latitude behind the cirrus boundary at approximately 2000Z. By that time, the surface low center had moved east-northeastward into north central South Carolina, but the cold cloud boundary moved more rapidly, nearly overtaking the low center. By 2100Z, **Figure 42c**, the surface center is still east of the cold cloud boundary, with a central pressure of 1006mb. The pressure has decreased only 3mb since 1200Z when the center was on the eastern boundary of the "leaf" pattern. This represents 21% of the total pressure decrease of this storm system. In comparison to other system developments, this is a relatively small amount of pressure decrease for this stage of the system evolution. One reason for this may be the behavior of the concave portion of the cold cloud boundary. It surged eastward very rapidly, not only overtaking the surface low center, but moving in advance of the middle cloud boundary. This can be observed on the visible image valid at 2130Z, **Figure 42d**. A lower middle cloud boundary, with tops in the 800mb to 700mb range, is identifiable at "R". This boundary, even after it emerged from under the cirrus edge, is very difficult to detect on infrared imagery. The middle topped altostratus clouds on the east side of the boundary are in the frontal inversion near 700mb, with top temperatures very similar to those of the clouds to the west which are between 850 and 900mb and under the inversion. In this case, at 0000Z, 2.5 hours after the visible image, the altostratus tops were near 0°C, and those to the west averaged between -2 and -3°C. By that time, the surface low center was to the rear of the cirrus boundary, but still in advance of the altostratus boundary.

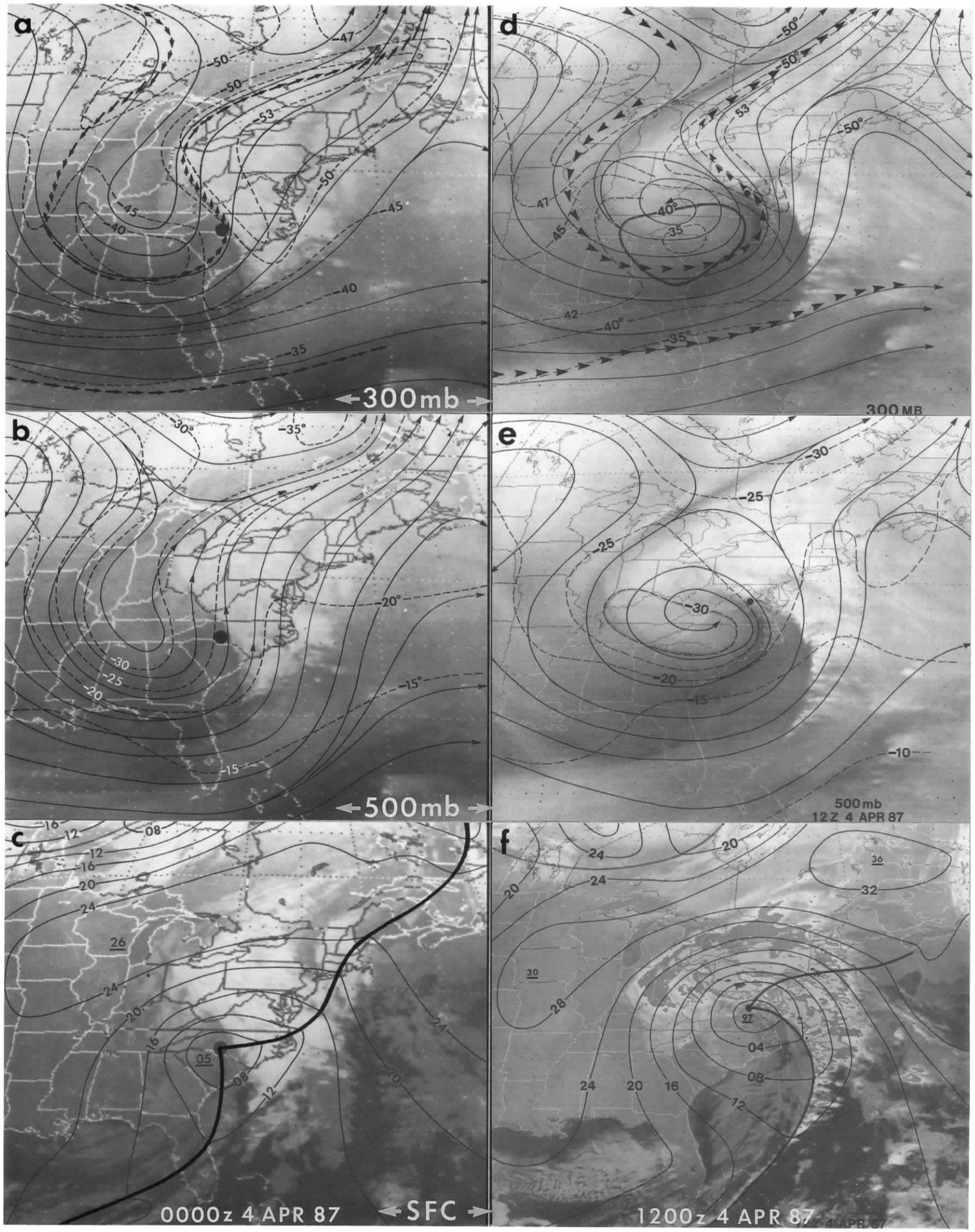

Figure 43

UPPER AIR AND SURFACE ANALYSES FOR TWO RADIOSONDE TIMES

Left Column Analyses: 0000Z 4 April 1987.
Fig. 43a and **43b**. 6.7μm 2300Z 3 April 1987.
Fig. 43c. Infrared 0000Z 4 April 1987.

Right Column Analyses: 1200Z 4 April 1987.
Fig. 43d. and **43e**. 6.7μm 1130Z 4 April 1987.
Fig. 43f. Enhanced infrared 1200Z 4 April 1987.

Upper air analyses: Streamlines (solid lines) isotherms (dashed lines). Axes of maximum wind speeds (arrowheads).
Surface analyses: isobars (thin lines) frontal positions (bold lines).

Related Surface and Upper Air Analyses

A well defined "leaf" system had formed; and, the cyclogenesis phase began at 1200Z. By 2000Z, the cloud pattern had attained the cusp stage. The system had undergone its first 12 hours of the cyclogenesis phase by 0000Z, April 4th. On the left column of **Figure 43**, three analyses valid at that time are superimposed on images. The 300mb and 500mb analyses are on the vater vapor image; and, the surface analysis is on an infrared image. On the right column, a similar set of analyses are valid 12 hours later at 1200Z 4 April. For that time, the surface analysis is on an enhanced infrared image.

0000Z 4 April 1987 - Left Column Analyses

During the first 12 hours of cyclogenesis, the shape of the "cold cloud shield" has changed, and the cloud top temperatures have become colder. The "cold cap" tropopause over the "cold cloud shield" has become higher and colder. Although it is revealed as an area of significantly colder air at 300mb, it is better defined on the 250mb analysis (not shown). The concave portion of the rear boundary of the "cold cloud shield", which had similar characteristics to a "dry surge" boundary, has moved rapidly eastward. The part of the "cold cloud shield" adjacent to the concave rear boundary had become narrower, as is common during this phase. However, as the system approached the coast, new deep convective weather formed offshore; and, that part of the "cold cloud shield" became wider again. Therefore, the shape of this particular cold cloud pattern has been modified, for this phase of development.

Whereas the southern part of the rear boundary of the "cold cloud shield" surged eastward, a portion just north of the inflection point has fallen back with respect to the southern part, and is no longer moving with an eastward component. The upper air ridge has begun to "build back". Although the upper air trough has remained open at 500mb and at higher levels, a low has closed at 700mb, with a center over eastern Kentucky and easterly winds over Ohio. The apex, or tip, of the cusp in the middle level clouds and moisture is located over north central Georgia. This is very near the point of maximum 500mb vorticity, as located on the NMC LFM absolute vorticity analysis (an empirically common relationship). The western boundary of the middle level clouds and moisture extends from the cusp apex northward to the northwestern corner of Ohio. The northern part of this "head" boundary (labeled "H" on **Figure 41c**) has become nearly stationary at 0000Z. It began to move westward just after 0000Z.

In cyclogenesis cases, such as this one, in which the cusp boundary occurs first at middle levels and emerges from under the higher cirrus boundary; a later second cusp formation usually occurs on the rear boundary of the "cold cloud shield". This higher cusp formation is correlated to several significant changes at upper tropospheric levels. The jet stream "breaks", a col forms as the upper tropospheric cyclone closes, and aircraft turbulence is commonly reported in the area of the cusp formation. Typically, these significant changes in the upper troposphere occur very rapidly; often between the 12 hourly radiosonde times. In this particular case, the 0000Z upper air measurements were made during the cusp formation period. The maximum convex curvature of the "cold cloud shield" boundary is located near the northwestern corner of Ohio at 0000Z. On the infrared image of **Figure 43c**, two hook-shaped areas of cirrus clouds are present over southwestern Ohio, suggesting that cirrus may be falling back in weakening high level flow over the top of the middle level moisture. By 0300Z, just three hours later, a well defined apex and cusp shape had formed on the cirrus boundary. Generally, prior to such high level cusp formations, in the area where the convex curvature of the "cold cloud shield" is increasing rapidly; the vertical depth of the strong jet stream winds decreases with time. In this case at 0000Z, just prior to the cusp formation, the amplifying boundary was located nearly over three radiosonde sites. The following wind reports from those sites indicate a shallow maximum wind zone with relatively large vertical shear - especially above the levels of maximum wind speed.

	Flint, Michigan	Dayton, Ohio	Huntington, WVA
250mb Wind	195°/015 kts	185°/016 kts	195°/047 kts
Maximum Wind	195°/103 kts at 297mb	170°/065 kts at 304mb	165°/097 kts at 317mb
400mb Wind	190°/041 kts	165°/040 kts	170°/057 kts
500mb Wind	190°/014 kts	200°/016 kts	175°/046 kts

During cyclogenesis, near the time of the cusp formation on the rear boundary of the "cold cloud shield", aircraft turbulence is commonly reported at moderate or severe intensities through relatively deep layers in the vicinity of the amplifying boundary. In this case, there were three reports of severe aircraft turbulence between 33,000 and 35,000 feet, each very near the high level moisture boundary. Two were near the Indiana-Ohio border at 1700 and 1800Z, and the third was near Lansing, Michigan at 2000Z.

Consider the upper air analysis features in relation to the cloud and moisture patterns during this period of rapid change with time. The "cold cloud shield" is associated with the newly amplified ridge in the 500mb and 300mb streamline patterns. Although the upper air trough has become very narrow over the Great Lakes area, between the "build-back" eastern ridge and the upstream ridge, the cyclone has not closed at 500mb or above. Easterly winds have not yet developed between the "build-back" ridge and the trough. At 0000Z, the only upper tropospheric flow of easterly component is on the western side of the trough, where the upstream ridge has moved eastward more rapidly than the base of the trough. At 300mb, the axis of maximum winds extends across the base of the trough parallel to the dark band "K" and intersects the rear boundary of the "cold cloud shield" near the surface low center. Downstream from the intersection, the axis of maximum winds shifts significantly to the left to a position over northwestern Ohio. From central North Carolina to northwestern Ohio, the axis of maximum winds is nearly coincident with the concave portion of the "cold cloud shield" boundary; but, both of these features are across the streamlines at a significantly large angle. From the region of maximum convex curvature in the high level moisture boundary (near the northwestern corner of Ohio), northeastward into Canada, the axis of maximum winds is parallel to the flow, both of which are parallel to the adjacent moisture boundary. At this stage of cyclogenesis, near the time of the high level cusp formation, but prior to the jet stream break, the significant leftward shift in the axis of maximum winds is common.

Changes 0000Z-1200Z 4 April 1987

During the 12-hour period between the times of the left and right columns of **Figure 43**, the surface low deepened 8mb and moved from central North Carolina to Northern Virginia. During the night, a line of new deep convective clouds developed near the surface frontal position to the rear of the concave boundary of the "cold cloud shield". This caused a retrogression of the rear edge of the "cold cloud shield", such that it was again over the surface low center and near the surface frontal location. Such reformations of convective weather to the rear of existing convective clouds is typical along the dry surge regions of storms during the cyclogenesis phase. By 1200Z, the surface low pressure center and front are near the cold cloud boundary formed by the new deep convective weather. The original rear edge of the "cold cloud shield" is over central New Jersey at 1200Z.

Just after 0000Z, a cusp formed on the high level "cold cloud shield" boundary. The northern end of the "head" boundary "H" that formed the western edge of middle tropospheric moisture building back around the developing low, accelerated westward. Higher level clouds and moisture near the newly formed cusp also moved westward. During the 12-hour period, the westward moving high level moisture moved rapidly over the middle level moisture; and, by 1200Z, both the middle and high moisture regimes have reached eastern Illinois.

1200Z 4 April 1987 - Right Column Analysis

Note that the 1130Z water vapor image, shown with the 300mb and 500mb analyses of **Figure 43d** and **43e**, is also shown without overlays as **Figure 44a**.

Whereas the northern end of "head" boundary "H" moved westward to Illinois, the southern tip moved eastward into west central North Carolina. As a result, the boundary rotated cyclonically to a generally northwest-southeast orientation. The moist air on the northeast side of that boundary has moved around the poleward side of the developing cyclone from the eastern side. The northern part of the moist regime, over Indiana, Ohio, and northern Kentucky is at high levels; and, is a part of the "cold cloud shield" that moved westward over the middle level moisture. By 1200Z, the upper air cyclone has closed in the middle and upper troposphere. Note that the region of cyclonically curved flow on the 300mb and 500mb streamlines is partly light and partly dark on the water vapor image.

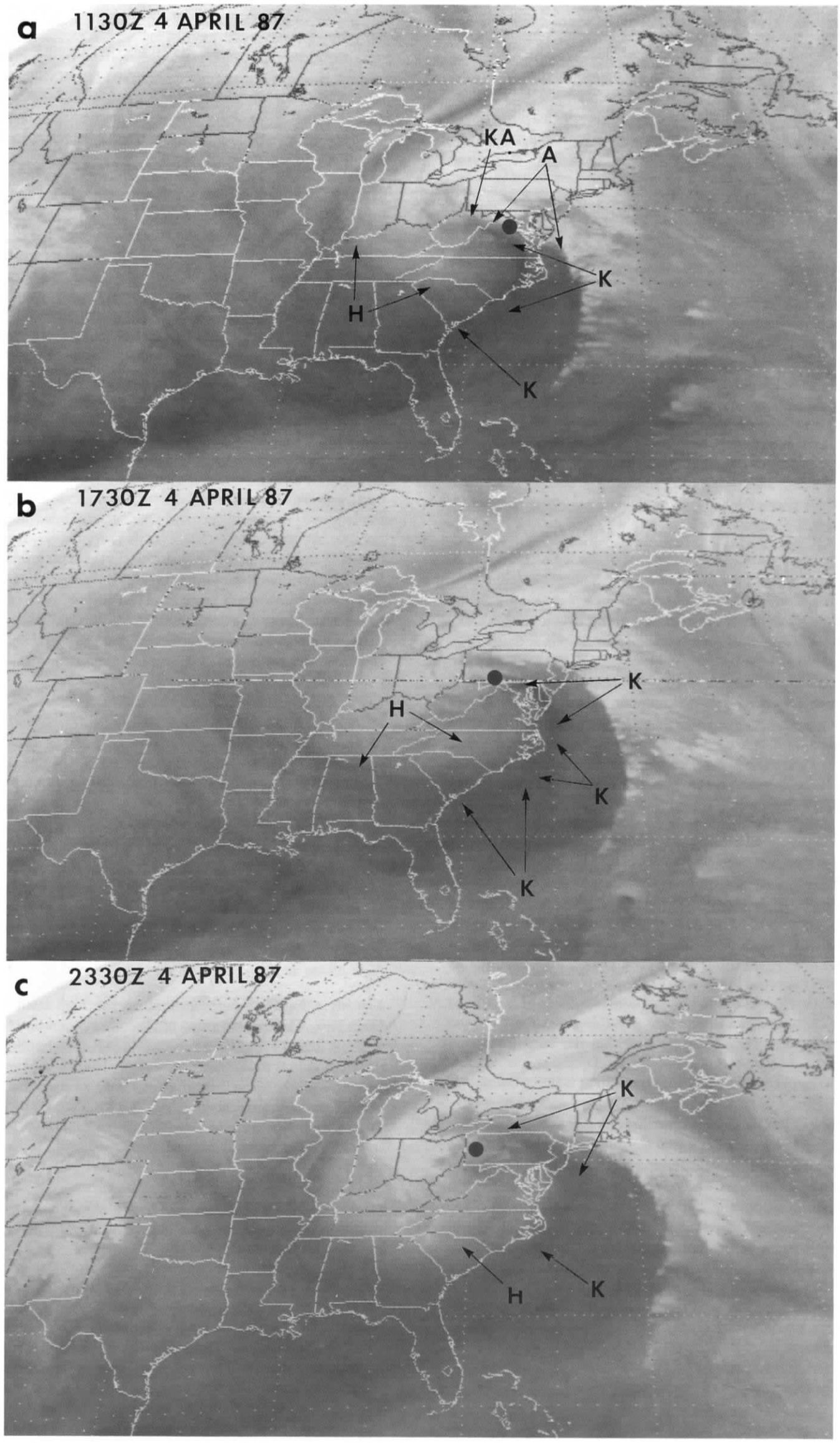

Figure 44 **SECOND SEQUENCE OF WATER VAPOR IMAGES - 4 APRIL 1987**
Sequence of 3 GOES East 6.7μm images from 4 April 1987 - 1130Z - 1730Z - 2330Z. Black dots indicate positions of the surface low pressure center, interpolated to image times from surface analyses and storm track analysis.

The central portion of the cyclone is dominated by the light gray shades of the moisture regime that built-back around the low from the downstream side. In the middle troposphere, that moisture is associated with warm air advection, as a thermal ridge "builds-back" around the northern side of the low. In the upper troposphere, above 400mb in this case, that moisture is associated with cold advection of the "build-back" ridge, above the middle level warm advection. Much of the radiation arriving at the satellite is originating from the very cold higher level moisture and the associated cold cirrus clouds, that are moving around the northern side of the cyclone center from the east. Therefore, the warm advection associated by the mid-tropospheric "build-back" ridge or thermal ridge is implicitly revealed on the satellite imagery; whereas, the moisture in the cold advection above is explicitly observed.

On the 300mb analysis, a break is indicated in the axis of maximum winds on the northeastern side of the cyclone. The apex of the cusp that formed on the "cold cloud shield" has moved to southeastern Illinois from western Ohio, where it formed shortly after 0000Z. The axis of maximum winds no longer follows along the edge of the "cold cloud shield"; however, the two remaining jet stream branches to the north and south of the "build-back" ridge can be connected across western Pennsylvania to Lake Huron, where the wind speeds are still nearly 70 knots across the ridge. In this case, the upstream ridge has partly "rolled over" to the northern side of the new low; and, a break has also occurred on the jet stream branch on the western side of the trough. Therefore, the new low has become "cut-off". Some upper air lows do not become "cut-off" during their existence. Compared to others that do "cut-off", the low in this case became "cut-off" very early. Such early "cutting-off" of the upper air low generally implies that the surface low will move more slowly, have a shorter than normal period of deepening, and is less likely to deepen rapidly.

On **Figure 44**, water vapor images are shown at 6 hour intervals. The image on **Figure 44a**, was also shown with analyses on the right column of **Figure 43**. Note on that first image that boundaries "K" and "A" approach each other with a relatively small angle, compared to the situation 12 hour prior to this image. The intersection is over northern Virginia, just west of the analyzed surface low center, indicated by a black dot. To the west of the point of intersection, the dark band "K" extends parallel to "A" for a distance of approximately 120 nautical miles across part of West Virginia. At the time of the image, the surface low pressure center was nearly coincident with boundary "A" and moving toward the north-northeast (for surface center track and pressure changes, see **Figure 46**). Our rule for estimating the position of the surface low center is as follows. Determine the intersection point of feature "K" and boundary "A". The low center is likely to be just under the high cloud boundary, and approximately one degree of latitude in the equatorward direction along that boundary. If a middle cloud boundary is present to the rear of the high cloud boundary, the middle cloud boundary should be used.

At the time of the first image, our rule also indicates that the surface low pressure center should be deepening (minimum central pressure decreasing with time). It is likely to stop deepening, if the dark band (or the forward boundary of that band, if it is significantly wide) moves on the right side, or hooks in advance, of the center of the surface low. However, to apply that empirical relationship requires knowledge of the location of the surface low center. Generally, that position cannot be explicitly observed on infrared or visible satellite imagery. If the position is not known, the following rule can be applied. Usually the dark band "K" and boundary "A" will intersect at decreasing angles with time as the storm evolves, and, the two features will become parallel to each other on their forward ends. Once the parallel distance becomes 200 miles or greater (3 degrees of latitude may be used), the low will likely stop deepening. Once that amount of parallel distance is attained, the intersection rule for locating the center, no longer applies. The low will likely be somewhere along the segment of parallel boundaries; however, we have no technique for estimating where along that segment.

In the case shown, after 1130Z, the high boundary "A" moved northward more rapidly than the surface front; and, new deep convective clouds formed along the surface frontal position. By 1730Z (**Figure 44b**) the dark band "K" had overtaken the surface low center. The surface low reached its minimum central pressure at 1800Z. By 2330Z, the dark band "K" had moved on the right side of the low center and extended in advance (moved westward more rapidly than the low center). By 0000Z, the low had filled 4mb, from its 1800Z minimum. Our empirical rules using the dark band or slot estimate when the low will "stop deepening". They do not predict or estimate the "filling". However, when the upper air systems become slowly moving, and the jet stream core "hooks" to the right of the surface center, immediate filling is common. The 4mb increase, in this case, may have been related to the associated convective weather, and to the fact that the low moved westward to higher terrain.

Boundary Evolutions - Water Vapor Imagery

It is useful to consider the changes in the moisture patterns during the cyclogenesis phase of the storm evolution. Although the cyclogenesis phase ended at 1800Z by our definition, we shall extend this discussion of patterns to 2330Z. On the first image of **Figure 41**, when the "cold cloud shield" was in the "leaf" configuration, there were two primary boundaries. The moisture regime of the trough was bounded on the western side by dark band "K", and on its eastern side by the rear boundary of the "leaf" with its concave and convex portions. At the end of the first 12 hours (**Figure 41c**) a third significant boundary had formed. The mid-tropospheric head boundary "H" had formed on the western side of moist air and clouds building back around the newly forming low. Also, by this time, the dark band "K" had rotated around the southern side of the trough to the rear of the surface cold front; whereas, the concave part of the "cold cloud shield" boundary "A" had moved in advance of the surface front. Therefore, in the first 12 hours, the situation had become more complex. During the next 12 hours, convective clouds formed near the surface front, causing the boundary of the "cold cloud shield" "A" to retrograde to that position, and hold as new high clouds and moisture were produced by the deep convective cells.

Consider the image of **Figure 44a** in regard to the boundaries and moisture patterns. The upper air cyclone has closed and is becoming "cut-off". High level moisture and clouds have built back over the middle level moisture that had initially built back. The head boundary "H" has become a vertically deeper interface, and moved westward into Illinois. Some of the "build-back" moisture has begun to rotate around the new upper air low to the position over western North Carolina. The moisture regime originally associated with the middle tropospheric cold air trough has become very narrow along "D-C", where it has become elongated between the upstream and "build-back" ridges. It is also beginning to narrow around the southern and eastern sides of the storm. In those quadrants, the cold moisture regime is bounded on its outer side by the jet stream axis and by the moisture feature "K". It is bounded on its inside (northern and western sides) by the "head" boundary "H", the edge of the return moisture building back around the storm. Note on **Figure 44a**, that the cold trough moisture regime is present over parts of the Carolinas between boundaries "K" and "H". To the west of there, on the southern side of the low, boundary "K" became indistinct as darkening occurred in the jet stream zone. Six hours later, at the time of **Figure 44b**, boundary "K" intersects the coast near Savannah, Georgia; and, the jet stream position has remained nearly stationary to the west of there. However, boundary "H" has expanded westward and southward, causing a further narrowing of the cold air moisture regime that initially dominated the area between the "leaf" and the upstream ridge. By the time of **Figure 44c**, boundary "H" extends from southeastern Missouri to central Georgia, then across the Carolinas to eastern Virginia. By this last image time, very little of the original cold trough moisture regime remains. The cyclonic flow pattern of the upper air system has become dominated by the lighter gray shades of the moist air that built back around the low from the ridge of the eastern side.The return moisture is located in the thermal ridge at middle levels and in the cold air above the level of maximum winds (at 300mb and above in this case).

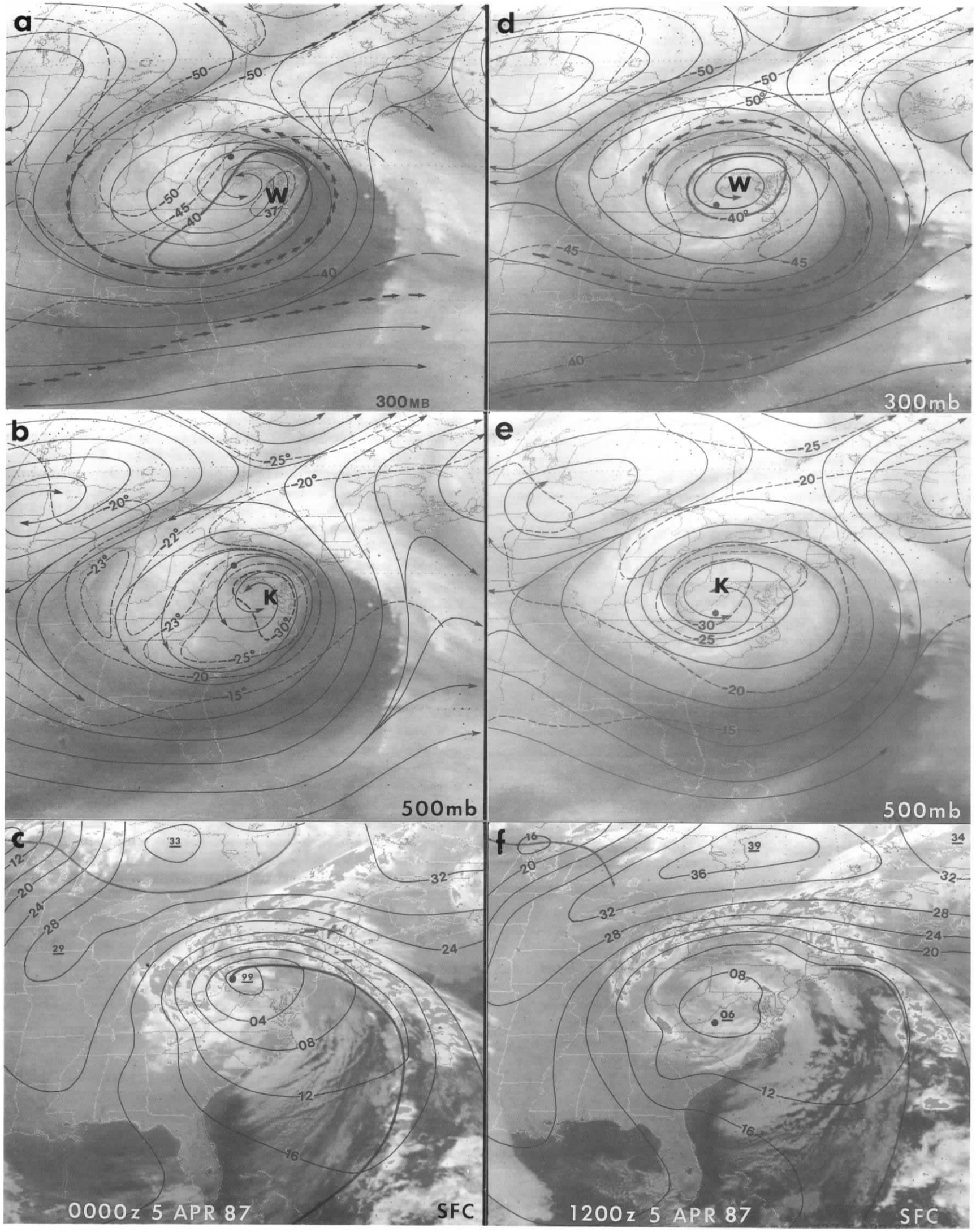

Figure 45

UPPER AIR AND SURFACE ANALYSES FOR TWO RADIOSONDE TIMES

Left Column Analyses 0000Z 5 April 1987.
Fig. 45a and **45b**. 6.7μm 2330Z 4 April 1987.
Fig. 45c. Enhanced IR 0000Z 5 April 1987.

Right Column Analyses 1200Z 5 April 1987.
Fig. 45d and **45e**. 6.7μm 1130Z 5 April 1987.
Fig. 45f. Enhanced IR 1200Z 5 April 1987.

Upper air analyses: Streamlines (solid lines), Isotherms (dashed lines). Axes of maximum wind speeds (arrowheads).
Surface analyses: isobars (thin lines), frontal positions (bold lines).

d. The Mature Storm Phase

0000Z 5 April 1987 - Left Column Analysis

Consider the images and analyses on the left column of **Figure 45**, which are valid at the end of the sequence of **Figure 44**. The light gray shades of the "head" moisture pattern are primarily within a region of warm advection at 500mb and cold advection at 300mb. The warmer moist mid-tropospheric air has arrived from the northwest over Greensboro, North Carolina. During the past 12 hours, the 500mb temperature increased 4°C, and the dewpoint depression decreased 7°C. At 0000Z, the Greensboro winds veered from 270° to 340° between 11,000 and 23,000 feet. Just below that layer, an inversion was present from 766-734mb. An even greater change occurred at Nashville, Tennessee, where the 500mb temperature increased 9°C and the 300mb temperature decreased 8°C as the warmer air overlain by cooler air moved from the north over the station. At Nashville, the winds veered from 335° to 020° between 13,000 and 27,000 feet above a 700-661mb inversion.

At 500mb, warmer air has built back around the northwestern side of the low. The air temperatures of the cold air part of the cyclone have increased with time; and, the thermal trough has become narrow around the southern side of the low. The "cold cap" tropopause has weakened; however, at 300mb, cold air has moved back around the northwestern side of the cyclone, over the warmer air at 500mb. Recall that the leading part of the dark band "K" had extended around the northern side of the low to northwestern Pennsylvania. The jet stream core has extended across New Jersey to near Buffalo where three levels of maximum winds were reported - all below 300mb; 110°/89kts at 356mb, 110°/85kts at 486mb, and 065°/68kts at 875mb. Such lower levels of maximum winds are common in the dry slot zones around mature storm systems.

The same water vapor image shown on the left column of **Figure 45** has been used to display the storm track. On **Figure 46**, the "track" of the surface low center is shown by dots at 3 hour intervals to the position near Pittsburgh, which is the location corresponding to the image time - 0000Z 5 April. Positions after the image time are shown by open circles. Pressure decreases are shown by black numbers between positions; and, pressure increases are shown by white numbers between 3-hourly positions. The last 4 positions are at 6-hour intervals. Analyses at 1200Z 5 April, are shown on the right column of **Figure 45**.

1200Z 5 April 1987 - Right Column Analysis

During the 12 hours after the image time of **Figure 46**, the core of the upper air low became vertical and nearly stationary over western Virginia. The surface center moved around the western quadrant of the upper center into southwestern Virginia, and filled an additional 7mb to 1006mb. The surface analysis valid at that time is shown as **Figure 45f**. The low has filled 11mb during the 18 hours since minimum pressure. Note that the surface pressure gradient has weakened significantly near the center; whereas, it has remained strong over the Great Lakes and southern Canada under the cold cloud band. This is characteristic of the mature storm phase.

On the upper air analyses, a large relatively strong cyclonic system is present. The dry slot, although not as distinct or well defined as on prior images, has rotated around the low into North Carolina. At 300mb, the axis of maximum winds with speed greater than 70 knots, extends around the low into northern Kentucky. The coldest air at 500mb and the warmest at 300mb now occupy the core region of the cyclonic circulation. It's likely that the isotherm patterns would form a more asymmetric spiral configuration related to the moisture pattern. However, with the radiosonde density, a tedious analysis using vertical cross sections and time changes is required for reliability. In mature storm cases, where this was done, the spiral moisture pattern is associated with similar configurations in the thermal and humidity fields. If the "cut-off" upper air low remains undisturbed, the spiraled moisture pattern on the imagery tends to lose its distinctiveness with time, merging into a homogeneous medium gray shade core. The thermal fields also lose their spiral configuration and form a cool middle level core overlain by a warm core at higher levels.

At this time, the cold core is also present at 700mb and 850mb with minimal temperature advection near the center. The surface low is on the southern side of the upper air low and still moving; but, it is inside the temperature gradient zones under the cold air. As shown on **Figure 46**, the surface center was identifiable during the next 24 hours. It moved eastward across southern Virginia to Delaware, and the pressure increased to 1009mb - the same pressure as its initial value. The system evolved to an upper air "cut-off" low - completing its surface cyclone phase.

In this case, the system was permitted to evolve to a very mature stage. The resulting "cut-off" low on the water vapor imagery had a "moist" core, dominated by moisture accumulated in the center from the "build-back" process. Many storm systems do not evolve to this degree of maturity. They may be "sheared out" by a stronger upstream system, or dominated by a new short wave entering the upstream circulation. This often results in the development of a new low on the eastern side of the original one before it completes its evolution. Also, in this case, the building back of the downstream ridge was significant to the system evolution. Although the upstream ridge was also significant, since it "rolled over", contributing to the cutting off process; it did not prevent the downstream thermal ridge from building back around. Generally with system developments, both the upstream ridge and the "build back" of the downstream ridge contribute to the warm mid-tropospheric air surrounding the upper air cyclone. Generally, the greater is the role played by the "build-back" ridge, the more significant is the surface low development. Perhaps this correlation should be stated in reverse.

We shall now show a cut-off low development in which the "roll-over" upstream ridge dominated the evolution.

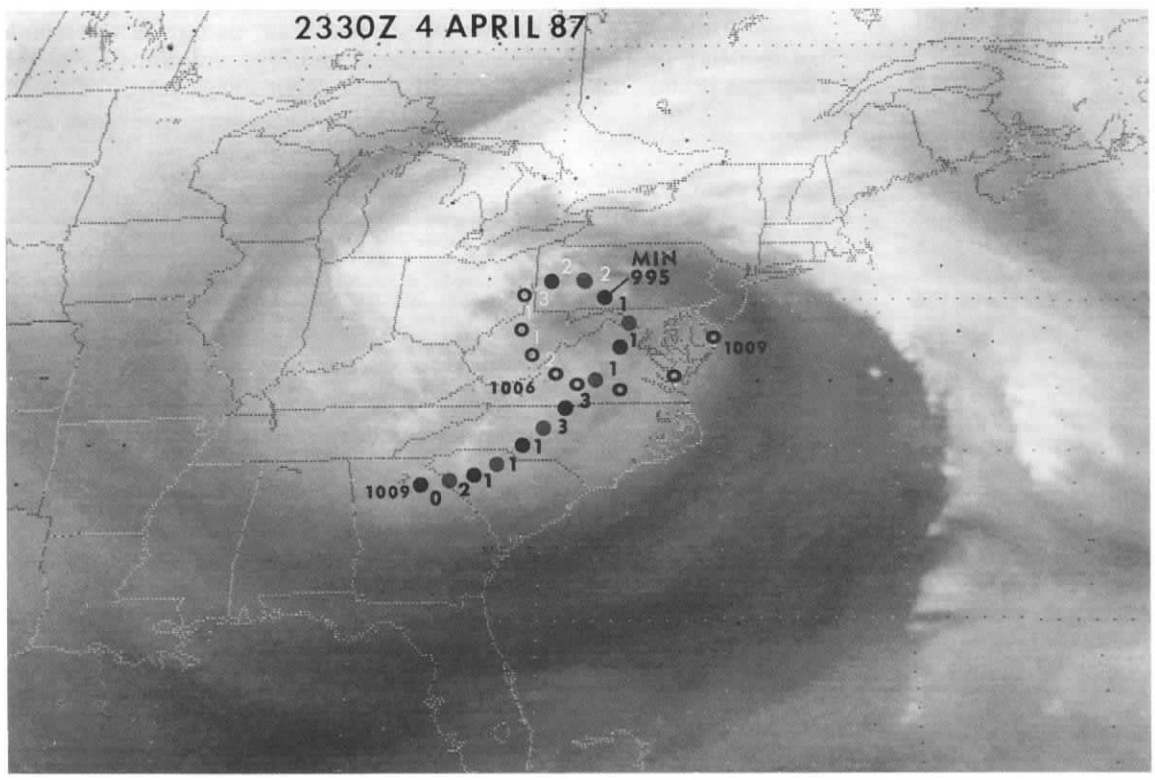

Figure 46

STORM TRACK ANALYSIS
6.7μm image, 2330Z 4 April 1987, GOES East. Surface low pressure center positions at 3 hour intervals. Numbers between the dots indicate the 3 hour change in the central pressure in millibars (black = decrease; white = increase). The northernmost solid dot near Pittsburgh is valid at 0000Z 5 April 1987 (30 minutes after the image time). Positions after that time are shown as open circles. The initial position near Athens, Georgia is valid at 1200Z 3 April (1009mb). Minimum pressure 1800Z 4 April 995mb (3rd from last solid dot - 5.5 hours prior to image time). The last position (1009mb) over Delaware is valid at 0000Z 6 April (24.5 hours after image time).

2. A "CUT-OFF LOW" DEVELOPMENT WITH A DARK CORE REGION

In the last cyclogenesis case, the system evolved to a "cut-off low" with a relatively moist core region. The moisture arrived there by rotating around the poleward side of the upper air low from the downstream side.

Consider another development which occurred later in the same month. On **Figure 47**, water vapor images are shown in sequence at 6-hour intervals. On all of the images, selected surface features are shown. On the 1130 and 2330Z images, 300mb analyses are superimposed. All analysis features are valid 30 minutes after the associated water vapor image.

At the time of the first image, an upper air trough extends from Hudson Bay to Arizona. During the 24 hours prior to this time, the trough in Canada moved rapidly eastward, the low over northwestern Mexico became "cut-off", and the trough over the western United States elongated into a cyclonic shear zone with significantly stronger winds on the forward side. A closed upper low had been present along the trough over the western U.S. As that system became "sheared out" in advance of the rapidly approaching upstream ridge, its moist head region dominated the remaining trough zone. The remaining moist cold air is present, elongated along the trough from northeastern Colorado to northern Minnesota. A dark band along the northwestern boundary of that moisture is identified as "K" on **Figure 47b**. A new jet stream branch has hooked across the upstream ridge into western South Dakota; and, a new pattern of cold topped clouds with precipitation has formed over Iowa and Wisconsin.

By 1730Z, the cold clouds have extended northward, and the surface winds have changed from northerly to northeasterly over southern Minnesota and western Wisconsin. A surface trough has formed from central Illinois to northwestern Iowa. The boundary along the eastern side of the dark band "K" has become more distinct. A small triangular dark area has formed over northeastern Colorado at "D" where the narrow dark band "K" intersects the dark band extending from Arizona to central Nebraska. Such "dry delta" features are an indication that the jet stream may be branching across the trough near that location.

By 0000Z 22 April, the jet stream branch across the ridge has extended parallel to "K" into western Nebraska, but there were no indications in the radiosonde data that it had crossed the trough. However, at 500mb, a closed low has formed over northeastern Nebraska, and there are indications that a speed maximum may be located across the trough over northwestern Kansas. The cirrus boundary on the east side of the trough has formed a low amplitude "S" curvature, with an inflection point over northwestern Iowa; and, a small dark region has formed over eastern Nebraska.

By 0530Z, **Figure 47d**, this dark region has become larger and a cusp appears to be forming on the cirrus boundary - or cold moisture boundary - over Minnesota. Although the pressures have lowered slightly in the surface trough over Illinois and eastern Iowa, there are no distinct surface low centers present. However, the trough has built back into the cold surface ridge. During the 12-hour period between **Figures 47b** and **47d**, the curvature of feature "K" and the "S" shaped cirrus boundary east of there has increased. This implies development has continued. The "dry delta" area has moved eastward, but has not increased in size. However, its size in the middle troposphere may be obscured by higher level moisture. Notice that the high level moisture boundary extending from northeastern New Mexico to northwestern Iowa appears to cross over the features extending from the north over Kansas.

By 1200Z 22 April (**Figure 47e**), the low has closed at 300mb, and has already become "cut-off". The jet stream branch which had crossed the upstream ridge has not persisted across the ridge. The primary jet stream along the northern side of the upstream ridge has continued to extend eastward across Canada. Although only a minor jet stream branch crossed the ridge, it was sufficient to initiate the new development. However, the advection of cold mid-tropospheric air into the rear of the developing system has not continued. The warmer air of the upstream ridge has "rolled over" adjacent to the downstream ridge north of Minnesota and Lake Superior.

The downstream upper air ridge has amplified over Wisconsin and eastern Minnesota; and, a "break" has developed in the jet stream. The boundary along the northern edge of the building ridge has the characteristics of a "head" boundary. Only a narrow dark zone is present along the boundary. Although the "cusp" has formed on the high level moisture boundary over Minnesota, the high level clouds and moisture have not hooked westward around the northern side of the low. The boundary extending southwestward from the col to the western side of the low was a part of feature "K" between the warm mid-tropospheric air of the upstream ridge and the cold air of the trough. That part of the low is bounded by the upstream ridges and a segment of the upstream jet branch is still present along the boundary.

The core of the "cut-off" low is predominately cold in the middle troposphere surrounded by warmer air. Approximately half of that warmer air is that of the upstream ridge on the west side and half is that of the downstream ridge. The core has warmed at 300mb. At Omaha, Nebraska, near the center of the upper air low, the 500mb temperature was -25°C with a 3.2°C dewpoint depression. The air below 500mb was very moist; but, 30°C dewpoint depressions were reported from 459mb upward. The 300mb temperature was -38°C, a relatively warm value.

By 1730Z, **Figure 47f**, the high level cusp has become better defined with cirrus clouds filled in to the apex which has moved slightly westward. This implies that the middle level thermal ridge may be building back around the northern side of the low. By 2330Z, **Figure 47g**, the low has moved slowly southeastward and the 300mb streamline pattern has become more rounded in shape. The moisture building back from the downstream ridge has extended around to northeastern Kansas. And, by 0530Z, the last image time, that moisture has extended southward over northeastern Oklahoma and southwestern Missouri. At that time, a band of cold clouds was present along the moist band, along that portion from Minnesota to northeastern Kansas. The "head" boundary has extended around the west side of the low, but the "head" moisture pattern consisted of only a narrow band.

In this case, surface cyclogenesis occurred; but, the surface development was weak and delayed. At the time of the first image, a cold surface ridge with 1035mb pressures extended from northwestern Minnesota to northeastern Colorado. Between 1200Z 21 April and 0000Z 22 April - **Figures 47a** and **47c** - the surface frontal trough remained nearly stationary over the Illinois area, and a trough built back into the ridge over Iowa. This change was primarily a reconfiguration of the isobaric pattern. The ridge moved eastward to the north and slightly eastward to the south. There were pressure decreases of about 1mb over northwestern Iowa. During the next 12 hours, between **Figures 47c** and **47e**, pressures decreased along the trough over eastern Iowa by 4-5mb. There was still no closed center there by 1200Z (**Figure 47e**), although a weak center was formed along the frontal trough on the Indiana-Kentucky border. By 1800Z 22 April, **Figure 47f**, 12 hours after the cusp stage has been attained, a closed center had formed on the Iowa-Illinois border, and the frontal low dropped 2mb in central pressure. By 0000Z 23 April (**Figure 47g**), the new low center had fallen back to the moisture boundary and deepened 1mb. Its pressure did not decrease after that. The net decrease in the surface pressure was about 7mb; but, the surface center had not formed until near the end of the pressure decrease period. This type of delay in the surface low formation is common with many high plains developments in which the upper air development is well to the west of the boundary layer trough. Surface pressures decrease in a typical location with respect to the upper air system, but that location is to the west of the initial surface trough. The pressure decreases occur within a portion of the cold boundary layer high to the west of the trough. With time, a new low may form to the west of the trough, or the trough may widen westward; however the surface development is delayed with respect to the evolution of the upper air system. In this case, a new low formed, but the development was short lived and weak, as the upper air system quickly became "cut-off".

The relatively weak surface development can be correlated with the image features. There was no significant "head" pattern in the clouds or moisture building back around the closed low; and, the core of the low was predominately dark on the water vapor imagery.

Figure 47 ➤

CYCLOGENESIS - DARK CORE EVOLUTION
Sequence of 8 images at 6-hour intervals, 6.7μm GOES East.
Left Column: 300mb analyses superimposed on images. Streamlines (solid lines), Isotachs (dashed lines - knots), Axes of maximum 300mb wind speeds (arrowheads where 70 knots or greater). Images, labeled by analysis times, are valid 30 minutes prior to those times.
Right Column: Image times are labeled.
Both Columns: Dots are surface low pressure center positions, bold dashed lines are surface trough axes, bold solid lines are surface frontal positions.

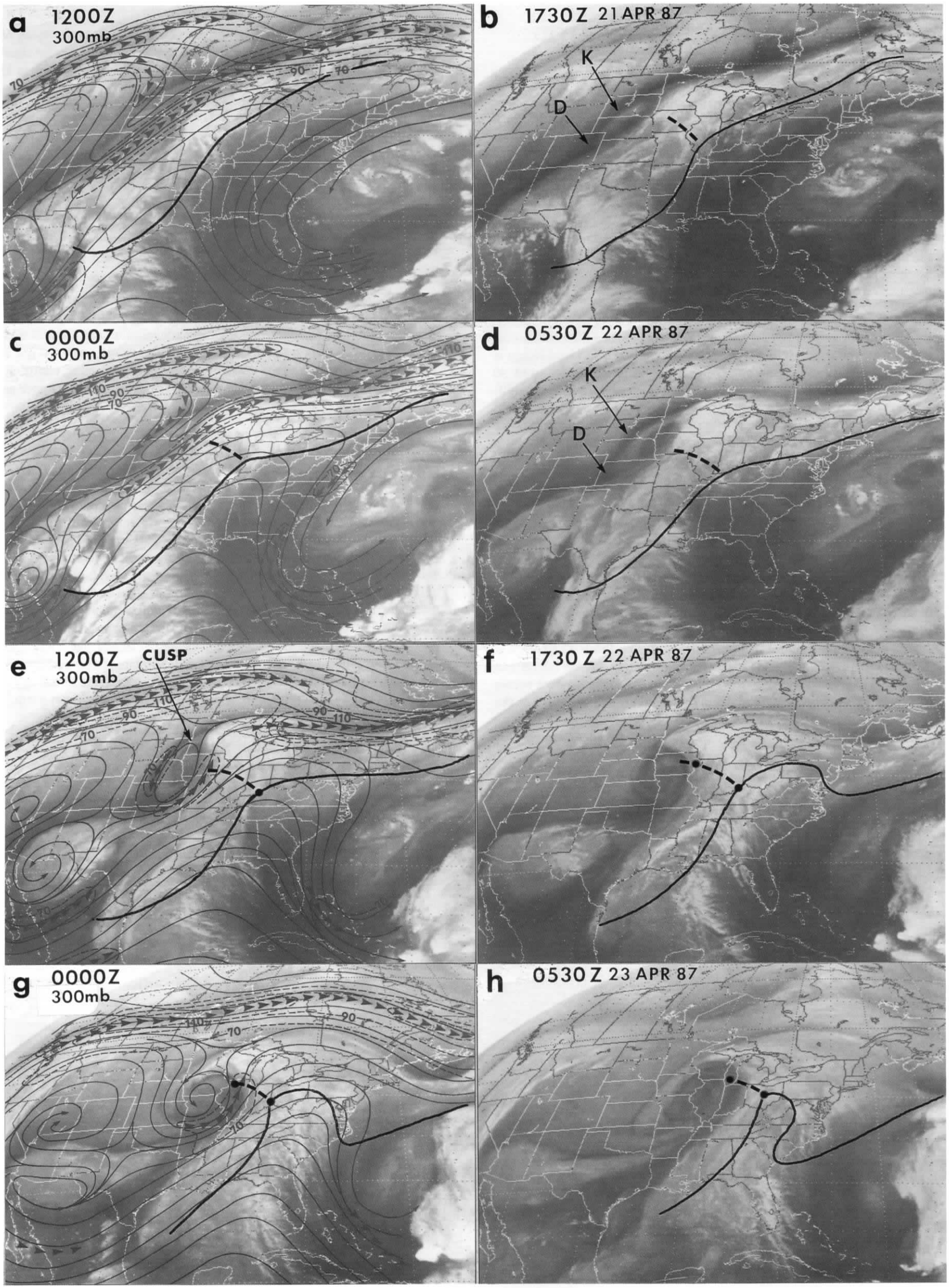
a
1200Z
300mb
70
90
70
b
1730Z 21 APR 87
K
D
c
0000Z
300mb
110
90
70
110
70
d
0530Z 22 APR 87
K
D
e
1200Z
300mb
CUSP
110
90
70
90
110
70
f
1730Z 22 APR 87
g
0000Z
300mb
110
90
70
70
h
0530Z 23 APR 87

3. A DEVELOPMENT WITH VERY RAPID DEEPENING SURFACE CYCLOGENESIS

a. A "Very Rapidly Deepening" Storm - The Surface Low Center Track

In a study of surface cyclogenesis over the North American data network during a six year period, we categorized developments by the rate of pressure change at the surface low centers. A "maximum deepening period" was defined as the specific 12 hour period with the maximum decrease of surface central pressure. If the central pressure decreased 12-23mb during the 12 hour "maximum deepening period", the storm was categorized as "rapidly deepening". If the pressure decreased 24mb or more, the storm was designated "very rapidly deepening".

On **Figure 48**, a "track" of surface low center positions is shown. Positions are shown at 3-hour intervals; and, white digits between the positions indicate the 3-hour pressure decreases. The enhanced infrared image is valid near the time of minimum central pressure, which occurred 30 minutes later. The last position was adjusted for the 30 minute time difference. The "maximum deepening period" occurred between 0900Z and 2100Z 25 November 1983. On the figure, the positions at those times are indicated by two arrows. During that period, the central pressure decreased 25mb, and the center propagated at an average speed of 48 miles per hour. This rapid speed of movement is typical of rapidly deepening surface centers. Both the speed and the deepening rate are related to the type of upper air system which is commonly present.

The surface low formed at nearly the same location as the 3-5 April 1987 system already discussed. That system deepened only 8mb during its "maximum deepening period"' and moved at a speed of 23 mph during the period. The system shown here deepened 12mb during the first 12 hours of its track, reaching a central pressure of 995mb and the location near Wallops Island, Virginia. During the following 12 hours, it deepened 25mb. It is likely significant that the track during those 12 hours was primarily offshore, except for a short portion across Rhode Island and eastern Massachusetts. After that, the system moved northward across Maine into New Brunswick and deepened another 4mb from 970 to the 966mb minimum at 0300Z on the 26th.

Although storms tend to deepen more rapidly as they cross the coast, or along portions of their tracks near the coast; this is not necessary for significant deepening. The storm of 25-26 January 1978 deepened 30mb in 12 hours as it moved from eastern Mississippi to southern Ohio at an average speed of 47 mph. However, no water vapor imagery were available for that case.

b. The "Leaf" Phase of Development

On **Figure 49**, water vapor images are shown at 6 hour intervals. Since no water vapor image was received at 1730Z on the 25th, an 1800Z infrared image has been substituted. Surface and 300mb analyses are shown on enhanced infrared sectors at 12 hour intervals on **Figure 50**; and intermediate surface analyses are shown on **Figure 51**.

At 0000Z 25 November, there is a strong surface low over northwestern Ontario. That system was also a rapidly deepening storm, having deepened 19mb in 12 hours, and reaching a minimum pressure of 968mb 18 hours prior to this time. Although there is an associated closed low at 300mb, the jet stream over the upstream ridge has been digging, contributing to a vertically deep cold frontal zone with a high amplitude upper air trough to its rear side.

Note on the 2330Z water vapor image, **Figure 49a**, that the rear border of the frontal zone moisture has formed an "S" curvature with an inflection point over Alabama. The curvature had just become apparent at 2100Z and has amplified rather rapidly. That change implies development. Another favorable implication is the existence and characteristics of the dark area at "KA". This triangular dark feature is similar to those observed with other cases previously discussed. The dark area is located to the rear of that part of the high level moisture boundary with maximum concave curvature. A second middle level moisture boundary - to the rear of the higher one - forms the southeast border of the dark area. We estimate the top of the middle level moisture to be near 600mb. The southwest boundary of the triangular dark area extends northward as a narrow dark band "K". This feature extends northward to Canada, but is very faint on our original image; therefore, its location is indicated by several arrows. It is generally parallel to the jet stream on the upstream side of the upper air trough, but on the cyclonic shear side of the axis of maximum winds.

The dark area "KA" is apparently just on the left side of the jet axis at the base of the trough. The 500mb wind at Lake Charles, Louisiana was northwesterly at 100 knots. In this case, the jet stream winds are significantly stronger than those of the 3-5 April 87 case. The 500mb trough temperatures are slightly warmer in this case, and the temperatures of the adjacent ridges are significantly warmer.

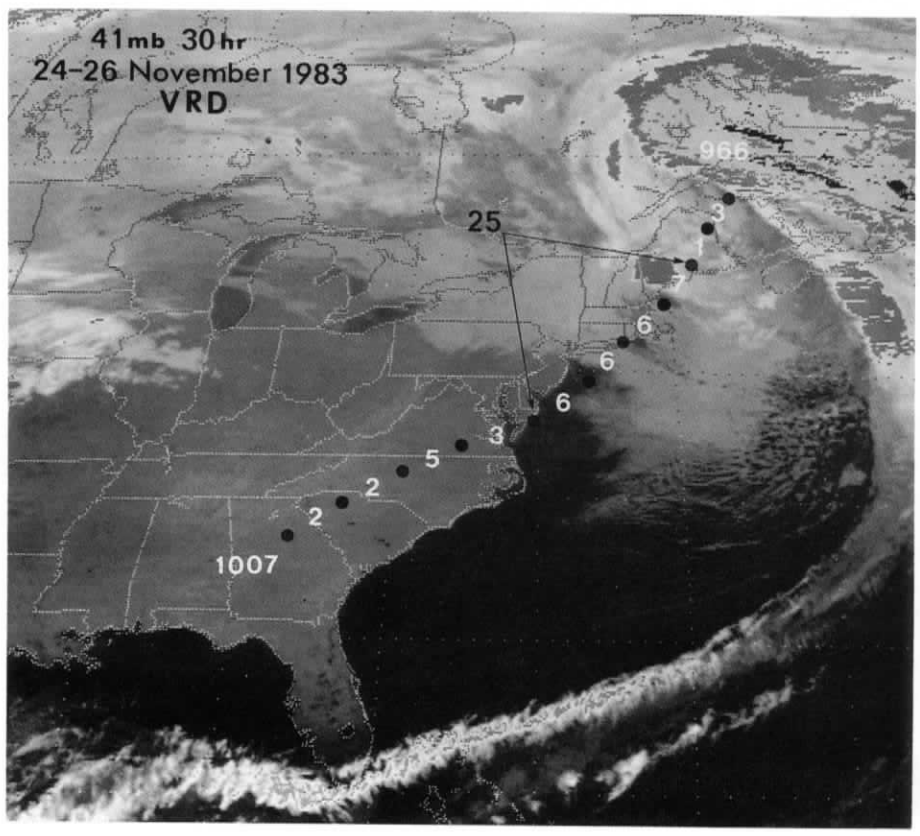

Figure 48

STORM TRACK
Enhanced infrared image (MB curve) 0230Z 26 November 1983, GOES East. Positions of the surface low pressure center at 3-hour intervals are shown as black dots. Numbers between dots indicate the 3-hour pressure decrease in millibars. Positions between arrows indicate the 12-hour period during which the greatest decrease in pressure occurred - 25mb/12 hours defined as "very rapid deepening" ("VRD"). The initial position (1007mb) is valid at 2100Z 24 November 1983.

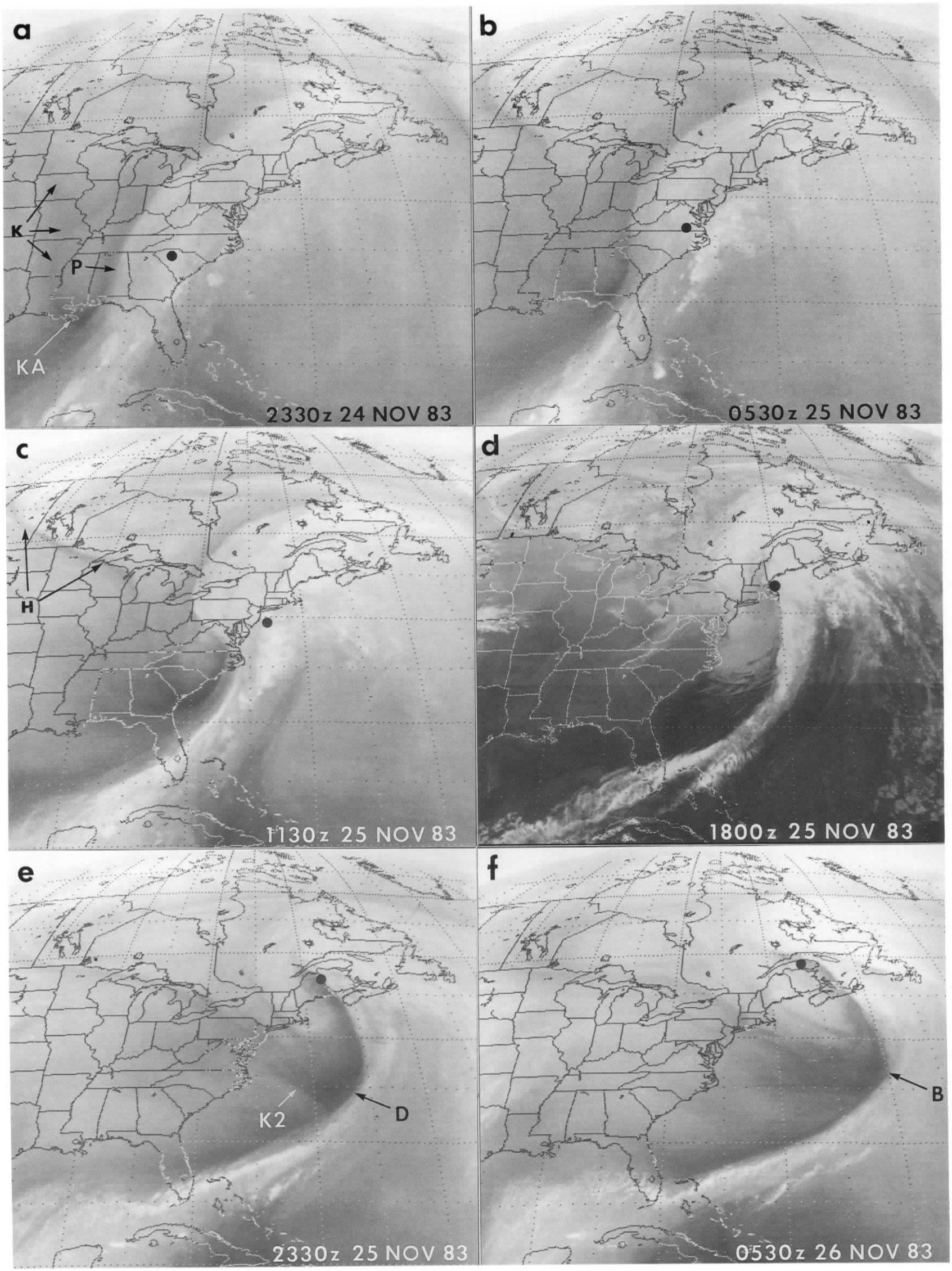

Figure 49 **SEQUENCE OF WATER VAPOR IMAGES**
Sequence of 6.7μm images at 6-hour intervals, GOES East. Times and dates labeled on images. No 6.7μm images was received for 1730Z 25 November 1983 - an 1800Z infrared image has been substituted. Surface low center positions, interpolated to image times, are shown by black dots.

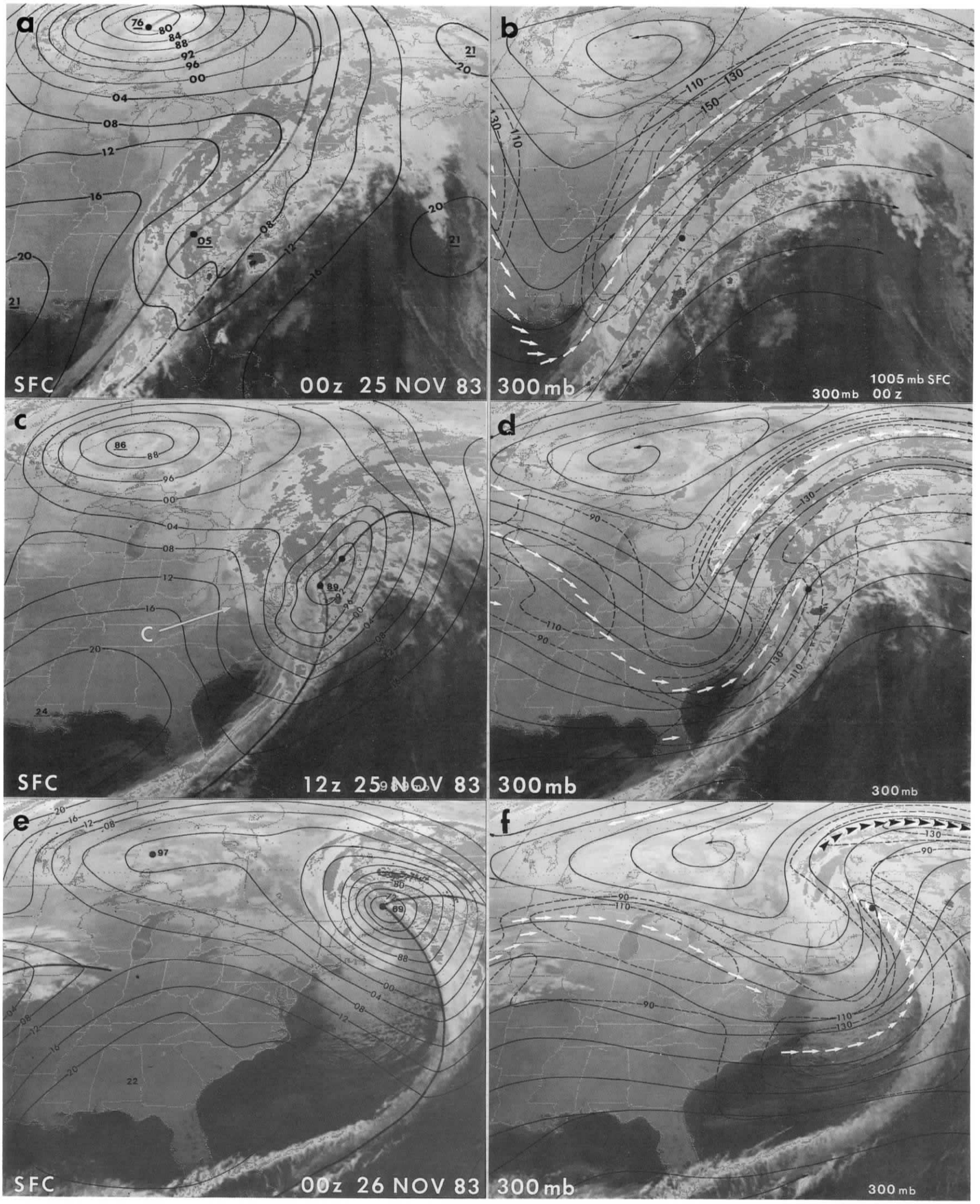

Figure 50 SURFACE AND 300mb ANALYSES AT 12 HOUR INTERVALS

Left Column - Surface Analyses
Isobars - thin solid lines
Frontal Positions - bold solid lines
Images - Enhanced Infrared (MB Curve)

50a. 0030Z 25 Nov 83 Image with 0000Z Analysis
50c. 1230Z 25 Nov 83 Image with 1200Z Analysis
50e. 0000Z 26 Nov 83 Image with 0000Z Analysis

Right Column - 300mb Analyses
Streamlines - thin solid lines
Isotachs - dashed lines
Axes of Maximum Winds - arrows

50b. 2300Z 25 Nov 83 Image with 0000Z Analysis
50d. 1200Z 25 Nov 83 Image with 1200Z Analysis
50f. 2300Z 25 Nov 83 Image with 0000Z Analysis

The 0000Z surface analysis is shown on **Figure 50a**. During the 12 hours previous to this, a line of heavy thunderstorms had formed just in advance of the surface front from the central Gulf of Mexico into western South Carolina; and moved eastward across Georgia and northern Florida. Some of their effects were to change the surface temperature, pressure, and winds; which made the task of surface analysis difficult. And, their cloud features complicated the task of image interpretation. A relatively well defined low level cloud boundary formed and moved in advance of the thunderstorms, probably as a result of the rain cooled low level outflow. Over northern Florida, surface temperatures decreased approximately 20°F, and the pressures increased as the line passed. From the satellite imagery, it would be normal to interpret this forward low level cloud border as the surface frontal position. However, the original surface frontal trough and wind shift line remained nearly stationary from 1500Z until 2100Z over Apalacheecola and central Georgia. Across that line, the temperatures decreased approximately 10°F from east to west. Any low level cloud features that might have been present at that location were obscured by high clouds spreading back from the thunderstorms, as the cells moved to the right of the high level wind directions.

During the early "'leaf" phase, it is common for the surface pressures to begin to lower along the frontal trough in advance of the inflection point. Often, this lowering of the pressures causes a retrogression or slowing of the frontal trough in that area; whereas, pressures continue to lower in advance of the trough. This results in a widening of the surface trough, even without the presence of deep convective clouds in advance of the front. When the thunderstorms are present, a double trough structure is typical - probably because a mesoscale ridge forms under the rain cooled air.

There are some other aspects of this case which are significantly different from the 3-5 April 87 case previously discussed. In this case, from 1800-0000Z, as the "S" curvature formed on the rear boundary of the frontal zone clouds, the minimum surface pressures along the frontal zone trough from central Pennsylvania to central Georgia decreased by approximately 4mb. The surface front did not exhibit the early curvature as in the last case. Perhaps related to this, is the fact that there is no break in the high clouds north of the inflection point. The clouds and associated well defined rear boundary extend to the primary upper air ridge over Labrador. For this reason, the cloud pattern is not referred to as a "baroclinic leaf". However, the frontal zone cloud pattern can be considered to be in a "baroclinic leaf phase", and many of the rules relating the clouds to the circulation systems may be used.

One of these rules is used to locate the "incipient position" of the new surface low center. At 0000Z, based upon the amplitude of the rear boundary on the water vapor image, and upon the relative widths of the cloud pattern on the infrared image, no well defined surface center would be expected. We can apply the incipient position rule, assuming we had no knowledge of the surface data and analysis. The inflection point is well defined at "P" on **Figure 49a**. The forward edge of the cloud system can be "located" on the infrared image, **Figure 50a**, by smoothing the irregularities and ignoring the thunderstorms that just formed along the coast of Georgia. This produces an incipient position over central South Carolina, 100 nm southeast of the position shown on the surface analysis. This difference, or error, may be attributed to the presence of the low level cloud boundary produced by the thunderstorms in advance of the front. Using a single still image, that edge would likely be interpreted as the forward edge of the leaf pattern.

At 0000Z, the minimum pressure along the frontal trough was 1005.2mb reported at Greenville, South Carolina, very near where the low center is shown on the analysis. The low is not yet well defined in the surface winds or in the isobaric pattern. However, from hindsight, we recognize that this was indeed, the incipient low position. If the "incipient position" rule using the inflection point was applied, with knowledge of the surface frontal trough position, that trough should have been used instead of the cloud edge. By that method, the incipient position would have been indicated very near the analyzed low center of **Figure 50a**. In real time, without the benefit of hindsight, the significance of an analyzed center along the surface trough is increased, if that location coincides with the incipient position determined from the satellite image.

The surface analysis for 0600Z 25 November, is shown on **Figure 51a**. The rear border of the frontal zone moisture and cold clouds has amplified, and the inflection point has moved to western North Carolina. The "incipient position" applied from the satellite imagery alone is about 50 nm to the southeast of the analyzed center over southern Virginia. A new line of thunderstorms had formed offshore in advance of the surface trough. The primary cloud edge of the "**leaf**" system was identifiable to the west of those thunderstorms. The central pressure of the primary surface center over southern Virginia had decreased 7mb during the 6-hour period. However, there is still an elongated trough zone along that portion of the cloud system northeast of the inflection point. Pressures have also dropped along that segment of the trough from central North Carolina to southern Maine. A second 999mb center is located over New Jersey. No significant center along the trough is well defined in the surface wind field. Therefore the incipient position from satellite imagery is still useful to imply which low center, or position along the trough is most likely to develop.

c. The "Leaf" to "Open Comma" Transition

Shortly after 0600Z, the incipient position rule was no longer applicable, for two reasons. When the rear boundary of the leaf pattern amplifies toward a true "S" shape, the cloud pattern widens adjacent to the convex part of the boundary and narrows adjacent to the concave part. The "cold cloud shield" pattern approaches a comma shape. During this transition phase, the surface low center falls back relative to the moving cloud system. The low center is not along the forward edge of the cloud pattern; and, the incipient position rule is no longer valid. Secondly, the rule usually cannot be applied because of the new shape of the "cold cloud shield" and the irregular conditions of the forward edge of that pattern. We have observed that the transition phase, with the low falling back under the cloud pattern, is likely to begin when the maximum width of the "cold cloud shield" reaches twice that adjacent to the inflection point. That relationship is not a highly reliable one; but, it is the best we are able to devise using the satellite imagery alone. In the case shown here, by 0900Z, the transition phase was underway and the incipient position rule was no longer useful.

By 1200Z, the rear boundary had amplified to an "S-like" shape, and the "cold cloud shield" was approaching a comma shape. (See **Figures 49c, 50c**, and image on this page.) By our definition, the transition phase ends when the "cold cloud shield" pattern reaches the "cusp" stage. This was defined on page 133. From hindsight in this case, we know that the "cusp" stage was attained between 1200Z and 1500Z. After the "cusp" stage, the surface low center is usually located just under the rear boundary of the "cold cloud shield", near the intersection of that boundary and the upstream axis of maximum winds. Using water vapor imagery, the intersection of the boundary and the "K" band is a reliable indicator. Applying the "K" band intersection concept with the 1130Z water vapor image, our technique would have estimated the surface low position at the northeastern corner of North Carolina, south of Norfolk, Virginia. However, the system has not yet reached the "cusp" stage, and the rule is not intended for use prior to that. Note that the surface low center was located just off the New Jersey coast at 1200Z. This is a relatively large distance from the rear edge of the "cold cloud shield". The following factors were involved. The system had entered its "very rapidly deepening" phase at 0900Z. During such periods of storm development, the cloud patterns change very rapidly with time, and are usually moving rapidly. In this case, a middle level boundary (with cloud and moisture tops near 600mb) was present to the rear of the "cold cloud shield" boundary. By 1200Z, a cusp apex had formed on that emerging boundary at "C" over west central Virginia. Although this was, indeed, the initial cusp formation, the angle at the apex had not reached 90° or less; therefore, it did not qualify as the "cusp stage" by our definition. A cirrus cloud band was coincident with the concave moisture boundary of the "cold cloud shield". By 1230Z (**Figure 50c**) a break had formed in this cirrus band over southeastern Virginia and eastern North Carolina. To the northeast of that break, toward the surface low center and under the jet stream zone, the high clouds were dissipating rapidly. This process of dissipation and downward vertical motion is causing the rear boundary of the "cold cloud shield" to rapidly overtake the surface low center position, at rates greater than the cloud element motions and related wind speeds. Such dissipation is a common process with many cases of cusp formation (see drawing 2, page 133).

By 1500Z, the part of the "cold cloud shield" boundary with the maximum concave curvature had accelerated northeastward nearly to the surface low position, and, cusps had formed on the "cold cloud shield" boundary and the middle level boundary to its rear. By 1800Z, high clouds had fallen back over the middle level cusp position near New York City (see **Figure 49d**).

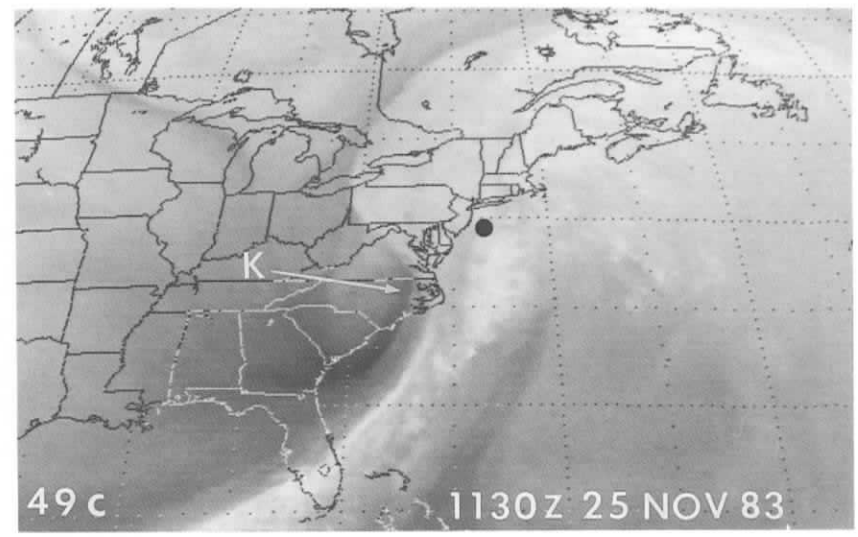

At 1200Z, the upper air system was not closed at 500mb. The open trough configuration is also present at 300mb, shown on **Figure 50d**. Notice on the water vapor imagery that the "head" boundary of the upper air system over Canada has pushed southwestward and become well defined, at "H". This has prevented the upper air ridge over the western United States from "rolling over" to the north of the trough of the eastern developing system, thereby contributing to the trough remaining open. Also, the western U.S. ridge has been blocked from building northward, and the jet stream zone between that ridge and the eastern trough is rotating counterclockwise. This type of circulation environment tends to "swing" the eastern trough around the northern low and keep it open, until its own "build-back" downstream ridge forms back around the north side.

At 1200Z, the 300mb axis of maximum winds shifts markedly to the left between the maximum concave and maximum convex portions of the high moisture boundary. The upstream and downstream axes of maximum winds nearly overlap. The wind speeds over New England in advance of the upstream segment decrease significantly, and those over West Virginia and southwestern Pennsylvania to the rear of the downstream segment increase even more markedly. This configuration is characteristic of the "open comma" system. The upper air streamlines have much less amplitude than that of the rear boundary of the cloud system. The wind directions tend to be parallel to the developing "dry slot" and parallel to the boundary along the "head" of the developing ridge, but across that portion between these features at large angles. The boundary becomes perturbed in the relative motion field of the system. In the area where the axis of maximum wind shifts to the left, significant positive vorticity advection and cold air advection are present at 500mb. As the slot forms, these become concentrated in advance of the slot. The mid-tropospheric thermal ridge "falls back" on the left side of the slot, and the upper air wind speeds decrease with time between the slot and the axis of the thermal ridge. The term "open comma" refers to the open trough condition, in which the cusp forms and falls back in the relative motion with respect to the moving system, instead of moving back with respect to the earth's surface. At 1200Z, the "cusp" and "slot" have not quite formed; the system is in a state of transition.

The 1800Z surface analysis is shown on **Figure 51b**. The low has deepened 12mb during the six hour period, and is now located under the high clouds just in advance of the newly formed dry slot. The apex of the high cloud "cusp" is located near New York City. The middle cloud "cusp" feature has apparently become covered over by the higher one. It can no longer be identified on any of the various forms of imagery available to us near that time.

d. The "Slotted Storm" Phase

By 0000Z November 26th, the surface low center has moved back over land to northeastern Maine. Although its analyzed center was nearly under the dry slot on the water vapor image, the pressure decreased another 3mb during the following three hours, reaching a minimum of 966mb at 0300Z.

Although a relatively large amplitude "build-back" ridge has formed over Quebec Province, a closed low has still not formed in either the 300mb or 500mb streamline fields. The upstream jet stream has continued to rotate counterclockwise, swinging the open trough into a northwest-southeast orientation.

On the 300mb analysis, shown on **Figure 50f**, we used the computer analysis of the isotach field at the base of the trough, since data were missing from Wallops Island and Cape Hatteras radiosonde sites. It is likely that the new speed maximum approaching the trough from the northwest over Pennsylvania had become the primary upstream jet stream branch, and had extended southeastward farther than shown. There are three reasons for this suggestion. The extension of the northern speed maximum across the trough would correlate with the presence of boundary "K2" on the 2330Z water vapor image of **Figure 49e**. There is also a dark triangular shaped area to the northeast of this boundary where it approaches the frontal zone moisture boundary. This feature, labeled "D" on **Figure 49e**, is likely a similar dark region as the "dry delta" feature shown on **Figure 32** with the "roll-over" cycle case, although this one is larger. Secondly, new convective clouds have begun to form along the frontal zone, at "V", between 38 and 45° latitude. This new line of convective clouds has formed to the rear and southward from the previously existing convective clouds along the front, and can be seen on the 0000Z enhanced infrared image of **Figure 50e**. And, thirdly, on the 0530Z water vapor image of **Figure 49f**, a bend in the curvature of the frontal boundary has developed at "B" near 36° latitude. All of these changes indicate that a new jet stream speed maximum had approached the eastern side of the trough, and that lowering surface pressure would likely be present along that part of the frontal trough just in advance of the bend in the curvature (to the north).

By 0530Z - the time of the last water vapor image - the dry slot had moved to the right of the main surface low center which began to fill slowly near that time.

It should be mentioned that during the later times of this series of images, the cloud and moisture patterns appear more elongated than normal, because of the perspective on the satellite map projection.

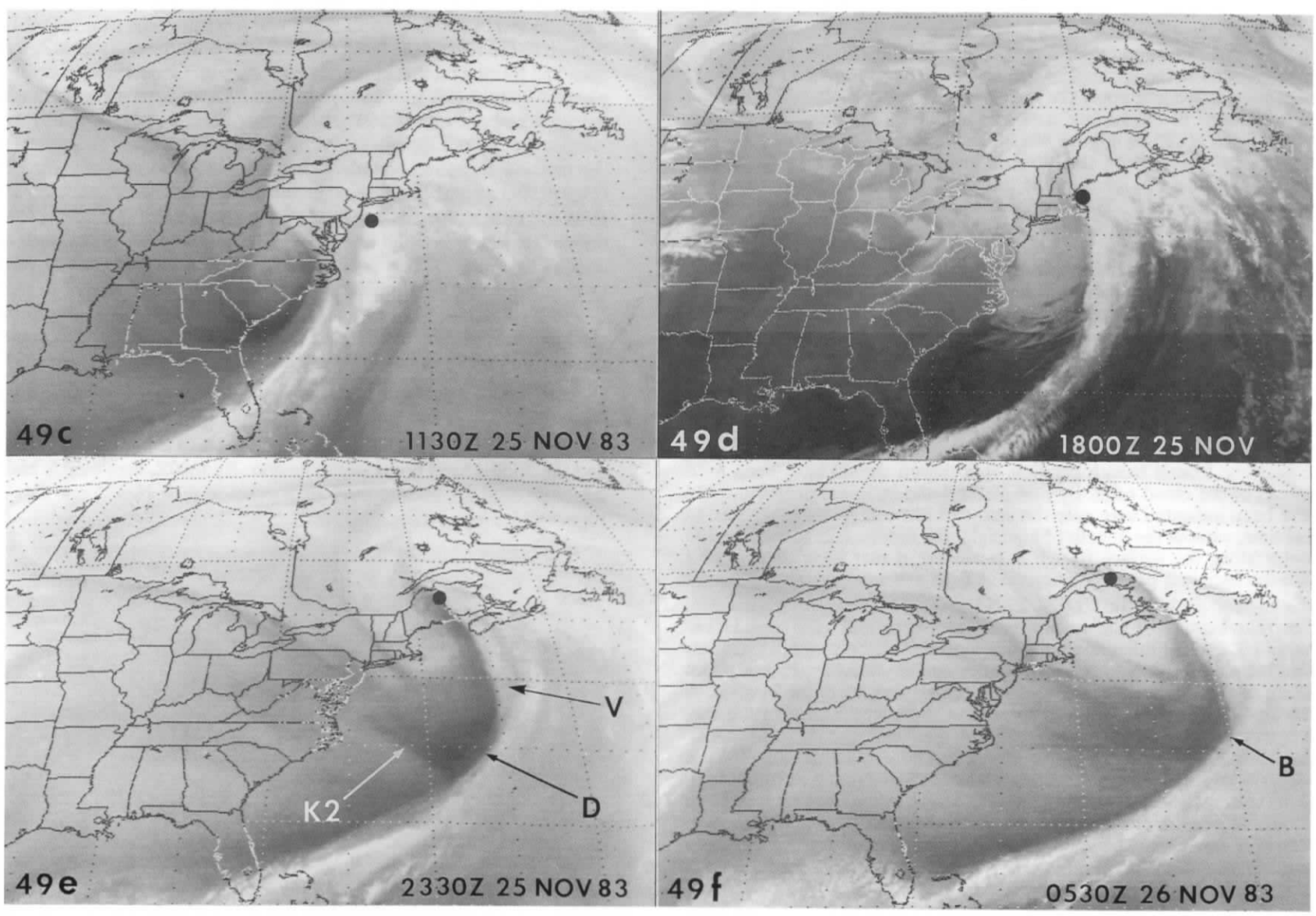

Figure 49 c-d-e-f Repeated

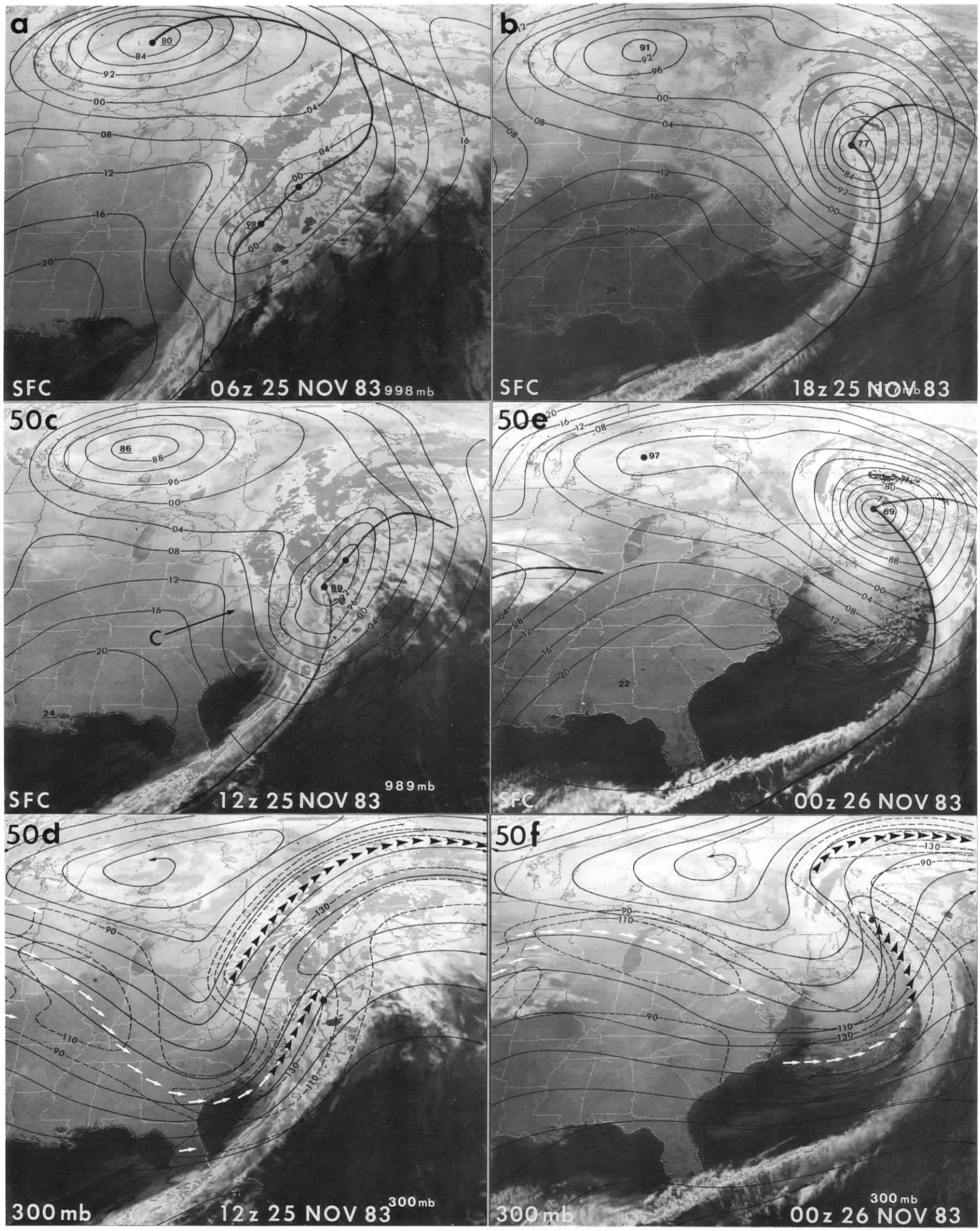

Figure 51 **INTERMEDIATE SURFACE ANALYSES WITH REPEATED PANELS OF FIGURE 50**
Top 2 Panels
51a. Surface Analysis on 0600Z 25 Nov 83 Enhanced IR Image
51b. Surface Analysis on 1800Z 25 Nov 83 Enhanced IR Image

Lower 4 Panels
Figures 50c, e, d, and **f, REPEATED**, and reconfigured for comparison to intermediate analyses.

SECTION D

MOISTURE PATTERNS OF SPECIFIC CIRCULATION SYSTEMS AND FEATURES

Finally, we are able to address some of the "simpler" questions such as: What do lows look like on water vapor imagery? How does "the jet stream" appear on water vapor imagery?

1. CYCLONES - THEIR PATTERNS ON WATER VAPOR IMAGERY

Most closed cyclone patterns observed on 6.7μm water vapor imagery are vertically deep systems, or shallow upper air systems. The exceptions are very rare, and consist of special cases at high latitudes during winter seasons where the atmosphere is very dry, and radiation from the boundary layer clouds and moisture patterns can penetrate to the satellite.

As at high latitudes, there are cases at middle and low latitudes in which closed synoptic scale cyclones of significant strength are present at the surface and in the boundary layer, without their circulations extending above that layer. These occur when rapid changes in the middle and upper troposphere cause the upper air portion of the system to accelerate rapidly away from the lower level cyclonic circulation, which has insufficient time to weaken. These "vertical separation" events are most common at subtropical latitudes, where vertically deep tropical systems moving within the easterlies suddenly encounter strong westerlies. When such shallow low level cyclones exist, they cannot be detected on the water vapor imagery.

There are other cyclonic systems which are vertically deep in the atmosphere, but have only low level clouds. Those generally are revealed in water vapor imagery.

How do lows or cyclones appear on water vapor imagery? The answer is: in many ways, or not at all. This subject has been addressed implicitly in the previous sections; however, we shall summarize and compare the various water vapor patterns of cyclones here.

a. Combination Moist-Dry Core Systems - the Most Common Condition

The moisture - or gray shade - pattern shown on **Figure 52a** is an example of one of the most common types observed. The core region of the upper air cyclonic flow is part moist and part dry. Generally, as in this case, the moist portion is relatively warm in the middle troposphere, and has "built back" around the cyclone from the downstream ridge. Although the moisture is moving back in cyclonic flow, it is associated with a thermal ridge in the middle level temperature field. Therefore, the cyclonic flow tends to increase with height on the inner border of the moist zone, and decrease with height on the outer border. In conjunction with this, the cyclonic circulation usually extends farther from the center at low levels than it does at high levels, on the moist side of the system. The dark portion is usually associated with drier cooler air in the middle troposphere, which has been advected into the system from upstream, while active sinking was in progress.

When systems are moving and changing rapidly, the light and dark portions of the cyclonic flow often correspond better to the warm and cold advection patterns than to the thermal ridge and trough.

In the case shown here, the moist portion has built back onto the west side of the upper air low. This was related to the initial orientation of the system as it developed. In many cases, in which a low is approximately half moist and half dry, the moist portion would be on the poleward side, and the dry on the equatorward side, when the development occurs within the westerlies.

The combination moist-dry pattern shown on **Figure 52b** is an example of "reverse image" type of upper air closed low. In the westerlies, these types of systems occur on moisture boundaries with the moist air to the west and the dry air to the east, and within an initially southerly component wind field. Or, without regard to compass orientation, the moist air is on the left of the wind directions and the dry air is to the right. When the perturbation forms, the moist air surges forward, and the dry air falls back.

Although we do not understand these systems well, we have observed the following. At 500mb, the moist side tended to be cool, and the dry side was warm. Over land during the warm seasons, or over warm ocean waters, convective weather tended to form under the moist portion of the system. If such a low was moving poleward along the boundary, the forward portion of the low had clear sky conditions, followed by convective weather in the rear portion.

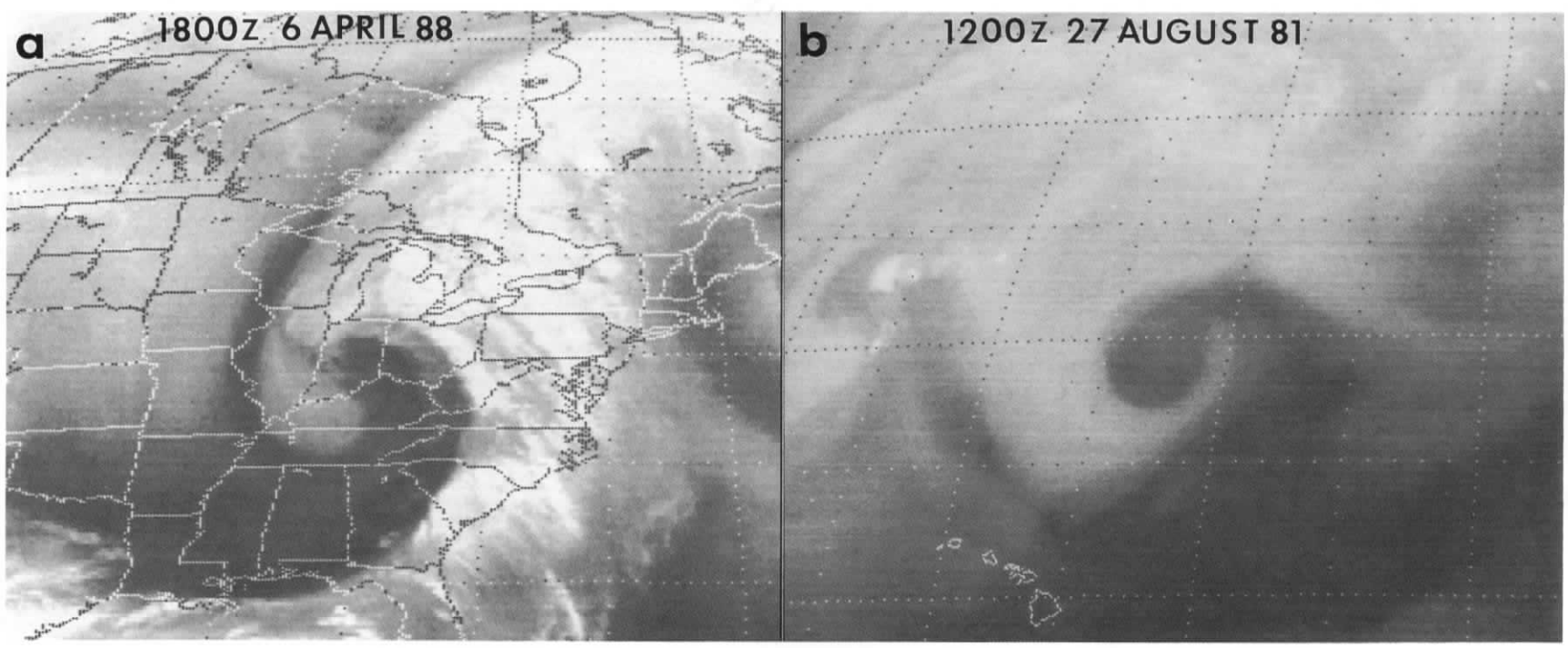

Figure 52 COMBINATION PATTERNS
Fig. 52a. 6.7μm image, 1800Z 06 April 1988, GOES West. **Fig. 52b.** 6.7μm image, 1200Z 27 August 1981, GOES West.

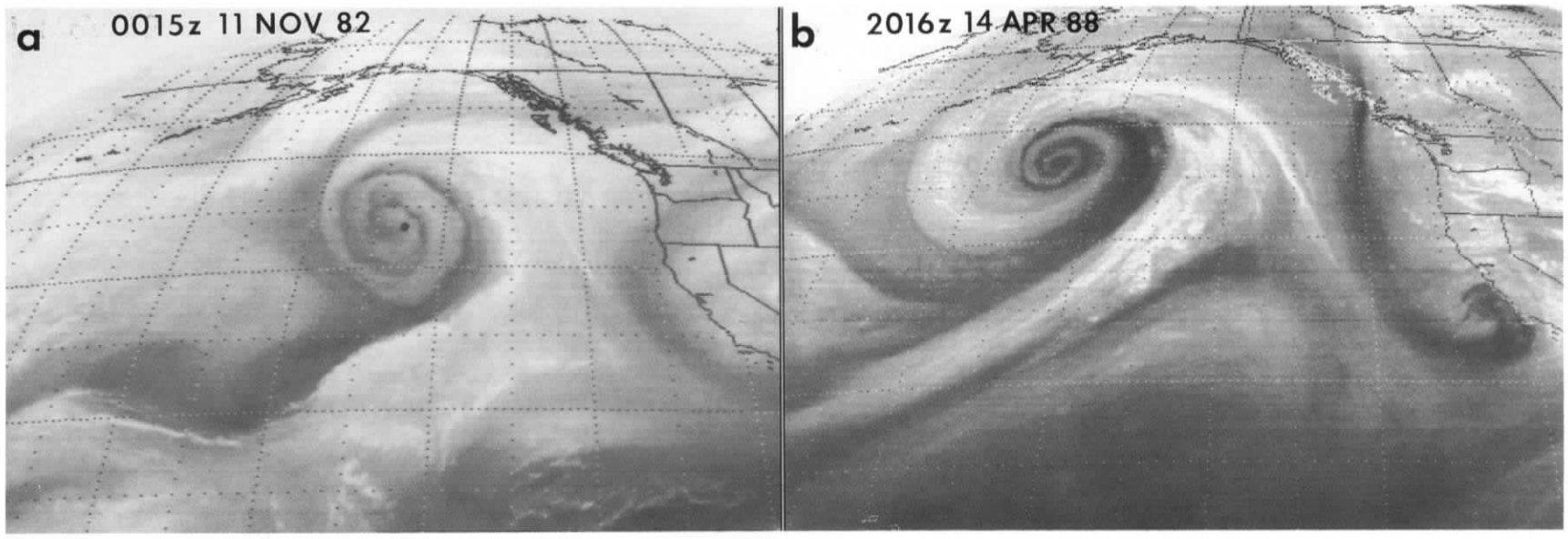

Figure 53 SPIRAL MOISTURE PATTERNS
Fig. 53a. 6.7μm image, 0015Z 11 November 1982, GOES West. Black dot at surface low pressure center.
Fig. 53b. 6.7μm image, 2016Z 14 April 1988, GOES West.

b. Spiral Moisture Patterns with Cyclones

Although these are also combination patterns, they deserve a special category for discussion purposes. Spiral patterns are observed with relatively shallow upper level lows; however, they are most common with mature phases of winter storm type systems, in which a significant "build-back" ridge is involved with the system development.

A spiral moisture pattern on water vapor imagery is an indication of the condition of the upper air cyclone. It indicates that the upper air low has closed and remained undisturbed for a period sufficient for the moisture to spiral around the center.

Whether or not a spiral moisture pattern is present with a storm system, or absent, is not well correlated with conditions of the associated surface low pressure systems. For example, we found no significant correlation between the presence of a spiral pattern and: (1) the rate of deepening of the surface low center, or (2) the minimum pressure of the surface low center. However, considering only those storm systems which did have a spiral moisture pattern, we found relationships between surface low conditions and features of the water vapor imagery.

An example of a spiral water vapor pattern is shown over the northeastern Pacific Ocean on **Figure 53a**. In this case, the moist band has spiraled two revolutions around the center. The surface low center at the time of the image was located near the black dot with a central pressure of 998mb. It had reached a minimum pressure of approximately 990mb between 18 and 24 hours prior to the image time. The spiral pattern formed primarily after the surface low had reached its minimum pressure. This has been observed with all cases we examined with adequate surface data. The spiral pattern developed after the surface low stopped deepening, and usually while it was filling significantly. However. most of those cases were over land, or just offshore.

Another example is shown on **Figure 53b**. In this case, also over the northeastern Pacific Ocean, the storm system was very intense. Although the available surface data were relatively sparse and poorly located with respect to the center, there is little doubt that the surface low deepened very rapidly and reached a minimum central pressure of at least 950mb.

In this case, the moist band has also spiraled two revolutions around the center. The primary differences between this pattern and the first one, are that this spiral pattern is much better defined, and formed more rapidly. This spiral completed two revolutions in approximately 12 hours; the pattern of **Figure 53a** required 24 hours to complete two revolutions.

This relationship is consistent with other cases. Many rapidly deepening storms with low minimum pressures do not develop spiral water vapor patterns. When a spiral pattern does develop with an intense storm, it is likely to form more rapidly and be better defined. The mere fact that a spiral pattern is observed on water vapor imagery, it is not an indication of an intense storm system. If that pattern is very well defined and spiraled rapidly, it is an indication that the associated storm is intense.

The most revolutions around a center that we observed were three. Usually, by the time the moisture and adjacent dry slot complete between one and two revolutions, the edges become irregular, and the moist portions merge with the dry portions. Thus, the patterns lose definition, and change to a relatively uniform core area with medium to light gray shades. Within the limitations of the radiosonde network, we have observed a correlation between the spiral identity and the mid-tropospheric temperature field. While the spiral pattern is well defined and rotating around the low, there are significant temperature differences within the cyclonic wind region occupied by the spiral. In some cases, when the system is large with respect to the density of the radiosonde network, the temperature differences form a spiral pattern of thermal ridge and thermal trough. In other cases, the differences are present, although the density of reports is not sufficient to analyze the thermal pattern. During the evolutions of the systems, as the spiral pattern loses identity on imagery and forms a uniform gray shade; the associated mid-tropospheric temperature differences within the core area of the cyclone also decrease. The thermal ridge and thermal trough spiraling around the low in the middle troposphere lose their identity, apparently by mixing or radiation effects. The core regions of the upper air lows evolve to relatively homogeneous moist cool conditions after the spiral patterns dissipate. This implies that a very strong storm system, with relatively large temperature gradients and rapid rotation, would be more likely to develop a well defined spiral pattern with greater revolutions before mixing is able to modify the system's core.

Note that the mid-tropospheric thermal ridges and thermal troughs spiraled around a cyclone were not necessarily coincident with the spiraled light and dark gray shades on the imagery. In many cases, the moisture spiral correlated better with temperature advection patterns. In other cases, the vertical location of the moist layers was a factor affecting correlations with analyzed temperature fields.

Clouds with middle level tops, primarily altostratus, are often observed with the moist bands of spiral patterns. They are usually present over only a part of the pattern at a given time, and are very difficult to identify without infrared imagery. Therefore, they are not likely a significant factor in the definition of the spiral patterns on the water vapor imagery.

We must emphasize that many spiral patterns on water vapor imagery form after the associated surface low pressure system has stopped deepening. In fact, it was observed, that the spiral patterns commonly developed after the surface low had nearly filled. The upper air cyclone continued to intensify, or maintain its strength. Other observed spiral patterns occurred with upper air lows that had no surface low developments.

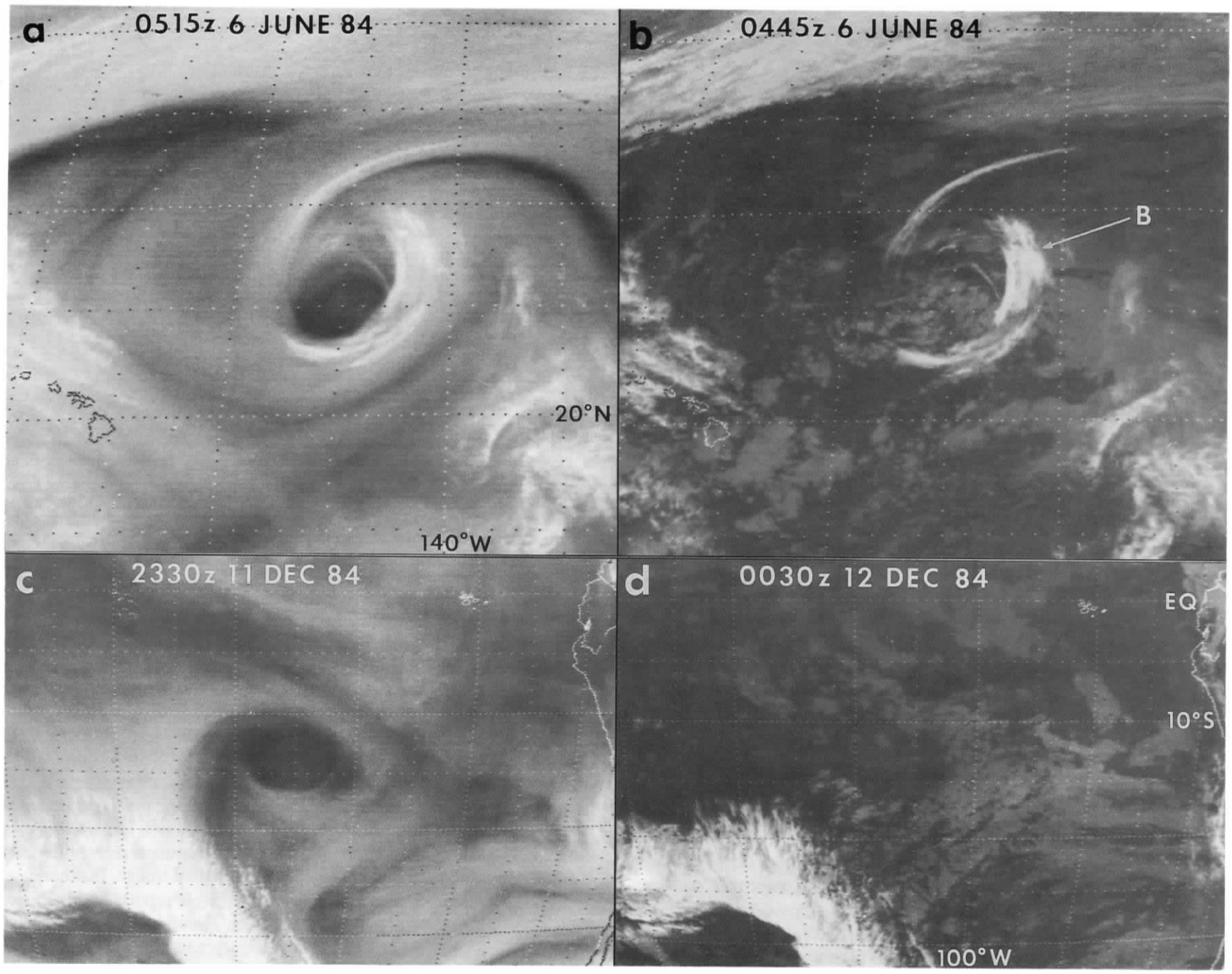

Figure 54 DARK CORE - CUT-OFF LOW PATTERNS
Fig. 54a. 6.7μm image, 0515Z 6 June 1984 GOES West. **Fig. 54b**. 11.2μm infrared image, 0445Z 6 June 1984.
Fig. 54c. 6.7μm image, 2330Z 11 December 1984, GOES Central. **Fig. 54d**. 11.2μm infrared image, 0030Z 12 December 1984.

c. Dark or Dry Core Cyclones

The core regions of some synoptic scale cyclones appear dark on water vapor imagery, relative to their surroundings. Most of these are closed upper air cyclones which formed without the development of an adjacent "build-back" ridge, and without surface cyclogenesis. Cyclones with associated surface cyclogenesis usually have well formed "build-back" ridges with significant development of cold clouds. The related upward vertical motions contribute high level moisture patterns in the upper air cyclonic flow.

Two examples of dark core upper air cyclones are shown on **Figure 54**, with both water vapor and infrared images. They represent two classical types of dark core systems. The cyclone shown on **Figures 54a** and **54b** is of the type formed from a pure "roll-over" process. The upstream ridge rolls over the base of a trough, with little or no "building back" from the downstream ridge side. Commonly, the clouds with such lows are similar to the case shown here. Bands of cirrus and some relatively high altostratus surround a core region free of middle and high clouds. Often, crescent shaped regions of thicker clouds form and rotate around the low in the left front quadrant of a speed maximum within the circulation field. The clouds at "B" on **Figure 54b** are of that type. Such dark core upper air lows are sometimes revealed by a pattern in the low cloud fields, although the cyclonic circulation does not extend downward to those levels. Apparently, the presence of the cold air in the lower middle troposphere changes the characteristics of the inversion at the top of the marine layer. In the case shown, the low clouds under the dark core form a distinct cellular pattern of stratocumulus, which is unique from the surrounding areas.

The system, shown on **Figures 54c** and **54d** west of South America, formed at the equatorward end of an inside boundary. Upper air lows of this type with dark core regions often form as the high closes. The upstream ridge moisture often "hooks" cyclonically around the closing low to the poleward side, with no ridge building on its local eastern side. In the case shown, that moisture has rotated around to the southwest side. No middle or high clouds are present with the system shown, but a rounded clear region is present under the dark core, as a pattern in the marine layer cloud field.

In some cases, relatively dark core regions do occur when the system development included a "build-back" ridge and surface cyclogenesis. An example over the central United States was shown on **Figure 47**. Although the ridge built to the cusp stage, and weak surface cyclogenesis occurred; the "roll-over" upstream ridge dominated the process, preventing the "build-back" ridge and surface cyclogenesis processes from advancing beyond the cusp stage. Although some high level moisture did rotate around the "cut-off" low, the core area remained relatively dry in the upper middle troposphere.

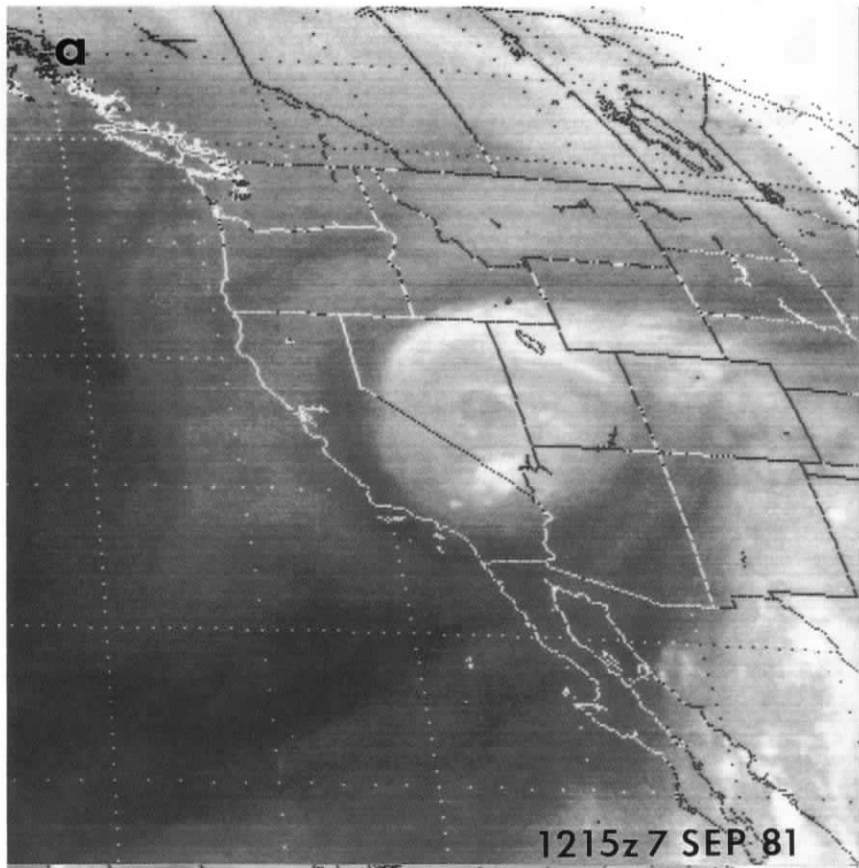

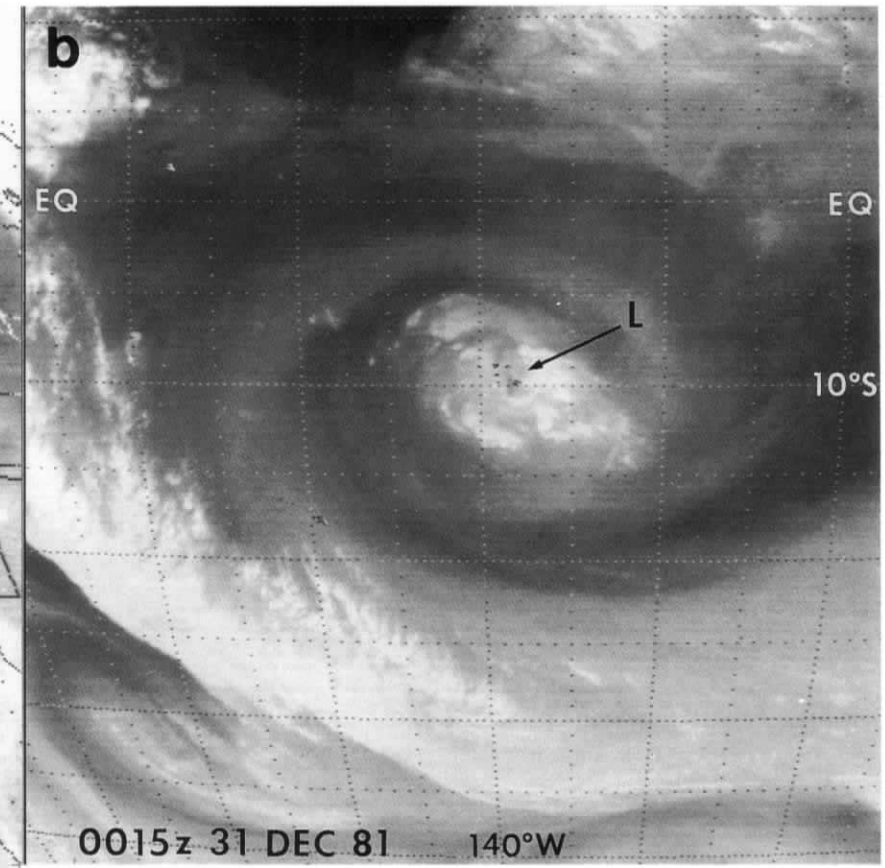

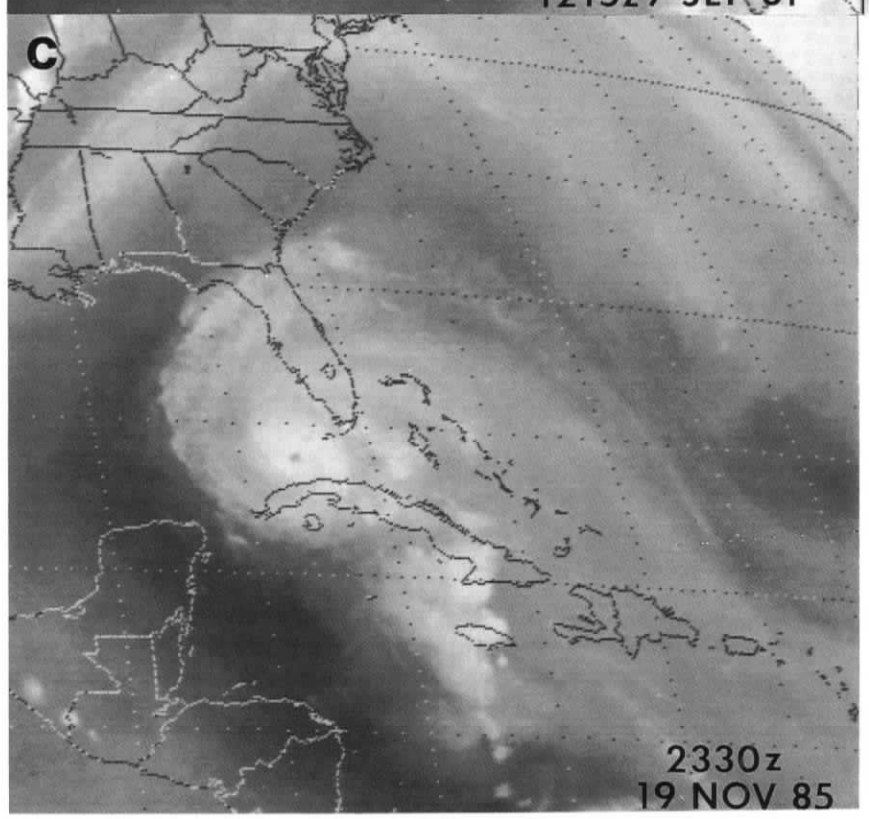

Figure 55

MOIST CORE PATTERNS
Fig. 55a. 6.7μm image, 1215Z 7 September 1981, GOES West.
Fig. 55b. 6.7μm image, 0015Z 31 December 1981, GOES West - southern hemisphere view.
Fig. 55c. 6.7μm image, 2330Z 19 November 1985, GOES Central.

Most cyclones with dark synoptic scale core regions are "cut-off" lows. The relative darkness of the core on the water vapor imagery depends upon the moisture conditions of both the original trough, and the adjacent ridges. When a portion of a relatively dry trough becomes "cut-off", and surrounded by high cold ridge moisture, the residual conditions of the core cause it to appear darker. However, in many cases, this residual dryness in the upper middle troposphere is not the only factor. Often, during the "cutting off" phase of the low formation, darkening with time occurs in the core region. Although the vertical layers involved and the overall depths of the closed cyclonic circulations vary considerably from case to case, the thermal structures of "cut-off" lows consist of a warm core cyclone overlying a cold core portion. On the average, the reversal of the baroclinic zone occurs near 400mb. During the early part of the "cut-off" low stage - as the system is forming, the upper warm portion becomes warmer and extends downward, lowering the level of the thermal gradient reversal. During this time, the core region is likely to become darker with time on the water vapor imagery. We do not adequately understand why this darkening occurs. Since the systems are not symmetrical and not totally stationary, the changes with time of the three dimensional thermal structure are very difficult to analyze from standard radiosonde data. The readers may make the same assumptions that we can.

d. Light or Moist Core Cyclones

These can be divided into three basic types. In the most common type, the moisture "building back" from the downstream ridge dominates the pattern. Usually this moisture "builds back" in a thermal ridge portion of the cyclonic flow, with colder drier air entering the circulation from the other side. With time, the moist portion then dominates the cyclonic core region.

An example is shown on **Figure 55a** over the western United States. In this case, at 500mb, the moist core region is colder than the surrounding ridge. The upstream ridge was warm and unusually dry.

The overall temperature configurations of moist core cyclones vary greatly depending upon the type of environment and the evolution of the system. In most cases, the lighter gray area of the core is warmer than the narrow remaining darker part of the cyclonic flow, cooler than the downstream ridge, and equal or slightly warmer than the upstream ridge. However, the relative temperature differences of these different parts of the system structure vary from case to case.

A second type of moist or light core cyclone is illustrated on **Figure 55b**. In this case, over the southern Pacific Ocean, the "cut-off" low at "L" has an area of deep convective clouds under the core region. The clouds are referred to as "core convection". Core convection is most often observed with upper air cold lows over warm ocean waters, especially when the low moves toward warmer sea surface temperatures. In this case, the low moved northwestward over warmer water. The 500mb temperatures within the core area ranged from -10°C and -12°C, compared to -4°C to -6°C over the surrounding areas.

In such cases, the deep convective clouds which form within the relatively unstable air under the cold core, cause the core region to become more moist with time, as moisture accumulates at upper levels from the upward vertical motions. Core convection occasionally occurs over land during summer seasons and over tropical latitude continents. In those cases, it forms and dissipates diurnally, but the moisture tends to accumulate aloft.

The third basic type of moist core cyclones on water vapor imagery is the tropical cyclone. An example is shown on **Figure 55c**. Although the outer portions of the synoptic scale rounded pattern of most tropical cyclones consist of high level ridges wrapped around the pattern, the inner core regions surrounding the eye are cyclonic through a very deep vertical layer.

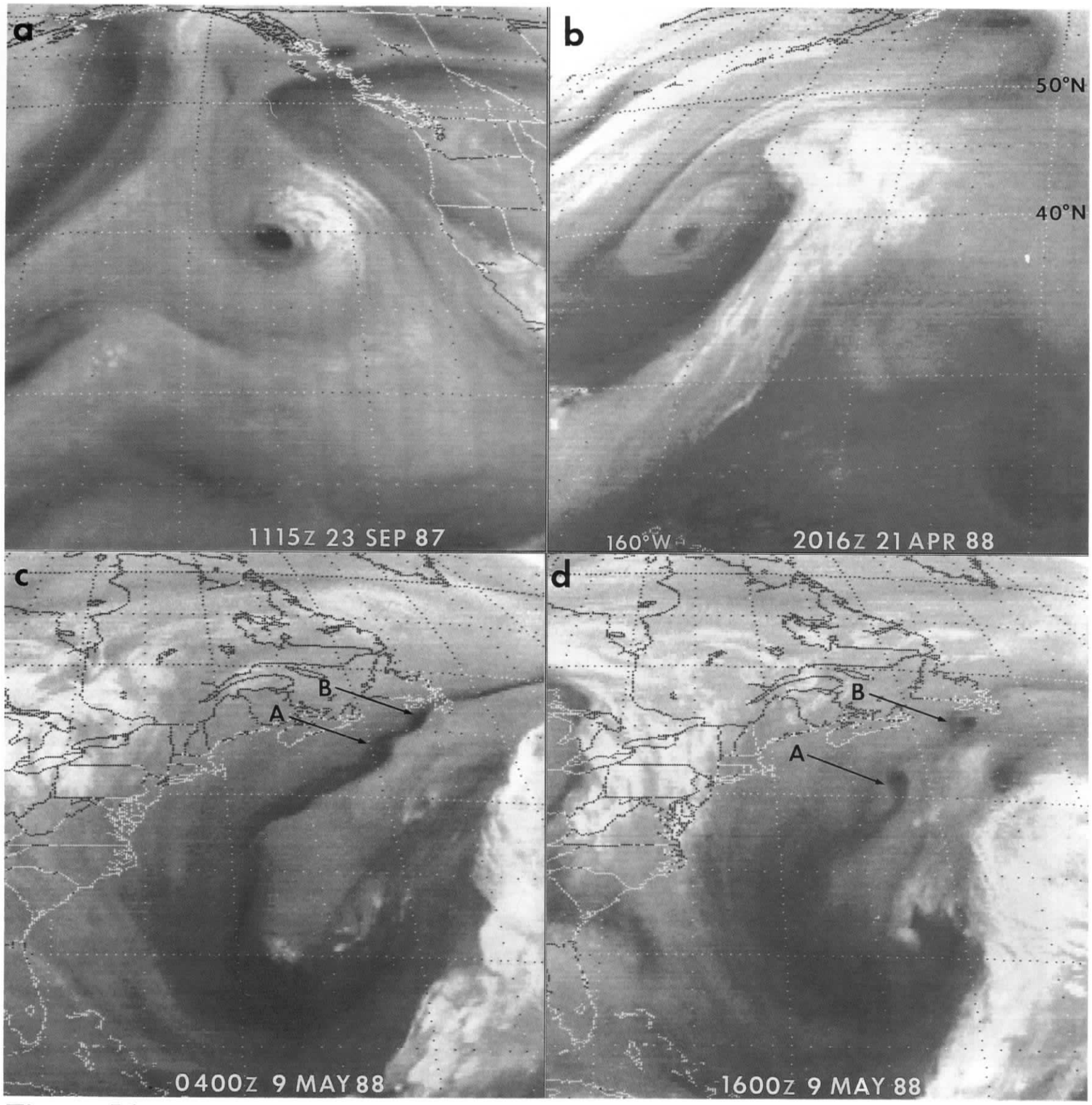

Figure 56 **VORTICITY EYE FEATURES**
Fig. 56a. 6.7μm image, 1115Z 23 September 1987, GOES West.
Fig. 56b. 6.7μm image, 2016Z 21 April 1988, GOES West.
Fig. 56c and 56d. 6.7μm images, 0400Z and 1600Z 9 May 1988, GOES East.

e. "Vorticity Eye Features"

Another type of dark cyclonic core feature has been observed relatively frequently on water vapor imagery; however, these are of sub-synoptic or mesoscale. We refer to them as "vorticity eye features". They consist of very dark small circular areas, and generally form within larger scale upper air cyclonic circulation systems. Because of their size, upper air data are not sufficiently dense for reliable analysis; however, the features appear to be located near the centers of mid-tropospheric cyclonic vorticity maxima.

A relatively large example is shown on **Figure 56a** over the northeastern Pacific Ocean at 40°N. In this case, the dark core is approximately 100 miles across. The core is associated with a "cut-off" low system.

Another example is shown on **Figure 56b**. In this case the dark core feature is within the cyclone of a winter storm type system. The core formed on the water vapor image after the surface low reached its minimum pressure. It remained relatively well defined on the images for a 72-hour period, with an average diameter of approximately one degree of latitude. Other cases have been observed to last 12 to 18 hours at diameters ranging from 15 to 20 miles.

Similar eye features often form when upper air moisture boundaries around a cyclone weaken, become perturbed, and break down into cyclonic eddies. An example, showing such formations, is shown on **Figures 56c** and **56d**. On the first image, a cyclonic system over the western Atlantic Ocean has weakened, and the boundary on the northwestern side of the "head" moisture pattern has become perturbed. The perturbations at "A" and "B" formed eddies with dark core features. These are shown on another image 12 hours after the first, on **Figure 56d**.

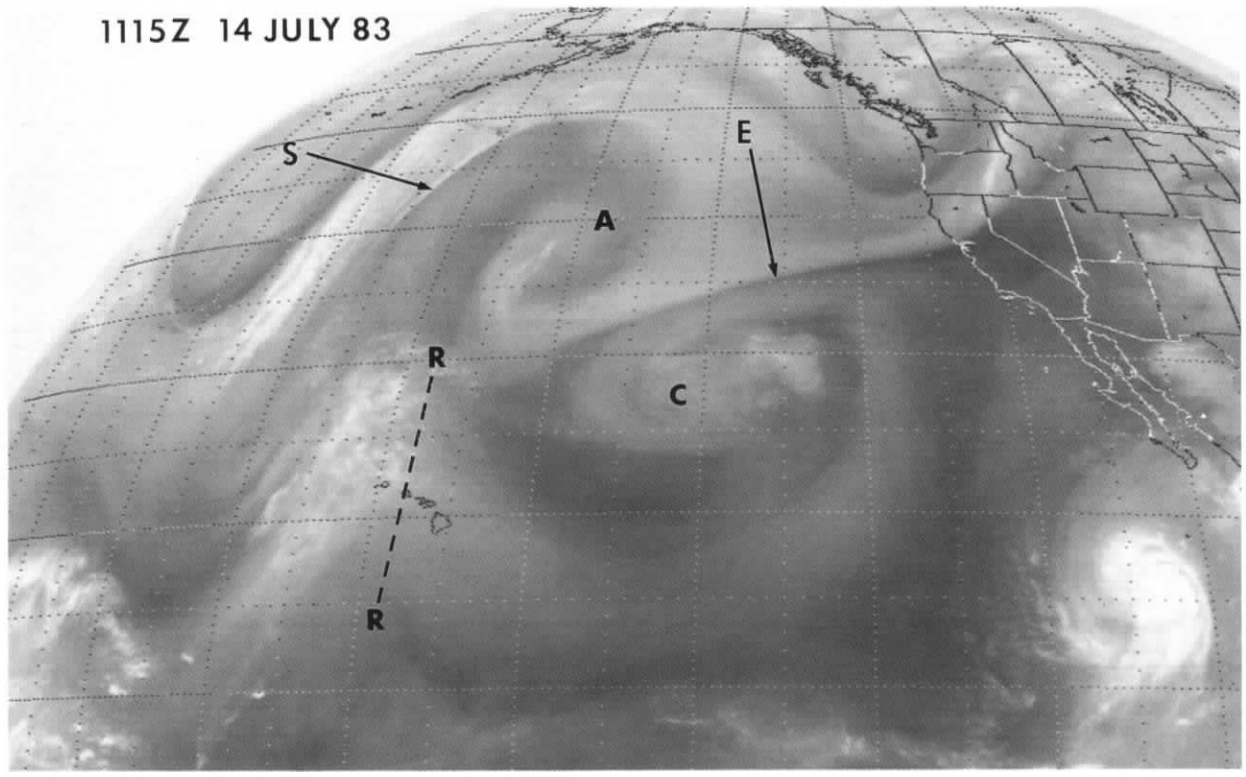

Figure 57 ADJACENT ANTICYCLONE AND CYCLONE PATTERNS
6.7μm image, 1115Z 14 July 1983, GOES West. Dashed line "R-R" - open ridge axis.

The eye features appear to be upper air mesoscale systems with active sinking maintaining the dry core region. Although we do not sufficiently understand the features, they are commonly observed; and may prove to be of some practical significance. With imagery observed at one hour interval time-lapse motion, the dark cores appeared to form at locations with maximum cyclonic rotation. When observed over the continental data network, with surface and upper air analyses, they appeared best related to the 500mb vorticity maxima, although their small size prevented reliable analysis. In most cases, the cores formed by moisture encircling an adjacent dry area or the end of a slot. However, their relatively long existence, compared to the small size, implies active sinking is involved rather than simply residual dry air.

2. ANTICYCLONES AND RIDGES

The water vapor image patterns associated with anticyclones and ridges are as variable as those with cyclones and troughs. Low level "cold core" highs are generally not revealed explicitly on 6.7μm imagery, although their positions can sometimes be inferred by upper air features.

Generally, the upper air ridges and anticyclones tend to have lighter gray shades than the troughs and cyclones. Frequently with upper air ridges, the tropopause is high, cold, and has a distinct temperature minimum. Moisture from upward vertical motion spreads within the high cold layer; and, cirrus clouds tend to spread and persist. However, with closed anticyclones, the gray shades are often similar to those of adjacent upper air cyclones. The circulation system must be identified by the pattern. On **Figure 57**, a closed anticyclone was centered near "A" in the 250mb wind field, to the north of a closed cyclone at "C". The gray shades of the moisture moving around the anticyclone are only slightly lighter than those of the moisture around the cyclone. Within the upper air easterly flow between "A" and "C", a well defined boundary is present at "E". The moisture on the north side of "E" is likely significantly higher and colder than that to the south, although the gray shades are only slightly lighter. Although it has become nearly stationary at the time of the image shown, boundary "E" was a "return moisture" boundary.

Also on **Figure 57**, there is an open upper air ridge system over the Hawaiian Islands. The ridge axis in the 250mb wind field is shown by dashes. The moisture pattern is typical of open ridges. On the upstream side of the ridge axis, the moisture is vertically deep, and high clouds are common. On the downstream side the gray shades on the image darken gradually downstream. The middle troposphere is usually dry, with high level moisture decreasing in vertical depth downstream.

A discussion of different types of water vapor image patterns observed with upper air ridges and anticyclones follows. Since many examples were present on the figures of previous sections, we shall refer to those, adding new figures only when necessary.

a. Closed Anticyclones

An example of a closed upper air anticyclone was shown on **Figure 57** with its 250mb streamline center near "A". The presence of a well defined "inside boundary", at "S", is an indication on the imagery that the system is closed.

When upper air anticyclogenesis occurs, it is common that darkening occurs in the region where the upper air winds rotate anticyclonically with time. This usually begins on the southeast portion of the amplifying upper air ridge (northeast portion in Southern Hemisphere); then moves westward as darkening continues and forms the "inside boundary". The region of drier air often rotates anticyclonically around the western side of the high, forming a spiral pattern with the adjacent moisture. Generally such spiral patterns are not as well defined as those with upper air cyclones: and rarely complete more than one revolution of the center before losing their identity. The spiral process is slower, as the associated upper air wind speeds are significantly less, than those with cyclones.

An example of an upper air anticyclogenesis was shown and discussed in Section B-2. The associated water vapor imagery of the resulting anticyclone are illustrated with upper air analyses on **Figures 20** and **21**. As discussed in that case over the radiosonde network, the moisture moving around the high within the easterlies was generally at high levels, with dry air in the lower middle troposphere. In many cases of spiraled moisture patterns with cyclones, the vertical moisture distribution is reversed. The air is generally dry in the upper troposphere; and the moist bands on the imagery reveal moisture, or higher levels of moisture, in the lower middle troposphere. However, with cyclonic spiral patterns, there appears to be much more variability in the associated vertical moisture distributions than with anticyclones.

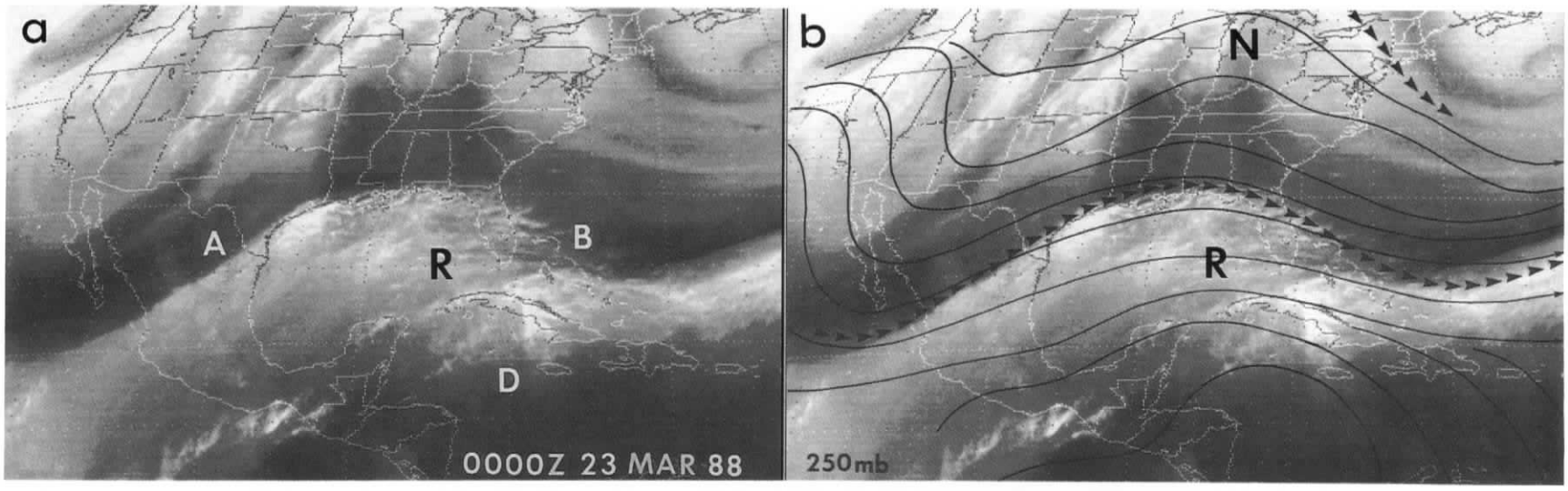

Figure 58 BASIC RIDGE PATTERN
Fig. 58a. 6.7μm image, 0000Z 23 March 1988, GOES East.
Fig. 58b. Same image with 250mb analysis. Streamlines - solid lines. Axes of maximum 250mb wind speeds - arrowheads.

b. Open Ridges

Basic Convex Poleward Boundary

The moisture pattern labeled "R" on **Figure 58** is associated with an open upper air ridge system. The poleward side boundary of the moisture regime is well defined with a convex curved shape. The following features are typical of such ridge systems. The moisture boundary is coincident with the jet stream axis of maximum winds. The western upstream segment of the boundary, labeled "A", is along the 250mb axis of maximum winds; but, those features are not parallel to the streamlines. The boundary and the axis of maximum winds shift to the left along the streamlines in the downstream direction (see **Figure 58b**). The eastern downstream boundary is angled across the flow and has a ragged edge of cirrus cloudiness. The edge is parallel to the axis of maximum winds, which shifts to the right in the downstream direction.

In this case, the gray shades on the southern side of the moisture regime darken gradually in the equatorward direction, with a ragged cirrus edge at "D". Some open ridge moisture regimes do have a well defined boundary on the equatorward side, in addition to that on the poleward side. An example will be shown.

Note on the streamline pattern of **Figure 58b**, that the anticyclonic curvature is present from the western Caribbean Sea northward to the Great Lakes. From the streamlines or height contours alone, a single ridge is suggested. A second ridge, "N", is present in another jet stream branch at higher latitudes. The two upper air ridge systems, labeled "N" and "R", are in phase at the time of the image and analysis. They were moving at different speeds; one was amplifying and the other dampening. On the water vapor image, the separation of the ridges is vividly shown by the well defined moisture boundary. The ridges were separated by the jet stream axis along boundary "A-B", and by significant features of the vorticity, temperature, and wind speed fields.

Split Ridges - Apex on Poleward Boundary

The poleward side boundary of the moisture regime of **Figure 58** has a convex curvature on both its upstream and downstream segments. The two parts, together, form a generally arched shape boundary on the moisture regime. Another common type of poleward side boundary associated with open ridge systems involves a "pointed shape" or "apex" on the boundary. Often, the cold high clouds and moisture patterns form a "delta" or triangular shape with the apex on the poleward side. This type of corner or apex on the poleward sides of ridge moisture patterns is related to a col region in the upper air winds with four associated circulation systems. Consider the drawing of **Figure 59a**.

The shaded area represents cold high clouds and moisture that would appear as very light gray shades on a water vapor image. There are two ridges involved. The delta shaped moisture regime is associated with the southern "base ridge", labeled "RB" on the drawings. The ridge to the poleward side is labeled "RP". There are also two troughs labeled "TW" to the west and "TE" to the east. The streamlines represent flow in the upper troposphere. In many cases that general flow pattern would be present through a relatively deep layer of the middle and upper troposphere. The associated axes of maximum winds are indicated by arrowheads. When a corner or apex forms on the poleward side of the base ridge moisture regime, as shown, a col is usually present near the apex; and, the jet stream is "broken" into two branches along the upstream and downstream sides of the triangular moist pattern. Sometimes, a weaker high level jet stream zone remains between the two branches. This would be to the south of the apex with an anticyclonically curved shape.

One of the most common types of delta shaped moisture regimes occurs during the "cusp stage" of cyclogenesis. In those cases, the two boundary segments forming the apex have the same sign of curvature, as in the drawing of **Figure 59b**. With that configuration, the upstream side of the moisture regime "A" is concave, and the downstream side "B" is convex (from the moist side perspective). An excellent example of a "cold cloud shield" in the cusp pattern was shown as **Figure 47f**. The best pattern occurred at 1730Z, between radiosonde times. However, the relationship to the upper air analyses before and after the cusp stage were shown on **Figures 47e** and **47g**, indicating the common patterns.

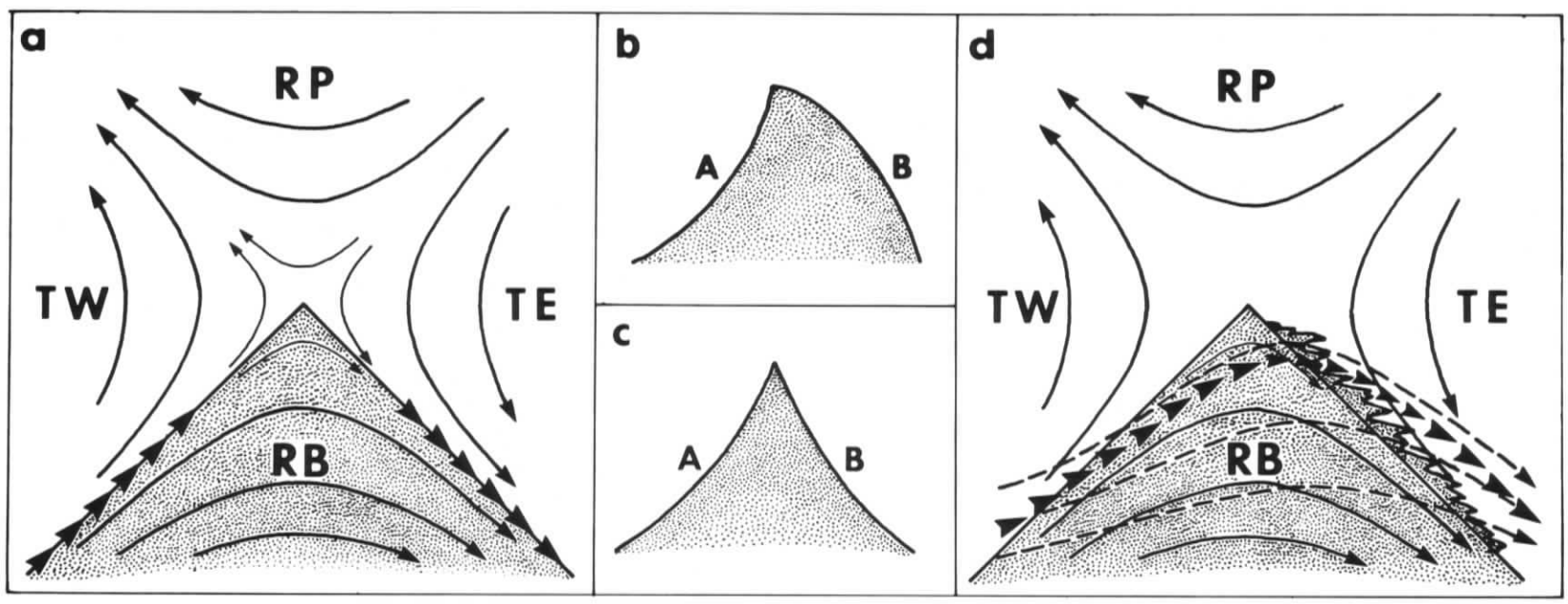

Figure 59 MODEL DRAWINGS - DELTA SHAPED OPEN RIDGE PATTERNS

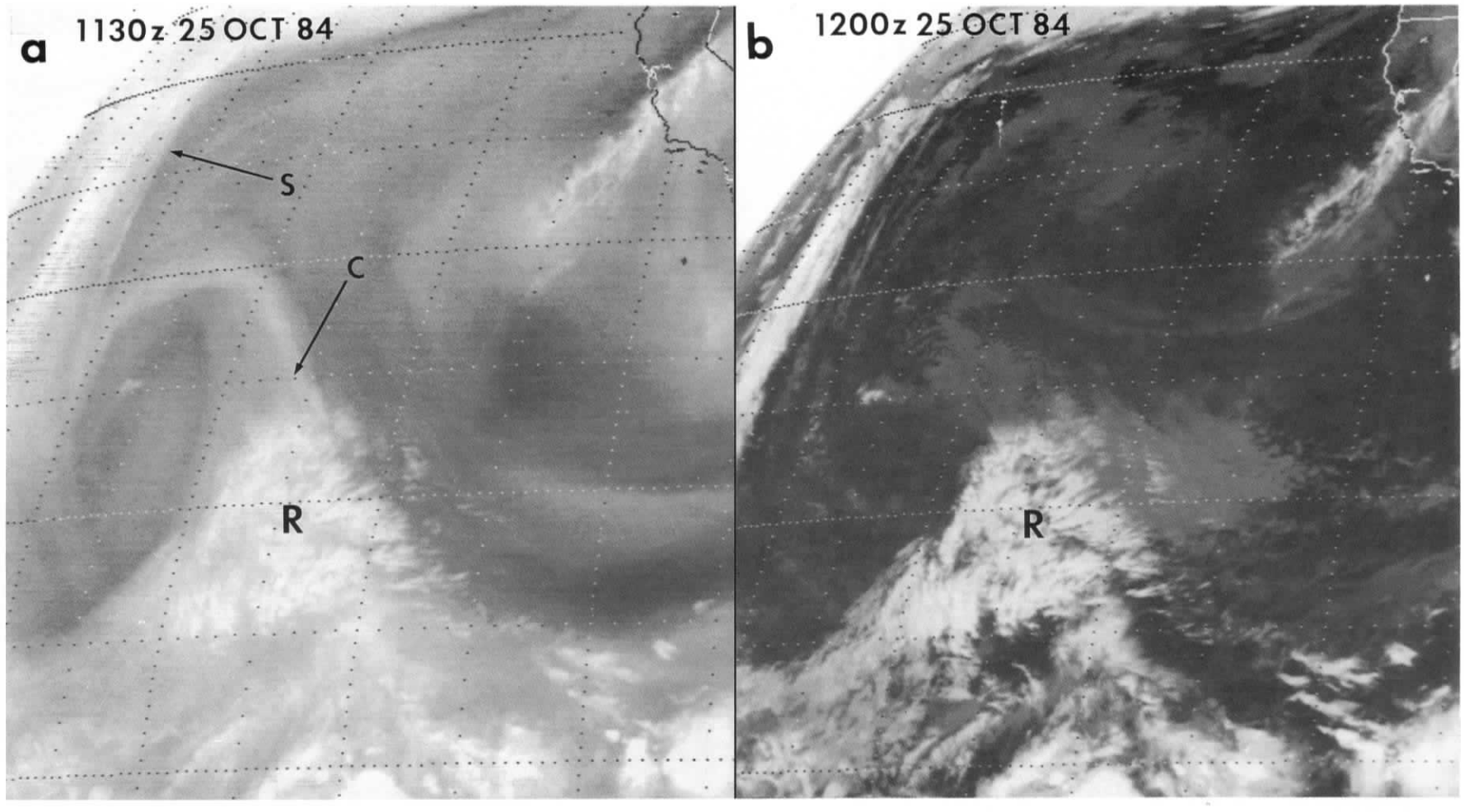

Figure 60 **SUBTROPICAL DELTA SHAPED RIDGE PATTERN**
Fig. 60a. 6.7μm image, 1130Z 25 October 1984, GOES Central.
Fig. 60b. 11.2μm infrared, 1200Z 25 October 1984.

We are aware of two other situations in which delta shaped moisture regimes are commonly present with base ridge systems. Both situations involve the basic set of four circulation systems indicated on the drawing of **Figure 59a**. Also in both situations, the eastern cyclonic circulation system (labeled "TE" on the drawing) is larger and stronger than with the cyclogenesis cusp stages. As a result, the eastern boundaries of the moisture regimes are often concave shaped; and, the patterns may appear similar to the drawing of **Figure 59c**.

One of the two common situations occurs at subtropical latitudes on the equatorward sides of the main polar jet stream zones. In such cases all of the four circulation systems (indicated on **Figure 59a**) are present; however, the two cyclonic circulations are often poorly revealed in the satellite imagery. This is a greater problem when imagery are not available in time-lapse motion. In many cases, the western upper air cyclone or trough is revealed on moisture patterns of still water vapor imagery; but, in many cases, the only indication of the four circulation systems and related col is a delta shaped area of cold clouds and moisture. An example of a subtropical case is shown on **Figure 60**. On the infrared image of **Figure 60b**, a triangular shaped area of cold clouds is present between 130° and 140°W, to the east of the Hawaiian Islands (labeled "R"). On the associated water vapor image (**Figure 60a**), the western cyclonic circulation pattern is relatively well defined in the moisture, in this case. However, the eastern trough is difficult to interpret on the still image. A closed anticyclone is present to the north in the "RP" location. Although this is implied by the inside boundary at "S", the eastern part of its pattern is not easily interpreted on the still image. In this case, the systems are complicated to the east side of the delta pattern. There are two short wave systems involved in the eastern trough; and, the systems are vertically out-of-phase between the middle and upper troposphere. The vertical phase aspect is a common type of complication; and, is illustrated in the model drawing of **Figure 59d**. In those situations the moisture boundary on the eastern side of the moisture regime is straight or concave in the middle troposphere. However, the flow of the upper troposphere crosses the boundary. The ridge in the upper troposphere is of less amplitude than that in the middle troposphere. In such cases, ragged cirrus cloud elements are present on the imagery across the general boundary shape. These are seen on the images of **Figure 60** and implied on the drawing of **Figure 59d** where the upper tropospheric streamlines are indicated as dashed lines. In this case, the solid streamlines would indicate the middle tropospheric flow of that portion of the circulation systems related to the base ridge. In such situations, the jet stream axis generally crosses over the base ridge moisture regime, as indicated by the arrowheads on **Figure 59d**. When a triangular shaped high cloud pattern or moisture regime is observed at subtropical locations, the delta shaped base ridge and its typical set of four circulation systems should be suspected. Other features and available upper air data may then be analyzed to complete the interpretation.

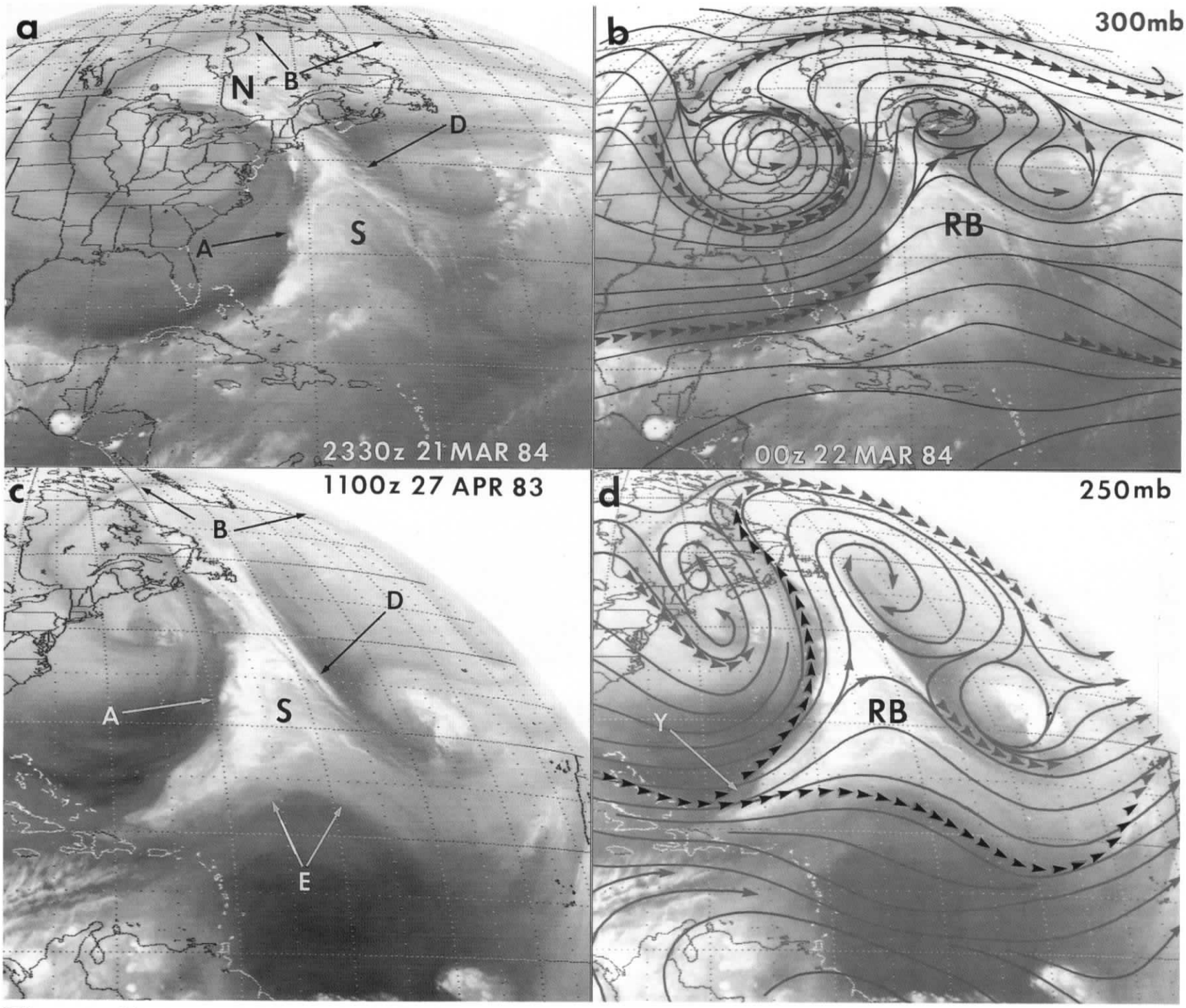

Figure 61 **SPLIT RIDGE PATTERNS WITH OMEGA BLOCKING REGIMES**
Fig. 61a. 6.7μm image, 2330Z 21 March 1984, GOES East. **Fig. 61b.** Same image with 300mb analysis.
Fig. 61c. 6.7μm, 1100Z 27 April 1983, GOES East. **Fig. 61d.** Same image with 250mb analysis.
Both analyses: solid lines - streamlines, arrowheads - axes of maximum wind speeds on the pressure surface.

The second common type of base ridge moisture regime involves the "split-ridge" systems of the "build-back" types of blocking regimes. Two cases are shown here on **Figure 61**. An initial discussion of such blocking regimes was presented at the end of Section B and illustrated on **Figure 37**. In such cases, the delta shaped base ridge moisture regime occurs after the mature phase of the blocking regime, when the three northern circulation systems have formed the "omega" pattern. In most of the cases, a true apex does not form at the poleward end of the base ridge moisture regime. Rather, a narrow band of high clouds and moisture remains, extending through the stretching axis of the cold region to the western side of the northern anticyclone. Recall that in these cases, the col forms when the northern anticyclone closes. This differs from the cusp formations associated with cyclogenesis, in which the col forms when the cyclone closes to the western side of the high level moisture regime. The "split-ridge" developments, such as these with the "build-back" evolution, are common, but less frequent than the "cusp" cases associated with cyclogenesis.

On the 300mb analysis of **Figure 61b**, the three closed circulation systems of the "build-back" blocking regime form the classical "omega" pattern; however, the fourth circulation system related to the col is also present as an open "base ridge" at "RB". In this case, a relatively wide band of high clouds and moisture extends through the col region, connecting the two primary ridge moisture patterns to the north and south ("N" and "S" on **Figure 61a**). Both the upstream and downstream sides of the moisture regime "S" have concave shapes. The upstream boundary at "A" is a type of "dry surge" boundary located between two jet stream branches. A case was shown on **Figure 7** of Section A. The concave shape of the eastern boundary at "D" is relatively common with omega configuration blocking regimes. Therefore, a moisture regime shape similar to that of **Figure 59c** is common with this type of blocking regime. Note that in this case, upper air data were insufficient to thoroughly analyze the jet stream branches associated with the two sides of moisture regime "S". There may have been stronger winds present near those boundaries.

A different case, with a similar blocking regime pattern, is shown on **Figures 61c**. Whereas on the first case (**Figures 61a-b**), there was no significant boundary on the southern side of the base ridge moisture regime, a boundary is present in that location in the second case, at "E". We have observed two situations in which such equatorward side boundaries are present with base ridge regimes. In one of those, the upstream jet stream divides into two branches, with one branch along the upstream side of the moisture regime, and the other along the equatorward side boundary. On the 250mb analysis of **Figure 61d**, a jet stream branch is indicated along boundary "E", with a split in the upstream jet at "Y". The second situation observed with boundaries on the equatorward side involves the extension of low latitude inside boundaries. In such cases, an inside boundary between easterly and westerly upper air wind regimes becomes extended poleward, then turned eastward anticyclonically into the open westerlies. The residually drier air, originally on the eastern side of the inside boundary is extended to the equatorward side of a base ridge moisture regime. In those cases, we are not aware of a jet stream presence along the boundaries involved.

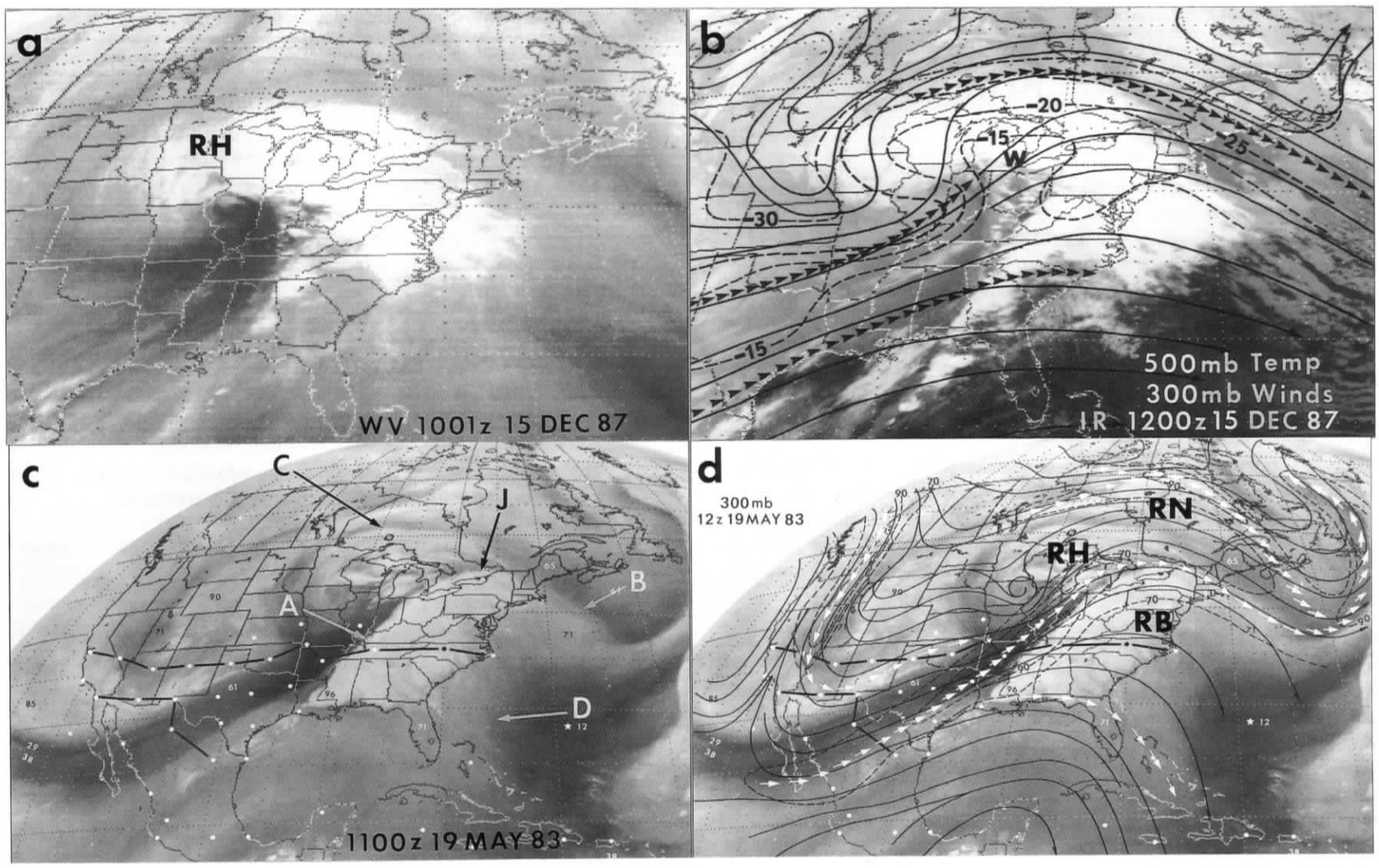

Figure 62

HEAD RIDGE PATTERNS
Fig. 62a. 6.7μm image, 1001Z 15 December 1987, GOES East.
Fig. 62b. IR Image, 1200Z 15 December 1987 with 300mb streamlines, 300mb axes of maximum winds, 500mb isotherms.
Fig. 62c. 6.7μm image, 1100Z 19 May 1983, GOES East.
Fig. 62d. Same image with 300mb analysis, Streamlines (solid lines), isotachs (dashed lines), axes of maximum 300mb winds (white arrows), cross section locations (white dots with straight black line segments) - Reference Part One **Figures 19-20.**

Head Ridges to Left of Primary Jet Axis

The "head" portions of the high clouds and moisture patterns of storm systems are a special type of open ridge system. The associated moisture regimes often have a rounded shape with a well defined boundary on the poleward side, but without a jet stream along that boundary. The "head" portion of the ridge moisture regime is on the left side (Northern Hemisphere) of the primary jet stream zone; or it is located between two jet stream branches - to the left front quadrant of an upstream branch and the right rear quadrant of a downstream branch.

Consider the system shown on **Figures 62a** and **b**. The analysis on the infrared image is a combination of two levels: 300mb streamlines and axes of maximum winds are shown with 500mb isotherms. The primary upstream branch of maximum winds extends from the southwest to northern Indiana. That portion of the cold clouds and moisture to the left of that jet stream branch is in the "head" position. It has "fallen back" or "built back" to the left side of the strong wind zone and associated region of dry air indicated by the dark area on the water vapor image of **Figure 62a**. Note that the portion of cold clouds and moisture is dominated by a thermal ridge at 500mb, and by anticyclonically curved flow at 300mb.

The upper air wind fields associated with the head portions of storm systems vary considerably. This variation is dependent upon the type of cyclogenesis involved, and the stage of evolution of individual cases because of the rapid changes with time during the cyclogenesis process. However, the head areas are usually associated with an area of minimum values of vorticity and a thermal ridge in the middle troposphere. In many cases, a thermal trough in the upper troposphere will be present over the thermal ridge. This condition is common when a portion of the "cold cloud shield" "builds back" after undergoing a cusp evolution, and especially so when thick cold clouds and precipitation are present in the head area.

Although not an application for water vapor imagery, it is worth noting that significant snowfall is common under the head ridge portions of storm systems, because the precipitation falls into equatorward flowing cold air at the surface layer.

Another example of a head ridge pattern is shown on **Figures 62c** and **62d**. The head portion is labeled "RH" on the image with the 300mb analysis. The head moisture regime has a well defined boundary along its northern side at "C", and is separated from ridge "RB" by a well defined cirrus cloud boundary and jet stream axis from "A" to "J". Twelve hours prior to the image time, ridges "RH" and "RB" were not separated. During the 12 hour period, an area of convective clouds formed on the forward side of the trough, ridge "RB" intensified, and the jet stream broke across the ridge from "A" to "B". This isolated the portion of the ridge on the left side of the new primary jet stream zone. In such cases of jet stream branches breaking across their downstream ridges, the moisture regime associated with the head portion of the ridge to the left side of the jet axis may persist with a well defined boundary along its poleward side. It is common that any jet stream branch along the eastern side of that poleward side boundary weakens with time after the upstream jet branch breaks across the ridge. In this case, a jet stream branch had been present along the eastern end of boundary "C". That branch dissipated; and, it did so very rapidly because of a coincidental feature. Ridge "RN" over Canada was moving eastward more rapidly than the systems over the United States. As it moved into phase with the U.S. ridge systems, its warmer mid-tropospheric air tended to merge with that of ridge "RH". The thermal trough between those systems weakened, reducing the baroclinity along the eastern end of boundary "C". Time changes of jet stream zones will be discussed in the next topic; and, the case shown here will be reviewed. However, it is important to recognize the moisture regimes of head ridges, and to differentiate them from other open ridges. The boundaries along their poleward sides may persist as well defined features without a significant jet stream branch present. This is especially true during late stages of the system evolution after the head moisture regime has become isolated on the left side of the primary jet stream zone, and often deformed from its initial shape and relationship to the overall storm pattern.

3. JET STREAMS - RELATED PATTERNS ON WATER VAPOR IMAGERY

a. Introduction

One of the most effective ways of using satellite imagery for weather forecasting is to observe the structure and behavior of the jet stream zones. Changes in the jet stream may be extrapolated to predict time changes in the related weather systems, and may be compared to computer model forecasts to provide an early indication of their validity. Location of the jet stream zones and their changes with time on satellite imagery is also highly useful for aviation support, especially over areas with sparse radiosonde data, and elsewhere during situations with rapidly changing conditions. However, such applications are dependent upon accurate interpretation of the image features related to the jet stream conditions.

Many examples relating jet stream conditions to features on 6.7μm imagery have been shown in the previous sections in context with other subjects. Here we shall consider the jet stream relationships explicitly, but in a summary format - referring to figures and discussions of other sections. Some imagery will be repeated here for convenience and comparison, and some new cases will be shown.

One of the problems of relating jet stream conditions to the patterns and features of satellite imagery is that the jet stream wind fields are complex. This can be readily noted by observing sets of radiosonde data using vertical cross sections and upper air analyses. By carefully combining such wind observations with water vapor imagery in time lapse motion, we are constantly reminded that the jet stream is not a "thing", but a condition of the air. As the imagery are viewed in motion, and the patterns and features are observed moving as a fluid, constantly deforming, accelerating, and decelerating. Each 12-hourly set of upper air data can be related to this fluid motion as a temporary set of conditions - "frozen in time". The related still satellite image can then be compared to the "synoptic" upper air data using the same fluid motion perspective.

Using this perspective, even a relatively uncomplicated speed maximum moving within the jet stream zone can be seen as a condition propagating along, as the warm and cool air along opposite sides moves as a fluid with different speeds and directions - constantly changing the density gradients and maintaining continuous local accelerations and decelerations as the air responds. In addition to the horizontal deformation, vertical motions cause rapid modification of the upper air temperatures, causing large accelerations and decelerations as the air motions respond to the rearranged temperature gradients. For example, if air is warmed to the left side of an existing speed maximum, the strong temperature gradient will reform to the left of the original one which weakens. Winds will accelerate at the new strong gradient, while weakening at the original position. During the finite length of time required for the transition, two speed maxima would be observed at a given moment in time. At that moment, a feature originally seen on satellite imagery associated with the initial speed maximum location, may no longer be discernible; whereas, the residual zone of strong winds there has not yet totally dissipated. Such common atmospheric behavior can cause difficulty in image interpretation, and in understanding the relationships between image features and the associated upper air data at a given analysis time. These difficulties can be reduced by using the "fluid" perspective - with continuous change with time in mind - while observing imagery.

Consider the example of a speed maximum "shifting" to the left due to vertical motions and warming along the left side of an initial speed maxima. In certain situations, this type of process apparently occurs in a continuous manner along jet stream zones. As the system propagates, the axis of maximum winds is continuously shifted to the left with time. As a result of this continuous shift in the temperature gradient and responding wind acceleration, the axis of maximum winds becomes reoriented from initially parallel to the associated winds, to across the winds. At a given time on a specific upper air pressure surface, such as 250mb, the axis of maximum winds is then oriented at an angle to the streamlines with the axis of maximum winds shifting to the right - looking downstream. If the resulting reoriented speed maxima is overtaking the downstream weather systems, it will produce a different effect than a speed maximum oriented parallel to the wind directions. This illustrates points: (1) that jet stream speed maxima change their structure with time as they propagate, and (2) these different jet stream structures are very significant to water vapor image interpretation and the system interactions observed on the imagery. Therefore it is useful to define three types of jet stream structure.

Three Types of Jet Stream Structure

Channeled Jet Structure

The axis of maximum winds is oriented nearly parallel to the wind directions on a given upper air pressure surface such as 300mb or 250mb.

The 500mb isotherms and vorticity isopleths tend to be parallel to the jet axis and to the wind directions. Although very strong temperature and vorticity gradients may be associated, advection is minimal at the synoptic scale.

There tends to be very little change of wind direction with height between the lower middle and upper troposphere.

Speed maxima of that nature tend to "extend" downstream, and smaller scale speed maxima within such a zone tend to follow one another, as opposed to successive ones moving significantly to the right or left of the previous one.

Linear shaped features on associated water vapor imagery tend to be parallel to the winds, and not rotating significantly with time.

NVA Type Advection Jet Structure

The axis of maximum winds is oriented across the flow at a significant angle. The orientation is such that the axis of maximum winds shifts to the right in the downstream direction when observed on an upper air constant pressure analysis such as 300mb or 250mb.

The 500mb isotherms and vorticity isopleths tend to be across the flow with significant advection of the positive temperature advection and negative vorticity advection sense. The strong temperature and vorticity gradient zones tend to be parallel to the axis of maximum winds, although the individual isopleths may be at slightly different angles.

Between the lower middle and upper troposphere, wind directions are likely to veer with increasing height.

Linear shaped features on the associated water vapor imagery tend to be oriented parallel to the axis of maximum winds, and not parallel to the wind directions. They are likely to be moving in a direction which is significantly different than their orientation.

The boundaries or elongated bands on the water vapor imagery are likely to be rotating clockwise as they move, during the formative phase of the NVA jet stream condition.

NVA jet stream conditions may be found on a synoptic scale at any location along the longwave scale jet stream zone; however, they are more frequent and most dramatically formed on the forward sides of upper air ridges.

PVA Type Advection Jet Structure

These are opposite to the NVA type conditions; therefore, will not be listed in detail.

The advection types of jet stream conditions vary greatly in the degree of crossing angle. Both are at times observed with the jet stream axes nearly orthogonal to the associated streamlines. The "channeled" condition, as defined, is an idealized situation. However, many jet stream segments occur and are maintained for significant periods of time in a nearly channeled configuration. In some cases, such as within a zonal longwave jet condition, a very nearly channeled condition can occur along a long portion of the axis for periods of 24 hours or longer. The greatest usefulness of the concept involves the degree of the differences, and the time change from one condition to another. This will be illustrated and applied in the discussion of the following cases relating water vapor imagery to jet stream conditions.

Another question significant to this discussion is: Which aspects of the jet stream shall be related to the water vapor imagery? Generally, we have found that, when people look at a satellite image and ask: "Where is the jet stream?", they mean "Where is the jet stream core or axis of maximum winds?" We shall emphasize that aspect in addition to the location of speed maxima along the axes of maximum winds, in cases where they can be reasonably estimated using still imagery. However, there are times, especially during the winter seasons, when the jet stream consists of a very wide zone of strong winds. In some of those cases, no single well defined core region is present. There may be multiple axes of maximum winds within the wide zone; and, in some cases, no well defined narrow core can be found in the radiosonde data. With these latter cases with no apparent well defined narrow core, a water vapor boundary is frequently present either along the poleward or equatorward side shear zone; however, we have not yet learned to distinguish the difference. Fortunately, during real time applications, the water vapor imagery is not used alone, but with knowledge of the past system evolution, and in conjunction with all available upper air observations.

Some General Observations on Relating Water Vapor Imagery And Jet Streams

The concepts and problems involved in locating jet stream conditions on water vapor imagery are very similar to those previously encountered using "window" infrared imagery. Water vapor imagery, in the 6.7μm band, is more useful for this task, primarily because it provides a more complete view of the upper air features. There are other advantages and some disadvantages in using water vapor imagery. The primary disadvantage is that it is more difficult to determine the heights of many features on water vapor imagery. Another is that certain types of cloud behavior can be related to conditions of the jet stream, and these often cannot be observed on water vapor imagery.

Parcel Motion Vectors

One method of locating jet stream conditions from satellite imagery is to observe an array of cloud or moisture element motion vectors. The motions of small elements or features of clouds or moisture can be measured between successive images, yielding quantitative values of speed and direction. On the average, such motion vectors are similar to the related upper air winds measured by radiosondes and aircraft. When the elements are carefully selected, and the time interval between images is small, the motion vectors will be very close in speed and direction to the associated winds. However, there are several problems involved. A component of the motions measured is contributed by local vertical motion effects on the elements being measured. Numerous observations in time-lapse motion from the ground indicate that vertical motions on the element scale have a significant effect on the speeds of motion of the elements. Even small patches of stratified clouds tend to form on one end while dissipating at the other, as they move. This is a greater problem with the cloud motions, than with the moisture element motions, and varies with different types of cloud elements at different locations with respect to the circulation systems. Another significant problem is that of assigning heights to the measured motions. Generally, this requires use of the satellite measured "brightness temperature" of the features being tracked, and some estimation of the specific vertical temperature sounding at the particular location. In the vicinity of jet stream core regions, with the related large vertical and horizontal temperature gradients and strong wind shears, both the vertical motion effects and the height assignment problem are significant. And even if the motion vectors obtained were perfectly accurate with respect to the wind field, the array of values across the core region would likely be at significantly different levels; therefore, not providing the kind of data field required for meaningful isotach analysis.

Another problem that is sometimes encountered when measuring element motions on water vapor imagery is that of distinguishing clouds from moisture parcels. In particular this involves clouds at some level below a layer of moisture, typically middle clouds under a layer of upper tropospheric moisture. The cloud elements provide cold sources for radiation. Radiation originating from the clouds is radiated from significantly cooler sources than the radiation passing upward adjacent to the clouds. As pointed out in Part One moisture in the upper troposphere is relatively translucent to the radiation arriving from lower altitudes (See Special Summary of Part One). Therefore the middle clouds can appear as colder (lighter) areas within the higher moist layer. On the water vapor imagery, without the benefit of coincident infrared or visible imagery, it is very difficult to distinguish the cloud effects from actual moisture parcels or moisture concentrations in the higher layer. If the motions of the cloud effects are tracked, the speeds and directions are those of middle clouds, which includes the local dissipation and growth effects, in addition to the fact that they are at a lower altitude.

Generally, it is difficult to accurately analyze jet stream axes by isotach analyses of element motion vectors. However, the data can be used to provide relative differences in wind speeds of jet streams, locate speed maxima along the jet stream zones, and often detect accelerations or change of strength with time. Element motion vectors provide very useful and quantitative information, often not available by other means; however, the data should be used with caution, recalling some of the problems mentioned here.

In the following illustrations, we shall address qualitative relationships between water vapor imagery and jet stream conditions, with primary emphasis on location of the jet stream core regions - or axes of maximum winds.

Generally, jet stream core regions can be located on satellite imagery more easily, and with less error, when the imagery are viewed in time-lapse motion. With still images viewed in time sequence, the task is more difficult; and, it is most difficult; using a single still image, without the benefit of knowing how the various patterns have been moving and changing with time.

Three Methods of Locating Jet Core Regions on Satellite Imagery

There are three basic methods which can be used in combination to locate jet stream core regions on satellite imagery:

(1)The jet stream core is located where boundaries across the flow are moving most rapidly. The boundary features involved must be those associated with upper level clouds or moisture, or those which are vertically deep in the troposphere.

(2)The jet stream core is located along an axis, across which upper level features are rotating in opposite directions due to horizontal shear. The concept involved is similar to that of method one; but, the shear method is most applicable to cirrus cloud features. The method is more applicable to "window" infrared imagery; but, many of the cirrus patterns will also be revealed in water vapor imagery.

(3)The jet stream core is located along linear shaped features, such as bands or boundaries in the upper air cloud or moisture fields. This is the most useful relationship using still imagery; however, many well defined boundaries are observed which are NOT associated with jet stream axes, and, some very well defined jet stream axes do NOT have well defined or distinct boundary or band features on the imagery.

On a typical water vapor image, there will be many well defined boundaries or banded features; and, only some of them are associated with jet stream axes. The problem is to determine which ones are, and which are not. Part of this problem can be resolved by recognizing common circulation patterns. This will be addressed by summary in the next section. However, such common patterns are not always present. In those cases, methods (l) and (2) can be used to help solve the problem.

If it is necessary to state one simple rule for locating jet stream axes on water vapor imagery, it is the following. Jet stream axes are located along upper air moisture boundaries, with the high level moist air on the right side and drier air on the left side (Northern Hemisphere). Unfortunately, the most simple relationships tend to be the least accurate.

Another over simplified relationship involves the fact that boundaries have two ends. Since "most" jet streams are located in wind fields of westerly component, the eastern end of a boundary is much more likely to be associated with a jet stream axis than the western end. In many cases, the western end lies through a col region. The primary exceptions to this rule involve cases of cyclogenesis or anticyclogenesis, when jet stream axes hook around the circulation and achieve an easterly component. Fortunately the associated patterns are usually recognizable on the associated imagery.

b. Jet Stream Conditions Related to Common Image Patterns

On a typical water vapor image, some of the moisture boundaries, or portions of boundaries are likely to be associated with jet stream axes. Others may be associated with very light winds, such as a col region. Often, features of the wind field can be estimated by the characteristics and behavior of the boundary, or by its location within a common recognizable pattern. The following cases illustrate many of the common patterns, and may serve as models to relate specific image features and their associated jet stream conditions.

Basic types of moisture boundaries observed on water vapor imagery were categorized and illustrated in Section A. Here, examples of each type are shown with related jet stream conditions summarized and compared.

Boundaries On The Forward Sides Of Upper Air Troughs

Typical examples are shown on **Figures 63**, **64**, and **65**. All of the cases involve troughs in the upper air westerlies; therefore, the "forward" side is the eastern side. The basic boundaries involved have a common characteristic. They are boundaries between drier conditions on the western, or upstream side; and upper air moisture on the eastern, or downstream side. Such boundaries usually have considerable high cloudiness on the moist side, and the moisture boundary is likely to be coincident with a cirrus cloud boundary. Therefore, the boundaries are often very distinct on the water vapor imagery, since the presence of the high clouds produces a large contrast in gray shades with the drier air side.

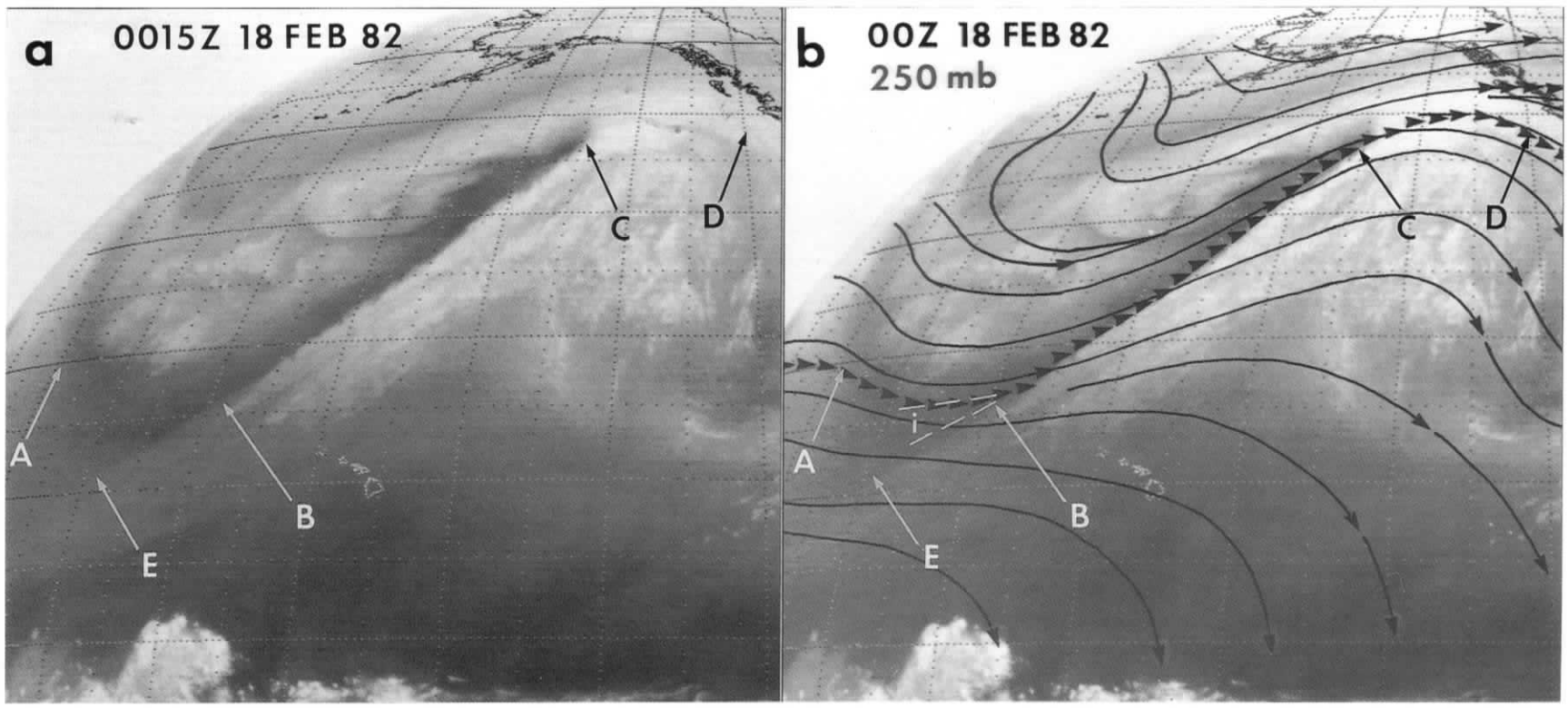

Figure 63 STRAIGHT BOUNDARY - FORWARD SIDE UPPER AIR TROUGH
Fig. 63a. 6.7μm image, 0015Z 18 February 1982, GOES West.
Fig. 63b. Same image with 250mb streamlines (solid lines), axes of maximum 250mb wind speeds (arrowheads).

STRAIGHT BOUNDARIES

Compared to other shapes of boundaries on the forward sides of troughs, our observations indicate that those which are nearly straight are most likely to be associated with a jet stream. A long portion of such boundaries is likely to be nearly coincident with the jet stream axis. The most difficult interpretation problems involve the conditions at the equatorward ends of the boundaries. Consider the example on **Figure 63a**, which was also shown on **Figure 4**. Here the 250mb axes of maximum winds are shown by arrowheads oriented parallel to the wind directions. The axis of maximum wind is divided into segments "A-B-C-D". The primary moisture boundary extends along "E-B-C". The upstream segment of the jet stream, "A-B", intersects or "approaches" the boundary near "B", and is parallel to the boundary from "B" to "C". The "E-B" portion of the boundary, which extends Equatorward of the jet stream intersection, is not parallel to an axis of maximum winds.

Generally, with straight boundaries, a part of the boundary is very likely to have a dark zone or slot along its western side. Often, that same portion of the boundary will have cirrus clouds along its moist eastern side. That part of the boundary with the adjacent slot is very likely to be coincident with the jet stream axis. However, in many cases, the dark slot does not extend along the entire boundary. There is likely to be a segment along the equatorward end of the boundary without a dark slot on its west side, or with a different dark zone than the one present farther to the poleward direction. This equatorward segment of the boundary may have an axis of maximum winds along it, or it may not. The equatorward ends of straight boundaries provide the primary interpretation problem. In the case shown on **Figure 63**, the boundary segment "B-C" does have a dark slot along its upstream side, and is coincident with the 250mb axis of maximum winds. There is no axis of maximum winds coincident with or parallel to segment "E-B" of the boundary.

Of the varied conditions observed near the equatorward ends of straight boundaries, the most common condition involves a jet stream branch approaching the boundary at some angle from upstream. For example, note that branch "A-B" of the jet stream intersects boundary "E-C" at an acute angle labeled "i". To the northeast of the intersection point "B", a jet stream branch is coincident to the boundary. During the process of image interpretation, an initial task is to locate the point of intersection "B" by conditions and features on the image. In cases in which the angle between the upstream jet axis ("A-B" in this case) and the boundary ("E-C" in this case) is large, there is often an abrupt difference in cloud conditions along the moist side of the boundary. Typically, high cold topped clouds are present poleward of the point of intersection, and low cloud tops are present equatorward of there. When the angle ("i" in this case) is small, there is often a gradual increase in cloud top altitudes in the poleward direction, or no high clouds present; therefore, no conditions on the moist side of the boundary imply the location of the intersection point. Furthermore, with straight boundaries, the angle of intersection is usually small. On the water vapor imagery, there are often features or conditions on the western side of the boundary to indicate the point of intersection. In the case shown, the conditions on the upstream side of the boundary are different. To the northeast of "B" the dark slot is present with a pattern of cold moisture and clouds on its west side. To the southwest of "B", a relatively wide dark area is present on the western side of the boundary. To the west of the boundary, the dark area and the region of cold moisture and clouds is separated by the upstream branch of the jet stream ("A-B"). Because of those different conditions of the upstream side of the boundary, a jet stream axis should be anticipated along that portion of the boundary east of the slot, but considered questionable along that portion east of the dark area. The following jet stream conditions may be considered: (1) most likely - a jet branch along "A-B" and not along "E-B", (2) second most likely - jet stream branches along both locations, (3) no jet stream branch west or south of point "B". If a wedge shaped area of moisture were present between "A-B" and "E-B", branches along both locations would be most likely. That would imply that a jet stream had branched across the upper air trough as illustrated and discussed in Section B (see **Figure 32**). The jet stream conditions along the equatorward ends of boundaries usually cannot be interpreted from a single water vapor image. Knowing the type of system evolution leading to that image is very useful. We shall expand upon this subject in discussions of other boundary shapes, and with the subject of changes with time.

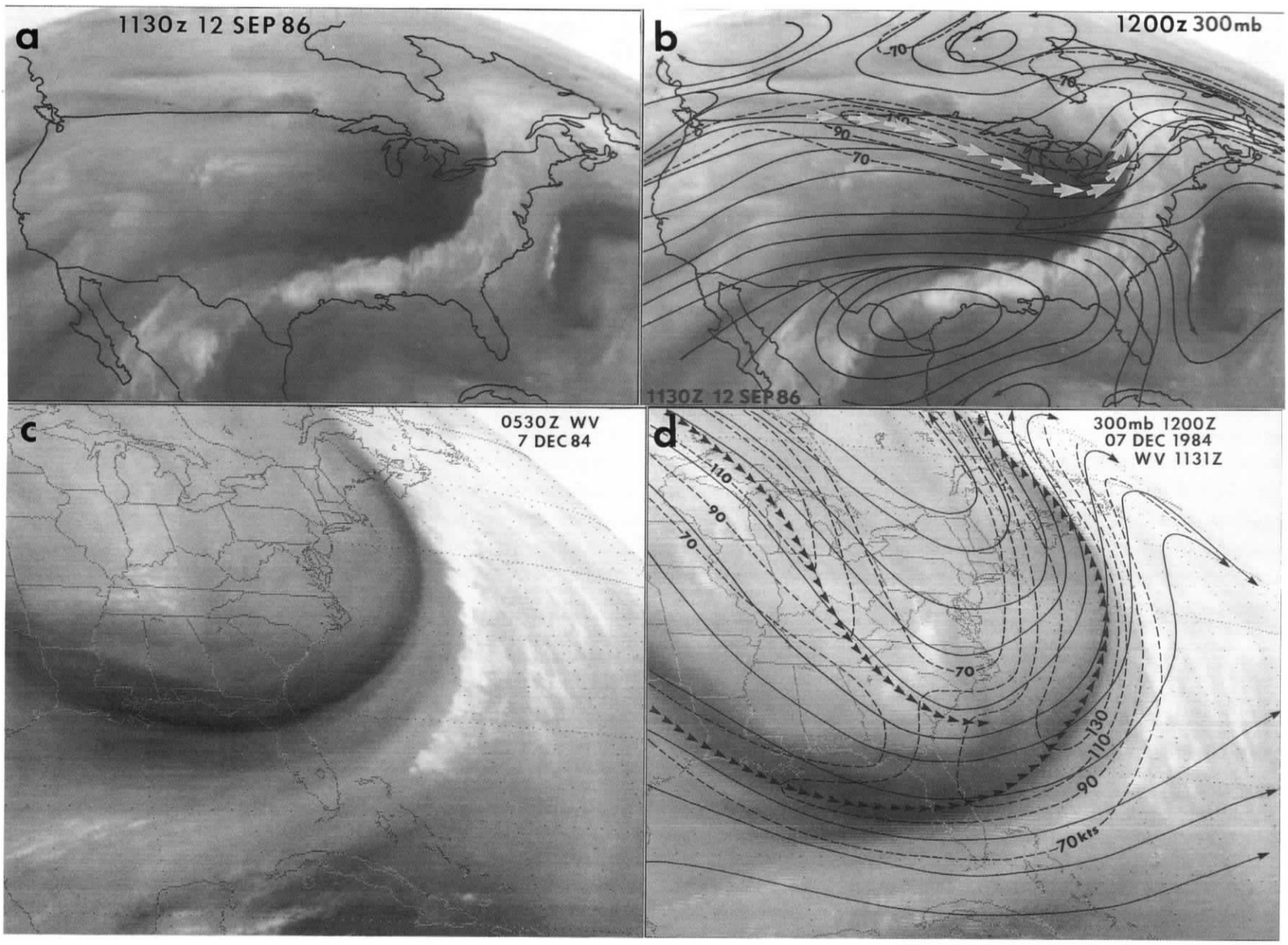

Figure 64

CURVED BOUNDARIES - FORWARD SIDES OF UPPER AIR TROUGHS
Fig. 64a. 6.7μm image, 1130Z 12 September 1986, GOES Central.
Fig. 64b. Same image with 300mb analysis.
Fig. 64c. 6.7μm image, 0530Z 7 December 1984, GOES Central.
Fig. 64d. 6.7μm image, 1131Z 7 December 1984, GOES Central with 1200Z 300mb analysis.
300mb analyses: streamlines (solid lines), isotachs (dashed lines), axes of maximum 300mb wind speeds (arrows).

"CYCLONICALLY" CURVED OR "CONCAVE" BOUNDARIES

Many of the boundaries on the forward sides of upper air troughs are curved concave from the perspective of the moist side. This curvature may be referred to as "cyclonic", although the upper air winds are usually not parallel to the boundaries. The two curved boundaries shown on **Figure 64** represent opposite extremes in regard to the associated jet stream conditions. One has a coincident parallel jet stream axis; the other does not. The case shown on **Figure 64a** and **64b** was also shown on **Figure 6** as an example of a "dry surge" type of basic moisture boundary. The case on **Figure 64c** and **64d** is a "parallel jet stream" type; it was not previously shown.

Characteristics of the two types of concave boundaries are summarized as follows.

The "Dry Surge" Boundary - Example On Figures 64a And 64b

CIRCULATION FIELD CHARACTERISTICS:

The upper air winds cross the boundary at relatively large angles, commonly in a diffluent streamline pattern. This can be seen on the 300mb analysis on **Figure 64b**.

The primary jet stream related to the system is upstream from the boundary. The boundary lies generally across the flow in advance of the jet stream. It has evolved into a curved shape by moving most rapidly in advance of the jet core region and less rapidly at the ends.

A jet stream axis is not likely to be parallel to such boundaries. If there is a jet stream axis of maximum winds parallel to - or coincident with - the boundary, it is usually along a relatively short segment near the poleward end. In the case shown here, a small part of the boundary north of Lake Ontario may have an axis of maximum winds parallel. When a jet stream axis is present near the poleward end, it is usually of the "PVA" advection type.

WATER VAPOR IMAGE CHARACTERISTICS:

Dry Surge boundaries usually move very rapidly. This can be determined from a sequence of images.

There is usually a relatively wide dark region to the rear of the boundary, often in an overall crescent shape, or an irregular shape. During the acceleration phase of the boundary's motion, darkening with time is likely to the rear of the boundary.

The rear edge of the dark region is likely to be irregular or diffuse, often with a gradual change from dark to light gray shades. Large scale moisture features to the rear of the dark region are likely to be generally orthogonal to the boundary - implying open westerly flow.

"Cyclonically" Curved Parallel Jet Stream Boundary - Figure 64c-64d

CIRCULATION FIELD CHARACTERISTICS:

This type of boundary is likely to be associated with a closed upper air low, or a high amplitude trough, as in the case shown here.

A jet stream axis is likely to be coincident with a large portion of the boundary. Such boundaries are usually moving, although not as rapidly as "dry surge" types. If so, the associated jet stream axis is likely to be coincident with the moisture boundary with a "PVA" type of jet structure. With cases which are nearly stationary, the jet stream axis is likely to be over the dry slot to the rear of the boundary, with a "channeled" type of structure.

In most cases, the upper air winds cross the boundary, often with very small angles near the poleward end, and at increasingly larger angles equatorward from there. With "channeled" type of jet structure and stationary cases, the wind directions as well as the jet axis will be nearly parallel to the boundary. Along portions of concave boundaries of this type, which are moving and rotating cyclonically with time, the wind directions tend to "back" with height within the upper troposphere below the level of maximum winds. Near the moisture edge, at the level of maximum winds, the directions will be nearly parallel to the boundary, but will be oriented across the boundary at levels just below that.

WATER VAPOR IMAGE CHARACTERISTICS:

Although less rapidly than "dry surge" boundaries, this type of boundary is likely to be moving. Commonly, the boundary will be "swinging" or rotating cyclonically with the poleward end moving very slowly, or "expanding" to a larger sized radius of curvature. In many cases, there is a "twisting" effect, with the poleward portion rotating more cyclonically, and some portion toward the equatorward end rotating very little, or even in the opposite direction.

The dry zone to the rear of the boundary is commonly in the form of a "slot". The slot is likely to be wider than those observed with "head" boundaries, and the rear edge of the slot is likely to be more distinct. The rear edge may have smaller scale irregularities, but generally parallel to the boundary on the forward side.

The larger scale overall pattern to the rear of the dark zone is likely to imply curvature of a closed low, or a high amplitude trough.

The jet stream relationships to most concave curved boundaries on the forward sides of upper air troughs are usually more complex than the two examples shown on **Figure 64.** Of all such curved boundaries, the most common type observed is a combination of the two types shown. The poleward part of the boundary will have a parallel jet stream, and the equatorward portion will have the characteristics of a dry surge type. This situation often occurs during cyclogenesis, as a dry surge boundary evolves to a parallel jet stream type.

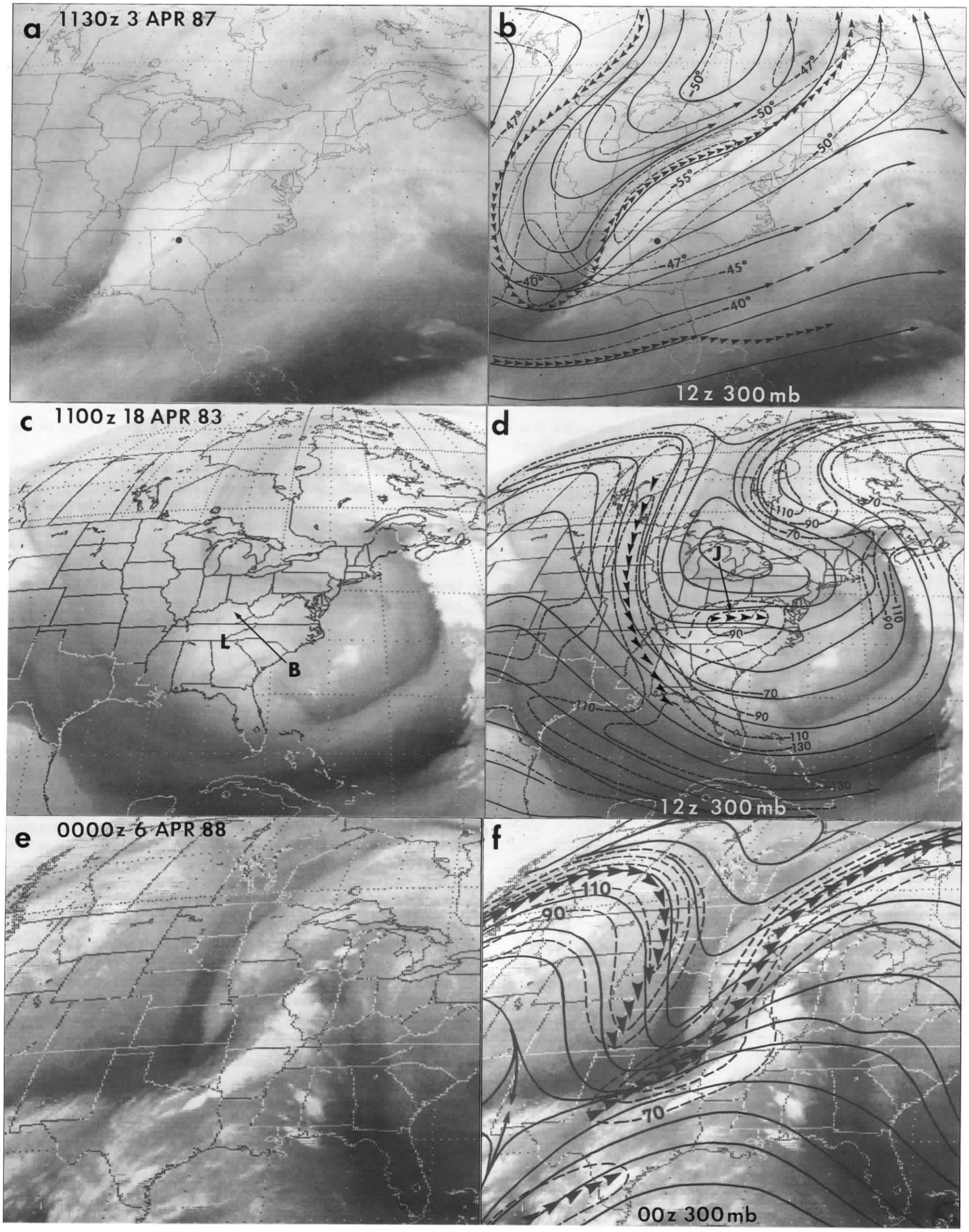
a
1130z 3 APR 87
b
-47°
-50°
-47°
-50°
-50°
-55°
-47°
-45°
-40°
-40°
12z 300mb
c
1100z 18 APR 83
L
B
d
110
90
70
J
90
70
110
90
110
130
130
12z 300mb
e
0000z 6 APR 88
f
110
90
70
00z 300mb

"CONVEX" AND "S" SHAPED BOUNDARIES

When a moisture boundary on the forward side of an upper air trough becomes slightly convex or "anticyclonically" curved, it is likely to have a coincident jet stream axis of maximum winds which is likely to be of the "channeled" type. On the GOES map projection, many slightly convex boundaries are actually straight or even slightly concave when compared to a "great circle" or when plotted on a "polar stereographic" map projection. When the convex, or "anticyclonic" curvature becomes large (smaller radius of curvature) or of greater amplitude, the boundary is most likely to be a part of an "S" shaped "baroclinic leaf" system, although the concave portion may be in some cases very short with respect to the overall length. When the curvature of such a boundary becomes very large, the boundary is no longer likely on the "forward" side of the trough. The trough along the west side of the boundary is likely stationary, or being "pushed" back to the west by a "building-back" upper air ridge. Such boundaries will be discussed in the category of "head" boundaries.

The "S" shaped boundaries are more frequently observed on water vapor imagery than on "window" infrared imagery. In many cases, the concave portion of the boundary is not present as a cloud edge because clouds are present only along the convex part of the boundary. However both portions of the boundary are revealed on water vapor imagery; and; the concave part is usually more distinct than the convex part. A dark area is likely to be present adjacent to the concave boundary. The convex part of the boundary is likely to be very well defined, but indistinct, on water vapor imagery; and, both well defined and distinct on infrared imagery.

Three examples of "S" shaped boundaries, or "baroclinic leaf" system boundaries, are shown on **Figure 65**. The most common type is shown on **Figures 65a** and b. The same system was extensively illustrated and discussed in Section C, and the leaf pattern was shown with surface and upper air analyses on **Figure 40**. A similar baroclinic leaf boundary, but with a rapidly deepening storm case, was shown on **Figure 49a** and **50b**. When baroclinic leaf systems form on the forward side of an upper air trough, there is usually a jet stream axis of maximum winds along the convex portion of the boundary, and along most of the concave portion. The concave portion has the characteristics of a "dry surge boundary" (a dark area is present on the upstream side, upper air winds cross the boundary at significant angles; and, the axis of maximum winds along the boundary shifts to the left). A "channeled" jet stream configuration is common along the convex portion of the boundary.

There are two other common types of baroclinic leaf types of moisture boundaries observed, which have different jet stream relationships. When the new development occurs to the left side (Northern Hemisphere) of the original downstream jet stream zone, or on the cold side of the vertically deep frontal zone; the leaf system will usually not have a jet stream present along its rear border. This type of development is common when a new jet stream speed maximum takes a track to the left, or cold side, of the existing downstream jet stream, or when a strong jet stream speed maximum branches across a trough and initiates development before arriving on the downstream side. In such cases, a new baroclinic leaf cloud system forms on the cold side of the pre-existing jet stream zone. During the process of development, a new jet stream segment is likely to develop along the downstream or poleward end of the leaf boundary; however, in the early stages, there is not likely to be a jet stream axis in that position. An example of such a leaf system is shown on **Figure 65c** and **d**. In this case, the system developed on the rear side of the trough as a new jet stream speed maximum formed and moved within the northwesterly flow. The cold cloud system is labeled "L" on **Figure 65c**. The jet stream on the western side of the trough crosses the western end of the newly formed "leaf" cloud system, and extends to southern Florida. However, a new jet stream branch has begun to form at "J", along the northern edge of the "leaf" cloud system. That edge, indicated at "B" on the water vapor image, was very distinct and well defined on the infrared image. Notice that the boundary is very indistinct on the water vapor image. This indistinctiveness of the convex part of the "leaf" boundary on water vapor imagery is very characteristic of the "cold air side" types of development. A very distinct cloud edge is likely on associated "window" infrared imagery.

With this type of "cold side" development, the "S" shaped "leaf" boundary is not initially coincident to an axis of maximum winds. The original jet stream zone crosses the concave part of the boundary, with most of the "cold cloud shield" forming on the left side of the jet stream axis. As the system develops, a new branch of maximum winds develops. This usually occurs after the "cusp stage" and along that part of the convex boundary downstream from the cusp apex. In the case shown here, the new speed maximum at "J" had formed earlier than normal, compared to the average of cases we observed. Generally, the "cold side" leaf systems can be recognized on imagery by their location with respect to other features and by the relative indistinctiveness of their convex boundaries on the water vapor imagery.

A third type of convex or "S" shaped boundary is illustrated on **Figure 65e and f**. We refer to this as a "split-leaf" pattern. There will be two adjacent and nearly parallel boundaries present and moving in conjunction with each other. As in the case shown, the jet stream axis of maximum winds is likely to be along the downstream boundary - usually the eastern one. With such systems, there will usually be a dry or dark slot dividing the two moist zones on the water vapor imagery. The associated cloud pattern is likely to extend across under the dry slot feature; therefore, the double structure is likely to be least distinct on visible imagery. There are often two high cloud patterns, with those on the right side of the jet axis higher and colder. As such systems evolve with time, with cyclogenesis occurring, the downstream portion usually rotates cyclonically with respect to the upstream portion, such that they are no longer parallel and tend to merge at the poleward end. The upstream portion on the left side of the jet axis becomes the comma "head" of the resulting storm pattern. Although we do not sufficiently understand this, the initial double pattern apparently represents a vertical separation - or offset - in the upper air baroclinic structure, perhaps related to the reversal of the sign of the baroclinity at the level of the jet stream core. However, when such "split-leaf" patterns are observed on water vapor imagery, empirical observations indicate that the jet stream axis is likely to be present along the forward or eastern of the two boundaries.

Figure 65

◄ **THREE TYPES OF BAROCLINIC LEAF PATTERNS**
Fig. 65a. 6.7μm image, 1130Z 3 April 1987, GOES East.
Fig. 65b. Same image with 1200Z 300mb analysis.
Fig. 65c. 6.7μm image, 1100Z 18 April 1983, GOES East.
Fig. 65d. Same image with 1200Z 300mb analysis.
Fig. 65e. 6.7μm image, 0000Z 6 April 1988, GOES East.
Fig. 65f. Same image with 0000Z 300mb analysis.
Analyses: Streamlines (solid lines), isotachs (dashed lines), axes of maximum 300mb wind speeds (arrowheads).

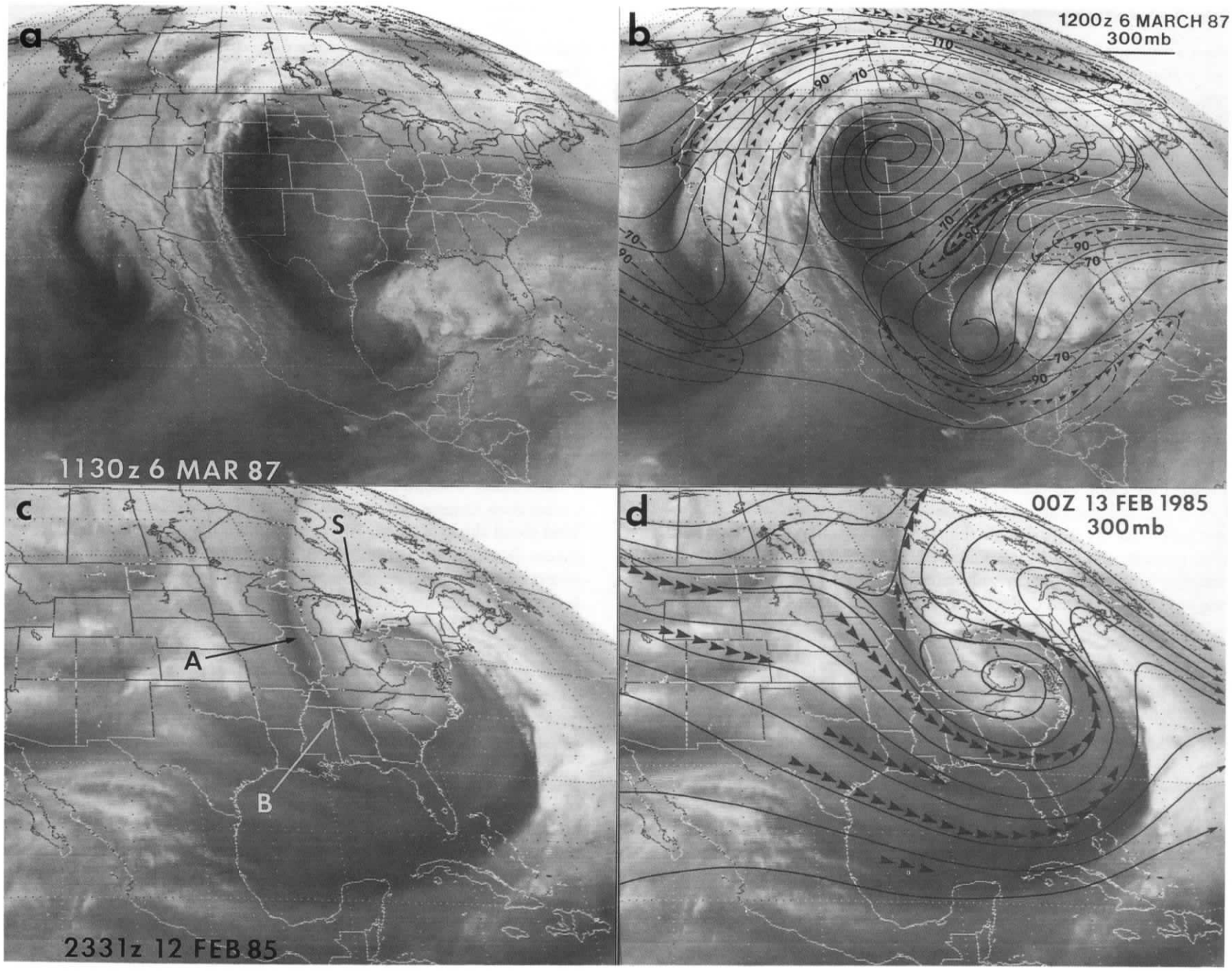

Figure 66

BLOCKING BOUNDARIES - TWO BASIC TYPES - INSIDE AND HEAD
Fig. 66a. 6.7μm image, 1130Z 6 March 1987, GOES Central.
Fig. 66b. Same image with 1200Z 300mb analysis.
Fig. 66c. 6.7μm image, 2331Z 12 February 1985, GOES Central.
Fig. 66d. Same image with 0000Z 13 February 1985 300mb analysis.
Analyses: Streamlines (solid lines), isotachs (dashed lines), axes of maximum 300mb wind speeds (arrowheads).

Boundaries Associated With Blocking Circulation Regimes

Two basic types of blocking regimes were introduced in Sections A and B. The associated primary moisture boundaries were the "head" boundary and the "inside" boundary. Both blocking regimes occur with the formation of upper air easterly winds, with the moisture boundaries forming on the western sides of the easterly wind regimes. "Head" blocking regimes occur with cyclogenesis. The easterly winds form as a ridge "builds back" from the eastern side to the poleward side of the closing cyclone. "Inside" blocking regimes form with upper air anticyclogenesis. The easterly wind regime is formed on the equatorward side of the closed anticyclone. "Head" and "inside" boundaries also occur in combinations. Two common types of combinations were illustrated in Section B with the "roll-over" and "build-back" cycles. Here we shall discuss the jet streams associated with the basic blocking regimes and several of their combinations.

Inside Boundaries - "Roll-Over" Ridge With Anticyclogenesis

An example originally shown on **Figure 20f**, is repeated on **Figure 66a**. The "inside" boundary is concave toward the east with moist air on the west and dry air on the east. Generally the dry region is relatively wide. Its eastern edge is often not parallel to its primary boundary on the west, and is likely to be irregular with a gradual moisture interface or feathered appearance. This is especially true during the early phase of the boundary. During that phase, the dry region is likely to have a crescent shape. During the later phases, the dark region is likely to become elongated parallel to the boundary forming a slot shape; however, the eastern edge of the dark region is likely to remain irregular or indistinct. In the case shown on **Figure 66a** and **b**, the dark region has become elongated, but has remained relatively wide.

Inside boundaries form in response to upper air anticyclogenesis. When the upper air high closes, the newly formed easterly winds on the Equatorward side of the high form a blocking regime in opposition to the upstream westerlies. A col pattern forms in the upper air wind field with its stretching axis coincident with a part of the inside boundary. A large portion of the length of inside boundaries is generally associated with relatively light upper air winds. However, as in the case shown, a jet stream axis of maximum winds is often present along the Equatorward end of the boundary. Along the poleward end of the boundary, which commonly rotates around the poleward side of the anticyclone, a separate speed maximum is sometimes present in the middle troposphere. When such speed maxima are present along the poleward end, the associated level of maximum wind is likely to be near or below 500mb. However, even at mid-tropospheric levels, speed maxima along the poleward ends of inside boundaries are observed much less frequently than at the equatorward ends.

With most inside boundary cases, there is some form of upper air wind speed maximum at the equatorward end. Even during summer seasons, with an inside boundary located at relatively low latitudes, there is generally an upper air speed maximum along the equatorward end. However, the intensity, vertical depth, and horizontal extent of the maximum wind zone are variable from case to case. The type of jet stream structure varies; but, the "channeled" type is most frequent.

From a single still water vapor image, it is very difficult to determine the relative strength of the equatorward end speed maxima, or their horizontal extent. Generally both of these factors are correlated to the size of the upper air trough or cyclone located on the equatorward side of the anticyclone. This size may usually be determined by the curvature of the moisture features in the area east of the inside boundary. Part of the upper air moisture patterns within the easterly flow between the anticyclone and the cyclone will often reveal anticyclonic curvature, and others cyclonic curvature. If the axis between those types of curvature is extrapolated westward to the boundary, that point along the boundary will be near the col region. This will provide some indication of the length of the jet stream segment along the equatorward end.

"Head" Boundaries - "Build-Back" Ridge With Cyclogenesis

An example of a "blocking regime" with a "head" boundary is shown on **Figure 66c** and **d**. The shape of the boundary is similar to that of the "inside" boundary of the last case, and the circulation systems on the east side of the boundary also consist of a ridge with a cyclone on its equatorward side. However, in this case, high level clouds and moisture dominate the eastern side of the boundary. The moisture moved back around the upper air low from the downstream ridge. At 500mb, the warmer air from the downstream ridge has moved around the west side of the low to southern Virginia and North Carolina.

With "head" boundaries, the primary jet stream position is along the poleward or eastern end of the boundary. In this case, as shown on **Figure 66d**, the axis of maximum winds at 300mb is nearly coincident with that portion of the boundary over Hudson Bay and northern Ontario. When the "head" boundary is associated with a "blocking" regime, as in this case, an even stronger jet stream is likely to be associated with the equatorward portion of the boundary. However, the axis of maximum winds of this jet - extending around the upper air cyclone - is not coincident with the "head" boundary itself, but is on the opposite side of the associated dry slot. When that "slot" is very narrow, as in the case shown, the jet axis may be very near the head boundary and extend parallel to the boundary around the southern side of the cyclone. Notice on **Figure 66c**, that a narrow elongated dark "slot" extends from northern Illinois, at "A", around the southern side of the cyclone. South of "A", the "head" boundary has become less well defined; the moist-to-dry interface is more gradual or less abrupt. In fact, over Alabama and Georgia - east of "B" - the moisture boundary on the southern side of the dry slot is better defined than the "head" boundary on the northern side of the slot. The col in the 300mb wind field is located over Wisconsin - just north of "A". Through the col area, and north of there, the dark slot is less distinct, and the boundary on the eastern side is better defined. The moisture interface to the west of the narrow slot is irregular and more of a gradual change. The 300mb axis of maximum winds from upstream "approaches" the dry slot near western Tennessee, and lies along the southern edge of the dark band around the cyclone.

Generally, when the downstream ridge "builds back" strongly forming a large head boundary oriented in a north-south direction, there are jet stream segments parallel to both ends. The poleward one will coincide with the head boundary. The equatorward one will be parallel to a portion of the head boundary, but on the opposite side of the associated dry slot. Often, along that portion of the equatorward end with the parallel jet stream, the equatorward or upstream side of the dry slot will be better defined than the "head" boundary side. The location of the col is difficult to determine on still imagery when the mid-tropospheric thermal ridge has moved cyclonically around the low. Two relationships may be helpful. Sometimes - as in the case shown - the head boundary will be most well defined near the col region, and remain well defined poleward of there. Therefore, if the "head" boundary becomes abruptly better defined poleward of a given location, the col is likely near there. The second relationship involves the leading part of the dry slot which has revolved around inside the cyclonic circulation. This may be revealed as a distinct "U" or "V" shape, or as a bend or apex. If the slot boundary is extrapolated across the high level moisture to the head boundary, this will often be near the col. In the case shown, the apex of the slot is at "S" over Lake Erie. Extrapolation of the boundary on the northern side of the slot across the moisture to the west, would intersect the "head" boundary over northern Illinois. Since the upper air wind speeds are weak in the col region, knowledge of its location is useful to determine where the jet stream is not associated with the boundary.

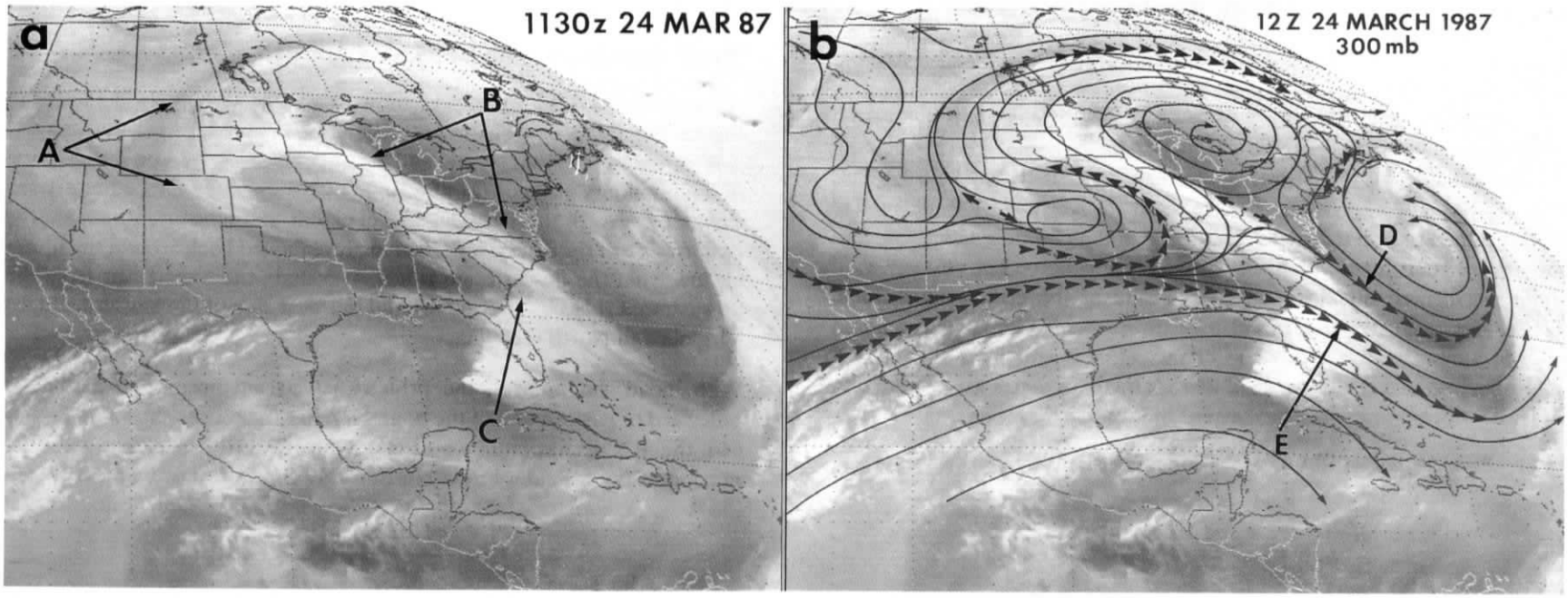

Figure 67 **COMBINATION BLOCKING REGIME - OMEGA TYPE**
Fig. 67a. 6.7μm image, 1130Z 24 March 1987, GOES Central.
Fig. 67b. Same image with 1200Z 300mb analysis. Streamlines (solid) axes of maximum 300mb wind speeds (arrowheads).

Boundary Combinations - "Head" And "Inside" - The "Omega Block"

"Head" and "inside" boundaries occur in combinations, two of which result in specific types of patterns or "signatures" which are commonly observed on water vapor imagery. The first of these is illustrated here, and is the water vapor pattern associated with the classical "omega block" set of circulation systems. The second type will be shown under the next topic.

On the last case of a "build-back" blocking regime shown on **Figure 66c** and **d**, the upper air ridge over eastern Canada had remained "open" and extended southeastward over the Atlantic Ocean. However, in other cases, the poleward portion of the "build-back" ridge may form a "closed" anticyclone. An example of that was shown on **Figure 37** of Section B. A new col and boundary formed in combination with the existing "head" boundary. Another example of the "omega" type combination of boundaries is shown here as **Figure 67**. The first boundary formed was the "head" boundary at "A" with a col in the 300mb wind field over eastern Colorado. An anticyclone has formed in the "build-back" ridge position over the Great Lakes. The col region associated with the closed high is over Ohio; and, an "inside" type of moisture boundary lies along the deformation zone of the col. The boundary "B" extends from the northeastern side of the closed low over Kansas to the southwestern side of an eastern closed low over the Atlantic Ocean. This combination type of moisture pattern is associated with a set of circulation systems of the classical "omega block" configuration. Although individual features vary, this set of image patterns represents the common signature of the "omega block" circulation pattern. The pattern on the imagery does not explicitly reveal the "omega" shape of the three primary closed circulation systems. The features are related better to the stretching axes of the three col regions and the related jet stream segments.

When interpreting such image patterns in regard to jet stream conditions, the relationships previously discussed for both types of "blocking" boundaries may be applied in combination. It is important to recognize the boundary "B" through the central col area as an "inside" boundary with weak winds along a large part of its length. There is likely to be a speed maximum along its equatorward or eastern end, as in the case shown. Also, in this case, the strong jet stream along the southern side of the western low is breaking across the open ridge at "C". This is a common occurrence in such situations, and often results in two jet stream branches parallel to one another, as at "D" and "E" on **Figure 67b**. Usually, after the two branches become parallel, the poleward branch weakens with time; however, a residual boundary may remain. Often the occurrence of the jet breaking across the open ridge can be detected on the imagery. The "inside" boundary ("B" in this case) continues to rotate into an extreme "negative tilt". Often a part of the drier air on the southern side of the western cyclone extends eastward, protruding into the ridge moisture. A break may occur in the high cloud pattern of the ridge.

Summary

With both basic types of blocking regimes, the upper air westerlies divide into two branches, around the poleward and equatorward sides of the blocking systems. The following jet stream conditions are common:

INSIDE BOUNDARIES - "ROLL-OVER" EVOLUTION

The primary jet stream is that in the poleward branch of westerlies around the anticyclone. The branch of westerlies is likely to be wide with strong winds and multiple axes of maximum winds. The cyclone on the equatorward side of the high is likely to become "cut-off " with a short weaker jet stream branch on its equatorward side. If the blocking regime persists, it is likely to extend eastward forming new "cut-off" lows and an elongated ridge.

HEAD BOUNDARY - "BUILD-BACK" EVOLUTION

The primary jet stream is that in the equatorward branch of the westerlies around the first closed cyclone. That branch on the equatorward side of the blocking regime is likely to be strong and wide. The anticyclone becomes "cut-off" with a short jet stream branch around its poleward side. If the regime persists, the block tends to retrograde westward at the latitude of the anticyclone; whereas, short wave troughs approaching from the west move south of the blocking easterlies. Their associated speed maxima tend to break across the open ridge to the south of the col (as at position "C" of **Figure 67a**); and, multiple axes of maximum winds are often present within the strong jet stream zone.

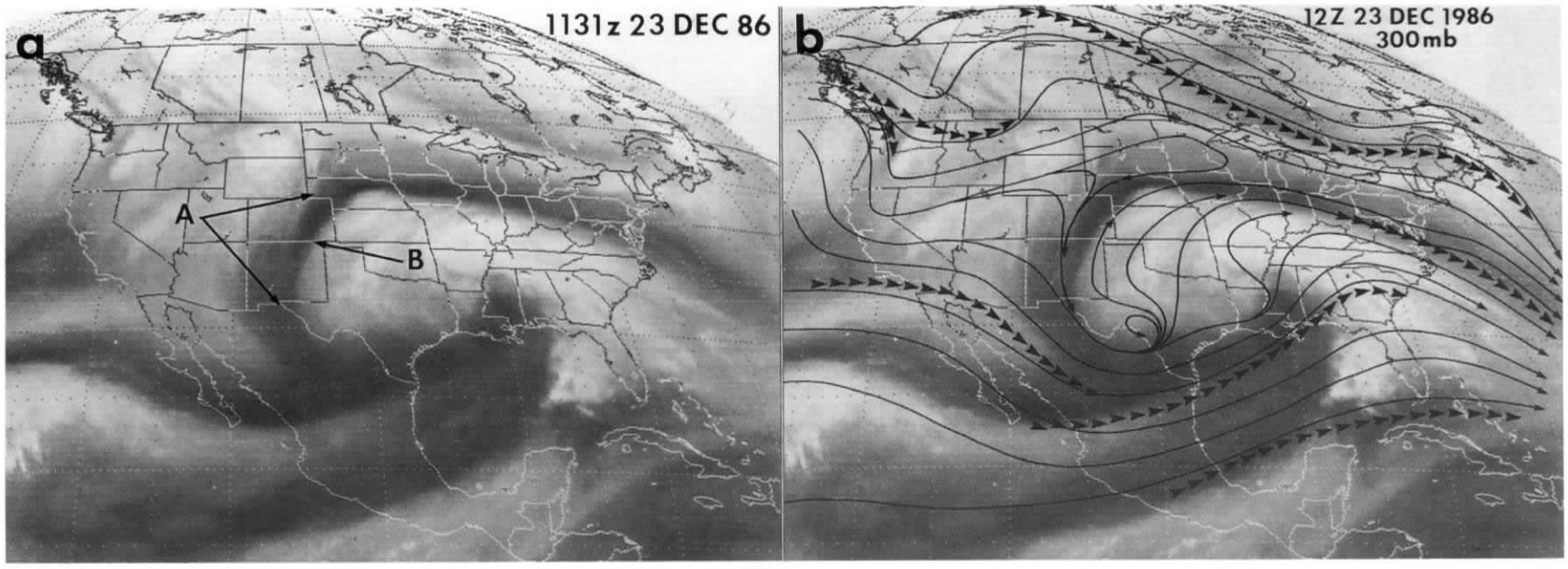

Figure 68 BOUNDARY ON WEST SIDE OF CLOSED LOW
Fig. 68a. 6.7μm image, 1131Z 23 December 1986, GOES Central.
Fig. 68b. Same image with 1200Z 300mb analysis, streamlines (solid lines), axes of maximum 300mb wind speeds (arrowheads).

Boundaries And Slots On The West Side Of Closed Lows

Conditions on the western sides of upper air cyclones vary considerably, both in regard to the water vapor image characteristics and to the jet stream conditions. On the imagery, there is usually some form of boundary or combination of boundaries curved convex from the east side perspective. Usually, there is some type of boundary formed on the eastern side of the moisture approaching in the upstream westerlies. Often that boundary will have moist air and light image gray shades on the west side and drier air with dark image gray shades to the east. The dark zone may be in the form of a slot with another region of lighter gray shades and moisture on the eastern side. However, the moisture forming the eastern side of the slot may be in cold air of the cyclone, or in a ridge built around the cyclone from the eastern side. The primary question to be addressed here is the following: is there a jet stream around the western side of the cyclone, or part of that side; and, which water vapor image feature may determine that.

One type of configuration which occurs on the rear side of storm systems, is a second type of combination of "inside" and "head" boundaries. In this case, a "head" boundary forms on the eastern side of an existing "inside" boundary. Generally, with the typical "inside" boundary, a large anticyclone is present to the poleward side of a closed low. Usually, there is a "build-back" type of ridge, on or around the eastern side of the low, and of similar scale as the low. Usually this ridge has been depressed equatorward by the equatorward flow around the eastern side of the anticyclone. However, in some cases, especially when intense convective weather is involved, the smaller "build-back" ridge grows rapidly and dominates the circulation pattern east of the inside boundary. The "head" boundary of the "build-back" ridge pushes westward, and becomes parallel to the inside boundary around the western side of the low. An example of such a resulting pattern is shown on **Figure 68**.

The "head" boundary "B" has become nearly parallel to the "inside" boundary "A". The upper air high, which originally caused the "inside" boundary, has opened and moved rapidly eastward to a position off the coast of New England. The ridge there had once been connected to the ridge extending from Arizona to Minnesota. The elongated dry zone between "A" and "B" is the remainder of the original trough which had been "rolled-over" by the upstream ridge. On the western side of the system, the air at 500mb is cooler along the dry zone than that of the moist areas to the west and east. The cool trough has weakened and elongated between the "build-back" ridge and the upstream ridge. Both boundaries and the cool drier air between them have curved anticyclonically around the northern side of the low, as the systems over Canada moved rapidly eastward.

As shown on the 300mb analysis, there is an axis of maximum winds present along the eastern end of the "head" boundary, from West Virginia toward the southeast. On the southwestern side of the system, a new jet stream branch has broken across the western ridge and extends around the southern side of the low. This was, in fact, the second branch to break across; and, the low is beginning to open and extend northeastward. A previously existing higher level subtropical jet branch is also present over southern Mexico. Of special significance, is the fact, that there is no jet stream located along either boundary of the dark band around the west and northwestern sides of the storm system. In such cases, in which the high cold moisture of the downstream ridge has "built-back" around the western side of a low, adjacent to the moisture of the upstream ridge, there is usually no jet stream associated with the dark zone or the boundaries of the two moisture regimes.

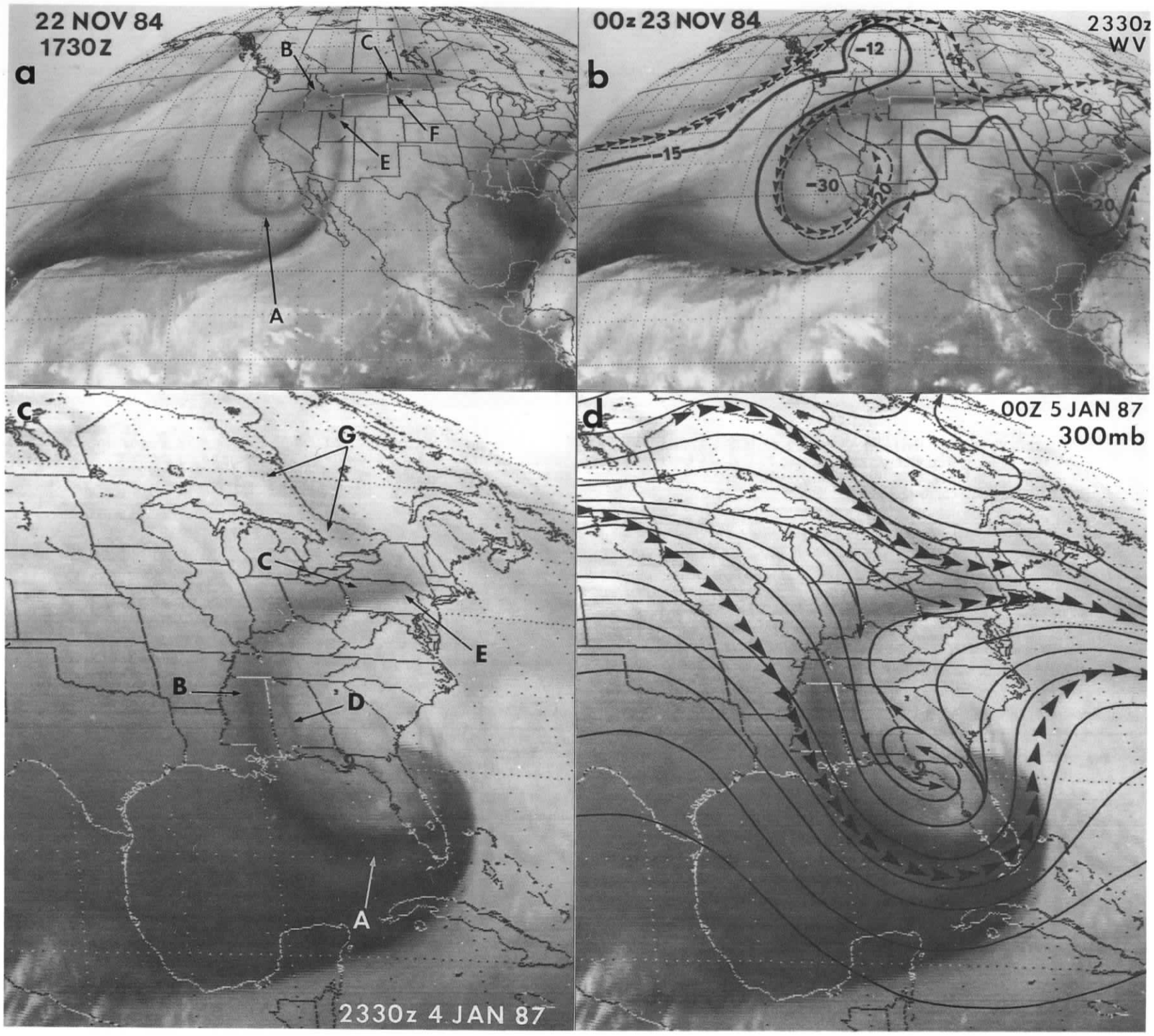

Figure 69

BOUNDARIES ON WEST SIDES OF CLOSED LOWS - VARIED JET CONDITIONS
Fig. 69a. 6.7μm image, 1730Z 22 November 1984, GOES Central.
Fig. 69b. 6.7μm image, 2330Z 22 November 1984, GOES Central, with 0000Z 23 November 1984 Analyses features. 500mb isotherms - 15°C (bold solid lines) -20°C (thin dashed lines), axes of maximum 300mb wind speeds (arrowheads), maximum and minimum 500mb temperatures with thermal highs and thermal lows.
Fig. 69c. 6.7μm image, 2331Z 4 January 1987, GOES Central.
Fig. 69d. Same image with 0000Z 5 January 1987 300mb analysis, streamlines (solid lines) axes of maximum 300mb wind speeds (arrowheads).

Other boundary features which are curved similarly on the upwind sides of upper air lows do have significant jet stream axes along most of their lengths. An example is shown on **Figures 69a** and **69b**. The imagery shown was previously shown on **Figure 29** as part of the series illustrating a "roll-over" circulation cycle. On the imagery, boundary "A-B-C" lies along the leading edge of the moisture of the upstream ridge. In this case, a jet stream axis of maximum winds is present along the "A-B" portion of the boundary. Along the "B-C" portion, there is no jet stream. There, the trough has elongated and weakened adjacent to boundary "E-F" with warm mid-tropospheric air from the downstream ridge on its southern side. In this case, the vertically deep warm air extending into the upper middle troposphere did not "build back" around the western side of the low. Although warmer air of a "head" ridge in the lower middle troposphere did rotate around to the western side, this had not built vertically upward. The air at 500mb adjacent to the boundary "A-B" has remained very cold -maintaining a strong temperature gradient along "A-B". The jet stream has continued very strong along the boundary with the warmer upstream ridge moisture.

In this case, and in the one shown on **Figure 68**, the boundary features were similarly curved around the western and northern sides of storm systems. They may be distinguished from classical inside boundaries by the absence of a wide dark area to the eastern sides, and by the dominating pattern of the upper air cyclones, as opposed to anticyclonically curved features. The presence or absence of a strong jet stream along the boundary is dependent upon whether the moisture on the eastern side of the boundary is that in the cold core trough or low, or that of a "build-back" ridge. If the downstream ridge with its warm air in the upper middle troposphere "builds back" around the western side of the low adjacent to the warm air of the upstream ridge, the trough elongates and weakens. The jet stream winds also subside, and no axis of maximum winds is present along that portion of the boundary feature. In image interpretation, this is best determined by observing the evolution of the features from a succession of images. If only a single still image is available, the presence or absence of the jet stream may be estimated by examining the gray shade pattern on the eastern side of the narrow dark band. If the gray shades indicate very high cold moisture, perhaps with cirrus clouds, the ridge has likely built around the low. In such cases the cold moisture pattern is relatively even in appearance, and without an abrupt change around the northern part of the low to the east side. If the moisture east of the dark band is of medium gray shades, or of a textured appearance, it is more likely in the cold upper middle troposphere of the trough or low. Also, in that case, there will likely be some type of interface or difference on the northern side of the low with an area of much lighter gray shades to the east of that interface.

The last two cases shown represent opposite extremes in regard to the jet stream conditions along the boundary feature on the upstream sides of the storm systems. In many similar systems, the downstream ridge is built partially around the closed low, and a jet stream is present along a portion of the curved boundary zone. Consider the example shown on **Figures 69c** and **69d**. In this case, over the southeastern United States, an elongated dry zone is similarly curved around the upstream side of the storm system. The moisture on the western side of the dry band is that of the upstream ridge; however, in this case, it is not - and had not been - an inside boundary. The system involved has not formed a "blocking regime", except in the relative motion sense to the north of the forming low. The system is moving eastward, and there is some doubt as to whether it has yet "closed" in the 300mb streamline field. Certainly, a portion of the trough has become very narrow and elongated between the two upper air ridges. A narrow dark zone is curved around the system from northeastern Pennsylvania to the Gulf of Mexico, and across Florida. On the east side of that dark zone, the downstream ridge has built back on the northern side of the low. On the northern side of the low, the cold clouds and high level moisture have built back to northeastern Alabama. The northwestern boundary of that cold moisture has built back to position "D-E" along the eastern side of the dark zone. The moisture just west of "D", and around the southern side of the low is in the cold air of the trough. An axis of maximum winds is present along that part of the dark zone. The jet stream across the upstream ridge approaches the dark zone at an acute angle over Arkansas, and lies along the western boundary of the dark zone from central Mississippi around the southern side of the low. Note that the western moisture boundary of the dark zone is well defined from "B" to "A", and around the southern side of the low. Along that portion, the eastern boundary is irregular and less well defined. Those characteristics are often observed along that portion of the dark zone with an axis of maximum winds along its western boundary. The portion of the dark zone from "B" to "C" adjacent to the "head" boundary has a poorly defined northwestern edge. The jet axis does not extend along that portion of the dark zone. However, there is usually a jet axis present, or forming, along some portion of the eastern end of the "head" boundary, "D-E". Typically, it is difficult to determine the location of the strong winds there from the characteristics of the "head" boundary itself; but, in many cases there will be a difference in the moisture pattern on the opposite side of the narrow dark band. In this case, a jet stream branch is present over Ontario at "G". This axis of maximum winds is along an interface between the moisture of the upstream ridge on its west side, and cooler air of a trough on its east side. On the imagery, slightly darker gray shades are present on the cool drier side. Opposite the "head" boundary, this interface is present over western New York state. West of there, warmer air from the upstream ridge is approaching the northwestern side of the dark band along "B-C". To the east, the cooler air of the Canadian trough was present adjacent to the "head" boundary. A jet stream branch is located along that "boundary, from western Pennsylvania eastward (between cooler air to the north and the warm air of the ridge to the south). Note that "moist wedging" has begun near "C", resulting in a double jet stream structure.

In summary, along the dark band and boundary features curved around the storm system, there are two segments with jet stream branches parallel to the dark zone. One is present along the "head" boundary side of the dark zone east of "C", where the mid-tropospheric warm air of the "build-back" ridge is adjacent to a relatively wide area of cold air to the north. The other is along the southwest side - the opposite side from the "head" boundary - to the south of "C", where the warmer air of the upstream ridge is adjacent to the wider area of cold air of the trough and low. That portion of the boundary zone from "B" to "C", where the warm air of the two ridges have approached and narrowed the trough, no jet stream winds are present along the dark zone.

Note also in this case, that where the jet stream branch crosses the upstream ridge from Montana to Arkansas, there are little or no indications of its presence on the water vapor imagery. This is common, especially when a new jet branch crosses the open ridge, or when a new one forms poleward of the original one. The water vapor imagery is not useful for locating such jet axes. One reason is that the jet stream zone itself tends to be wide without distinct narrow axes of strong winds. There are often multiple minor axes of maximum winds within the wide zone.

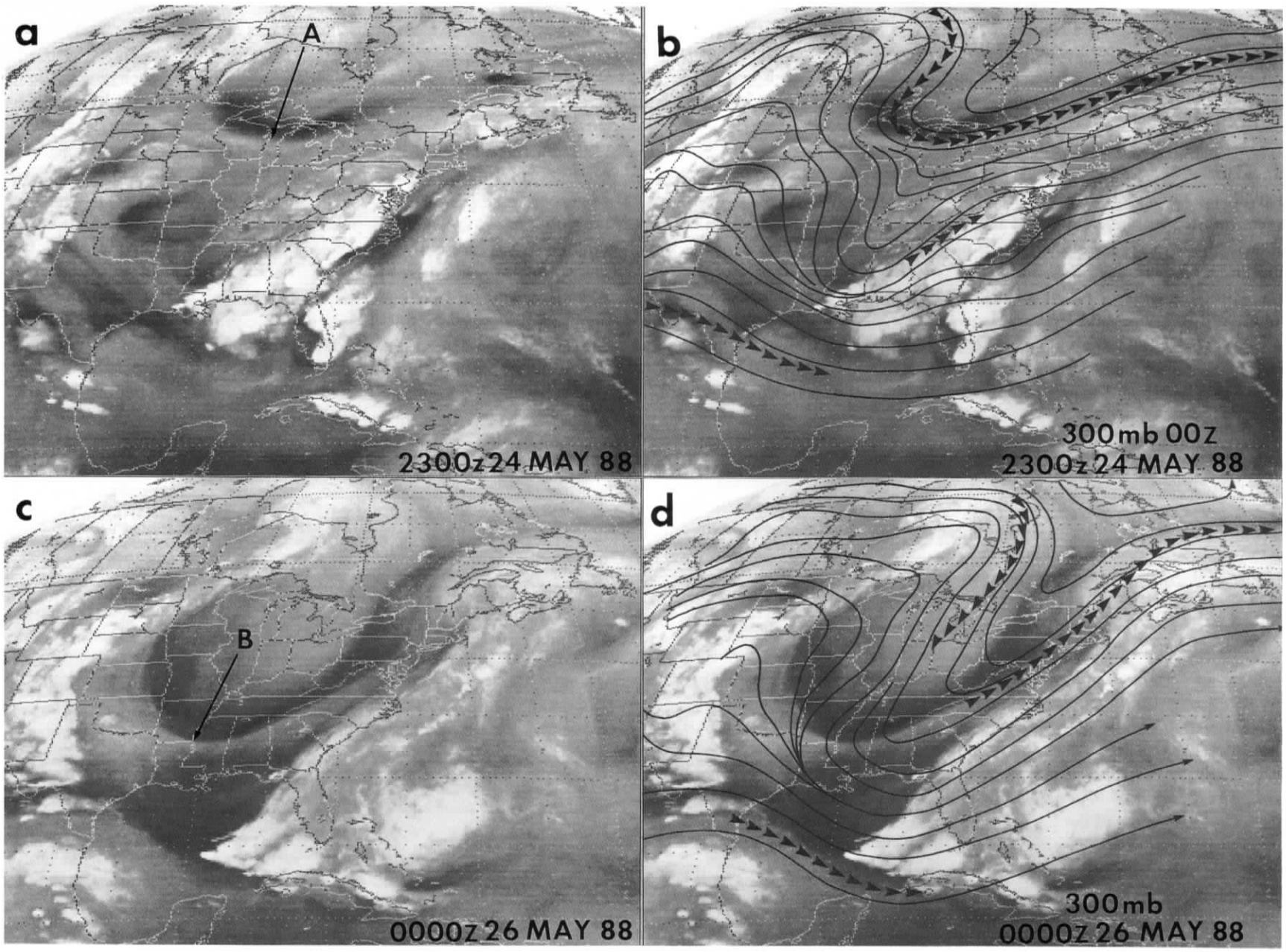

Figure 70 **BOUNDARIES AT THE BASE OF TROUGHS - CHANGE FROM PARALLEL JET TO BASE SURGE**
Fig. 70a. 6.7μm image, 2300Z 24 May 1988, GOES East. **Fig. 70b.** Same image with 0000Z 25 May 1988 300mb analysis.
Fig. 70c. 6.7μm image, 0000Z 26 May 1988, GOES East. **Fig. 70d.** Same image with 300mb analysis.
Analyses: Streamlines (solid lines), axes of maximum 300mb wind speeds (arrowheads).

Boundaries Oriented Generally West To East

Boundaries At The Base Of Troughs

Generally, such moisture boundaries are curved concave toward the poleward side. They may be curved generally parallel to the upper air streamlines which are curved cyclonically around a trough or low. Many of those types of boundaries are associated with jet stream axes of maximum winds. The primary exception is the "base surge" boundary.

Consider the case illustrated on **Figure 70**. On **Figures 70a** and **70b**, a boundary is present at "A" across the Great Lakes region. On the 300mb analysis, an axis of maximum winds lies along the boundary. The boundary and the associated jet stream are curved around the upper air trough over eastern Canada.

During the following 24 hours, the upstream ridge moved eastward and amplified. The winds along its forward side became more northerly with greater speeds. The same boundary - labeled "A" on **Figure 70a**, is shown 24 hours later on **Figure 70c**, labeled "B". As the boundary surged southward, the curvature increased, and the dark zone along its poleward side widened and became darker. On the 300mb analysis of **Figure 70d**, an axis of maximum winds is present from western North Carolina northeastward on the eastern side of the high amplitude trough. There are no strong winds along a large portion of the "base surge" boundary. In fact, the streamlines of the upper air wind fields cross the boundary along a large portion of its length - generally from Nebraska to northern Georgia.

The image interpretation concepts involved in distinguishing "base surge" boundaries from those with parallel jet streams, are similar with those used with boundaries on the forward sides of troughs. With base surge boundaries, generally, the dark zone on the poleward side of the boundary tends to be wide with a poorly defined or irregular rear edge. If the dark zone is narrow with a relatively well defined parallel edge on its poleward side, an axis of maximum winds is likely along the equatorward side boundary. Also, base surge boundaries tend to move rapidly equatorward. Another valuable key is the overall moisture pattern on the poleward side of the boundary. If the pattern implies that a trough or low is present, a jet stream is likely. If it implies a ridge dominates the region, a "base surge" boundary is likely.

Other examples of the formation and evolution of "base surge" boundaries were shown in previous sections on **Figure 9** and on **Figures 17** and **18**. Many moisture boundaries on the equatorward sides of troughs and lows were shown on the examples used for other purposes. The image features and jet stream conditions may be observed by reviewing the figures of previous sections.

Boundaries Over The Poleward Sides Of Ridges

Generally these have well defined jet stream axes nearly coincident with the boundaries. Also, the boundaries are often quite distinct because a cirrus cloud edge is often present along a large portion of the moisture boundary. Examples were shown in Section D2. **Figures 58** and **62** provide representative samples. Such curved boundaries - convex toward the poleward direction - have perhaps the best relationship with jet stream axes, compared to other boundary features on satellite imagery. However, there are exceptions and some complications. The jet axes slope with height; therefore, the axis of maximum winds on a specific upper air constant pressure analysis may not be coincident with the moisture boundary, or the relationship may vary along different parts of the same boundary. Generally, when exceptions were observed, the boundaries involved were not well defined, the curvature was of very large amplitude such as an apex, or when conditions were changing rapidly with time. We shall discuss the time change situations in the next section.

When the jet stream over the ridge is of "channeled" configuration, the cirrus clouds commonly extend downstream along the equatorward side of the jet axis, often to the base of the downstream trough. In other cases, when the configuration changes to an "NVA advection" type on the downstream side of the ridge, the cirrus dissipates. However, the moisture extending downstream can be observed on the water vapor imagery. When the cirrus boundary is aligned with the moisture boundary, a well defined jet stream axis is likely to be present along the downstream moisture boundary. Such a case was shown on **Figure 62**. The cirrus dissipated near the coast of southern New England, and the moisture boundary continued downstream with a similar radius of curvature. In cases where the cirrus dissipates, and the moisture boundary is equatorward of the cirrus edge, and perhaps with a different shape of curvature; the jet axis is not likely along the moisture boundary. An example of this was shown on **Figure 60**.

Straight Or Zonal Boundaries

With relatively straight boundaries oriented west-east, an associated jet stream axis is likely. This is especially valid, if the boundary has only a narrow dark band associated with the lighter gray shades on the equatorward side. With relatively straight zonal boundaries, the eastern portions are very likely associated with a jet axis. The western portions present the primary interpretation problem. Basically, the presence of a jet axis in that position depends upon the varying conditions on the poleward side. There is usually an upper air ridge on the equatorward side of the western portion. If there is also a ridge to the poleward side, such as in a "roll-over" situation, strong winds may not be present along that portion of the boundary. In those cases, there is likely to be on the poleward side of that western portion of the boundary either: (1) a wide dark zone of the type indicating that anticyclogenesis is taking place poleward of there, or (2) a narrow dark band with equally light or even lighter gray shades on the poleward side, indicating that ridge has "rolled over" to the poleward side. Generally, the presence or absence of a jet stream axis along the western end of a boundary can be determined better by examining the overall pattern on the poleward side, rather than features of the boundary itself. If those poleward side patterns indicate a trough, an associated jet stream is likely.

The primary exception to the foregoing rules occurs when a strong jet stream breaks through the ridge of a storm system. An example of this can be seen on **Figure 10**. In that case, a strong west to east oriented jet stream formed to the north of the inside boundary over the northeastern Pacific Ocean. This jet stream broke through the upstream ridge, and the high clouds and moisture of the "head" ridge extended eastward and persisted along the northern side of the jet stream. As a result, on **Figures 10b** and **10e**, the gray shades to the north of the relatively straight dark band are as light or lighter than those on the south side. Often, in such cases, there will be an initial jet stream branch along the eastern end of the head ridge on its poleward side; and when the jet breaks through the ridge, two jet branches are present during the transition. Usually the poleward of the two then weakens and the jet stream which has broken through to the equatorward side becomes the primary jet stream.

When two or more west to east boundaries are present generally parallel to one another, with the exception of "break-through" situations; the poleward one is likely associated with a jet axis. Those on its equatorward side are likely residual boundaries, or with weakening axes of maximum winds.

c. Change With Time and System Interactions

Constantly, within the jet stream zones, some branches are weakening or dissipating; whereas, others are intensifying or forming. They are also moving, or propagating, as their associated wind speeds change. Commonly, both the amount of movement and the changes of wind speeds with time are significant during the 12 hour time interval between radiosonde sets.

For example, during a 12 hour time interval, a zone of maximum wind speeds may move eastward and weaken significantly; while a second one forms to the west, and moves into a position near where the first one had been at the beginning of the period. Although the wind speeds of the second branch are intensifying, they have not yet reached the magnitudes initially observed with the first one at the beginning of the period. If this situation were observed with upper air data at 12 hour intervals, it may appear that the first zone of maximum winds had remained nearly stationary, perhaps retrograded slightly, and that its maximum wind speeds have decreased. The same conclusion could be made by comparing an initial radiosonde set and an accurate 12 hour upper air prog. Interpolation between the initial data and the 12 hour prog would imply that the winds had remained strong over the area; whereas, they had been significantly less at the mid-point of the time period. At the end of the time period, the second speed maximum is moving rapidly eastward and strengthening. Extrapolation of the initial data and prog would imply that the speed maximum is nearly stationary with weakening wind speeds. Although an experienced forecaster would likely detect the situation, more frequent information is highly useful for aviation support. Satellite imagery, available at more frequent intervals, may be used; and, water vapor imagery is particularly applicable. Even if upper air forecasts are available at more frequent intervals, such as 3 or 6 hours, the imagery will be useful to refine and evaluate the forecast results.

The imagery will not be useful in determining the wind speeds, except in a relative basis, such as distinguishing very strong from weak. However, if the initial radiosonde data are used to determine that a particular moisture boundary or feature is related to an axis of maximum winds, those associated speeds are initially known. The movement of the feature can be accurately observed on the subsequent imagery. Furthermore, observed changes on the imagery, during the movement, may be used to detect cases of significant wind speed changes along the axis of maximum winds.

The types of image changes useful in relation to changing jet stream conditions, involve system development and demise, and the complex interactions of adjacent systems as they move at different speeds and deform. Many of the more common types of changes and system interactions were illustrated and discussed in the previous sections. Those changes and their related image patterns will likely be recognized on future imagery. However, on a daily basis, many of the patterns and changes observed are likely to appear unique or unusual compared to those shown here, or recognized from past experience. Because of the large variety of system interactions, we shall not attempt to show numerous past cases for future reference. We will provide a set of general relationships that may be applied in conjunction with available upper air data and computer forecasts; and, we shall provide a few illustrations of typical changes and interactions.

For relating jet stream conditions to water vapor imagery, it is very useful to be able to identify the thermal ridges and thermal troughs which occupy the upper middle troposphere, generally between 600mb and 400mb. These can be related to the water vapor imagery; and, the changes with time of the associated thermal gradients are reasonably well correlated to changes of the jet stream conditions.

On water vapor imagery, the thermal ridges usually have lighter gray shades than their adjacent thermal troughs. High level moisture or cirrus clouds are commonly present within the very cold air above the thermal ridges. The air above the thermal troughs is relatively warm and dry. The moisture which contributes to the image gray shades is usually from air which is warmer than that above the adjacent thermal ridges. Therefore, the thermal trough patterns appear darker on the imagery. Note, however, that the very lightest and darkest gray shades are not generally at the centers of the thermal ridges and troughs. The darkest gray shades tend to be in the downstream portions of the thermal trough flow fields, and the lightest gray shades tend to be in the upstream portions of the thermal ridges. By using the relative gray shade differences, in conjunction with the patterns and their evolution, many of the thermal ridges and troughs can be identified from the imagery alone. If the imagery can also be compared with the latest set of radiosonde data, the relationships may be confirmed or refined.

Once the thermal ridge and trough patterns have been identified on the imagery, the motions must be taken into account. Those boundaries with the thermal trough on the left, and the thermal ridge to the right (Northern Hemisphere), are likely to have wind speeds increasing with height in the upper troposphere; and, are likely associated with an axis of maximum winds. If such a boundary, and its associated thermal gradient zone, is created; a jet stream branch is likely to form. If such a boundary and an associated axis of maximum winds are present, the wind speeds are likely to increase with time if the thermal ridge strengthens, the thermal trough strengthens, or both strengthen. The formations of thermal ridges and troughs, and the strengthening of those already present, can often be detected on the water vapor imagery. Also observed on the imagery, are the interactions of systems moving at different speeds and directions. Even if the intensities of the systems were not changing, a thermal trough on the left side of a jet stream boundary may be replaced by a thermal ridge, as systems move at different speeds. In most situations, this would cause the wind speeds to weaken significantly along the boundary.

Changes Associated With Thermal Ridge Developments

On **Figure 71a**, the low over southern Idaho has been moving slowly southeastward, as the open trough over the central states moved eastward. This has resulted in a wide complex jet stream zone across the southern United States and northwestern Mexico. Within the zone, a southern branch "A" extends across northwestern Mexico and the gulf coastal area; and, a northern branch,"C", extends around the western low, and across the south central U.S. to the base of the eastern trough.

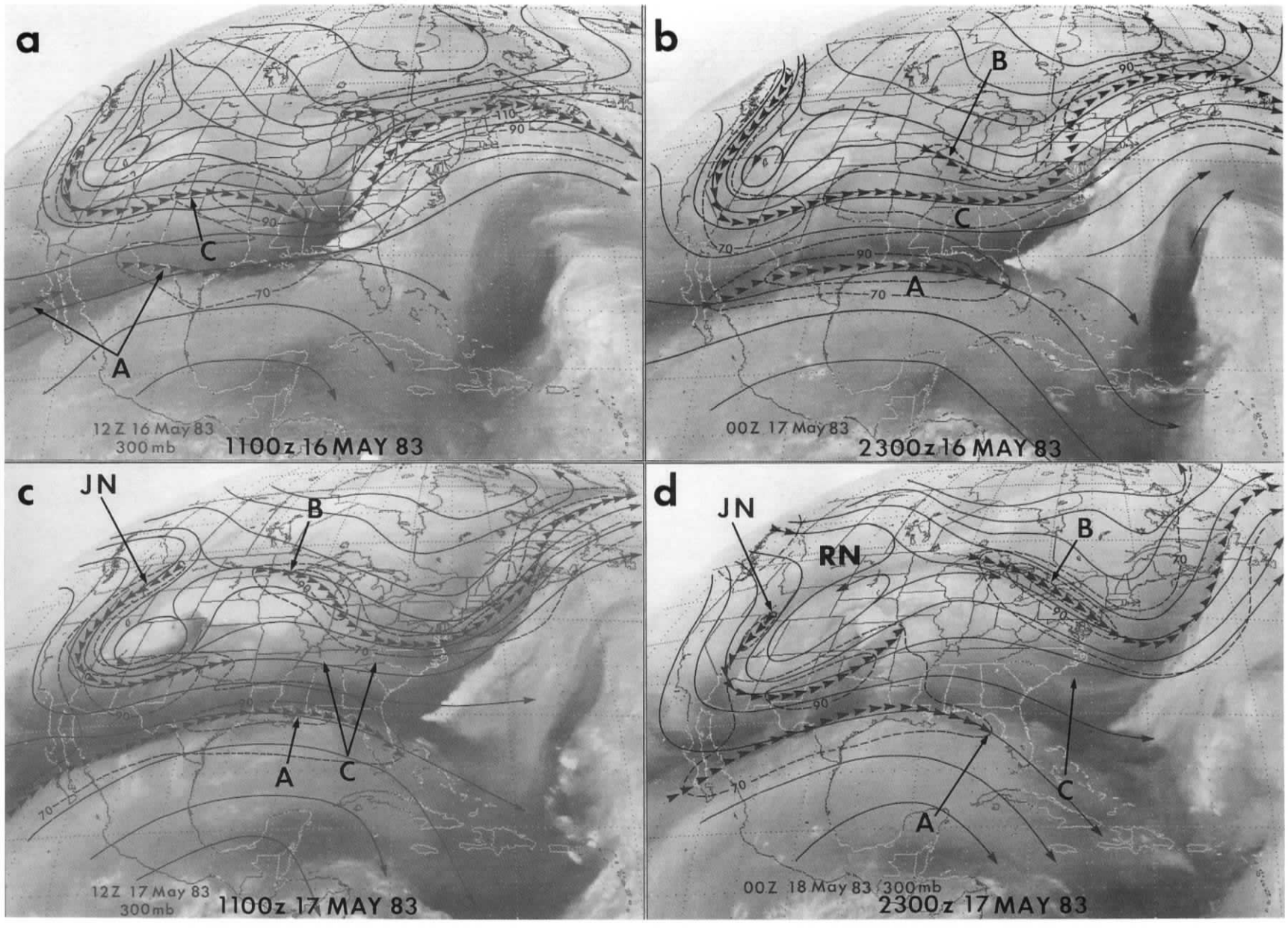

Figure 71 **FORMATION OF NEW JET STREAM BRANCH - THERMAL RIDGE DEVELOPMENT**
Sequence of 4 GOES East 6.7μm images with 300mb analyses superimposed. Image times are:
Fig. 71a. 1100Z 16 May 1983. **Fig. 71b.** 2300Z 16 May 1983.
Fig. 71c. 1100Z 17 May 1983. **Fig. 71d.** 2300Z 17 May 1983.
Analyses valid 1 hour later than images, streamlines (solid lines), isotachs (dashed lines), axes of maximum 300mb wind speeds (arrowheads).

On the first image, a region of high cold topped clouds has formed around the northeastern side of the Idaho low. The primary area of cold clouds is over Wyoming. This region of cloudiness is difficult to observe on the water vapor imagery, since no well defined moisture borders have formed. During the next 12 hours, the cloud region increased in size, and the amplitude of the anticyclonically curved streamlines increased, as the upper air ridge strengthened to the east of the low. During the second 12 hours, between **Figures 71b** and **71c**, the cloud region increased even more significantly, as deep convective clouds formed over the high plains. During this period, the upper air ridge extended eastward. The air temperatures in the ridge increased approximately 5°C between 500mb and 400mb. A "cold cap" feature formed at high levels - just below 200mb, where the air temperatures cooled by an average of 5-6°C. The cloud formation and ridge intensification, with the associated temperature changes, occurred to the left of the primary jet stream zone "C". Along the downstream portion of the new ridge, the upper air wind speeds increased on the left side. On **Figure 71c**, a new jet stream branch has formed at "B". The level of maximum winds in the new branch is near 250mb, with a maximum reported wind speed of 96 knots over central Minnesota. The 500mb and 400mb temperature gradients over that region increased; whereas, those over the Kansas, Missouri, Arkansas have decreased. There, the wind speeds decreased between 300mb and 250mb, but remained strong above 200mb. A weaker higher level axis of maximum winds remained at position "C" on the last two images.

During the last 12 hour period, the moisture extended downstream from the cloud region. The mid-tropospheric thermal ridge has extended downstream more rapidly than the cold trough over eastern Canada. At 500mb, the temperature gradient along the left side of the thermal ridge has increased. The level of maximum winds of branch "B" has lowered to near 300mb, and wind speeds have increased to a maximum of 120 knots. During the last 12 hours, the interaction effects of the thermal ridge moving adjacent to the eastern Canada thermal through have produced an additional increase of the wind speeds of branch "B".

Another example of interaction effects can be seen along the western part of the system on **Figure 71d**. The thermal ridge has elongated from western Colorado to Virginia. The upstream ridge, "RN", has "rolled over" along the northwestern side of the slow moving upper air low, with warmer mid-tropospheric air across Montana. The thermal trough between the two thermal ridges has weakened, and the wind speeds of the jet stream, "JN", on the west side of the low have weakened significantly.

When a new upper air ridge builds on the left side of the primary jet stream, as in this case, the jet stream zone changes with time. A new branch forms to the left downstream side of the new thermal ridge. To the right downstream side of the new thermal ridge, the wind speeds usually weaken in the 400mb to 250mb layer, but remain strong, or at times, even intensify at very high levels. Such new ridge formations are associated with significant new cloud production, and the production of a cold cirrus overcast. The new jet branch forms along the downstream left boundary of that cirrus. There is an empirical positive correlation between the amount and rate of cloud formation and the intensity of the wind field changes. Intense deep convective weather enhances the effects.

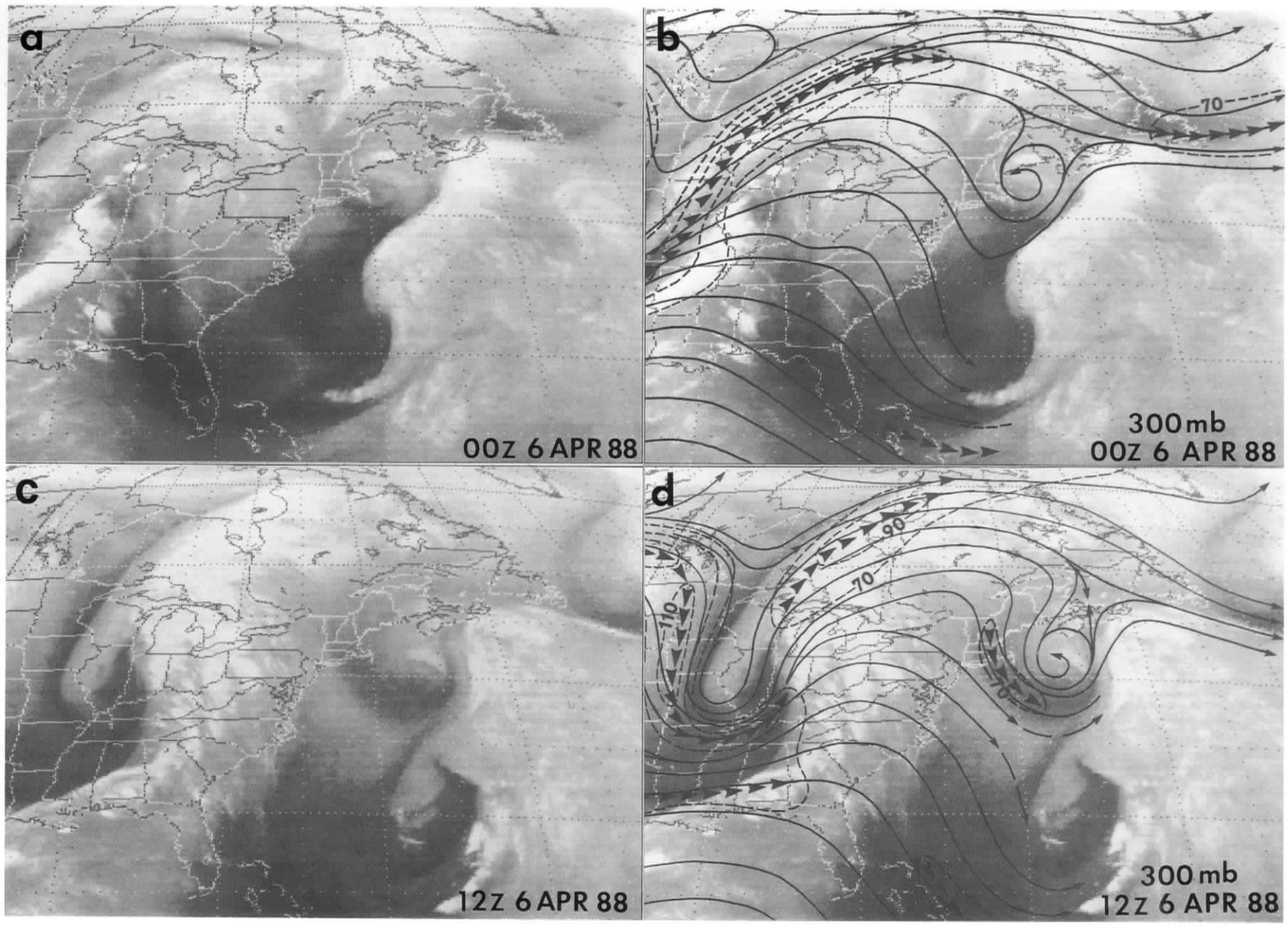

Figure 72 **INTENSIFICATION OF THERMAL LOW AND ASSOCIATED JET BRANCH**
Fig. 72a. 6.7μm image, 0000Z 6 April 1988, GOES East. **Fig. 72b.** Same image with 300mb analysis.
Fig. 72c. 6.7μm image, 1200Z 6 April 1988, GOES East. **Fig. 72d.** Same image with 300mb analysis.
Analyses: Streamlines (solid lines), isotachs (dashed lines), axes of maximum 300mb wind speeds (arrowheads).

Thermal Trough Intensification

At the time of the first image on **Figure 72a** and **b**, two upper air lows are present within the trough east of the United States. There have been relatively weak jet stream branches across the upstream ridge into both low circulations. During the 12 hour period shown on **Figure 72**, the northern low became "cut-off" and intensified. The 500mb temperatures in the core region decreased by approximately 4-5°C, with no detectible changes in the adjacent ridge temperatures. On the water vapor imagery, a dark region formed on the west and south sides of the low with a well defined boundary on its southwest side. A jet stream branch intensified along that boundary. At 300mb, wind speeds greater than 70 knots have formed on the southwest quadrant of the low. Although the low intensified within the trough position, it was to the right of the primary jet stream zone over the ridge in northeastern Canada. New or intensifying jet stream branches, such as that shown here with the low intensification, appear to be less frequent than those formed with new ridge formations. In this case, the ridge over eastern Canada intensified and closed. Images and 300mb analyses for the following 24 hour period were shown as **Figures 3** and **7**. As the anticyclone formed, the cyclonic circulation became larger, and the boundary with the intensified jet branch persisted. New jet branches with thermal trough intensification are prevalent in this situation with anticyclogenesis and a new col formation (**Figures 3** and **7**).

Interactions - Thermal Ridge And Thermal Trough

An example of a thermal ridge moving adjacent to thermal trough, and resulting intensification of a jet stream branch was shown on **Figures 71c** and **71d**. The warmer mid-tropospheric air from the intensified ridge over the central United States moved rapidly eastward. Thus, the thermal ridge extended eastward onto the right side of the slower moving thermal trough over eastern Canada. The thermal gradients and upper air wind speeds along the extended boundary increased. As is usually the case in such interactions, the warmer air of the thermal ridge moves rapidly on the equatorward side of a slower moving trough to the poleward side.

Another type of jet stream branch intensification occurs when a thermal trough on the poleward side of a ridge retrogrades - or "falls back" in a relative motion basis. An example of this was shown on **Figure 37**. During that sequence, as anticyclogenesis occurred over Canada, the winds over Quebec Province changed from northerly to nearly easterly. The cooler air between the Canadian ridge and the Atlantic low moved southwestward with respect to the moving ridge over eastern United States. Over the northeastern U.S., the mid-tropospheric temperature gradient increased; and, strong winds continued to form at the upstream end of the jet branch along the U.S. east coast. Usually in such cases, the maximum winds of the jet branch increase; however, in this case upper air data were not sufficient over the western Atlantic to verify this. That type of interaction, shown on **Figure 37**, is common on the downstream sides of intensifying ridges with mid-tropospheric flow rotating anticyclonically with time. The trough to the east of the ridge tends to hold or retrograde; and, the upstream end of the jet stream branch at the base of the trough intensifies. This type of change with time often occurs at the equatorward ends of "inside" boundaries during the formative phases, and is common with those particular "inside" boundaries of "omega" type blocking regimes.

Interactions - Thermal Ridge To Thermal Ridge

When two thermal ridges approach one another, causing the trough between to narrow and elongate, the associated jet stream branches usually weaken. There were many examples of this type of interaction in previously illustrated cases. A common example occurs with cyclone formations, in which the downstream ridge "builds back" and the upstream ridge "rolls over". The various patterns resulting from those interactions were discussed in the last section in regard to jet stream conditions. The changes with time with such interactions were better shown in Section B - Evolution of Features. The merging of the "roll-over" and "build-back" ridges is illustrated on **Figure 35**. In that case, the weak wind portion of the boundary extended with time over the western and central United States as the upstream ridge "rolled over" the downstream ridge. For example on **Figure 35**, Time T-10, the wind speeds between the two ridges have weakened from Oregon to Illinois.

A similar "roll-over" type of interaction occurs with systems moving in two branches of westerlies, when a ridge in the poleward branch rapidly overtakes a ridge in the equatorward branch. An example of this was shown on **Figure 47**. At the time of **Figure 47e**, a strong jet stream branch was present along the northern side of the eastern U.S. ridge. During the next 12 hours, the upstream Canadian ridge extended rapidly eastward. As the warm air of the Canadian ridge merged with the U.S. ridge, the trough between them elongated and weakened, and the jet stream branch weakened rapidly.

As noted, there is a significant exception to the general rule that jet streams tend to weaken between merging ridges. This occurs when a trough becomes elongated between a downstream ridge and an upstream ridge with a jet stream branch "hooking" anticyclonically equatorward on its eastern side. Generally, in such cases, the upstream ridge is a "closed" type. As opposed to an open ridge, the jet stream curves anticyclonically around the ridge. The ridge is likely to be very slow moving, or anticyclogenesis may be occurring. A jet stream branch is likely to "hook" around the ridge in a "channeled" or nearly "channeled" type of configuration. The downstream trough becomes elongated and narrowed, but changes to a strong cyclonic shear zone with jet streams in opposite directions on both sides. An example was shown on **Figure 20f**. In that case, as anticyclogenesis occurred, a jet branch "hooked" anticyclonically around its eastern side. The jet stream wind speeds were maintained on both sides of the upper air trough over the eastern United States.

Interactions - Thermal Trough To Thermal Trough

As with thermal ridges, the associated jet streams tend to weaken between two merging thermal troughs. The thermal ridge between the two troughs narrows and elongates. The three most common situations for this type of interaction are: at the western side of opening cut-off lows, with "split" ridge formations, and with jet stream "break-throughs" - in which a jet stream "breaks" across its downstream ridge. Both of the second two types tend to occur with "build-back" omega type blocking regimes. An example was shown on **Figure 67a** and **b**. The upper air ridge had already become narrow over the eastern United States between the two lows. In fact, a col was present in the 300mb wind field, centered over Ohio. A jet stream branch was present around the eastern side of the western low on the western side of the ridge, from Arkansas to Illinois to Iowa. On **Figure 73**, the 300mb analysis is shown on an image 12 hours after **Figure 67**. As the ridge continued to narrow between the two lows, the jet stream branch around the eastern side of the western low weakened. A short branch of maximum winds has remained over northern Iowa, where the upper air high remains wide to the north and east.

Also in this blocking regime case, a stronger speed maximum "broke" across the ridge over the southeastern states. In such cases, the jet branch on the equatorward side of the western low extends across the base of the ridge to the right side of the jet branch already present on the equatorward side of the eastern low. This results in two jet branches on the equatorward side of the eastern low. Usually the poleward of those two weakens and dissipates, as the thermal ridge between the two jet branches narrows and weakens.

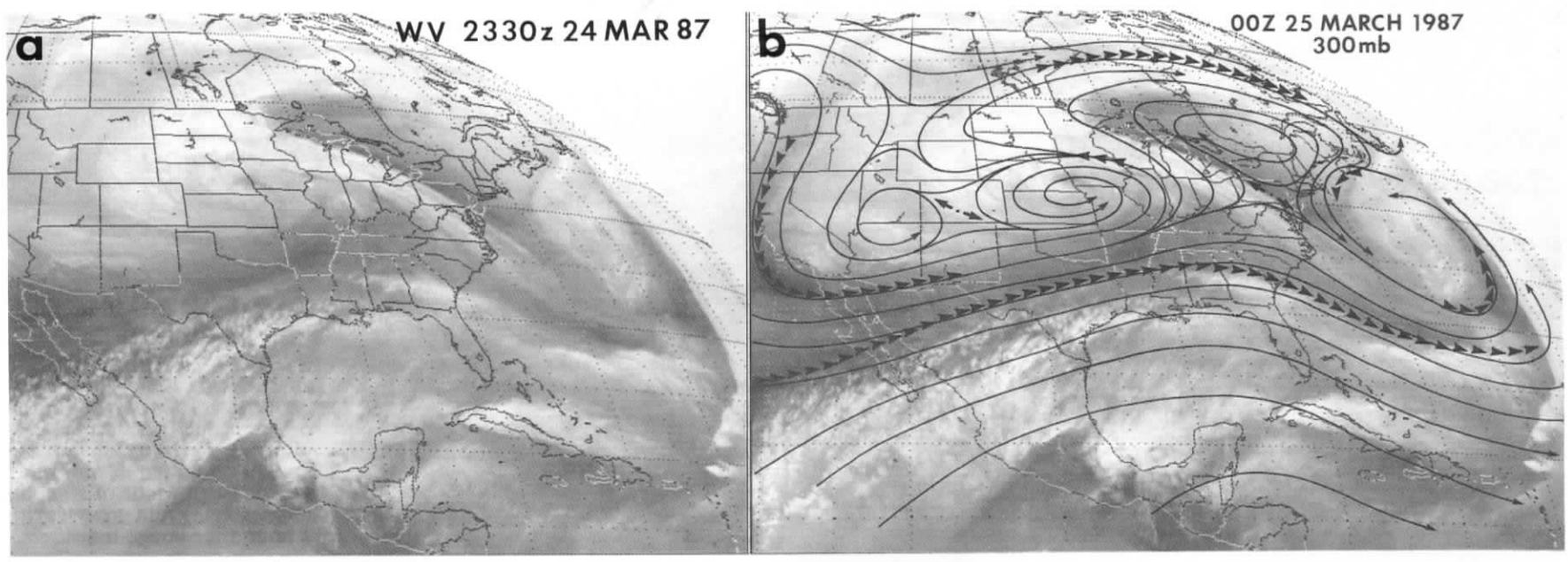

Figure 73

JET BREAKS ACROSS DOWNSTREAM RIDGE - OMEGA PATTERN
Fig. 73a. 6.7μm image, 2330Z 24 March 1987, GOES Central.
Fig. 73b. Same image with 0000Z 25 March 1987 300mb analysis, streamlines (solid lines), axes of maximum 300mb wind speeds (arrowheads).

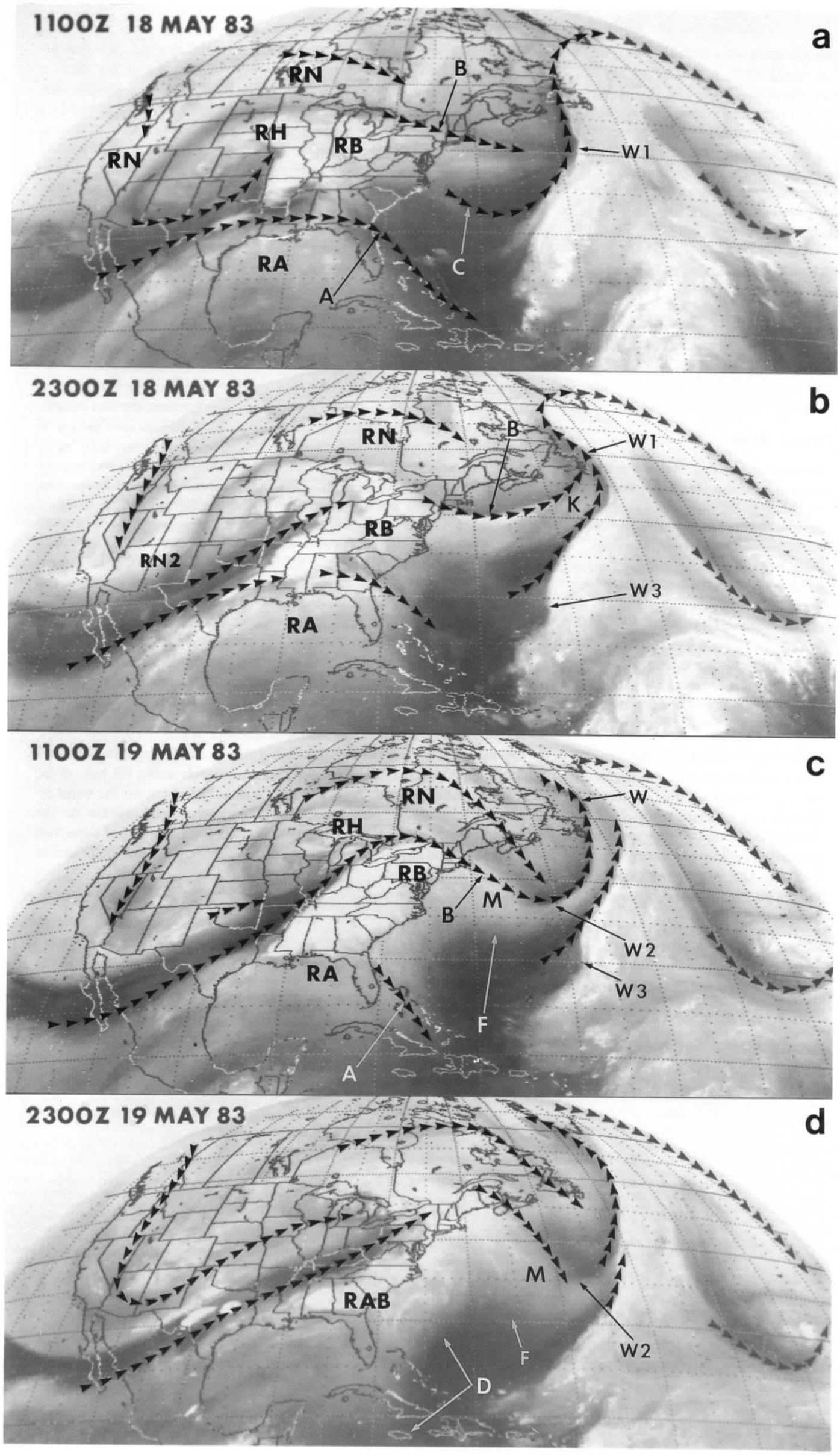

Figure 74

SYSTEM INTERACTIONS AND CHANGES
Sequence of four GOES East 6.7μm images at 12-hour intervals. Arrowheads indicate axes of maximum 300mb wind speeds (with winds of 70 knots or greater). From analyses 1 hour after image times.

A Summary Of Jet Stream Changes And Interactions

The four images of **Figure 74** were also shown on **Figure 11** as an introduction to boundary changes and residual effects. A sequence of 4 images at 12-hour intervals prior to those of **Figure 74**, was shown on **Figure 71**. Those images, with 300mb analyses superimposed, were used to illustrate the formation of a new jet stream branch.

In the discussion of **Figure 11**, emphasis was placed on the boundaries and changes over the western and central U.S. A jet stream branch, "digging" southward over the western states contributed to a "return moisture" boundary over northwestern Mexico, and caused the cyclone over the central U.S. to open and accelerate northeastward. Here, we shall emphasize the changes and interactions over eastern North America and the western Atlantic Ocean.

Consider the first image of the sequence - **Figure 74a**. In regard to the streamline curvature of the upper air flow, a large trough extends from eastern Canada, southward over the western Atlantic Ocean to the Dominican Republic. However the trough is complicated by several branches of maximum winds within its cyclonic flow pattern. A northern branch, "B", crosses the coast over New England. This axis of maximum winds developed and intensified during the sequence of images on **Figure 71**. It has become the primary branch entering the western side of the Atlantic trough. The two branches at "A" and "C" are weakening with time; however, both have wind speeds near 100 knots remaining, with levels of maximum winds between 250mb and 200mb.

An area of maximum wind speeds along jet branch "B" has moved eastward off the New England coast. In response to this, the boundary of high clouds and moisture on the eastern side of the trough has become perturbed at "W1". Also, an area of lighter gray shades on the image has extended eastward along the right side of the jet stream branch "B". The lighter gray shades are extended from the moisture regime of ridge "RB", and are associated with warmer mid-tropospheric air of the ridge. Thus, the image pattern implies that some of the warmer mid-tropospheric air from ridge "RB" has protruded eastward into the cooler air of the downstream trough. If the protrusion continues, the thermal field of the trough will be divided into two primary parts by the thermal ridge along the southern side of jet branch "B".

By the second image time, the moisture along the southern side of jet branch "B" has extended across the trough, and has nearly merged with the moisture on the eastern side of the trough to the south of "W1". In the area indicated by "K", the moisture that crossed the trough has moved adjacent to the moisture originally on the east side of the trough. Two boundaries are present with two axes of maximum winds. In such cases, while both boundaries remain well defined on the water vapor imagery, two axes of maximum winds are present with the one to the right side weakening with time. When the jet stream branch on the right side dissipates or loses identity, the two boundaries will have merged, or the one on the right side will have become very poorly defined.

Between the first two image times, ridge "RN" over Canada moved eastward into longitudinal phase with ridge "RB". When two ridges in separate branches of westerlies move into phase in this manner, it is common that the winds along the eastern sides of both ridges rotate anticyclonically with time. The equatorward component of the wind directions on the western side of the downstream trough increases. Features within the trough environment begin to accelerate equatorward. This process has begun by the second image time of **Figure 74**. A perturbation has begun to form along boundary "B" just east of New England. During the next 12 hours, the perturbation amplified and accelerated southeastward to position "W2".

During the same overnight period between **Figures 74b** and **74c**, a large area of convective weather formed along the eastern side of the opening central U.S. trough. Ridge "RB" intensified, and the jet stream along its western side "broke across" the ridge to connect with jet stream branch "B". This increased the wind speeds along the jet stream at "B" and probably contributed to the acceleration of perturbation "W2". It also caused a new surge of moisture from the ridge into the trough environment at "M".

At the second image time, the trough had become divided into two primary parts. However, the basic flow had remained westerly; and, the division was manifested in wind speeds, vorticity, and thermal fields. By the third image time, the division has become greater. The surge of moisture at "M" is associated with a significant protrusion of mid-tropospheric warm air across the trough. The northern edge of the warm air is along jet stream "B". That portion of the trough on the poleward side of "B" remains open. In this case, it has become subdivided by the additional jet stream branch from the Canadian ridge "RN". The southern side of the warmer air is represented on the imagery by the moisture edge at "F". In comparison to the boundary at "B", the edge at "F" is poorly defined. The gray shades darken gradually toward the south. In regard to the moisture pattern "M", we refer to the northern boundary along "B" as the "hard" side, and the edge at "F" as the "soft side". As the moisture regime "M" from the upstream ridge protrudes eastward into the trough, warmer air moves onto the poleward side of the slower moving cold air at the base of the trough. In such situations, the upper air winds near the "soft" edge "F" decrease speeds and rotate anticyclonically with time. The rotation is greater than would be attributed to the re-orientation of the trough and ridge systems. Upper air anticyclogenesis is in progress, although it may not continue to form a closed anticyclone. As the moisture regime of the upstream ridge "rolls-over" the trailing end of the trough, the upper tropospheric winds cross edge "F" from the moist side toward the dry side, and are rotating anticyclonically with time. At the third image time, they cross the edge from the northwest, then rotate to northeasterly by the 4th image time. During the 12 hours between the last two image times, the winds changed to easterlies in the dark area south of edge "F". In response, the western edge of the dark area became better defined and moved slightly westward; an inside boundary formed.

At the third image time, a weakening jet stream branch was present at "A" southeast of Florida. By the last image time, this speed maximum had moved southeastward with decreasing wind speeds. A small closed upper air low formed with its center just west of Puerto Rico. The trough has become divided into three basic parts: (1) a "cut-off" low at the equatorward end, (2) an open trough at the poleward end to the north of jet stream branch "B", and (3) a narrow elongated portion between the moisture regime "M" and the moisture regime of the downstream ridge between "G" and "E".

The division of a trough into three basic parts is common when a jet stream branches across a trough from the upstream ridge. Generally, the poleward part of the trough remains open, and is strengthened by additional cold air moving along the left side of the branching jet ("B" in this case). New cyclogenesis often occurs on the forward side of the open portion of the trough. In this case, cyclogenesis occurred with feature "W1". The resulting closed upper low is located southwest of Greenland at "L" at the last image time. It is common that a closed upper air low forms at the equatorward end of the trough. Usually this low is also "cut-off". The central part of the trough becomes elongated and narrow between the two merging ridges. On the water vapor imagery, a dark zone coinciding with the remaining thermal trough becomes narrow between the stationary or slower moving downstream ridge and the approaching moisture regime of the upstream ridge. The eastern side of this dark zone is usually well defined and coincident with a jet stream axis on the forward side of the trough. The western side of the dark zone is the leading edge of the moisture approaching from the upstream ridge. The features of this edge, and the jet stream conditions vary significantly. Generally, if the "soft" side of the moisture regime (edge "F" in the case shown) approaches and forms the rear boundary of the dark zone, the narrowing trough weakens; and the jet stream winds along its eastern side decrease with time. We believe this occurred in the case shown, although upper air data were not present in the exact locations to confirm the decreased speeds.

In some cases, the "hard" side of the approaching upstream moisture regime (boundary "B" in the case shown) forms the rear side of the narrow dark zone. In those cases, the jet stream "hooks" anticyclonically equatorward. Therefore, a jet stream axis is present on the western side of the narrow dark zone, with winds of nearly opposite direction of those with the jet axis on the eastern side of the zone. The trough narrows to a strong cyclonic shear zone; and, the wind speeds of the jet stream along the eastern side are maintained. Often in such cases, the gray shades of the narrow dark zone become darker with time, with relatively well defined and distinct boundaries on both sides. In cases with the "hooking" jet branches and "hard" boundary approaching the eastern side of the trough, the narrow "shear zone" part of the trough is relatively long compared to the other parts; and, cyclogenesis is not likely in advance of the open part of the trough. An example of the long "shear zone" type of trough division was shown on **Figure 10**.

This page intentionally left blank

SECTION E

TROPICAL APPLICATIONS

Although we have emphasized systems and features at middle latitudes, and over the North American radiosonde network; we examined water vapor imagery at all latitudes. Our observations at tropical latitudes included the U.S. GOES satellite areas, and approximately four years of METEOSAT imagery. We did not view water vapor imagery over longitudes between 60°E and 160°E.

Most of the concepts illustrated and discussed in the preceding sections are applicable at tropical latitudes. The primary differences are in the relative frequency of occurrence of specific types of features; and the fact that the image features at lower latitudes are related to circulation features at higher altitudes. Although jet stream wind speeds of greater than 100 knots are sometimes observed over the Equator, the upper air temperature gradients and wind speeds at low latitudes are usually less than those commonly observed at middle latitudes. Because of this, changes in the upper air conditions induced by vertically deep convective weather, are more prevalent and play a more dominant role than at middle latitudes. In this regard, those image features related to rapid amplification of upper air ridges, and blocking regimes with inside boundaries, are observed more frequently at lower latitudes.

We believe that water vapor imagery can be very useful for analysis and forecasting at tropical latitudes. Eventually, as our knowledge improves, the tropical applications of water vapor imagery may be more beneficial than at middle and high latitudes. With the relatively low density of radiosonde data over tropical areas, the imagery may be used to improve upper air analyses. These may be most directly applied in improved wind information for aviation support. However, the upper air circulation systems and their changes, are often of significant influence to surface weather conditions. The use of water vapor imagery to observe the upper air systems may be most applicable to improve local weather forecasts.

In this section, we will provide a summary of water vapor patterns and features at tropical latitudes. For the reader, this should provide an introduction to the common types of features and changes, and their potential applications. Since many of the features observed over low latitudes are similar to those already discussed, we shall show only a few of those, and emphasize others which are unique to tropical locations.

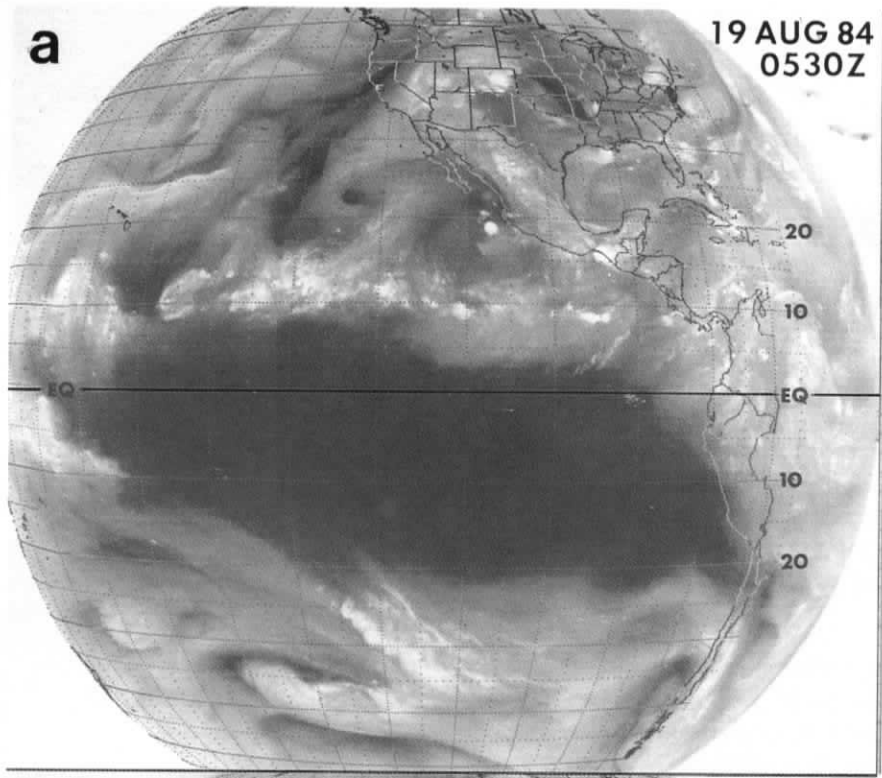

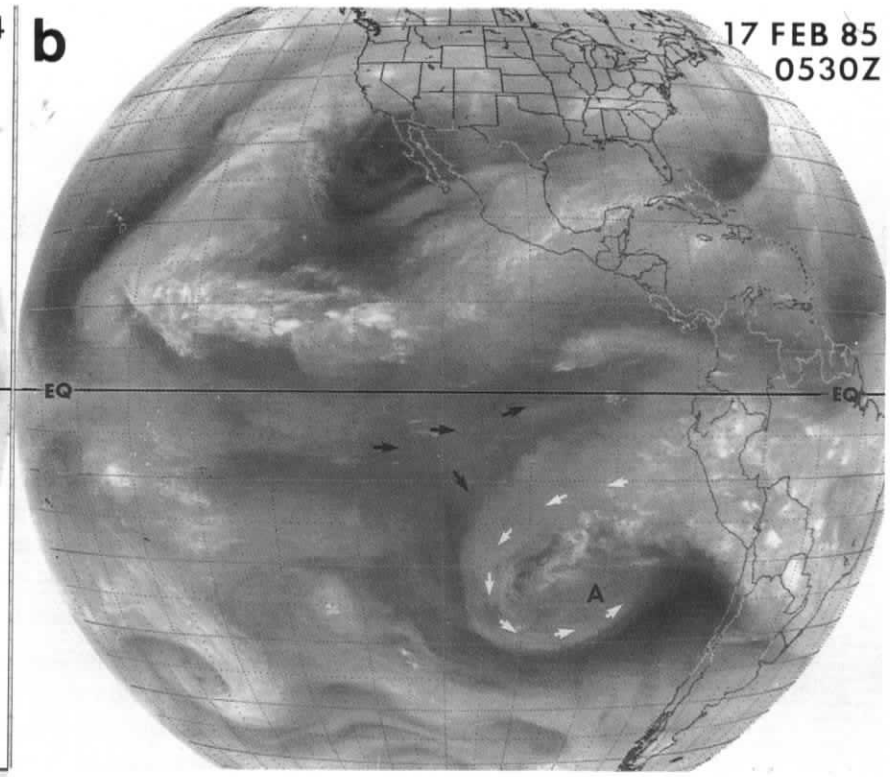

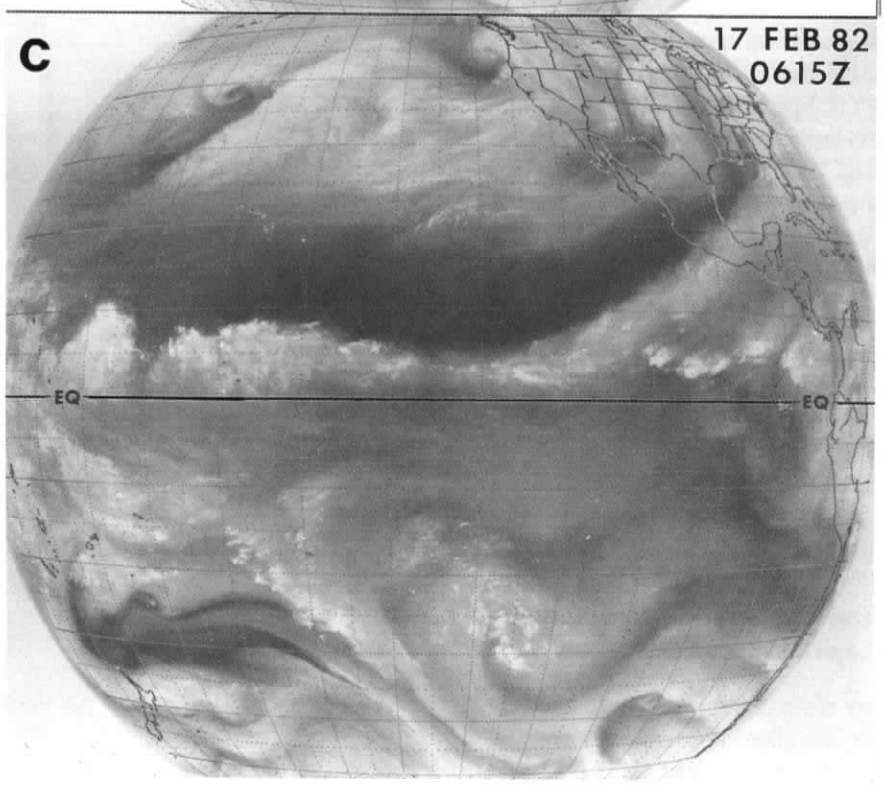

Figure 75

LARGE SCALE FEATURES - SEASONAL PATTERNS
Fig. 75a. 6.7μm image, 0530Z 19 August 1984, GOES Central (Satellite moving eastward).
Fig. 75b. 6.7μm image, 0530Z 17 February 1985, GOES Central. Black arrows - cirrus cloud motions. White arrows - 250mb wind directions, interpolated between analyses times.
Fig. 75c. 6.7μm image, 0615Z 17 February 1982, GOES West.

1. LARGE SCALE FEATURES

a. Large Tropical Dark Regions

In Section A, on **Figure 1b**, we showed an example of a boundary between moisture accumulated above the convective weather over South America, and the drier upper air westerlies over the southeastern Pacific Ocean. This was described as a "continental scale" feature, and is an example of a "large" scale tropical circulation pattern. Within the introduction to Section B, we referred to very large scale dark regions which are observed on water vapor imagery over subtropical latitudes. Although such regions are often "subtropical" in regard to their associated circulation systems, they are often "tropical" in regard to geographical location. An example is shown on **Figure 75a**. The large dark region is located primarily over the Southern Hemisphere, but extends across the Equator. Such large dark regions over tropical areas are most common during the winter season. Over those longitudes which we viewed on water vapor imagery, the large tropical dark regions were most commonly observed over the southeastern Pacific Ocean area - in the region shown on this case. They also tended to be larger and more persistent over this region. One reason for this is that the Intertropical Convergence Zone (ITCZ) convective weather regime remains on the northern side of the Equator, even during the Southern Hemisphere summer season. During years of climatological average sea surface temperatures, deep convective weather is rare between the Equator and 20°S, from the South American coast, westward to near 130°W. During those average years, deep convective weather is most likely during March and April, when a second ITCZ convective zone sometimes forms south of the Equator. Those convective regimes usually do not persist for more than a few days during each occurrence, and do not provide a persistent source of high level moisture. Therefore, in this eastern Pacific Ocean area, the large tropical dark regions tend to extend over a larger area, and remain residually dry for longer periods without being moistened by deep convective weather.

Note on **Figure 75a**, that the image over the summer hemisphere reveals many relatively small scale perturbations; whereas, large scale systems with a tropical dark region occupy the winter hemisphere. This set of conditions would have been our choice, if we were asked to guess the patterns over this region for some randomly chosen date in August. Although these may be the most typical conditions, the variability is of such a degree that the guess would be incorrect more than half of the time. For example, had we chosen a date one week prior to the time shown, or one week later, the large tropical dark region would not have been present. We shall return to this subject.

Consider a date approximately six months later than that shown, during the Northern Hemisphere winter season. An image valid on 17 February 1985 is shown on **Figure 75b**. Although large winter season types of systems are present over the Northern Hemisphere, no large tropical dark region is present. Several synoptic scale dark areas are present at different latitudes. Over the Southern Hemisphere, a large upper air anticyclone is present over the eastern Pacific Ocean. The system was centered at "A" in the 250mb wind field, interpolated between radiosonde times. Upper air moisture from the South American deep convective weather has moved westward around the anticyclone as indicated by the white arrows, which are similar to 250mb wind directions for the nearly stationary system. The black arrows indicate the directions of cirrus cloud elements valid at the time of the image, and reveal the split in the westerly flow on the western side of the anticyclone. Over the remainder of the Southern Hemisphere Pacific Ocean, small scale summer type systems are revealed by the water vapor patterns. Note that we have implied that there are additional factors than size to differentiate winter and summer season patterns on the imagery. In addition to being of large size or wave length, the winter season systems are more likely to consist of "open" troughs and ridges which are moving rapidly. On a single water vapor image, on which movement cannot be determined, the "open" patterns can often be revealed by elongated shapes of patterns with well defined boundaries on the western sides of moist areas and irregular or poorly defined edges on the eastern sides.

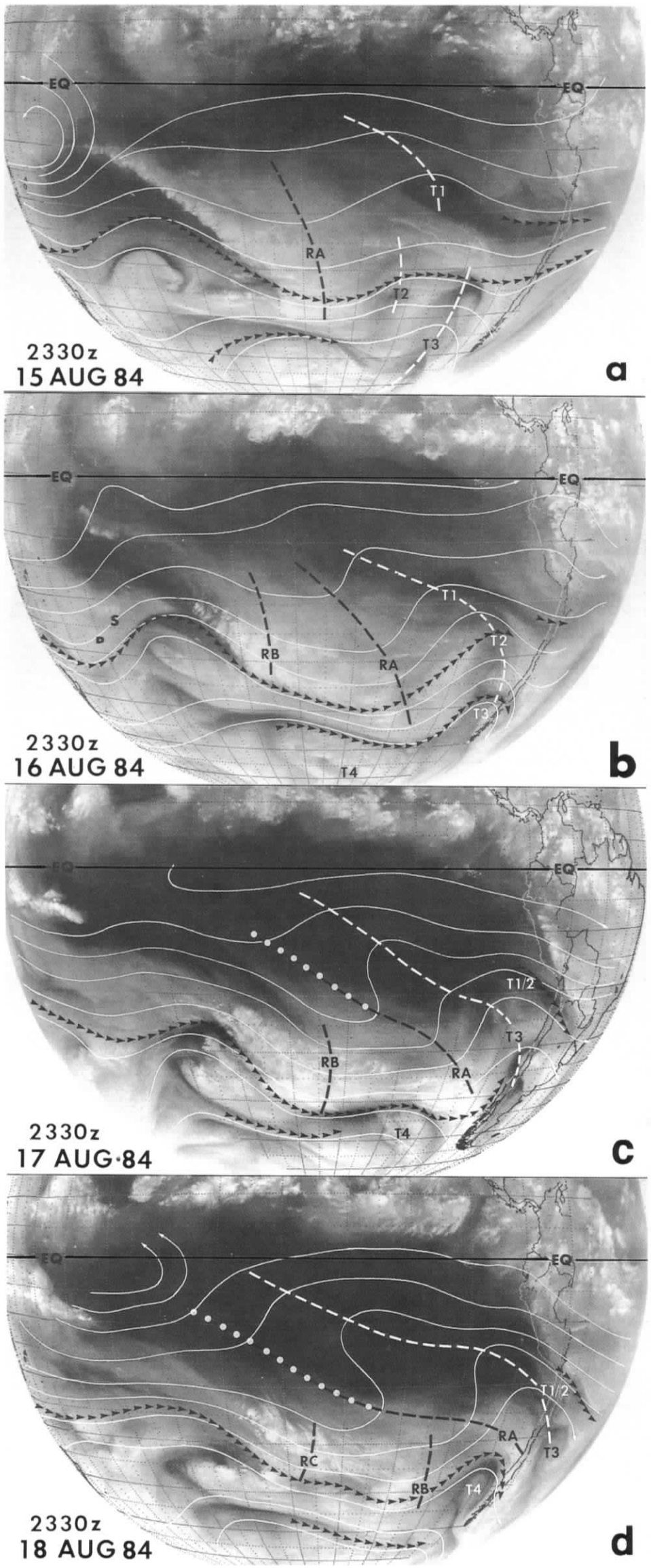

During the summer seasons, the systems sizes tend to be much smaller. Systems of the slow moving "closed" types are more prevalent. These are often revealed by their more rounded shapes, and by the well defined boundaries on the eastern sides of the moist patterns (the light shade areas). We shall address this subject again in our discussion of tropical cyclogenesis.

On **Figure 75c**, an image is shown three years prior to that of **Figure 75b**. On this February 17th, a large dark region is present over the tropical latitudes. The satellite was located at 135°W instead of at 115°W as in the first two cases; therefore, the view is farther to the west. In this case, with the dark region in the Northern Hemisphere, the dark area is not as large as in the first case. The ITCZ convective clouds are on the northern side of the Equator, limiting the southern extent of the dry region.

Consider, again, the large tropical dark region shown on **Figure 75a**. The dark region had reached its largest size on the 18th, and was decreasing slowly in size at the time of the image shown. On **Figure 76**, images are shown at 24-hour intervals during the period that the dark region formed. Streamline analyses of 250mb winds are superimposed on the images, and selected circulation field features are indicated. Troughs are indicated by dashed white lines and ridges by dashed black lines (with white dots where required). Axes of maximum 250mb winds are shown by arrowheads where wind speeds were greater than 70 knots.

On the first image, **Figure 76a**, a relatively narrow dark region has formed over the equatorial area. The dominant circulation feature is the ridge labeled "RA". This ridge has been increasing in amplitude and moving eastward. An area of relatively zonal and light westerly winds extends across most of the tropical region between the Equator and 20°S. On the next image, **Figure 76b**, ridge "RA" has moved eastward and amplified. The winds in advance of the amplifying ridge have turned more equatorward. This has caused the small trough systems "T2" and "T3" to move in paths turning to the left with time. Both of those systems have moved equatorward, and the overall trough patterns of systems "T1", "T2", and "T3" have merged in the streamline field, although their identities would likely be separate in the thermal and vorticity fields. Of most significance is the fact that the ridge "RA" has begun to "roll over" the downstream trough systems. This has contributed to a general "positive tilt" orientation in the large scale features. The systems are oriented with their poleward ends in advance of their equatorward ends.

By the second image time, ridge "RA" is near the end of its amplification phase; but a new ridge "RB" has formed, and is amplifying upstream from "RA". Therefore, during the next 24 hours, ridge "RA" continued to rotate. Note on the third image, **Figure 76c**, that the ridge axis "RA" has become generally parallel to the trough axis; and, both axes have continued to rotate to a greater degree of "positive tilt". Between the 2nd and 3rd image times, the short wave trough systems "T1" and "T2" continued to move northeastward; and, a new trough formed upstream in advance of ridge "RA". This new trough formed the primary trough axis in conjunction with trough "T3". In this type of situation, when an open ridge or succession of short wave ridges, "roll over" on the poleward side of an open trough, the trough is likely to increase in amplitude or extend its length in the streamline and height fields. The cooler mid-tropospheric air of the trough is overtaken on its poleward side by the warm air of the ridge. The winds between the ridge and the trough rotate anticyclonically with time. This reconfiguration of the flow field causes the trough to amplify "by default", without new or continued cold advection.

By the fourth image time of **Figure 76d**, the general trends have continued. A new short wave ridge "RC" has formed upstream from "RB" which accelerated eastward along with the poleward end of ridge "RA". The primary trough and ridge axes have rotated into an almost zonal orientation, and both have extended along the equatorward side of the primary jet stream zone.

Figure 76

FORMATION OF LARGE TROPICAL DARK REGION
Sequence of 4 GOES Central 6.7μm images at 24-hour intervals - southern hemisphere view. Analyses data valid 30 minutes after labeled image times: Arrowheads - axes of 250mb maximum winds with speeds of 70 knots or greater. White dashed lines - 250mb trough axes. Dashed black lines with white dot extensions into dark areas - 250mb ridge axes. Solid white lines - 250mb streamlines.

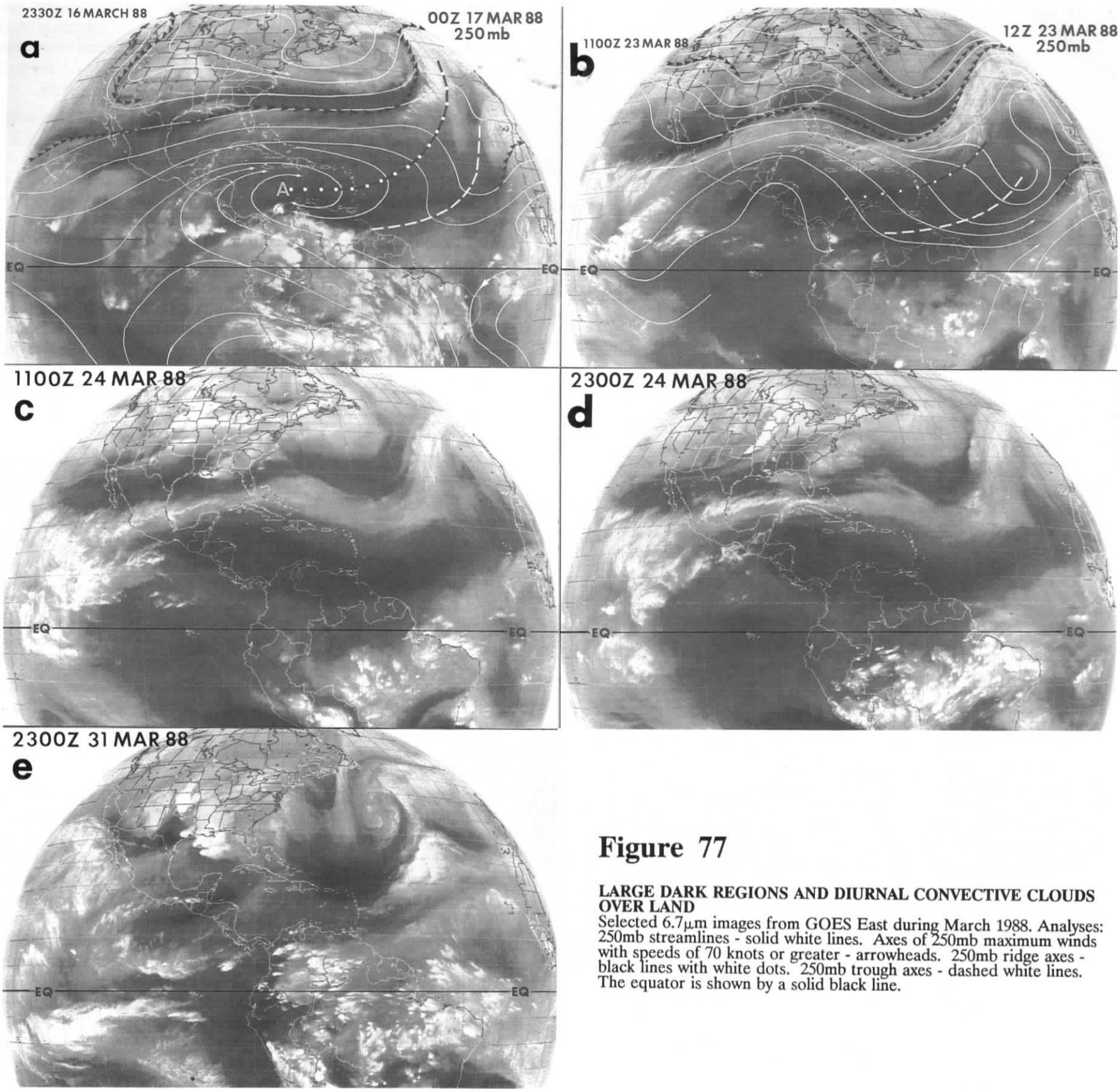

Figure 77

LARGE DARK REGIONS AND DIURNAL CONVECTIVE CLOUDS OVER LAND

Selected 6.7μm images from GOES East during March 1988. Analyses: 250mb streamlines - solid white lines. Axes of 250mb maximum winds with speeds of 70 knots or greater - arrowheads. 250mb ridge axes - black lines with white dots. 250mb trough axes - dashed white lines. The equator is shown by a solid black line.

During the three day period shown on **Figure 76**, the large dark region formed across the tropical latitudes. This type of change in the circulation systems is common to other cases of large tropical dark region formations. The darkening events occur when the warm mid-tropospheric air of an "open" jet stream ridge "rolls over" onto the poleward side of an open low latitude trough. As the equatorward component of the upper air flow increases between the ridge and trough, darkening occurs. When a single ridge is involved, the dark region is likely to be limited in its longitudinal extent. The long dark regions which extend and persist across a great east-west distance of the tropical latitudes, are usually formed as a series of short wave ridges follow the first. In these cases, the large scale ridge and trough axes become oriented in a zonal direction with the ridge along the poleward side of the trough. The associated short wave ridges, in those cases, may be best revealed in the vorticity field or as speed maxima moving along the jet stream zone. The associated jet stream zones are of the vertically deep "polar" type, which are present at subtropical latitudes most often during the winter or equinox seasons. Generally, the high vertically shallow "subtropical" types of jet streams, which are present over low latitudes at times during the summer seasons, are not associated with such darkening events.

The primary significance of the large tropical dark zones, which are relatively dry regions in the middle and upper troposphere, is their effect on the weather. Within the dark regions, middle and high clouds are absent; and, the formation of vertically deep convective clouds is rare. When deep convective weather does occur, it is likely to be near one of the edges of the dark region, or during the late stages of the period when the dry conditions have become residual, or are becoming modified. However, from case to case, the dark regions vary in size, persistence, and vertical depth of the dry conditions. The large strong cases, which appear very dark on the imagery are more likely to affect the local weather conditions than weak cases.

b. Dark Regions Over Land

During the month of March 1988, a succession of tropical dark regions formed over the Caribbean and tropical Atlantic Oceans. On many days, these dark regions extended over parts of northern South America and affected the weather conditions there. Persistent middle and high clouds, and deep convective weather, were not generally present over the Northern Hemisphere portion of the continent during most days of the month. An image valid on one of the generally convective days is shown on **Figure 77a**. A 250mb streamline analysis is shown on the water vapor image. In this case, a relatively large tropical dark region had been present on the 15th, and had extended over most of Colombia and Venezuela. The dark region was oriented generally northeast to southwest and associated with a single large ridge and trough system, rather than a series of short wave ridges. Late on the 15th, the southeastern boundary of the dark region began to move northward over Colombia and Venezuela, while the eastern portion over the Atlantic Ocean continued to move southward. By the time of the image shown on **Figure 77a**, the dark region has become relatively narrow and rotated to a generally east-west orientation. A region of deep convective weather with middle and high cloud debris has formed over most of Colombia and the southern portions of Venezuela. At the time of the image of **Figure 77a**, upper air blocking regimes were present with dual branches of westerlies just off the west coast of the United States and over the eastern Atlantic Ocean. Between those blocking regimes, a single primary jet stream branch is present from northern Mexico eastward over the western Atlantic. The maximum wind speeds along that branch are on that portion east of Florida, where the axis of maximum winds is shown with larger sized arrowheads. The ridge associated with the darkening event is shown by a black line with white dots; and, in this case, an anticyclone is present at the equatorward end of the ridge axis. The jet stream speed maximum and the center of the anticyclone have been moving eastward. On the right forward quadrant of the speed maximum, or to the east side of the associated anticyclone in this case, where the upper air flow has a northerly component; the dark region has been maintained and pushed southward. On the western side of the anticyclone, the upper air flow has a southerly component, generally into the jet stream zone. Over that region of the tropical area, upper air moisture is moving poleward into the jet steam zone. The area of transition between the flow out of the jet stream zone with the tropical dry zone, and the flow into the jet stream zone with upper air moist conditions, is near the center of the anticyclone and moving eastward. At the rear of this moving transition area, the tropical moisture is "returning" poleward, and convective weather conditions are moving northward.

In many similar situations, the related circulation system characteristics are more subtle than in this case. The amplitude of the related wind field may be less, with no anticyclone present. The speed maximum along the jet stream will be present, but the flow into and out of the jet stream zone may be difficult to detect. Generally, this can be seen on imagery in time lapse motion and the features are present in the upper air vorticity fields. However, the dark region can be observed and followed on water vapor imagery.

In regard to forecasting applications, we found that deep convective weather was not likely within the dry regions. If the dry region is present over land where the local convective weather is likely to occur during some diurnal cycle, deep convective weather is not likely to develop during its usual time - or at other times. Over the adjacent upper air moist regions, deep convective weather was much more likely, but it may not occur. Low level conditions would have to be taken into account for forecasting the deep convective weather within the moist regions. There was one situation in which deep convective weather was found to be favored within the upper air moist regions. This was the type of situation shown on **Figure 77a**, where the southern boundary of a dark region was "returning" northward. Deep convective weather was observed frequently within those particular portions of moist regions. We observed another related, but very specific, type of situation favorable for deep convective weather. This will be discussed in context with a different subject. Note that the foregoing discussion of deep convective weather occurrence relates only to the subject of large tropical dark regions and their adjacent moist regions. The concepts do not apply to convective weather associated with specific synoptic scale systems, such as upper air lows and tropical cyclones.

On the days following the image of **Figure 77a**, a new ridge developed along the jet stream zone over Mexico; and, a large dark region formed. This was maintained, or renewed, by a series of short wave ridges and speed maxima along the jet stream zone until the last few days of the month. On **Figure 77b**, another image and related 250mb analysis, are shown valid approximately one week after the time of **Figure 77a**. This shows one ridge of the sequence of such systems along the jet stream zone. By this time, a second jet stream branch was present across the northern United States and adjacent western Atlantic Ocean. At the time of the image, the short wave troughs and ridges of the two jet stream branches are in phase over the eastern United States and western Atlantic. Although this has amplified the cyclonically curved portion of the southern jet stream zone east of Florida, the winds have remained of northerly component over the tropical region to the southeast of the cyclonically curved jet segment.

An image, valid 24 hours later, is shown on **Figure 77c**. Note that a large dark region south of the jet stream zone extends over the northern part of South America. The 1100Z image time is during a diurnal minimum in the general convective weather cycle. With the knowledge that the southern edge of the dark region over South America is nearly stationary, we could forecast no afternoon and evening deep convective weather over the northern half of Colombia and most of Venezuela. The 2330Z image of **Figure 77d**, reveals no deep convective clouds over that region; however, none are present within the adjacent moist area south of the dry region either.

After another week, the jet stream conditions over the United States and the western Atlantic Ocean changed to a high amplitude environment. On **Figure 77e**, an image valid on March 31st, shows the related moisture conditions. No large tropical dark region is present; and, a moist upper air environment with deep convective clouds dominates the northern portion of South America.

The foregoing illustrations and discussions emphasized only one type of large scale circulation feature, but provides a sample of large scale tropical environments and interactions with the adjacent jet stream zones. Furthermore, the type of large dry zone illustrated is a type of circulation regime for which water vapor imagery is particularly applicable as an aid to analysis and weather forecasting.

2. SOME SYNOPTIC SCALE FEATURES AT TROPICAL LOCATIONS

Many of the features and patterns discussed in previous sections also occur at tropical latitudes. We found no significant differences in the characteristics of those features when they occur at different latitudes, except that the related circulation features were generally higher in the atmosphere. Even this difference was not always true. It depended upon the season of the year and the long wave circulation environment. Some examples shown in the previous sections were at tropical latitudes. The boundary on the forward side of the trough shown on **Figure 5** was referred to as an "ITCZ flare-up." We have observed those upper air trough features over most areas of the tropical latitudes during the winter seasons. Those observations included the Gulf of Arabia, the Bay of Bengal, and the south Indian Ocean on infrared imagery. Other examples shown included the "split" ridge case on **Figure 60**, east of Hawaii; and several summer season upper air cyclones in that same area. Here, we shall show some additional cases, primarily at lower latitudes.

a. An Upper Air Cyclone with Core Convection

One of the previously shown cases was an upper air low with "core convection". That same image, shown as **Figure 55b**, is repeated here on **Figure 78e**. On **Figure 78**, pairs of water vapor and infrared images are shown at 12-hour intervals. In this case, the "cut-off" low formed to the southeast of the position shown on the first image. The vertically deep convective weather developed in the core region after the system began to move slowly northwestward over an area of warmer sea surface temperatures. At the first image time, **Figures 78a** and **b**, the upper air cyclone is centered near 11°S, just east-southeast of the Marquesas Islands, and is moving slowly toward the west-northwest. The Marquesas Islands can be located on the infrared image by the small grid patterns at "M". The radiosonde site at Atouna, Marquesas Islands, is located by the black dot, labeled "A" on **Figure 78a**. Other radiosonde sites are Tahiti at "T", and Hao at "H". For comparison purposes, Atouna is located at a Southern Hemisphere latitude comparable to the Canal Zone in the Northern Hemisphere, and Tahiti is comparable to San Juan.

On the infrared images, the deep convective clouds within the core region of the upper air cyclone represent a relatively isolated cluster of cold clouds within a large area of lower clouds under the marine layer inversions. A key to forecasting such weather is to recognize its relationship to the upper air circulation system. With the water vapor imagery, this recognition is simple. When such core convection patterns are viewed on infrared or visible imagery in time-lapse motion, the individual cloud cells can be observed to move in a cyclonically curved pattern with respect to each other. Usually the individual cells do not persist for more than 1 to 2 hours. The anvil debris spreading from the tops of the cells moves in advance of the cells, indicating wind speeds increasing with height between the middle and upper troposphere. This implies a cold core cyclonic system rather than a warm core type, in which the anvil debris tends to fall back from the cell motions. Also, significant to the cold core convective systems, the high level debris does not usually persist. However, during the later stages of such a system, after the upper air environment becomes moist from the convective clouds, debris does tend to persist and spread, and merge with that of adjacent cells. This type of trend can be seen on the sequence of images shown on **Figure 78**.

Some of the upper air temperature and wind conditions associated with this low latitude system are shown on Table 1. The radiosonde data for Atouna, Tahiti, and Hao are valid near the image times of **Figure 78a** and **b**. On the left columns, air temperatures are shown with dewpoint depressions in brackets. Winds are shown on the right columns in degrees azimuth and knots. Comparing the temperatures at Atouna, which is close to the cyclone center, with the other sites, the colder air of the cyclone extends from 700mb to 250mb. The warmer core portion is evident at 200mb and 150mb. The largest temperature gradients around the low were likely near 400mb. As the cyclone drifted westward over the Marquesas Islands, after the time reported here, the 500mb temperature at Atouna reached a minimum of -11°C, but reports were only at 24 hour intervals, and the system was weakening. Note on Table 1, that the wind speeds at Atouna increased with height above the marine layer to a maximum of 115 knots at 205mb.

With the deep convective weather recognized as core convection, computer forecasts of the cyclone movement could be used to forecast the weather. If such computer forecasts were not available, or inaccurate, features on the water vapor imagery may be used to aid in the forecasting. The system could be tracked on successive images. The moisture boundary at "B" should be observed. Usually when such cyclones form, that boundary becomes better defined, and remains so while the system is cut-off. During summer seasons when cut-off cyclones often move westward during their mature phases, the identified boundary is likely to remain well defined during the westward movement, but lose definition if the system stops or opens and moves eastward. In this case, the cyclone moved westward until near the time of **Figure 78e**, then became stationary. It did not open and accelerate eastward, but slowly weakened over the Marquesas Islands. The boundary "B" lost definition between the last two image times of **Figure 78**, then became more irregular and indistinct as the dark bands around the west side of the cyclone moistened.

TABLE 1

0000 GMT 30 December 1981 Radiosonde Data

	TEMPERATURES AND DEWPOINT DEPRESSIONS						WINDS (KTS)		
	ATUONA 91925		TAHITI 91938		HAO 91944		ATUONA 91925	TAHITI 91938	HAO 91944
100 mb	-76.6°C	[ ]	-78.7°C	[ ]	-77.1°C	[ ]	MSG	200/16	130/44
150 mb	-64.7°C	[ ]	-66.5°C	[ ]	-69.3°C	[ ]	MSG	155/23	145/33
200 mb	-50.7°C	[ ]	-51.3°C	[ ]	-54.3°C	[ ]	200/115*	145/20	145/60
250 mb	-42.1°C	[5]	-39.9°C	[11]	-39.1°C	[10]	180/ 85	140/14	140/57
300 mb	-33.7°C	[7]	-29.1°C	[12]	-27.9°C	[10]	180/ 57	160/13	130/49
400 mb	-20.7°C	[5]	-13.5°C	[12]	-16.1°C	[13]	180/ 46	080/13	110/41
500 mb	-10.1°C	[8]	- 4.3°C	[11]	- 5.3°C	[14]	170/ 35	075/11	105/27
700 mb	+ 8.2°C	[7]	+11.4°C	[20]	+11.6°C	[24]	120/ 17	070/17	095/27
850 mb	+15.4°C	[3.4]	+16.8°C	[1.1]	+16.6°C	[3.8]	120/ 08	015/03	100/15
1000mb	+26.6°C	[8.0]	+27.2°C	[5.0]	+26.8°C	[4.8]	130/ 10	055/08	115/15

*205 mb (Max Wind)

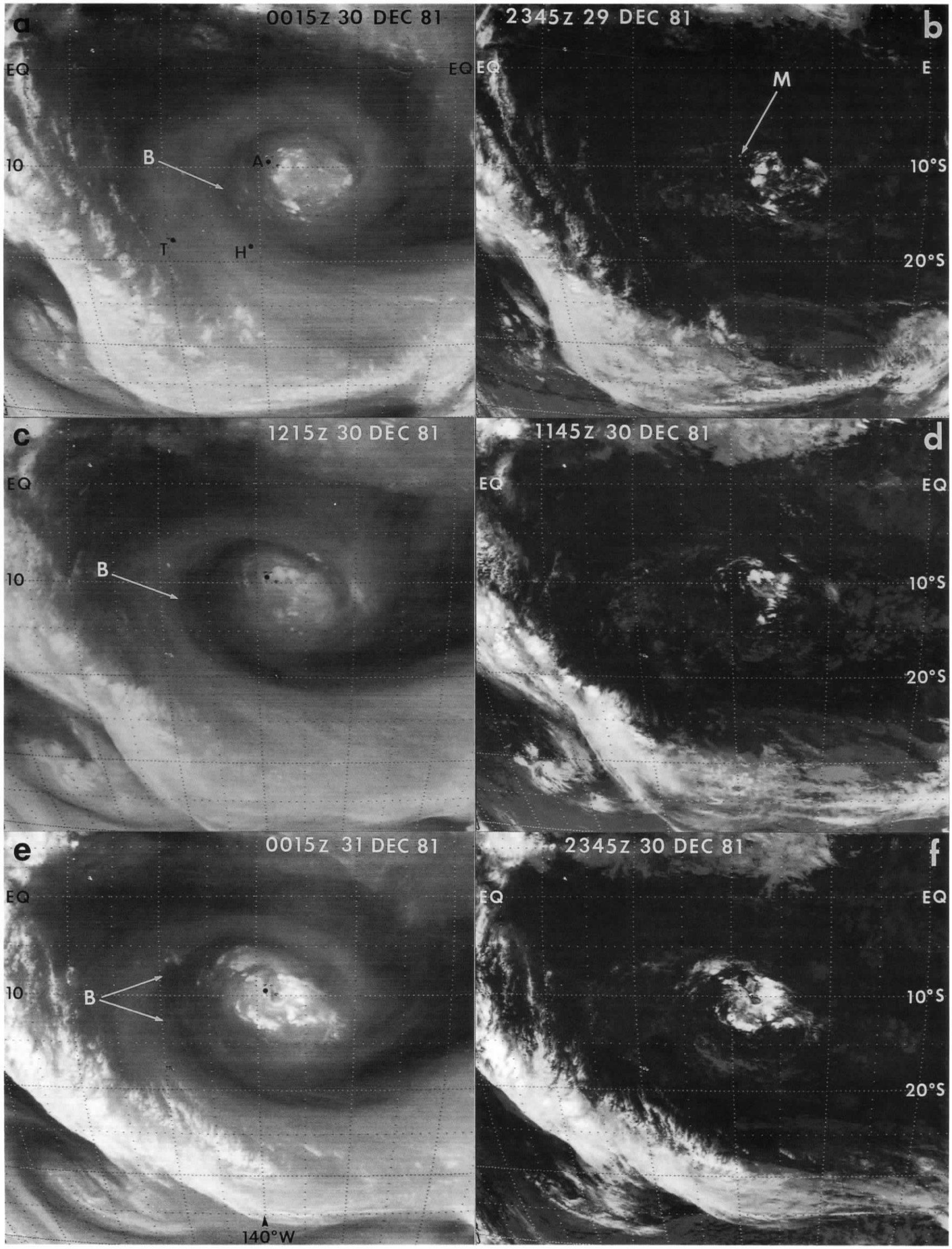

Figure 78

CUT-OFF LOW AT TROPICAL LATITUDES
Sequence of 6.7μm Water Vapor and 11.2μm Infrared image pairs at 12-hour intervals. Southern hemisphere view. Radiosonde sites labeled on **Fig. 78a.** A - Atuona (91925) T - Tahiti (91938) H - Hao (91944). Atuona location is shown by dots on **Figures 78c** and **78e.** Equator is indicated at "E".

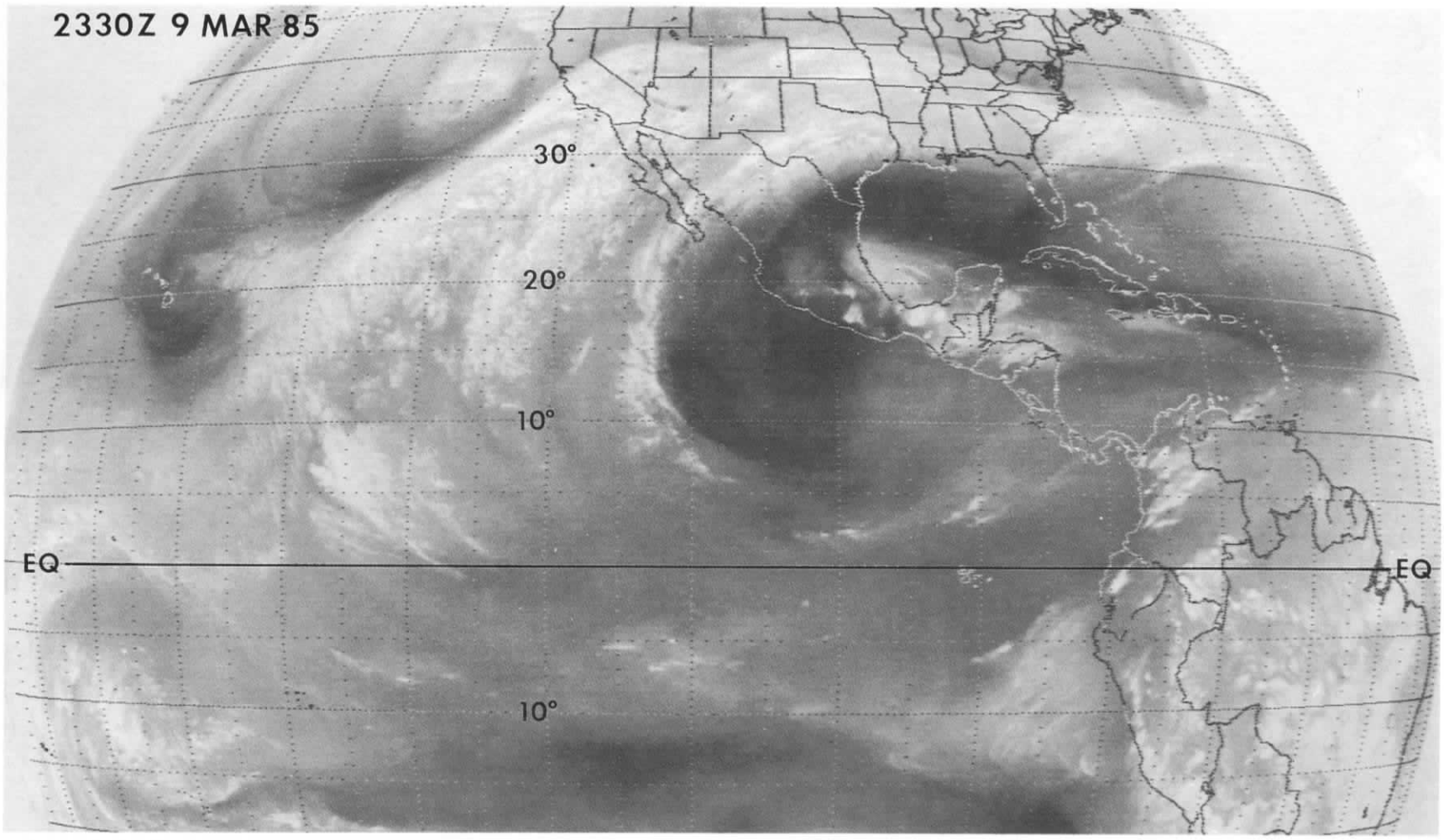

Figure 79 **LOW LATITUDE INSIDE BOUNDARY - NORTHERN HEMISPHERE**
6.7μm image, 2330Z 9 March 1985, GOES Central.

b. Inside Blocking Regimes at Low Latitudes

On **Figure 10**, of Section A, an example of an inside boundary was shown west of the Hawaiian Islands. With that case, during early December, the inside boundary and the dark region on its east side extended to approximately 7°N. Another low latitude blocking regime is shown on **Figure 79**. In this case, west of Central America, the inside boundary does not extend as far to the south. However, two factors of this case have contributed to very strong westerly winds over the equatorial latitudes. It occurred during March when relatively strong westerlies can occur in both hemispheres, and the blocking regime was dominated by cyclonic circulation. The col in the 250mb wind field was near 20°N along the inside boundary. This, in combination with relatively strong westerlies at low latitudes in the Southern Hemisphere, caused a zone of strong winds along the Equator from approximately the coast of South America to the west edge of this image. To the east of the blocking regime, the strong low latitude winds are from the southwest across northern Colombia. At the radiosonde site at Howard AFB, Canal Zone, the maximum winds reported were 230° at 73 knots at 200mb.

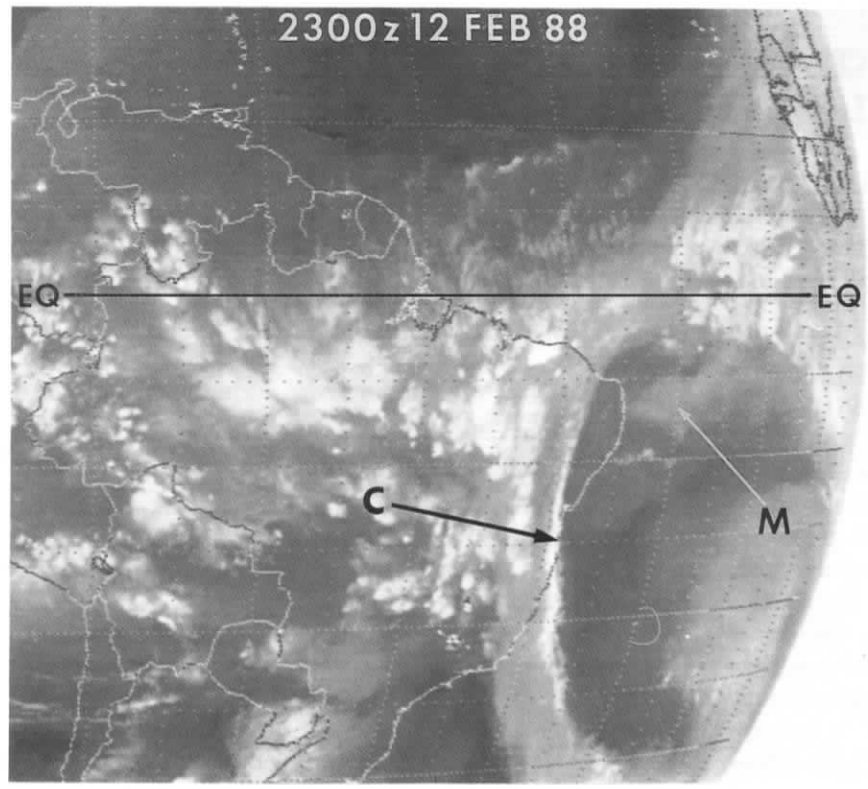

Figure 80 **LOW LATITUDE INSIDE BOUNDARY - SOUTHERN HEMISPHERE**
6.7μm image, 2300Z 12 February 1988, GOES East.

Another example of a low latitude blocking regime with an inside boundary is shown on **Figure 80**. This case in the Southern Hemisphere was dominated by the anticyclone on the east side of the inside boundary. The col in the 250mb wind field was located near 15°S, near "C". Although strong upper air westerlies were present at low latitudes in the winter season Northern Hemisphere, the summer hemisphere winds were relatively light. The inside boundary extended to approximately 3°S, but winds across and over the Equator were in the 30-40 knot range. Another application of such patterns on water vapor imagery, in addition to their upper air wind relationships, is that deep convective clouds are usually not present under the dark areas east of the inside boundaries. If afternoon and evening convective weather conditions are to be forecast based upon an early morning water vapor image, two factors should be considered. The dark areas can sometimes become narrow and elongated along the inside boundary, and this can occur relatively quickly. Secondly, moisture at middle levels often rotates around the cyclone within a portion of the easterly flow of the blocking regime. Diurnal convective weather often occurs over tropical land areas within those moisture patterns. In the case shown here, some moisture has rotated around the low, and is present in easterly flow at "M". However, it is over the ocean, and deep convective clouds are not present. Note that we implied an afternoon maximum for diurnal convective weather. This depends on local conditions, where in fact the maximum may occur at night or early morning from differential cooling effects.

3. SYNOPTIC SCALE FEATURES UNIQUE TO TROPICAL LATITUDES

a. A Base Surge Boundary and Weather Regime Change

In Section A, an example of a base surge boundary at tropical latitudes was shown on **Figure 9**. In that case, east of Hawaii, the base surge boundary reached 14°N at its southernmost position. Another tropical case is shown here on **Figure 81**. Images are shown at 12 hour intervals with 250mb axes of maximum winds indicated by arrowheads. In this case, the boundary moved to nearly 5°N. In addition to the lower latitude location, this base surge case is different from the one on **Figure 9** in another significant aspect. In our discussion of base surge boundaries in previous sections, we mentioned that base surges occurred in response to sudden increases in the equatorward components of the upper air flow; and, that there were many different types of circulation system changes that caused such increases. We identified several of the most common types in Section A. The recognition of one of those changes on imagery, upper air analyses, or computer progs, may allow us to anticipate a base surge event, or to identify the pattern at its earliest stages. It is also useful for tropical applications, to categorize the base surge or base darkening events themselves into two basic types. We discussed this difference and implied the significance in Section B; but here, we emphasize the concept. We shall refer to the two basic types of base surges as "direct" and "indirect". With the "direct" type, an initial moisture boundary is present and changes to a base surge boundary. Also, that initial boundary extends westward as a boundary of the ridge, or one of the ridges which amplifies to cause the base surge. In other words, a boundary which becomes a base surge boundary, is a downstream extension of the ridge which amplifies. In some cases, there may be another ridge in another branch of westerlies to the poleward side. The base surge cases of **Figure 9**, **Figure 18**, and **Figure 70** were of the "direct" type. Usually with the "direct" type, there is a jet stream branch along the initial boundary which becomes the base surge boundary. With the "indirect" type of base surges, either no boundary is initially present; or, the ridge which amplifies is not an integral part of the initial boundary, but is within a branch of westerlies poleward of the initial boundary. The case shown on **Figure 16** and the case shown here on **Figure 81** are examples of "indirect" types. With the "indirect" types of base surges which have initial boundaries, some have jet stream branches along the initial boundary, some do not, and in many cases a branch of maximum winds is present only along the eastern portion of the boundary. The "indirect" type base surge events are common at tropical latitudes because of the prevalence of well defined moisture boundaries along the poleward sides of the deep convective weather regimes, such as the ITCZ and tropical land masses.

Consider the March 1986 case shown on **Figure 81**. The boundary "B", along the northern side of the South American convective regime, is similar in nature to those of March 1988, shown on **Figure 77**. The boundary was related to a trough in the westerlies, which was "rolled over" by upstream ridges and rotated into a generally east-west position along the equatorward side of the jet stream zone. The boundary had a jet stream branch along its eastern end 24 hours prior to the time of **Figure 81a**. At the first image time, the 250mb winds along the boundary are relatively light westerlies. Along that portion of the boundary between the white arrows of "B", the winds are northwesterly, crossing the moisture edge from the dry side. West of there, the winds have a southerly component, crossing from the moist to the dry side; and, along the northeastern part of the boundary, the winds are nearly parallel. The dark zone along the poleward side of the boundary had been wider, but has narrowed during the past 12 hours by high level moisture approaching from the north. At the west end, the dark region extends into area of a weak upper air open trough at "T". This contributes to the convex curved shape of the western part of the boundary.

At the time of the first image, the base surge event is just beginning, and is not yet detectable by the boundary characteristics on the still image. The surge in the northerly component flow has already begun on the east side of the jet stream ridge "JR". That ridge has intensified significantly in conjunction with cyclogenesis over the central United States during the past 18 hours. Axes of maximum 250mb winds were shown on the images only on the east side of the ridge. Small short wave features and related speed maxima along that zone affected the details of the axis of maximum winds during the 36 hour period shown; however, the overall trend was that the jet stream rotated into a nearly north to south orientation and extended southward during the period.

By the second image time, the base surge is recognizable. A new dark area has formed at "D", and is moving southward. The moisture boundary has begun to change shape, moving southward at the white arrow and northwestward at the black arrow. During the next 24 hours the trend continued. The dark area "D" moved adjacent to the boundary, and both moved southward to near 6°N. With this, the dark region adjacent to the base surge boundary became wide. The convex western part of the boundary increased its curvature, became more rounded, and moved northwestward.

Note during the sequence of images, the change in cloud conditions under that portion of the moist region with the convex boundary. High clouds and areas of deep convective weather formed and persisted through the diurnal cycles. Within the first topic of this section, we discussed the probability of deep convective clouds forming under the moist regions adjacent to the large tropical dry zones. With our discussion of **Figure 77b**, we mentioned a related type of situation in which the probability of deep convective weather was high, and that specific types of situation would be illustrated. This is it. Often when the "indirect" type of base surge boundaries form, well defined convex portions of the boundary form at the east and west sides of the concave base surge portion. In the upper tropospheric wind fields, local synoptic scale ridges form at the two moist areas with convex boundaries. We refer to the eastern ones as "R1" ridges, and to the western ones as "R2" ridges. The ridge systems in the "R2" location are more common. This is related to the types of circulation changes which cause the base surges. In those cases, such as the one shown here, in which the base surge is caused by a polar jet stream extending equatorward directly into the environment next to the moist boundary, cyclogenesis usually occurs at the base of the "digging" trough on the east side of the jet stream. The "R1" ridge then takes the form of a "build-back" ridge associated with the cyclogenesis. In those cases, the "R1" ridges have the similar characteristics and behavior of mid-latitude "build-back" ridges associated with cyclogenesis except they are at a tropical location. We shall discuss the "R1" ridges further with later topics.

Once formed, the "R2" ridges at the western side of the base surge, usually move westward. The "R2" cloud system formations, with base surge events, represent a common type of development of synoptic scale systems in the tropical easterlies. Of primary significance, they often cause a change in the local weather regimes. In this case, prior to the images shown, an upper air dry region had dominated the weather conditions over southern Central America and northwestern Colombia. After the base surge and "R2" ridge formation, the weather regime changes to one of persistent high cloudiness and areas of deep convective weather. Also in this case, the "R2" system was blocked from moving on to the west. Upper air westerlies were present over the tropical eastern Pacific Ocean, and the weak trough and ridge systems there moved slowly eastward in predominantly southwesterly flow. By the last image time, the trough system "T" became narrow and elongated along the west side of the "R2" ridge. Afterwards, the "R2" pattern, itself, became stationary and elongated northeastward by the westerlies.

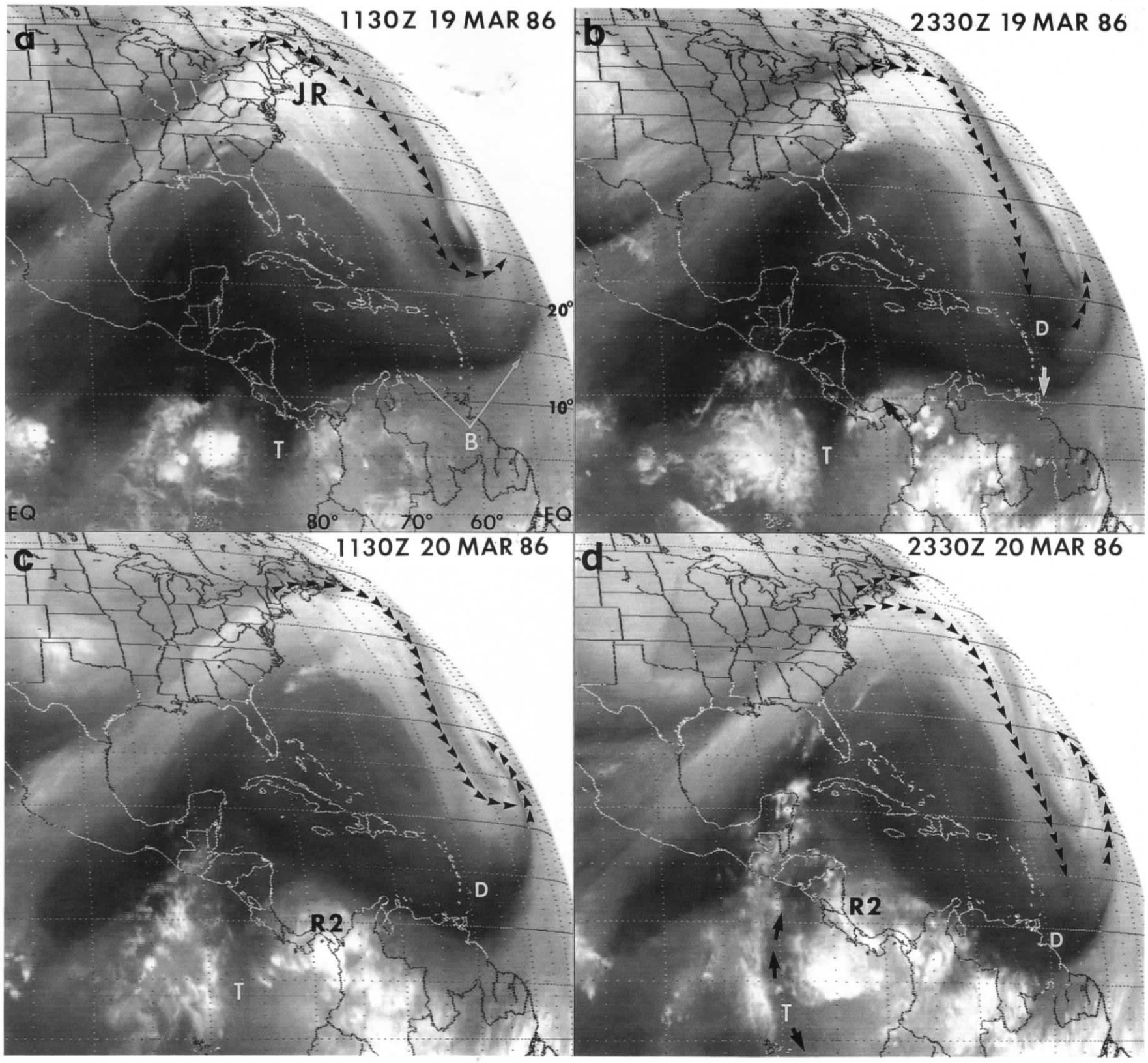

Figure 81 **WEATHER REGIME CHANGE WITH INDIRECT BASE SURGE**
Sequence of 4 GOES Central 6.7μm images at 12-hour intervals. 250mb axes of maximum winds over the Atlantic Ocean only - black arrowheads (from analyses valid 30 minutes after respective images).

When "R2" systems are allowed to persist for approximately 24 hours or longer with persistent deep convective weather in the moist pattern, a closed cyclone is likely to develop in the lower middle troposphere under the upper tropospheric ridge or anticyclone. With persistence, an inverted trough pattern is likely in the marine layer easterly wind field. During the winter and equinox seasons, such systems are likely to move only a short distance westward before encountering a trough in the upper air westerlies. The upper air ridge elongates on the eastern side of the approaching upper air trough and moves eastward with the trough. The vertically deep systems is destroyed; but, the marine layer portion of the systems often continue westward as an "easterly wave" system, usually without deep convective weather or high clouds.

During the summer seasons, with the upper air westerlies weaker, and often in the form of smaller scale "closed" and slow moving perturbations at low latitudes, the "R2" ridge locations represent an environment favorable for tropical cyclogenesis. This subject will be included with the last topic of this section.

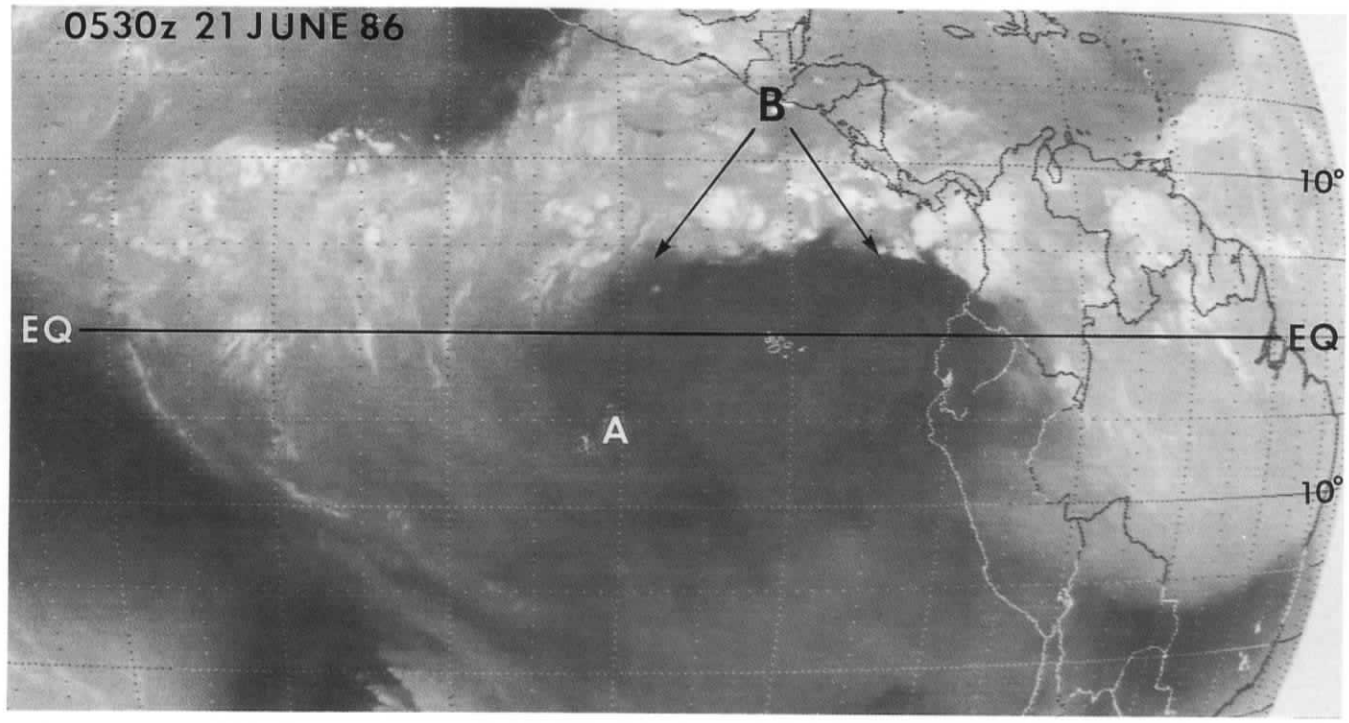

Figure 82 **BASE SURGE ACROSS THE EQUATOR**
6.7μm image, 0530Z 21 June 1986, GOES Central. "EQ" = equator.

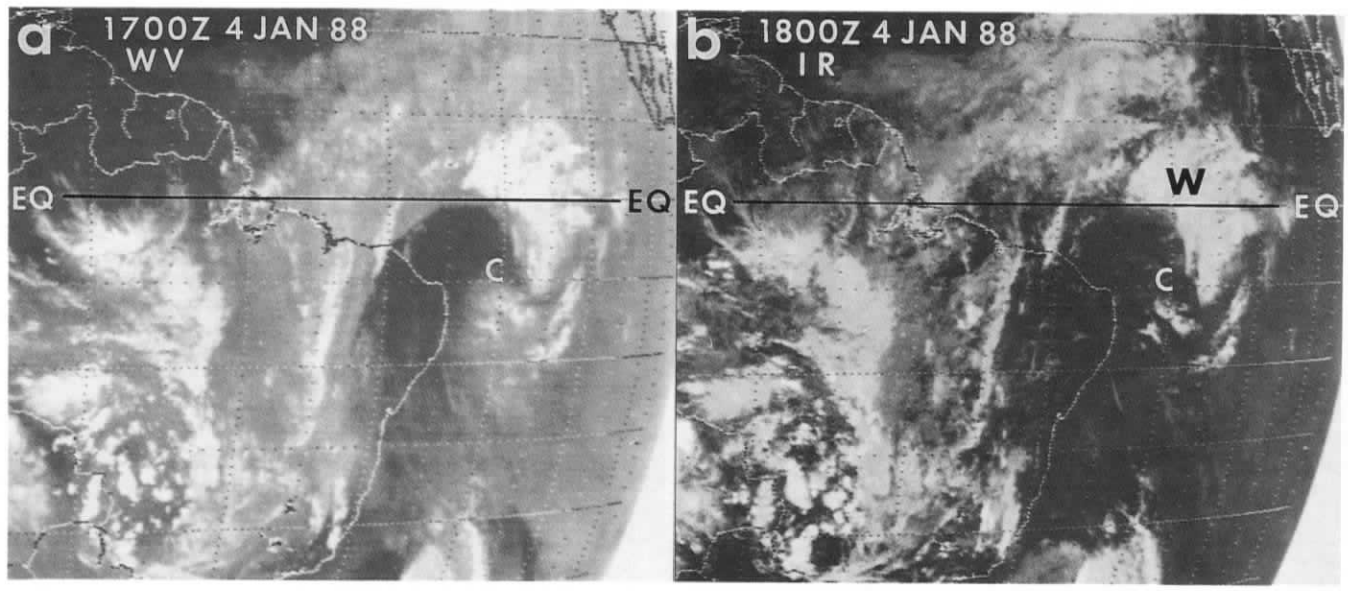

Figure 83 **SOUTHERN HEMISPHERE SYSTEM AFFECTS NORTHERN HEMISPHERE WEATHER**
Water Vapor - infrared image comparison.
Fig. 83a. 6.7μm image, 1700Z 4 January 1988, GOES East.
Fig. 83b. 11.2μm infrared image, 1800Z 4 January 1988, GOES East. "EQ" = equator.

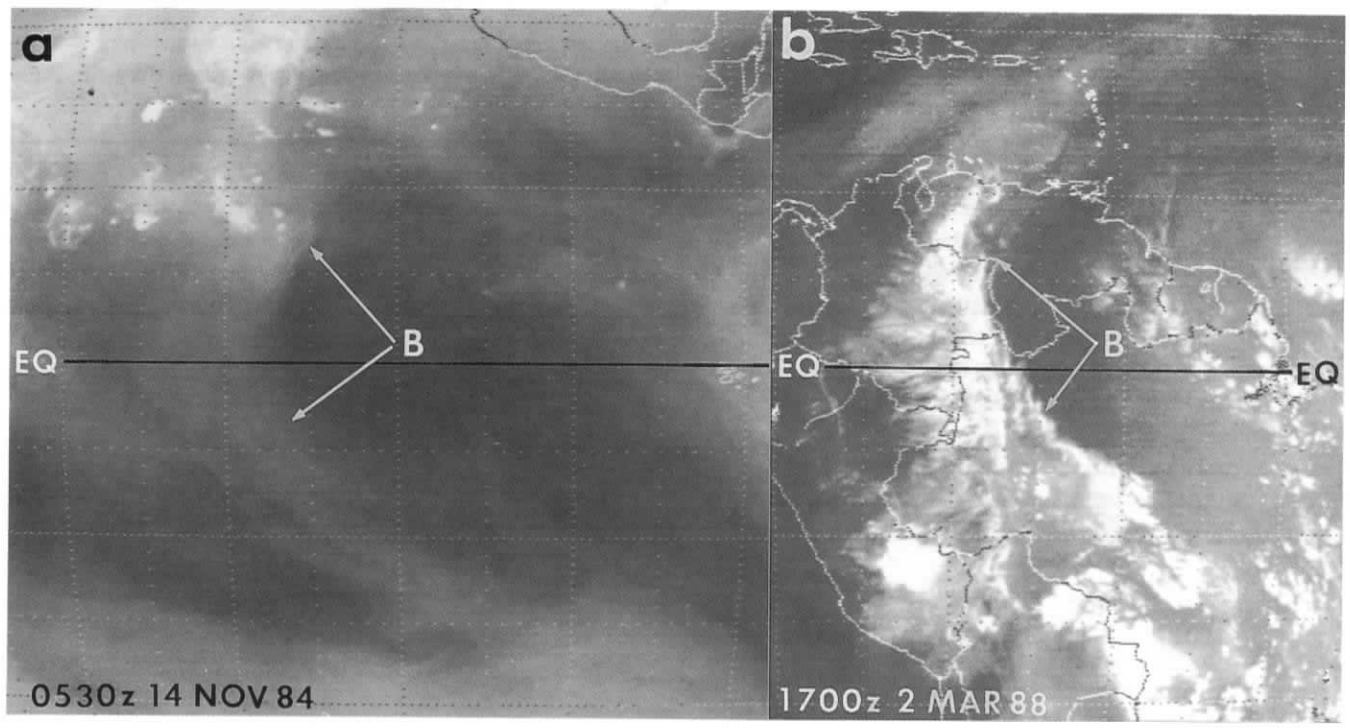

Figure 84 **BLOCKING REGIMES ORIENTED ACROSS THE EQUATOR**
Fig. 84a. 6.7μm image, 0530Z 14 November 1984, GOES Central.
Fig. 84b. 6.7μm image, 1700Z 2 March 1988, GOES East. "EQ" = equator.

b. Base Surge Across the Equator

On **Figure 82**, a base surge from the Southern Hemisphere has formed a base surge boundary at "B" in the Northern Hemisphere. An upper air anticyclone was centered near "A" in the Southern Hemisphere. This, in association with an open trough along the South American coast, contributed to the northward surge. Since the ITCZ convective weather region was initially north of the Equator prior to the surge, the event did not cause any reduction of convective weather. Often, along the southern side of the ITCZ in this area, shallow layers of cirrus and middle clouds spread equatorward from the ITCZ convective weather. The drier conditions of the base surge has eliminated or prevented those clouds.

With strong winter season base surges in the Northern Hemisphere, a break in the ITCZ convective zone is more likely. However, these surges do not have to cross the Equator to affect the convective weather, since that weather is generally located between 5°N and 10°N. Often, in those cases with the ITCZ convective weather break, the equatorward flow is dominated by the cyclonic flow of a trough, and there is an increase in the cold clouds on a segment of the ITCZ along the eastern side of the base surge boundary. Sometimes this type of cloud and weather increase is caused by Southern Hemisphere systems. Consider the next case.

c. Cloud Conditions Affected by System of Opposite Hemisphere

On the water vapor image of **Figure 83a**, an upper air cyclone is centered at "C", near 4°S off the eastern coast of Brazil. This low closed early on the previous day with its center near 8°S. Then, apparently in response to an increase in the northward flow on the east side of the adjacent ridge, the low moved toward the Equator. This caused a small sized base surge of the kind dominated by cyclonic upper air flow. An additional aspect of the surge is that it is the "direct" type. The base surge boundary is an extension of ridge boundary. Prior to the equatorward surge of the moisture boundary associated with the low, the ITCZ was located near the Equator, but on the Northern Hemisphere side. As the boundary approached, an area of deep convective weather formed rapidly at the ITCZ. This occurred only along that part of the ITCZ adjacent to the eastern half of the approaching base surge boundary. The convective clouds and spreading high clouds are identified on the infrared image of **Figure 83b** as "W". Although we have observed other similar occurrences, we are not certain of the reliability of this type of change for use in forecasting. However, once the event occurs and the weather is related to the low in the opposite hemisphere, forecasting movement or dissipation of the weather is likely. Note also, that the Southern Hemisphere upper air system is more easily recognized by the patterns on the water vapor image than, on the infrared image.

d. Dry Blocking Regimes Across the Equator

On **Figure 84**, two examples are shown with blocking boundaries extending across the Equator. These are a special type of inside boundary. Dark regions with upper air easterly flow are present on the eastern sides of the boundaries. However, the circulation systems involved consist of closed anticyclones adjacent to each other on opposite sides of the Equator. As at other latitudes, the boundaries form in response to a formation or intensification of the easterly upper air winds. In the cases we observed with adequate upper air data, an anticyclone was already present in one hemisphere; then, an anticyclone formed at nearly the same longitude in the other hemisphere. In the case shown on **Figure 84a**, over the eastern Pacific Ocean, an anticyclone formed in the Northern Hemisphere, with a low latitude ridge already present in the Southern Hemisphere. The easterly winds were primarily on the north side of the Equator. The opposite type of formation conditions occurred with the case over South America, shown on **Figure 84b**. In that case, more upper air moisture, and persisting high clouds from the deep convective weather were present on the western side of the boundary. The boundary appears more distinct. The primary significance of such boundaries is that deep convective clouds usually do not occur within the dark regions on their eastern sides. The boundaries also imply a blocking situation between regions of westerly and easterly upper air winds; however, those winds are usually very light.

e. Perturbations on the ITCZ Moisture Boundaries

The upper air moisture accumulated above the deep convective weather along the ITCZ tends to spread both northward and southward. Often there are well defined boundaries formed along the edges of this moisture regime. Usually, the well defined boundaries can be associated with some specific type of upper air circulation feature which is not unique to tropical latitudes. The boundary may be a specific type of head boundary, formed as the convective moisture is blocked by general ambient flow in the equatorward direction. Or, the circulation feature may be a low latitude jet stream branch, or an upper air trough extended in an east-west orientation. However, the perturbations that occur along these boundaries form some of the most significant tropical weather systems, and often develop characteristics unique to tropical latitudes.

By the term "perturbation", we refer to a "set" of conditions consisting of an intrusion of drier air into the moisture regime adjacent to a protrusion of moist air away from the moisture regime. Although the specific wind fields vary considerably, the intrusion-protrusion moisture patterns are usually associated with some type of upper air trough and ridge couplet. The trough and adjacent ridge may form and amplify together, or one may initiate the other. During the system evolution, either the trough or ridge may dominate the other.

On **Figure 85**, four examples of ITCZ moisture boundary perturbations are shown. Three water vapor images are shown for each case. Although the time intervals between images are consistent within each case, they vary for the different cases. All of the examples shown are northern hemisphere systems; however, two are along the northern side, and two are along the southern, equatorward, side. For each case, images were selected to show movement and pattern changes of the system. It was not our intention to show the initial formations, or complete system evolutions; nor to address any case in detail.

Poleward Side Perturbations

Most of the perturbations along the ITCZ moisture regime are on the poleward side, where a boundary is more commonly present, and subject to intrusions from the adjacent jet stream zones. Most commonly, a trough forms first and initiates or contributes to the amplification of an adjacent ridge. (A very significant exception to this is the "R2" type of ridge development, which was introduced with the previous topic.) In many cases, especially when deep convective weather is involved, the trough may initiate the development, but the ridge then dominates the system evolution.

Considering all seasons of the year, the most common type of poleward side perturbation involves upper air westerly winds along the boundary zone. In those cases, a trough "digs" or extends equatorward into the moisture regime. Dry air intrudes into the moisture on the west side of the trough, and moisture moves poleward between the trough and a building ridge on its eastern side. Those systems usually move eastward or remain nearly stationary. If the ridge becomes dominant, and the trough weakens or "cuts-off", the system may move westward; but, it also becomes separated from the primary moisture regime. Since the pattern evolutions and related circulation systems of these types of perturbations are similar to systems elsewhere in the westerlies; and many examples are included with other topics, we will not show this common type here. The two cases shown here involve dominant upper air easterly wind regimes more common during the summer seasons.

Consider the first row of images, labeled a,b,c on **Figure 85**. This case occurred during June, west of Central America. An elongated anticyclone was present from "D" eastward across southern Mexico; and, vertically deep easterly winds dominated the ITCZ moisture regime, including its northern boundary. The image view includes the western two thirds of the anticyclone area and the upper air easterly wind regime along its southern side. Just to the west of the view, an upper air trough is present at low latitudes; and, a large region of upper air moisture has extended northeastward between that trough and the west side of the anticyclone, and crosses over the Baja Peninsula and northwestern Mexico. A jet stream branch (with the 250mb axis of maximum winds indicated by white arrows on **Figure 85a**) extends from the eastern side of the trough, around the northern side of the anticyclone. As this jet stream branch extended southeastward over the Gulf of Mexico, the eastern end of the anticyclone moved southward. The upper air winds, just west of southern Mexico, changed from easterly to southeasterly; and, a trough formed in the upper air easterlies. The trough axis is shown on **Figure 85a** by a dashed white line labeled "T". Small arrows show 250mb wind directions. On the eastern side of the trough axis, where the easterly flow is across the moisture boundary from the southeast, the moisture has protruded northward and forms a ragged edge at "G". To the west of the trough axis, the winds have become northeasterly toward the moisture spreading from the convective weather. There, a relatively well defined moisture boundary has formed at "B". The moisture boundary extends around the western side of the dry area "D", and becomes nearly parallel to the jet stream zone, near "E". Along the western and northern side of the dry area, the 250mb winds cross the boundary at small angles from the dry toward the moist side.

During the period shown by the second two images, the open trough in the easterlies forms a closed low. By the second image time, the moisture boundary to the west of the trough axis has become better defined; and, the well defined portion has extended westward to "B". By the upper air data time at 1200Z, the well defined part of the boundary has extended to the northeast, to a point again labeled "B". As the cyclone closed, a new col formed in the upper air winds. It is centered near "C" and is indicated by large white arrows along its stretching axis. A well defined portion of the boundary is along the deformation zone (the stretching axis of the col). During the period shown, the moisture which protruded northward on the eastern side of the trough axis, has formed a more organized pattern, "hooked" around the northern side of the newly formed low. The protruded moisture pattern is located generally between the low and a ridge on its east side. Although the upper air flow associated with the pattern is partly cyclonically curved, and partly anticyclonic, we tend to associate the protruded portion with a ridge, and have labeled the pattern as "R" on **Figure 85c**. The two reasons for this involve observations of other similar systems. The patterns tended to be associated with a "thermal" ridge in the upper middle troposphere (the 500mb to 400mb range), even where the upper air flow was cyclonically curved. And, secondly, in cases where deep convective weather formed within the moist pattern, a ridge or anticyclone formed in the upper level winds coincident with the moisture pattern. In this case, there were no mid-tropospheric data available, and deep convective weather remained generally south of the protruded moisture pattern.

Note in this case, that the overall moisture pattern was very similar to the "inside" boundary cases shown in previous sections. This is a special type of inside boundary common to low latitude regions, especially during the summer seasons. The boundary "B", that was extended around the western side of the dry region, represented a "blocking regime" between regions of easterly and westerly wind regimes at similar latitudes. This was true at the first image time before the closed low formed. The easterly winds extended to the Equator; therefore, no col is present in the wind field. The westerlies and easterlies merge in a confluent pattern between southwesterlies and southeasterlies. By the last image time, after the low closed, a col formed, and the boundary became better defined. With this type of inside boundary blocking regime, there is not an equatorward side branch of westerlies, at least not in the same hemisphere. The resulting inside boundary moisture pattern appears very similar on the water vapor imagery, when a low forms at the equatorward end of the inside boundary, as in this case. Note that in both types of cases, the moisture protrusion located on the east side of the low, has a special significance. We refer to this pattern, identified at "R" in this case, as an "RE1" system. This will be discussed in the last topic on tropical cyclogenesis.

A second example of a poleward side perturbation, shown on **Figures 85 d, e,** and **f**, occurred during August over the Atlantic Ocean north of South America. One day prior to the first image time, the overall circulation pattern of this case was similar to that of the first case. The anticyclone was smaller; the westerly wind systems to the west of the perturbation were weaker; and, the systems in the westerlies to the north were moving eastward. The perturbation in this second case was moving westward; whereas, the one in the first case evolved in a nearly stationary position. On the first image, **Figure 85d**, boundary "B" (equivalent to boundary "B" of the 1st case) has rotated anticyclonically, as the trough in the westerlies farther to the north moved eastward. The axis of the anticyclone extends southeastward from its western end, identified at "R". The upper air low associated with the dry side of the moisture perturbation is labeled "T1". During the past 24 hours, it has moved toward the northwest and decreased in size. In this case, deep convective weather has been present within the moist side of the perturbation.

By the second image time, boundary "B" has continued to rotate anticyclonically, as the southern end moved westward, and the northern end moved eastward. A trough to the west of the moving perturbation has two small closed cyclones at "T2" and "T3". That trough has been nearly stationary; and, as the perturbation moved westward, the dry pattern associated with trough "T1" has become blocked and elongated in a northeast-southwest orientation. During the period between the 2nd and 3rd images, the "T1" dry zone narrowed and disappeared between adjacent moist zones. Also, during that period, deep convective weather increased and persisted within the moist pattern of the perturbation. A larger area of anticyclonic flow with increased wind speeds formed at high levels, and dominated the circulation field of the moist convective pattern.

In this second case, deep convective weather formed and persisted within the moist side of the perturbation. The system moved westward; and, the upper air ridge became the dominant circulation feature. The trough on the west side weakened and "sheared out" in advance of the developing ridge. In both cases shown, the dry portion of the pattern was on the west side, and associated with a trough as the system evolved. The moist pattern was on the eastern side, between the trough and the adjacent couplet ridge. Such a configuration is common to perturbations along the poleward sides of the ITCZ moisture regimes.

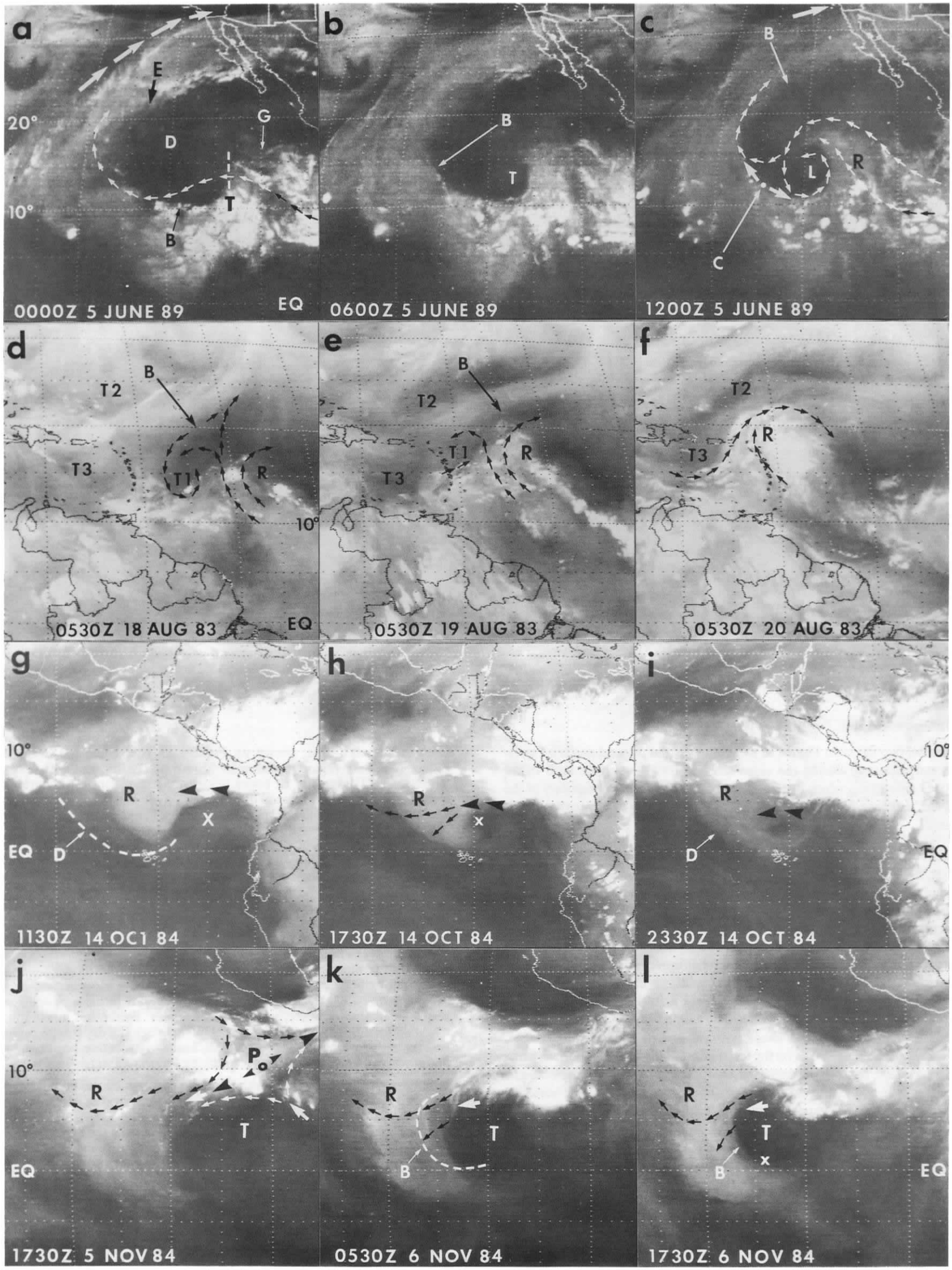

Figure 85 **PERTURBATIONS ON OPPOSITE SIDES OF THE NORTHEN HEMISPHERE ITCZ MOISTURE REGIME**

Four sequences of three 6.7μm images arranged in rows. Small arrows indicate upper tropospheric wind directions (derived from 250mb analyses and motion vectors of cirrus and high level moisture). Large white arrows on **Figures 85a** and **85c** indicate 250mb axes of maximum winds. "EQ" = equator.

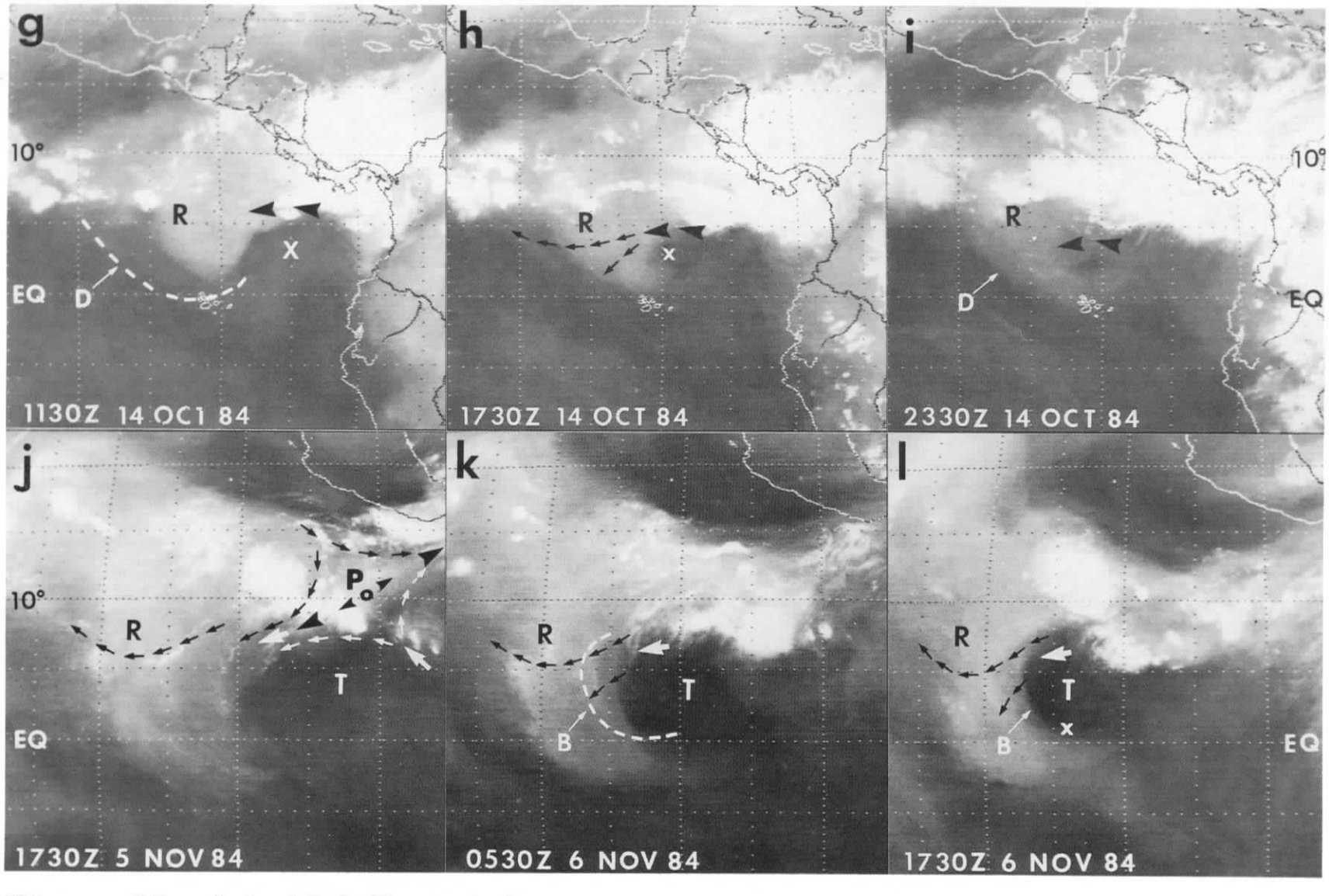

Figure 85 g-h-i, j-k-l Repeated

Equatorward Side Perturbations

The last two cases on **Figure 85** are both over the tropical eastern Pacific Ocean area, and during the same season of 1984. Also, in both cases, upper air easterly winds were present along the southern boundary of the ITCZ moisture regime; however, the origins of the two cases were different.

In the case shown in **Figure 85g, h, i**; upper air easterly winds were present over the ITCZ area shown. These were bounded on the north side by a ridge axis near 15°N, and on the south by an east-west oriented trough axis just north of the Equator. Prior to the first image time, a speed maximum formed within the easterlies, perhaps resulting from deep convective weather over the western Caribbean and southern Central America. By the 1st image time, this speed maximum has moved westward; and, a perturbation has begun to form along the southern boundary of the ITCZ moisture regime. On the images, large black arrowheads indicate the approximate locations of the speed maxima within the easterlies. These were estimated, based upon the image patterns and their changes with time. Note that the small arrows on the last 6 images indicate 250mb wind directions, and are based upon upper air analyses and high cloud motions. The "X" symbols are estimated locations of the maximum cyclonic vorticity, based upon the moisture patterns and their movement. On the image of **Figure 85g**, a dry region is present to the south of the speed maximum in the easterlies. West of there, in advance of the speed maximum and trough on its left side, the moisture has protruded southward. The ridge axis in the 250mb wind field is near "R". During the sequence of images, the moist area with "R" moves westward and partly equatorward. Boundary "D" on **Figure 85i** has been superimposed as a dashed white line on **Figure 85g** to show the movement of the advancing edge of the moisture. A part of the moist area moved west, and part rotated cyclonically around the vorticity maximum, and enclosed a small dark area by the last image time. The perturbation surged westward, then slowed between the last two image times, as the low apparently closed with a very small area of weak westerly winds just north of the Galapagos Islands. This was implied since some of the moisture moved eastward just south of the vorticity maximum.

Consider the last case, shown on **Figures 85 j, k, l**. On the image of **Figure 85j**, a col region is shown by 250mb wind directions with a center near "P". During the 12 hours prior to this first image, the stretching axis of this col has rotated anticyclonically. It was originally oriented northeast-southwest, and represented a significant boundary between moist air on the northwest side, and dry air on the southeast side. Even the ITCZ deep convective clouds were absent on the southeastern side. On the dry side, the upper air southeasterly flow split at the col with a ridge to the right (toward the northeast) and a trough to the left (toward the southwest). As a trough in the westerlies moved eastward over Mexico, the col axis rotated, and the ridge on the east side of the col weakened. Deep convective clouds formed along the ITCZ on the southeast side of the col. These events occurred leading to the time of the first image. As the col is continuing to rotate, the cyclonic portion of the flow on its south side is moving westward, and the moist area on its west side is beginning to hook around cyclonically on the south side. Again, as in the previous case, the trough moves westward and forms a closed low, with a small area of westerlies near the Equator. By the last image time, a well defined boundary had formed at "B" between the dry trough region and the moisture on its west side. This boundary location has been superimposed on the second image to show the movement.

In both of the last two cases, with the perturbations on the equatorward side of the ITCZ moisture regime, the moisture protruded southward on the western side of the upper air trough. The moist area moved westward in advance of the dry area associated with the troughs. This configuration is opposite to those with the perturbations on the poleward side of the moisture regime. With those systems, moving westward, the dry region was on the west side in advance of the moisture.

In the cases shown here on the equatorward side of the ITCZ moist regime, the deep convective clouds did not form within the moist patterns protruding southward on the west sides of the trough. In this area, deep convective clouds would have been unlikely south of the ITCZ position because of the cooler sea surface temperature there. We have observed similar cases along the northern coast of South America, in which middle clouds and some convective weather did form around the west side of the troughs and propagated westward with the perturbations. In those cases the deep convective clouds were near or over land; and, water vapor imagery was not available.

4. WATER VAPOR IMAGE PATTERNS RELATED TO TROPICAL CYCLOGENESIS

By "tropical cyclogenesis", we refer to the development of the intense vertically deep cyclones which, in their mature stages, are defined as "hurricanes" and "typhoons". While observing water vapor imagery for general purposes, we noticed that certain common patterns on the imagery were present in the environments of forming tropical cyclones. It appeared that water vapor imagery might be applied to forecasting or understanding tropical cyclogenesis, at least with certain types of formation. Therefore, we again viewed all available water vapor imagery to specifically observe the relationships with tropical cyclones. We concluded that in certain situations, specific types of pattern changes on the imagery could be used to reliably forecast tropical cyclone developments; and, that those cases represented only a small percentage of all developments. However, there were many situations in which the pattern changes on water vapor imagery could be used in conjunction with other information to improve the forecasting of tropical cyclone development. Specifically, certain patterns and changes on the water vapor imagery within the environment of developing cloud systems were identified as favorable or unfavorable for continued development. Relative to other types of information, we found the water vapor imagery to be most useful during the very early stages of tropical cyclone development. Although the water vapor imagery may be applied at later stages of tropical cyclone evolutions, its value decreases relative to other satellite imagery, upper air analyses, and computer models, because their usefulness increases.

Here we shall summarize our observations by presenting the most common patterns and changes relating to tropical cyclone development with emphasis on the early formation phases. We also emphasize those types of development for which we believe water vapor imagery is most useful.

Prior to discussing the applications of water vapor imagery, it is useful to address some of the empirical relationships associated with tropical cyclone development and their cloud patterns observed on visible and infrared imagery. Satellite imagery has been extensively used to identify and observe tropical cyclones. Subjective techniques using visible and infrared imagery, and objective methods using infrared derived temperatures were developed by Dvorak (1984) to estimate the surface central pressures of tropical cyclones.

From the perspective of viewing tropical cyclogenesis cloud patterns on satellite infrared and visible imagery, we have identified two conditions common to all cases. These may be combined in the simple phrase: "organized deep convection". Vertically deep convective clouds were present and persisting in an organized synoptic scale pattern. Generally, the patterns were of rounded shape or in the form of bands curved around a small central location. When questioned on this subject, Dvorak (1988) agreed that it was consistent with his observations. We believe these observed conditions are also requirements for development, although they may not be the only ones.

Tropical cyclone developments may be divided into types, according to their specific circulation environments. We have divided developments and those various types into two basic categories, related to the "organized deep convection" conditions. Although the dynamic processes involved are likely the same, the categories are useful for analysis and forecasting using satellite imagery. With some cases of tropical cyclone formation, the "organization" element occurs first, followed by the presence of vertically deep convective weather. We refer to this sequence of development as "Category I". An organized synoptic scale circulation system, such as an "easterly wave system" is present and subsequently develops deep convective cloud conditions. In this category, we include those cases in which deep convective weather develops in conjunction with the formation of the circulation system. In other cases, referred to as "Category II" developments, the organization condition occurs after the presence of deep convective weather. An area of deep convective weather, such as an ITCZ convective regime, may be present with organized behavior only at the meso or convective scales. The convective cloud behavior appears random at larger scales, with individual cells and clusters failing to persist in any particular area, but reforming nearby as initial ones dissipate. A synoptic scale circulation system may then form within the convective regime, providing organization to a portion of the deep convective clouds. Those clouds then persist in a pattern consistent with the new circulation system.

In summary, and for reference purposes, the two basic categories of early stage tropical cyclone formation are:

Category I

An organized circulation system is initially present; then, deep convective clouds form and persist within the organized pattern.

Category II

A deep convective environment is initially present, but without synoptic scale organization. Then, a synoptic scale system forms within the convective environment.

Once an organized pattern of deep convective clouds has formed, by either of the categories just defined, the system may continue to evolve to a tropical cyclone. However, its evolution may be disrupted. Most systems which reach the "organized deep convection" phase, do not continue to the named "tropical storm" stage. Satellite imagery, including water vapor imagery, may be used to detect environmental conditions which positively or negatively affect the continued evolution.

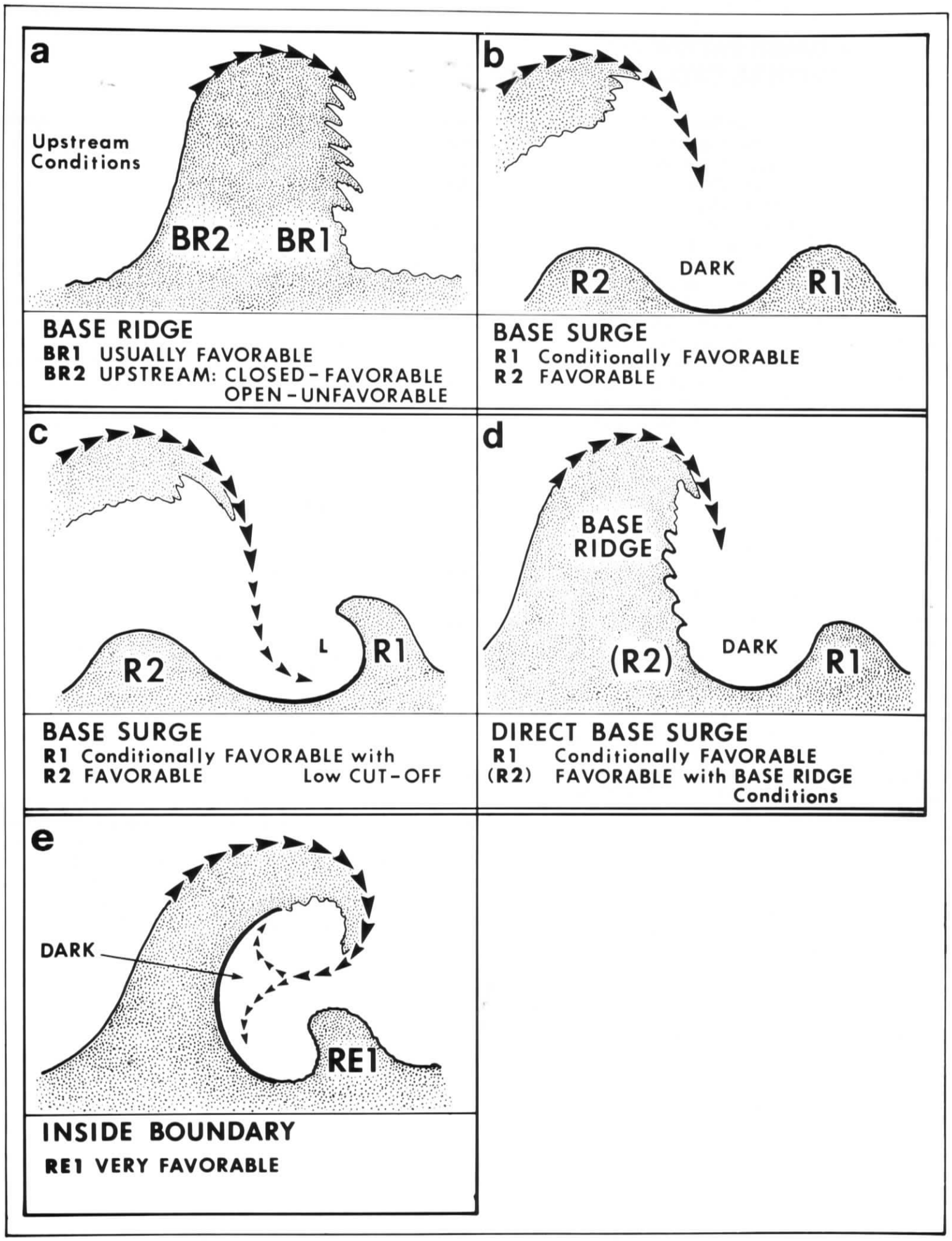

Figure 86 MODEL MOISTURE PATTERNS FAVORABLE FOR TROPICAL CYCLONE FORMATION
Shaded areas indicate high cold moist conditions that would appear light gray on 6.7μm image displays. Arrowheads indicate jet stream axes. Patterns are northern hemisphere configurations.

a. Model Patterns of Favorable Image Conditions

The organized deep convective cloud patterns that are incipient to tropical cyclogenesis usually form under the moist areas of the water vapor imagery. Those moist areas were most commonly associated with upper air ridges or anticyclones of a synoptic scale. Although a cyclonic circulation system may be present, or forming, under the pattern within the lower troposphere, we are able to identify only the upper anticyclonic portion on satellite imagery. Therefore, we refer to the patterns as "ridges". The simple upper air ridge or anticyclone pattern is not likely to apply to the system at later stages, if the system evolves and intensifies as a tropical cyclone; however, here we are concerned with the very early stages. Once we identified those early stage convective systems that later evolved to tropical cyclones, we were able to identify many others, in which the evolution was disrupted prior to the named tropical storm stage. From those two sets of cases we were able to identify certain common patterns and changes on water vapor imagery which were either favorable, or unfavorable for formation and continued evolution.

Drawings on **Figure 86** may be used to summarize some of the most common types of water vapor image patterns favorable for synoptic scale organization of deep convective weather regimes.

Figure 86a

We refer to the pattern on **Figure 86a** as a "base ridge". With these patterns, the moist regions from the ITCZ, or another low latitude deep convective regime, extend poleward to near the axis of maximum winds of a jet stream branch in the westerlies. In some cases, the jet stream branch may also be present along portions of the western and eastern borders of the moisture pattern in addition to the poleward side. These ridge patterns are relatively large features compared to the sizes of the incipient organized convective patterns of tropical cyclones. However, many tropical cyclones form within the moisture patterns of "base ridges". A base ridge pattern is a more favorable location for tropical cyclogenesis than other general locations within the ITCZ convective regimes. Within the base ridge regime, development is more likely at the equatorward end where the ITCZ convective weather is more prevalent, but formations are relatively common elsewhere within the equatorward two thirds of the patterns. With tropical cyclone formations of base ridge patterns, the systems tend to evolve more slowly than with the other common patterns to be shown here.

The base ridge locations may become either more or less favorable for development, depending upon the image conditions farther to the west or northwest. We will show two cases on imagery, and discuss these conditions.

Figure 86b

The drawing on **Figure 86b** represents a situation following an "indirect" base surge with convex boundary segments on both sides of the concave surge portion. If the base surge occurred into a large regime of deep convective weather conditions, high clouds and convective weather will be likely on the moist sides of both convex boundary segments. Even when deep convective weather conditions were not initially present along the moist side of the boundary, they are likely to form in the "R1" and "R2" locations. Both the "R1" and "R2" locations are favorable for tropical cyclone formation. The "R2" location is more favorable than the "R1" location. As in all of the locations shown and discussed here, there are other factors such as the geographical location and the season of the year. If the convective system has formed, or is moving, over land or relatively cool sea surface temperatures, a negative influence will be present, which will outweigh the favorable upper air environment indicated by the water vapor image pattern. Furthermore, after the initial formation of the "R1" or "R2" ridge pattern; the environmental upper air conditions may change, or the pattern may move into the influence of less favorable upper air conditions. Consider the case shown on **Figure 82**, in which an "R2" cloud pattern formed. In that case during March, the convective weather never became well organized, and the system formed over the land areas of Colombia and southern Central America. Also, as the system moved westward, it quickly encountered a large eastward moving upper air trough/ridge system in the low latitude westerlies. This caused the "R2" pattern to halt and "shear out" to the northeast. In that same region during July, August, and September, "R2" systems may form in nearly the same location, or over the western Caribbean, and move westward across the Central American isthmus to the eastern Pacific Ocean where tropical cyclogenesis proceeds. Even during those months, the low latitude upper air conditions to the west of the "R2" system, must be favorable for continued development. However, a strong open upper air westerly system is less frequent at those latitudes during the summer season. Note that the formation or movement of "R1" and "R2" weather over land will not destroy them, but it will prevent the evolution of a tropical cyclone. In some cases, "R1" and "R2" do persist over tropical land areas, as significant deep convective weather systems with well defined mid-tropospheric cyclones and upper tropospheric anticyclones. The "R2" locations are more favorable for tropical cyclone development than the "R1" locations, because of their position with respect to the circulation pattern which caused the initial base surge. Upper air easterly winds, or very light westerlies are likely adjacent to the "R2" position, since a large upper air ridge or anticyclone is present poleward of there during the surge event. Thus, the "R2" location is isolated or "protected" from open upper air troughs and their associated mid-tropospheric cold advection, at least during the initial stages. The upper air environments to the poleward side of the "R1" locations are more variable. Using a Northern Hemisphere perspective as in the drawings, the base surge is caused by an acceleration of northerly component flow. Since this flow is generally on the east side of a ridge and the west side of a trough, there is often a trough to the northwest side of the "R1" location. Some base surges result from a temporary condition, such as a single short speed maximum in the jet stream over the ridge, or two ridges in the westerlies moving into, then out of, phase. In those cases, the trough to the northwest side of the "R1" location is present only briefly, or remains strong only briefly. In those cases, a rounded shape of "R1" system is likely, and subsequent westward movement and development are more likely.

Figure 86c

In other base surge cases, in which a strong digging trough or extending jet stream are involved, the "R1" ridge system forms as a "build-back" ridge related to the base of the "digging" trough. This type of situation is shown on the drawing of **Figure 86c**. Tropical cyclogenesis can occur with such systems. If so, it will be a "hybrid" type which occurs after the related upper air trough becomes "cut-off" or significantly weakened. An example of this type of formation will be shown on **Figure 90**, as an example of a Category I development.

Figure 86d

This drawing represents conditions with a "direct" type of base surge at a tropical location. Since the ridge on the west side of the base surge boundary is the one causing the surge, the resulting ridge in the "R2" position is that same ridge. At low latitudes, it most likely could be considered a "base ridge", as shown on **Figure 86a**. There were indications that a tropical cyclogenesis in the "base ridge" location was more likely after the occurrence of a base surge on its east side; however, the cyclogenetic potential was still largely dependent upon upper air conditions to the west of the "base ridge". On the drawing of **Figure 86d**, the "R1" pattern is shown as the rounded convex boundary shape; however, it could also be the "build-back" type in these circumstances.

Although not shown on the drawings of **Figure 86**, it is relatively common during the summer seasons along the ITCZ convective regimes, for a "direct" type of base surge to form on the eastern side of a strengthening tropical cyclone. Often, these create an "R1" ridge system with deep convection on the east side of the base surge boundary. Those types of "R1" systems are also favorable for tropical cyclogenesis. However, upper air conditions are often unfavorable to the poleward side of the new "R1" system. A ridge or anticyclone is often present at latitudes just poleward of the tropical cyclone, since the environment was obviously favorable. In conjunction with this, there is often an open trough to the east, on the poleward side of the new "R1" system. Overall, the favorability for tropical cyclogenesis with this special type of "R1" ridge is approximately the same as for the other convex boundary types, as depicted on **Figure 86b**.

Figure 86e

In the situation shown on **Figure 86e**, an inside boundary forms on a "base ridge" moisture pattern, as a result of anticyclogenesis. The primary surge in the upper air flow is toward the west, in the form of easterlies on the south side of the anticyclone, instead of toward the south as in the base surge cases. The dark region and concave moisture boundary will be along the east side of the "base ridge". A new trough is likely at the southern end of the dark region, where the easterly winds turn cyclonically southward. Often a ridge forms on the east side of the new low. We refer to this ridge as the "RE1" location. It is also very favorable for tropical cyclone development. A case will be shown as **Figure 88**.

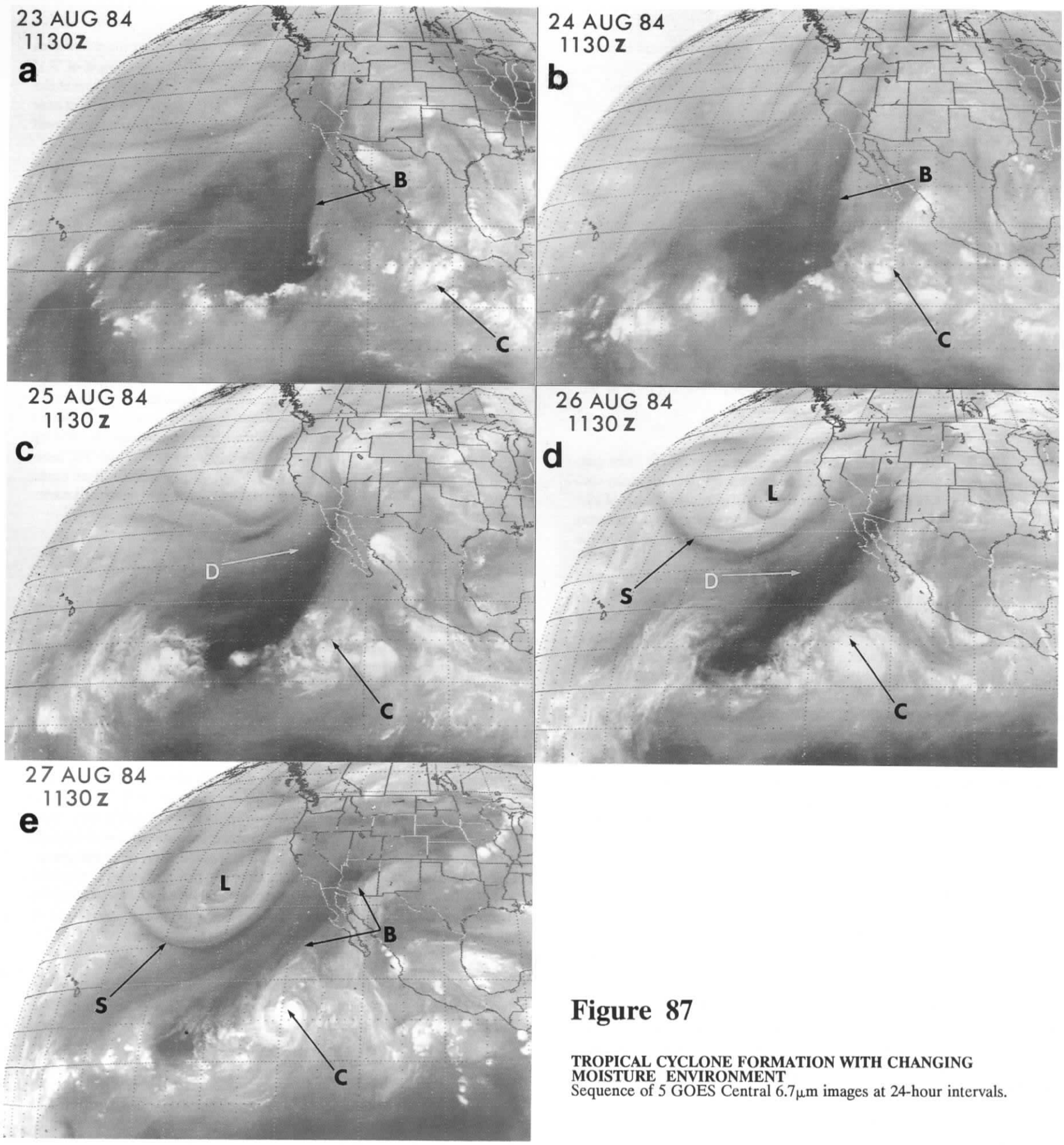

Figure 87

TROPICAL CYCLONE FORMATION WITH CHANGING MOISTURE ENVIRONMENT
Sequence of 5 GOES Central 6.7μm images at 24-hour intervals.

b. A Tropical Cyclone Formation in the "Base Ridge" Location

On **Figure 87**, five water vapor image are shown at 24 hour intervals. A tropical cyclone formed in the "base ridge" location. For illustrations in this and previous sections, we chose cases which were relatively "simple" and well defined, so that the particular concepts involved could be shown without complications and distractions. This case has some of the complexity of the typical water vapor images observed on a daily bases. It was chosen because five separate conditions were present, which have been observed to be individually favorable for tropical cyclone development. We would have been very disappointed had development not occurred.

The most reliable indications of tropical cyclone development on satellite imagery are the observations of the convective cloud conditions using visible and infrared imagery. The fundamental question for the observer is: are deep convective clouds formed and persisting in an organized pattern? The trend in the behavior of this convective pattern can then be extrapolated as a basic forecast. If the convective clouds are persisting, and becoming better organized with time, that basic extrapolation may be for development. Then, the patterns on the water vapor imagery may be considered as an additional factor. Is the convective cloud system at a location within the water vapor image patterns, which is considered favorable for development? Is it moving into such a location? What types of changes with time are occurring on the water vapor imagery, which may detract from or enhance the favorability? In this manner, knowledge from the water vapor imagery may be combined with information from other sources to confirm or modify the forecasts.

Consider the case shown on **Figure 87**. At the first image time, a large high amplitude upper air ridge system extends from the north central United States southward into the ITCZ convective regime. This ridge is complicated by several short wave features, however it is revealed as a large moist region on the image with a "base ridge" pattern at the tropical latitudes. With other factors being equal, unfamiliar, or ignored, a "base ridge" moisture region is generally favorable for tropical cyclone formation. Any deep convective weather occurring within the region merits more attention than within the convective regime in general. In this case, convective clouds can be seen on the first image at several locations along the ITCZ area. The area at "C" has been more persistent. Deep convective clouds have been recurring in the same general region; and, an area of middle and high cloud debris has been persisting within stable layers in the vicinity of the recurring convective cells. Sometimes those areas of stable middle and high clouds will reveal a pattern on still images before one can be identified in the convective cells. Also, when viewed in time-lapse motion, the deep convective cells may be moving in a cyclonic rotation with respect to each other, and cirrus debris may be seen to fall back with respect to the cell motions. Both of these are an early indication of synoptic scale organization required for development. The pattern indications in this case, at the time of the first image, were of the type which are very common in the ITCZ region without continued development in most cases. However, those that do develop appear very similar at this early stage.

The degree of favorability within a "base ridge" pattern can be significantly modified by considering the conditions to the west of the ridge. Usually there will be a reasonably well defined moisture boundary at the tropical latitudes on the west side of the ridge moisture. This is identified at "B" in this case. There will be a relatively darker area on the west side of that boundary. The key question involves the characteristics of the western edge of that dry or dark area. If the dark region extends with little change for a long distance to the west, such as 20° of longitude or greater, then no additional information can be added to the degree of favorability of the "base ridge" moist area. We found no significant correlation in those cases.

If the west side of dark area has no well defined boundary, but gradually becomes lighter to the west, this implies an "open" circulation pattern between the trough and the upstream ridge. This is unfavorable for development within the "base ridge" moist area, especially if the incipient deep convective weather area is near the western edge of the moist area. This condition is present on the first image of **Figure 87**, to the west of boundary "B". However, this "unfavorable" influence is not as great as it might be, since the primary convective cloud region at "C" is located approximately 10° of longitude east of boundary "B". The net results from the two conditions identified on the water vapor image are about zero. The favorability of the base ridge location is offset by the degree of unfavorability of the conditions farther to the west. Therefore, it is necessary to use the trends of the deep convective weather as a forecast; or perhaps, to supplement this with the computer model forecasts of the upstream trough and ridge systems.

In this regard, the best applications of the water vapor imagery are usually obtained by observing the changes with time on a series of images. In this case, we would specifically look for changes in the character of the moisture pattern between the trough dark area, and the lighter moist area of the ridge farther to the west. Is a well defined edge beginning to form there? If so, the upstream systems are changing from moving "open" types to slower moving "closed" types; and, conditions for development in the "base ridge" area are favorable. Although "open" and "closed" systems were discussed in the previous sections, it is useful to summarize some aspects for use here, and in the following cases. With "open" cases, the upper air flow is generally across the ridge and trough axes. The related moisture patterns are generally oriented with the ridge and trough axes, with flow across the edges. In the westerlies, the western boundaries of moist patterns are well defined, and the eastern edges are poorly defined or gradually changing in gray shades. The mid-tropospheric isotherms tend to have greater amplitude than the streamlines, so that significant thermal advection is present. With "closed" patterns, the upper air flow is generally around the periphery of the related toughs and ridges, generally more parallel to the axes of those features; or around closed lows and highs. Well defined boundaries are likely on the eastern sides of moist areas as well as the west sides. Although significant thermal gradients may be present, the flow is nearly parallel to the isotherms with little thermal advection, and slow moving or stationary systems. One of the most useful simplified statements we can make in regard to tropical cyclogenesis is that it is more likely with "closed" circulations in the upper air environment, and less likely with an "open" upper air environment. In most geographical areas, this applies most to the environment to the west and north of the incipient deep convective system, where significant mid-tropospheric cold advection is likely to be present, and approaching.

By the time of the second image, **Figure 87b**, the conditions to the west of the "base ridge" have not changed significantly. The deep convective cloud pattern "C" has propagated westward. Although the deep convective cells have not persisted to any significant degree during the period, the pattern has become slightly better organized. The cells present at any given time are better arranged in a banded pattern, and some of the cirrus debris is persisting in patterns suggesting a weak upper level anticyclonic system. The very fact that the system persisted for the 24 hour period is a positive sign for development. However, with the convective system closer to the western boundary of the moist area, the conditions on the water vapor imagery west of there must be given more emphasis.

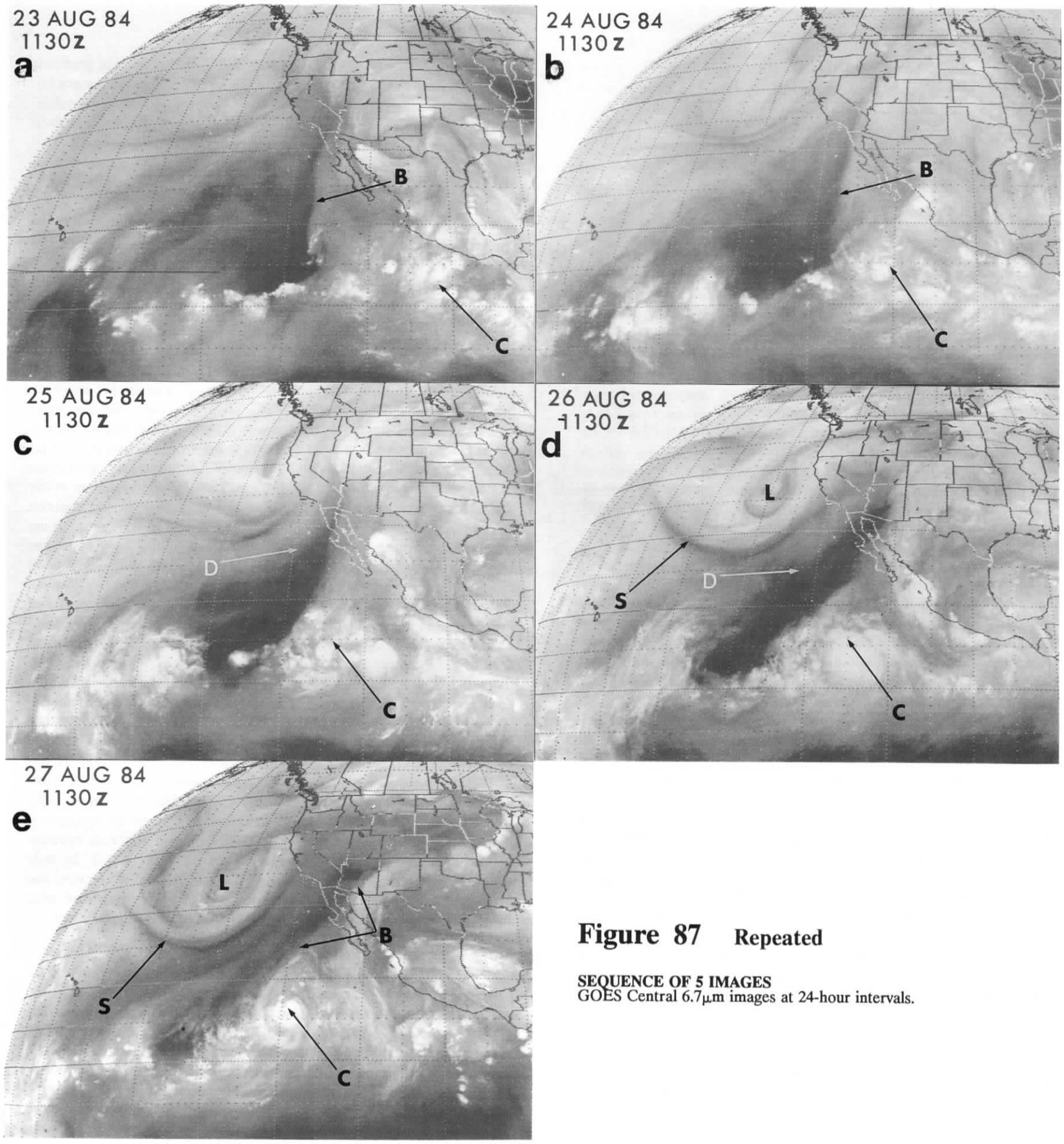

Figure 87 **Repeated**

SEQUENCE OF 5 IMAGES
GOES Central 6.7μm images at 24-hour intervals.

Although it is relatively easy to identify the type of upstream upper air systems on the water vapor imagery, it is very difficult to determine the strength - the wind speeds and temperature gradients. However, the effects of the upstream system on the tropical cyclone formation, are dependent upon the intensities of both the upper air system approaching and the tropical cyclogenesis processes. For example, in the case shown here, the convective cloud system has been moving westward and gradually improving its pattern. Therefore, we can conclude that the strength of the open upper air conditions to the west have been such as to permit the westward movement and the improvement trend. This type of "balance" between the opposing processes of unknown individual intensities, is probably of significance to our observation that changes with time in the water vapor environment are more useful indications than the types of patterns. We also observed that when a tropical convective cloud pattern and an "open" type of upstream upper air system are becoming closer, the negative effects of the open environment are likely to increase, even with no apparent changes with time in the "open" conditions.

In the case shown here, at the time of **Figure 87b**, the convective pattern is moving westward toward the unfavorable upper air environment. We would expect some destructive or weakening effects in the convective system, during the next 24 hour period, unless the environmental conditions become more favorable, or less unfavorable. Six hours after the second image time, some increase in the gradients could be observed between the dark area and the lighter gray shades to the west of there. By the third image time, a boundary "D" has formed on the northern portion of the west side of the dark area. South of there, the western edge of the dark area became slightly more distinct, but irregular. Overall, the change with time has been away from unfavorable conditions, or toward favorable ones, therefore a favorable change. The pattern of the convective system continued to improve, with both the convective cells and the high cloud debris appearing in a more organized pattern. By the fourth image, **Figure 87d**, the boundary "D" has become more distinct along a relatively long extent, and better defined. The conditions have changed to such an extent that the upstream pattern would now be considered the favorable "closed" type. At the fourth image time, the pattern on the still image is favorable; and, the changes with time during the past 24 hours have been favorable. The convective system "C" continued to improve, but not at a rate significantly greater than it had been undergoing previously. During the last 24 hours, the pattern of system "C" improved significantly to a tropical cyclone pattern. Note that our analyses of the condition of the convective pattern "C" were based upon infrared and visible imagery, not shown here. System "C" was named Tropical Storm Lowell, 12 hours prior to the last image, and designated a hurricane 24 hours after the last image time.

In this case, a tropical cyclone development occurred in a "base ridge" location, which is regarded as a generally favorable location, because many formations were observed in that water vapor image environment. The upper air conditions to the west of the "base ridge", which have been observed to be very significant to the degree of favorability of the "base ridge", changed from unfavorable to favorable during the period of development. •

Three other environmental conditions occurred in this case, each of which were individually correlated positively with tropical cyclone developments in other cases. None of the three are as strongly correlated to development as the other conditions discussed here, or in the discussion of the model patterns of **Figure 86**. All are regarded, by us, as "clues" favorable to development. All three factors are identifiable at their earliest phase on **Figure 87c**, and very recognizable on **Figure 87d**. In order of their "value" in regard to tropical cyclone formation, they are as follows: Consider **Figure 87d**. A "cut-off" upper air low has become well defined in the water vapor image pattern at "L". We have observed that the formation of a "cut-off" low to the northwest of an incipient convective cloud pattern, is a favorable indication. The favorability is strengthened, if the image pattern of the "cut-off" low becomes more rounded with time, if well defined boundary features form on its west side, and if the system remains stationary with respect to the formative tropical convective pattern, or moves westward. The second environmental feature is the "return moisture boundary" at "S". Such boundaries were first discussed in Section A. The boundary has a convex curvature - from the moist side perspective, and is moving equatorward. As is characteristic of such boundaries, it is moist on the poleward rear side, with a narrow dark region along the equatorward side of the boundary. Such "return moisture boundaries" were also observed to be a favorable clue to tropical convective system formations. In those cases, the "return moisture boundaries" were observed to enter the northwestern quadrant of the tropical convective system, from the north. A critical condition of this "favorability" was that the extrapolated path of the "return moisture boundary" was to the west side of the tropical convective pattern. In this case, both the "return moisture boundary" and the "cut-off" low were moving southwestward, in conjunction with each other, as parts of the same overall circulation pattern. This behavior most likely caused the formation of boundary "D" in this case. This is a common result of such a southwestward "digging" process; but, by no means the only way in which boundaries such as "D" form. The "digging" systems likely caused an amplification in the upper air trough and adjacent ridge system east of Hawaii, and caused the winds along the western side of the dark region (near "D") to rotate cyclonically with time, from westerly across the edge to southwesterly nearly parallel to the edge. In other cases, when occurring individually, both the "return moisture boundaries" and the "cut-off" low formations, are indications of the tropical system environments changing from "open" to "closed" configurations. A "cut-off" low is itself a closed system, and when moving westward, implies an anticyclone dominating the polar jet stream zone in the longitudes to the west of the tropical convective pattern. Similarly, a "return moisture boundary" generally is involved with a southward moving anticyclone which changes the open troughs in its path to cyclonic shear zones. Again the trend is for systems to change from open to closed in the environment of the tropical convective pattern.

The third condition which occurred at the time of **Figure 87d**, was that the primary moisture boundary "B" had rotated anticyclonically with time. This had begun 24 hours prior to that, as the equatorward end of the boundary moved westward, and the poleward end moved eastward. This type of rotation of the western boundaries of "base ridges" is a relatively weak indication of development. The anticyclonic rotation of those boundaries has been observed with developing tropical convective systems; and, in the absence of other more significant information, can be a sign of development, if not actually a favorable condition useful for forecasting. Often, the equatorward ends of such boundaries will move westward as a result of the westward moving convective weather system. This was true in the case shown here. This is an indication that the deep convective cloud system is not being blocked by a strong open upper air trough to its west side.

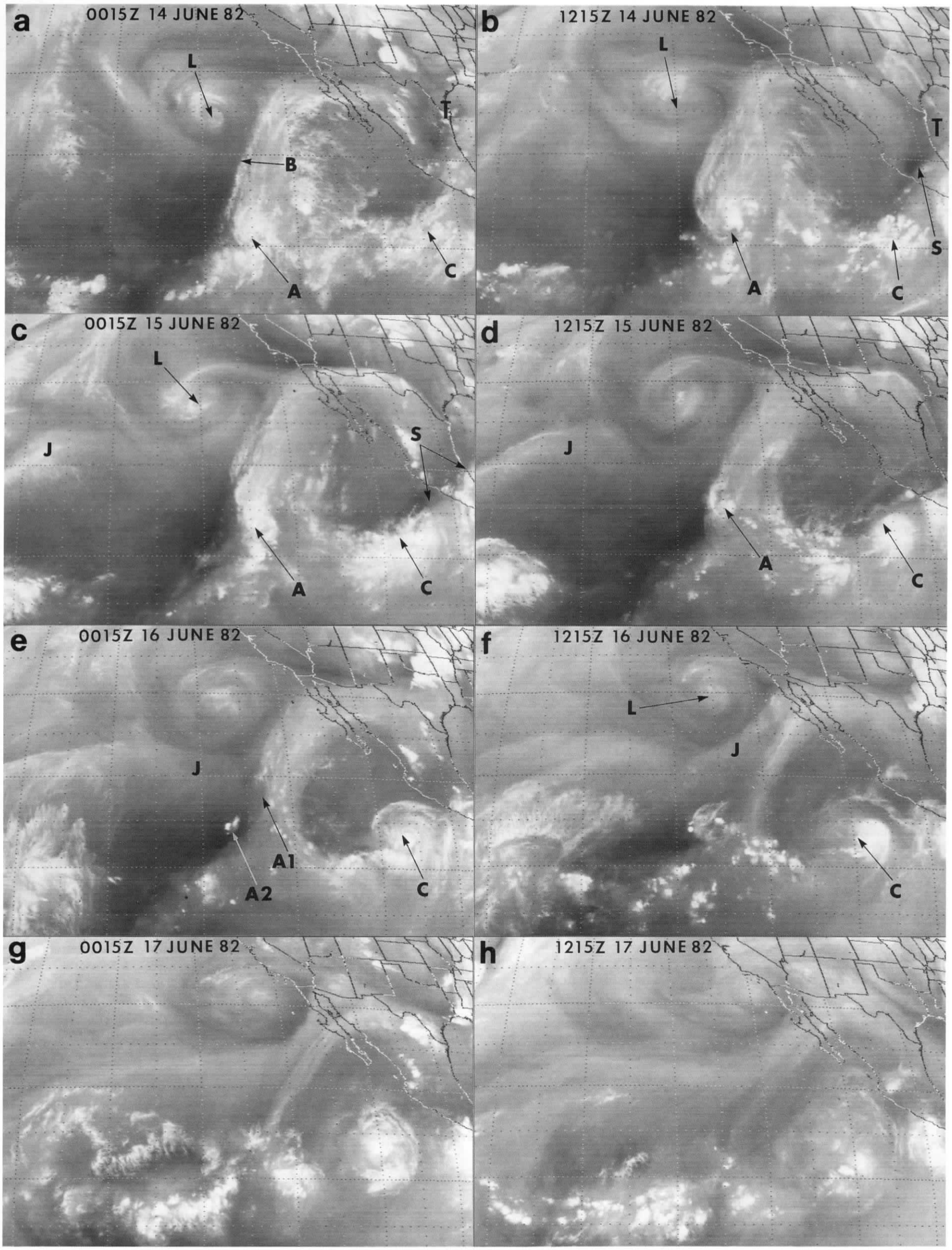
a
0015Z 14 JUNE 82
L
B
T
A
C
b
1215Z 14 JUNE 82
L
T
S
A
C
c
0015Z 15 JUNE 82
L
J
S
A
C
d
1215Z 15 JUNE 82
J
A
C
e
0015Z 16 JUNE 82
J
A1
A2
C
f
1215Z 16 JUNE 82
L
J
C
g
0015Z 17 JUNE 82
h
1215Z 17 JUNE 82

c. An "RE1" Formation and Westerly Jet Stream Break-Through

The case shown on **Figure 88** was also chosen because there were several types of circulation environments and interactions. The water vapor images are in sequence at 12-hour intervals. With this case, in mid June, the upper air wind systems were stronger than those involved in the last case.

On the first image, **Figure 88a**, a "base ridge" pattern is present to the west of Mexico. In this case the jet stream branch on the poleward side of the ridge is near 30°N. High clouds and convective weather are present along the ITCZ convective zone along the southern side of the ridge, and extended northward along the western side of the ridge. A boundary at "B" with cirrus clouds associated is present along the west side of the "base ridge" moisture regime. To the west of that boundary, an upper air low at "L" has become "cut-off" from the polar jet stream zone, and an "open" upper air trough extends southward from the low within the dark region at low latitudes on the west side of the ridge. The upper air trough system is not vertically shallow and limited to high levels, but is relatively deep within the middle troposphere. Therefore, the dark region has an effect on the deep convective weather, similar to those discussed in the first topic of this section. The ITCZ convective weather is suppressed, with only a few small areas present, and south of 10°N. The convective regime is significantly different than that on the south side of the "base ridge" on the eastern half of the image. On the northwest part of the image, an area of high cold clouds and moisture is present. Those clouds are associated with a complex high amplitude ridge system which extends from low latitudes east of Hawaii, over the northeastern Pacific. Similarly, a jet stream, with a low latitude branch to the west, extends around the poleward side of that ridge system, then equatorward along the west coast of the United States. It was the northeastern part of that jet stream ridge system that "rolled over" the "cut-off" low at "L".

At the time of the first image, there were three areas within the "base ridge" moisture regime with persisting deep convective clouds. One of those patterns near the western part of the ridge, at "A", has persisting convective weather and a relatively well organized pattern. Convective clouds have been generally persistent in the area at "C", but organization has been relatively poor. A third area of deep convective weather persisting in a rounded pattern is just off the eastern edge of the image, along the southern coast of Mexico. With the static view of the first image alone, that easternmost convective pattern appeared to have promise for development. At that image time, there is a trough in the westerlies over northeastern Mexico, at "T", and moving eastward. Once that trough passes eastward out of the northern quadrant of the convective pattern, the convective system is likely to move westward away from the coast, and onto the south side of the large "base ridge" system. That better environment, with the already persisting organized convective weather, would likely result in development.

Figure 88

CHANGING MOISTURE ENVIRONMENT AND DEVELOPMENT IN THE ER1 POSITION
Sequence of 8 GOES Central 6.7μm images at 12-hour intervals.

Before discussing the changes with time and the system evolutions, consider the environment of the convective system "A". According to our previous discussions of **Figures 86** and **87**, there are two favorable conditions and one unfavorable observed on the water vapor image, to be combined with current trend of the convective weather and organization of system "A". The fact that it is within the "base ridge" moisture regime is favorable. There is also a newly formed "cut-off" low in its northwestern quadrant. This is moving slowly westward and is a favorable condition; but, it should be given less weight than the moisture patterns of the upper air systems to the west of the "base ridge", at the same latitudes of "A". These are unfavorable, with the gradual change of gray shades on the western side of the dark zone. Furthermore, the upper air westerly winds are relatively deep and strong, as indicated by the effect on the convective weather, and the fact that system "A" has become stationary. We would have guessed that, under these conditions, system "A" was "in trouble". With the trough at such a low latitude, it could amplify and change to a "closed" type of system, causing system "A" to accelerate northward, while maintaining its intensity or even developing. However, there are no indications of this "closing" of the trough. If it intensifies as an "open" trough system, it is likely to cause the convective system to "vertically shear". The upper air ridge portion will move eastward in advance of the strengthening "open" westerlies; and, the lower portion in the marine layer will move westward as a "wave" or shallow cyclonic system in the easterlies.

By the second image time, **Figure 88b**, the pattern of system "A" appears on the water vapor image, to show no significant change, with perhaps a small northward movement. To the west, the dark area has decreased in size by moisture approaching from the west with an "open" type of pattern. Overall, the water vapor image conditions are unfavorable for development of system "A". Unless more information, such as computer upper air progs, or some changes noted on the upper air analyses on imagery farther to the west, is available; we would suggest a "trend" forecast for system "A", based upon the convective pattern.

Consider the other convective system to the eastern part of the "base ridge" pattern. During the 12 hour period, there was an increase in the upper air winds over Mexico, on the northeast side of the ridge. The trough "T" moved southeastward. In response, a well defined boundary formed at "S". Although the eastern deep convective pattern has moved westward enough to show on the eastern edge of the second image, it is now in an unfavorable position with respect to the "digging" trough. If the trough continues to move southeastward, with its western end over Mexico remaining strong, any development of the convective system will be halted or delayed.

By the third image time, the movement and shape of boundary "S" imply that the trough remained relatively strong. The organization of the eastern convective system has been adversely affected. During the same period, the deep convective weather has become more persistent with system "C", and the pattern has become better organized. Note on the first two images, that the cirrus clouds on the eastern side of the "base ridge" cloud area, formed a ragged pattern, suggesting that the upper air flow crossed the ridge axis in an "open" upper streamline configuration. By the third image, the cirrus clouds in the same area have begun to form a curved pattern, suggesting a possible inside boundary formation. By the 4th image on **Figure 88d**, that pattern is vividly indicated. An inside moisture boundary has formed, and darkening has occurred on its eastern side. The ridge has changed from an "open" pattern to a "closed" anticyclone, with newly formed upper air easterly winds over a part of the dark area south of the new upper air high. This change in the image pattern, with the implied new circulation pattern, was observed to be favorable for tropical cyclone formation within the convective regime along the south side of the new dry area. Usually a new trough will form at the southern end of the inside boundary, and a new "RE1" type of ridge pattern will form to the east of the trough. That "RE1" ridge location is very favorable for development. If one or more deep convective systems are already under way along the southern side of the dark area, during the inside boundary formation, they should be considered as favorable locations. If the new low forms at the southern end of the inside boundary, that convective system closest to the "RE1" location is in the most favorable location. In this case, convective system "C" was in that favored location. By the time of **Figure 88e**, the improved organization of system "C" can be seen on the water vapor image. The system developed in the "RE1" location as the anticyclone closed and the inside boundary formed.

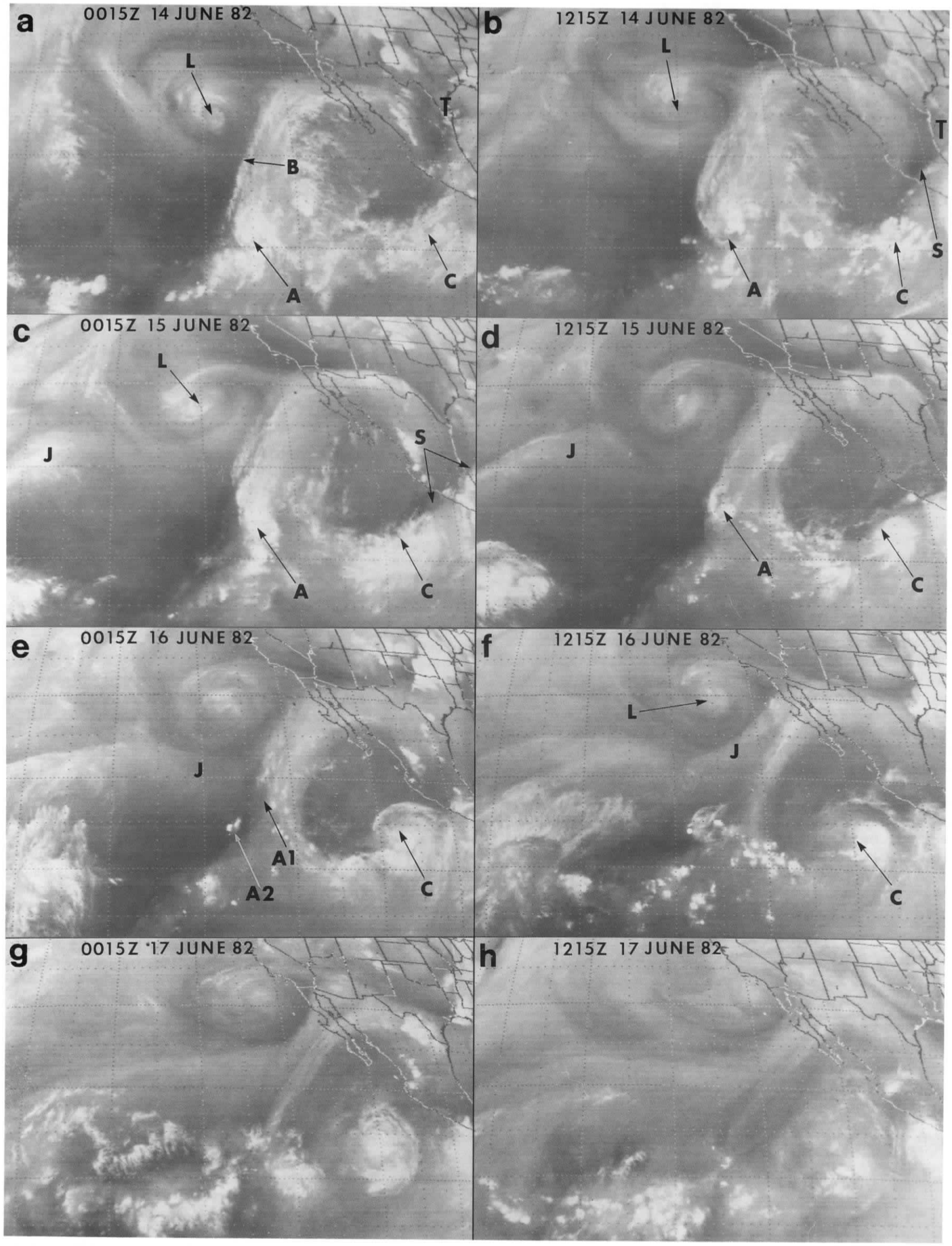

Figure 88 **Repeated**

SEQUENCE OF 8 IMAGES
GOES Central 6.7μm images at 12-hour intervals.

We interrupted our discussion of the deep convective system "A" after the time of the second image. Between the 2nd and 3rd image times, some significant changes have begun in the environment to the west of the "base ridge" system. The "cut-off" low, which was moving slowly westward, became stationary near 130°W. Secondly, a jet stream branch over the Hawaiian Islands (just west of the image areas) began to break across the mid Pacific ridge, which extended from low to mid-latitudes. On the third image, **Figure 88c**, a region of high level moisture and cirrus clouds is present at "J" on the west side of the image. This is within the upstream ridge, along the southern side of the axis of maximum winds of the jet stream branch breaking across that ridge. In association with this jet stream branch, extending eastward across the ridge, the wind speeds will increase at tropical latitudes on the rear side of the trough south of the "cut-off" low. The increased wind speeds cannot be detected on the still image of **Figure 88c**; but, the effects can be seen by the changes of the high cold cloud pattern of system "A". The western border of those clouds has moved eastward, and the pattern has elongated in a south-north orientation. System "A" is still a significant vertically deep weather system at the image time; however, its pattern change indicates it has encountered a problem. Since such pattern changes are common, and often temporary, with early stage tropical cyclone systems, as they encounter different environmental conditions; it is very useful to recognize the feature or condition in the environment which is causing the problem. Will the change continue, or be temporary? In this case, we have already anticipated and identified the problem. The "open" ridge-trough system already present in the upstream westerlies has intensified with the jet stream break-through. Conditions have become very unfavorable for system "A". If the computer progs of the upper air systems have sufficient data to be accurate, they may be useful to forecast the unfavorable circulation conditions. A primary question to answer from those progs is: will the jet stream extend northeastward, opening the "cut-off" low and causing it to accelerate eastward? If so, the ridge may "roll over" the position of system "A", allowing it to survive, and perhaps strengthen. Or, the open westerly ridge-trough system to the south of the low may move eastward, with the jet stream extending eastward on the south side of the low. By the fourth image time, this second alternative is indicated on the image. The cold moisture pattern, "J", has extended eastward. The western edge of the dark area has remained "soft"; and, the cold cloud pattern of system "A" has diminished in size.

During the next 12 hours, the cold cloud pattern of system "A" moved northward and dissipated. By the time of **Figure 88e**, system "A" had undergone a "vertical separation". The low level part of the system moved toward the west-southwest, and is identified at "A2". It has moved under the upper level dry air conditions shown by the water vapor image; and is identified as a pattern of marine layer clouds observed on the infrared and visible imagery. Several deep convective cells are formed just to the north side of the cyclonic vorticity center indicated by the low clouds. The upper tropospheric part of the system moved toward the north-northeast in advance of the strengthening upper air trough, to the "A1" position. Usually, when such a "vertical separation" occurs, the thermal ridge, which was initially curved around the convective system in the upper middle troposphere, is weakened and removed from the upstream side, where the upper air trough is approaching. It remains on the downstream side, where cold topped convective clouds often persist. In this case, the deep convective weather with the upper level system dissipated. A large area of middle clouds above the marine layer remained under the upper level westerlies on the northern side of the low level center. These are not identifiable on the water vapor image.

The band of moisture associated with the jet stream branch has extended across the trough to the south side of the low "L" by the time of **Figure 88e**. By the next image, its effects on the "base ridge" pattern are evident. The elongated band of upper air moisture on the west side of the anticyclone has narrowed rapidly, and rotated anticyclonically. In this case, the point of rotation is near the south end which has remained nearly stationary. Also, on the image of **Figure 88f**, the low "L" has moved eastward in response to the intensified westerlies. By the image of **Figure 88g**, the trends have continued; and, by the time of the last image, the anticyclone has opened and moved eastward. The upper air winds to the northwest and north of system "C" have changed to westerlies, as the jet stream extended eastward at low latitudes. Most of the deep convective clouds associated with system "C" have dissipated; and, the upper air pattern has become disorganized, although an area of high level moisture remains. After this sequence, system "C" remained only as a low level cloud system, separated from its upper level moisture regime.

At the time of the last image, the low level cyclonic system "A2" is still identifiable on infrared imagery with some non-persisting deep convective cells; and, the only organized pattern with significant deep convective weather is the one originally near the southern coast of Mexico. It survived the effects of the "digging" trough and remained nearly stationary east of system "C".

d. A Base Surge Effect on an Existing Organized Convective System

When base surges, or inside boundary formations occur in a convective environment, deep convective clouds often persist in newly organized patterns at the "R1", "R2", or "RE1" locations. In the last case, shown on **Figure 88**, the organized deep convective cloud pattern, "C", was already present near the "RE1" location, when the inside boundary formed. System "C" then proceeded to evolve rapidly in the favorable "RE1" location. Such interactions involving previously existing deep convective patterns, and forming "R1", "R2", and "RE1" features identifiable on water vapor imagery, are relatively common events associated with tropical cyclone formations. In some cases, an existing deep convective cloud system will move into the favorable location created by a nearby inside boundary formation or base surge event.

An indirect type of base surge event was shown on **Figures 16** and **17** of Section B. Although that case was shown because it was over the United States and Mexico upper air networks, it also occurred at relatively low latitudes during the tropical cyclone season. On **Figure 16**, water vapor images were shown at 12-hour intervals, during the period in which a base surge boundary formed over Oklahoma and northern Texas, then moved southward to northern Mexico, where it interacted with the northern moisture boundary of the ITCZ convective regime. During the period shown, and days prior to that, the ITCZ convective clouds were generally north of 10°N, and relatively active with a large region of high level moisture accumulated over the convective regime. Also during this period, only one area within the eastern Pacific convective regime was present with the deep convective weather persisting and organized in a synoptic scale pattern. On **Figure 16**, this pattern is present just off the southwestern coast of Mexico between 100°W and 110°W. Although the deep convective clouds were reforming in a curved band pattern, with an anticyclonic cirrus pattern, they were not persisting well. Such patterns can often occur for a week or 10 days, without ever developing further. However, by the last image time of **Figure 16**, the convective clouds began to persist, and the cirrus persisted in a large area with the plumes forming an anticyclonic pattern.

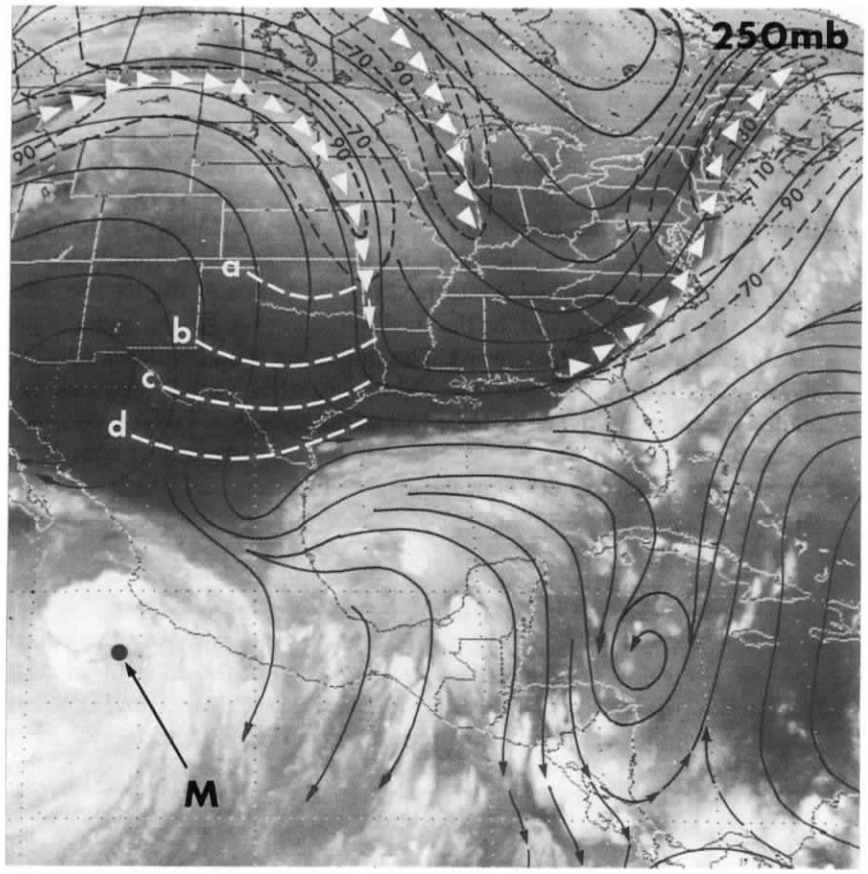

Figure 89

TROPICAL CYCLONE DEVELOPMENT IN THE R2 POSITION
6.7μm image, 2330Z 5 September 1984, GOES Central with 0000Z 6 September 1984 250mb analysis. Solid black lines - streamlines. Dashed black lines - isotachs (knots). White arrowheads - axes of maximum 250mb wind speeds (for speeds greater than 70 knots). Dashed white lines - base surge boundary locations at 12 hour intervals. Same times as images **Figure 16** [a = 2330Z 3 September, b = 1130Z 4 September, c = 2330Z 4 September, d = 1130Z 5 September].

We have observed that when a new base surge boundary forms with a deep convective cloud pattern already present in its southwestern quadrant, that convective system is likely to develop, and in many cases, rapidly. The convective weather system needn't be directly in the "R2" location, just south of the convex portion of the boundary to the west of the concave base surge part. A line may be extrapolated equatorward through the center of the concave part of the base surge boundary and its adjacent dark region on the poleward side, implying the primary direction of movement of the base surge, were it to continue moving equatorward. We observed that development was likely, if the center of the convective system was to the west of this line. The generally rounded poleward edge of the convective pattern, in these cases, may not coincide with the convex boundary of the "R2" location. It may be equatorward of there, or also farther to the east, such as to be out of phase with the curvature of the moisture boundary of the base surge. Note that this concept applied only in cases in which an identifiable organized convective pattern was present prior to the occurrence of the base surge.

In the case shown on **Figure 16**, the deep convective pattern of the ITCZ regime was in this type of favorable location. On the last image of **Figure 16** "R1" and "R2" locations are identified. These are based upon the pattern of the moisture boundary on the water vapor image, without consideration of the related upper air circulation systems, which may not be known in many cases. The favorability for development of the convective system, was considered even better in this case, because the convective system was moving northwestward toward the "R2" location; and, the jet stream ridge, which initiated the base surge, was moving eastward as an open system. With such eastward movement of the ridge, the jet stream was not likely to "hook" anticyclonically and push the base surge boundary back to the west side of the convective system. On **Figure 89**, an image is shown, valid 12 hours after the last one of **Figure 16**. Shown on the image, are 250mb streamlines, axes of maximum winds, isotachs, and positions of the base surge boundary for the image times of **Figure 16**. The 250mb data were valid at 0000Z, on the 2330Z 5 Sept 84 image. The convective system was named Tropical Storm Marie at 1800Z on the 5th. The surface center location is shown by a dot at "M" on **Figure 89**. The base surge event ended at the time of the image shown. The tropical storm system continued to move northwestward, and was designated a hurricane at 00Z on the 7th, approximately 24 hours after the image of **Figure 89**.

e. A Category I "Hybrid" Type of Tropical Cyclone Development

On **Figures 90** and **91**, images are shown at 12-hour intervals with 300mb analyses superimposed. The same sequence of **Figure 90** is continued on **Figure 91**. The first image of **Figure 90** is valid 12 hours after the image of **Figure 89**; however, the image is a close-up view located farther to the east. As the large open upper air ridge, which initiated the base surge event, moved eastward, a series of jet stream speed maxima formed and moved along the downstream side of the ridge system. Two of those are indicated by 300mb axes of maximum winds on the west side of **Figure 90a**, labeled "1" and "2". It was an earlier speed maximum zone along the axis of maximum winds, "1", which initiated the base surge event associated with the development of tropical storm Marie. The two axes of maximum winds are on the western side of the trough extending from eastern Canada to the Gulf of Mexico. High cirrus clouds are present along most of the moisture boundary on the forward side of the trough; and, several areas of deep convective cloudiness are present farther to the east, generally along a surface frontal trough zone.

During the period between the 1st and 4th images of **Figure 90**, cyclogenesis occurred at the base of the trough. The evolution of the cloud patterns and upper air circulation systems was a common type of mid-latitude development, referred to by Weldon as a "branching jet cyclogenesis". In those cases, the upstream jet stream is "split" into two branches, one equatorward to the rear side of the developing low, and the other extending to the left (Northern Hemisphere) along the newly building ridge. Or, quite commonly, two speed maxima in sequence, move in different directions. The first moves to the right, to the rear of the new low, and the second moves to the left on the poleward side of the newly forming "build-back" ridge. In this case, speed maxima in the two jet stream branches shown on the first image, evolved in that manner. With this type of cyclogenesis, the portion of the upper level trough directly involved with the cyclogenesis, closes early and usually becomes "cut-off" from the jet stream zone.

In this case, by the second image time, the boundary on the forward side of the upper air trough had become perturbed into an "S" shape, entering the "baroclinic leaf" phase of development. The jet stream branch, "1", had extended southward to the rear of the southern portion of the trough; and, branch "2" was forming the upstream side of a northern portion. By the third image time, a low had closed, and had become "cut-off" as the winds of the "1" speed maximum weakened to less than 50 knots. The cloud pattern had formed a "cusp" feature just off the northeast Florida coast. It was not until the 4th image time, when a closed surface low was indicated on the NMC analyses. The 1014mb center location is indicated by a dot on the image of **Figure 90d**. This surface low formation was later than we would have expected based upon the cloud pattern evolution. However, our relationships between cloud patterns and surface low formation were based upon sample cases, heavily biased toward the winter halves of the years, with primarily stronger vertically deep jet stream zones. In any case, a surface low was analyzed at 00Z on the 8th, then subsequently moved westward toward the Florida coast. Generally, during cyclogenesis, the surface low positions redevelop back toward the upper air trough in a relative sense as both systems move. However, in this case, the upper air low became "cut-off" and nearly stationary; therefore, the westward movement of the surface low center toward the upper air low would not be unusual. By the 4th image time, a moist area had built back around the upper air low from the eastern side. These areas are usually associated with a thermal ridge in the middle troposphere. Although radiosonde data were not available in the correct locations to verify that at the 4th image time, it was considered likely based upon subsequent analyses. By the 5th image time, **Figure 90e**, deep convective clouds had formed in the moist portion of the low, and a weak ridge had formed over that area in the upper troposphere. This ridge is shown on the 300mb wind field analysis. This tended to divide the cold parts of the trough into two parts. At this same time, the system was named Tropical Storm Diana, with a surface low center of 1008mb just on the southeast side of the deep convective weather. By the time of **Figure 90f**, the surface low was centered under a region of convective weather and cold cloud tops, over the ocean east of the Florida coast. During this phase, the upper air systems become very complex with an organized structure on the subsynoptic scales. The 300mb streamlines in the weak wind field area are largely estimated, and drawn with dashed lines. We believe they are reasonably correct until the time of **Figure 90f**, and inadequate in detail after that.

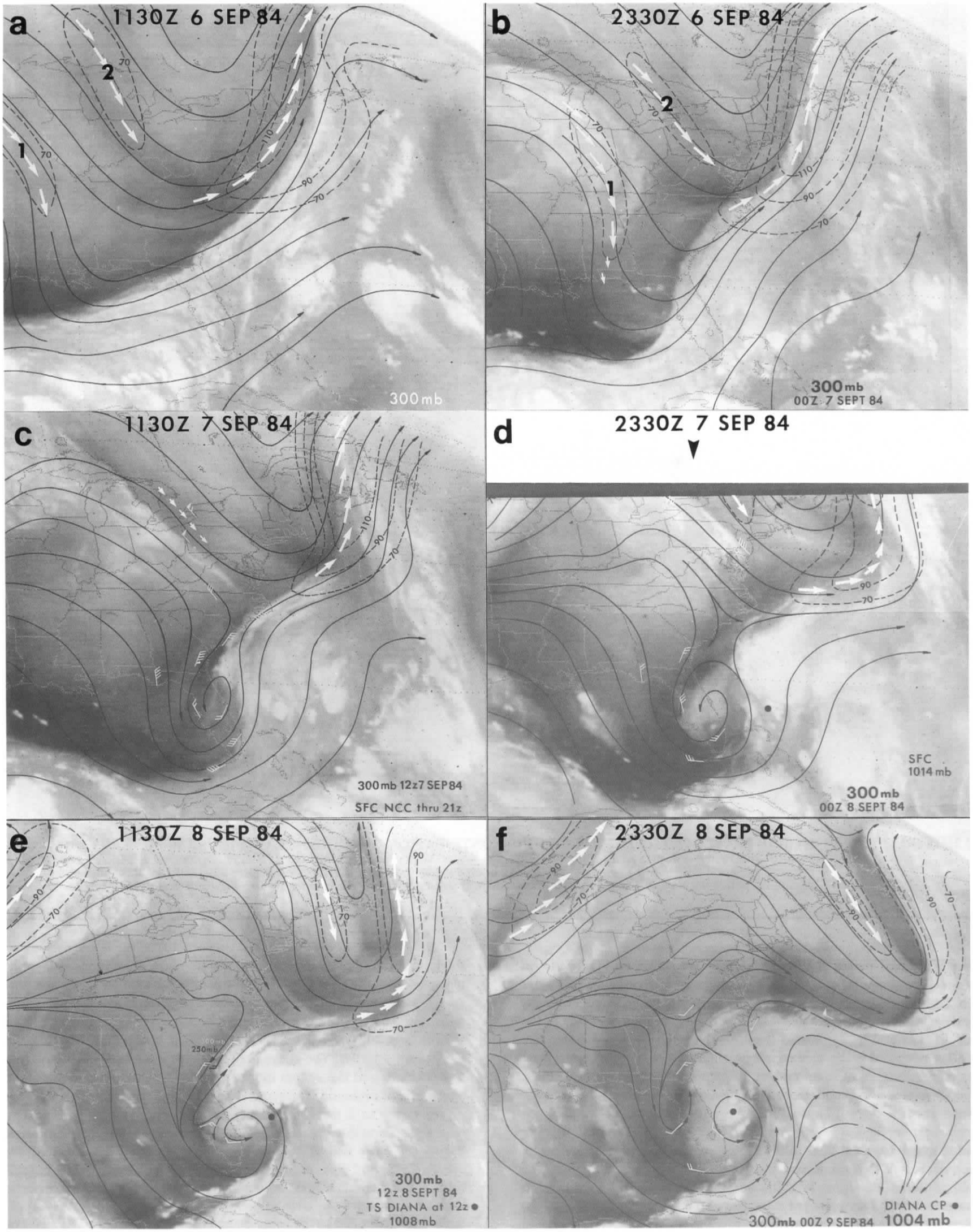

Figure 90

HYBRID DEVELOPMENT IN R1 POSITION
Sequence of 6 GOES Central 6.7μm images at 12 hour intervals, with 300mb analyses superimposed. Streamlines - black lines, Iostachs - dashed black lines, axes of maximum 300mb wind speeds - white arrows. Selected 300mb winds plotted in white symbols. Black symbol on **Fig. 90e** is 250mb wind. Analyses and wind reports are valid 30 minutes after Water Vapor images.

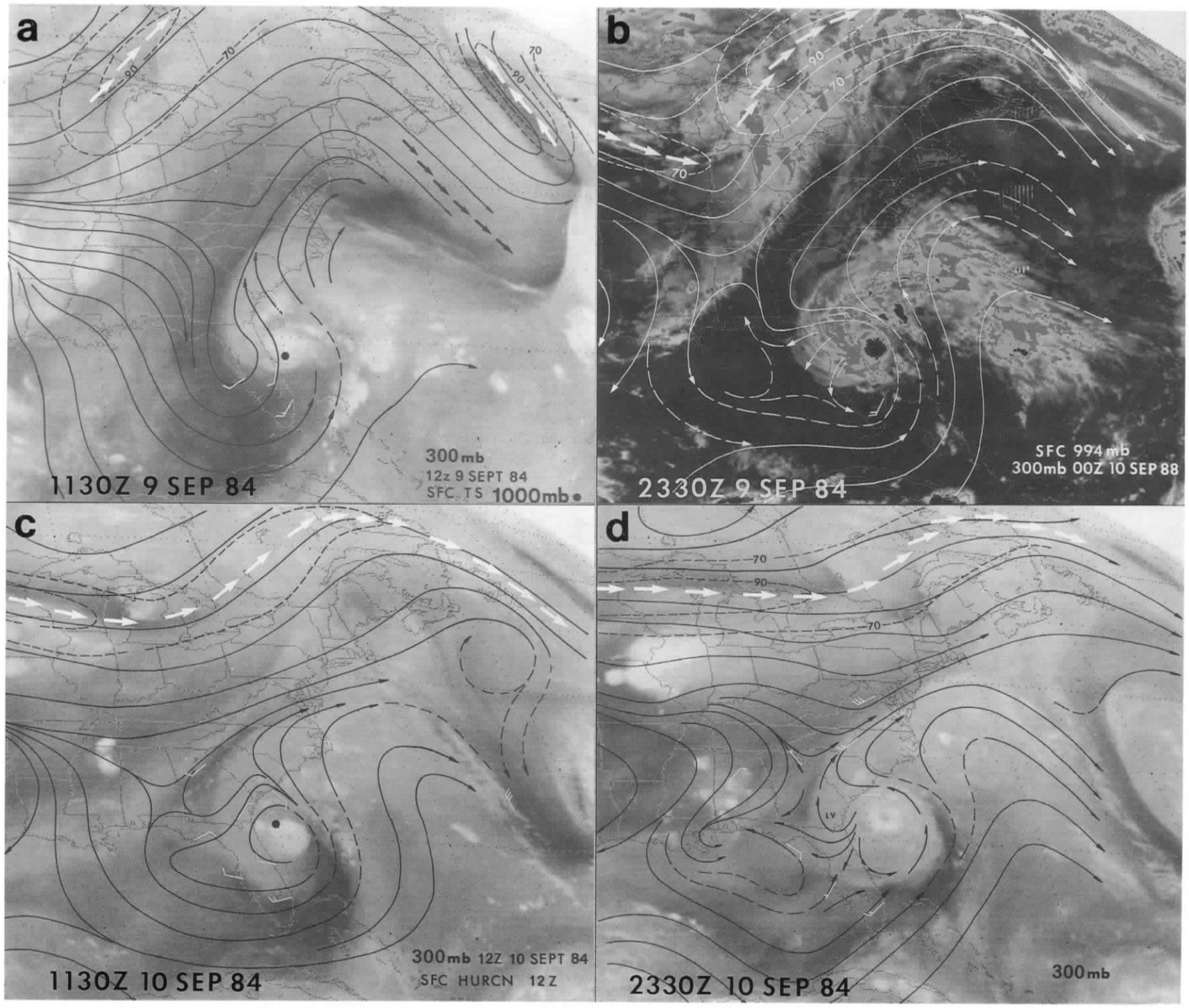

Figure 91 **HYBRID DEVELOPMENT IN R1 POSITION - CONTINUATION OF SEQUENCE ON FIGURE 90**
Images and 300mb analyses at 12-hour intervals. No Water Vapor was received for 2330Z 9 September 1984. An enhanced infrared image ("MB" curve) valid at 2300Z has been substituted. Black arrows on **Figure 91a** indicate a 300mb axis of maximum winds with speeds less than 70 knots. 300mb streamlines are white lines on the **Figure 91b** infrared image.

Four additional images at 12-hour intervals are shown on **Figure 91**. An infrared image was substituted for a missing water vapor image on **Figure 91b**. By the first image of **Figure 91**, the large jet stream ridge, originally over the western United States, has "rolled over" to the north side of the "cut-off" low and its associated tropical storm system. Deep convective weather persisted in the core region over the surface low, protected from the cold advection of open mid-tropospheric troughs in the westerlies. The low intensified, and moved northward. It was named Hurricane Diana near the time of **Figure 91c**. An eye formed shortly after that, and can be seen on the water vapor image of **Figure 91d**. The central pressure had reached 980mb at 00Z on the 11th, near the time of that last image; then decreased to a minimum value of 949mb, 24 hours after that. The cold portion of the upper level low became very complex on the last few analyses shown. The westward extension of the trough was caused by the effects of a large convective complex system over the south central United States during the period.

We have referred to these types of tropical cyclone formations as "hybrid" types, because the system in which the convective weather forms and persists is a mid-latitude type system located over warm sea surface conditions. Even after the deep convective weather forms in the organized environment and persists, the related upper air system may reopen to the upstream westerlies. The convective weather then moves off the surface low position, and the system moves out with a subsequent mid-latitude storm type of evolution. The systems were called "hybrids", since they may evolve either to a tropical cyclone, or to a winter storm type system, depending upon the interactions with the environmental jet stream zones during the early and middle phases. These types of development are usually Category I types of formation. The deep convective weather usually forms and persists within the thermal ridge portion of mid-tropospheric cyclonic flow, after the circulation system has formed. Water vapor imagery can be applied to the analyses and forecasting of such systems. For tropical development, the upper air trough must weaken, and be in some way blocked from continued cold air advection into its upwind side. Usually the trough closes and becomes "cut-off", surrounded by warm mid-tropospheric ridges. The water vapor imagery may be used as it might be applied to "cut-off" lows and their potential "opening". Although the water vapor imagery is useful, we believe it is more useful in applications to the Category II formations.

REFERENCES

1. Weinreb, M.P. and M.L. Hill, 1980: Calculation of atmospheric radiances and brightness temperatures in infrared window channels of satellite radiometers. NOAA Tech. Rept. NESS 80, National Oceanic and Atmospheric Administration, U.S. Department of Commerce, Washington, D.C., 40 pp.

2. Weinreb, M.P., Fleming, H.E., McMillin, L.M., and Neuendorfer, A.C., 1981: Transmittances for the TIROS Operational Vertical Sounder. NOAA Tech. Rept. NESS 85, National Oceanic and Atmospheric Administration, U.S. Department of Commerce, Washington, D.C., 60 pp.

3. U.S. Standard Atmosphere, 1962: U.S. Government Printing Office, Washington, D.C., National Aeronautics and Space Administration, United States Air Force, United States Weather Bureau, December 1962.

4. Weldon, R., 1979: Satellite Training Course Notes, Part IV Cloud Patterns and the Upper Air Wind Field. Applications Division, NESS, National Oceanic and Atmospheric Administration, U.S. Department of Commerce, Washington, D.C., 80 pp.

5. Dvorak, V.F., 1984: Tropical Cyclone Intensity Analysis Using Satellite Data. NOAA Tech. Rept. NESDIS 11, National Oceanic and Atmospheric Administration, U.S. Department of Commerce, Washington, D.C., 47 pp.

Susan and I are grateful to David Brown, Frances Holt, Donald Miller, and Vince Oliver for their reviews of the draft manuscript, and their valuable suggestions for improvement.

We also thank Tina Cashman and Sherri Weldon for their typing skills; Phil Golden for the massive photo reproduction task, and Paige Bridges for drafting support and completion of the final layout.

Our special gratitude is extended to Michael Weinreb and Arthur Neuendorffer who provided the RADCOM program and aided us in its use.

I would like to express my sincere appreciation to Vince Oliver and Vern Dvorak for the many discussions of atmospheric behavior and meteorology during the research and production phases of this report. Their experience and knowledge have certainly contributed to my understanding and ability to communicate my observations. Many of the complex concepts and relationships presented in Part Two of this report have been improved or refined by our discussions. Thank you.

Roger Weldon
21 March 1991